

Part 1: Towards the Synthesis of Pyrene Zigzag Cyclacenes

**Part 2: New Methods for the Synthesis of Conjugated
Polymers**

by

Rafael Alberto Mirabal

A thesis

presented to the University of Waterloo

in fulfillment of the

thesis requirement for the degree of

Doctor of Philosophy

in

Chemistry

Waterloo, Ontario, Canada, 2021

©Rafael Alberto Mirabal 2021

Examining Committee Membership

The following served on the Examining Committee for this thesis. The decision of the Examining committee is by majority vote.

External Examiner: Dr. Graham J. Bodwell
Professor-Memorial University of Newfoundland and Labrador

Supervisor: Dr. Derek J. Schipper
Associate Professor- University of Waterloo

Internal Member: Dr. J. Michael Chong.
Professor- University of Waterloo

Internal Member: Dr. Gary Dmitrienko
Professor Emeritus-University of Waterloo

Internal Member: Dr. Adrian Schwan
Professor- University of Guelph

Internal External: Dr. Yuning Li
Professor-University of Waterloo

Author's Declaration

I hereby declare that I am the sole author of this thesis. This is a true copy of the thesis, including any final revisions, as accepted by my examiners.

I understand that this thesis may be made electronically available to the public.

Abstract

Part 1:

Carbon nanotubes (CNTs) are allotropes of carbon that have emerged as candidates for implementation in electronic devices ranging from transistors to solar cells. Unfortunately, the behavior of CNTs is highly dependent on their structure and modern synthetic methods for generating CNTs are not able to provide uniform samples for electronic applications. Recently, the synthesis of cycloparaphenylenes (CPPs), which closely resemble metallic CNTs, has been elucidated and has since been further expanded to allow for the CPPs of varying diameters and subunits. More importantly, CPPs were also shown to allow for the controlled bottom-up synthesis of CNTs, opening the door towards the concise synthesis of CNTs.

Herein, we will outline our synthetic attempts towards the synthesis of zigzag cyclacenes and how the creation of a zigzag nanobelt could bring forth the defined synthesis of semiconducting zigzag nanotubes. Drawing inspiration from previous attempts at cyclacenes and the successful synthesis of CPPs, we set out to construct a zigzag macrocycle using a Diels-Alder approach with pyrene as the backbone of the cycle. We were able to successfully construct the cyclic precursor to the cyclacene following numerous attempts; however, isolation of the fully aromatized product was not accomplished because the strain exhibited by the cycle led to an over reduction.

Our search to create cyclacenes led us towards phosphonium salts as a new method for the mild creation of benzyne. Unfortunately, the phosphonium benzyne performed poorly due to regioselectivity issues, but in trying to create the aryl phosphonium salts, we created a new route towards these compounds. Herein, we will describe our development of a metal free synthesis of aryl phosphonium salts. When aryl halides are irradiated with UV light in the presence of a phosphine, the two species can couple leading to the formation of the phosphonium salt. The reaction is amenable to a variety of phosphines and can proceed with aryl chlorides, iodides, bromides, and pseudohalides.

Part 2:

Conjugated polymers have gained a great deal of interest as these compounds can be used as active materials and enable the creation of lightweight, flexible, and low-cost electronic devices. Critical to the advancement of these technologies is the creation of new synthetic methods and facile access to material. Herein, we will outline the development of new synthetic techniques for the creating conjugated polymers.

First, we will discuss the development of a new metal free dehydrative polymerization of thiazole *N*-oxides. Drawing inspiration from nature and from the industrial synthesis of commodity polymers, such as PET and nylon-6,6, we developed a new transformation that can dimerize thiazole *N*-oxides in the absence of a metal with the formal loss of water being the sole byproduct. This methodology was later extended onto bifunctional monomers and allowed for the synthesis of conjugated polymers in quantitative yield and good molecular weights.

Secondly, we will discuss the design and synthesis of a new palladium precatalyst for the synthesis of conjugated polymers through direct arylation polymerization. Conjugated polymers are mostly synthesized using transition metal couplings such as Stille or Suzuki couplings; however, these methods require pre-functionalization and can leave behind toxic byproducts. Direct arylation polymerization has recently emerged as a new technique for synthesizing conjugated polymers; however, the nature of the propagating species means that conjugated polymers created this way are more prone to branching/crosslinking defects. We designed a palladium precatalyst specifically for direct arylation polymerization that can reduce unwanted functionalization while providing good molecular weights, high yields, lower loadings, and improved thermal properties.

Acknowledgements

This has been a long and grueling journey and I can't imagine having been able to complete this immense task without the help of the people that I've met along the way and my friends and family. First and foremost, I would like to thank my parents Rafael and Tania, my sister Nicole, and my grandparents Alberto, Lobelia and Mery. You have all been incredibly supportive and invested in my studies and I cannot thank you guys enough for your love and support.

Derek, thanks for giving me the opportunity to work in your lab, I am glad I decided to stick around. I still remember the day you offered me a full-time position back when I was volunteering the summer of my 3rd year. I remember telling my friends and family almost immediately, I could not tell you how happy I was to be given the opportunity to work in a real research lab. Thanks for all the support over the years, fun questions in group meeting, Christmas parties, etc. You have been a great boss, mentor, and friend.

I would also like to give thanks to all the members of my committee, I consider myself truly lucky to be able to attend a university with such great scientists at the helm. Dr. Chong, thanks for being such a great teacher, you were the first introduction I got to organic chemistry (Please don't look at my 264 grade) and you were also the last lecturer I had in my graduate career. Thanks for all the great advice over the years, the many lectures, and a wide array of chemicals you let me borrow from your lab, no matter how silly my idea was. Dr. Dmitrienko, thanks for all the great advice and for being a fantastic committee member. I really wished I had the opportunity to attend one of your lecture/courses is not often you get to learn from such a talented chemist. Dr. Schwan, thanks for being a great teacher, I truly enjoyed all of your lectures. Hopefully we can get the school to pay for another lunch, I'm thinking maybe we can do Red House next time. Finally, I'd also like to thank my external committee members Dr. Bodwell and Dr. Li, thank you for taking the time to read my thesis and for being a part of my committee.

Throughout my tenure in the Schipper lab a lot of people have come and gone but each member has left a positive impact on both the lab and I. Firstly, I would like to thank Dr. Mike Emmett, you were responsible for training my when I was green as grass and luckily you and I got along well. I learned a lot from you, and I don't think I really got the chance to say thanks. Tianyu and Luke, thanks for being the upmost example of what a grad student should

be and just an overall fun bunch. Dr. Selmani, thanks for being such a great friend and mentor. It's weird not having you around, you were always the person I could go to for chemistry questions or to get sidetracked for the whole day. I really hope you and the wife are doing well over in LA and that our paths cross once more. Rob, I think you and I learned roughly at the same time that conjugated polymers are somewhat migraine inducing, it was really great to go on that journey alongside you. Thanks for being a good friend and tolerating my antics, I hope the band can get back together soon and release that album. Dr. Sinclair, I don't think I have ever argued with anyone as much as I have with you, but I think those conversations made me a better person and chemist, so I thank you for that. Thanks for being such a good friend and pretty much paving the way for me. Sara, you brought so much life and energy into the lab, I truly miss having you around. Thanks for being such a great friend and lab mate.

Wayne, we started grad school at roughly the same time, and we did our undergrad together, so you were my oldest friend in the lab. We had some fun times together and I hope you are doing well, let me know if you ever cash in on bitcoin so we can celebrate. Dr. Snowden, you are an exemplary scientist and one of the hardest workers I know. I wish you the best of luck on your post doc and all your future endeavors. Jianan, my cyclacene brother and the fastest googler in the west, you are one of the smartest guys I know, I truly believe you can wrap up this cyclacene synthesis for us. It is a shame we were not the first ones to reach the cyclacenes but I'm proud of how far we got. Thanks for being such a good friend and coworker. Sarah, thanks for being such a good and compassionate person, science could truly benefit from more people like you. Javan, you are truly a great friend, few people possess that trait. Thanks for being someone I could always talk to and for being the only other metalhead in the lab, we will release that album one day. Dr. Ghods, your time in the lab was short but I learned a lot while you were around. Thank you for being supportive and for being someone to look up to.

I would also like to acknowledge some of the new recruits at the Schipper lab. Mila, since day one you and I have been good friends. It's great to have someone around that understands my sense of humor. Thanks for being a lot of fun, I have full confidence that you will amount to great things (hopefully you will be Dr. Milos in 3 years' time). Boris, you are such a nugget of joy and positivity that was sometimes very needed in the lab. I hope you continue to be awesome and that your chemistry brings only quantitative yield. Gigi, you have grown so much these

last couple of years, I was thrilled when I heard you were rejoining the lab. I wish you the best of luck and may your chemistry bring only high yields.

Throughout the years I had the opportunity to mentor several gifted students. I'm still very amazed that I was put in charge of all these folks when they were all very independent from the start. Thank you, Amelia, David, Peter, Nooran, Lukas, Chris, Daniel, Scotty and Jack. You are all great people and great chemists and I'm sure you will become pioneers in your fields.

Finally, I'd like to thank my family away from home. To the goon squad, Garner, Gene, Dom, Jen, Will, Christian, Ryan, Dalia, Sam, Tori, Eric, Yaro, and Wanning. You guys are the best friends anyone could ever ask for, I know that we will always be in touch and wish you all the best. In particular, I would like to thank the Keats way house: Ryan, you are quite frankly the smartest guy I know, thanks for being such a great friend, coming to God knows how many shows with me and for always being willing to discuss chemistry. Dalia, I think you are my oldest friend from undergrad, you are both smart and kind, and tolerate a great deal of crap from us. Thanks for always being there for me, and for putting up with all the chemistry talk that occurred at the house. Christian, I think you have published more than all of us put together and that is not a small feat. You are incredibly knowledgeable, tolerate nonsense from no one and are always willing to tell it how it is. Thanks for being such a great friend and roommate. Lastly, I would like to thank my loving girlfriend, Alex. We started talking right about when I started writing this thesis and you have been nothing but supportive. I don't think I would have been able to do this without you always cheering on. Last but not least, I'd like to thank my two kittens Betsy and Francis. It is crazy how much joy a pet can bring into a house.

Dedication

Dedicado a mis abuelos/ Dedicated to my grandparents,

Rafael, Mery, Alberto, & Lobelia

TABLE OF CONTENTS

Examining committee membership.....	ii
Authors declaration.....	iii
Abstract.....	iv
Acknowledgements.....	vi
Dedication.....	ix
List of figures.....	xiii
List of tables.....	xv
List of abbreviations.....	xvii
List of schemes.....	xx

Part 1: Carbon Nanotubes and its Fragments 1

1.1 Carbon Nanotubes.....	1
1.2 Band structure of CNTs and Graphene.....	2
1.3 Applications of Carbon Nanotubes.....	4
1.4 Synthesis of Carbon Nanotubes.....	5
1.4.1 Electric Arc Discharge.....	6
1.4.2 Laser ablation.....	7
1.4.3 Chemical Vapour Deposition.....	8
1.5 Purification of carbon nanotubes.....	9
1.6 Sorting of CNTs.....	10
1.7 Carbon Nanotube Transistors.....	11
1.8 Templating techniques for the precise synthesis of CNTs.....	12
1.9 Fragments of Carbon Nanotubes.....	15
1.9.1 Paraphenylenes and Cycloparaphenylenes.....	15
1.9.2 Template synthesis of CNTs using CPPS as a template.....	17
1.9.3 Properties and applications of CPPs.....	18
1.9.4 Bottom-up approach of CNTs using CPPs.....	20
1.9.5 Polycyclic aromatic hydrocarbons, acenes, and cyclacenes.....	22
1.9.6 Properties of acenes.....	22
1.9.7 Synthesis of linear acenes.....	27
1.9.8 Applications of acenes.....	28
1.9.9 Predicted properties of cyclacenes.....	29
1.10 Attempted synthesis of cyclacenes.....	31

Part 2: Attempted synthesis of Pyrene Zigzag Cyclacenes..... 38

2.0 Motivation.....	38
2.1 Design of pyrene cyclacene and retrosynthesis.....	39
2.2 Synthesis of starting materials.....	41
2.3 Initial attempts at cyclization.....	44
2.4 Pyrene face blocking.....	46
2.4.1-Face blocking with an inorganic molecule.....	48
2.4.2 Organic face protecting group.....	50
2.4.3 Face blocking groups using pyrrole.....	55

2.5 Pyrene cyclophane scaffold for cyclacene synthesis.....	58
2.6 Stepwise cycle formation using an orthogonal reactivity approach.....	62
2.7. Computational studies on pyrenecyclacenes.....	69
2.8 Reduction to cyclacenes.....	71
2.9 First reported synthesis of cyclacenes.....	74
2.10 Synthesis of larger cyclacenes.....	76
2.11 Synthesis of pyrenols.....	77
2.11.1 Oxidation of pyrene boronic esters.....	77
2.11.2 Sulfonate fusion.....	80
2.11.3 Metal catalyzed synthesis of PAH alcohols.....	81
2.11.4 Photocyclization of aromatic haloketones to PAH alcohols.....	84
2.12 Conclusion.....	87
Part 1: Metal free synthesis of phosphonium salts.....	88
3.1 Phosphorus compounds in organic chemistry.....	88
3.2 Phosphonium Salts.....	89
3.3 Synthesis of phosphonium salts.....	91
3.3 Benzynes from phosphonium salts and applications towards the synthesis of cyclacenes.....	96
3.4 Synthesis of aryl phosphonium salts through alkali butoxide electron transfers.....	102
3.5 Light as a tool in organic synthesis.....	105
3.6 Photophosphorylation of aryl halides with triphenylphosphine under uv light.....	110
3.7 Photophosphorylation of aryl halides with tributylphosphine under UV light.....	116
3.8 Phosphorylation of aryl halides with trioctylphosphine and tricyclohexyl phosphine under UV light.....	123
3.9 Conclusions and outlook.....	128
Part 2: Dehydration polymerization of conjugated polymers.....	130
4.1 Conjugated polymers.....	130
4.2 Properties and Application of conjugated polymers.....	130
4.3 General polymer terminology.....	131
4.4 Conjugated polymer design and bandgap engineering.....	133
4.4.1 Bond length alternation.....	135
4.4.2-Planization and rigidification.....	136
4.4.3 Electron donating/withdrawing effects.....	137
4.4.4 Acceptor-Donor motifs.....	138
4.4.5 Intramolecular interactions.....	139
4.5 Synthesis of conjugated polymers.....	140
4.5.1 Metal catalyzed polycondensation of conjugated polymers.....	141
4.5.2 Direct arylation.....	144
4.6 Condensation polymerization of commodity polymers.....	147
4.7 Dehydration polymerization of poly(hetero)arenes.....	148
4.8 Conclusions.....	156
Part 2: Design of a new palladium precatalyst for direct (hetero)arylation polymerization.....	158
5.1 Direct (hetero)arylation polymerization.....	158
5.2 Effect of the ligand on direct (hetero)arylation polymerization.....	160
5.3-Side reactions and defects of direct (hetero)arylation polymerization.....	162
5.3.1 Homocoupling.....	163
5.3.2 Branching and Cross-linking.....	164
5.3.3 End group defects.....	166

5.3.4 Residual metal defects.....	167
5.4 Catalyst design in direct (hetero)arylation polymerization.	167
5.5 Buchwald Precatalysts	168
5.6 Design of a Palladium Precatalyst for Direct (hetero)arylation polymerizations	170
5.7 Conclusions and outlook.....	181
Supporting Information	182
6.0 General considerations	182
6.1 Synthetic procedures- Chapter 2.....	183
6.2 Synthetic procedures- Chapter 3.....	222
6.3 Synthetic Procedures- Chapter 4.....	247
Photo/Electrochemical Properties – Small Molecules	273
Photo/Electrochemical Properties - Polymers	274
6.4 Synthetic Procedures-Chapter 5.....	292
6.5 NMR Spectra for Novel Compounds.....	302
7.0 References	397
Appendix-Cartesian Coordinates for Compounds in Computational Study	422

List of Figures

Page	Entry	Title
1	Figure 1.1	Structure of single-walled carbon nanotubes and multi-walled carbon nanotubes (MWNT)
2	Figure 1.2	Schematic structure of graphene chiral indices (left). Schematic representation of armchair CNTs denoted by (n,m) A , zigzag CNTs denoted by $(n,0)$ B and chiral CNTs where $(n \geq m \geq 0)$ C
3	Figure 1.3	(a) Real space representation of graphene lattice. Unit cell is shown in dashed rhombus with non-equivalent point A and B. (b) Reciprocal space representation of graphene lattice. High symmetry points (Γ , K, M) in Brillouin zone are labelled.
3	Figure 1.4	(a) Brillouin zone of graphene with conic energy dispersion at K points, allowed k_{\perp} states are indicated by the dashed lines. Zoom in of energy dispersion and cross sections along K point for metallic CNTs (b) and semiconducting CNTs (c).
5	Figure 1.5	Schematic describing the general methodology behind common CNT synthetic methods.
6	Figure 1.6	Schematic representation of the experimental setup for electric arc discharge.
7	Figure 1.7	Schematic representation of a laser ablation experimental setup.
8	Figure 1.8	Schematic figure of a chemical vapour deposition reaction setup.
11	Figure 1.9	Schematic representation of a CNT transistor.
15	Figure 1.10	Cyclic paraphenylenes (CPPs) as the shortest section of an armchair CNT (left); Cyclacenes as the shortest segment of a zigzag CNT.
15	Figure 1.11	Examples of different CPPs and LPPs.
22	Figure 1.12	Structure of common PAH, acenes and cyclacenes.
23	Figure 1.13	Clar aromatic sextets for pentacene and pyrene.
24	Figure 1.14	Chemical modification of acenes with bulky groups to prevent formation of endoperoxides and dimers.
25	Figure 1.15	Clar sextet analysis between a linear acene and a benzoannulated acene.
27	Figure 1.16	A -Schematic representation of an acene bottom contact organic field effect transistor.; B - Schematic representation of an acene organic light emitting diode.
28	Figure 1.17	Structure of anthracene chromophore for blue OLED.
28	Figure 1.18	A -Structures of [14]annulene and [10]trannulene. B - Structure of [10]cyclacene highlighting the behavior of the macrocycle as two bonded [10]trannulenes, possible theoretical resonant structures of cyclacenes with bond lengths
31	Figure 1.19	A -Structure of theoretically predicted closed shell $[5.7]_n$ cyclacene and its use as a CNT heterojunction. B -Structure of theoretically predicted closed shell benzocyclacenes.
37	Figure 1.20	Conjugated macrocycles synthesized on the path towards zigzag cyclacenes.
39	Figure 2.1	2D representation of a cyclacene vs a pyrene cyclacene.
44	Figure 2.2	Possible stereoisomers from Diels-Alder cyclization of 2.9 with benzoquinone.
77	Figure 2.3	Fluoride activated pyrene benzyne precursors.
88	Figure 3.1	Structure, oxidation state and nomenclature for common phosphorus compounds found in organic chemistry.
89	Figure 3.2	Top; equilibrium between tetra and pentacoordinated forms of tetraphenyl phosphonium bromide. Bottom; examples of phosphonium salts and their application.
103	Figure 3.3	Coordination complexes between potassium <i>tert</i> -butoxide and nitrogen heteroaromatic molecules
130	Figure 4.1	Early examples of conjugated polymers.
131	Figure 4.2	Molecular weight distribution in polymer science.
132	Figure 4.3	Branching and homocoupling defects (Left). Possible dyads in polyalkylthiophenes.
133	Figure 4.4	Band gap in small molecules versus the solid state.
134	Figure 4.5	Aromatic vs quinoidal form in conjugated polymers.
134	Figure 4.6	Schematic representation of all the contributions to the bandgap in conjugates polymers. X is a heteroatom such a O, N, S, Se, etc.

135	Figure 4.7	BLA in polythiophene (A) versus polyisothionaphthalene (B).
136	Figure 4.8	Destabilization of aromatic resonance through oxidation of polythiophene to poly(thiophene-S,S-dioxide) (PTdO).
136	Figure 4.9	Covalent and non-covalent modifications to induce planarity in conjugated polymers.
137	Figure 4.10	Effect of increasing electron withdrawing group strength on conjugated polymer band gap.
138	Figure 4.11	Molecular orbital diagram for donor-acceptor conjugated polymers.
139	Figure 4.12	A - Lamellar structure of regioregular poly(3-hexylthiophene). B - Different effects on intermolecular interactions in the solid state.
142	Figure 4.13	Schematic representation of homopolymerization and copolymerization for Stille and Suzuki cross coupling
158	Figure 5.1	Comparison between traditional cross coupling reactions and direct(hetero)arylation.
160	Figure 5.2	Effect of coordinating ligands on CMD transition state.
162	Figure 5.3	Defects associated with conjugated polymers synthesized through DARp.
165	Figure 5.4	β -branching prevention by bulky ligands and carboxylic acids.
166	Figure 5.5	End group defects in traditional couplings and direct(hetero)arylation
173	Figure 5.6	Time vs. molecular weight plots for PF8BT synthesized under conditions A, B and C.
174	Figure 5.7	^1H NMR of the aromatic region of PF8BT at 80 °C in deuterated 1,1,2,2-tetrachloroethane (TCE).
175	Figure 5.8	Possible defects present in PF8BT .
176	Figure 5.9	^1H NMR of the aromatic region of PF8BT made using condition C at 80 °C in deuterated 1,1,2,2-tetrachloroethane (TCE). Arrows indicate defect NMR signals.
177	Figure 5.10	UV-VIS spectrum of PF8BT synthesized through conditions A, B, and C.
178	Figure 5.11	Time vs. molecular weight plot for PF8BT synthesized with condition D .
181	Figure 5.12	Candidates for new series of DHAP precatalysts.
217	Figure S1	Geometry optimized structure for 10-pyrenecyclacene (2.118)
218	Figure S2	Bond lengths in 2.118
222	Figure S3	Strain analysis for pyrene cyclacenes.
299	Figure S4	Differential calorimetry data for PF8BT made with conditions A, B, and C.

List of Tables:

Page	Entry	Title
70	Table 2.1	Summary of theoretical calculations on cyclacenes and pyrenecyclacenes.
71	Table 2.2	Summary of NICS(0) values for [10] and [20] pyrenecyclacenes.
85	Table 2.3	Summary of optimization of photocyclization of α -haloketones. Reactions were irradiated in a 10 mL quartz test tube overnight with 1-([1,1'-biphenyl]-2-yl)-2-bromoethan-1-one(1 equiv), Base (2 equiv) in solvent [0.2 M]. Yield in parenthesis indicates isolated yield.
104	Table 3.1	Reaction optimization for the metal free synthesis of aryl phosphonium salts using <i>tert</i> butoxide bases.
110	Table 3.2	Optimization for the UV synthesis of tetraphenyl phosphonium iodide from iodobenzene and triphenylphosphine. Reactions were performed in 0.2 M concentration for 18 h.[a]-reaction performed under UV light using a handheld TLC light for 4 h.
113	Table 3.3	Optimization of photophosphorylation of bromobenzene with triphenylphosphine. Reactions were carried out at 0.2 M for 18 h; Yields were determined by ^{31}P NMR using triphenyl phosphate as an internal standard. [a]-reaction was carried out for 36 h.
116	Table 3.4	Optimization of photophosphorylation of bromobenzene with PBU_3 . Reactions were performed at 254 nm with 1 equiv of bromobenzene, 3 equiv of PBU_3 in MeCN [0.2 M] for 18 h.
120	Table 3.5	Optimization of photophosphorylation of bromobenzene with PBU_3 . Reactions were performed at 254 nm in MeCN [0.2 M]. Yields were determined by ^{31}P NMR with triphenyl phosphate as an internal standard. [a]- reaction was carried out in the absence of stirring.
122	Table 3.6	Optimization for photophosphorylation of aryl chlorides with tributyl phosphine. Reactions were carried out with 1 equiv of the aryl chloride, 3 equiv of the phosphine in MeCN [0.2 M] for 18 h at 254 nm. Yields were determined by ^{31}P NMR using triphenyl phosphate as an internal standard.
123	Table 3.7	Condition screening for the photophosphorylation of chlorobenzene with $\text{HBF}_4\text{PCy}_3/\text{DIPEA}$ (1:1 ratio) under 254 nm. Reactions were carried out in MeCN [0.2 M]. [a]- 2 equiv of NaI was added to the reaction mixture. [b]-Reaction was reacted at [0.1 M] concentration.
125	Table 3.8	Condition screening for the photophosphorylation of chlorobenzene with TOP. Reactions were carried out in MeCN [0.2 M] under 254 nm light. [a] - ^{31}P yield determined using triphenyl phosphate as an internal standard. [b]- reaction ran at [0.1 M] concentration.
148	Table 4.1	Optimization of thiazole dimerization. 1 equiv of 4,5-dimethylthiazole <i>N</i> -oxide was reacted with 1.5 equiv of base in 0.25 M solvent. Initial optimization carried out by Dr. Michael R. Emmett.
173	Table 5.1	Summary of results for PF8BT polymerization under different conditions. Molecular weights were estimated by GPC with THF at 35 °C against polystyrene standards.
174	Table 5.2	Differential calorimetry data for PF8BT synthesized through conditions A, B, and C.
176	Table 5.3	Percentage of impurities present in PF8BT synthesized through conditions A, B, and C.
177	Table 5.4	Maximum absorption wavelengths for PF8BT synthesized with conditions A, B, and C
179	Table 5.5	Molecular weights and yields for polymerization of PDOF-TP with precatalyst 5.39 .
218	Table S1	Cavity size and wagging bend angle for 2.118
218	Table S2	Thermochemistry for [10]cyclacene.
218	Table S3	FMOs for [10]cyclacene.
219	Table S4	FMOs for [10]pyrenecyclacene
221	Table S5	Thermochemical data for 2.118 triplet.
221	Table S6	FMOs for 2.119 triplet.
221	Table S7	Thermochemical data for cyclacene species used in strain analysis.
221	Table S8	FMO comparison for pyrenecyclacenes of varying sizes.
221	Table S9	Strain and thermochemical comparison between cyclacenes and pyrenecyclacenes of varying sizes.
294	Table S10	Time vs. Molecular weight data for PF8BT using $\text{Pd}(\text{OAc})_2/\text{P}(\text{o-anisyl})_3$

295	Table S11	Time vs. Molecular weight data for PF8BT using Pd(OAc) ₂ /P(<i>o</i> -anisyl) ₃
296	Table S12	Time vs. Molecular weight data for PF8BT using precatalyst (5.39)
297	Table S13	Time vs. Molecular weight data for PF8BT using precatalyst (5.39) with LiO ^t Bu as an additive.
298	Table S14	Crystal and structure refinement data for 5.39 . Crystal structure of material was elucidated with the aid of the SQUEEZE function.
302	Table S15	Table of contents for compound NMR spectra.
424	Table S16	Cartesian coordinates for [10]pyrenecyclacene.
426	Table S17	Cartesian coordinates for [15]pyrenecyclacene.
430	Table S18	Cartesian coordinates for [20]pyrenecyclacene.
436	Table S19	Cartesian coordinates for [25]pyrenecyclacene.
442	Table S20	Cartesian coordinates for [10]cyclacene.
444	Table S21	Cartesian Coordinates for [20]cyclacene.

List of Abbreviations

AFM	Atomic force microscopy
Ad	Adamantane
BC	Benzoannulated cyclacene
BLA	Bond length alternation
bpy	Bipyridine
CMD	Concerted metalation deprotonation
CNTFET	Carbon nanotube field effect transistor
CNT	Carbon nanotube
COD	1,5-Cyclooctadiene
CPPs	Cycloparaphenylene
CVD	Chemical vapour deposition
Cy	Cyclohexyl
dba	Dibenzylideneacetone
DCE	1,2-Dichloroethane
DCM	Dichloromethane
DCTB	trans-2-[3-(4- <i>tert</i> -Butylphenyl)-2-methyl-2-propenylidene]malononitrile
DDQ	2,3-Dichloro-5,6-dicyano-1,4-benzoquinone
DEHA	Bis(2-ethylhexyl) adipate
DFT	Density functional theory
DHAP	Direct(hetero)arylation polymerization
DI	Deionized
DIPEA	Diisopropylethylamine
Dipytet	3,6-di(pyridin-2-yl)-1,2,4,5-tetrazine
DMAc	Dimethyl acetamide
DMDO	Dimethyldioxirane
DMF	Dimethylformamide
DMSO	Dimethyl sulfoxide
DNA	Deoxyribonucleic acid
dppe	1,2-Bis(diphenylphosphino)ethane
dppf	1,1'-Bis(diphenylphosphino)ferrocene
DSC	Differential scanning calorimetry
dtbpy	4,4-Di- <i>tert</i> -butyl-2,2'-bipyridine
EDG	Electron donating group
EDOT	3,4-Ethylenedioxythiophene
EWG	Electron withdrawing group
FET	Field effect transistor
FMO	Frontier molecular orbital
GPC	Gel permeation chromatography
HiPco	High pressure carbon monoxide
HMDS	Hexamethyldisilazane
HMPA	Hexamethylphosphoramide
HOMO	Highest occupied molecular orbital
HPLC	High pressure liquid chromatography
HRMS	High resolution mass spectrometry
HWE	Horner-Wadsworth Emmons
ICP-MS	Inductively coupled plasma mass spectrometry
IDC	Iterative-convergent/divergent
IPA	Isopropyl alcohol
ITO	Indium tin oxide

LPP	Linear paraphenylenes
LUMO	Lowest unoccupied molecular orbital
MALDI-TOF	Matrix assisted laser desorption ionization- time of flight
<i>m</i> -CPBA	<i>m</i> -Chloroperbenzoic acid
MMPP	Magnesium monoperoxyphthalate
M _n	Number average molecular weight
MS	Mass spectrometry
MWCNT	Multi-walled carbon nanotubes
M _w	Weight average molecular weight
MW	Microwave
NBS	<i>N</i> -bromosuccinimide
NDA	Neodecanoic acid
NICS	Nucleus-independent chemical shift
NMR	Nuclear magnetic resonance
NOE	Nuclear Overhauser effect
OFET	Organic field effect transistor
OLED	Organic light emitting diode
OPV	Organic photovoltaics
P3HT	Poly(3-hexylthiophene)
PAH	Polycyclic aromatic hydrocarbon
PCDPP	Poly[<i>N</i> -9''-heptadecanyl-2,7-carbazole-3,6-bis(thiophen-5-yl)-2,5-dioctyl-2,5-dihydropyrrolo[3,4-]pyrrole-1,4-dione]
PCE	Power conversion efficiency
PDI	Polydispersity index
PDOF-TP	Poly(dioctylfluorene tetrafluorobenzene)
PEG	Polyethylene glycol
PEPPSI	Pyridine-enhanced precatalyst preparation stabilization and initiation
PET	Poly(ethylene terephthalate)
PF8BT	Poly(9,9-dioctyl-2,7-fluorene-alt-2,2'- bithiophene)
PF8BT	Poly(dioctylfluorenebithiophene)
Pin	Pinacol
Piv	Pivalic, Pivaloyl
PMMA	Poly(methyl methacrylate)
ppy	2-Phenylpyridine
PTdO	Poly(thiophene- <i>S,S</i> -dioxide)
RB	Round bottom
RCM	Ring-closing metathesis
rr	Regioregularity
SET	Single electron transfer
SWCNTs	Single walled carbon nanotubes
S _N Ar	Nucleophilic aromatic substitution
TBAF	Tetrabutylammonium fluoride
TBAI	Tetrabutylammonium iodide
TCB	1,3,5-Trichlorobenzene
TCE	1,1,2,2-Tetrachloroethane
TEA	Triethylamine
TEMPO	(2,2,6,6-Tetramethylpiperidin-1-yl)oxyl
TFA	Trifluoroacetic acid
TFE	2,2,2-Trifluoroethanol
TGA	Thermogravimetric analysis
THF	Tetrahydrofuran
TLC	Thin layer chromatography
TM	Transition metal

T _m	Melting temperature
TMS	Trimethylsilyl
TON	Turnover number
TOP	Trioctylphosphine
TPD	Thienopyrrolodione
TPO	Triphenylphosphine oxide
TfOH	Triflic acid
UV	Ultraviolet
UV-Vis	Ultraviolet-visible

List of Schemes:

Page	Entry	Title
12	Scheme 1.1	Synthesis of specific type nanotubes using template technique.
13	Scheme 1.2	Metal free "cloning" CVD growth of CNTs.
14	Scheme 1.3	Schematic representation of seeded CVD growth of capped CNTs using an open C ₆₀ fullerene as the seed.
16	Scheme 1.4	Jasti <i>et al.</i> synthesis of [9], [12] and [18]CPP.
17	Scheme 1.5	-Yamago <i>et al.</i> synthesis of [8]CPP using a Pt tetracoordinate approach.
18	Scheme 1.6	Schematic representation of the well-defined growth of CNTs using CPPs as seeds/templates.
19	Scheme 1.7	Host-guest chemistry of [10]CPP to form shortest fullerene-peapod.
19	Scheme 1.8	Yamago synthesis of the green OLED [4]cyclo-9,9-dipropyl-2,7-fluorene.
20	Scheme 1.9	Scholl cyclodehydrogenation of CPPs to form ultrashort-CNT fragments.
21	Scheme 1.10	Synthesis of CPP 1.18 .
24	Scheme 1.11	A -Formation of endoperoxides in acenes. B - Self dimerization of pentacene.
25	Scheme 1.12	Matrix assisted synthesis of heptacene.
26	Scheme 1.13	Synthesis of twisted heptacene using a Diels-Alder approach.
27	Scheme 1.14	Synthesis of first isolatable and crystalline nonacenes.
28	Scheme 1.15	Rapid synthesis of pentacene.
32	Scheme 1.16	Stoddard and coworkers' synthesis of [12]collarene.
34	Scheme 1.17	Corey and coworkers' synthesis of [8]cyclacene precursors.
35	Scheme 1.18	Gleiter and coworkers' synthesis of [6.8] ₃ cyclacene
36	Scheme 1.19	Itami and coworkers' attempted synthesis of [12]benzocyclacenes.
39	Scheme 2.1	Retrosynthetic analysis of [9]benzocyclacene.
40	Scheme 2.2	Proposed synthetic pathways towards macrocyclic precursor to pyrene cyclacene.
41	Scheme 2.3	Synthesis of pyrenofurans.
43	Scheme 2.4	A -Synthesis of dipytet. B -Dipytet mediated synthesis of benzofurans.
44	Scheme 2.5	Attempted cyclization of bisdiene 2.9 with <i>p</i> -benzoquinone.
45	Scheme 2.6	Attempted synthesis of cyclacenes using an AB approach.
46	Scheme 2.7	Attempted synthesis of cyclacenes using an AA-BB approach.
46	Scheme 2.8	Schematic representation of possible reaction outcomes for AA-BB cyclization approach.
47	Scheme 2.9	Possible reaction outcomes after the formation of diad 2.22 .
48	Scheme 2.10	Directing role of Cr(CO) ₃ in [4+2] Cycloadditions.
48	Scheme 2.11	Attempted synthesis of pyrene-chromium complexes.
49	Scheme 2.12	<i>In situ</i> synthesis of 2.30 followed by reaction with bisdiene 2.9 .
50	Scheme 2.13	<i>In situ</i> synthesis of 2.31 for the directed cyclization of 2.7
51	Scheme 2.14	Schematic representation of an organic face blocking group directing the reaction towards a cyclic product. Blue bar represents a pyrene furan/dibromide, red bar represents a new pyrene unit, grey box represents organic face blocking molecule.
51	Scheme 2.15	Schematic representation of a face grouping molecules ability to prevent endoperoxide and dimer formation.
52	Scheme 2.16	Retrosynthetic analysis for the synthesis of an organic face protected pyrene using perfluorobiphenyl.
52	Scheme 2.17	Attempted synthesis of 2.37 and 2.38 .
53	Scheme 2.18	Attempted synthesis of 2.38 using alkyl chloride 2.40 .
53	Scheme 2.19	Attempted synthesis of face protected pyrene using perfluorobiphenyl.
54	Scheme 2.20	Open vs closed equilibrium for alkylated pyrene.
55	Scheme 2.21	Retrosynthetic analysis for faced blocked pyreno-pyrrole.
55	Scheme 2.22	Attempted synthesis of tethered pyrene.
56	Scheme 2.23	Control reactions for the synthesis of a tethered pyrenopyrrole.
56	Scheme 2.24	Prior reports using pyrroles as dienophiles in [4+2] cycloadditions with benzyne.

57	Scheme 2.25	Successful cycloaddition of <i>N</i> -methylpyrrole with a benzyne dienophile.
58	Scheme 2.26	Alternate RCM pathway for the synthesis of a pyrene-cyclophane.
58	Scheme 2.27	Pyrene labelling and effect of bulky electrophiles on the regiochemistry of pyrene.
59	Scheme 2.28	Ir C-H activation of pyrene.
59	Scheme 2.29	Retrosynthetic analysis for a pyrene cyclophane using a RCM approach.
61	Scheme 2.30	Attempted synthesis of pyrene cyclophane 2.71 .
61	Scheme 2.31	Bromination control experiment of 2,7-dimethoxypyrene.
62	Scheme 2.32	Attempted bromination of 2,7-bis(pinacolato)boronpyrene and alternate pathway using trifluoroborate salts.
63	Scheme 2.33	Schematic representation of orthogonal reactivity to achieve the stepwise construction of a cyclacene.
63	Scheme 2.34	Attempted synthesis of pyrene diad 2.89 .
64	Scheme 2.35	Attempted synthesis of pyrene diad 2.90 .
64	Scheme 2.36	Synthesis of benzobisoxadisiloles.
65	Scheme 2.37	Benzyne generation through benzooxadisiloles and <i>o</i> -bis(trimethylsilyl)benzene.
66	Scheme 2.38	Synthesis of pyrene benzooxadisiloles.
67	Scheme 2.39	Attempted orthogonal synthesis of pyrene diads.
67	Scheme 2.40	Synthesis of bistriflate 2.110 .
68	Scheme 2.41	Synthesis of [10]tetraepoxy pyrenecyclacene 2.113 .
69	Scheme 2.42	Synthesis of orthogonally reactive pyrene benzyne precursors.
70	Scheme 2.43	Comparison between [12]BC and [10]pyrenocyclacene.
71	Scheme 2.44	NICS analysis of [20] and [10]pyrenocyclacene.
72	Scheme 2.45	Attempted reduction of tetraepoxycyclacene to 2.119 .
73	Scheme 2.46	Partial deoxygenation of 2.1123
73	Scheme 2.47	Oxidation of 2.120 .
74	Scheme 2.48	Successful synthesis of pyrene cyclacenes.
74	Scheme 2.49	Itami and coworkers' synthesis of zigzag carbon nanobelt.
75	Scheme 2.50	Chi and coworkers' synthesis of a [12,0] CNT sidewall fragment.
77	Scheme 2.51	Attempted synthesis of [20]pyrenocyclacene.
78	Scheme 2.52	Synthesis of pyrenols from pyrene boronic esters.
79	Scheme 2.53	Attempted synthesis of a pyrene bistriflate.
80	Scheme 2.54	Synthesis of brominated pyrene <i>anti</i> -diol anti-2.239 .
80	Scheme 2.55	Synthesis of pyranine using sulfonate fusion.
80	Scheme 2.56	Attempted synthesis of pyrenols using sulfonate fusion.
81	Scheme 2.57	Proposed synthesis of PAH alcohols using a metal catalyzed intramolecular ring closing strategy
82	Scheme 2.58	Proposed catalytic cycle for the metal catalyzed synthesis of PAH alcohols.
83	Scheme 2.59	Synthesis of PAH cyclization precursors.
84	Scheme 2.60	Attempted synthesis of PAH using a transition metal catalyzed ring closing.
84	Scheme 2.61	A-Synthesis of 9-phenanthrol using a photochemical approach.
86	Scheme 2.62	Thermal control reaction for photocyclization of α -haloketones.
86	Scheme 2.63	Attempted synthesis of bispyrenol.
88	Scheme 3.1	Reactions mediated by phosphorus compounds.
90	Scheme 3.2	A - Generic catalytic cycle for phosphine organocatalysis. B - Intramolecular Rauhut-Currier reaction by Wang et al. C : Asymmetric example of Morita-Baylis Hillman reaction as reported by Huang and Shi.
91	Scheme 3.3	Synthesis of methyltriphenylphosphonium bromide via nucleophilic attack of PPh ₃ on methyl bromide.
91	Scheme 3.4	Synthesis of (dihydroxynaphthalen-2-yl)phosphonium triflate via conjugate addition.
92	Scheme 3.5	A -Charette and Marcoux's synthesis of aryl phosphonium salts using either a Ni or Pd catalyst. B -Catalytic cycle for the metal catalyzed synthesis of aryl phosphonium salts. C - <i>In situ</i> formation of Ni(I) catalyst for the Ni catalyzed synthesis of aryl phosphonium salts.

93	Scheme 3.6	A -Benzyne mediated synthesis of aryl phosphonium salts. B -Synthesis of aryl phosphonium salts through reaction of benzyne with triphenylphosphine oxide.
94	Scheme 3.7	Umpolung strategy for the synthesis of phosphonium salts and phosphines.
95	Scheme 3.8	A - Synthesis of aryl phosphonium light using a Ru photocatalyst under visible light. B - Synthesis of aryl phosphonium salts under metal/catalyst free conditions utilizing 400 nm (purple) light.
96	Scheme 3.9	(Left) Catalytic cycle for the synthesis of tetraaryl phosphonium salts using a Ru photocatalyst under visible light. (Right) Metal free synthesis of aryl phosphonium salts using visible light.
97	Scheme 3.10	A - Initial attempted synthesis of a [9]epoxycyclacene using an AB-cyclization triggered by a lithium halogen exchange with <i>n</i> -BuLi. B - First successful cyclization of a pyrene epoxycyclacene in our laboratory using a benzyne triggered by the addition of fluoride. C - Proposed monomer with orthogonal benzyne reactivity for the stepwise construction of a pyrene cyclacene.
98	Scheme 3.11	Nucleophilic arylation with tetraarylphosphonium salts.
98	Scheme 3.12	Formation of benzyne through the elimination of a phosphonium salt. Target benzyne precursors for the stepwise formation of pyrene cyclacenes.
99	Scheme 3.13	Attempted synthesis of pyrene arylphosphonium salt through metal catalyzed cross-coupling.
100	Scheme 3.14	A -Attempted synthesis of phosphonium benzyne precursor through metal catalyzed synthesis of tetraaryl phosphonium salts. B -Possible reduction mechanism for the metal cross coupling of 1,2-dihalobenzenes.
101	Scheme 3.15	A -Synthesis of phosphonium benzyne precursor. B -Attempted Diels Alder reaction with furan and Cs ₂ CO ₃ generated benzyne.
101	Scheme 3.16	Possible degradation pathways for 3.14 under Cs ₂ CO ₃ .
102	Scheme 3.17	General scheme for the radical coupling of a phosphine to an aryl radical to form an aryl phosphonium salt.
102	Scheme 3.18	<i>tert</i> -Butoxide mediated radical coupling of aryl halides with aromatics and heteroaromatic groups.
104	Scheme 3.19	Optimized conditions for the synthesis of tetraarylphosphonium salts from aryl iodides and potassium <i>tert</i> -butoxide.
105	Scheme 3.20	A - Test reaction for the determination of a radical or benzyne mechanism. B - Mechanistic rationale for the formation of observed regioisomers.
106	Scheme 3.21	Radical cyclization of aryl iodides using a [Ir(ppy) ₂ (dtbbpy)]PF ₆ photocatalyst.
106	Scheme 3.22	Homolytic dissociation of aryl halides under ultraviolet irradiation.
107	Scheme 3.23	A - Intermolecular photocyclization for the formation of biphenyls. B - Intramolecular photocyclization of phenyl pyrazoles
108	Scheme 3.24	A - Traditional Miyaura borylation of bromobenzene with pinacol borane. B - UV light synthesis of aryl boronates from aryl fluorides.; C - Synthesis of aryl iodides from aryl triflates under UV conditions.
109	Scheme 3.25	Synthesis of a calcium antagonist via UV coupling of H-Phosphonates.
110	Scheme 3.26	UV mediated aromatic "Finkelstein" of 4-bromoisoquinoline.
111	Scheme 3.27	Proposed mechanism for the synthesis of quaternary phosphonium salts via UV light.
111	Scheme 3.28	Control reactions for the UV synthesis of tetraaryl phosphonium iodides.
112	Scheme 3.29	Substrate scope for photophosphorylation of aryl iodides with triphenylphosphine. Reactions were carried out in DMSO [0.2 M] with 1 equiv of the aryl iodide and 3equiv of triphenyl phosphate at 300 nm. Yields were determined by ³¹ P NMR using triphenyl phosphate as an internal standard.
114	Scheme 3.30	Proposed mechanism for <i>in situ</i> aromatic "Finkelstein" followed by our photophosphorylation to form tetraphenyl phosphonium iodide.
114	Scheme 3.31	Substrate scope for the photophosphorylation of aryl bromides under UV irradiation. Reactions were performed with 1 equiv of aryl iodide, 3equiv of PPh ₃ in MeCN [0.2 M] for 18 h. Purity was determined by ³¹ P NMR after isolation of the phosphonium

		salt. A - Reaction was carried out with 1 equiv of 4-iodotoluene, 3 equiv of PPh ₃ and 3 equiv of NaI in acetone [0.2 M] at 350 nm for 18 h.
116	Scheme 3.32	Control reactions for photophosphorylation of aryl halides. A - 1 equiv of PPh ₃ was irradiated at either 350 nm or 254 nm for 18 h in MeCN [0.2 M].; B - 1 equiv of triphenylphosphine oxide was irradiated at 254 nm for 18 h in MeCN [0.2 M]. Yields were determined via ³¹ P NMR with triphenyl phosphate as an internal standard.
116	Scheme 3.33	Control reaction of PBu ₃ under UV radiation. 1 equiv of PBu ₃ was irradiated at 254 nm in MeCN [0.2 M] for 18 h. Yield was determined via ³¹ P NMR with triphenyl phosphate as an internal standard.
117	Scheme 3.34	Photophosphorylation of aryl bromides with PBu ₃ . Reactions were performed at 254 nm with 1 equiv of the aryl bromide, 3 equiv of PBu ₃ in MeCN [0.2 M] for 18 h. Yields were determined by ³¹ P NMR with triphenyl phosphate as an internal standard.
118	Scheme 3.35	Photophosphorylation of aryl chlorides with PBu ₃ . Reactions were performed at 254 nm with 1 equiv of the aryl chloride, 3 equiv of PBu ₃ in MeCN [0.2 M] for 18 h. Yields were determined by ³¹ P NMR with triphenyl phosphate as an internal standard.
118	Scheme 3.36	Reactions were performed at 254 nm with 1 equiv of the aryl halide/pseudohalide, 3 equiv of PBu ₃ in MeCN [0.2 M] for 18 h. Yields were determined by ³¹ P NMR with triphenyl phosphate as an internal standard.
121	Scheme 3.37	Test reaction for the origin of PBu ₄ Br impurity. Reaction was carried out 1 equiv of PhPBu ₃ Br, 2 equiv of PBu ₃ in MeCN [0.2 M] under reflux for 18 h. Yield was determined by ³¹ P NMR using triphenyl phosphate as an internal standard.
121	Scheme 3.38	Isolatable tributyl phosphonium salts synthesized through UV phosphorylation. Reactions were carried out 3 equiv of phosphine, 3 equiv of DIPEA and 1 equiv of the aryl chloride in MeCN [0.2 M] under 254 nm for 36 h. a -synthesized using 3 equiv of PBu ₃ .
123	Scheme 3.39	Isolatable tributyl phosphonium salts synthesized through UV phosphorylation. Reactions were carried out 1 equiv of phosphine, 1 equiv of DIPEA and 1 equiv of the aryl chloride in MeCN [0.2 M] under 254 nm for 18 h
124	Scheme 3.40	Reaction scope for the photophosphorylation of aryl halides with HBF ₄ PCy ₃ . Reactions were carried out with 1 equiv of aryl halide, 3 equiv of HBF ₄ PCy ₃ , 3 equiv of DIPEA in MeCN [0.2 M] under 254 nm for 18 h. Bromobenzene was irradiated for 36 h.
125	Scheme 3.41	Possible radical pathways during homolytic cleavage of chlorobenzene.
127	Scheme 3.42	Reaction scope for the photophosphorylation of aryl chlorides with TOP. Reactions were carried out with 1 equiv of aryl chloride and 3 equiv of TOP in MeCN [0.2 M] under 254 nm light.
128	Scheme 3.43	UV photophosphorylation of 1,4-dichlorobenzene. Reaction was ran with 1 equiv of the 1,4-dichlorobenzene. 3 equiv of TOP in MeCN [0.2 M] under 254 nm irradiation for 18 h.
140	Scheme 4.1	Overview of traditional synthetic techniques for the preparation of conjugated polymers.
141	Scheme 4.2	Generic catalytic cycle for transition metal cross-couplings.
142	Scheme 4.3	Synthesis of polyalkylthiophene via Negishi and Kumada cross-couplings.
143	Scheme 4.4	Example of a Stille homopolymerization (top) and a Suzuki one pot homopolymerization.
143	Scheme 4.5	Pre-functionalization of Pd catalyzed cross coupling monomers for Stille (A) and Suzuki (B).
144	Scheme 4.6	Drawbacks of Pd catalyzed polycondensations; Stille copolymerization resulting in the formation of stoichiometric amount of toxic organotin waste (A). Protodeboronation of a bifunctional Suzuki monomer (B).
145	Scheme 4.7	Direct arylation of benzothiazole with 4-bromotoluene and catalytic cycle for direct arylation.
146	Scheme 4.8	Synthesis of polythienopyrrole through direct arylation and Stille polycondensations.

147	Scheme 4.9	Synthesis of biopolymers and commodity polymers through dehydration polymerization.
148	Scheme 4.10	Traditional synthesis of conjugated polymers versus dehydration polymerization for the preparation of conjugated polymers. Z is a carbon or heteroatom, Y is a heteroatom, X is a halide.
149	Scheme 4.11	Proposed mechanism for dehydrative dimerization of 4,5-dimethylthiazole.
149	Scheme 4.12	Thiazole dehydration substrate scope general outline.
150	Scheme 4.13	Synthesis of thiazole <i>N</i> -oxide precursors by direct arylation. Reactions were carried out with 1.5 equiv of thiazole, 1 equiv of aryl bromide, 1.5 equiv of K ₂ CO ₃ , Pd(OAc) ₂ (2 mol%), PCy ₃ HBF ₄ (4 mol%), 0.3 equiv of PivOH in DMAc [0.5 M] for 20 h at 100 °C
151	Scheme 4.14	Oxidation of thiazole with <i>m</i> CPBA. Oxidations were carried out with 1 equiv of thiazole, 1.5 equiv of <i>m</i> CPBA in DCE [0.33 M] for 2-4 h.
152	Scheme 4.15	A -Oxidative ring opening of benzothiazoles. B -Directed oxidation of thiazoles through a diphenyl carbinol. C -Oxidation of thiazoles with Rozen's reagent.
153	Scheme 4.16	Reaction scope for the dehydrative coupling of thiazole <i>N</i> -oxides. Reactions were run with 1 equiv of <i>N</i> -oxide and 1.5 equiv of LiO ^t Bu in THF [0.25 M].
154	Scheme 4.17	Dehydrative cross couplings of thiazoles. Reactions were run with 1 equiv each of <i>N</i> -oxide and 3.0 equiv of LiO ^t Bu in THF [0.25 M].
155	Scheme 4.18	Dehydration polymerization of thiazole <i>N</i> -oxides.
156	Scheme 4.19	Deoxygenation of thiazole dehydration dimers and polymers.
158	Scheme 5.1	Lemaire and coworkers' synthesis of polyalkylthiophenes.
159	Scheme 5.2	Ozawa and coworkers' synthesis of highly regioregular poly(3-hexylthiophene) through direct arylation.
159	Scheme 5.3	A - Ozawa and coworkers' synthesis of PDOF-TP 5.8 . B - Leclerc and coworkers' synthesis of PCDPP 5.11 .
161	Scheme 5.4	Examples of ligand free direct arylation in small molecules (A) and in conjugated polymers (B).
162	Scheme 5.5	Mixed ligand polymerization of 5.20 .
163	Scheme 5.6	Homocoupling pathways in transition metal catalyzed couplings as exemplified by Still coupling.
164	Scheme 5.7	Free energy of activation (ΔG_{298} , kcal mol ⁻¹) for C-H activation via CMD for thiophene.
165	Scheme 5.8	Copolymerization of fluorene and bithiophene using β -protected monomers.
166	Scheme 5.9	Removal of end group defects by end capping Br-terminus. 1-AdCOOH- 1-adamantencarboxylic acid.
168	Scheme 5.10	Dual catalytic direct arylation polymerization of P3HT .
169	Scheme 5.11	A -Buchwald precatalyst generations I, II, III. B - Mode of activation for Buchwald precatalyst.
169	Scheme 5.12	Suzuki coupling of unstable boronic acids with Buchwald precatalysts.
170	Scheme 5.13	Buchwald precatalyst for direct (hetero)arylation polymerization.
171	Scheme 5.14	Synthesis of direct arylation Buchwald precatalyst.
171	Scheme 5.15	Synthesis of PF8BT .
179	Scheme 5.16	Synthesis of PDOF-TP using precatalyst 5.41 .
180	Scheme 5.17	Synthesis of P3HT with precatalyst 5.40 .

CARBON NANOTUBES AND ITS FRAGMENTS

1.1 CARBON NANOTUBES

Carbon nanotubes (CNTs) are allotropes of carbon in which the carbon atoms are arranged in a rolled graphitic sheet that takes the form of a 1-dimensional tube composed solely of sp^2 carbons in a hexagonal pattern.¹⁻³ CNTs can exist in various forms with lengths in the micro to centimeter range and diameters in the nanometer range. There are two main types of CNTs with single walled carbon nanotubes (SWCNTs) comprised of a sole graphitic sheet rolled into a tube and multiwalled carbon nanotubes (MWCNTs) which are a series of CNTs arranged within each other much like concentric rings within a tree trunk (**Figure 1.1**).

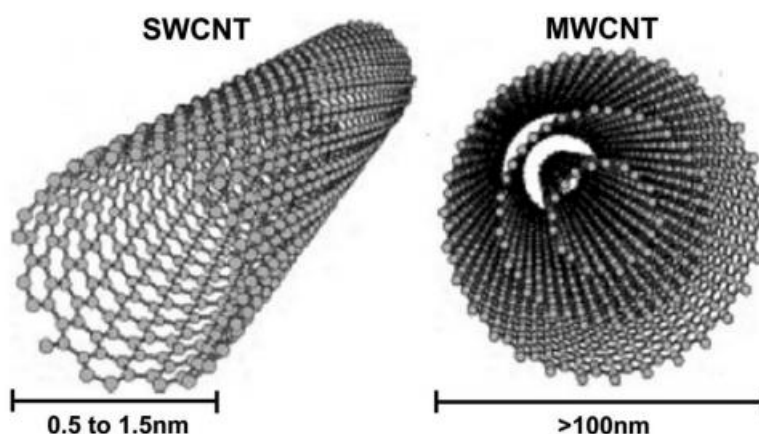


Figure 1.1- Structure of single-walled carbon nanotubes and multi-walled carbon nanotubes (MWCNT).⁴

CNTs can also exist in either open or capped⁵ forms and the cavity within the cylinder can also be occupied by molecules such as fullerenes.⁶ In addition to the CNTs listed above, different edge chiralities arise from SWCNTs and can have a great effect on the CNTs' properties. When describing CNTs two integers (n,m) are used to describe the shape and direction of the CNT. These integers originate from the graphene unit cell from which the CNT is "rolled up" and are referred to as the chiral indices. There are three types of CNT chiralities that can be described by these indices: zigzag ($n,0$), armchair ($n=m$) and chiral ($n \neq m$). **Figure 1.2** highlights how these chiral indices can be used to describe a CNT as well as schematic representations of each type of CNT chirality.

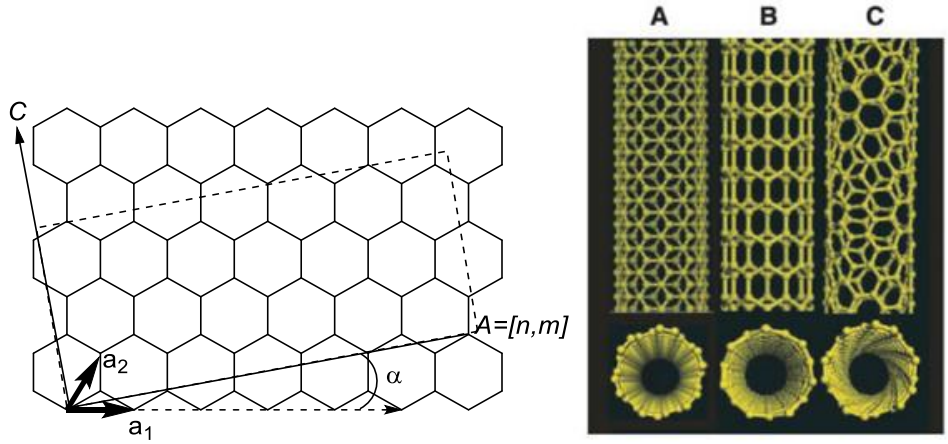


Figure 1.2- Schematic structure of graphene chiral indices (left). Schematic representation of armchair CNTs denoted by (n,m) **A**, zigzag CNTs denoted by $(n,0)$ **B** and chiral CNTs where $(n \geq m \geq 0)$ **C**.²

For a given CNT, the chiral indices indicate the perimeter of the tube denoted by \vec{A} . The perimeter vector of the CNT refers to the length of the graphene sheet and is defined by: $\vec{A} = (n, m) = n\vec{a} + m\vec{a}$, where the magnitude of A is defined by $A = a_0(n^2 + m^2 + nm)^{1/2}$ and $a_1 = a_2 = a_0 = 0.246nm$, the value of the latter value is obtained from spacing in a graphene sheet.⁷ The tubule axis, C , runs perpendicular to the perimeter vector, \vec{A} , and is the axis on which the CNT is rolled up from the graphene sheet. The diameter of the tube, d , can also be derived from the chiral indices following the equation $d = \frac{A}{\pi} = \frac{a_0}{\pi} \sqrt{n^2 + m^2 + nm}$. Finally, helicity, α , describes the angle on which the graphene sheet is rolled up but is more specifically defined as the angle between the perimeter and basis vector denoted by the equation $\alpha = \cos^{-1} \frac{2n+m}{2\sqrt{n^2+m^2+nm}}$. From the helicity equation, we can see how two special cases arise, one where $(n \geq 1, m=0)$ which gives rise to zigzag CNTs and a $\alpha=0^\circ$ and a second case where $(n=m)$ resulting in an armchair CNT with $\alpha=30^\circ$.⁷

1.2 BAND STRUCTURE OF CNTS AND GRAPHENE

As stated previously the structure and chirality can have a great effect on the properties of the CNT and consequently the application the material is used for. To understand how CNTs behave, it is necessary to first understand the band structure of graphene as the approximations used to understand the band structure of CNTs stems from graphene. Much like CNTs, graphene is also an allotrope of carbon in which a series of sp^2 carbons are arranged in hexagonal pattern in a single sheet. Being solely composed of carbon, the $2s$, $2p_x$ and $2p_y$ are hybridized and responsible for the σ -bonding while the remaining $2p_z$ orbital exists out of the plane and makes up the π -orbitals

responsible for the band structure in graphene. The π -orbitals lie near the Fermi-level for graphene and dictate all electronic transport within the material.⁸

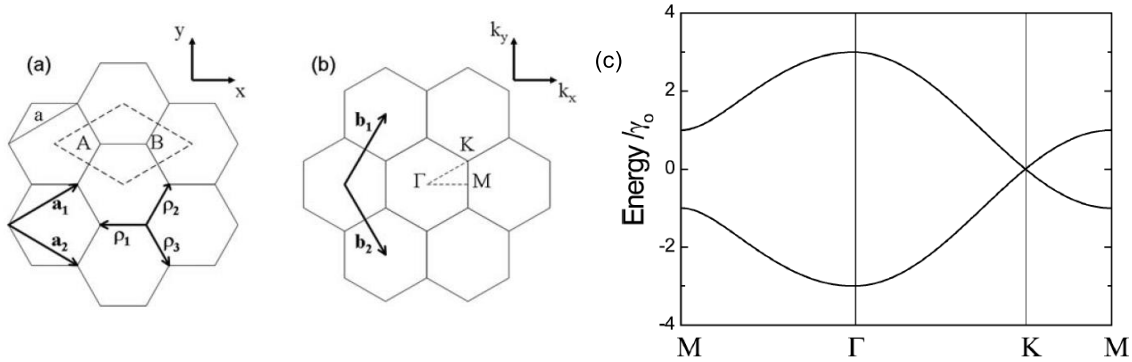


Figure 1.3- (a) Real space representation of graphene lattice. Unit cell is shown in dashed rhombus with non-equivalent point A and B. (b) Reciprocal space representation of graphene lattice. High symmetry points (Γ , K, M) in Brillouin zone are labelled. (c) Band structure for graphene.⁸

Looking at the band structure for graphene we can observe that the valence and conduction band meet at the symmetry point K in the Brillouin zone (**Figure 1.3B-C**). Usually, this would mean that the solid behaves as a metal; however, the density of states for electrons at the Fermi level for graphene is zero. This means that there are no available states for the electrons to occupy and allow for conduction. Therefore, graphene acts as a zero-bandgap semiconductor.⁹

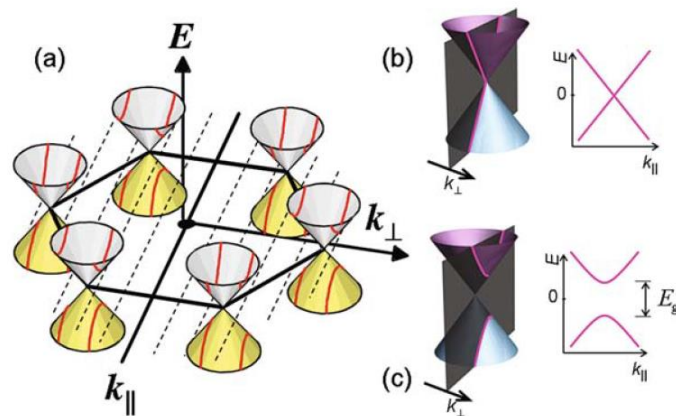


Figure 1.4-(a) Brillouin zone of graphene with conic energy dispersion at K points, allowed k_{\perp} states are indicated by the dashed lines. Zoom in of energy dispersion and cross sections along K point for metallic CNTs (b) and semiconducting CNTs (c).

Graphene is a 2-dimensional material and while a CNT is technically 3-dimensional, the band structure analysis is performed under the assumption that CNTs are infinitely long 1-D rolled up sheet of graphene with two

associated wave vectors. The wave vector k_{\parallel} runs parallel to the CNT axis and is assumed to be continuous as the CNT is considered to be infinitely long. While the wave vector k_{\perp} runs along the circumference of the CNT and is restricted by the circumference of the tube and thus follows the boundary condition $k_{\perp} \cdot A = \pi d k_{\perp} = 2\pi l$, where d is the diameter of the tube and l is an integer. This boundary condition leads to quantized values for k_{\perp} and depending on the allowed values of k_{\perp} the CNT either behaves like a metal or semiconductor. **Figure 1.4** provides a visual example of how k_{\perp} affects the resulting electronic behavior. If k_{\perp} bisects the K point perfectly then the valence and conductance band overlap leading to metallic behavior. Unlike graphene, CNTs can have electronic states at the Fermi level meaning the CNT displays conductive behavior. If the allowed k_{\perp} state pass nearby the K points, then two distinct valence and conductance bands form, leading to a non-zero band gap semiconductor. The bandgap for a semiconducting nanotube is inversely proportional to its diameter and range from 0.2-0.9 eV for CNTs ranging from 0.8-3 nm diameters.⁸

Without delving too far into the solid-state physics of the CNTs, the equation $n - m = 3q + p$ where q is an integer, can be used to predict the electronic nature of a CNT. If $p=0$ then at least one k_{\perp} bisects the K point perfectly and the CNT displays metallic behavior. If $p=1,2$ then k_{\perp} does not intersect K perfectly leading to semiconducting behavior. Based on the previous equation we can see that all armchair ($n=m$) CNTs will exhibit metallic behavior while zigzag and chiral nanotubes can behave either as metals or semiconductors. When dealing with MWCNTs, the behavior of this material is always metallic. This is due to the large number of tubes that reside in MWCNTs, if just one of these tubes is metallic in nature, then the entire bundle acts as a metal. Due to the way these CNTs are synthesized (See **Section 1.3**) it is difficult to control leading to any MWCNTs exhibiting metallic behavior.¹⁰

1.3 APPLICATIONS OF CARBON NANOTUBES

CNTs possess several unique properties that make these compounds such interesting materials. To begin, CNTs have great mechanical properties such as being incredibly strong, exhibiting tensile strengths that are 10-fold higher than common industrial fibers.¹¹ Additionally, CNTs are lightweight and stretchy displaying a high Young's modulus of approximately 0.64 TPa,¹² meaning the material can withstand a significant amount of elastic stretching before breaking. This value approaches the Young modulus of other well-known materials such as silicon-carbide

nanorods.¹³ CNTs also experience ballistic electron transport, which allows CNTs to carry vast amounts of electric currents with little to no heating.^{14,15} CNTs are also great thermal conductors with the individual thermal conductivity for a MWCNT surpassing the values for both diamond and graphite.¹⁶ As a bonus, CNTs have also previously been shown to function as superconductors at low temperatures (0.55 K to 5 K), with the superconductive temperature changing depending on how the CNT was grown.¹⁷

Due to the unique properties of CNTs, the material has been utilized for a wide number of applications including but not limited to composites,¹⁸ coatings,¹⁹ films,²⁰ microelectronics,^{21,22} electrochemical devices,²³ energy storage,²⁴ biosensors and medical devices,²⁵ hydrogen storage,²⁶ sensors,²⁷ and probes.²⁸ Typically, MWCNTs are reserved for more structural applications as they can be fabricated at low cost, whereas SWCNTs are often utilized for electronic or device applications where the parameters need to be more tightly controlled.^{2,3} Due to the correlation between structure and properties for CNTs, it is important to be able to control the type of CNT utilized for certain applications, a challenge that may prove difficult due to the common high energy synthesis used to create CNTs.

1.4 SYNTHESIS OF CARBON NANOTUBES

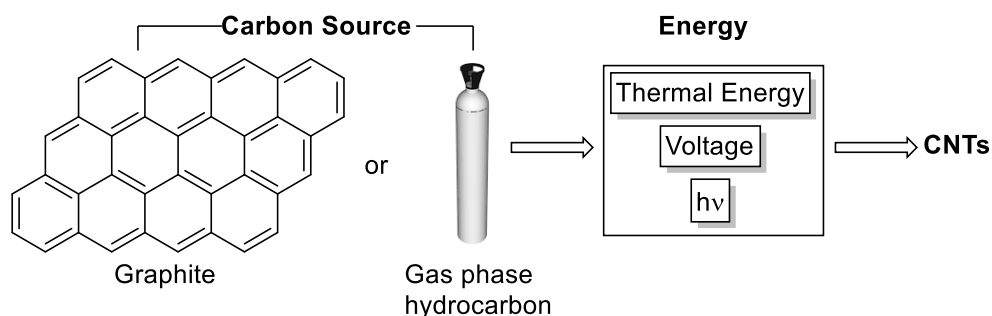


Figure 1.5- Schematic describing the general methodology behind common CNT synthetic methods.

There are 3 main methods by which CNTs are synthesized: arc discharge, laser ablation and chemical vapour deposition (CVD). Out of all 3 methods, CVD is the most popular method for synthesizing CNTs.²⁹ The principle behind the formation of the CNTs is the same for all three methods whereby a carbon source, either solid or gaseous, is introduced to a vast amount of energy, forcing the carbon atoms to cluster to form CNTs alongside other allotropes of carbon such as graphites and fullerenes (**Figure 1.5**). Herein, we will briefly describe each method with particular

interest on CVD as this method offers the most versatility for the synthesis of CNTs and may offer an elegant solution to the selectivity problem presented by these methods.

1.4.1 ELECTRIC ARC DISCHARGE

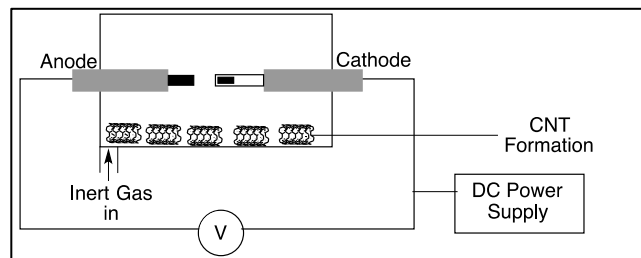


Figure 1.6- Schematic representation of the experimental setup for electric arc discharge.

Arc discharge is the oldest method for synthesizing carbon nanotubes and was the method Iijima used in his seminal publication identifying carbon nanotubes.¹ The method operates by evaporating a carbon sample into a plasma via the passage of voltage (~ 20 V), **Figure 1.6** provides a simplified schematic of the experimental setup. The anode and cathode are composed of high purity graphene doped with a metal catalyst, voltage is passed through the electrodes creating supercritical carbon, the metal catalyst within the sample then helps direct the carbon atoms to form CNTs and other carbon allotropes. The reaction is carried out in a steel chamber under an inert atmosphere (typically He or Ar at 50-600 Torr) and the carbon plasma can reach temperatures of 2000-3000 °C.²⁹ The type of catalyst used as well as the current, temperature, carrier gas and voltage are all parameters that can affect the type of CNT synthesized from arc discharge. Of particular importance for arc discharge are the voltage, which must be held constant in order for the arc to remain stable, and the pressure of the inert gas in the reaction chamber.³⁰

Typical yields for arc discharge reactions are around 30% yield for SWCNTs and usually results in short tubes with a large number of impurities when compared to other methods.³¹ Arc discharge is also somewhat unselective with the synthesized tubes having a random distribution of length, diameter, and chirality.³¹ The reaction parameters can be altered for arc discharge to yield better results, for example, Shi *et al.* demonstrated how by utilizing a precise composition of Co, Y, and Ni they were able to produce SWCNTs in a 70-90% yield at a gram scale.³² Other techniques for controlling arc discharge make use of a water-cooled electrode to control the temperature of the plasma³³ or a rotating electrode to create a uniform carbon vapor that nucleates at a carbon collector located at the periphery of the carbon plasma.³⁴

1.4.2 LASER ABLATION

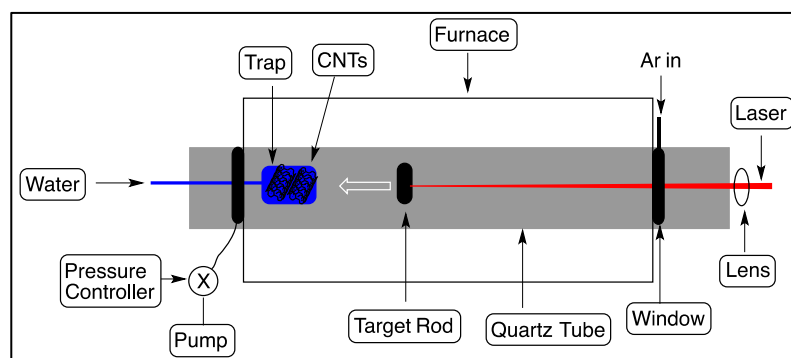


Figure 1.7- Schematic representation of a laser ablation experimental setup.

Laser ablation is a more modern but less commonly used way of synthesizing CNTs. Similarly, to arc discharge, the method uses a laser to evaporate a target sample that is then deposited on a cooled target upon which the CNTs form (**Figure 1.7**).^{29,35} The target is composed of graphene which if pristine leads solely to the formation of MWCNTs and when doped with metal particles leads to the formation of SWCNTs.³⁵ Consequently, the sample purity for laser ablation is extremely important as even small amount of metal particles present in the graphite can lead to the formation of SWCNTs.

Laser ablation was initially developed as an alternative to arc discharge; this new method used a more precise power source and was able to proceed more selectively, provide greater control over growth conditions, allow for continuous operation, and furnish CNTs of better quality and in higher yield.³⁵ Unfortunately, the appeal of this method was also its greatest drawback as it required specialized equipment and was difficult to scale up making it unappealing for an industrial like setting.

Laser ablation usually produces highly ordered tubes ranging from 0.81 nm to 1.51 nm in diameter with the outcome highly dependent on the reaction temperature.³⁶ The type of CNTs synthesized during laser ablation are usually metallic with a particular propensity to create (10,10) armchair nanotubes specifically.³⁷ However, methods do exist that are more selective towards semiconducting CNTs but the selectivity does not exceed 50%.³⁸ This makes laser ablation particularly unsuitable for creating CNTs for material applications as pure semiconducting CNTs are required.

1.4.3 CHEMICAL VAPOUR DEPOSITION.

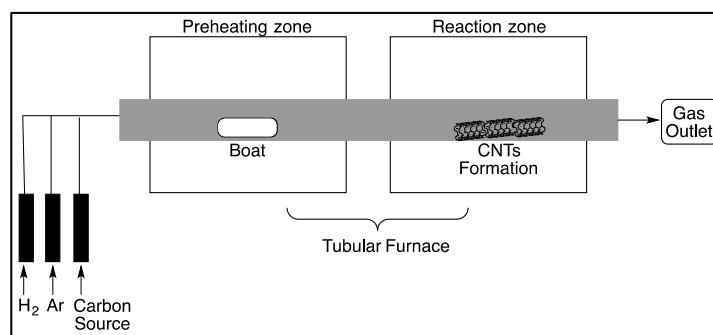


Figure 1.8- Schematic figure of a chemical vapour deposition reaction setup.

Chemical vapour deposition (CVD) is the most common way by which CNTs are synthesized. Laser ablation and arc discharge both suffer from similar drawbacks including large energy requirements which are not economical for industrial scale production. Additionally, high purity graphite samples and high temperatures are needed for the reaction to yield the desired CNTs. Lastly, arc discharge and laser ablation leave behind a large number of carbon and metal by-products that can be difficult to fully remove. CVD allows for a cost-effective method of creating CNTs that can be highly tuned to a specific type of chirality or tube type, uses cheap raw material in the form of gases, and can be easily adapted for high volume production.

CVD operates by using a metal catalyst to help induce a thermal dehydrogenation and to “crack” the hydrocarbons to help coat a surface in which the CNTs can begin to grow. **Figure 1.8** provides a general schematic for a CVD setup, a carbon source is used in the form of a gas (for example benzene, ethylene, ethanol, etc.), a carrier gas such as Ar gas and hydrogen gas which acts as a reducing agent. The boat contains the catalyst (metal or organometallic compound such as ferrocene) that helps crack the hydrocarbons and the CNTs are deposited in the next chamber with the aid of the carrier gas. Aside from being a scalable method, CVD can also be used to coat surfaces with CNTs for various applications.

CVD is highly tunable. Different parameters can be applied such as the type of hydrocarbon used, metal or organometallic catalyst, carrier gas, and growth temperature can select for a specific type of tube and chirality.³⁹ The substrate on which the CVD growth is carried out is highly important and can have a drastic effect on the resulting CNTs. A good example can be seen in the use of a floating zeolite catalyst that was doped with Fe particles, the zeolite holds on to the metal particles such that the diameter is controlled and the CNTs grow without bundling

or interfering with one another leading to an almost 1-D material.⁴⁰ More importantly, however, CVD is one of the only methods that can reliably and reproducibly synthesize semiconductive tubes required for electronic applications in respectable yields.^{41,42}

One of the most popular uses of CVD is HiPco process developed by Richard Smalley at Rice University. High pressure carbon monoxide (HiPco) uses a high pressure of CO (30-50 atm) with catalytic clusters of Fe at high temperatures to induce clustering of iron which then serve as catalysts for the CNTs to grow on. This process allows for SWNTs of high purity (~97%) and rates as high as 450 mg/h or 10 g/day.⁴³

1.5 PURIFICATION OF CARBON NANOTUBES

Although methods for the synthesis of CNTs have considerably improved in terms of yield and selectivity, often CNT samples need to be purified before they can be introduced for device purposes. When referring to CNTs, an impurity is anything that is not a CNT, such as metal particles, carbon soot, or other carbon allotropes. The purification steps required for CNT samples can be laborious and potentially introduce defects into the CNTs. Consequently, the price of CNTs is currently quite high with high purity samples of SWCNTs costing around 750 \$/g and samples with significant impurities costing roughly 60 \$/g. Bulk MWCNTs, whose applications require fewer specific properties, cost around 100 \$/kg, a value that is roughly 1-10 times the cost of commercially available carbon fiber.⁴⁴ Herein, the methods by which CNTs are purified and isolated will be briefly outlined.

There are three main ways by which CNTs are purified including physical, chemical methods or a combination of both. Physical methods, as the name implies, relies on the physical properties of the CNTs such as magnetism, aspect ratio, specific gravity, and physical size to purify the CNTs and include techniques such as filtration,⁴⁵ centrifugation,⁴⁶ and high temperature annealing.⁴⁷ These techniques are not destructive in nature and impart no defects on the CNTs but are less effective than the chemical purification. Chemical purifications usually refer to the selective oxidation of the carbonaceous impurities and metal particles left over from the synthesis and are faster and more effective than physical techniques. Unfortunately, chemical purification techniques often introduce defects into the CNTs, consequently a hybrid approach involving both methods is often required to minimize defects and purify the CNTs.⁴⁸

1.6 SORTING OF CNTs

The above-mentioned purification techniques serve to remove non-CNT impurities left over from the synthesis including carbon soot, fullerenes, and metal contaminants. Ideally, after the purification process what is left over should be solely CNTs. Unfortunately, due to the high varieties of chiralities, sizes, diameters, and lengths the remaining CNTs need to be sorted to attempt to select for a specific type of tube. This process is referred to as sorting and there are several methods by which this can be accomplished.

One of the most important types of sorting is separating metallic tubes from semiconducting tubes. This is critical when constructing transistors with CNTs as the inclusion of a single metallic CNT will prevent the transistor from functioning. Luckily, the removal of metallic CNTs can be accomplished by passing an electrical current through the metallic CNTs which then break down due to Joule heating leaving only behind semiconducting CNTs which are not affected by the current.⁴⁹ Unfortunately, after this point we are left with several semiconducting CNTs with varying band gaps. Thus, further sorting is needed especially when constructing CNT devices.

The sorting CNTs is a very active area of nanotechnology with several techniques available to separate tube chiralities (See **Section 1.1**). One of the first ways CNTs were sorted was via DNA wrapping followed by ion exchange chromatography. It was previously known that DNA was able to form higher order structures with CNTs thus several short DNA strands were engineered to bind to a specific type of CNT chirality and were then isolated following ion-exchange chromatography.⁵⁰ The method is selective towards semiconducting CNTs and can even separate tubes that possess the same diameter but different chiralities. The method is not perfect however, as the yields for the separation are low (maximum 10%) and SWCNTs irreversibly bind to the ion-exchange resin affecting the resolution of the separation after each run.

There are several more ways by which CNTs can be sorted.⁵¹ The Schipper group recently reported a sorting method where an iptycene, a 3D bicyclic aromatic compound, tweezer was used on a functionalized surface to align and sort CNTs by both length and diameter.⁵² It should be noted that most of these methods are not applicable to large scales, are costly or may be specific to certain chiralities, thus a more concise synthesis of the CNTs could prove key for the large-scale synthesis of CNTs.

1.7 CARBON NANOTUBE TRANSISTORS

As the limits with regards to silicon-based electronics begin to be reached, alternative new materials are required to further miniaturize and optimize modern electronic devices. Due to their unique properties, CNTs are “new” promising materials that have already displayed their potential as semiconductors in field effect transistors (FETs) and have even been shown to out-perform silicon FETs.⁵³ The unique properties of CNTs including high current-carrying capacity, high carrier velocity and good electrostatics thanks to their thin bodies, make CNTs particularly suited towards materials applications.⁵⁴

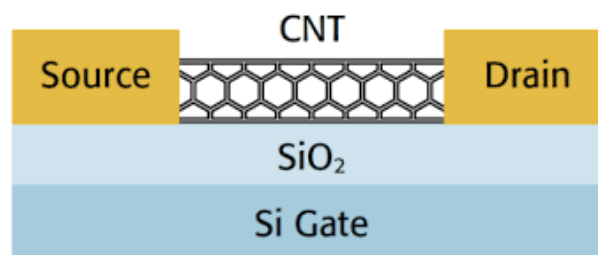


Figure 1.9- Schematic representation of a CNT transistor.

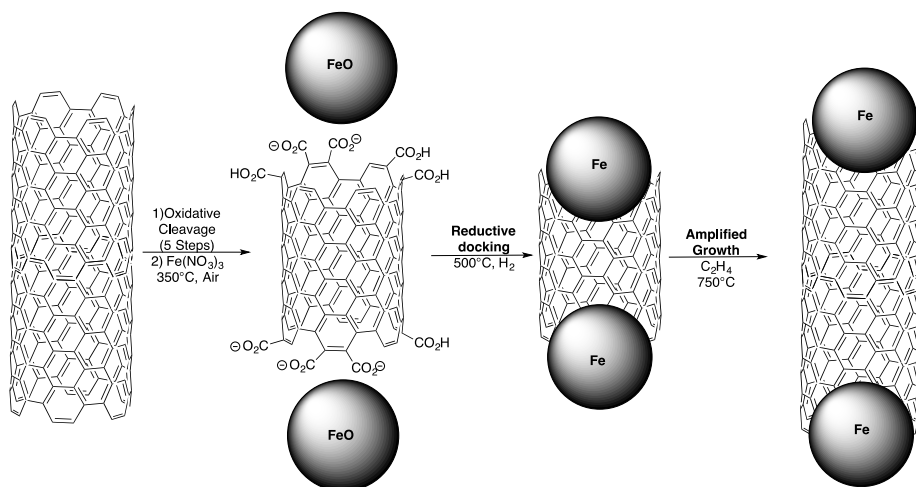
CNT transistors are one of the most synonymous devices associated with CNTs, a schematic representation of a CNT transistor is highlighted in **Fig 1.9**. In essence, a transistor operates as a tiny switch that can assume either an on or an off position. When voltage or electric field is applied onto the device, the semiconducting material, in this case a CNT, can allow the flow of current from the source to the drain, however, in the absence of a voltage or electric field the device then remains off. Several of these transistors are placed onto a chip which a computer can then interpret as binary (1 or 0) depending on the state of the transistor. This is the most basic way by which a computer operates and there are already examples in the literature where computers have been constructed using only CNT field effect transistors (CNTFETs).^{21,22} Field effect transistor (FET) simply refer to a transistor that operates using an electric field rather than a voltage. Although simplistic in its construction, there are several hurdles that need to be overcome before CNTFETs become fully complementary to silicon electronics. The core issues that must be addressed before CNTs become the mainstay for transistors and other devices include purification, sorting, and alignment.

The alignment of the CNT is required for the device to operate correctly. The CNTs must be aligned correctly between the source and the drain. The Schipper group recently showed an elegant solution to this problem,⁵² but other alignment techniques exist.⁵⁵ Secondly, the purity of the CNTs is important as any remaining metal impurity can substantially hinder the devices performance. Finally, the tubes need to be sorted for a specific type. If a single metallic tube is found within the transistor the device can short circuit and lower the I_{on}/I_{off} ratios drastically.⁵⁶ Furthermore, the band gap of CNTs varies depending on the chirality and diameter. Thus, a specific type of semiconductive tube must be sorted for to obtain ideal device performance.

Most of the roadblocks that prevent CNT devices from truly expanding stem from the synthesis of the material, as even the best methods are rather unselective. Although sorting and purification methods exist, there are often low yielding and expensive leading to a product cost that is not feasible for mass production. Thus, a more concise synthesis of CNTs is highly desired.

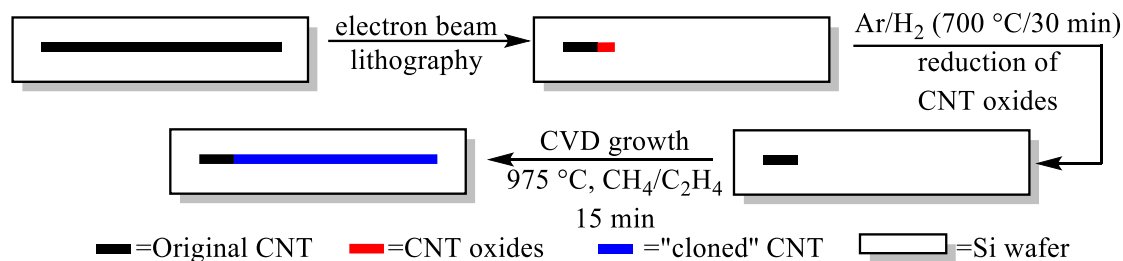
1.8 TEMPLATING TECHNIQUES FOR THE PRECISE SYNTHESIS OF CNTs

Although widely used, CNT synthesis techniques such as CVD and laser ablation do not currently allow for the precise synthesis of a nanotube with a specific chirality and type. There are, however, methods by which the CVD process can be “seeded” to guide to reaction to provide a specific type of CNT with the chirality and diameter matching that of the seed.



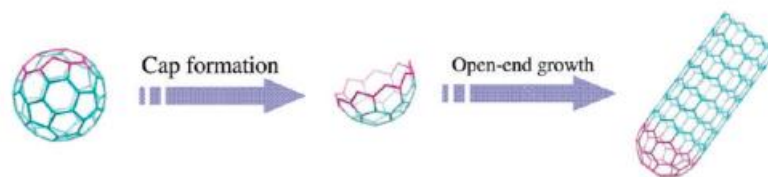
Scheme 1.1- Synthesis of specific type nanotubes using template technique.⁵⁷

The first example of specific CNT growth mediated by a template or seed molecule was reported by Smalley *et al.*⁵⁷ For this synthesis, the authors prepared ultrashort CNTs starting from HiPco synthesized CNTs and were able to showcase that the ultrashort CNTs served as templates as were thus elongated into CNTs with the same height and orientation as the seed CNTs (**Scheme 1.1**). The CNTs were chemically cleaved using previously established methodology and then were docked with an Fe particle inside the CNT that served as the catalyst for the CVD growth. In theory, this procedure could be repeated indefinitely but the methodology suffers from low yields (max 3%) and would require a pristine CNT sample to be of value, raising the cost of the reaction. Additionally, the CNTs that are successfully elongated from the reaction now have an Fe particle embedded within the CNT, which can be removed chemically at the risk of introducing defects into the newly formed CNTs.



Scheme 1.2- Metal free "cloning" CVD growth of CNTs.⁵⁸

The group of Yao *et al.* showed a similar report where they were able to "clone" SWCNTs starting from an ultra-short CNT under metal free conditions (**Scheme 1.2**).⁵⁸ For this synthesis the authors grew ultra-long CNTs on Si wafers and then cut those CNTs using electron beam lithography. After the tubes were cleaved, the CNTs were subjected to reductive conditions to remove any pendant COOH or OH groups resulting from the cleavage. This was then followed by the CVD growth of the seeds which was able to elongate the cleaved CNTs albeit in a low yield. Although the methodology for extending the tubes is not yet applicable to larger scales, it does raise some questions about the mechanism by which the CNTs grow, as Smalley *et al.* required the catalyst for the reaction to proceed, whereas the cloning method did not.⁵⁷ The authors claimed that the reaction was carried out 100% metal free although it should be noted that trace amounts of metal particles can have an effect on the reaction as seen in methods like arc discharge or laser ablation. If truly metal free then it does indicate that the metal impurities from CNT synthesis could in theory be negated entirely, removing the need for chemical treatment of CNTs.



Scheme 1.3- Schematic representation of seeded CVD growth of capped CNTs using an open C_{60} fullerene as the seed.⁵⁹ Reprinted with permission from Yu *et al. Nano Lett.*, **2010**, 10, 3343-3349.

The use of ultra-short CNTs as CVD shows promise, however, for it to be of any use we would require facile access to pure CNT samples and the CNTs themselves would have to survive all chemical transformations with little to no defects. Thus, alternatives for templates or seeds for CVD are highly desired. One template molecule shown to work as a CVD seed for the synthesis of CNTs is opened C_{60} fullerene caps. Fullerenes are similar to CNTs as they are also an allotrope of carbon. In this case the carbon atoms are arranged in a hollow sphere composed of hexagons and pentagons.⁶⁰ If one were to closely observe a capped CNT then it would become apparent that the cap of the CNT resembles a C_{60} fullerene. Thus, it stands to reason that this molecule could be used as a seed for CVD. Yu *et al.* displayed the use of opened C_{60} fullerenes as a method to produce uniform CNTs, which was also able to proceed under metal free conditions.⁵⁹ This methodology offered less control than previous methods with the diameter of the grown tubes not being uniform and highly dependent on the prior oxidative treatment of the open C_{60} cages. The method, however, did offer advantages as the seed was a small molecule and therefore offered easier handling compared to the insoluble CNTs. The main drawback of this seed, however, was that the seed itself is difficult to modify to yield different diameters and chiralities and thus the number of tubes that could be made from fullerenes would be limited.

Although the report from Yu *et al.* on a C_{60} seeding method was able to display how a small molecule could provide good control over the growth of CNTs, a molecule that could be better tuned is still highly coveted as it would provide a means for controlling CNT chirality and diameter.

1.9 FRAGMENTS OF CARBON NANOTUBES

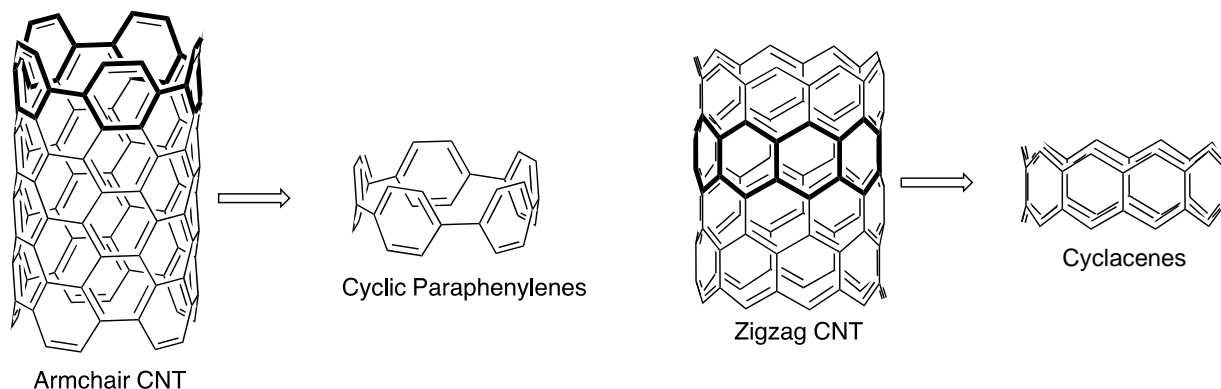


Figure 1.10- Cyclic paraphenylenes (CPPs) as the shortest section of an armchair CNT (left). Cyclacenes as the shortest segment of a zigzag CNT (right).

Much of the difficulty regarding CNT synthesis stems from a lack of knowledge regarding the mechanism by which the CNTs grow. Although, several growth models⁶¹⁻⁶⁴ have been put forth it remains unclear as to how CNTs grow and thus control of the reaction remains a challenge. Researchers have turned their gaze towards the bottom-up synthesis of CNTs with the hope of using standard synthetic procedures that would provide control over the growth of the CNTs. In doing so, two potential candidates that could be used to study the formation of CNTs have been proposed. The first one being cycloparaphenylenes (CPPs) that can be thought of as the smallest section of an armchair CNT and the second candidate being cyclacenes, which can be thought of as the smallest section of zigzag CNT. Both these compounds could provide valuable information with regards to CNT synthesis but may also yield similar properties that mirror their parent CNT thus negating the need for synthesizing CNTs.

1.9.1 PARAPHENYLENES AND CYCLOPARAPHENYLENES

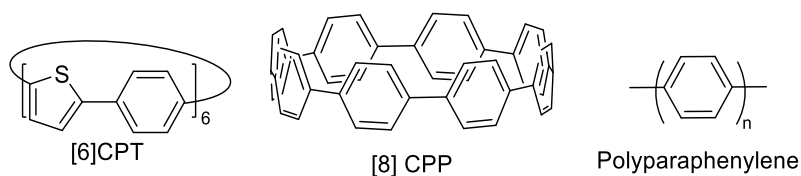
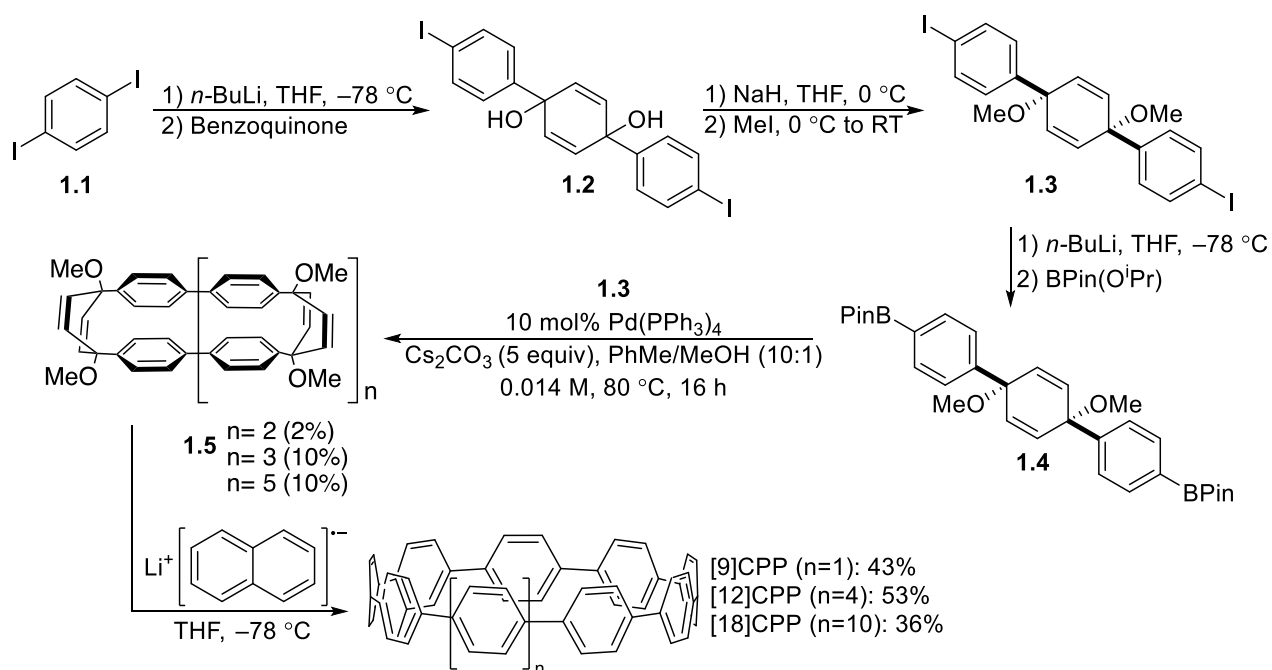


Figure 1.11- Examples of different CPPs and LPPs.

Paraphenylenes are a series of aromatic rings that are bonded via σ -sigma bonds connected via a 1-4-linkage. Within this family of compounds are linear paraphenylenes (LPPs), which exists as polymers or oligomers, and cyclic paraphenylenes (CPPs) as well as heterocyclic CPPs (**Figure 1.11**). LPPs are some of the oldest known

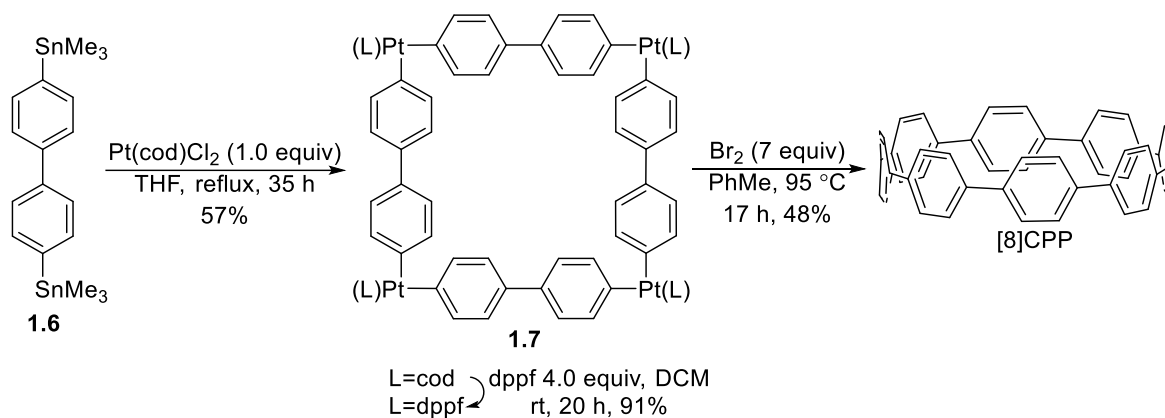
examples of conjugated polymers. Unfortunately, the material often suffers from undesirable properties including poor solubility and low molecular weights. Consequently, LPPs have seen little application in organic electronic devices, although recently new synthetic methodologies have come to fruition allowing for polymeric LPPs to be synthesized.^{65,66} Cycloparaphenylenes are the cyclic analogues of LPPs and are a relatively new type of compound with the first successful synthesis reported in 2008 by Jasti *et al.*⁶⁷ Since the initial report by Bertozzi, the field of cycloparaphenylenes has grown, with multiple reports highlighting how to achieve different diameters and incorporate different atoms within the CPP,⁶⁸ some CPPs are now commercially available making them attractive substrates for potential CNT amplification and synthesis.



Scheme 1.4- Jasti *et al.* synthesis of [9], [12] and [18]CPP.⁶⁷

Herein some of the strategies that were used to synthesize CPPs will be briefly highlighted starting with Bertozzi's seminal synthesis of [9], [12] and [18]CPP. The synthetic route is highlighted in **Scheme 1.4**. First, 1,4-diodobenzene **1.1** was subjected to a lithium-halogen exchange and then used as a nucleophile to attack benzoquinone yielding the *syn*-diol **1.2**. The reaction is selective for the *syn* diol due to electrostatic interactions present in the transition state. The diol **1.2** was then methylated followed by the conversion of the aryl iodides to aryl boronates using another lithium halogen exchange in the presence of BPin(OⁱPr). With the aryl boronate **1.4** and

aryl iodide **1.3** in hand a Suzuki coupling was performed to form the macrocycle **1.5**. The use of the syn-dimethoxycyclohexadiene **1.3-1.4** is critical to the formation of the CPP as it provided the proper bend for the macrocycle to exist before it was aromatized to the fully conjugated CPP. The macrocycle **1.5** was then reduced to the CPP using lithium naphthalenide to yield the CPPs in a 43-53% yield.



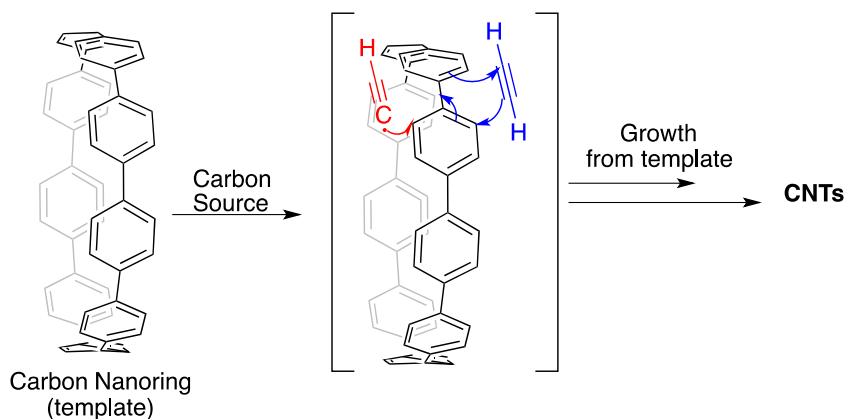
Scheme 1.5- Yamago *et al.* synthesis of [8]CPP using a Pt tetracoordinate approach.⁶⁹

The second example makes clever use of the square planar geometry of Pt to align the fragments of the CPP together which upon a reductive elimination led to the formation of [8]CPP.⁶⁹ The synthetic procedure is outlined in **Scheme 1.5**. 4,4'-Bis(trimethylstannyl)biphenyl **1.6** was reacted with one equivalent of Pt(cod)Cl₂ yielding the square planar metallocycle **1.7** which was then reductively eliminated with the aid of bromine to yield [8]CPP in 49% yield. This methodology has the advantage of proceeding in less steps, but it does make use of stoichiometric amount of an expensive Pt reagent. Yamago's synthesis of CPPs operates differently than Jasti's synthesis but operates on a similar principle. The key to successfully constructing CPPs, for all methods, lies in properly arranging the coupling partners in the right geometry before proceeding to construct the fully conjugated product.

1.9.2 TEMPLATE SYNTHESIS OF CNTS USING CPPS AS A TEMPLATE.

Much like the previously described template method described in **Section 1.6**, it has been shown that CPPs can be used as molecular templates for the precise growth of CNTs. In 2013 the Itami group was able to demonstrate the use of [9] and [12]CPPs as seeds for CVD growth with the resulting tubes displaying similar diameters and heights compared to the original seed (**Scheme 1.6**).⁷⁰ The methodology itself is not perfect as the CPPs begin to break down

under the growth temperatures and give rise to side products such as LPPs and double-walled CNTs. Furthermore, the reaction can currently only be carried out at very low scales with the yield of the growth currently being unknown. Nonetheless, this report is a pivotal as it displays how a small molecule, whose properties can be controlled using traditional synthetic techniques, can be used to direct the growth of CNTs into the desired chirality and diameter.



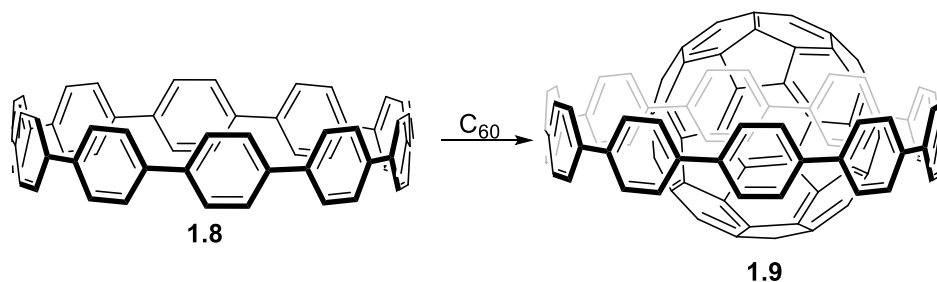
Scheme 1.6-Schematic representation of the well-defined growth of CNTs using CPPs as seeds/templates. ⁷⁰

Ideally, if the CNTs from the templating method were produced at high yields when using CPPs as seeds this would provide a concise route to create armchair CNTs. Unfortunately, metallic CNTs do not fare well in materials applications such as CNT transistors. Therefore, a macrocycle that closely resembles zigzag CNTs may be the key for the concise synthesis of semiconducting CNTs using a small molecule template.

1.9.3 PROPERTIES AND APPLICATIONS OF CPPS

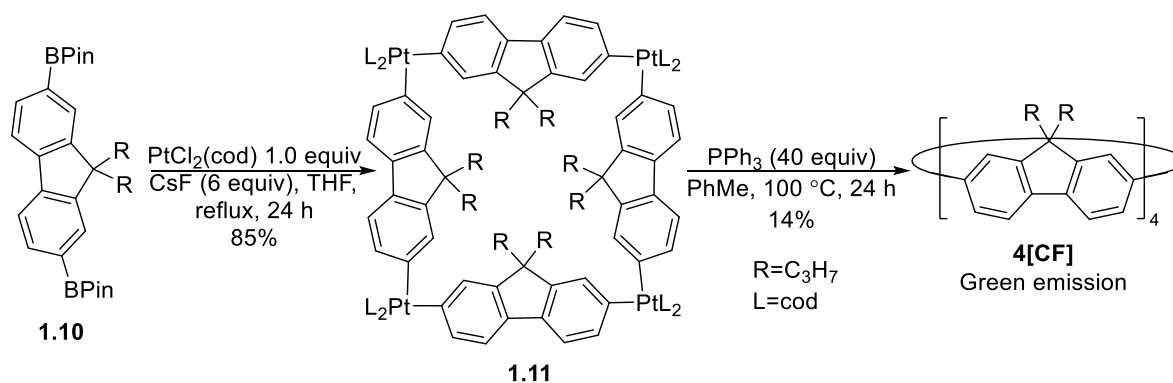
Aside from serving as a model compound for the shortest possible armchair CNT, CPPs exhibit a host of interesting properties and applications. To begin, CPPs all exhibit non-zero dihedral angles between adjacent rings, which means that the aromatic moieties that compose the cycle do not lie perfectly flat with each other but rather exist in a staggered conformation.⁶⁷ Initially, it was predicted that the dihedral angle would be zero allowing for good strong electronic interactions with the adjacent rings. However, it is not surprising that the dihedral angle is non-zero as linear oligophenylenes, such as biphenyl, also possess a non-zero dihedral angle at roughly 45°. ⁷¹ The absorption and emission spectra are also interesting, with CPPs exhibiting a uniform absorption maximum ($\lambda_{\text{max}}=340$ nm) regardless of the cycle size but an increasing Stokes shift with decreasing size.^{67,72} Finally, it should be noted

that in contrast to armchair CNTs, CPPs behave as semiconductors with a bandgap ranging from 0.59-0.85 eV, with the smaller rings exhibiting smaller HOMO-LUMO gaps.



Scheme 1.7- Host-guest chemistry of [10]CPP to form shortest fullerene-peapod.⁷³

In terms of applications, CPPs have similar properties to their armchair CNT counterparts that allows CPPs to partake in host-guest chemistry. In 2001 Yamago and co-workers were able to demonstrate CPPs ability to encapsulate C_{60} to form the shortest fullerene-peapod (**Scheme 1.7**).⁷³ This finding is significant as the ease of accessibility of CPPs provides a range of diameters that could be used to selectively encapsulate molecules such as fullerenes and CNTs, this in turn could provide a solution to the sorting problem for CNTs and higher fullerenes.



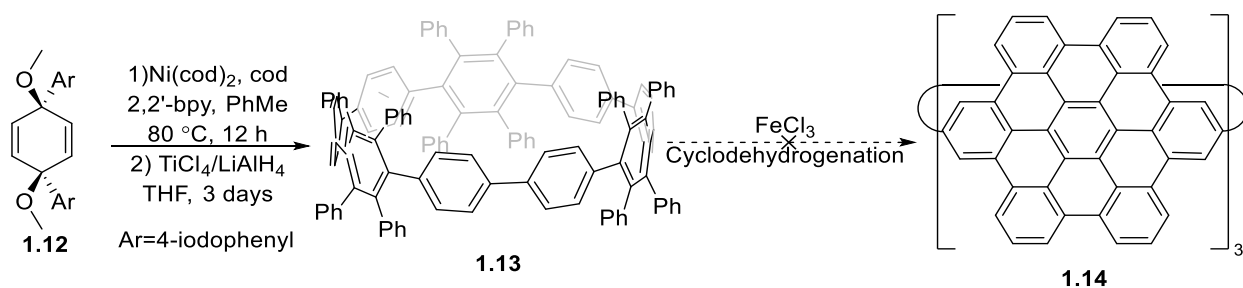
Scheme 1.8- Yamago synthesis of the green OLED [4]cyclo-9,9-dipropyl-2,7-fluorenylene.⁷⁴

Even though CPPs closely mirror CNTs and can behave as semiconductors they have found little application in the field of organic electronics. One of the few reports of CPPs being used in an electronic application is by Huang and co-workers, in which the authors utilized Yamago's CPP methodology to synthesize a CPP with a fluorene as the repeating unit.⁷⁴ The authors then showcased the ability to use this material as an organic light emitting diode (OLED) as the material showed a strong green emission. 4[CF] served as an example of how strain can be utilized to tune

the photoelectronic properties of a material as the linear 4-oligofluorene emits blue light whereas the cyclic analogue emits green light.

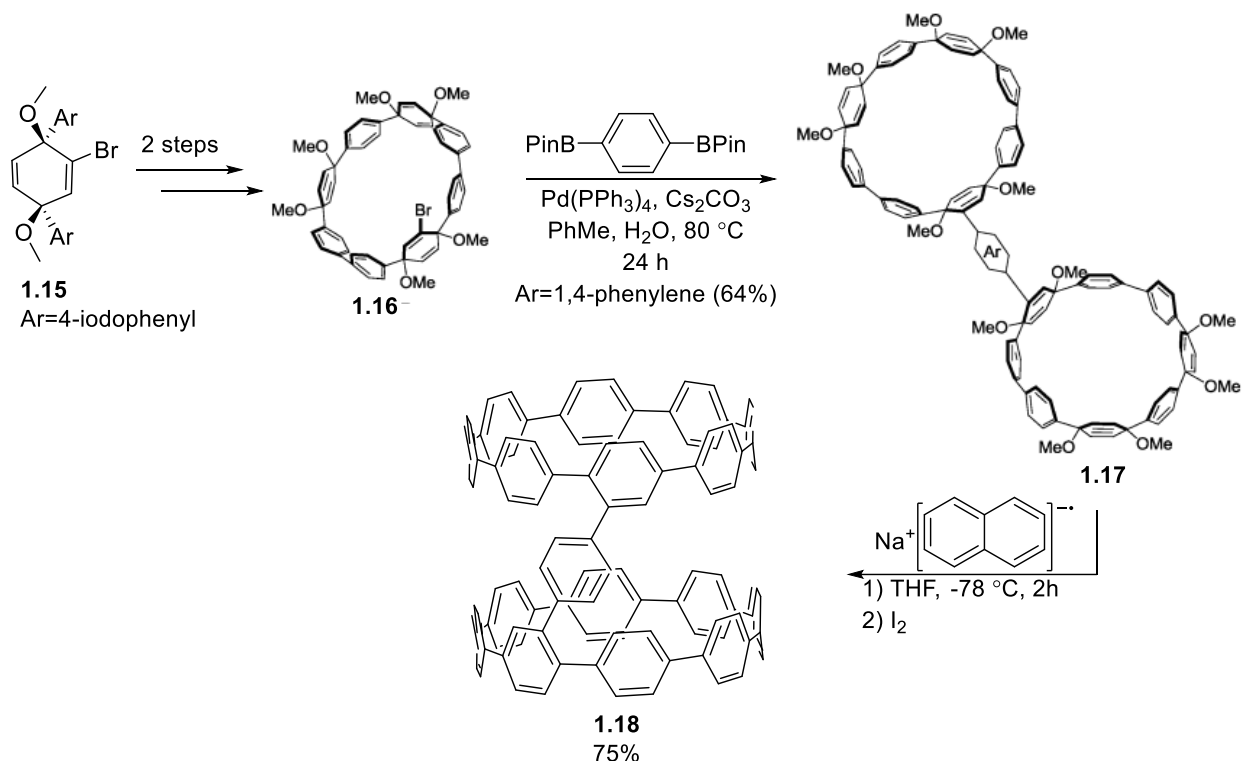
1.9.4 BOTTOM-UP APPROACH OF CNTs USING CPPs

Given the wide availability and multiple synthetic approaches for constructing CPPs, the nanoring seemed like a logical starting point to attempt the bottom-up synthesis of CNTs. Several groups began to investigate how to expand CPPs in more than one dimension to begin to approach the full structure of CNTs and create techniques for the 3-dimensional expansion of these cycles.



Scheme 1.9- Scholl cyclodehydrogenation of CPPs to form ultrashort-CNT fragments.⁷⁵

Taking inspiration from techniques used to create graphene nanoribbons (GNRs) and nano-graphenes (NRs), Müllen and coworkers set out to create a CPP that could undergo a cyclodehydrogenation reaction, such as a Scholl reaction, and in turn yield a CPP that is conjugated in 3-dimensions (**Scheme 1.9**).⁷⁵ A CPP containing a 1,2,4,5-tetraphenylbenzene subunit was synthesized following a procedure similar to Jasti's original synthesis of CPPs with the exception of using a Ni mediated Yamamoto coupling instead of a Suzuki coupling. After aromatization with TiCl₄/LiAlH₄, the authors arrived at the CPP **1.13** and proceeded to try the cyclodehydrogenation under several oxidative conditions. Unfortunately, the reaction yielded a complex mixture of products due to partially dehydrogenated products as well as other impurities present in the reaction mixture. The difficulty in this pathway lies in the lability and orientation of the pendant phenyl groups of the CPP, the reaction must proceed multiple times and the phenyl groups must be at the correct spot for the reaction to work. Although, the fully cyclodehydrogenated CPP was observed by MALDI-TOF MS, or an isomer thereof, the compound was not successfully isolated.



Scheme 1.10- Synthesis of CPP **1.18**.⁷⁶ Adapted with permission from Xia *et al.* *J. Am. Chem. Soc.* **2012**, *134*, 19709.

The same year as the report from Müllen and coworkers, Jasti and coworkers attempted a different approach towards the bottom-up synthesis of an armchair CNT.⁷⁶ The authors hypothesized that late-stage functionalization of the CPP would prove difficult and thus opted to construct the 3-dimensional structure first before aromatizing to the CPP. The synthetic scheme is highlighted in **Scheme 1.10**. Starting with a brominated cyclohexadiene **1.15**, the first macrocycle **1.16** was reached following a Suzuki cyclization. Macrocycle **1.16** was then dimerized by performing another Suzuki coupling with 1,4-phenylenebis(boronic acid) pinacol ester which was followed by reduction to the CPP **1.18** using sodium naphthalenide in a 75% yield. The authors also created a second CPP dimer using a naphthalene linker unit in 48% yield following the outlined synthetic procedures. The synthesis of the dimerized CPP proved to be simple enough and proceeded in good yield, but the valuable information resided in the conformation of the two CPPs rings relative to each other. Gratifyingly, both theoretical calculations and X-ray analysis seem to suggest that the CPP rings exist on top of each other indicating that if a CPP dimer was constructed without the addition of an aryl linker it may lie in the correct conformation for a cyclodehydrogenation to take place similarly as outlined by Müllen and coworkers.⁷⁵

1.9.5 POLYCYCLIC AROMATIC HYDROCARBONS, ACENES, AND CYCLACENES

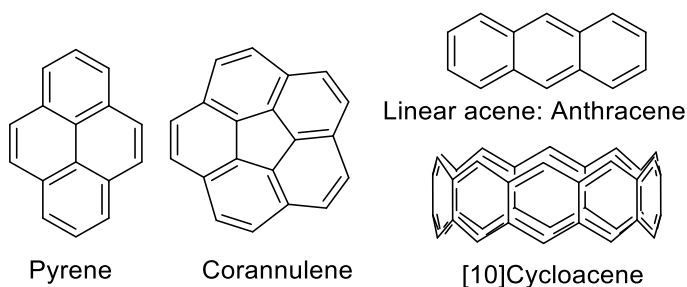


Figure 1.12- Structure of common PAHs, acenes (anthracene) and cyclacenes ([10]cyclacene).

A polycyclic aromatic hydrocarbon (PAH) is a substance solely composed of carbon and hydrogen where the atoms are arranged in a series of aromatic rings. The compounds discussed thus far fall under the PAH category, although the term usually refers to molecules such as pyrene, corannulene, anthracene, etc (**Figure 1.12**). Within this family of compound lie the acenes, a type of PAH in which a series of benzene rings are linearly fused to each other.⁷⁷ Acenes exhibit interesting optoelectronic and solid-state properties making them prime candidates for the construction of organic electronics. For this reason, a great deal of research has been dedicated towards the synthesis of acenes and construction of devices with such materials.⁷⁸ Within this family of compounds lie cyclacenes, which closely resemble the shortest possible zigzag CNT, and until recently,^{79,80} the synthesis of these macrocycles remained elusive due to the high reactivity and strain predicted to be exhibited by these compounds. To understand why cyclacenes have remained such elusive targets, one must first take a step back and understand the chemistry of linear acenes as much of the reactivity of these compounds directly translates to their cyclic counterparts.

1.9.6 PROPERTIES OF ACENES

Small acenes occur naturally and can be extracted from petroleum but any acene larger than tetracene must be synthesized in the lab. Pentacene is one of the most commonly made synthetic acenes and displays great hole transport semiconducting properties which are important to for organic field effect transistors (OFETs) applications.⁸¹ Additionally, pentacene is a good candidate for studying singlet fission, a process which is critical towards the development of better solar cells.⁸² The properties of pentacene sparked renewed interest in the

synthesis of longer acenes; however, the same properties that make pentacene appealing also make the isolation of longer acenes difficult.⁸³

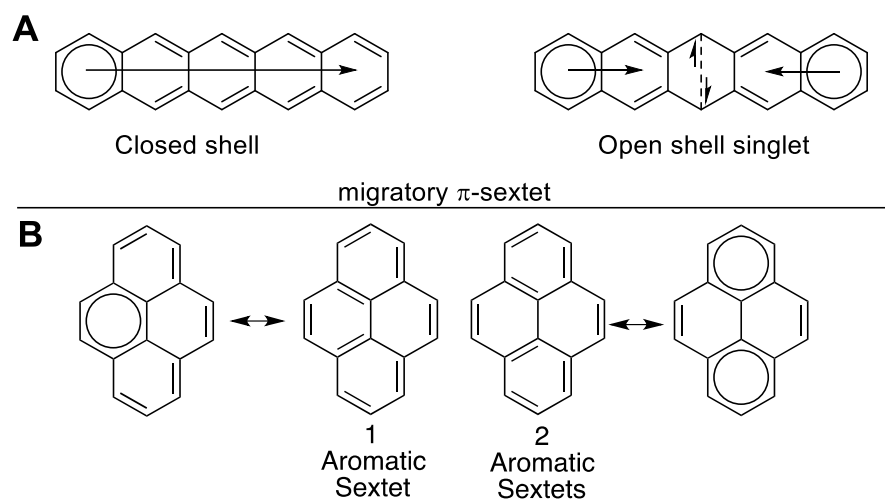
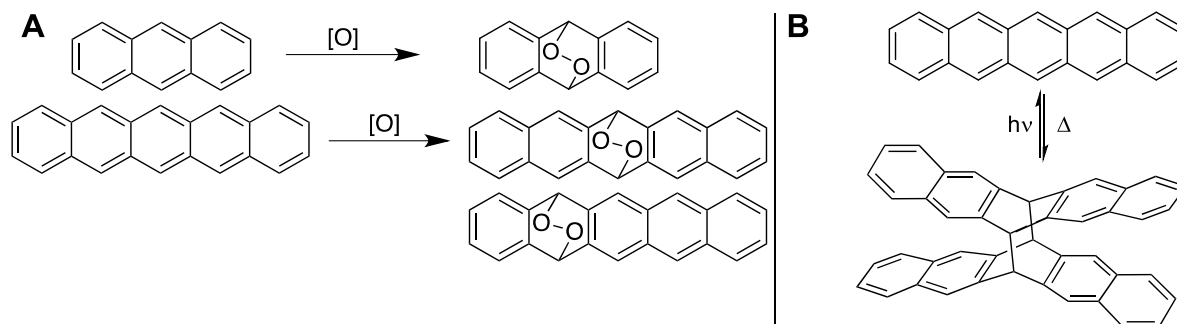


Figure 1.13-Clar aromatic sextets for pentacene **A** and pyrene **B**.

When dealing with PAHs a good way to describe stability is by applying Clar's aromatic π -sextet rule. This rule states that a PAH will be stable if it can maximize the number of Clar sextets or Kekulé aromatic rings within the molecule.⁸⁴ When this analysis is applied to acenes we can observe that regardless of the length, acenes can only have one aromatic Clar sextet (**Figure 1.13A**). In contrast, a PAH like pyrene contains two Clar sextets, this not only accounts for the high stability of the molecule but also helps to predict the reactivity of pyrene (**Figure 1.13B**). As acenes begin to "grow", the molecule will have a higher propensity to adopt a configuration that maximizes the number of Clar sextets. Thus, longer acenes will form a reactive open shell singlet or biradical electronic configuration.⁸⁵⁻⁸⁷



Scheme 1.11-A-Formation of endoperoxides in acenes. B- Self dimerization of pentacene.

This open shell singlet configuration is the main deterrent for creating higher acenes. As a result of the reactivity of the biradical state, longer acenes tend to dimerize⁸⁸ or react with singlet oxygen⁸⁹ (**Scheme 1.11**). The reactivity patterns of the dimerization or oxidation are dictated by Clar's rule with the major product maximizing the number of aromatic rings that share a Clar sextet. This unwanted reaction breaks the planarity of the acene and consequently leads to a material that is no longer useful for applications such as in OFETs. Additionally, the dimerization and oxidation reactions of acenes are accelerated by light, which could be quite problematic for a semiconducting material found in organic solar cells.

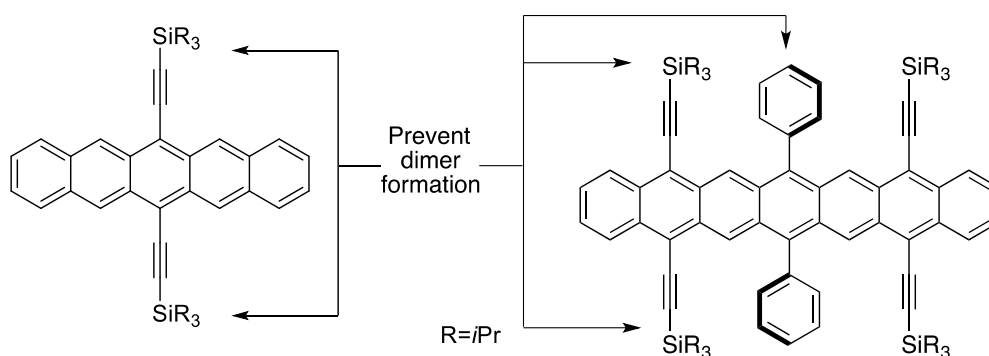
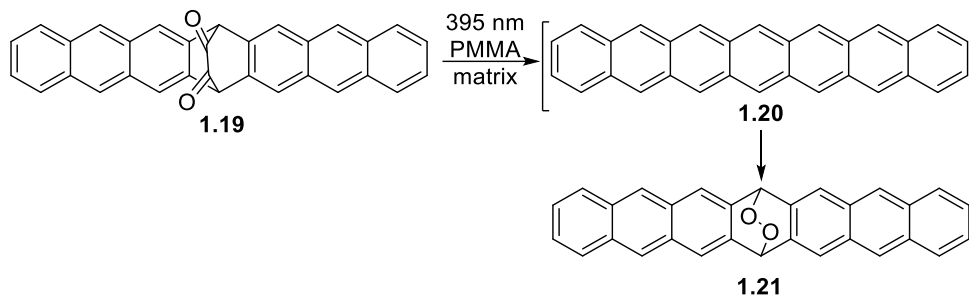


Figure 1.14- Chemical modification of acenes with bulky groups to prevent formation of endoperoxides and dimers.^{90,91}



Scheme 1.12- Matrix assisted synthesis of heptacene.⁹²

Some work has been published regarding the design of longer acenes with bulky groups to prevent dimer and endoperoxide formation. The addition of these groups allows for these acenes to remain stable under irradiation⁹⁰ and have even permitted for the isolation of the longest acene to date (heptacene)⁹¹ for a long enough time to allow for a full characterization (**Figure 1.14**). Other methods for the synthesis of longer acenes use surface conditions on a matrix to synthesize acenes as large as dodecacene.⁹³ The use of these techniques does not provide the means for isolation or a more in-depth study of the material but proves that these compounds can exist under the right conditions. An example of matrix assisted synthesis is highlighted in **Scheme 1.12**. The synthesis of heptacene was carried out on a poly(methyl methacrylate) (PMMA) matrix in an attempt to prevent any oxidation or dimerization.⁹² The sample was irradiated at 395 nm to trigger the expulsion of two CO molecules from the diketone bridge and was analyzed via MALDI-TOF MS and ¹H NMR. Although the acene itself was not observed, the endoperoxide was seen by MALDI-TOF MS and NMR, along with other oxygen adducts, indicating that the bare heptacene formed but immediately oxidized.

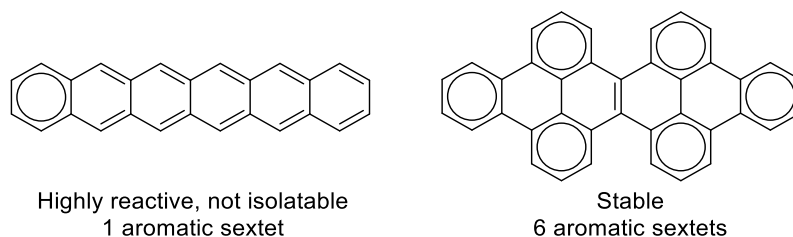
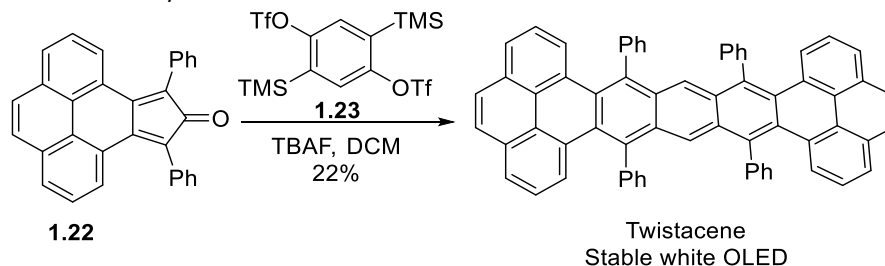


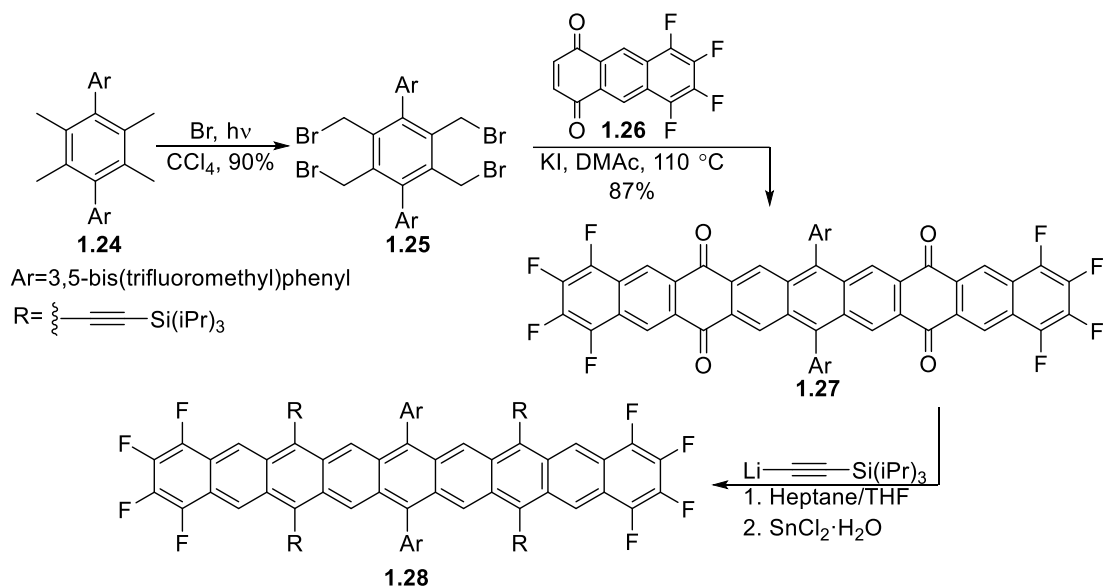
Figure 1.15- Clar sextet analysis between a linear acene and a benzoannulated acene.⁹⁴



Scheme 1.13- Synthesis of twisted heptacene using a Diels-Alder approach.⁹⁵

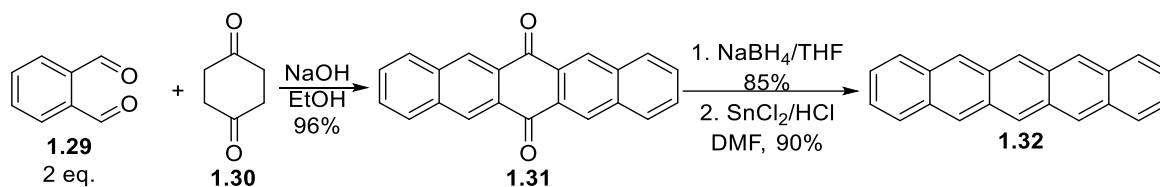
A way to avoid the triplet character of larger acenes is to introduce more Clar sextets onto the acene chain by annulating the molecule. **Figure 1.15** shows how by introducing a pyrene moiety into the acene chain five more Clar sextets are introduced into the molecule that consequently allows the molecule to be bench stable. The effect of additional annulation had been known since Clar's initial analysis of PAHs;⁹⁴ however, the additional annulation can affect the optoelectronic properties due to the additional conjugation. An alternative strategy to imbue acenes with more stability is to twist the acene backbone, thus preventing any dimerization or oxidation, although the twisting must be moderate to maintain good communication between all the acene aromatic rings. Wudl and coworkers demonstrated the synthesis of a heptacene "twistacene" which featured two pyrene moieties at the ends of the acene chain and a slight twist in the main acene backbone (**Scheme 1.13**).⁹⁵ The synthesis of the acene proceeded via a benzyne Diels-Alder reaction with a pyrene cyclopentadienone **1.22**, that after forming the Diels-Alder adducts expels CO to aromatize the acene. The "twistacene" exhibited good stability and did not succumb to oxidation or dimerization even after a 3-year period. Additionally, the compound did not degrade until 400 °C when analyzed by thermogravimetric analysis (TGA) and exhibited strong electroluminescence when utilized in an OLED which produced white light.

1.9.7- SYNTHESIS OF LINEAR ACENES



Scheme 1.14- Synthesis of first isolatable and crystalline nonacenes.⁹⁶

Two syntheses by which acenes are made have been discussed hitherto. The general methodology by which they are constructed is mostly the same where a cycloaddition constructs the ring system and the non-conjugated acene is then either reduced or oxidized (depending on the acene precursor) to yield the fully aromatic acene. Anthony and coworkers' synthesis of nonacene **1.28** provides an excellent example of this approach and is highlighted in **Scheme 1.14**.⁹⁶ Following a bromination, a Cava reaction was triggered with the addition of KI creating a diene from **1.25** that proceeded to perform a Diels-Alder reaction with the dione **1.26** yielding quinone **1.27** in 87% yield. The authors then installed alkynyl groups by reacting the alkynyl lithium with quinone **1.27** and followed this step with a reduction with SnCl_2 to reach nonacene **1.28**. The purpose of the alkynyl groups was to further prevent the acene from dimerizing or oxidizing while also providing a group that may aid with the crystal packing of the molecule. The poor stability of the acene did not allow for an accurate determination of the yield although the authors were able to grow suitable crystals for single X-ray diffraction analysis.



Scheme 1.15- Rapid synthesis of pentacene.⁹⁷

The construction of acenes is not limited to cycloaddition approaches. Pentacene can be synthesized rapidly over two steps using an aldol condensation methodology in which 1,4-cyclohexanone **1.30** is reacted with 2 equivalents of 1,2-phthalaldehyde to yield the quinone **1.31**. A reduction with NaBH₄/SnCl₂ conducted on **1.31** can then be used to yield pentacene from inexpensive starting materials.⁹⁷ The Schipper group required large amounts of pentacene for a series of projects and used this method to obtain an otherwise costly material from inexpensive materials over three steps.

1.9.8- APPLICATIONS OF ACENES

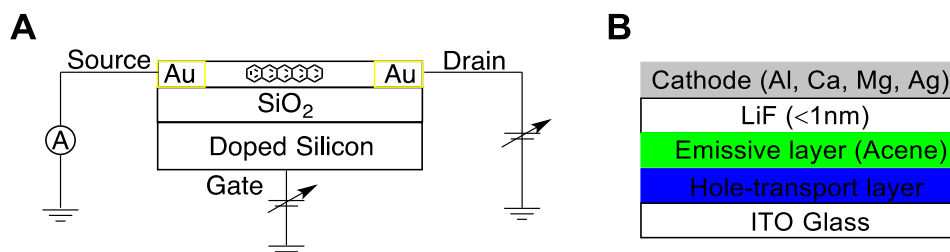
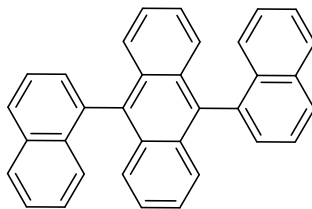


Figure 1.16-A-Schematic representation of an acene bottom contact organic field effect transistor. **B-** Schematic representation of an acene organic light emitting diode.⁷⁸

There are two main applications in which acenes are used in electronic devices: field effect transistors and organic light emitting diodes, although acenes have found limited use in organic solar cells as well. OFETs with acenes can be constructed in a bottom contact configuration (**Figure 1.16 A**) or top contact configuration, with the former providing an easier route towards device fabrication but the latter yields better device performance.⁷⁸ Pentacene is the most common acene used in FETs with some reports showing excellent hole mobilities⁸¹ and ambipolar charge transport.⁹⁸



1.29

Figure 1.17.-Structure of anthracene chromophore for blue OLED.

For OLEDs, acenes serve as the emissive layer of the device which is sandwiched between the hole transport layer and a layer of LiF (**Figure 1.16 B**). Typically, the OLEDs are constructed on an indium tin oxide (ITO) glass coated surface, the purpose of which is to oxidize the emissive layer with the aid of the hole transport layer.⁷⁸ A standard acene OLED is the anthracene derivative **1.29** that was used to create a blue OLED. The naphthyl ligands have a structure that prevents the anthracene from crystallizing creating an amorphous solid with higher luminescence.⁹⁹

1.9.9.-PREDICTED PROPERTIES OF CYCLACENES

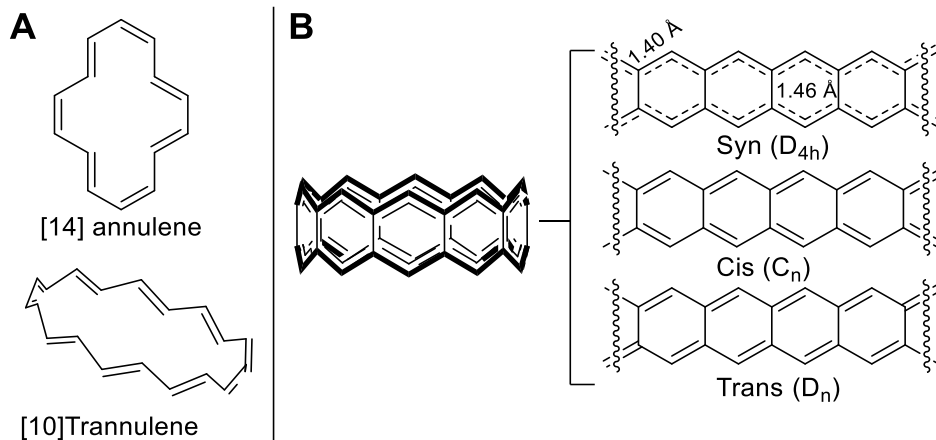


Figure 1.18-A-Structures of [14] annulene and [10]trannulene. **B-** Structure of [10] cyclacene highlighting the behavior of the macrocycle as two bonded [10] trannulenes, possible theoretical resonant structures of cyclacenes with bond lengths.¹⁰⁰

As a consequence of the similarity of cyclacenes to semiconducting zigzag CNTs, high symmetry, appealing structure, and elusiveness with regards to synthesis, cyclacenes were an interesting class of compound to investigate theoretically. To investigate the nature of cyclacenes, Kim and Choi performed a study that was similar to an earlier theoretical investigation on annulenes.¹⁰⁰ Annulenes are monocyclic hydrocarbons that are fully conjugated or have the maximum number of double bonds within the cycle, a common example of an annulene would be benzene although it is not commonly referred to as such. Other examples of annulenes include [14]annulene and [10]tranannulene (**Figure 1.18A**).¹⁰¹ Annulenes possess very similar properties to cyclacenes as they are both fully

conjugated systems that, as a result of ring strain and bond angle constraints, fail to fully follow Hückel's rules for aromaticity. When Kim and Choi analyzed cyclacenes they found that the macrocycle behaves as two trannulenes that were held together in place by a sigma bonding network. Much like the annulenes, cyclacenes can exist as 3 resonant structures, outlined in **Figure 1.18B**, with the *syn*-resonance structure being the most stable of the three. The structure of the optimized *syn*-resonance structure displayed different bond lengths between the two types of bonds in the molecule, this contrasts with aromatic molecules such as benzene where all bond lengths are the same thus indicating that the strain of the cycle influences the aromaticity.

Kim and Choi also modelled the compound in both a singlet and triplet state and found that as the cycle grows the cyclacene was more likely to behave like a triplet with the singlet-triplet energy gap decreasing with increasing size. This singlet-triplet gap decreased rapidly as the cycle grew displaying an almost non-zero metallic singlet-triplet.¹⁰⁰ The likelihood of a cyclacene existing as a triplet is the most likely reason behind the lack of synthetic procedures as such a species would be highly reactive. This trend mirrors what is observed with longer linear acenes. While cyclacenes are most likely not stable, NICS analysis did predict the molecule to be aromatic following a trend similar to that observed with triplet trannulenes. Finally, Kim and Choi noticed that there was a difference in stability between even and odd cyclacenes, with even cycles exhibiting a higher level of stability than odd cycles. These results were further expanded upon by Nendel and coworkers, who confirmed the tranannular nature of the cyclacene as well as its dependence with ring size and if the cycle was had an odd or even number of rings.¹⁰²

At this point all theoretical investigations pointed towards an unstable aromatic molecule that would exist in a triplet state. Another study by Houk and coworkers further examined the triplet state and found that rather than a closed singlet state, cyclacenes would exist as an open shell singlet, meaning that two unpaired electrons occupy different orbitals with opposing spins.¹⁰³ The analysis was further expanded to short CNT fragments and it was found these molecules would also behave as open shell singlets with the edges of the macrocycle behaving as radicals.¹⁰³

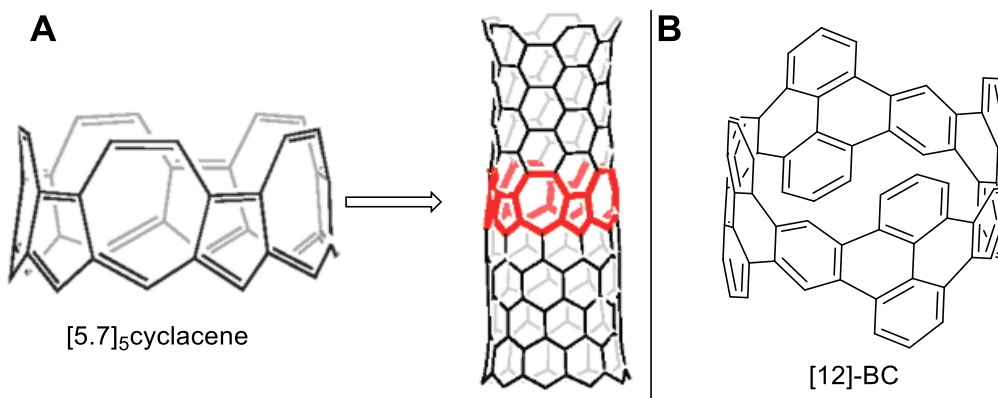
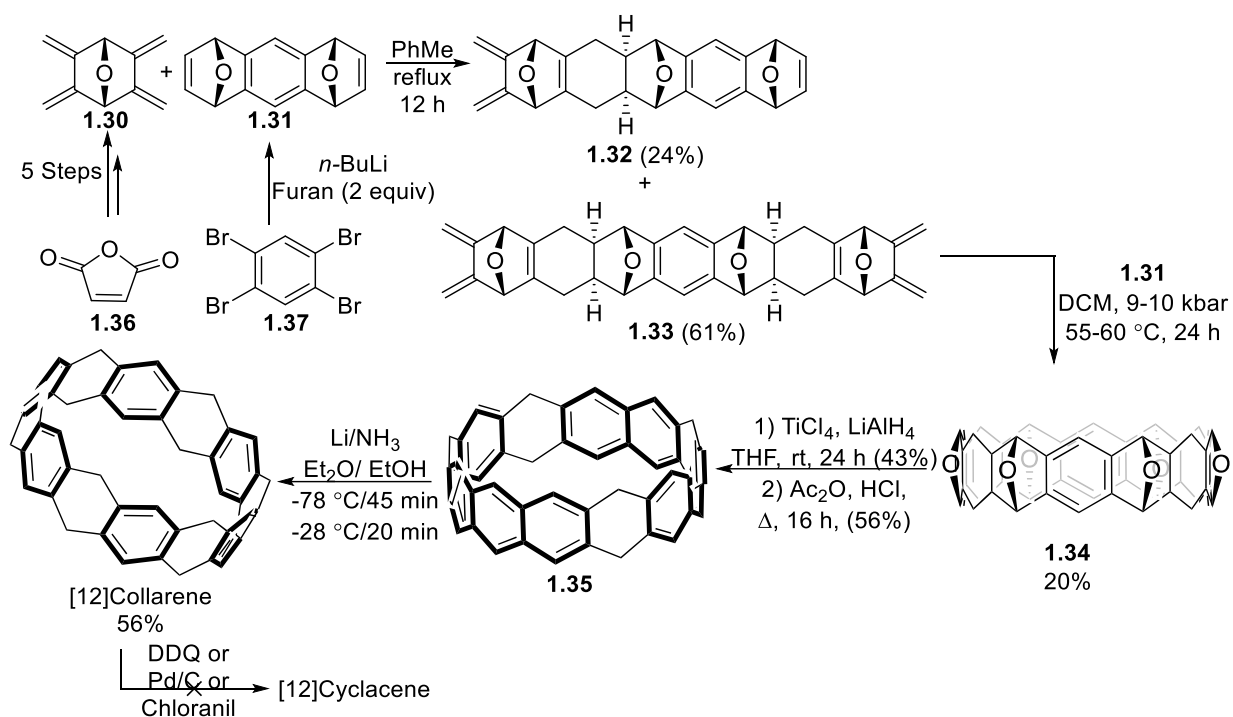


Figure 1.19-A-Structure of theoretically predicted closed shell $[5.7]_n$ cyclacene and its use as a CNT heterojunction,¹⁰⁴ reprinted with permission from *Org. Lett.*, **2011**, 13, 6220-6223. **B**-Structure of theoretically predicted closed shell benzocyclacenes.¹⁰⁵

Only two reports were able to demonstrate computationally that a zigzag edged nanobelt would not exist as a triplet. The first report was by Jasti and coworkers, where the authors proposed that a $[5.7]_5$ cyclacene, an isomer of $[10]$ cyclacene based on azulene, would adopt a closed shell state (**Figure 1.19A**).¹⁰⁴ The azulene cyclacene has a zigzag edge and although it does not exactly match a zigzag CNT, the macrocycle closely resembles a heterojunction between two edge chiralities in a CNT. The second report was by Itami and coworkers where the authors predicted that including pyrene in the backbone of the cyclacene would allow for the cycle to exist as a closed singlet (**Figure 1.19B**).¹⁰⁵ The benzoannulated cyclacene 12[BC] was not only predicted to be more stable than its parent cyclacene but also possessed less strain, lower HOMO-LUMO levels, and behaved as a semiconductor.

1.10 ATTEMPTED SYNTHESIS OF CYCLACENES

Seeing the vast applicability that cyclacenes could potentially present several groups have previously attempted to synthesize cyclacenes. The nanohoop not only represents an important step towards the concise synthesis of nanotubes but also represents a synthetic challenge as imbuing high levels of strain and breaking the planarity of an aromatic system is a worthy challenge. Herein, some of the attempts at synthesizing a fully conjugated cyclacene will be outlined.

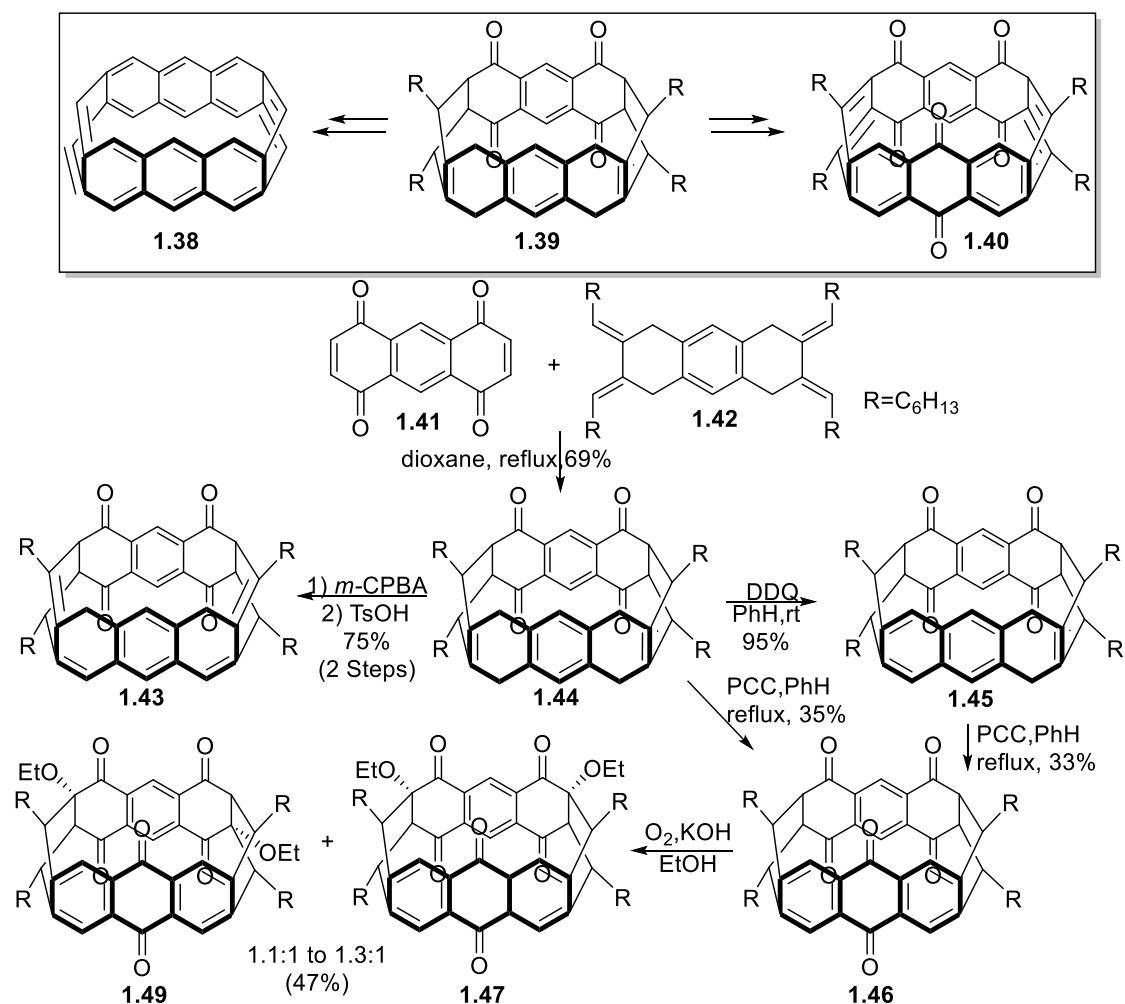


Scheme 1.16- Stoddard and coworkers' synthesis of [12]collarene.^{106–108}

The first attempt at cyclacenes was reported by Stoddart and coworkers. For this synthesis, the authors chose to pursue the cyclacene using a Diels-Alder approach (**Scheme 1.16**).^{106–108} Critical to this approach was the use of the *syn*-diendoxide **1.31**. For the cyclization to be a success, the endoxide oxygen bridges must possess a *syn* relationship to each other, the use of **1.31** ensured that some bias already existed for the product to be able to cyclize in the later steps. Prior experiments revealed that to minimize steric interactions, the endoxide bridges will preferentially lie *syn* to each other. Additionally, all adduct must lie in the *exo*-configuration for the curvature of the molecule to allow cyclization.¹⁰⁹ Since the reaction is carried out under high temperature and pressure conditions and the Diels-Alder reaction is reversible, the reaction eventually reached the required stereochemistry to properly cyclize. The first Diels-Alder reaction was able to proceed yield the mono-adduct **1.32** and bis adduct **1.33** in a 24% and 61% yield, respectively. The first Diels-Alder proceeds much faster (>100 times) than the second Diels-Alder, thus the reaction can be easily controlled by tuning the equivalents of the reactants. Both the mono-adduct and the bis adduct are then reacted once more under high pressure to reach the macrocycle **1.34** in a 24% yield, the stereochemistry and cyclic nature of the product were then unambiguously assigned via single crystal X-ray crystallography.

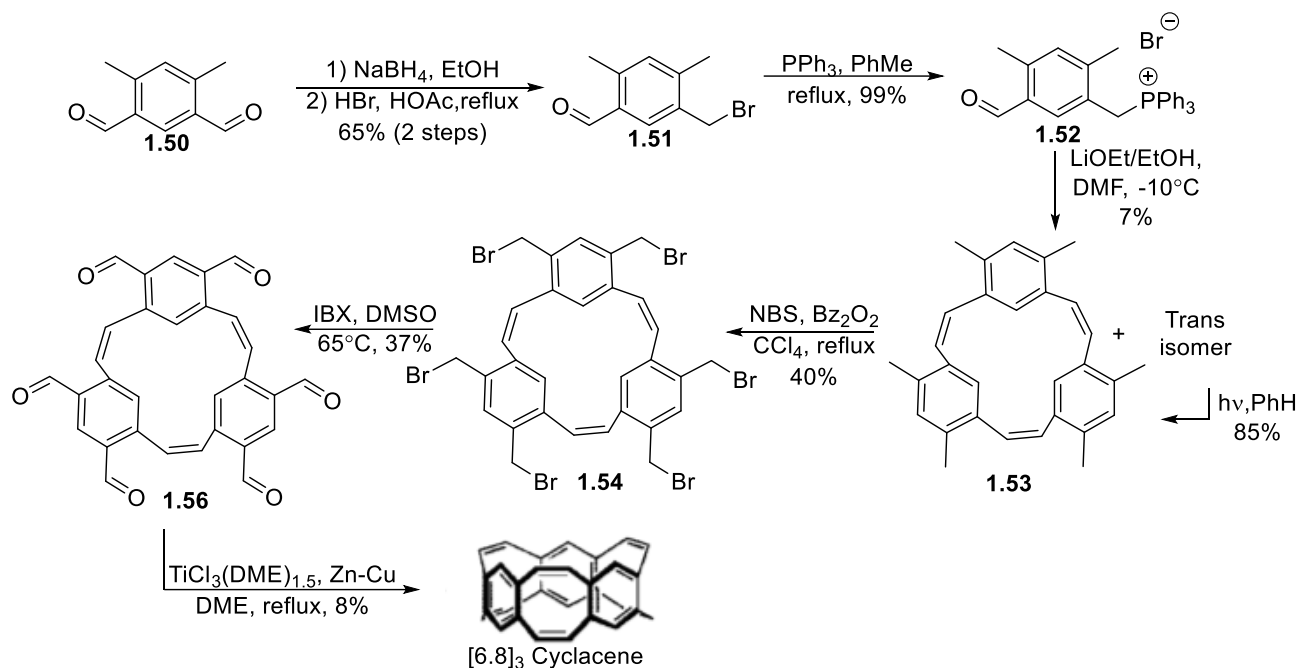
The aromatization of macrocycle **1.34** was then attempted following a series of deoxygenations, first with $\text{TiCl}_4/\text{LiAlH}_4$ followed by Ac_2O to remove the remaining endoxides. The resulting macrocycle **1.35** was then successfully synthesized and was composed of an anthracene, benzene, and naphthalene separated by cyclohexadiene units. The observed aromatic subunits were somewhat unexpected which hints at an acid catalyzed isomerization to maximize the number of Clar sextets present in the cycle. At this point the authors reduced macrocycle **1.35** via a Birch reduction to yield [12]collarane, a highly symmetric precursor to a [12] cyclacene where benzene rings alternate with cyclohexyl rings. Oxidations of the [12]collarene to the [12]cyclacene were attempted with different oxidants to no avail, although oxidations of macrocycle **1.35** were not discussed by the authors it is likely that those oxidations would not yield the cyclacene due to the high reactivity of the product.¹¹⁰

One of the other commonly cited examples is Cory and co-workers' synthesis of a macrocyclic cyclophane which could function as a precursor for [8]cyclacene.^{111,112} Similarly to Stoddart and co-workers' earlier report, the authors opted to construct the cyclacene using a Diels-Alder approach. In contrast to the report by Stoddart however, Cory and co-workers utilized a more flexible bisdiene **1.42** that did not match the dienophile in size but provided enough flexibility to allow for the cyclization of a smaller [8]cyclophane **1.44** (**Scheme 1.17**). The macrocyclization was performed by reacting **1.42** with quinone **1.41** in refluxing dioxane and was able to yield cyclophane **1.44** in a 69% yield.



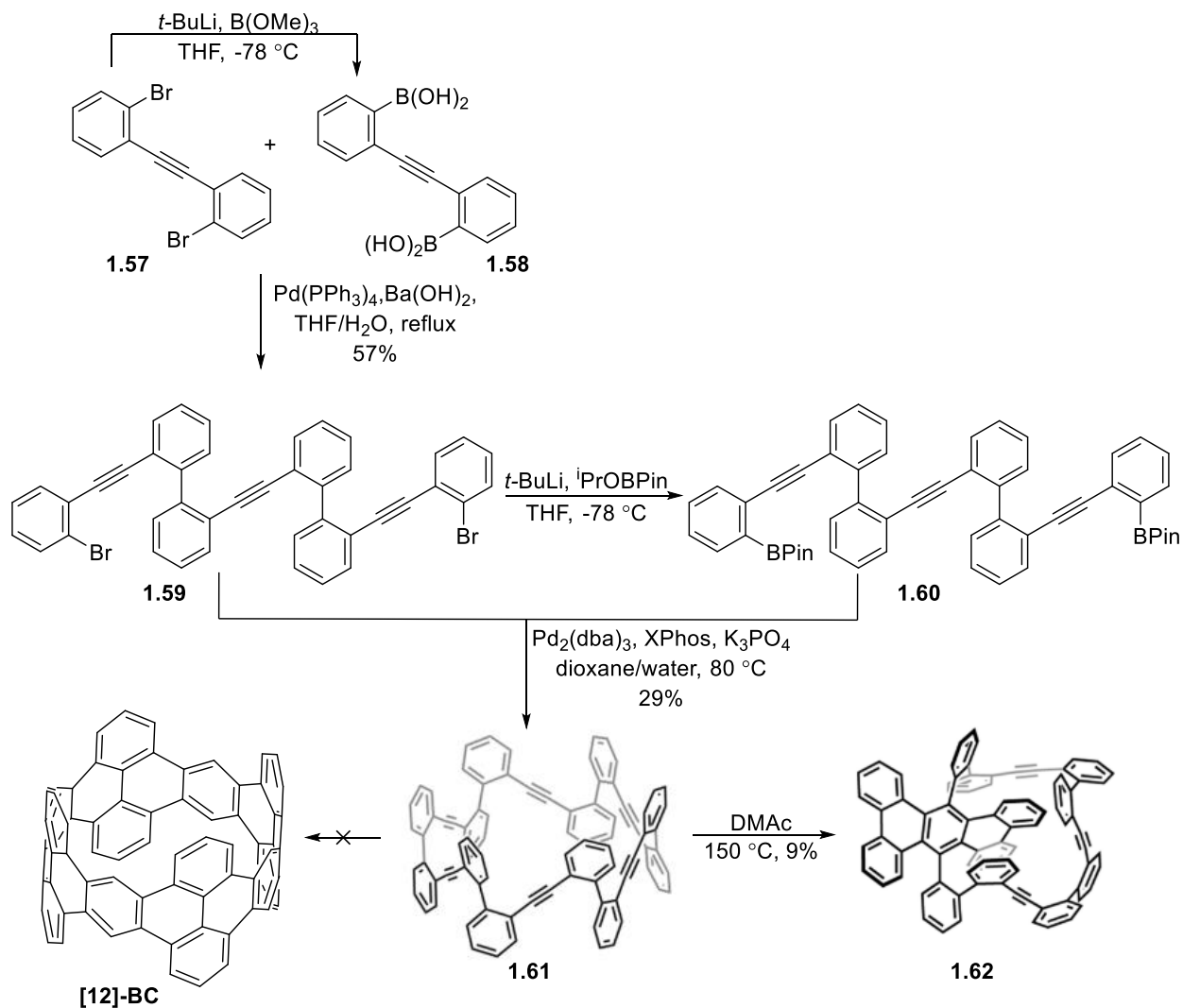
Scheme 1.17- Cory and coworkers' synthesis of [8]cyclacene precursors.^{111,112}

With the cyclophane precursors in hand, the authors then set out to attempt to aromatize the macrocycle, initially targeting the quinoidal acene **1.40** which should be electronically complementary to the fully reduced [8]cyclacene **1.38**. The authors experimented with different ways to aromatize the cycle and found that using *m*-CPBA/TsOH they were able to oxidize some of the unsaturated bonds in the cyclophane. Likewise, they found that DDQ was able to convert **1.44** into the naphthalene **1.45** in high yield. Further oxidation of the naphthalenophane **1.45** did not yield the anthracene or the desired tetraquinone but instead gave triquinone **1.46** in 33% yield. When starting from compound **1.44**, the DDQ oxidation led to the same product in a 35% yield. Further attempts to oxidize the product resulted in mixtures of unwanted products as seen in the formation of products **1.49** and **1.47**. No further attempts to aromatize this cyclophane have been reported since.



Scheme 1.18- Gleiter and coworkers' synthesis of [6.8]₃cyclacene.¹¹³

Although partially conjugated zigzag edges had been successfully synthesized, there had yet to be a report that highlighted a fully conjugated macrocycle that possessed a zigzag edge or cyclacene character. Then in 2008, Gleiter and coworkers were able to capitalize on the flexibility of a cyclooctatetraene and synthesize a macrocycle that was fully conjugated across the ring.¹¹³ The cyclophane backbone of the cyclacene was created using a Wittig cyclization and the second strand of the cycle was constructed using a McMurry coupling. Both reactions result in unsaturated bonds thus no additional transformations were required to aromatize the molecule and following the McMurry coupling the cyclacene was already fully conjugated. If the [6.8]₃ cyclacene was to be expanded via a method like CVD, the nature of the resulting CNT is unclear. This example however, served to show how different ring sizes could allow for a cyclacene and was later expanded upon by the theoretical work carried out by Jasti and coworkers.¹⁰⁴



Scheme 1.19- Itami and coworkers' attempted synthesis of [12]benzocyclacenes.¹⁰⁵

The last example to be highlighted is Itami's attempted synthesis of [12]benzocyclacenes.¹⁰⁵ Having previously performed theoretical calculations to predict the stability of the benzoannulated cyclacenes, Itami and coworkers set out to synthesize [12]BC using a benzoannulation technique on **1.61** which was constructed following a series of Suzuki couplings (**Scheme 1.19**). Several reaction conditions were screened to convert **1.61** into [12]BC following prior reports for cyclizing aryl acetylenes,^{114,115} but only resulted in complex mixtures and the desired [12]BC were never observed. The precursor **1.61** was also found to yield an unexpected product (**1.62**) if heated in DMAc at $150\text{ }^\circ\text{C}$ for two days. This product was formed via a formal [2+1+2+1] cycloaddition and the mechanism for the cyclization was ascertained following DFT calculations.

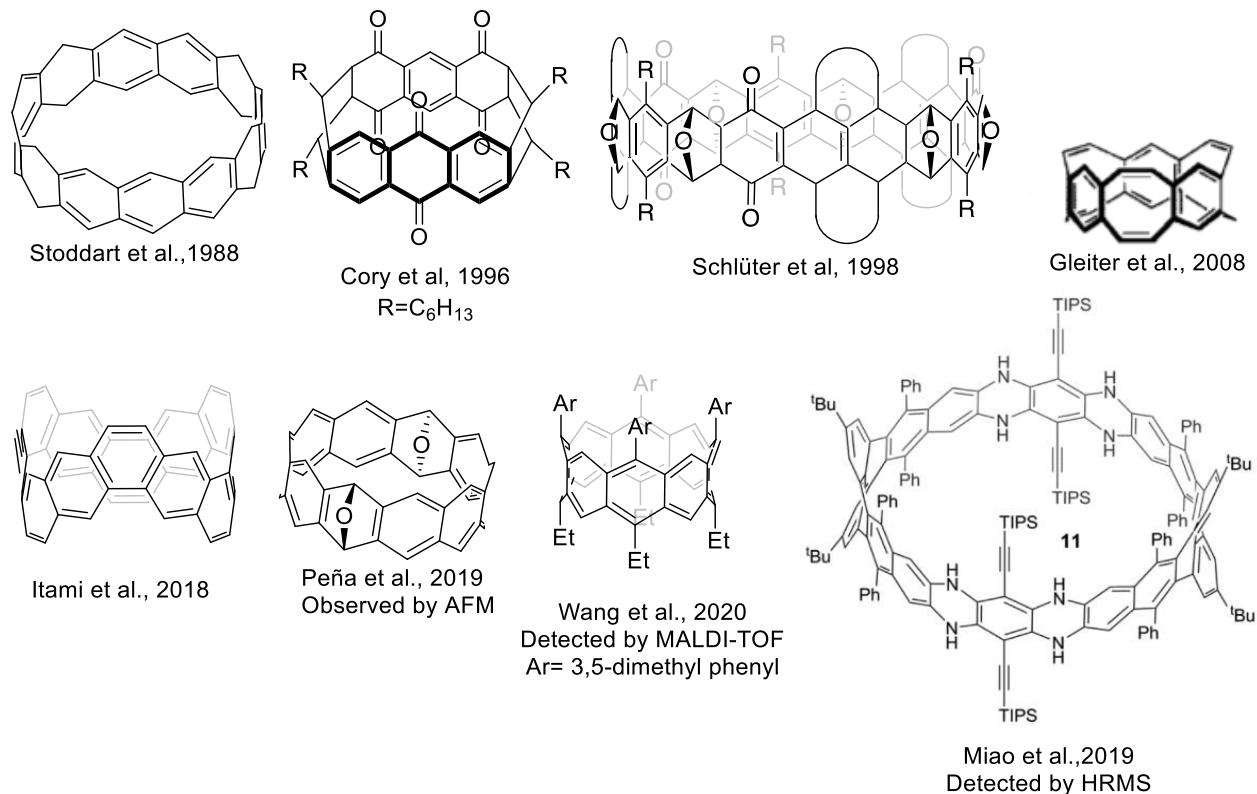


Figure 1.20- Conjugated macrocycles synthesized on the path towards zigzag cyclacenes.^{107,111,113,116–119}

A lot of variety exists with regards to the different synthetic pathways by which chemists have attempted to create cyclacenes.^{107,111,113,116–119} Usually, researchers that take on this challenge are able to construct a cyclic precursor but fail to aromatize the molecule. Other groups will take a more non-conventional approach such as surface chemistry¹¹⁸ or laser ionization,¹²⁰ with the latter allowing for the observation of an [8]cyclacene by MALDI-TOF MS. **Figure 1.20** highlights some of the macrocycles that have been made so far in an attempt to create cyclacenes. Of particular interest are the cycles created by Itami¹¹⁷ and Gleiter,¹¹³ as both of these macrocycles exemplify a fully conjugated edge around the cycle, hinting that provided the right conditions cyclacenes may in fact be isolatable.

PART 1: CHAPTER 2

ATTEMPTED SYNTHESIS OF PYRENE ZIGZAG CYCLACENES

2.0 MOTIVATION

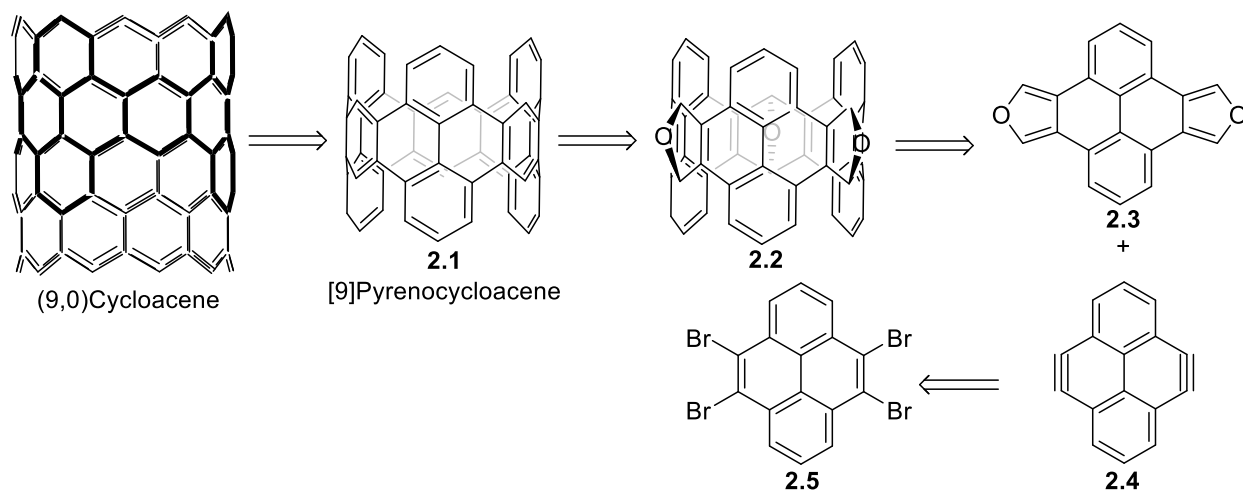
The previous chapter highlighted the importance of carbon nanotubes and the potential impact they can have on the future of field effect transistors.^{2,3,21,22} The current synthesis of CNTs is problematic as a result of the high amount of energy introduced into the system causing the reaction to be unselective towards which allotrope of carbon is made.^{29,121} Although the selectivity of CNT synthesis has improved and purification^{46,48} and sorting⁵¹ methods are available, the cost and availability of pure semi-conducting CNTs is a hurdle for the advancement of CNT electronic materials.

Small molecules that resemble CNTs may offer a solution to the synthesis problem as these molecules have previously been shown to direct the CVD growth^{57,70} of CNTs with the resulting tubes matching the diameter and chirality of the seed. Thus, researchers turned their attention towards CPPs, which closely resemble armchair CNTs, and cyclacenes, which closely resemble zigzag CNTs, as potential seed molecules from which the CNTs can grow. CPPs were first synthesized by Jasti and coworkers⁶⁷ and since their inception multiple synthetic routes have been created providing easy access to CPPs of different sizes and diameters. The accessibility of CPPs has increased to the point that these cycles are now commercially available.

Cyclacenes on the other hand are a much more elusive species that remained unreachable until only recently.^{79,80,122} The wide availability of a zigzag cyclacenes could provide precise access to semiconducting CNTs and could potentially exhibit interesting properties of its own that could allow the molecule to be used in semiconductor applications. Thus, given the impact such a molecule could have on the field of CNT electronics, we set out to design a synthesis that would yield an isolatable and stable zigzag cyclacene. Herein, the synthetic strategies and rationale behind our attempt for the synthesis of zigzag cyclacene will be discussed.

2.1 DESIGN OF PYRENE CYCLACENE AND RETROSYNTHESIS.

When designing a candidate for our cyclacene, we had to consider why prior synthesis failed to give out the fully conjugated cyclacene. Prior computational studies revealed that cyclacenes would behave as open singlets consequently forbidding isolation due to the high reactivity of the species. Thus, it is not surprising that cyclacene precursors, such as Stoddart's [12]collarene,¹⁰⁷ (**Scheme 1.16**) were not able to be aromatized to the cyclacene due to the ring's high reactivity. Indeed, cyclacenes have been observed by MALDI-TOF MS indicating that the species may exist briefly but enough long to be of use.¹²⁰



Scheme 2.1-Retrosynthetic analysis of [9]benzocyclacene.

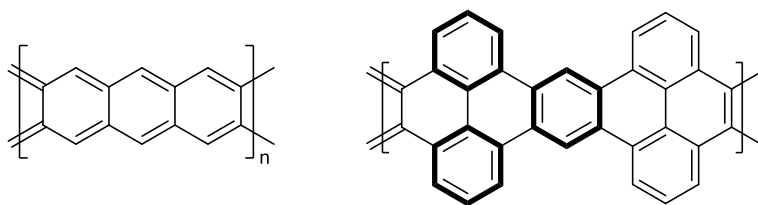
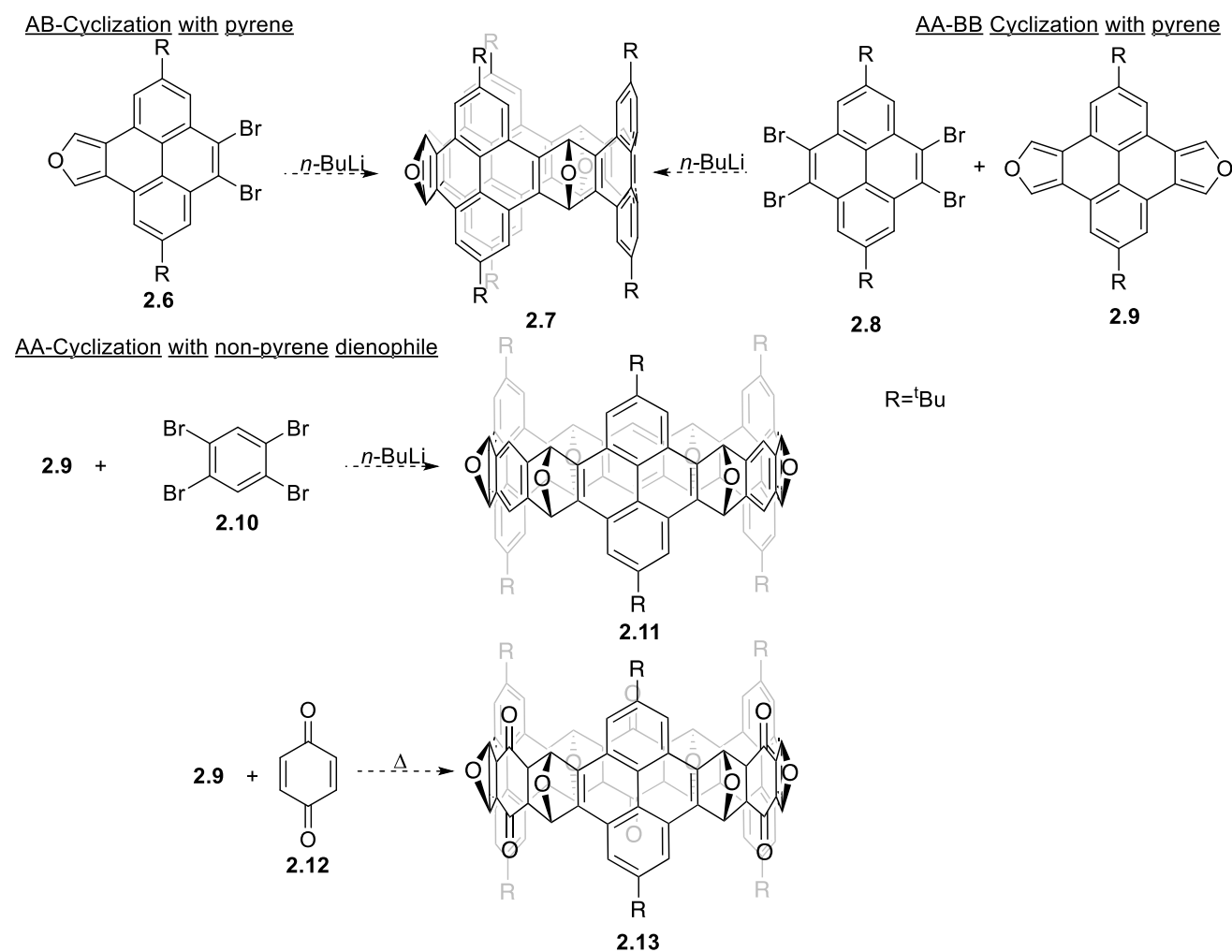


Figure 2.1-2D representation of a cyclacene vs a pyrene cyclacene. Clar sextets are represented by bolded bonds.

When we looked at acenes for inspiration, we observed that if an acene was annulated, then the benzoannulated acene would be more stable than the linear acene (**Chapter 1-Figure 1.14**). Thus, we envisioned using pyrene as the backbone of our cyclacene which should stabilize the cyclacene by creating Clar sextets within the cycle (**Figure 2.1**). Pyrene offers several advantages for our synthesis: the chemistry and transformations are well known, the starting material is inexpensive, has been previously predicted to give rise to a stable cyclacene,¹⁰⁵ and was shown to be flexible as to allow for the synthesis of strained cyclophanes.¹²³⁻¹²⁶

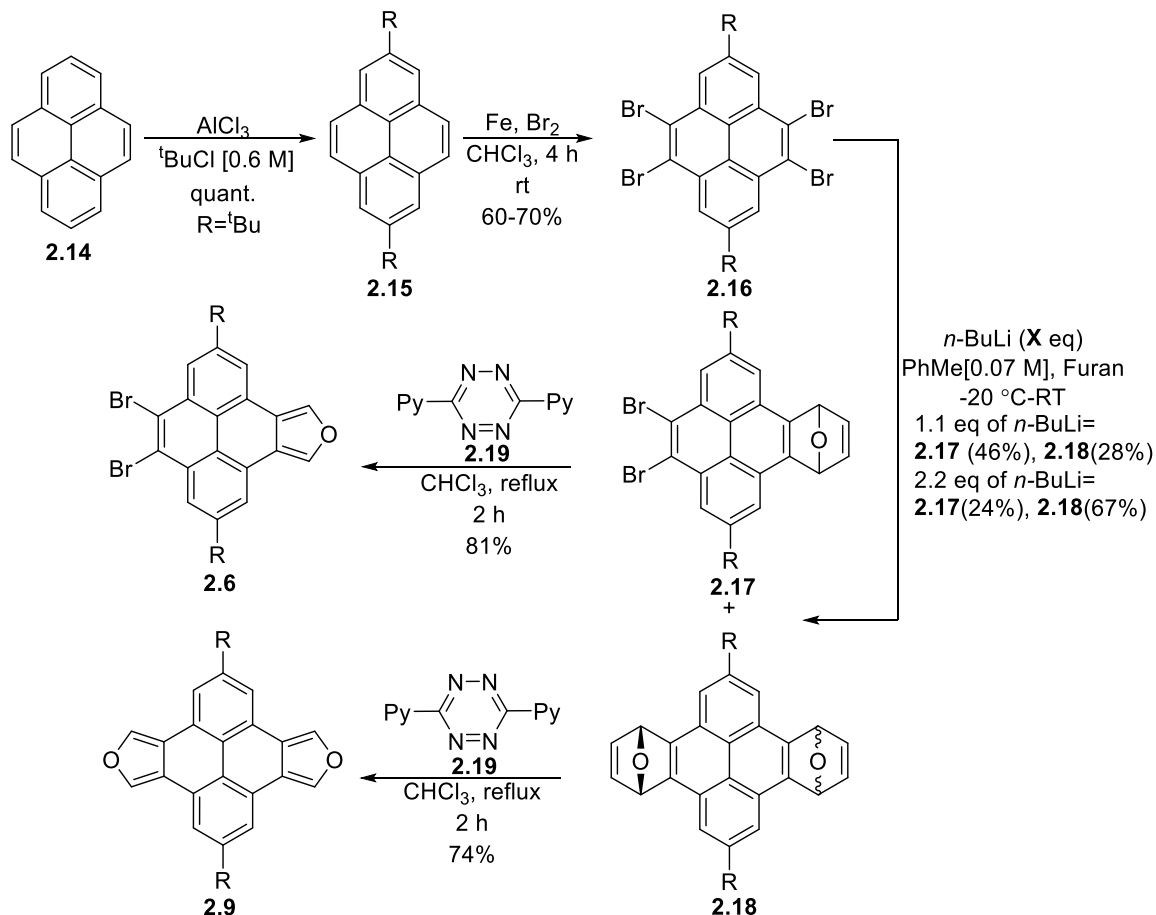
Our retrosynthetic analysis is shown in **Scheme 2.1**. The target for our synthesis was pyrene cyclacene **2.1**, which can be seen as a small segment of a zigzag CNT. To reach this compound we proposed a Diels-Alder approach to construct the double stranded cycle following a similar procedure to those reported by the groups of Cory and Stoddart.^{107,109,111,112} We hypothesized that the cycle would be constructed from cyclizations between pyrenofurans **2.3**, thus before we reached **2.1**, the cycle would have to be reduced from the epoxycycle **2.2**. The epoxycycle can be constructed from bisdienophile **2.3** and a dienophile such as the pyrene bisbenzyne **2.4**. The required starting materials for the cyclization would then be synthesized from the tetrabromopyrene **2.5**. It should be noted that since we are proceeding through a Diels-Alder approach the final ring size for the product is unknown since the reaction can potentially yield cycles of different ring sizes.



Scheme 2.2-Proposed synthetic pathways towards macrocyclic precursor to pyrene cyclacene.

Following our retrosynthetic analysis, we proposed four possible synthetic pathways to try and reach the pyrene cyclacene precursor (**Scheme 2.2**). The first synthetic pathway would utilize an AB cyclization using monomer **2.6** as both the diene and dienophile to reach cycle **2.7**. The Diels-Alder reaction would proceed through a benzyne intermediate created from lithiation of **2.6** via a lithium-halogen exchange followed by elimination. Similarly, an AA-BB approach can also be used to construct the cycle by reacting bisfuran **2.9** with tetrabromopyrene **2.8**. Once again, this cyclization proceeds via a lithium halogen exchange/elimination to create the benzyne dienophile. We also hypothesized that the cycle could be reached using a non-pyrene dienophile, although this does increase the likelihood that the product may behave as an open singlet due to the larger exposed zigzag edge. For this approach, we could react the bisfuran **2.9** with commercially available dienophiles such as tetrabromobenzene **2.10** or benzoquinone **2.12** to reach cycles **2.11** and **2.13**, respectively.

2.2 SYNTHESIS OF STARTING MATERIALS



Scheme 2.3-Synthesis of pyrenofurans.

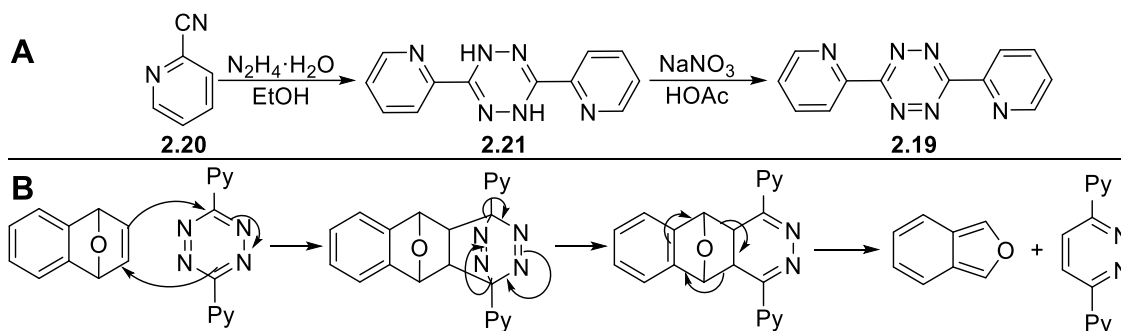
The synthesis of the starting materials can be seen in **Scheme 2.3** and closely follows a previously published synthesis of **2.9** outlined by Dibble and coworkers.^{124,127} Commercially available pyrene was first *tert*-butylated at the 2 and 7 positions using ^tBuCl and AlCl₃ in a quantitative yield. The role of the *t*-Bu serves two purposes: first it grants solubility to the pyrene and secondly it blocks the most reactive positions with regards to electrophilic aromatic substitution, the latter becomes important in the next step as the ^tBu groups direct the bromination towards the desired positions. 2,7-Di-*tert*-butylpyrene **2.15** was then brominated with elemental bromine and iron powder in CHCl₃ with yields ranging from 60-70%.

The bromination of **2.15** was one of the initial hurdles for this project as we experienced batch to batch variability with some reactions providing little to no yield or inseparable impurities. Furthermore, initial attempts to run the reaction at large scales proved difficult due to mixing issues brought about by the Fe powder interfering with the magnetic stirring. These issues were eventually remedied as we learned that the reaction was sensitive to the solvent and the reaction time. Literature preparations typically ran the bromination of **2.15** in CCl₄, a rather expensive and ozone depleting substance. Thus, in an attempt to perform the reaction in a cost-effective manner we initially carried out the reaction in DCM. The reaction was able to proceed in DCM, but the batch variability was problematic with most reactions yielding an inseparable mixture of products. Changing the solvent to CHCl₃ allowed for the reaction to proceed more cleanly and with less variability. Additionally, we also concluded that the ideal reaction time was 4 h based on a prior report.¹²⁸ With those two variables changed, we were now able to reliably and cleanly synthesize **2.16**, oftentimes not requiring any further purification after quenching the reaction. The nature of the side products is unclear, but the most likely candidates are pyrenes with varying levels of bromination.

Tetrabromopyrene **2.16** was then subjected to the first Diels-Alder cyclization with furan via a lithium-halogen exchange to yield the monoendoxide **2.17** and the diendoxide **2.18**. The reaction proceeds by creating a benzyne following lithiation/elimination which then reacts through a cycloaddition with furan to yield the endoxide. Initially, the observed yields for the reaction were not ideal (<20%) but were improved upon by adding a large excess of furan, which escapes from the reaction due to its high volatility, and a more controlled addition of *n*-BuLi. Both compounds were of use to us, and we could select for one endoxide over the other depending on the equivalents of *n*-BuLi used; however, both products were always observed. For the di-endoxide, both the *syn*- and *anti*-diendoxide

2.18 eluted at roughly at the same time on the column with occasional runs providing some resolution between the two diastereomers. Literature on similar compounds suggests that the ratio between *syn* and *anti* is roughly 1:1.¹⁰⁸

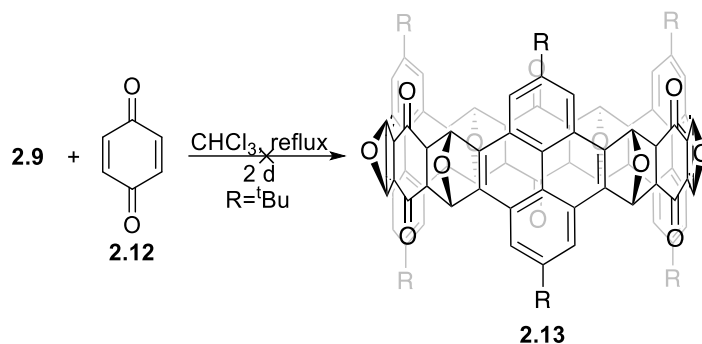
The pyrenofurans **2.6** and **2.9** can then be reached by reacting the endoxides with dipytet **2.19**, which yields a pyrenofuran following a series of cycloadditions driven forward by the expulsion of nitrogen. The furans were furnished in good yields and exhibit good stability compared to other benzofurans. Initially, we were concerned about the stability of these furans as other benzofurans are highly reactive but gratifyingly observed no decomposition even when the furans were left on the bench for long periods of time. When we first reacted **2.6** and **2.9** with dipytet, we did so at room temperature for 18 h, but with the assurance that the product would not decompose we performed the reaction in refluxing CHCl_3 and were able to retain the same yield in a shorter reaction time.



Scheme 2.4-A-Synthesis of dipytet. B-Dipytet mediated synthesis of benzofurans.

Dipytet **2.19** was also synthesized in our lab due to the high commercial cost of the compound. **2.19** can be easily synthesized following a condensation of hydrazine with 2-cyanopyridine to yield **2.21** which is then oxidized with NaNO_3 to yield dipytet **2.19**. The mechanism by which dipytet functions and its synthesis are highlighted in **Scheme 2.4**.

2.3 INITIAL ATTEMPTS AT CYCLIZATION



Scheme 2.5- Attempted cyclization of bisdiene **2.9** with *p*-benzoquinone

Now having a good grasp on the synthesis of the pyrenofurans **2.9** and **2.6**, we set out to attempt to cyclize our pyrene monomers to construct our cycle. We first set our sights on the macrocycle **2.13**, taking inspiration from Cory and coworkers' attempted synthesis of cyclacenes. We hoped that our pyrene bisdiene would provide enough flexibility when combined with *p*-benzoquinone. Additionally, we hypothesized, perhaps wrongly, that the quinoidal nature of the cycle would provide stability to the macrocycle thus allowing for facile transformation to the cyclacene. We reacted benzoquinone with bisdiene **2.9** in refluxing CHCl_3 for two days; however, we were unable to successfully extract anything resembling a macrocycle out of the reaction mixture (**Scheme 2.5**). We did observe the formation of some new spots by TLC but were not able to isolate any cyclic products through chromatography.

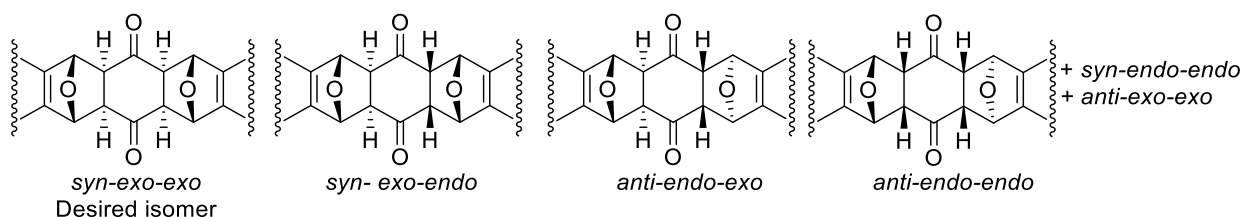
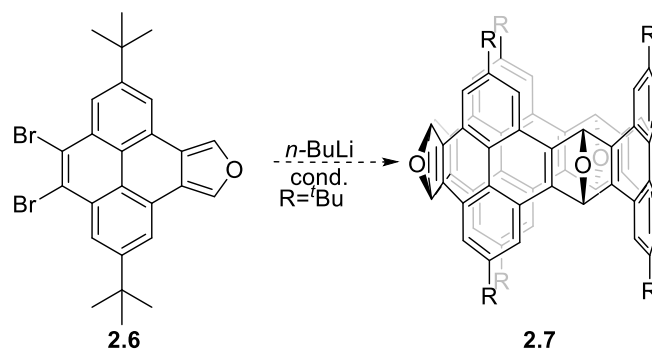


Figure 2.2-Possible stereoisomers from Diels-Alder cyclization of **2.9** with benzoquinone **2.12**.

Our reaction conditions were based on observations made by Stoddart and coworkers; they observed that the desired isomer was the most thermodynamically stable thus given enough time the reaction should obtain the desired stereochemistry.¹⁰⁹ Unlike Stoddart, however, we did not have the stereochemistry of our endoxide bridges set before cyclization therefore upon performing the Diels-Alder reaction there are 6 possible isomers that can form

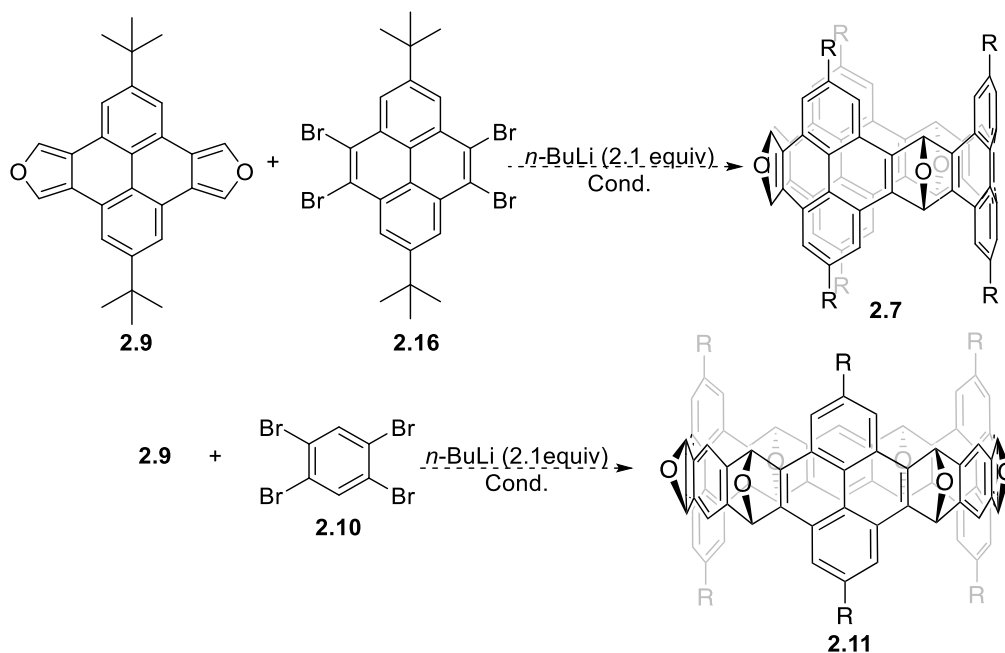
(Figure 2.2). We tried to account for this by running the reaction over a long time period; however, this was somewhat of a “shotgun” approach as several pieces needed to fall perfectly into place for this approach to work.



Scheme 2.6- Attempted synthesis of cyclacenes using an AB approach.

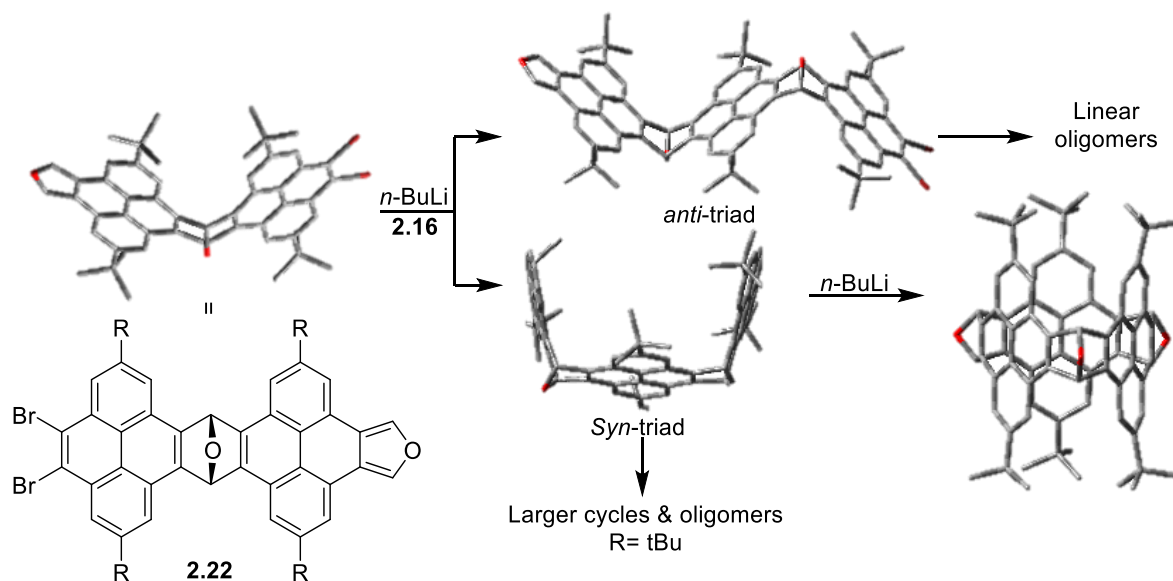
Given the high number of isomers that can be formed during the reaction with a dienophile like benzoquinone, we decided to perform our cyclizations using benzyne as our dienophile. Since the reacting benzyne orbitals are parallel to the plane of the aromatic ring then no *endo* or *exo* isomers can form limiting the number of isomers that can form to just *syn* and *anti*. Additionally, the high reactivity of the benzyne species should provide a significant driving force for our Diels-Alder cyclizations to proceed. Thus, we set out to attempt the AB cyclization of pyrenofuran **2.6** with *n*-BuLi. This cyclization was attempted under numerous conditions including different temperature, concentrations, solvents, slow addition of *n*-BuLi, and different equivalents of *n*-BuLi. Despite our best efforts, the reaction was only able to give complex mixture which were difficult to analyze by any spectroscopic method (**Scheme 2.6**).

We also attempted the cyclization following an AA-BB cyclization which granted us an additional level of control with the way that reagents were introduced. The reaction was attempted with tetrabromopyrene **2.16**, bisfuran **2.9** and *n*-BuLi; however, no set of conditions was able to grant any cyclic product. Similarly, the reaction was tried with 1,2,4,5-tetrabromobenzene **2.10** and bisfuran **2.9** under *n*-BuLi but once again the product was not observed or isolated (**Scheme 2.7**).



Scheme 2.7-Attempted synthesis of cyclacenes using an AA-BB approach.

2.4 PYRENE FACE BLOCKING

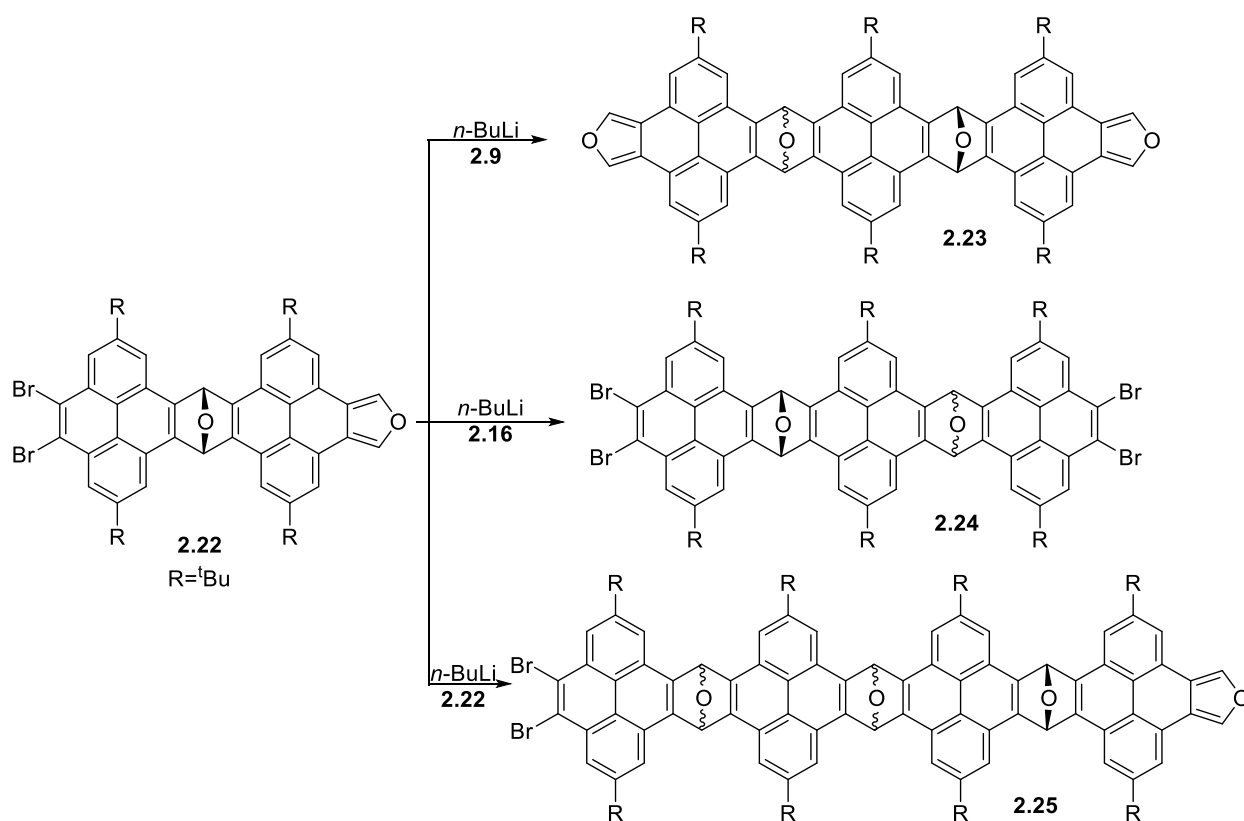


Scheme 2.8- Schematic representation of possible reaction outcomes for AA-BB cyclization approach.

When we performed these initial cyclizations we did observe the starting materials being consumed, thus it was very likely that the reaction was indeed proceeding but not making the desired products. Given that our macrocyclic precursors (**2.6**, **2.9**, and **2.16**) were flat and had no pre-existing curvature, the reaction was unselective towards the formation of the desired *syn* diastereomer. This lack of selectivity results in the proliferation of

unwanted isomers and products that are ultimately inseparable from the desired product. **Scheme 2.8** provides a representation of the possible reaction outcomes. When the diad **2.22** forms, the reaction can then proceed to yield a *syn*-triad or an *anti*-triad, since either outcome is equally likely, a mixture of both is formed. The reaction can then proceed with either triad resulting in a mixture of linear and cyclic products, as well as larger cycles and oligomers.

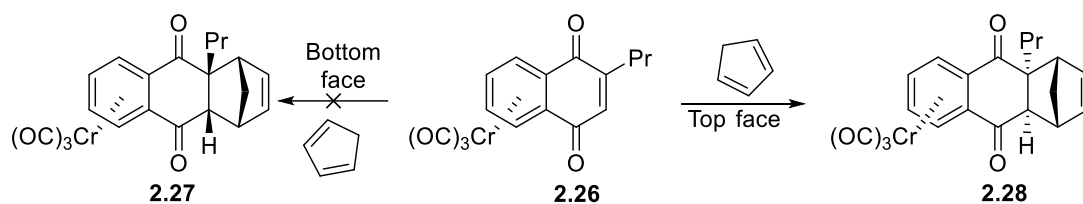
This problem is further aggravated by the larger number of products that can form following the production of **2.22**. **Scheme 2.8** provides an idealized scenario which can still lead to several unwanted products; however, the complexity of the reaction is much more harrowing. **Scheme 2.9** shows a more accurate representation of the reaction, once **2.22** forms the diad can react with one of 3 possible partners due to the bifunctional nature of the molecule. All possible outcomes can yield the desired cycle; however, after each addition two or three new isomers are created which can react further. Consequently, several products are made that make isolation of a cycle, if any, extremely difficult. Thus, if we hope to isolate a cyclacene using this approach, we need to impart some selectivity on the cyclization.



Scheme 2.9- Possible reaction outcomes after the formation of diad **2.22**.

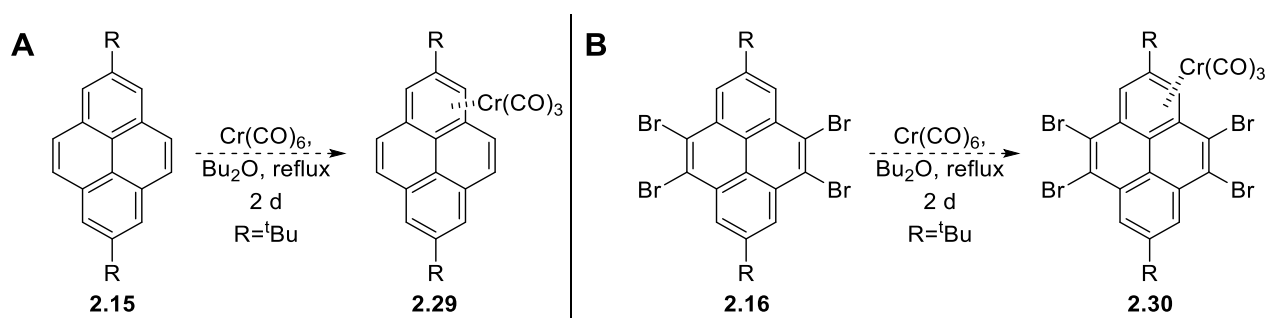
As an initial strategy towards promoting cyclization, we sought to protect one of the faces of our pyrene monomers to promote the sole selection of the desired *syn*-diastereomer. This face group would either be an organic or an inorganic molecule that would then be removed after the cyclization.

2.4.1-FACE BLOCKING WITH AN INORGANIC MOLECULE



Scheme 2.10- Directing role of $Cr(CO)_3$ in [4+2] cycloadditions.¹²⁹

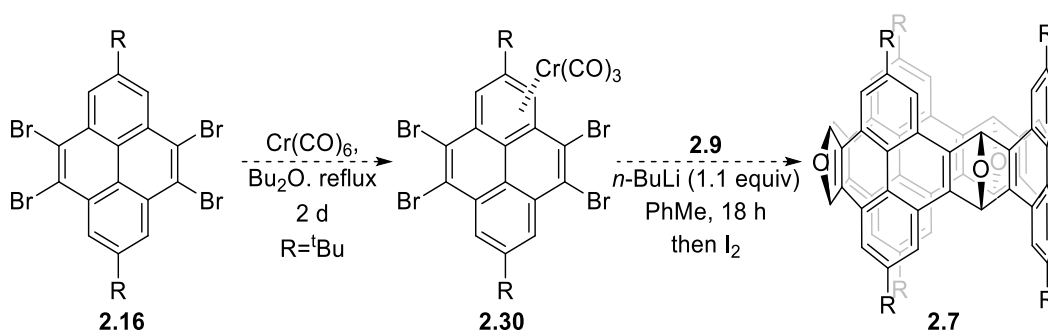
For our initial attempts at a face blocking group. We set our sights on the use of an inorganic molecule as we could potentially attach it to our pyrene monomers without creating any additional bonds and could then remove it easily via the addition of an oxidant. Chromium complexes have been previously shown to form complexes with the π -system of aromatic molecules and can be used as a way to induce selectivity in prochiral molecules.¹³⁰ For example, Dötz and coworkers demonstrated how [4+2] cycloadditions could be influenced by the presence of a $Cr(CO)_3$ moiety. The steric bulk of the $Cr(CO)_3$ leads cycloadditions of naphthoquinone to yield perfect *anti*-selectivity between the chromium and cyclopentadiene (**Scheme 2.10**).¹²⁹ Using the previous example as an inspiration, we hypothesized that the *anti*-directing role of the Cr would lead to endoxides with *syn* relationships to each other and consequently a cyclic molecule.



Scheme 2.11- Attempted synthesis of pyrene-chromium complexes.

When examining the literature, we were pleased to observe that pyrene-chromium complexes have been previously reported. To further reinforce Clar's sextet law, the addition of the $\text{Cr}(\text{CO})_3$ occurred in the most aromatic ring of the pyrene and similarly for other PAHs.¹³¹ We began our investigation into pyrene-chromium complexes by reacting 2,7-di-*tert*-butyl pyrene **2.15** with $\text{Cr}(\text{CO})_6$ in refluxing Bu_2O for two days and observed that the light yellow solution slowly converted to a bright green solution (**Scheme 2.11-A**). 2,7-Di-*tert*-butylpyrene **2.15** was used initially as opposed to our cyclization precursors as we were unsure if the *t*-Bu groups would allow for the Cr to bind to the pyrene. Additionally, we feared furans **2.9** and **2.6** would break down at the reaction temperatures and did not want to waste precious starting material at this stage in the project. We attempted the isolation of compound **2.29** but were unable to recover the Cr-pyrene compound. We suspect that **2.29** degraded when subjected to column chromatography. While the colour change does indicate the formation of **2.29**, as these complexes are highly coloured, the additional bulk around the Cr might weaken the already weak interaction between the pyrene and $\text{Cr}(\text{CO})_3$ causing **2.29** to be more sensitive than the previously reported pyrene-Cr complexes.

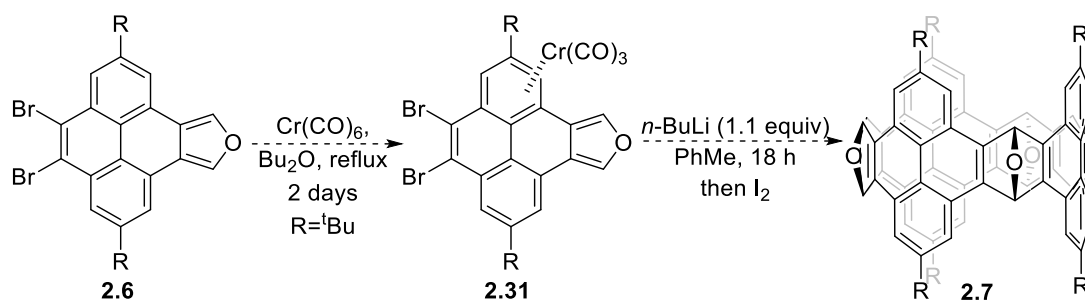
We also attempted to attach $\text{Cr}(\text{CO})_3$ onto **2.16**, which if successfully functionalized would allow for use in the cyclization. Once again, we observed a change from yellow to green but were unable to isolate the compound. The additional bulk caused by the four bromine atoms may weaken the pyrene-Cr bond further and disallow for its isolation. Furthermore, the electron-withdrawing nature of the bromines might lessen the overall reaction yield.



Scheme 2.12-*In situ* synthesis of **2.30** followed by reaction with bisdiene **2.9**.

Given the apparent instability of the compound we decided to take a different approach to try and install $\text{Cr}(\text{CO})_3$ on our molecule. Based on the colour change we knew that some of the starting material was turned into the chromium complex. We also understood that these compounds exhibit different degrees of air sensitivity.

Therefore, it was possible that degradation in air led to a drastic reduction of the yield. Thus, rather than attempting to isolate the compound we sought to create the pyrene-chromium complex and immediately expose this compound to our cyclization conditions. Our hope was that the added influence towards cyclization may promote the formation of a cycle enough for us to observe and isolate it. With this in mind, we reacted **2.16** with $\text{Cr}(\text{CO})_6$ for two days in refluxing Bu_2O and following this reaction we removed the solvent under reduced pressure and introduced bisdiene **2.9**, toluene, and $n\text{-BuLi}$ to the reaction vessel (**Scheme 2.12**). After the reaction time elemental iodine was added to the mixture to remove any Cr still bound to the products. The reaction appeared to proceed more cleanly (As seen by TLC and our Combiflash chromatogram) but we were still unable to assign any of the isolated compounds as our desired cycle.



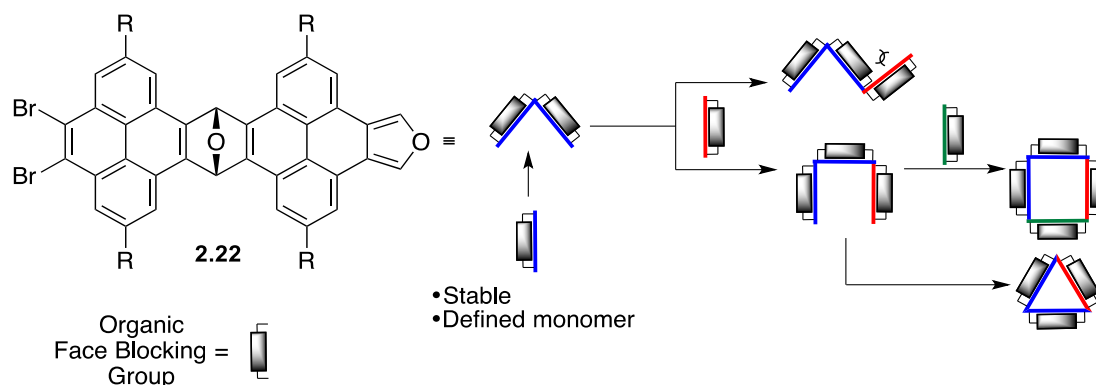
Scheme 2.13- *In situ* synthesis of **2.31** for the directed cyclization of **2.7**

We also attempted to install $\text{Cr}(\text{CO})_3$ on the monofuran **2.6**, our logic was that this pyreno furan should be the more stable than **2.9** and would be more likely to survive the reaction (**Scheme 2.13**). Once again, we opted not to isolate the compound and reacted **2.6** with $\text{Cr}(\text{CO})_6$ for two days, after which exchanged the solvent to PhMe and added $n\text{-BuLi}$. To our dismay the reaction once again returned several products, and we were unable to assign any of the isolated compounds as cyclic or otherwise.

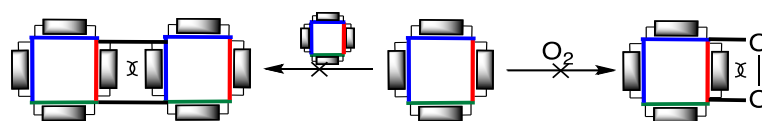
2.4.2 ORGANIC FACE PROTECTING GROUP

Given the inherent instability of the arene chromium complexes, we set our sights on an organic molecule that could protect one face of our pyrene monomers (**Scheme 2.14**). This method, although more synthetically taxing, could be more beneficial as the organic face blocking group may protect against unwanted dimerization or

oxidation that the cyclacene may experience (**Scheme 2.15**). Moreover, the face blocking group does not introduce more metals into the synthesis and may serve as a springboard to further grow CNTs from cyclacenes.

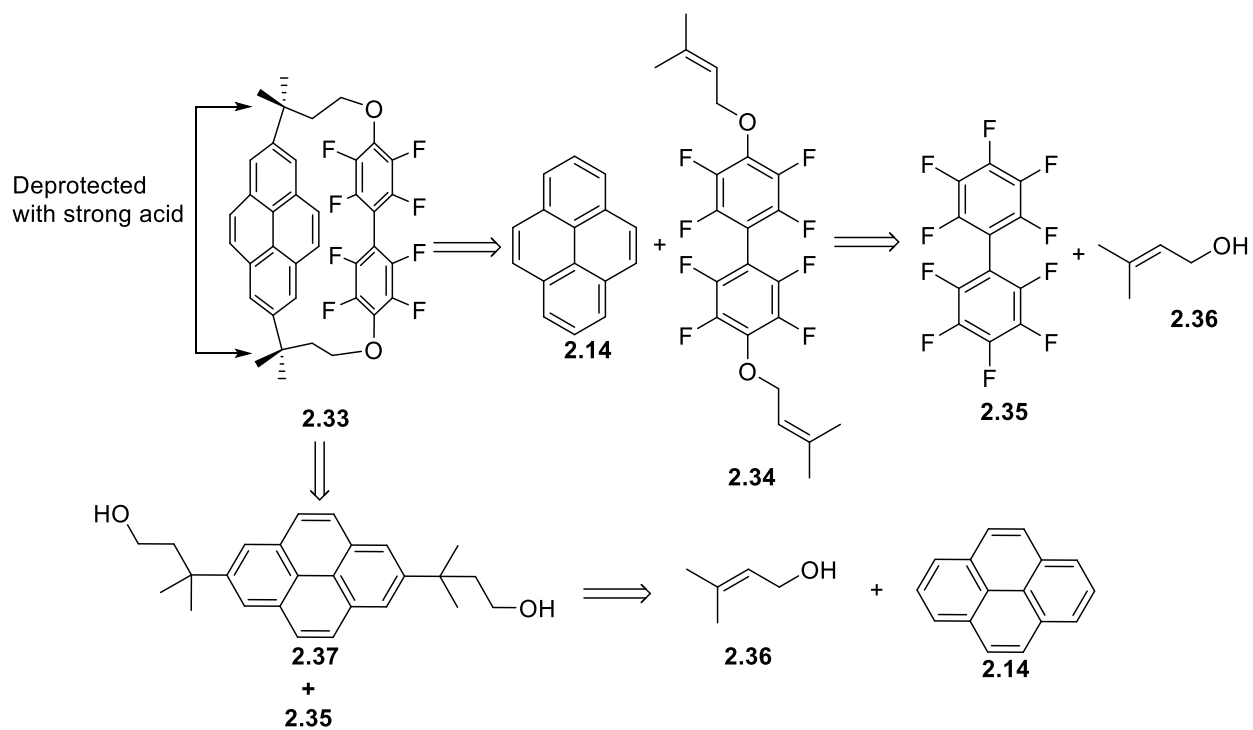


Scheme 2.14- Schematic representation of an organic face blocking group directing the reaction towards a cyclic product. Blue bar represents a pyrene furan/dibromide, red/green bar represents a new pyrene unit, grey box represents organic face blocking molecule.

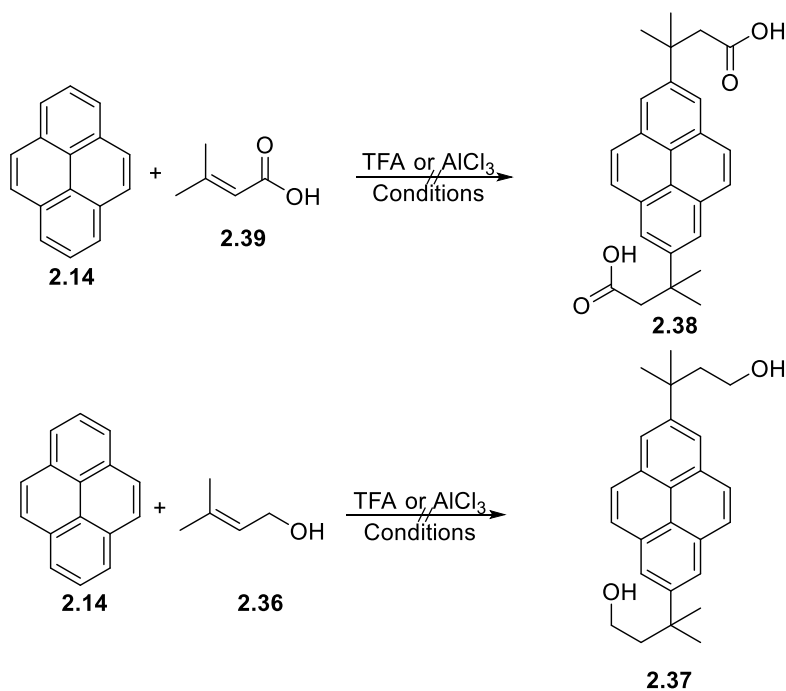


Scheme 2.15-Schematic representation of a face grouping molecules ability to prevent endoperoxide and dimer formation.

For the design of our face blocking molecule, we envisioned functionalizing pyrene with an aromatic molecule which would be later cleaved by the addition of acid. We arrived at compound **2.33** pictured in **Scheme 2.16**. The purpose of the perfluorinated biphenyl is to provide a π stacking partner that matches the pyrene in size which should allow us to form the pyrene cyclophane by bringing both molecules together.¹³² For the retrosynthesis of **2.33**, we envisioned **2.34** adding to the pyrene via a Friedel-Crafts alkylation. Compound **2.33** could then be easily synthesized from commercially available perfluorobiphenyl **2.35** and prenyl **2.36** through an S_NAr reaction. Alternatively, **2.37** could be synthesized from the Friedel-Crafts alkylation of pyrene, arriving at **2.37** which could then be cyclized through an S_NAr reaction with perfluorobiphenyl **2.35**.



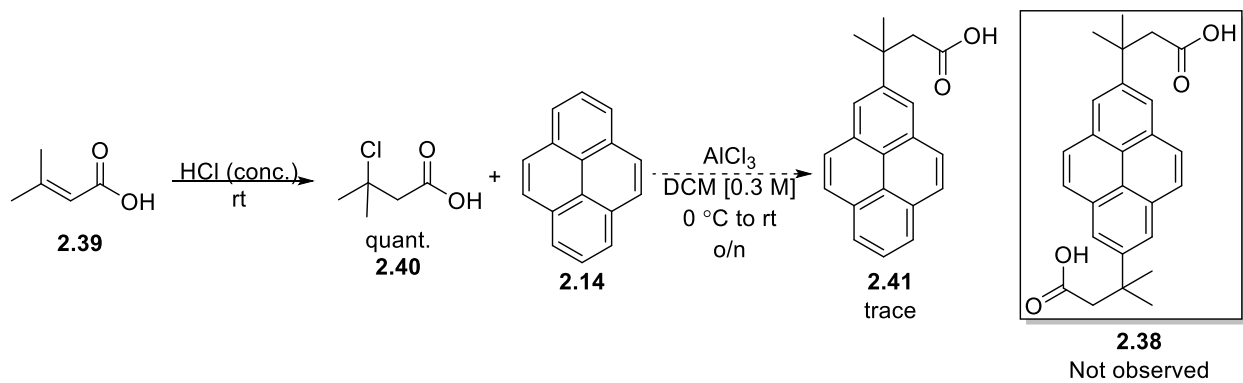
Scheme 2.16- Retrosynthetic analysis for the synthesis of an organic face protected pyrene using perfluorobiphenyl.



Scheme 2.17- Attempted synthesis of **2.37** and **2.38**.

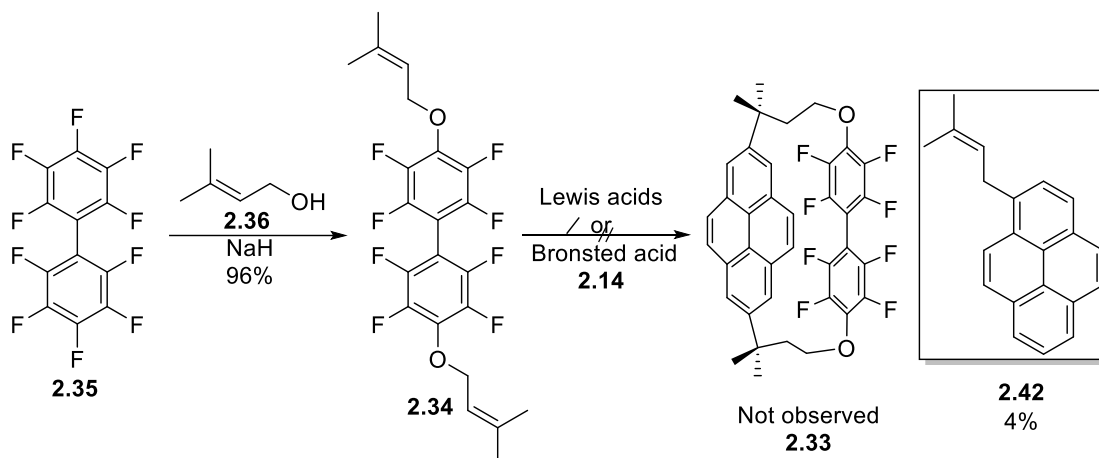
We began by targeting compound **2.37** by attempting Friedel-Crafts alkylation on pyrene with prenol **2.36** or dimethyl acrylate **2.39**. Despite screening multiple sets of conditions, we were unable to successfully isolate

either compound **2.37** or **2.38**. The acrylic acid **2.39** was used as a way to decrease the nucleophilicity of the oxygen which we feared could be problematic. With both compounds we did see conversion of the starting material, but multiple products were present by TLC and any attempt at isolation resulted in indiscernible spectra.



Scheme 2.18- Attempted synthesis of **2.38** using alkyl chloride **2.40**.

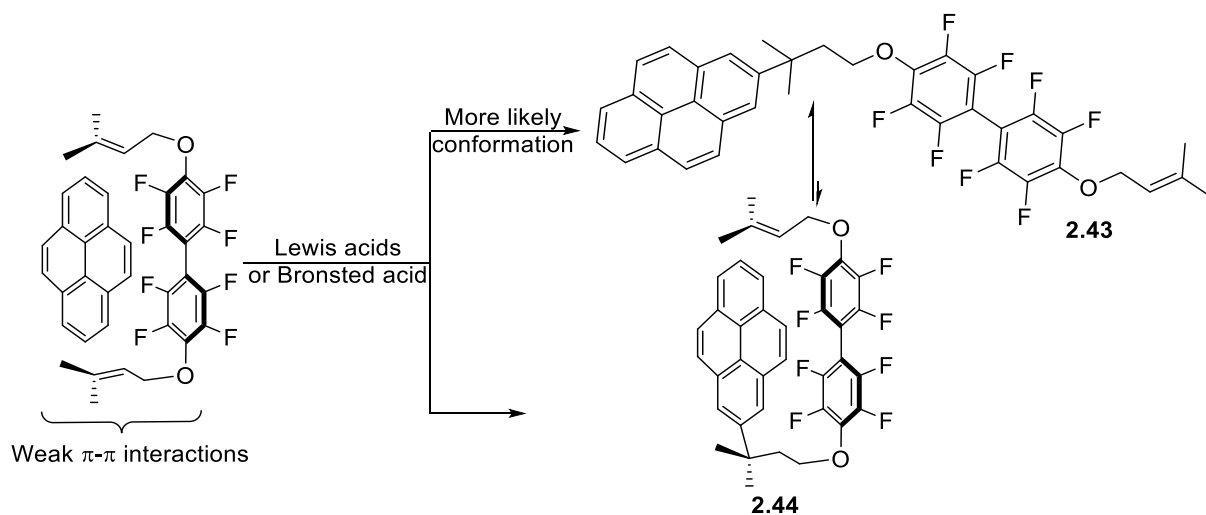
We feared that the acrylic acid and prenyl were not strong enough electrophiles for the reaction to proceed. In an attempt to create a better electrophile, we converted the acrylate to the alkyl chloride **2.40** by stirring the acrylate in concentrated hydrochloric acid. The reaction was able to produce the chloride **2.40** in quantitative yield. This compound was then reacted with pyrene, and we were able to observe the formation of the mono-functionalized pyrene by TLC-MS in trace amounts (**Scheme 2.18**). Further attempts at increasing the yield of the reaction of pyrene and **2.40** were unsuccessful or unable to yield any alkylated product.



Scheme 2.19- Attempted synthesis of face protected pyrene using perfluorobiphenyl.

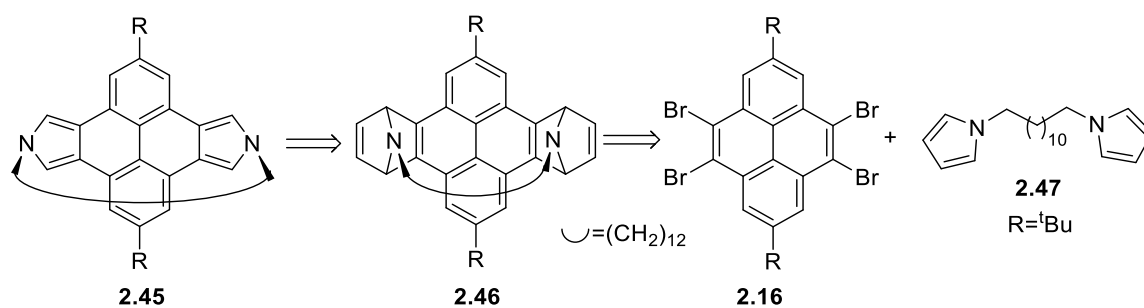
We suspected that part of the reason why we were unable to form our cyclophane was due to the nucleophilic oxygen present in both the prenyl **2.36** and the acrylic acid **2.39** which may undergo a solvolysis reaction leading to the formation of an ether.¹³³ Thus, we opted to perform the S_NAr first which should prevent the oxygen from interfering with the Friedel-Crafts alkylation. To that end, we reacted prenyl **2.36** with perfluorobiphenyl and NaH and were delighted to observe the formation of **2.34** in a 96% yield (**Scheme 2.19**). Following this result, we then attempted the Friedel-Crafts alkylation on pyrene with **2.34** but were unable to create the cyclophane **2.33** despite screening multiple conditions. The only compound observed from our attempt to make the cyclophane is **2.42** by a mechanism that remains unclear. It is possible that a Friedel-Crafts reaction between the prenyl group, either from **2.34** or residual prenyl from the S_NAr , and pyrene led to **2.42**. Previous experiments between pyrene and prenyl failed to give **2.42** as a product. Thus, it was unexpected that **2.42** was only observed when pyrene was reacted with **2.34**.

Looking back at this face blocking group we can hypothesize two reasons why our synthesis was unsuccessful. Firstly, biphenyl groups are twisted to minimize steric interactions,⁷¹ this means that despite being the same size as the pyrene any π -stacking interactions are disrupted by the twist in perfluorobiphenyl. Secondly, since the π -stacking interactions are weak it is likely that if the alkylation proceeded it would yield a linear product rather than a sandwiched one (**Scheme 2.20**). This linear product (**2.43**) can then react further and yield oligomeric products which may why we observed complex TLCs for this reaction.



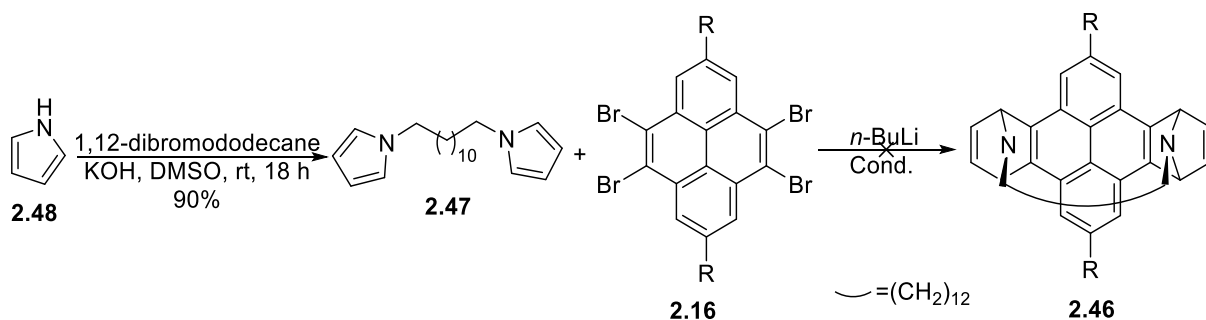
Scheme 2.20- Open vs closed equilibrium for alkylated pyrene.

2.4.3-FACE BLOCKING GROUPS USING PYRROLE.



Scheme 2.21- Retrosynthetic analysis for faced blocked pyreno-pyrrole.

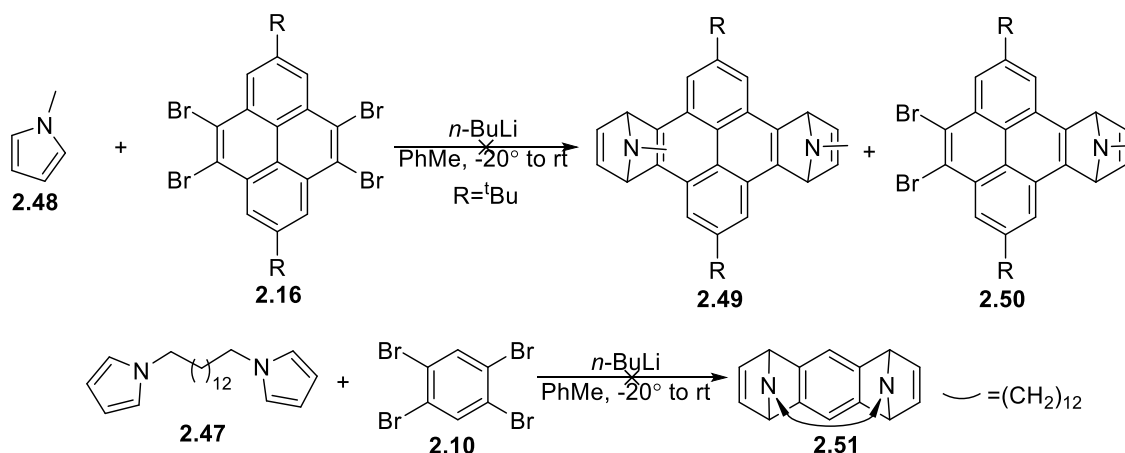
Our current synthesis involved the use of pyrenofurans as the dienes for our cyclization. Unfortunately, the furans offer limited functionalization as no more bonds can be created at the oxygen. Pyrroles, on the other hand, offer a reactive handle on the nitrogen that can be functionalized; we therefore hypothesized that we could use this nucleophilic nitrogen as a means of protecting one of the faces of our pyrene. Similarly to benzofurans, pyrroles can participate in cycloadditions and may serve as an alternative to our current method.^{134,135} We targeted **2.45** as our benzopyrrole face protected molecule and pictured the retrosynthesis following a similar pathway as the pyrenofurans. Compound **2.45** can be derived from the di-amino pyrene **2.46** and that compound can then be obtained from the [4+2] cycloaddition of **2.16** with **2.47** (**Scheme 2.21**).



Scheme 2.22- Attempted synthesis of tethered pyrene.

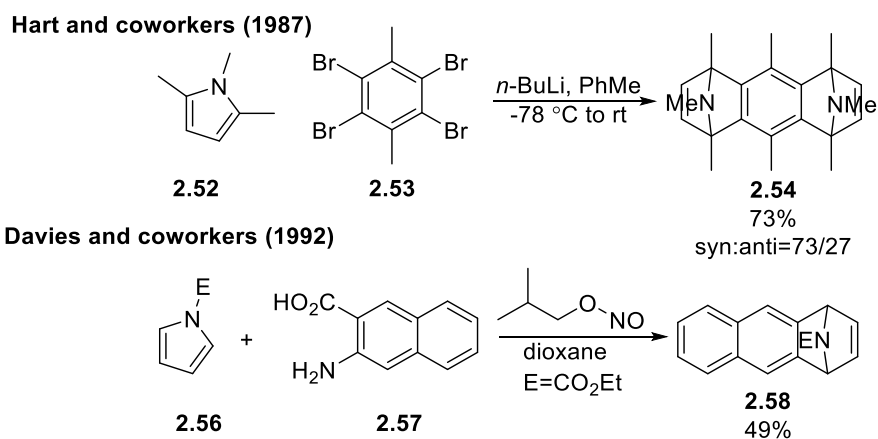
We began our synthesis by reacting pyrrole with 1,12-dibromododecane to yield the alkyl linked dipyrrole **2.47** in a 90% yield (**Scheme 2.22**). We opted to do this reaction as the first step as we hoped that tethered pyrroles would preferentially yield the *syn*-isomer negating the need to separate the diastereomers. We then attempted to react **2.47** with **2.16** by introducing *n*-BuLi to the reaction mixture but to our dismay, observed no product; neither **2.46**

nor the mono adduct were seen for the reaction. Although a reaction did occur, it only gave a complex mixture of products.



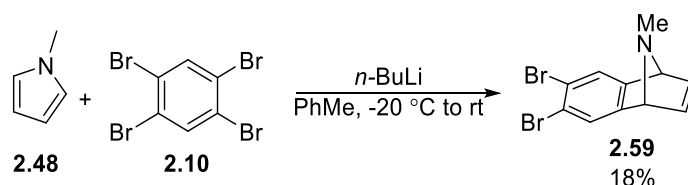
Scheme 2.23- Control reactions for the synthesis of a tethered pyrenopyrrole.

After failing to synthesize **2.46** we took a step back and attempted to get a handle on the reactivity. We performed a control in which we reacted commercially available *N*-methylpyrrole **2.48** and **2.16** following a lithium halogen exchange with *n*-BuLi. The goal of this experiment was to assess the reactivity of **2.16** benzyne towards pyrrole (**Scheme 2.23**). Unfortunately, this too was not able to proceed and no adducts were successfully isolated or identified. Much like previous benzyne reactions with **2.16**, the starting material was being consumed but not being converted to the desired products. The goal of our second control reaction was to test if our linked pyrrole would allow for the formation of a cyclophane (**Scheme 2.23, bottom**), this however, failed to give out any adducts.



Scheme 2.24-Prior reports using pyrroles as dienophiles in [4+2] cycloadditions with benzyne.^{134,135}

Prior reports had previously showcased that pyrroles can indeed react with benzyne to form 1,4-amines; thus we were somewhat puzzled by the lack of reactivity we observed (**Scheme 2.24**).^{134,135} The main difference between the literature reports and our system was the use of 2,5-substituted pyrroles. This substitution on the pyrrole may be key as pyrrole can be lithiated by *n*-BuLi which could be problematic as this species could attack the benzyne.¹³⁶ Similarly, the resulting 1,4-amines may be nucleophilic enough to attack any newly formed benzyne and yield rearrangement products that further complicate the nature of the reaction mixture.¹³⁷ A strategy to prevent nucleophilic attacks by the amines would be to cap the amine with an electron withdrawing group to limit the nucleophilicity of the nitrogen, this strategy has previously allowed for the isolation of similar products to what we were targeting.¹³⁵

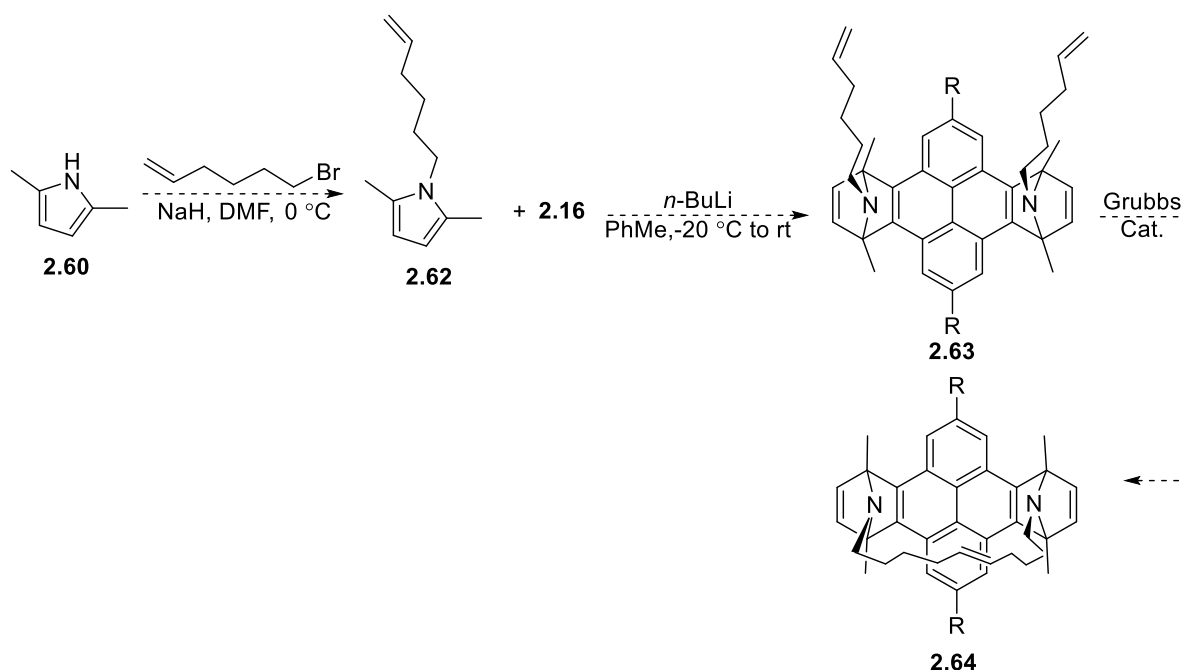


Scheme 2.25- Successful cycloaddition of *N*-methylpyrrole with a benzyne dienophile.

Despite the poor reactivity of pyrrole with benzyne created with a lithium halogen exchange, we were able to observe one adduct from the [4+2] cycloaddition of *N*-methylpyrrole **2.48** with tetrabromobenzene **2.10** in a 18% yield (**Scheme 2.25**). Further attempts to improve the yield of the reaction or convert the 1,4-amine into the benzopyrrole were unsuccessful. We did attempt to acylate pyrrole but were faced with similar problems when we attempted the cycloaddition. Additionally, we had trouble working with pyrrole as the substance can easily oxidize or polymerize under air further complicating our reaction environment.

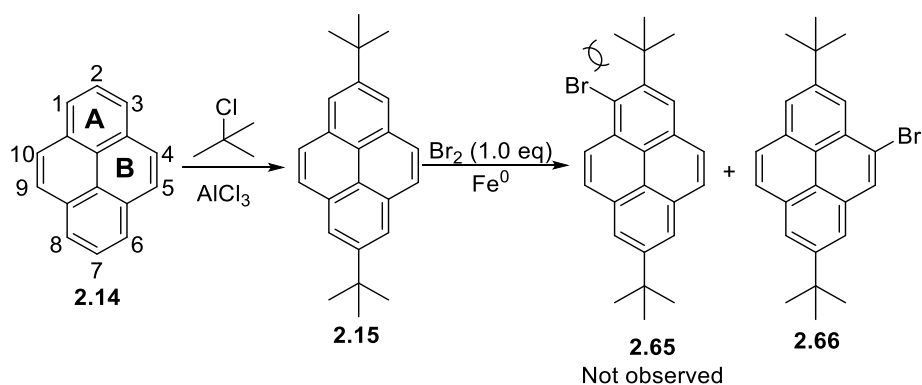
Even though our pyrrole pathway was not successful, it may still be worth revisiting, as the right pyrrole may be key in getting the cycloaddition to proceed. One potential pathway to form the pyrene cyclophane using pyrroles would be to utilize a ring closing metathesis (RCM) to perform the cyclization (**Scheme 2.26**). So far, RCM has been the only method to prove successful in the synthesis of a pyrene cyclophane in our hands (see **Section 2.5**), so it stands to reason that it may be successful if performed intramolecularly with the pyrroles. This pathway is

promising but it does require the separation of *syn*-isomer from the other diastereomer which can greatly affect the overall yield of the reaction.



Scheme 2.26- Alternate RCM pathway for the synthesis of a pyrene-cyclophane.

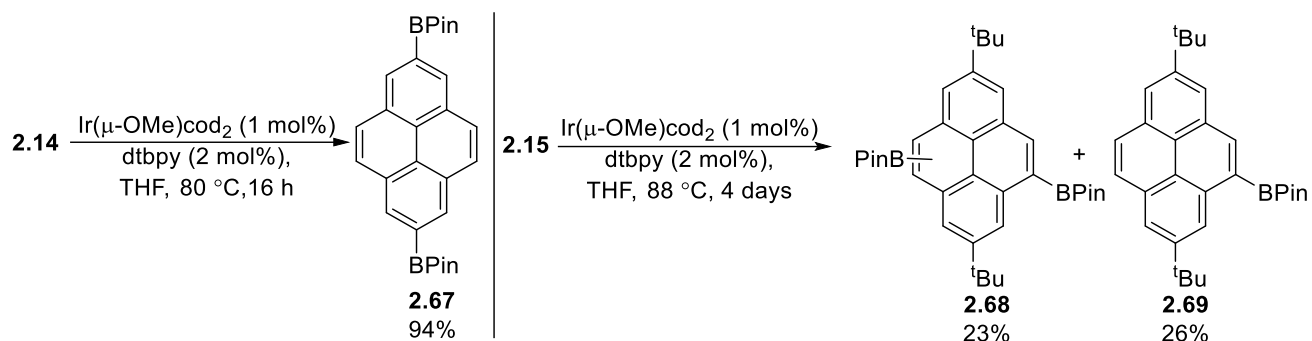
2.5 PYRENE CYCLOPHANE SCAFFOLD FOR CYCLACENE SYNTHESIS.



Scheme 2.27-Pyrene labelling and effect of bulky electrophiles on the regiochemistry of pyrene.

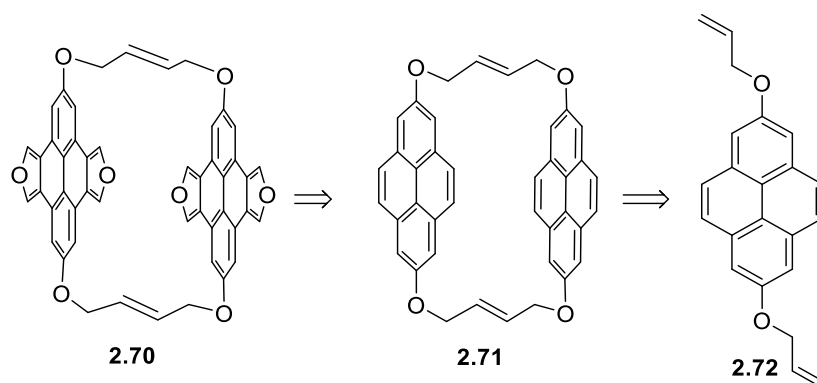
The most reactive positions in pyrene for electrophilic aromatic substitution chemistry are the 1, 3, 6, and 8 positions. Consequently, any chemistry not performed on those positions requires the use of protecting groups to direct the chemistry on the less reactive rings. For example, our synthesis of **2.6** and **2.9** necessitates the addition of a ^tBu group to sterically block the reactive positions and direct electrophiles towards the less reactive 4,5,9, and 10

positions. The large size of the *t*-Bu groups disallows a reaction at the 1, 3, 6, and 8 positions (**Scheme 2.27**). This is problematic as it limits chemistry to only bulky electrophiles when attempting electrophilic aromatic substitutions on pyrene.



Scheme 2.28- Ir C-H activation of pyrene.^{138,139}

An alternative to Friedel-Crafts reactions on pyrene is to perform C-H activation on pyrene using an Ir catalyst.^{138,139} This reactivity opens new doors as the 2 and 7 positions of the pyrene, which can now be functionalized with groups other than bulky electrophiles. Alternatively, if the 2,7-positions are blocked with bulky groups then more forcing conditions can be used to functionalize the 4, 5, 9, and 10 positions without being solely limited to electrophilic aromatic substitution. The Ir catalyzed C-H of pyrene replaces a hydrogen for a Bpin group which can then be oxidized or transformed into several other functional groups via transition metal couplings (**Scheme 2.28**).

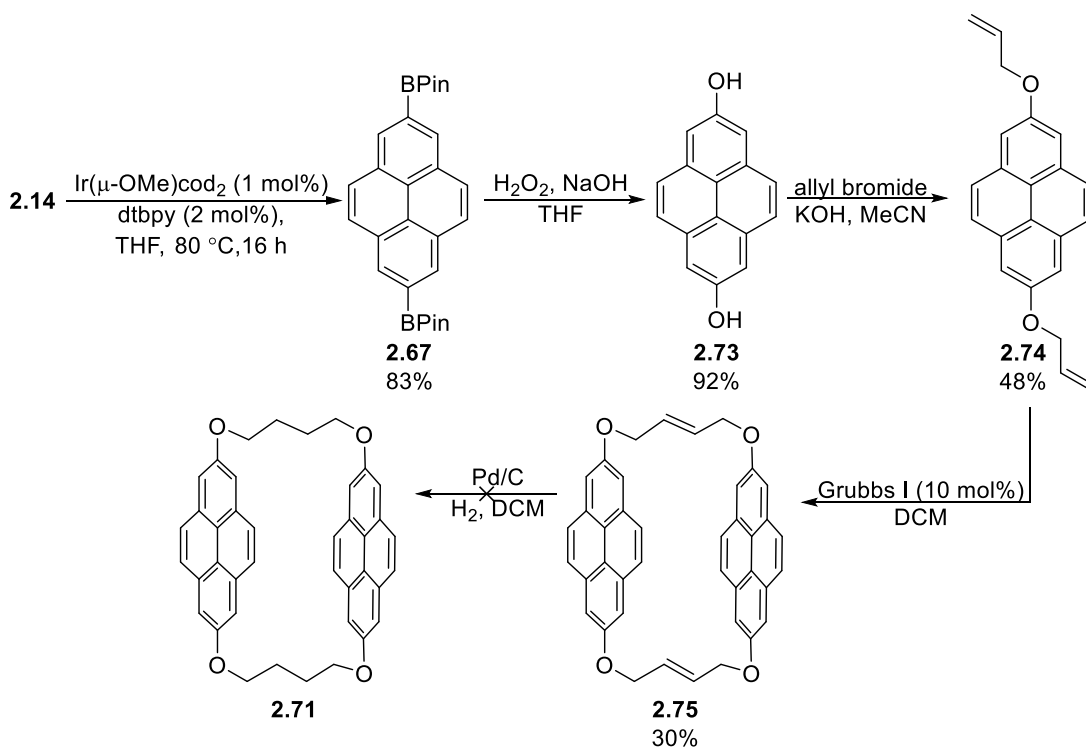


Scheme 2.29- Retrosynthetic analysis for a pyrene cyclophane using a RCM approach.

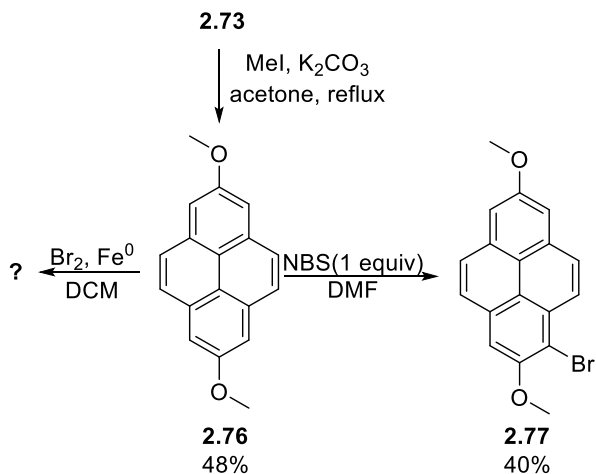
Having been previously unsuccessful at installing other electrophiles at the 2 and 7 positions, we saw this as an opportunity to install functional groups that could allow us to block one face of the pyrene using a RCM approach. However, rather than just blocking one face with an alkyl tether, we saw the opportunity to create a cyclophane that was primed for cyclization. Our target was a molecule like **2.70**. With the pyrenofurans already in place the likelihood that the molecule could cyclize upon introducing a benzyne seemed promising as the pieces for the cycle would be aligned. The only drawback with the method was that aromatic carbon oxygen bonds can be difficult to selectively remove, although examples do exist in the literature.¹⁴⁰

We began our investigation by performing a retrosynthetic analysis of **2.70** (**Scheme 2.29**). We hypothesized that the furans would have to be installed after the cyclophane was made since a blocking group for the 2 and 7 positions is needed to direct the bromination. Thus, **2.70** would originate from the pyrene cyclophane **2.71** which would be synthesized from **2.72** through a RCM. The main hurdle in this synthesis was whether the alkoxy tether would influence the bromination to occur at the desired positions, nonetheless we set out to try and synthesis the pyrene cyclophane **2.70**.

First, we performed a C-H activation on pyrene following the procedure outlined by Marder and coworkers¹³⁹ and arrived at **2.67** in an 83% yield (**Scheme 2.30**). We then converted **2.67** to the 2,7-pyrene-diol **2.73** with NaOH/H₂O₂ in a 92% yield. This was then followed by the alkylation of the diol **2.73** with allyl bromide, which proceeded in a 48% yield to yield the RCM precursor **2.74**. For the RCM we attempted the dimerization with Grubbs I, II, and III but surprisingly Grubbs I was the only catalyst that allowed us to observe cyclophane **2.75** in a 30% yield. We suspect that our Grubbs II and III catalysts had “died” as in theory they should be more reactive than Grubbs I. With the cyclophane **2.75** in hand, we attempted to reduce the alkene tether to the fully saturated alkane but were only able to retrieve starting material from the reaction. We are unsure why the reaction was not able to proceed but one possible hypothesis is that the geometry of the cyclophane disallows proper interaction with the catalyst and consequently led to no reaction.



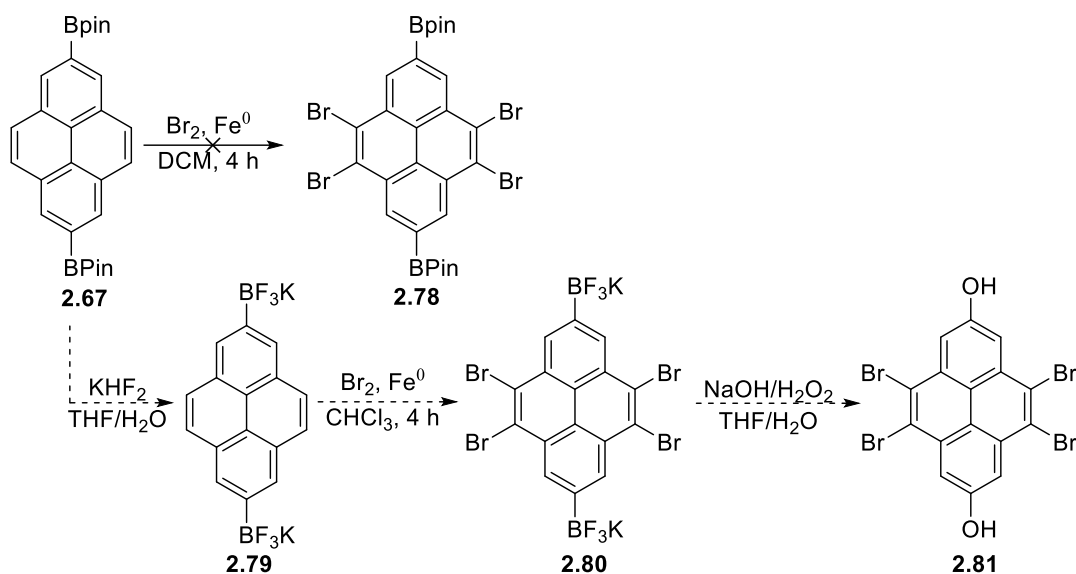
Scheme 2.30- Attempted synthesis of pyrene cyclophane **2.71**.



Scheme 2.31- Bromination control experiment of 2,7-dimethoxy pyrene.

Before we explored other possible reduction conditions for the alkene, we wanted to first make sure that the bromination would proceed as desired. To that end, we synthesized **2.76** as a model compound to observe if the bromination would take place in the A or B ring of pyrene. **2.76** was synthesized via the methylation of **2.73** with MeI and K₂CO₃ in a 43% yield (**Scheme 2.31**). **2.76** was then subjected to bromination conditions first with our standard bromination conditions using an excess of bromine in the presence of iron was tested but gave a complex

mixture of products. Secondly, we tried brominating with NBS, a much milder reagent, and observed the formation of a monobrominated product in a 40% which by NMR is most likely **2.77**.



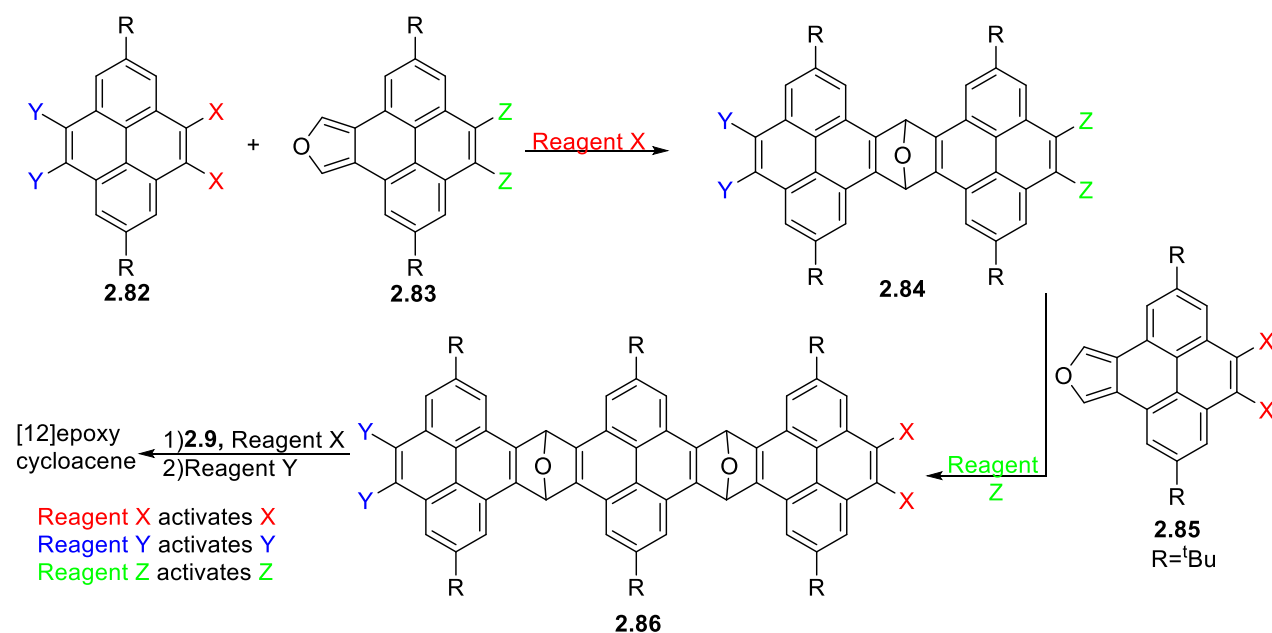
Scheme 2.32- Attempted bromination of 2,7-bis(pinacolato)pyrene and alternate pathway using trifluoroborate salts.

This result indicated that macrocycle **2.71** would most likely yield an undesired regioisomer upon bromination, which consequently would not be able to be converted to the furans or bromides. Our only hope would be to brominate pyrene prior to oxidizing **2.67** to the pyrene diol **2.73**. Thus, we subjected **2.67** to Br_2 in the presence of Fe powder in DCM and unfortunately observed a mixture of products (**Scheme 2.32**). When we conducted this experiment, we still had not fully optimized this reaction; therefore, it is possible that the right conditions may permit the reaction to proceed. Alternatively, the **2.67** could be transformed to **2.79** with the addition of KHF_2 creating a more stable borate that could tolerate the bromination conditions.

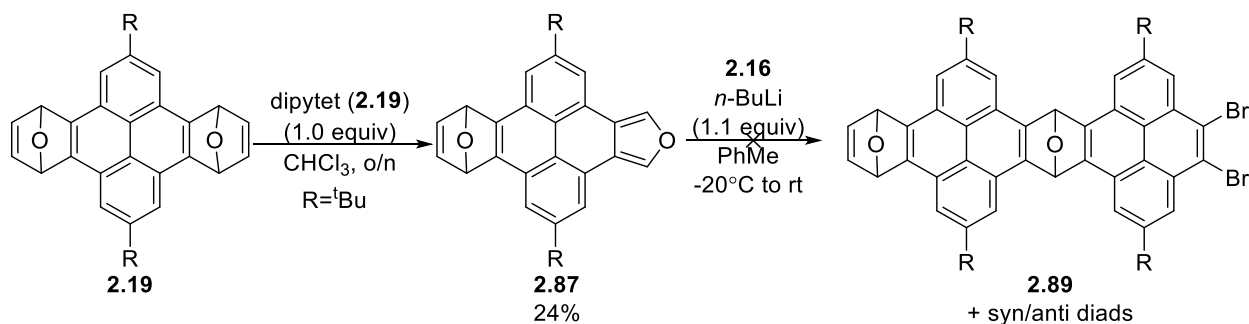
2.6 STEPWISE CYCLE FORMATION USING AN ORTHOGONAL REACTIVITY APPROACH.

So far, all our attempts to create a cyclacene gave unsatisfactory results. We attempted directing the cyclization by blocking one of the faces of our pyrene cyclization precursors but observed similar results, providing only complex mixtures while consuming our starting materials. It was clear at this point that a one-shot cyclization would likely not be possible, so we decided to tackle our cyclacene synthesis using a stepwise approach. The bifunctional nature of our cyclization precursors (**2.6**, **2.9**, and **2.16**) meant that the reaction could proceed undesirably; thus, to gain more control over the reaction benzynes with orthogonal reactivities would be required.

Scheme 2.33 highlights how an orthogonal pathway would function: For this hypothetical reaction, we have three benzyne precursors that can be activated with orthogonal reactivity, meaning that only one type of benzyne will be created while the other benzyne precursors remain inert to the activation conditions. Therefore, for our hypothetical reaction scheme, reagent X would only form one of the benzyne on **2.82** leading to **2.84** as the sole product. This process would be repeated until a molecule has the proper orientation to facilitate the cyclization and in theory could be repeated indefinitely to reach a variety of cyclacene sizes.

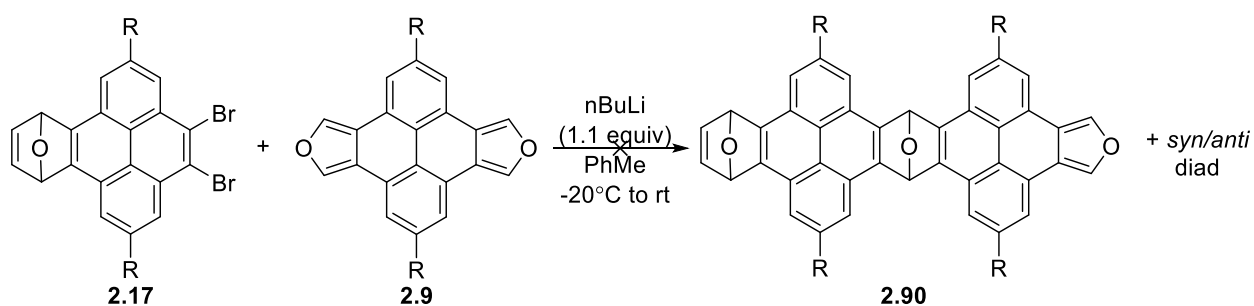


Scheme 2.33-Schematic representation of orthogonal reactivity to achieve the stepwise construction of a cyclacene.



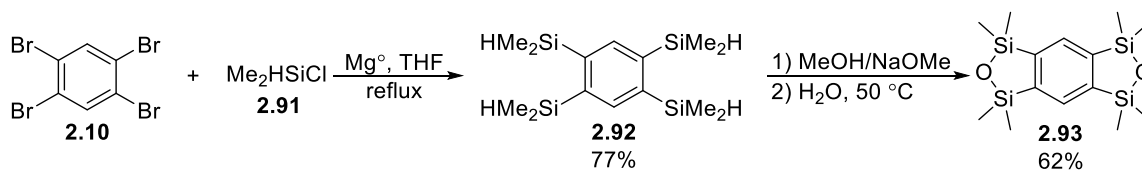
Scheme 2.34-Attempted synthesis of pyrene diad **2.89**.

Our first attempt at the stepwise synthesis of cyclacene involved the monofuran **2.87**. The idea behind using this molecule was to create a diene that only had one reactive site while the other endoxide could be later converted to the furan with dipytet **2.19**. Monofuran **2.87** was reached in a 24% yield following the reaction of diendoxide **2.18** with dipytet. Although only one equivalent of dipytet **2.18** was used, the reaction still produced a considerable amount of difuran **2.9** (Scheme 2.34). **2.9** and **2.87** are similar in polarity which makes the isolation of **2.87** challenging and thus part of the reason for the low yield. Monofuran **2.87** was then reacted with tetrabromopyrene **2.16** and *n*-BuLi in toluene; however, no mono or diad adducts were isolated or observed. Even though we limited the reactivity of the cycloaddition partners the reaction was still not able to proceed cleanly, this is most likely due to the large number of diastereomers that can form from the reaction.



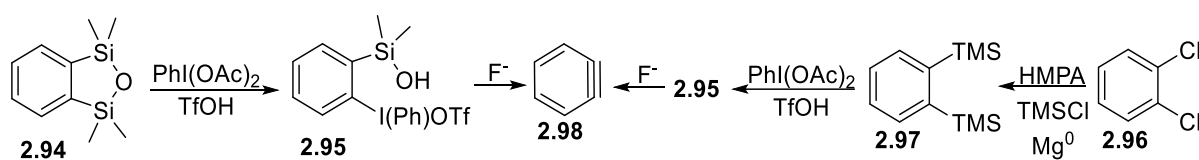
Scheme 2.35- Attempted synthesis of pyrene diad **2.90**.

With a similar thought in mind, we attempted to synthesize **2.90**. We reacted **2.17** with difuran **2.9** under one equivalent of *n*-BuLi but were unable to successfully isolate anything that we could call an adduct (Scheme 2.35). Once again, we suspect that the reaction gave a complex mixture due to the larger number of diastereomers possible between the mono adduct and diad adducts. One possible way to limit the number of products would be to immediately expose the reaction mixture to an excess of dipytet **2.19** which would considerably reduce the number of products and change the polarity of the compounds, potentially allowing for their separation.



Scheme 2.36- Synthesis of benzobisoxadisiloles.¹⁴¹

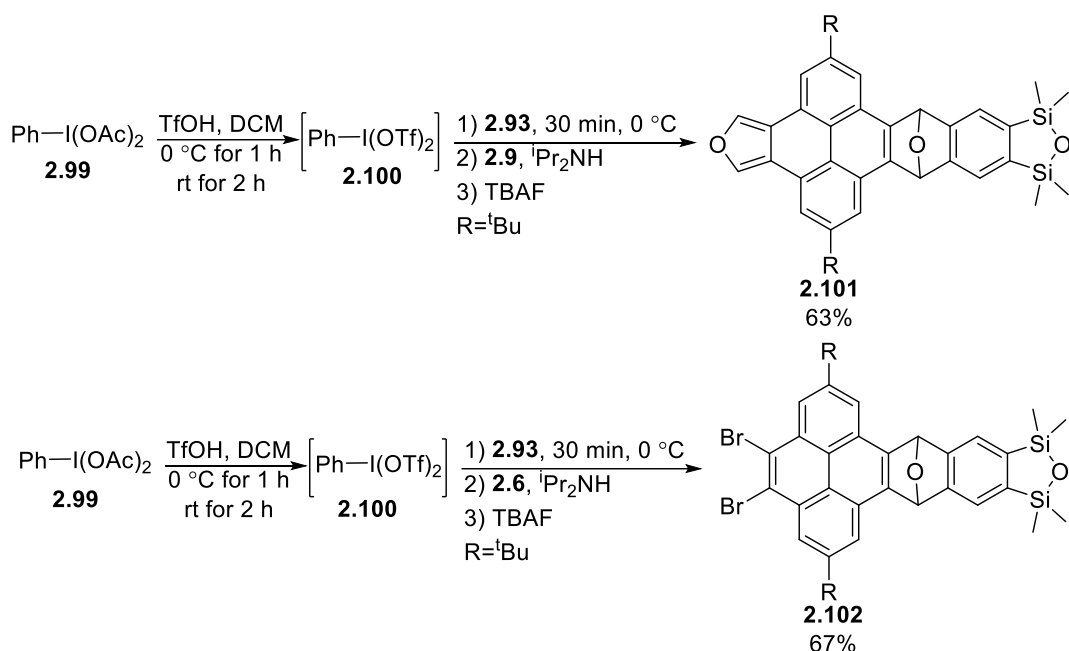
Next, we wanted to create a cycle stepwise using two different benzyne precursors. For this method we envisioned having a benzyne activated by a lithium-halogen exchange, while the other benzyne would be created with the addition of fluoride. Our first candidate for a fluoride activated benzyne were benzobisoxadisiloles, as these benzyne precursors could be synthesized rapidly at high yields. The synthesis on benzobisoxadisiloles is outlined in **Scheme 2.36** and was synthesized according to a procedure by Lee and coworkers.¹⁴¹ First, tetrabromobenzene **2.10** was subjected to a Grignard reaction with dimethylchlorosilane **2.91** leading to the tetrasilated benzene **2.92**. An oxidation was then performed with MeOH/NaOMe to yield the benzobisoxadisiloles **2.93** in a 62% yield.



Scheme 2.37- Benzyne generation through benzooxadisiloles and *o*-bis(trimethylsilyl)benzene.¹⁴¹

Benzooxadisiloles **2.94** on their own are not able to create a benzyne, it must first be oxidized to **2.95** at which point a fluoride source is introduced forcing the formation of the benzyne. **2.97** can also be reached by using **2.96** as the precursor, however, HMPA is required for the synthesis. Benzooxadisiloles offer a safer and greener alternative that does not require the use of highly carcinogenic HMPA and operates on the same mechanism (**Scheme 2.37**).

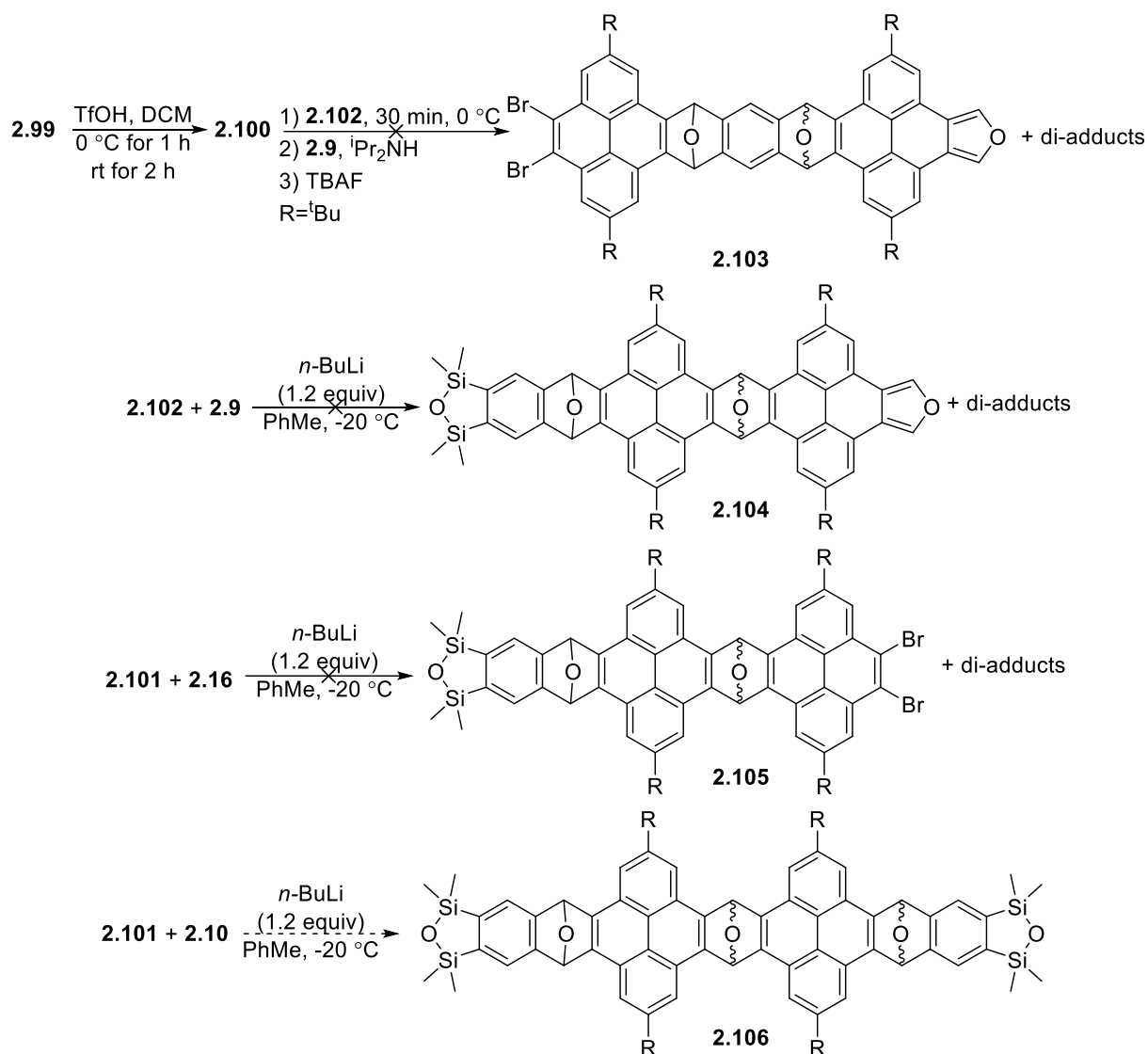
With the benzobisoxadisilole **2.93** in hand we set out to try and form a [4+2] adduct with our cyclization monomers, with the end goal of creating a pyrene molecule that can form benzyne orthogonally with the addition of *n*-BuLi or fluoride. Following the benzyne conditions outlined by Lee and coworkers,¹⁴¹ we exposed difuran **2.9** and monofuran **2.6** to benzobisoxadisilole benzyne and were pleased to observe a 63% and 67% yields for adducts **2.101** and **2.102**, respectively (**Scheme 2.38**). So far, this was the first successful example of a pyrene Diels-Alder reaction with something other than furan. It should be noted that both our group and the Lee group were unable to ring open the benzobisoxadisilole more than once even with an excess of **2.100**.¹⁴¹ This worked to our benefit as the reaction would stop after the first benzyne cycloaddition allowing for easy isolation.



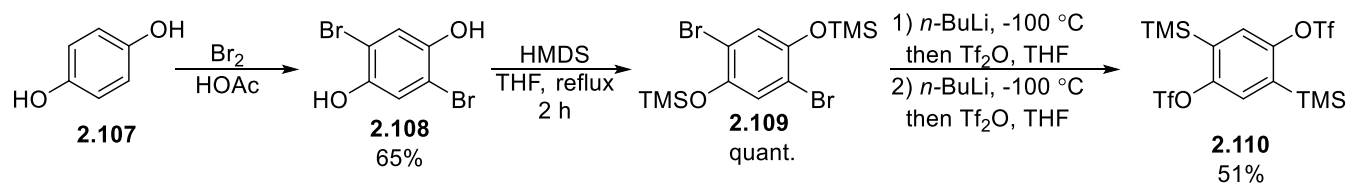
Scheme 2.38- Synthesis of pyrene benzoaxadisiloles.

Next, we sought to add one more pyrene unit to our newly formed adducts to construct a pyrene diad.

Scheme 2.39 outlines all the different combinations attempted to form pyrene diads (**2.103-2.105**), unfortunately regardless of the adduct combinations or conditions no products were observed in any of the reactions. We tried creating benzyne using the benzoaxadisilole conditions as well as the lithium halogen exchange conditions but both methods returned mostly starting material. An additional spot was observed by TLC/CC but it was undiscernible by NMR. At the time, it is unclear whether it was a decomposition product or a mixture of all the possible adducts from the reaction since it can proceed more than once. Later experiments made use of MALDI-TOF MS as a way of identifying the adducts when the NMR was unclear; however, at the time we did not have access to the spectrometer. The only combination not attempted was **2.101** with **2.102**, which if successful would only be able to proceed once. The only problem being that 3 possible diastereomers would be possible and might be difficult to separate based on our previous results.



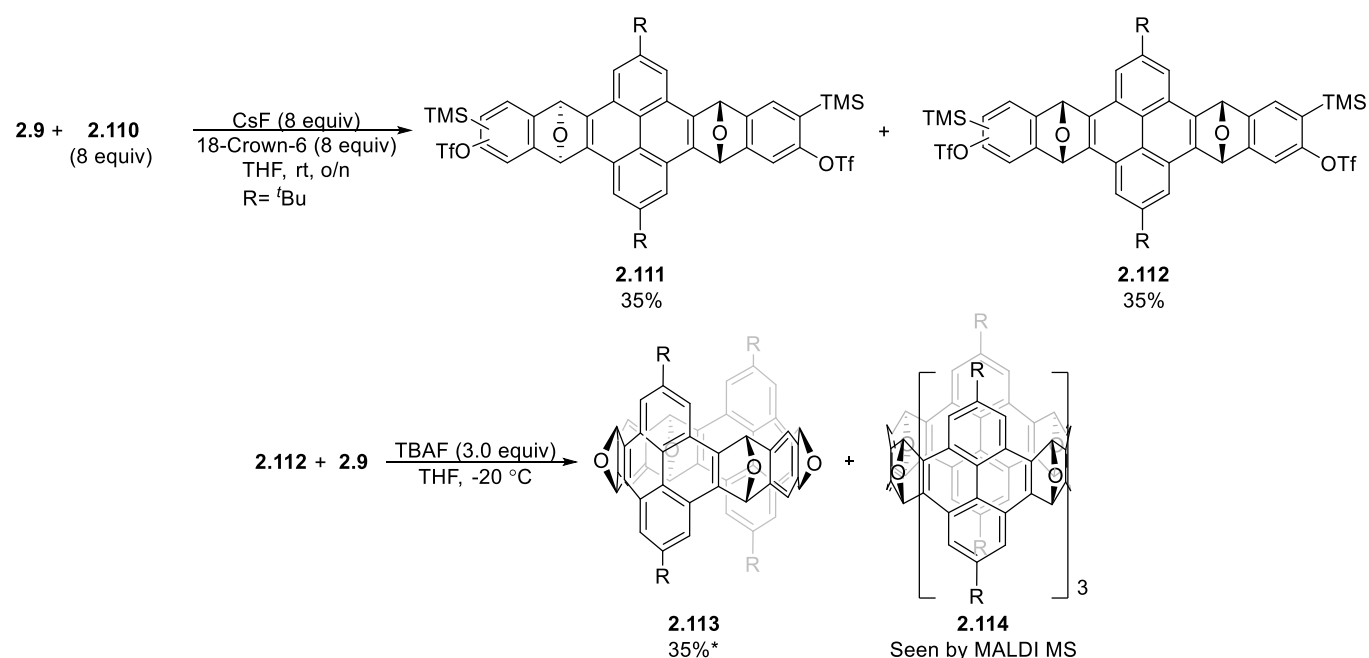
Scheme 2.39-Attempted orthogonal synthesis of pyrene diads.



Scheme 2.40-Synthesis of bistriflate **2.109**.

After seeing modest success with fluoride generated benzyne, we decided to continue exploring this approaching with a different fluoride initiated benzyne. We turned our attention towards bistriflate **2.110**, which offers a stable compound that can be isolated and activates readily upon the addition of fluoride. We initially pursued the benzoaxadisilole pathway instead of the use of TMS-triflates as the synthesis of the benzoaxadisiloles was

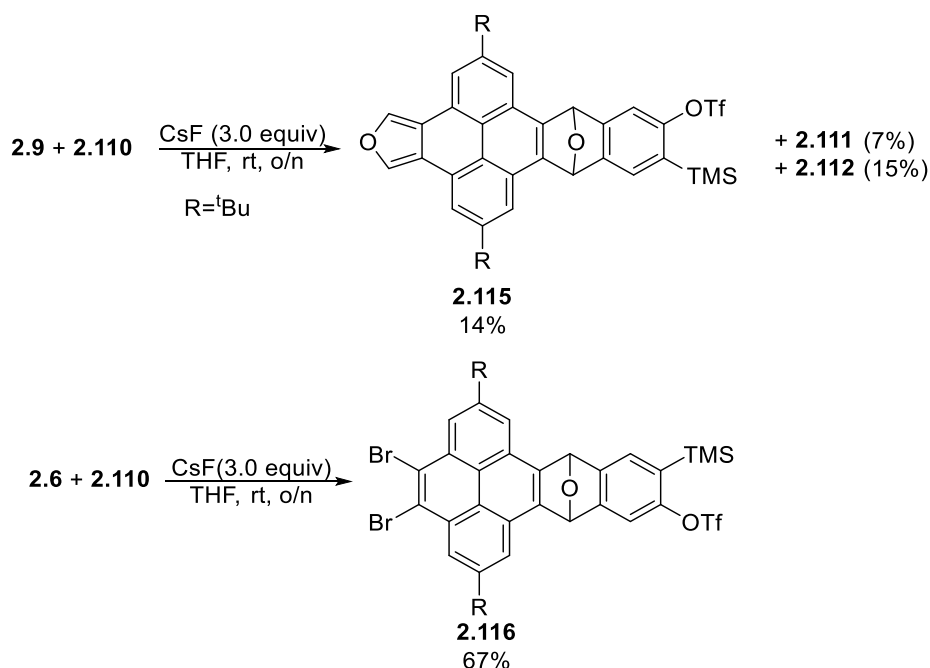
simpler, it did however require several components to form the benzyne whereas this method only requires the sole addition of fluoride. The synthesis of **2.110** is outlined in **Scheme 2.40**. First hydroxyquinone was brominated in acetic acid with elemental bromine to yield **2.108** in a 65% yield. **2.108** Was then silylated using HMDS in refluxing THF to give the disilyl ether **2.109** in quantitative yield. **2.108** was then converted to the bistriflate **2.110** in a 51% yield following a retro-Brook rearrangement and a triflation of the phenols. This transformation had to be conducted stepwise and with the utmost care with regards to the temperature; if the reaction temperature was not properly controlled it would result an insoluble gel.



Scheme 2.41- Synthesis of [10]tetrabenzotetraepoxycyclacene **2.113**. (*) denotes a crude yield.

Following the isolation of bistriflate **2.110**, we proceeded to react this molecule with difuran **2.9** and were pleased to observe the formation of diadducts **2.111** and **2.112** in an equal yield of 35% for each diastereomer (**Scheme 2.41**). Similarly, to the benzooxadisilole, the benzyne was only able to form once per molecule regardless of the excess of fluoride present in the reaction mixture, which was beneficial as it only limits the expected products to the *syn/anti*-diastereomers. We were then able to separate the diastereomers by column chromatography and after isolating the *syn*-adduct **2.112** we reacted the compound with difuran **2.9** and were thrilled to observe the formation of the [10]tetrabenzotetraepoxycyclacene **2.113** in a crude yield of 35%. The formation of the cycle was confirmed by MALDI-TOF MS and later ¹H-NMR. We report a crude yield as the isolated cycle was always

accompanied by impurities visible by NMR that could be removed if the product were subjected to several rounds of chromatography (approx. 6% yield after purification), other purification techniques such as recrystallization and size exclusion chromatography were also attempted but were unsuccessful.



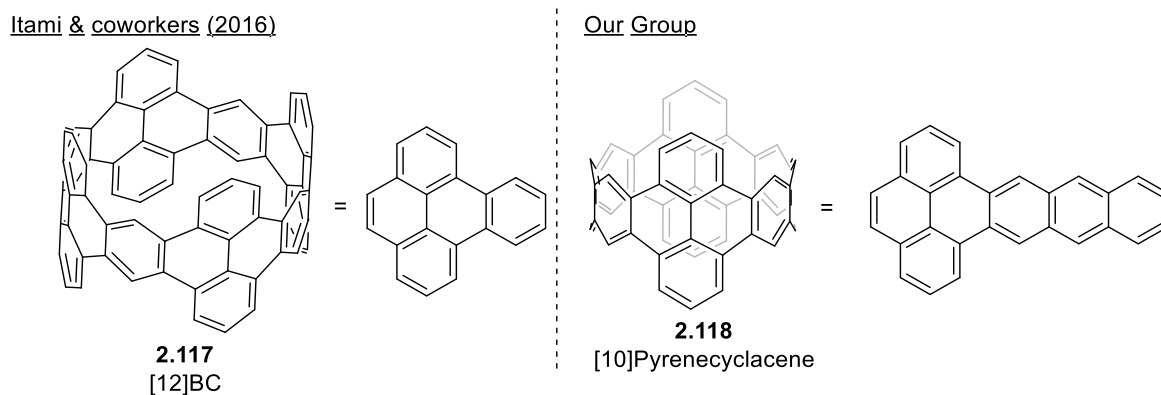
Scheme 2.42- Synthesis of orthogonally reactive pyrene benzene precursors.

We also attempted reacting monofuran **2.6** with bistriflate **2.110** as well as difuran **2.9** with 1 equivalent of bistriflate **2.110** to create stepwise monomers (**Scheme 2.42**). These reactions were successful, but we encountered low yields when trying to build our cyclacene step by step and once we observed that **2.112** plus **2.9** was able to reliably create **2.113** we abandoned these routes for the faster method towards the cyclacene.

2.7. COMPUTATIONAL STUDIES ON PYRENECYCLACENES

We were now close to our long sought synthetic target, the only remaining hurdle was reducing **2.113** to the cyclacene which aside from all the challenges we met up to this point maybe the most challenging as the strain or instability of acene may not allow the reaction to proceed. As the possibility of reaching the cyclacene became a reality we undertook a theoretical study of our cyclacene to assess the stability and strain of our molecule. Previously, Itami and coworkers modelled a similar cyclacene and predicted that the pyrene backbone of the molecule would reduce the strain of the ring and eliminate the radical character of the acene,¹⁰⁵ thus we had reason

to believe our molecule would be stable. However, our cyclacene would contain larger sections of “exposed” acene which may behave differently to Itami’s and coworkers benzocyclacene (**Scheme 2.43**).



Scheme 2.43- Comparison between [12]BC and [10]pyrenocyclacene.

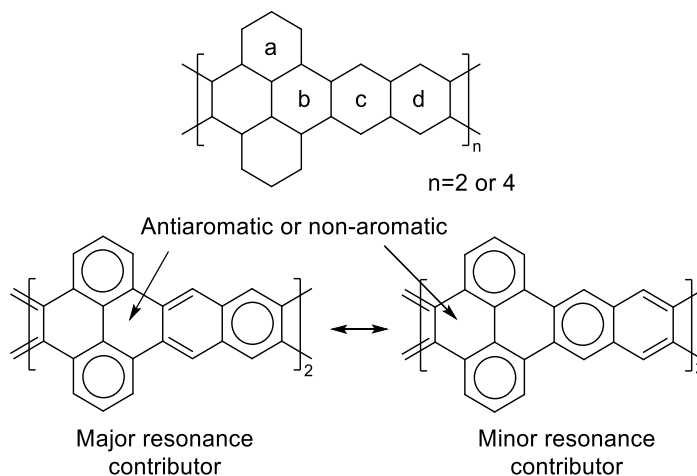
To get a handle on the stability and strain of our predicted cyclacene we performed a similar theoretical analysis to Itami and coworker’s study of [12]BC on **2.118**. We performed DFT calculations on **2.118** using an unrestricted UB3LYP/6-31G(d) basis set and compared the results against the non-benzannulated cyclacenes; the results are summarized in **Table 2.1**. From our calculations we can predict that **2.118** will be less strained and possesses a wider band gap compared to the cyclacene analog of the same size. Additionally, none of the calculations performed resulted in the formation of a triplet state indicating that the pyrenocyclacene will adopt a closed singlet.

Compound	Strain Energy (kcal/mol)	Orbital Energy (eV)		
		HOMO	LUMO	HOMO-LUMO Gap
[10]Pyrenocyclacene	121.26	-4.72	-2.05	2.67
[10]Cyclacene	132.43	-3.92	-2.92	1.00
[20]Pyrenocyclacene	60.63	-4.85	-2.19	2.67
[20]Cyclacene	66.22	-3.90	-3.23	0.67

Table 2.1- Summary of theoretical calculations on cyclacenes and pyrenocyclacenes.

We also performed a NICS(0) analysis on [10] and [20]pyrenocyclacene to examine the aromaticity within the cycle (**Scheme 2.44**). From the NICS(0) analysis we observed that the most aromatic region of the pyrenocyclacene is the D ring, which would compose the center ring in the bridging anthracene subunit. The remaining rings are also aromatic with the exception of the B ring which exhibit antiaromatic or non-aromatic character by NICS(0).^{142,143} Initially this was cause for concern, but it is not unusual for PAHs to exhibit alternating

aromatic and antiaromatic rings.¹⁴⁴⁻¹⁴⁷ Based on the NICS analysis we can hypothesize what the dominant resonant structures are which align with the structures we initially predicted following Clar's sextet rule.



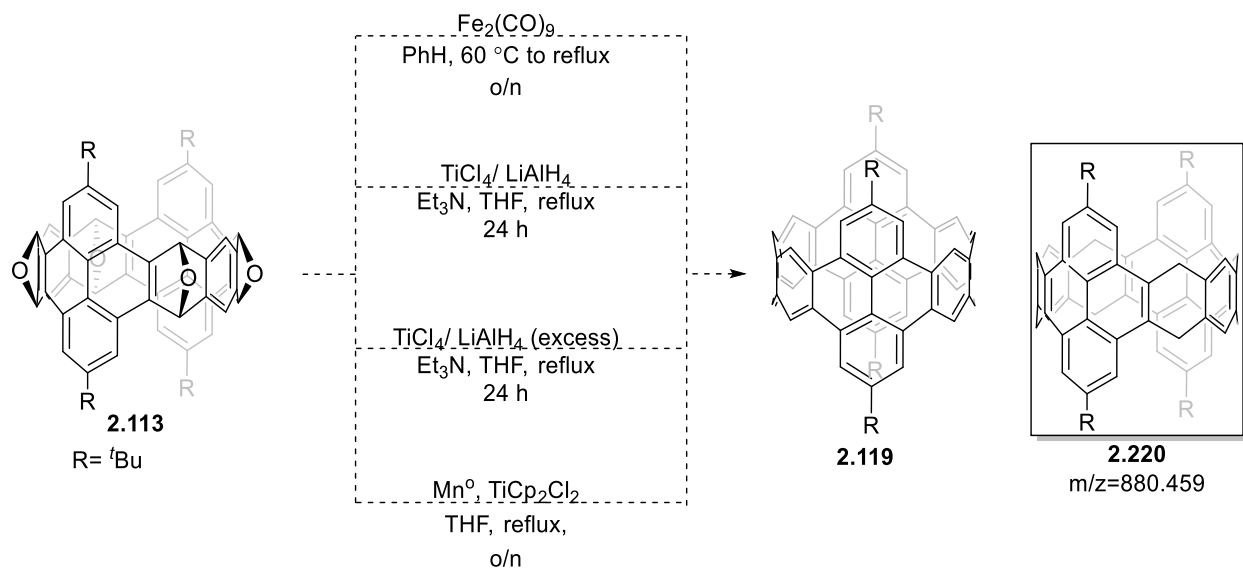
Scheme 2.44-NICS analysis of [20] and [10]pyrenecyclacene.

Ring	[10]pyrenecyclacene NICS(0)	[20]pyrenecyclacene NICS(0)
A	-6.28	-6.11
B	1.44	2.80
C	-7.21	-7.47
D	-10.75	-10.44

Table 2.2- Summary of NICS(0) values for [10] and [20]pyrenecyclacenes.

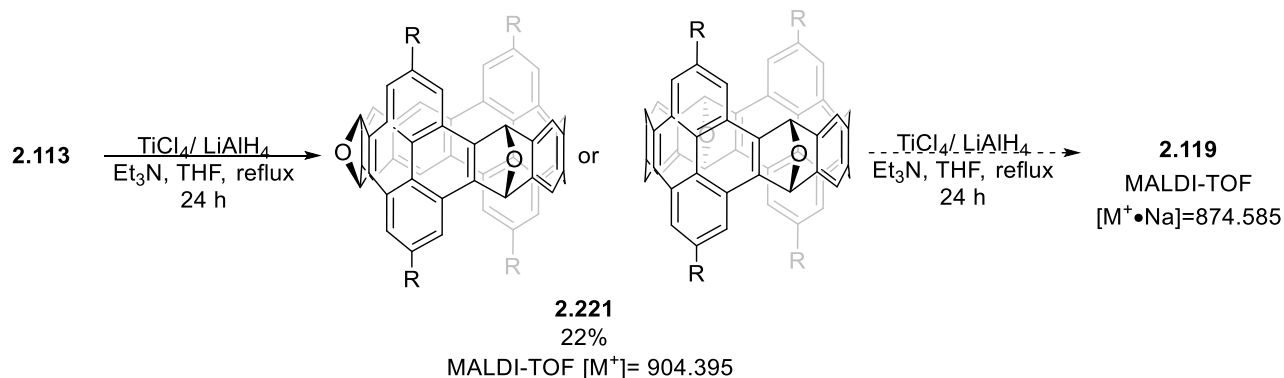
2.8 REDUCTION TO CYCLACENES

With the epoxycyclacene **2.113** in hand and with theoretical evidence suggesting that **2.113** would be stable, we undertook the challenge of reducing the cycle down to the fully conjugated cyclacene. **Scheme 2.45** highlights all the different reduction conditions we exposed **2.113** to. To our dismay, we were not able to observe the fully conjugated cyclacene from any reducing conditions. When we performed the reductions, we often observed the formation of a less polar spot compared to the starting material, however all our attempt to isolate clean product were fruitless. We tried a variety of techniques including preparative TLC, preparative HPLC and size exclusion chromatography but were never able to obtain good separation between our desired product, if any, and the rest of the unknown compounds.

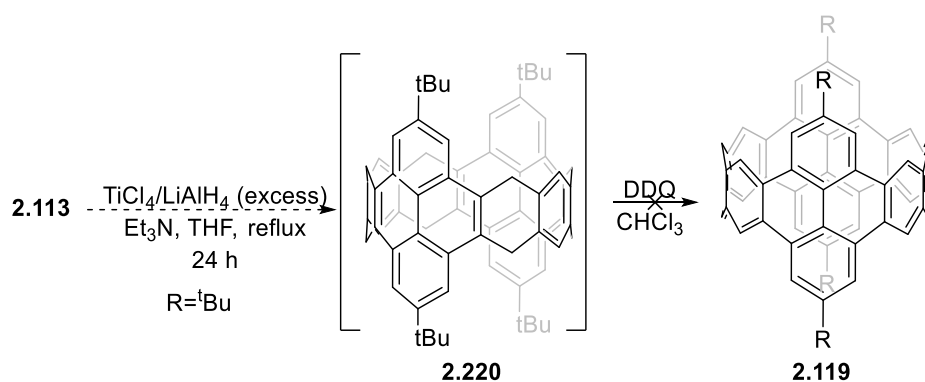


Scheme 2.45- Attempted reduction of tetraepoxycyclacene to **2.118**.

To attempt to analyze the reaction mixture, we separated the components of the reaction mixture as well as we could and analyzed them by MALDI-TOF MS. Usually, we observed the mass of remaining **2.112** and a mass corresponding to **2.120**. The latter compound is interesting as it hints to an over-reduced compound, meaning that at some point we reached our desired cyclacene **2.119** but the reduction continued until **2.220** was created. Attempts at carrying out the reduction with lower equivalents were partially successful and we were able to isolate **2.221** in a crude 22% yield (**Scheme 2.46**). At this point we believe that the regioisomer with the adjacent oxygens is the more likely product, however, further spectroscopic evidence, such as COSY or ^{13}C NMR, are needed to fully assign the structure. We attempted to reduce **2.221** further but were not able to observe the fully deoxygenated products. When analyzed by MALDI-TOF MS we did see a small peak which could correspond to the sodium adduct of the fully conjugated sample, but we were not able to confirm this finding by ^1H -NMR.



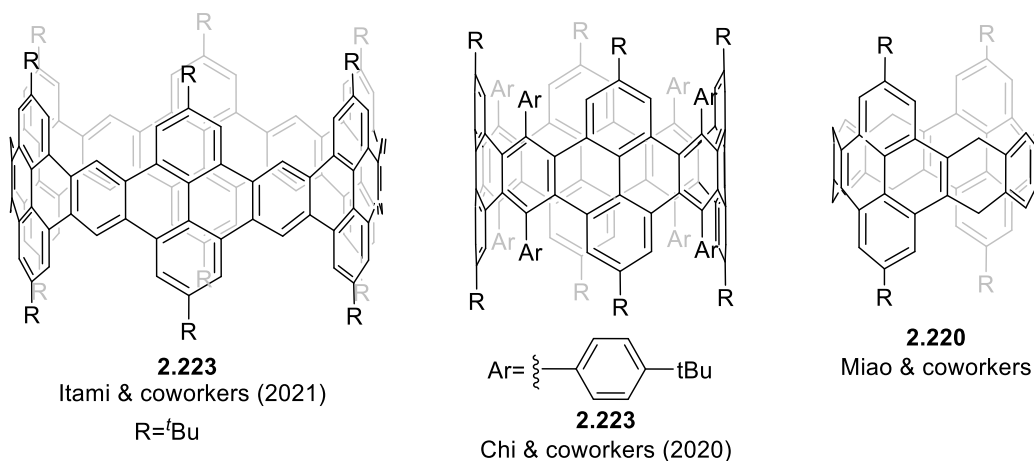
Scheme 2.46- Partial deoxygenation of **2.112**.



Scheme 2.47- Oxidation of **2.119**.

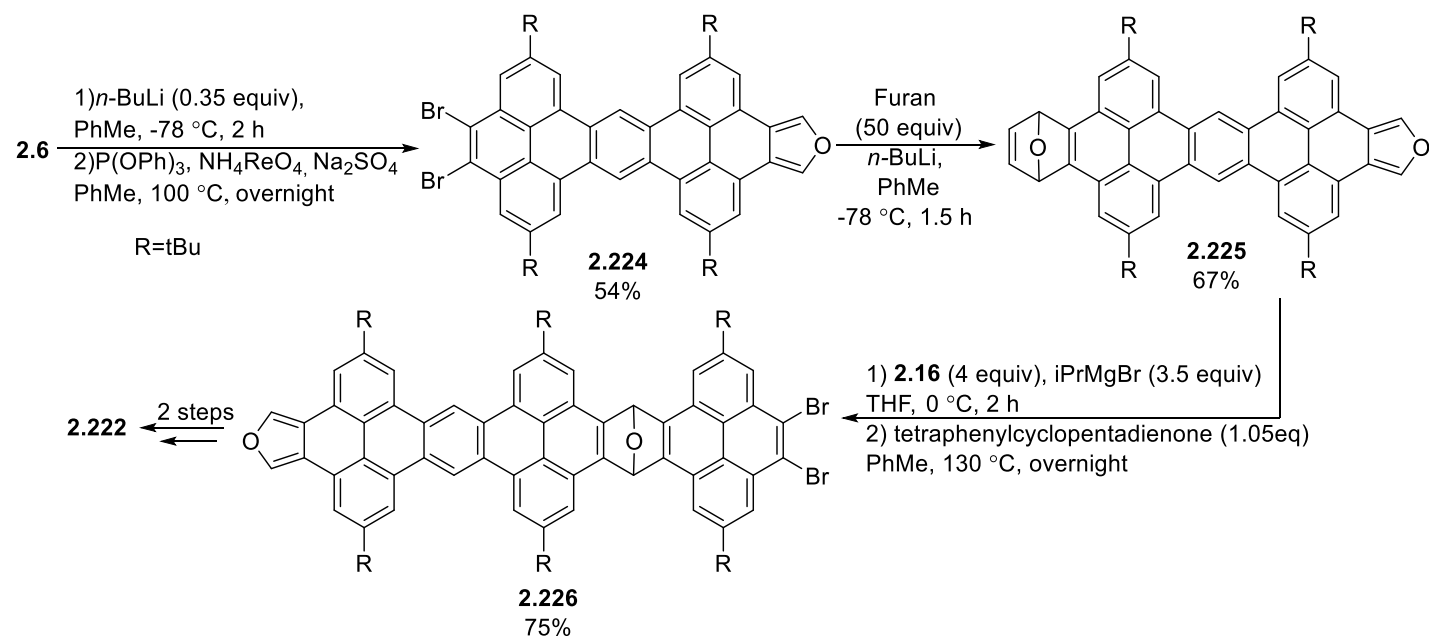
Since we appeared to be making a mixture of partially deoxygenated and over-reduced products, we decided to force the reaction to over-reduce and then attempt to oxidize the cycle back into the fully conjugated **2.119**. To that end, we reacted **2.113** with an excess of reducing agent, removed the starting materials from the reaction mixture, and subjected the remaining products to an overnight oxidation by DDQ (**Scheme 2.47**). This time by TLC there appeared to be no reaction and the NMR of the starting material remained unchanged. We suspect that the over-reduction is favoured to release some of the strain in the cycle which consequently makes it difficult to oxidize back to **2.119**. It should be noted that although we saw **2.220** by MALDI-TOF MS we were never able to get an accurate yield for this side product, thus the amount of over-reduction is unclear. Our hope with the oxidation was to potentially convert the over-reduced product to **2.119** which in turn could allow for an easier isolation of the product.

2.9 FIRST REPORTED SYNTHESIS OF CYCLACENES



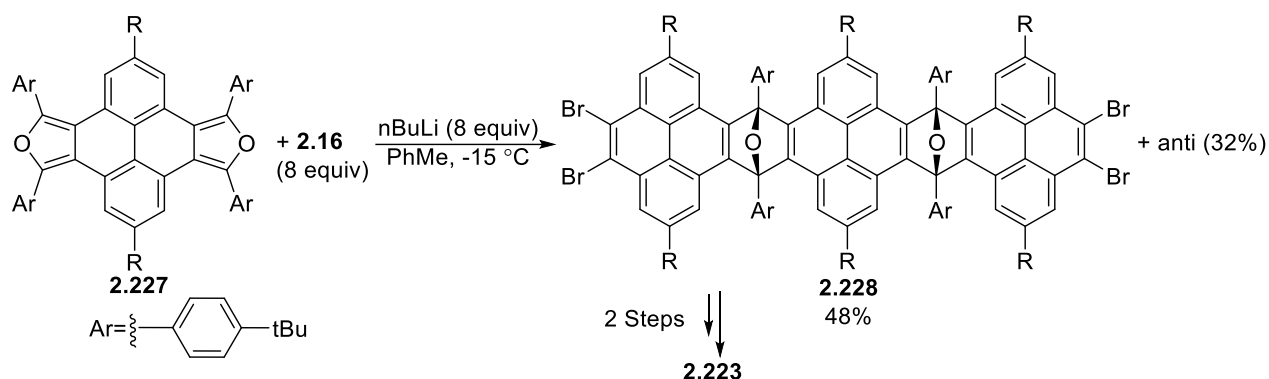
Scheme 2.48- Successful synthesis of pyrene cyclacenes.^{79,80,122}

As we approached the conclusion of our synthesis of cyclacenes we became aware of three publications that arrived roughly at the same time and reported the synthesis of cyclacenes using pyrene as the backbone of the cycle.^{79,80,122} We were somewhat heartbroken that two other groups managed to reach cyclacenes before us but were nonetheless pleased that our initial hypothesis of constructing cyclacenes using a pyrene backbone was indeed correct (**Scheme 2.48**).



Scheme 2.49- Itami and coworkers' synthesis of a zigzag carbon nanobelt.⁸⁰

The groups of Itami and Chi both used similar approaches to our group to construct the double stranded cycle, both groups made use of benzofurans and [4+2] cycloadditions to construct the double stranded cycle. The key steps for each synthesis are highlighted in **Scheme 2.49** and **Scheme 2.50**: Itami and coworkers recognized that for the cycle to form some type of curvature needed to exist on the cyclization monomers, thus they utilized a stepwise approach and eventually synthesized **2.226** which contained a single endoxide ring that provided enough curvature for the cyclization to proceed.⁸⁰ Key to their synthesis is the exclusion of any reactions that would yield diastereomers, for example, **2.224** was isolated as the acene rather than the endoxide to limit the number of products in the next step, similarly, **2.226** was isolated as the furan rather than the diendoxide.



Scheme 2.50- Chi and coworkers' synthesis of a [12,0] CNT sidewall fragment.⁷⁹

Chi and coworkers' synthesis of [12]cyclacene followed a similar pathway to our approach (**Scheme 2.50**). For this synthesis, the authors reacted **2.227** with a large excess of tetrabromopyrene **2.16** to create **2.228** plus the *anti*-diastereomer in good yield.⁷⁹ **2.228** was then reacted once more with **2.227** to yield the cycle and following reduction the cyclacene was reached. Like us, the authors reported over-reduction of the cyclacene, to mediate the reduction the authors installed 4-*tert*-butylbenzene groups on the benzofurans which helped prevent the over-reduction of the cyclacene.

There was one more report on the synthesis of cyclacenes published by Miao and coworkers,¹²² which unfortunately outlined the exact same synthesis we had tailored. To make matters worse, the authors reported that the fully conjugated cyclacene was not possible with our system and that the over reduced cycle **2.220** was the only

product from the reduction. The authors report a 92% yield for **2.220** and although we used different reduction conditions, we were only able to observe **2.220** by MALDI-TOF MS.

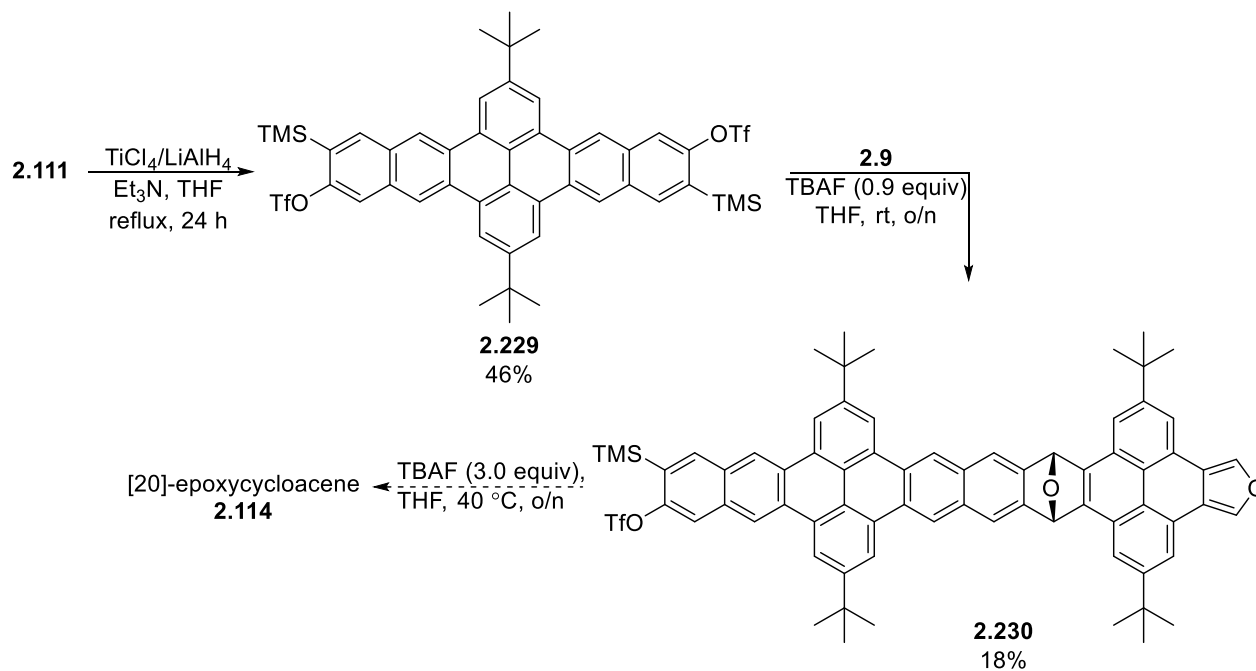
The main takeaway from Itami's and Mia's successful synthesis was that the [4+2] cycloaddition of pyrenofurans and benzyne is somewhat reluctant to proceed and thus must be carried out with large excess of one of the reactants. Furthermore, the conditions by which the benzyne form vary for each different precursor. For example, the Itami group utilized different organometallic reagents to carry out each [4+2] cycloadditions. We briefly experimented with different organometallic reagents to trigger the elimination on **2.16** but obtained mostly unchanged results. Lastly, the curvature of the cyclization monomers was crucial to achieve cyclization. We also arrived at this conclusion as our only successful cyclization was with **2.112** which contained a *syn* geometry between the endoxides, meanwhile carrying this reaction out with flat monomers never allowed for any cyclic product.

2.10 SYNTHESIS OF LARGER CYCLACENES

Given that Miao and coworkers' report on the exact same molecule we were pursuing proved unsuccessful, we set our sights on the construction of larger cyclacenes. Our previous theoretical analysis indicated that the electronics of the cyclacene remained mostly unchanged between the [10]pyrenocyclacene and the [20]pyrenocyclacene but the strain between these two cycles was significantly reduced. Therefore, we hypothesized that [10]pyrenocyclacene's **2.118** propensity to over-reduce may be due in part to the molecule wanting to reduce ring strain and that a larger cyclacene would not be subject to the same effects.

Inspired by the recent successful synthesis of cyclacenes, we designed a new synthesis to construct [20] cyclacene that avoided the creation of several diastereomers with a single curvature point to promote the cyclization. The synthetic route is highlighted in **Scheme 2.51**. We started with the *anti*-bisadduct **2.110** and subjected the compound to a reduction under low valent titanium which produced acene **2.228** in a 46% yield. From our previous synthesis we had stockpiled large amounts of **2.110** as it is made at roughly the same yield as the *syn*-bisadduct **2.111**. The reaction should proceed with either diastereomer but we choose **2.110** as it allows us to show how either diastereomer can be used to construct a cyclacene. Acene **2.228** was then reacted with difuran **2.9** in a [4+2] cycloaddition furnishing **2.229** in a 18% yield. Finally, we attempted to cyclize **2.113** with TBAF in THF but were not able to observe cycle **2.113** either by NMR or MALDI-TOF MS. Due to time constraints the synthetic pathway was

not explored further but this might garner a re-examination as it seems a likely route to construct a larger cyclacene. One thing to note is that as the acene grows it become less and less reactive thus more forcing conditions may be needed to arrive at the cyclacene.



Scheme 2.51- Attempted synthesis of [20]pyrenecyclacene.

2.11 SYNTHESIS OF PYRENOLS

2.11.1 OXIDATION OF PYRENE BORONIC ESTERS

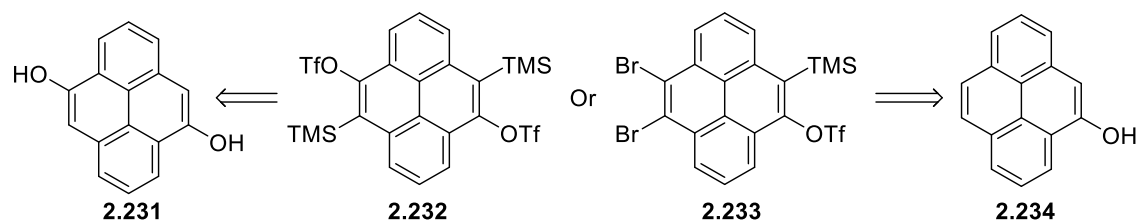
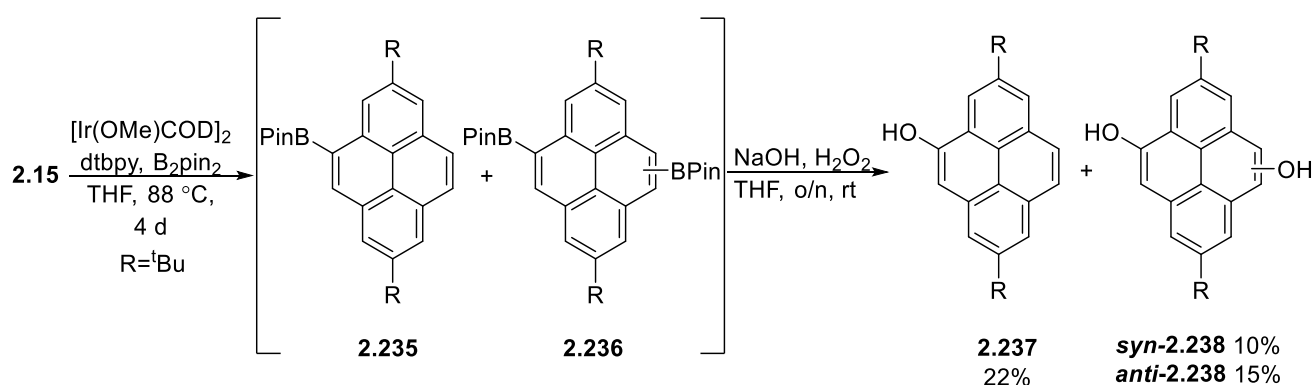


Figure 2.3-Fluoride-activated pyrene benzyne precursors.

Our experience with benzyne created via lithium halogen exchange on pyrene made us wonder if it was possible to create a fluoride activated benzyne directly on pyrene. This was motivated by how cleanly benzyne formed when we reacted bistriflate **2.110** with fluoride versus when we made benzyne on pyrene with *n*-BuLi. We were unsure if the basicity and nucleophilicity of *n*-BuLi was to blame for the poor reactivity and if adding a milder activating agent, such as fluoride, would ensure a cleaner reaction.

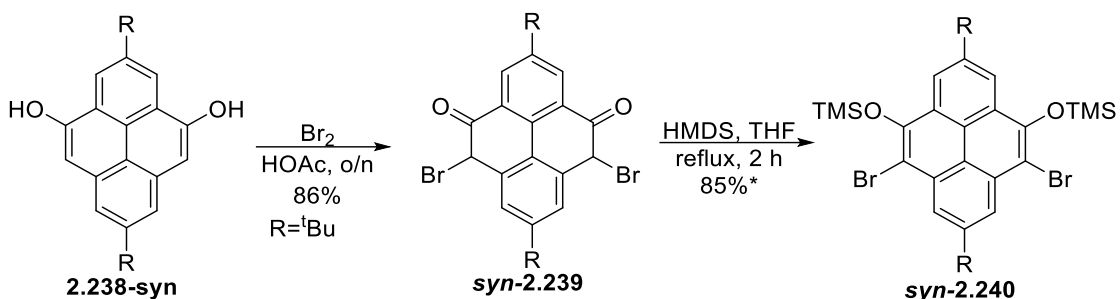
We set our sights on **2.231** and **2.233** and we thought that the best way to reach these targets was to perform the exact set of transformations used to reach bistriflate **2.110** (see **Scheme 2.40**), therefore we would have to find an efficient way to construct pyrenols (**Figure 2.3**). In terms of oxidizing pyrene, there are few reports present in the literature but none of the oxidations directly reach the pyrenols.^{148–152} Previously, we had performed an Ir catalyzed C-H activation on pyrene that results in the formation of pyrene-boron esters and thought this would be a great starting point for synthesizing the pyrenols as the aryl boronic esters can be easily transformed to the phenols if treated with peroxide.



Scheme 2.52- Synthesis of pyrenols from pyrene boronic esters.

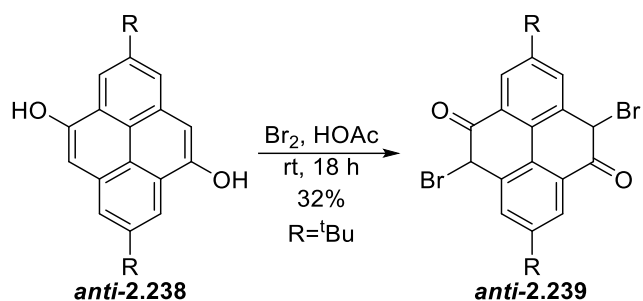
We began our synthesis of pyrenols by performing a borylation on 2,7-di-*tert*-butyl pyrene **2.15** with an Ir catalyst following the procedure outlined by Marder and coworkers (**Scheme 2.52**).¹⁵³ Rather than isolating the pyrene boronic esters **2.235** and **2.236**, we opted to introduce the peroxide after the reaction time and after several rounds of purification we arrived at the pyrenol **2.237** and dipyrenols **2.238** in a 22% and 25% yield respectively. For the pyrene diols **2.238**, the more polar compound was the *syn*-diol (*syn*-**2.237**) while the less polar compound was the *anti*-diol (*anti*-**2.237**). In our hands this reaction proved somewhat difficult to carry out and we often saw batch to batch variability with some trials yielding product while other trials contained only starting material. Additionally, this reaction was a rather expensive way of creating this product due to the high catalytic loading of the catalyst. Nonetheless, we proceeded with our synthesis of pyrene bistriflates using the pyrenols on hand and reacted *syn*-**2.238** with Br_2 in acetic acid (**Scheme 2.53**). The *syn*-diol was initially utilized we had an easier time isolating the regioisomer in comparison to the *anti*-adduct. The more nucleophilic pyrenol did not require the addition of Fe for

the bromination to proceed and furnished the tautomerized diphenol **syn-2.238** in an 86% yield. Since the bromination was carried out in acetic acid **syn-2.238** tautomerized to the keto form. Since the chemistry should remain the same for both keto/enol forms, we continued using this method with acetic acid as the solvent made for easy isolation of the brominated products.



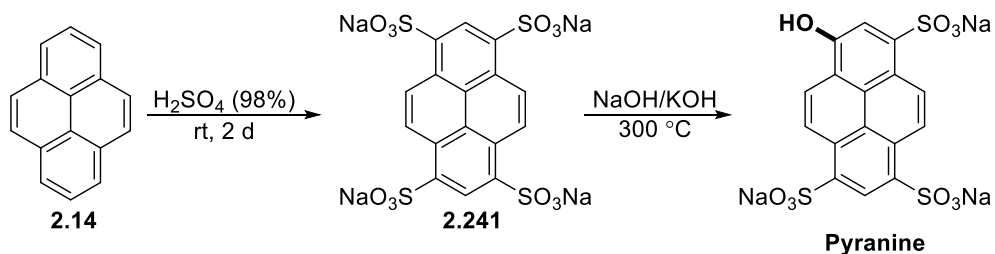
Scheme 2.53-Attempted synthesis of a pyrene bistriflate.*Crude yield of **2.240**; compound decomposed over time

We then attempted the silylation of **2.239** using HMDS in refluxing THF but we began to run into problems, although we did observe **syn-2.240** by NMR it was accompanied by various impurities which despite several purification attempts, we were not able to remove. Prior experience with the retro-Brook rearrangement made it clear that for the next step to proceed we needed clean starting material, fearing losing all our starting material we did not attempt the next step. It is unclear what the impurity was but it may be possible that **syn-2.239** decomposed under the reaction conditions as similar compounds like 9-phenanthrol decompose in aerobic conditions.¹⁵⁴ Alternatively, it may be possible that **syn-2.240** tautomerized to the keto form due to the lability of the TMS group, later experiments outlined in **Section 2.11.4** show that pyrene-diols prefer to reside in the keto form, further supporting this theory. The transformations shown in **Scheme 2.53** were also attempted on **syn-2.238** but due to difficulties with purification we were not able to obtain sufficient material to carry out the remainder of the synthetic route.



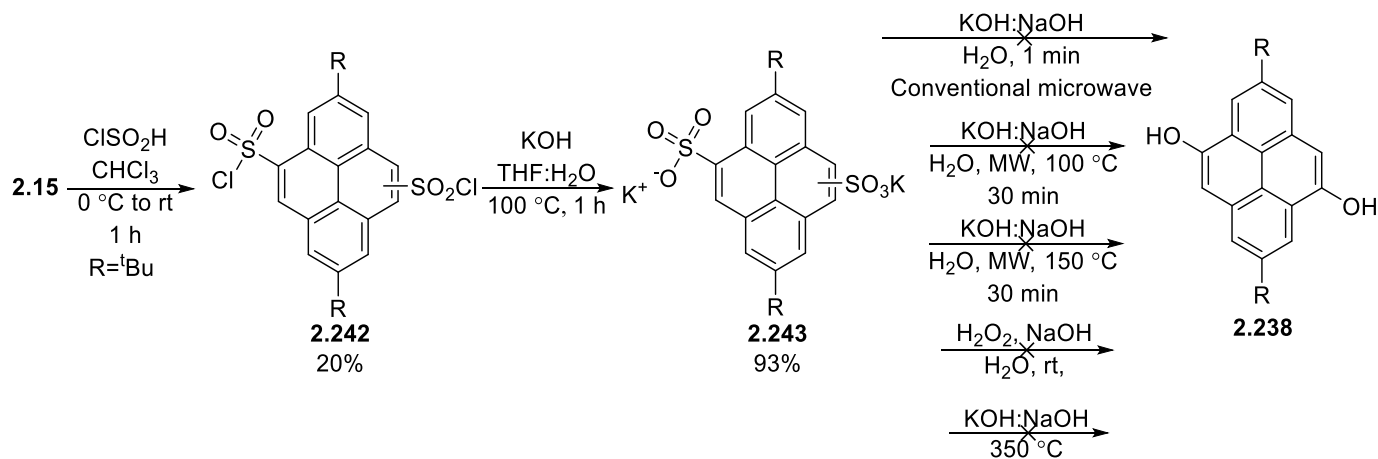
Scheme 2.54- Synthesis of brominated pyrene *anti*-diol **anti-2.239**.

2.11.2 SULFONATE FUSION



Scheme 2.55- Synthesis of pyranine using sulfonate fusion.¹⁵⁵

Due to the high cost and long reaction times for the Ir catalyzed pyrenol synthesis, we decided to pursue alternatives that either proceeded quickly or with a lower cost. One of the most appealing methods was sulfonate fusion, a process by which an aryl sulfonate reacts with molten hydroxide to yield phenols in a short amount of time.¹⁵⁶ This was a very old reaction that had been previously used as the main method for synthesizing phenols and was even demonstrated to work on pyrene (**Scheme 2.55**).^{155,157}

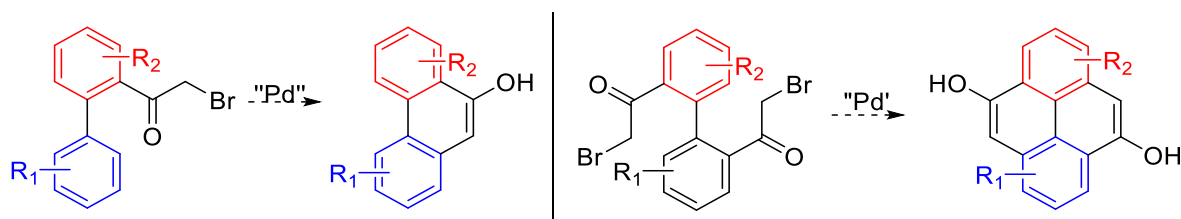


Scheme 2.56- Attempted synthesis of pyrenols using sulfonate fusion.

Our attempted synthesis of pyrenols via sulfonate fusion is highlighted in **Scheme 2.56**. Given the fast reaction times for the sulfonate fusion, our goal was to create a synthetic pathway to the pyrenols that would proceed using inexpensive reagents in a short amount of time (approximately 3 h to reach pyrenols). We began our synthesis with the sulfonylation of 2,7-di-*tert*-butylpyrene **2.15**, once again the *t*Bu groups were required to direct the electrophile towards the desired positions. We attempted numerous sulfonylation conditions but ultimately settled on chlorosulfonic acid in CHCl₃ which produced **2.242** in a 20% yield. The sulfonyl chlorides were then converted to the sulfonate **2.243** in a 93% yield with KOH and finally we attempted the sulfonate fusion using a variety of conditions but were unable to convert the sulfates into the pyrenols.

We tried numerous conditions under microwave¹⁵⁸ and thermal conditions^{155,157,159} but were unable to convert to the pyrenols. Some reactions were met with explosive results and any left-over starting material was difficult to remove from salt/hydroxide mixture due to its high polarity. Sulfonate fusion had been previously carried out on molecules such as naphthalene and pyrene so we had reason to believe the reaction would proceed.^{155,158} One possible hypothesis was that since the reaction is thought to proceed via an S_NAr mechanism¹⁶⁰ and we were conducting the reaction on the less aromatic rings of pyrene then it was difficult for this mechanism to occur. This hypothesis is somewhat supported by the sulfonate fusion being possible in pyranine which possesses the sulfonate groups in aromatic rings of pyrene.¹⁵⁵

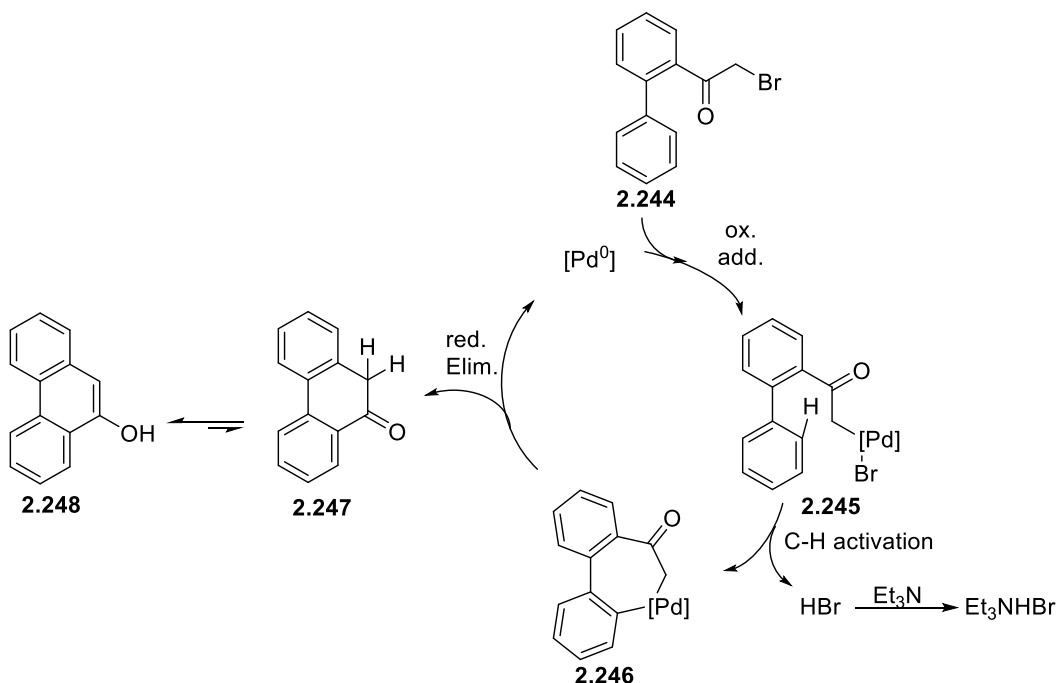
2.11.3 METAL CATALYZED SYNTHESIS OF PAH ALCOHOLS



Scheme 2.57-Proposed synthesis of PAH alcohols using a metal catalyzed intramolecular ring closing strategy.

Sulfonate fusion proved to be an attractive pathway for synthesizing phenols unfortunately the pyrene reactivity worked against us and disallowed the formation of the pyrenols. We decided to take a more modern approach and milder approach for constructing our pyrenols following a metal catalyzed ring closing reaction (**Scheme 2.57**). Prior reports have made use of transition metal coupling to induce intramolecular cyclization^{161,162} and we hypothesized that we could utilize a similar method to synthesize pyrenols. We envisioned using α -

haloaromatic ketones to create our pyrenols. This methodology would introduce additional steps, but it does possess the advantage of offering variety for the substrates rather than being limited to just pyrene thus allowing for the creation of new PAH alcohols. Furthermore, if successful the reaction would allow for the creation of a pyrene diene/dienophile that is free of *t*-Bu which are usually introduced to direct the synthesis.

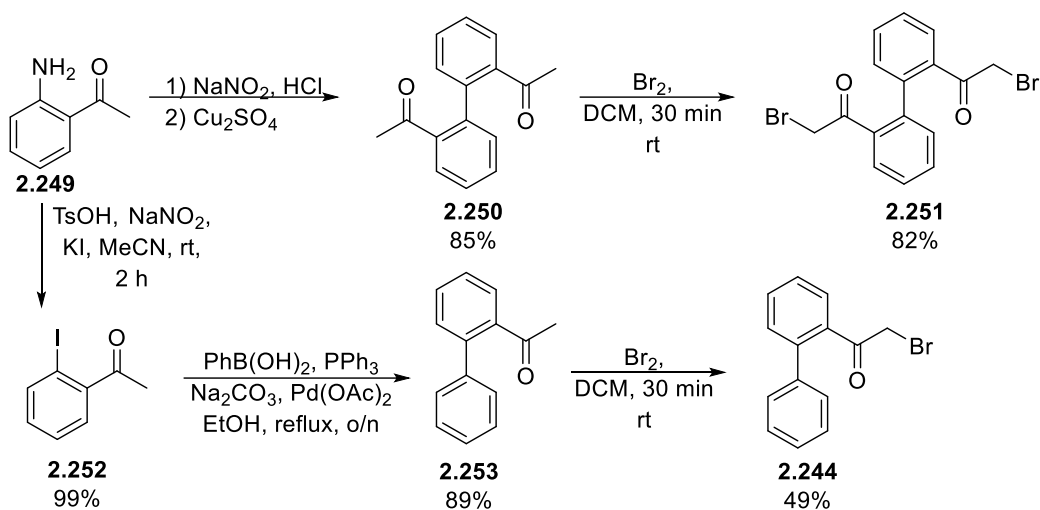


Scheme 2.58-Proposed catalytic cycle for the metal catalyzed synthesis of PAH alcohols.

Scheme 2.58 outlines our proposed catalytic cycle: first an oxidative addition would occur on **2.244** leading to **2.245**. The metalated compound would then perform a C-H activation promoted by the close proximity of the metal center to the aromatic ring. Upon deprotonating the aromatic ring, palladacycle **2.246** would form and this species would then reductively eliminate to regenerate the catalyst and form ketone **2.247** which would then tautomerize under base to yield the PAH alcohol **2.248**.

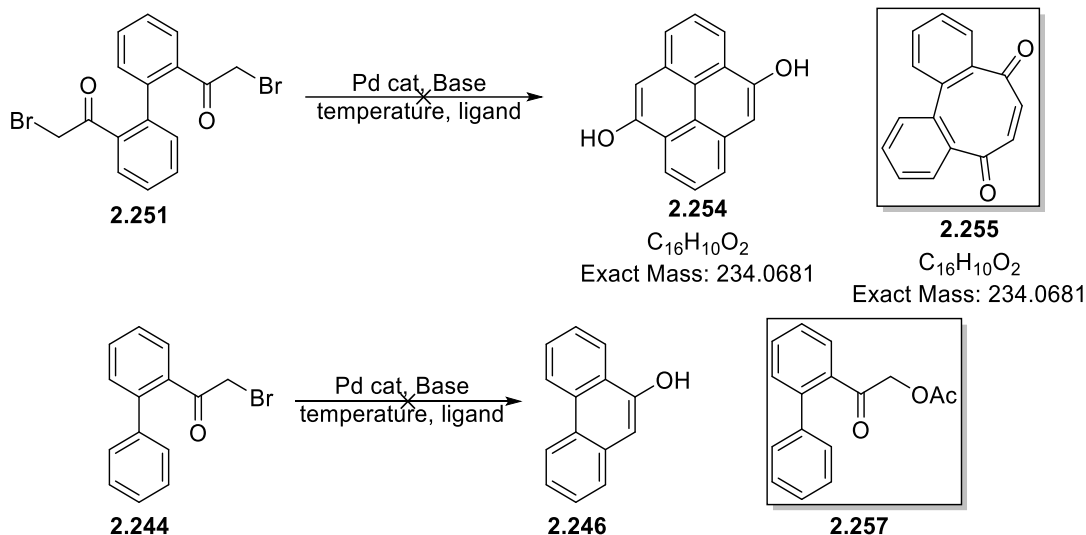
The synthesis of the starting material is outlined in **Scheme 2.59**: 2'-aminoacetophenone **2.249** was subjected to an oxidative coupling to yield biphenyl **2.250** in 85% yield. This ketone was then brominated with Br₂ in DCM to create **2.251** in an 82% yield. **2.251** serves as the precursor for bispyrenol but for our initial optimization we wanted to utilize **2.244** as our model compound since it only possesses one reactive site. To synthesize **2.244**, we

once again started with 2'-aminoacetophenone **2.249** and performed a Sandmeyer reaction to reach **2.252** in quantitative yield. **2.252** was then arylated in 89% yield via a Suzuki coupling which was then followed by a bromination leading to **2.244** in a 49% yield



Scheme 2.59-Synthesis of PAH cyclization precursors.

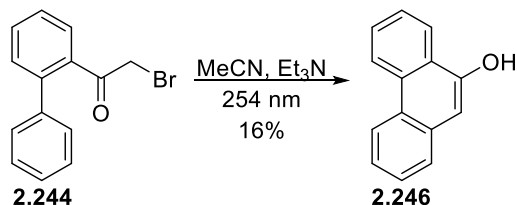
With the starting materials on hand, we attempted numerous conditions but were not able to detect the formation of product. We screened different parameters including Pd catalyst, temperature, ligand, and base but none of our conditions gave 9-phenantrol **2.248** or bispyrenol **2.254** (**Scheme 2.60**). Often the highly electrophilic α -haloketones would react with the base leading to compounds like **2.257**. The reaction conditions also allowed for the formation of **2.255** which appeared promising when analyzed by MS due to having the same mass as our desired product. Further analysis revealed this was a somewhat known reaction that occurs when **2.251** is introduced to a metal.¹⁶³ Due to the myriad of side-reactions possible when these compounds were introduced to our reaction conditions we ultimately abandoned this reaction pathway as we soon after discovered a metal-free way to carry out this cyclization.



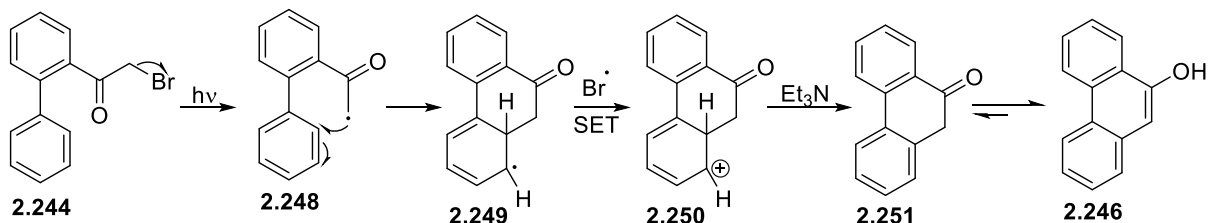
Scheme 2.60-Attempted synthesis of PAH using a transition metal catalyzed ring closing.

2.11.4 PHOTOCYCLIZATION OF AROMATIC HALOKETONES TO PAH ALCOHOLS

A



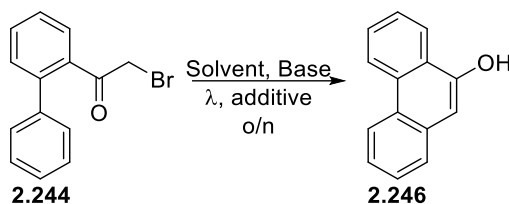
B



Scheme 2.61-A-Synthesis of 9-phenanthrol using a photochemical approach. **B**-Proposed mechanism for the photochemical synthesis of PAH alcohols.

We were not quite ready to give up on creating a new method for the synthesis of PAH alcohols, we still had plenty of starting material left over from our attempts to cyclize using a metal catalyst and were eager to try different routes. Previously, we had some success using photochemistry to promote our reactions (See **Chapter 3**) and were curious if α -haloketones behaved similarly to aryl halides when exposed to UV light. Gratifying, we found α -haloketones will dissociate and phototautomerize when exposed to UV light^{164,165} which led us to believe that if a radical was created α to the ketone then it could lead to a PAH alcohol. Thus, we exposed **2.244** to 254 nm irradiation and were pleased to observe the formation of 9-phenanthrol in a 16% yield (**Scheme 2.61A**).

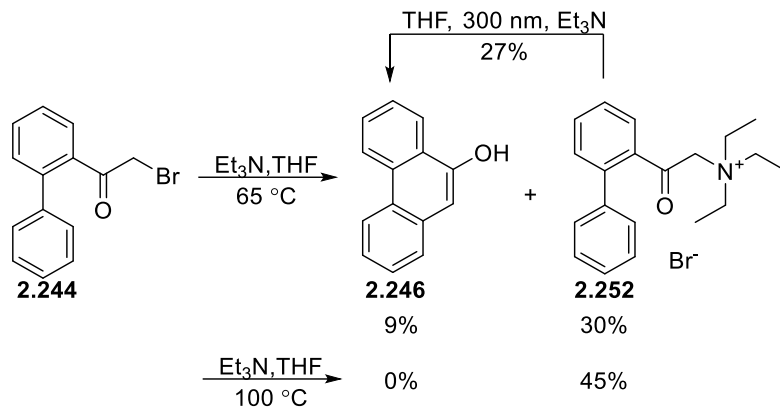
Our proposed mechanism is outlined in **Scheme 2.61B** and proceeds as follows: UV irradiation on **2.244** induces a homolytic cleavage creating radical **2.248** plus a bromine radical, the newly formed organic radical then attacks the adjacent aryl group creating a new 6-membered ring (**2.248**). A single-electron transfer then follows creating a cation **2.250** which then is rearomatized by a base (either Br⁻ or Et₃N) arriving at ketone **2.251**. The ketone can then be tautomerized to the phenanthrol **2.246** under base or light.



Entry	Solvent	Wavelength (nm)	Base	Additives	Yield (%)
1	MeCN	254	TEA	-	16(14)
2	MeCN	300	TEA	-	42
3	MeCN	350	TEA	-	36
4	THF	300	TEA	-	66
5	THF	300	DIPEA	-	53
6	THF	300	-	-	37
7	THF	300	-	KI (1equiv)	21
8	THF	300	TEA	KI (1equiv)	50
9	THF	300	DIPEA	KI (1equiv)	37
10	THF	300	DIPEA	TBAI (1equiv)	49

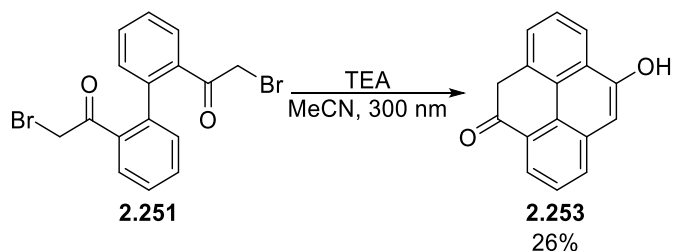
Table 2.3-Summary of optimization of photocyclization of α -haloketones. Reactions were irradiated in a 10 mL quartz test tube overnight with 1-([1,1'-biphenyl]-2-yl)-2-bromoethan-1-one (1 equiv), Base (2 equiv) in solvent (0.2 M). Yield in parenthesis indicates isolated yield.

Delighted with the successful formation of 9-phenanthrol **2.248**, we set out to optimize the reaction. A summary of the optimization conditions is highlighted in **Table 2.3**. First, we examined the effect of different wavelengths on the reaction and found 300 nm to be the best wavelength for the reaction (**Table 2.3-Entry 1-3**). Next, we experimented with the solvent and after a thorough screening we arrived at THF as the ideal solvent which provided a 66% yield (**Table 2.3-Entry 4**). We then screened different bases and ran the reaction in the absence of base. Next to TEA, DIPEA performed the best with a slight drop in yield to 53%, while running the reaction in the absence of base nearly halved the yield (**Table 2.3-entry 5-6**). We tried running the reaction under Finkelstein conditions by adding an equivalent of iodide, which would convert the alkyl bromide to the iodide *in situ* and in turn provide an easier bond to homolytically cleave. All attempts to perform an in-situ Finkelstein resulted in a drop in yield (**Table 2.3-entry 7-10**) regardless of the iodide source.



Scheme 2.62-Thermal control reaction for photocyclization of α -haloketones

Reaction optimization is still being carried on in our laboratory at the time of writing this thesis, we are exploring the effect of concentration of the reaction as well as beginning to investigate the functional group tolerance of the reaction. We also performed a series of controls of the reaction outlined in **Scheme 2.62**: We first tested if the reaction needed light to proceed and found that it was indeed able to proceed, albeit at low yields, thermally. Additionally, we found that TEA can perform an S_N2 on **2.244** leading to the ammonium salt **2.252**. This salt is still able to homolytically cleave under light but to a lesser extent than the aryl halides, consequently DIPEA is still being considered as the base for the reaction due its decreased nucleophilicity.



Scheme 2.63-Attempted synthesis of bispyrenol.

Before fully optimizing the reaction, we also attempted the photocyclization of **2.251** to see if we would observe the bispyrenol **2.252**. To our surprise when **2.251** was irradiated under UV we observed **2.253** as the product in a 26% yield. It is unclear at the moment as to why this tautomer is the favoured product of the reaction and currently our group is investigating how to further optimize the reaction (**Scheme 2.63**). Our photochemical method is still in its infancy and may prove to be a powerful way to synthesize PAH alcohols in the future.

2.12 CONCLUSION

CNTs are a class of materials that may revolutionize the transistor and consequently electronics and computers alike. We hoped to address the synthesis problem for semiconducting CNTs by creating the first examples of zigzag cyclacenes. Although, we were not successful in synthesizing our cycle, other groups used similar methodologies to synthesize the first examples of cyclacenes, which like us, relied on the use of a pyrene backbone to suppress the molecules triplet character, and provide flexible scaffold to the cycle.

When Bertozzi and coworkers successfully synthesized CPPs, the field exploded, and now multiple sizes of these macrocycles are commercially and synthetically available. Thus, there is still plenty of work to be done regarding cyclacenes. We tried to address some of the synthetic challenges when trying to construct these cycles to attempt to alleviate the difficulty in their synthesis and provide new routes towards these compounds.

Some of our chemistries may merit revisiting, in particular the synthesis of larger cyclacenes (**Section 2.10**) and the synthesis of cyclacenes using a pyrene cyclophane (**Section 2.5**). New techniques will ensure a variety of cyclacenes will be available and will thus help us understand how to build CNTs from the bottom up.

PART 1: CHAPTER 3

METAL FREE SYNTHESIS OF PHOSPHONIUM SALTS

3.1 PHOSPHORUS COMPOUNDS IN ORGANIC CHEMISTRY

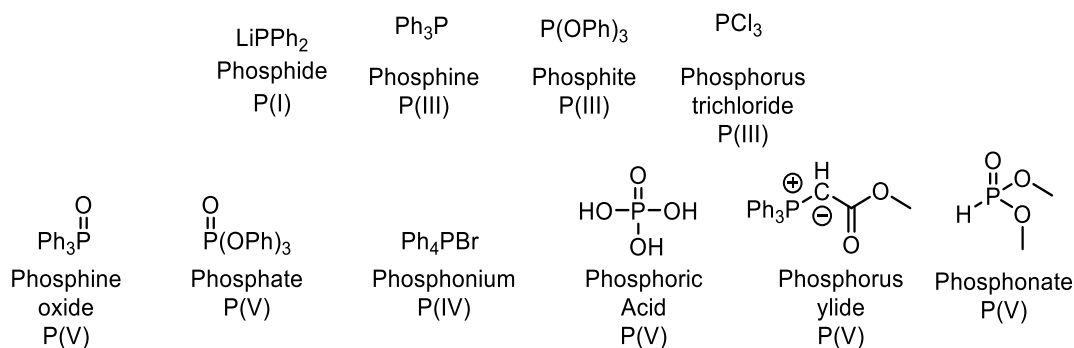
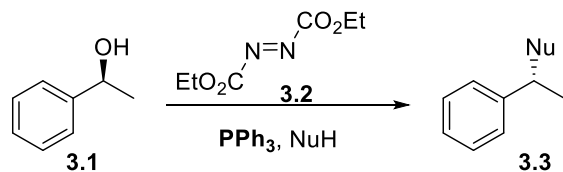


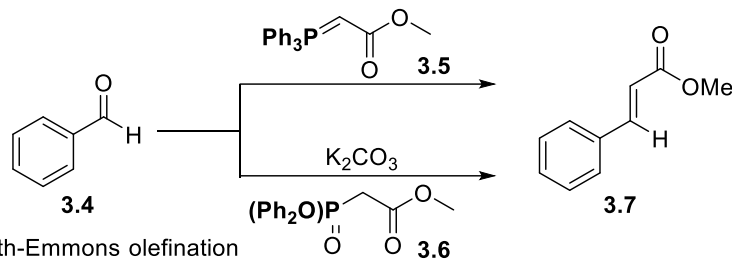
Figure 3.1-Structure, oxidation state and nomenclature for common phosphorus compounds found in organic chemistry.

Mitsunobu



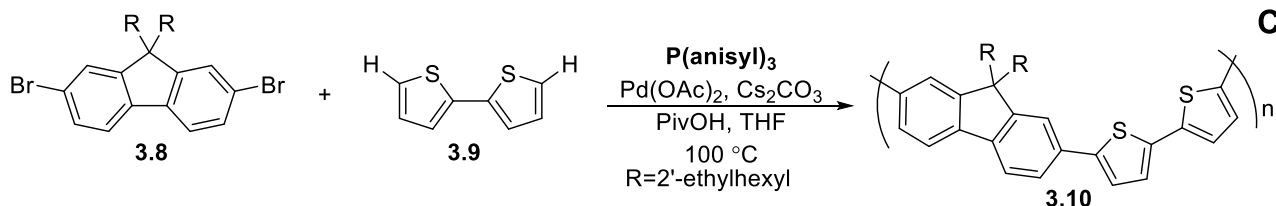
A

Wittig Olefination



B

Horner-Wadsworth-Emmons olefination



C

Phosphines as ligands for direct arylation polymerization

Scheme 3.1- Reactions mediated by phosphorus compounds.

Phosphorus compounds can serve for a wide variety of applications and adopt multiple forms with varying oxidation states. Some of the most common forms of phosphorus are highlighted in **Figure 3.1**. Typical oxidation state of phosphorus compounds varies between P(III) and P(V) although in some cases P(I) can be reached. Several

well-known reactions in organic chemistry rely on the use of a phosphorus compound as a key reactant for the reaction to proceed. For example, the Mitsunobu (**Scheme 3.1A**) reaction requires the use of a phosphine (typically PPh_3) in order to functionalize an alcohol into a good leaving group such that upon nucleophilic attack the alcohol is expelled in the form of triphenylphosphine oxide.^{166,167} This classic reaction proceeds through an $\text{S}_{\text{N}}2$ mechanism resulting in substitution of the alcohol with inversion of stereochemistry.^{166,167} The Wittig olefination (**Scheme 3.1B-top**)^{168,169} and Horner-Wadsworth-Emmons (HWE) olefination (**Scheme 3.2B-bottom**)¹⁶⁹ serves as another classic example of the use of phosphorus in synthesis. In this case, a phosphorus ylide is responsible for the reactivity and provides the driving force for the reaction via the release of phosphine oxide or a water-soluble phosphate for the Wittig olefination and HWE olefination, respectively. Additionally, phosphines have found a great deal of use as ligands for transition metal catalysis, often the structure of the ligands can have a great effect on the reactivity of the catalyst.¹⁷⁰⁻¹⁷⁴ **Scheme 3C** highlights a modern application of a phosphine ligand for the synthesis of the conjugated polymer poly(9,9-dioctyl-2,7-fluorene-alt-2,2'-bithiophene) (**PF8BT**) through direct arylation. For this example, the $\text{P}(o\text{-anisyl})_3$ ligand aids in the C-H activation step of the catalytic cycle and has been shown to be the ligand of choice when creating conjugated polymers via direct arylation.¹⁷⁴

3.2 PHOSPHONIUM SALTS

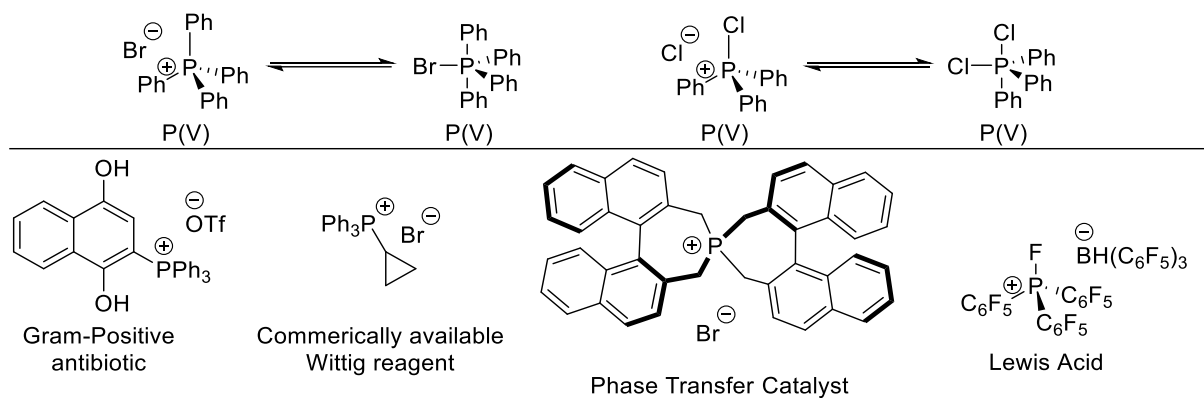
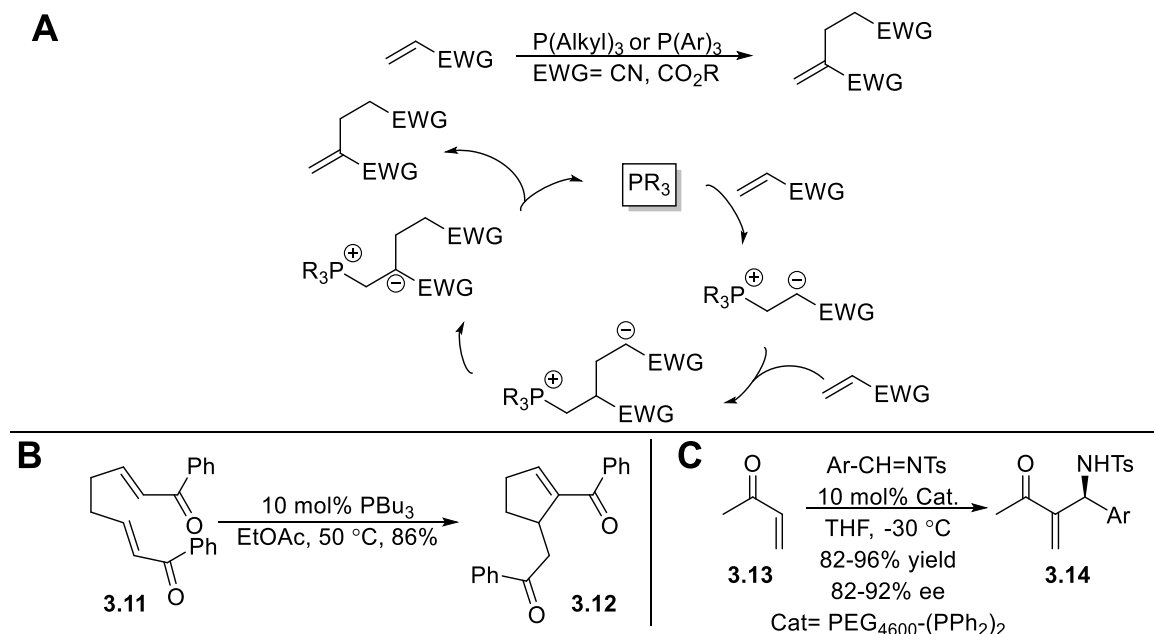


Figure 3.2-(Top) equilibrium between tetra and pentacoordinated forms of tetraphenyl phosphonium bromide. (Bottom) examples of phosphonium salts and their application.

Phosphonium salts are phosphorus compounds in which a positively charged phosphorus atom is bound to four substituents. Typically, the substituents are alkyl or aryl groups; phosphonium salts can also be observed with

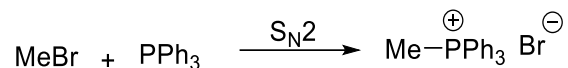
other heteroatoms such as nitrogen,^{175,176} sulfur or oxygen¹⁷⁷ as well as halides.^{178–181} Depending on the nature of the phosphonium salt, the compounds can exist in an equilibrium between the tetravalent and pentavalent form. The equilibrium is dictated by the nature of the solvent with more polar solvents favouring the charged tetracoordinated conformation while less polar solvents favour the pentacoordinate form(**Figure 3.2**).^{178–181}

Phosphonium salts are typically associated with the Wittig olefination but can be serve for a wide variety of applications including as Lewis acids,¹⁸² reagents,^{168,169} ionic liquids,^{183–186} as moieties for drug delivery,¹⁸⁷ antibiotics,¹⁸⁸ electrolytes,¹⁸⁹ soluble supports¹⁹⁰, pseudo halides for metal catalyzed cross couplings^{191–193}, reactants for the construction of biaryl systems¹⁹⁴ and as phase transfer catalysts.¹⁹⁵ Phosphonium salts can also be observed as intermediates in phosphine mediated organocatalysis.¹⁹⁶ For example, in the Rauhut-Currier reaction phosphines serve as an organocatalyst to aid in various conjugate additions by creating a phosphonium salt as a key intermediate which can then be expelled back as the phosphine to complete the catalytic cycle (**Scheme 3.2A**).¹⁹⁷ The reaction can be carried out with a wide variety of phosphines and can serve as method for the reaction enantioselectively (**Scheme 3.2**).



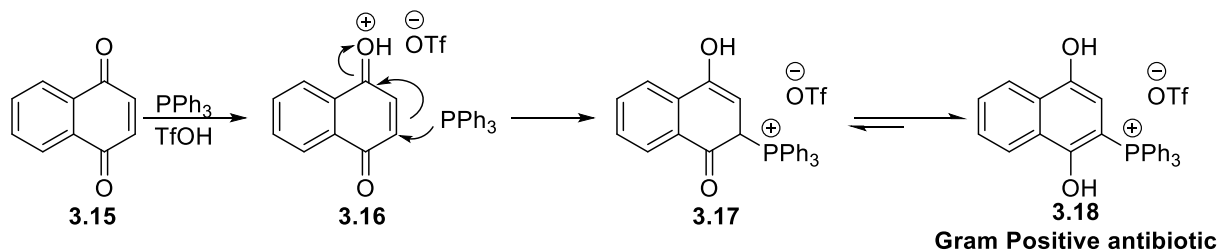
Scheme 3.2-A: Generic catalytic cycle for phosphine organocatalysis.¹⁹⁶ **B:** Intramolecular Rauhut-Currier reaction by Wang *et al.*¹⁹⁸ **C:** Asymmetric example of Morita-Baylis Hillman reaction as reported by Huang and Shi.¹⁹⁹

3.3 SYNTHESIS OF PHOSPHONIUM SALTS



Scheme 3.3-Synthesis of methyltriphenylphosphonium bromide via nucleophilic attack of PPh₃ on methyl bromide.

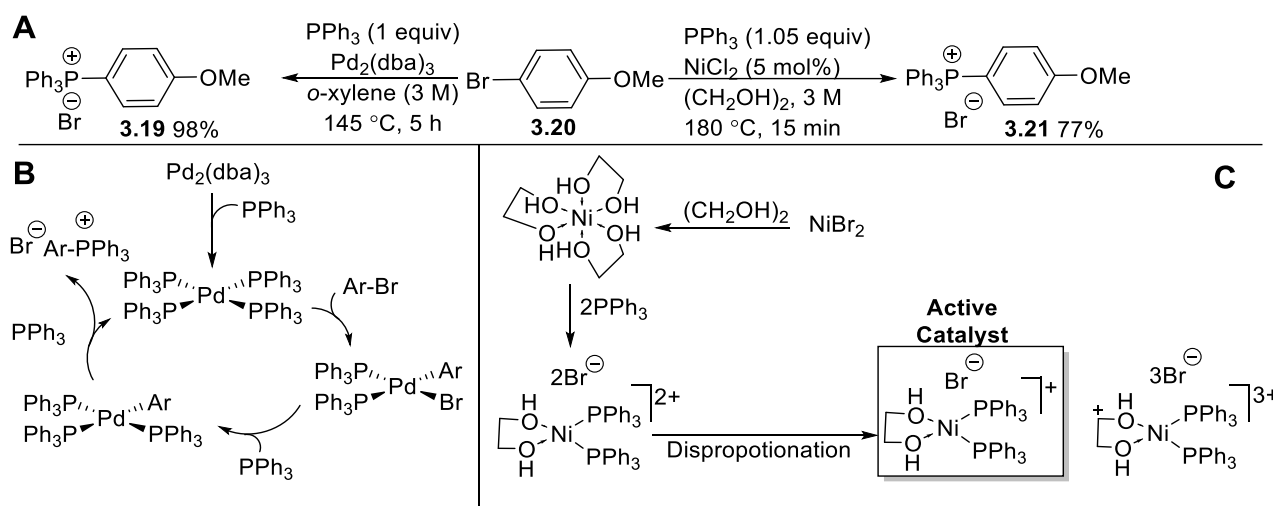
The synthesis of phosphonium salts changes depending on the type of phosphonium salt being created. Alkyl phosphonium salt can be easily generated by performing a S_N2 attack on an alkyl halide and as such are the most common of these salts with a majority of these substrates being commercially available (**Scheme 3.3**).^{200,201} The synthesis of aryl phosphonium salts on the other hand can be more challenging as simple substitutions are not always possible. In some instances, the nucleophilicity of phosphines can be taken advantage of in order create phosphonium salts via conjugate addition similarly to how phosphines serve for organocatalysis. An example of this can be seen in the synthesis of (1,4-dihydroxynaphthalen-2-yl)phosphonium triflate **3.18** (**Scheme 3.4**). PPh₃ was reacted with triflic acid to create triphenylphosphonium triflate that then performs a conjugate addition on 1,4-dihydroxynaphthalene to create a 1,4-dihydroxynaphthylphosphonium salt.¹⁸⁸ The ensuing phosphonium salt was then tested for antimicrobial activity as phosphoniums are known to penetrate the cell wall of the mitochondria and thus can serve as a method of targeted drug delivery.^{187,188}



Scheme 3.4- Synthesis of dihydroxynaphthalen-2-yl)phosphonium triflate via conjugate addition.¹⁸⁸

The most common way of synthesizing aryl phosphonium salts is by utilizing metal mediated cross-coupling. The initial discovery of this chemistry was established by Horner, who utilized nickel catalysts to create the arylphosphonium salts.²⁰²⁻²⁰⁴ Horner's methodology, however, suffered from high catalytic loadings and high temperatures, which greatly limited the applicability of the reaction. It was not until 40 years later that the

methodology was improved upon by Charette and Marcoux who displayed the synthesis of aryl phosphonium salts using either a palladium or nickel catalyst to perform a coupling reaction between a phosphine and an aryl halide to create an aryl phosphonium salt (**Scheme 3.5A**).^{205,206} The initial advancement was performed using Pd₂(dba)₃ as the catalyst and the authors showed that the coupling was able to proceed with aryl bromides, iodides and triflates and tolerate a wide range of functional groups. For the reaction to proceed a high temperature of 145 °C was required as well as a high boiling non-polar solvent such as toluene or xylenes. The use of a non-polar solvent helps drive the reaction forward as the resulting phosphonium salts precipitate out of solution.²⁰⁵ The catalytic cycle for the reaction is as follows: an oxidative addition occurs between the aryl halide and the catalyst; this is then followed by a ligand exchange and a reductive elimination yielding the phosphonium salt and regenerating the catalyst (**Scheme 3.5B**).

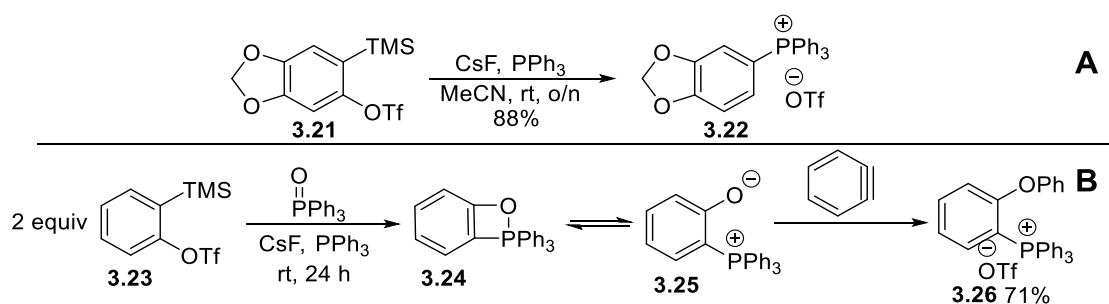


Scheme 3.5- A-Charette and Marcoux's synthesis of aryl phosphonium salts using either a Ni or Pd catalyst. B- Catalytic cycle for the metal catalyzed synthesis of aryl phosphonium salts. C- *In situ* formation of Ni(I) catalyst for the Ni catalyzed synthesis of aryl phosphonium salts.^{205,206}

That same year, another example of metal mediated synthesis of phosphonium salts was reported by the same group, only this time the reaction relied on the use of a nickel catalyst.²⁰⁶ Similar to the Pd catalyzed coupling, the reaction needed to be performed at high concentrations and at high temperatures, but the solvent was swapped for ethylene glycol. Whereas previously the coupling relied on the solubility of the phosphonium salts to drive the reaction, the nickel catalyzed couplings instead made use of a highly reactive complex formed between the metal center and the ethylene glycol to propel the reaction. The authors noted that the addition of ethylene glycol greatly improved the catalyst's turn over numbers (TON), and if the reaction was performed in other polar solvents, then

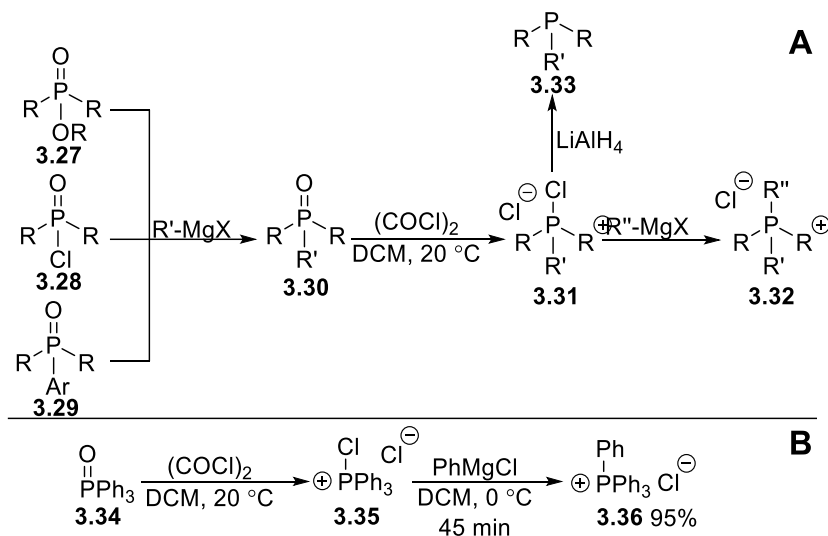
the reactivity would shut down or give poor yields. The mechanism of the formation of the active species for the Ni catalyzed synthesis of phosphonium salts is highlighted in **Scheme 3.5C**. As the Ni halide dissolves in ethylene glycol, it forms an octahedral complex with the ligand; PPh₃ can coordinate more strongly to the Ni center and thus displaces the glycol ligand. A disproportionation reaction then follows leading to the active Ni(I) species. It is believed that the Ni(I) complex is the active catalyst as it is the most reactive, however, Ni (II) and Ni (III) complexes also allowed for the reaction to proceed when isolated and re-introduced back into the reaction. Aside from the *in-situ* formation of the active catalyst, the Ni catalyzed synthesis of phosphonium salts follows the same catalytic cycle as the Pd catalyzed method outlined in **Scheme 3.5B**. The Ni system proved to be more versatile than its Pd counterpart as the reaction was able to functionalize aryl chlorides, bromides, iodides and triflates as well as display a similar functional group tolerance as the original reaction.

In addition to the metal catalyzed coupling other methods are available for the synthesis of aryl phosphonium salts. One of the simplest methods would be through the addition of a phosphine onto a benzyne. An example of this can be seen in **Scheme 3.6A**, where cesium fluoride was used to trigger an elimination that led to the creation of a benzyne. This was then followed by a nucleophilic attack of a phosphine onto the benzyne to create the salt. The reaction allows for a simple procedure to generate aryl phosphonium salts and allowed for several aromatic substrates and phosphines in moderate to high yield.¹⁷⁶ Although simplistic, this method suffers from two main drawbacks: firstly, for the reaction to proceed 2-(trimethylsilyl)aryl triflates are required. These substrates are easily converted into benzyne but are synthetically taxing to create greatly limiting the scope of the reaction. Secondly, the nature of the benzyne allows for the nucleophilic attack to occur at either end of the benzyne consequently this can create a mixture of regioisomers that cannot be separated through normal means.



Scheme 3.6-A-Benzyne mediated synthesis of aryl phosphonium salts.¹⁷⁶ **B**-Synthesis of aryl phosphonium salts through reaction of benzyne with triphenylphosphine oxide.²⁰⁷

Benzyne can also react with phosphine oxides to create aryl phosphonium salts. This unique reactivity utilizes 2-(trimethylsilyl)aryl triflates in tandem with phosphine oxides to generate a phosphonium salt with an adjacent phenyl ether.²⁰⁷ The mechanism of the reaction is hypothesized to proceed through an oxaphosphetane intermediate with benzyne that upon opening reacts with another equivalent of benzyne leading to the phosphonium salt (**Scheme 3.6B**).

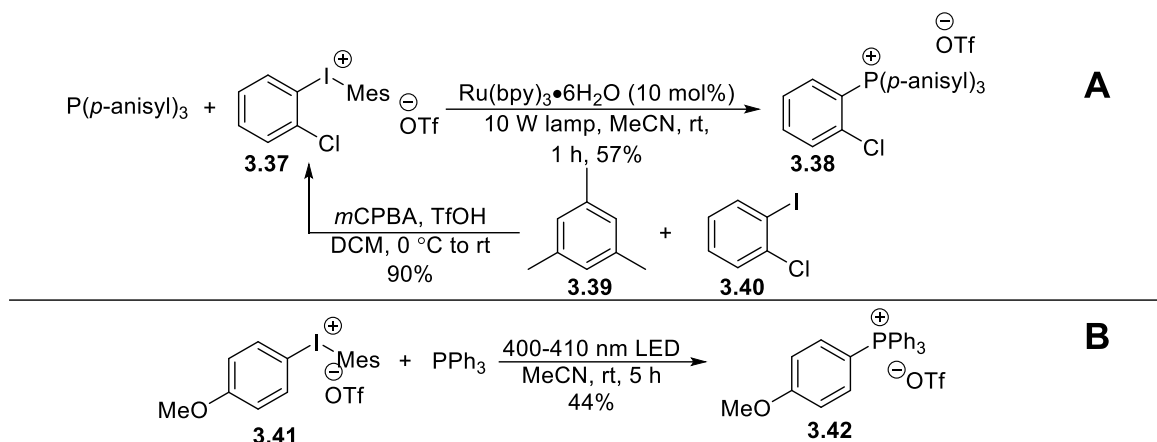


Scheme 3.7- Umpolung strategy for the synthesis of phosphonium salts and phosphines.^{181,208}

One of the most versatile techniques for the creation of phosphonium salts is through phosphine oxides as the molecules can be easily substituted to create various substituted phosphines and quaternary phosphonium salts. The general methodology is highlighted in **Scheme 3.7A**, where an alkyl or aryl Grignard can be used to displace a group on the phosphorus center to create a new phosphine oxide.^{181,208} The leaving group for the attack can be a halogen such as a chloride, an alkoxy/ phenoxy group and in some cases an aryl group can also be displaced. The substitution of an aryl group can occur in phosphines oxides through the use of strong nucleophiles such as organolithiums and Grignard reagents. This chemistry is somewhat unique to phosphine oxides as aryl groups are usually poor leaving groups and do not submit to substitutions.²⁰⁹ Once the desired phosphine oxide is reached, it can be converted into the corresponding chlorophosphonium salt by deoxygenating with oxalyl chloride at room temperature. This chlorinated salt can then be converted back to a phosphine by means of a reduction with LiAlH₄ or transformed into a phosphonium salt via a Grignard reagent this time replacing the chlorine. Additionally, the use

of this methodology allows for the creation of unique phosphine ligands starting from inexpensive phosphine oxides.

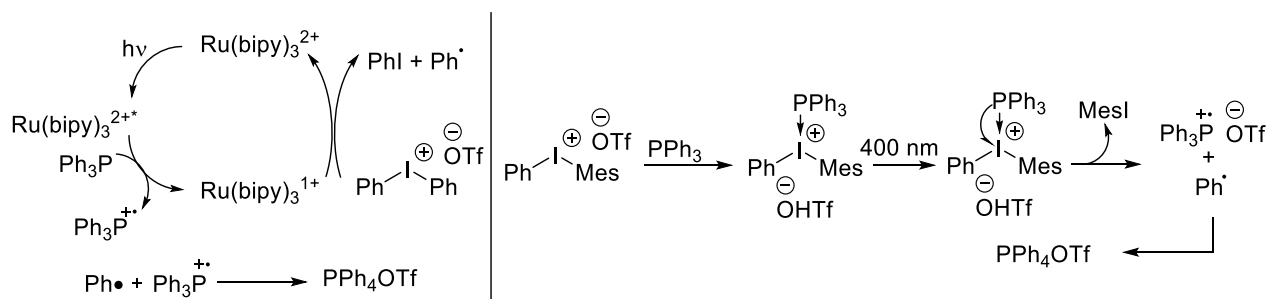
Scheme 3.7B highlights an example of the synthesis of a phosphonium salt starting from the easily available triphenylphosphine oxide to reach the tetraphenylphosphonium chloride in a 95% yield over two steps.



Scheme 3.8- A- Synthesis of aryl phosphonium light using a Ru photocatalyst under visible light.²¹⁰ **B-** Synthesis of aryl phosphonium salts under metal/catalyst free conditions utilizing 400 nm (purple) light.¹⁷⁵

Finally, one of the more modern ways of creating phosphonium salts is through photocatalysis (**Scheme 3.8A**). In a 2016 report, the synthesis of arylphosphonium salts was reported using a ruthenium photocatalyst. The reaction was proposed to proceed through a radical pathway under visible light and furnished a wide variety of phosphonium salts in high to moderate yields.²¹⁰ Unlike the previously mentioned synthesis of phosphonium salts, the use of photocatalysis allowed for a mild method for creating arylphosphonium salts. However, this came at a price as the reaction required a relatively high catalytic loading and utilized diphenyl iodonium triflates which, similarly to 2-(trimethylsilyl)aryl triflates, can be synthetically taxing to make and are limited by the availability of aryl iodides. Soon after the Ru photoredox synthesis of arylphosphonium salts was reported, a similar method was reported which excluded the use of a catalyst and was able to yield arylphosphonium salts solely under light (**Scheme 3.8B**). Starting from diphenyliodonium triflates the reaction was able to yield arylphosphonium salts by simply irradiating the iodonium triflates under 400 nm light in the presence of a phosphine.¹⁷⁵ The reaction proceeded with modest to high yields and surpassed the previously established methodology by displaying a large functional group tolerance and reaction scope. Once again, the main drawback of the reaction was the use of diphenyl iodonium triflates, which allows the reaction to proceed due to the weak carbon iodide bond. The mechanisms for both reactions are highlighted in **Scheme 3.8**. The reaction proceeds by creating an aryl radical under light. For the Ru

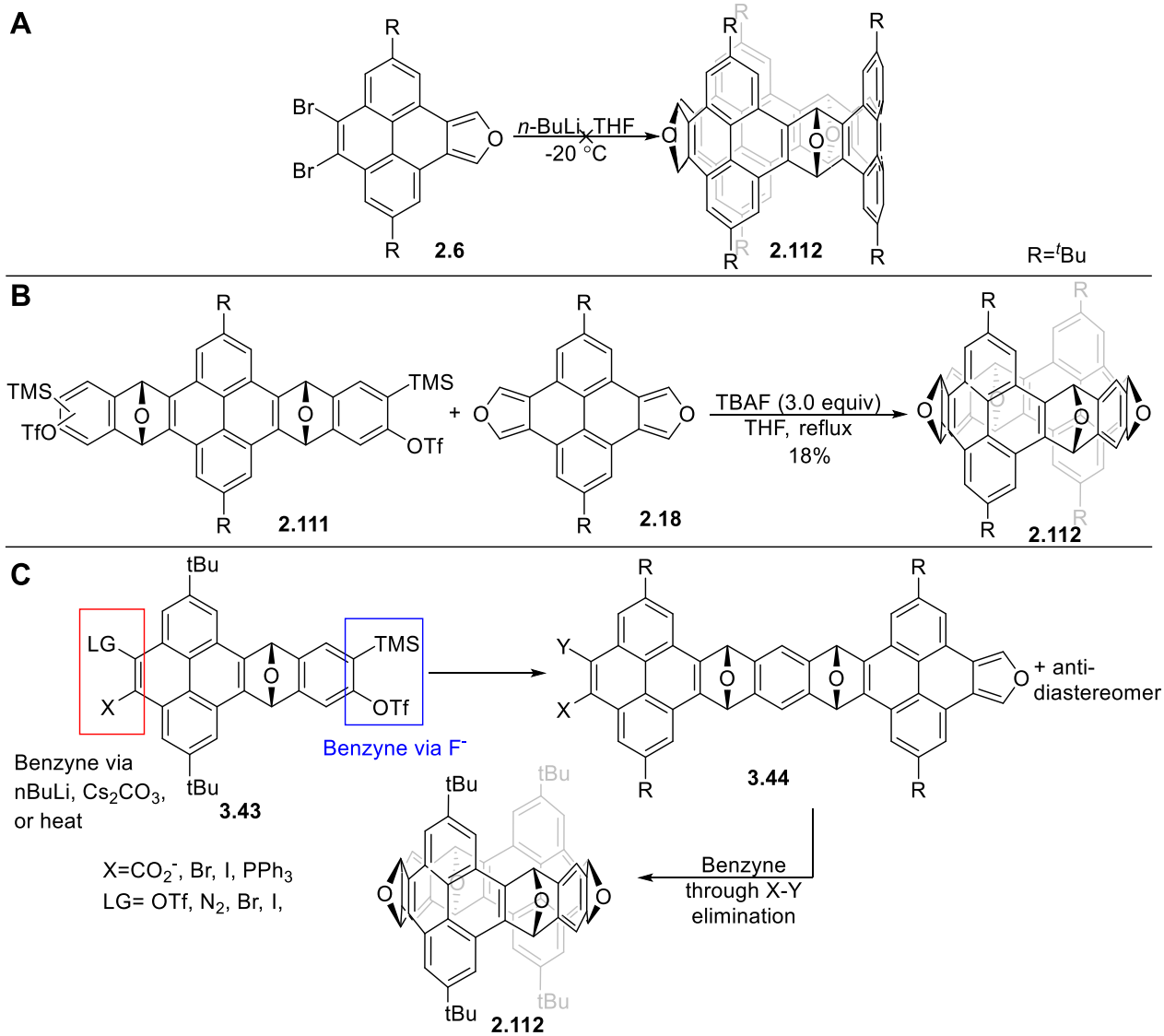
catalyzed method, the Ru center was proposed to create both the phosphorus radical cation and the aryl radical. While the metal free version of the reaction relies on a single electron transfer from the phosphine to the iodonium which is promoted by using a higher energy wavelength than in the Ru catalyzed example. For both examples the mesityl group serves as a dummy group and is usually not transferred, this is due to both steric and electronic factors.



Scheme 3.9- (Left) Catalytic cycle for the synthesis of tetraaryl phosphonium salts using a Ru photocatalyst under visible light.²¹⁰ (Right) Metal free synthesis of arylphosphonium salts using visible light.¹⁷⁵

3.3 BENZYNES FROM PHOSPHONIUM SALTS AND APPLICATIONS TOWARDS THE SYNTHESIS OF CYCLACENES

As we began exploring different pathways to create cyclacenes it became apparent that the formation of benzyne through a lithium halogen exchange was problematic specially when dealing with larger molecules. Samples subjected to a lithium halogen exchange resulted in either low yields or an inseparable mixture of products (**Scheme 3.10A**). It remains unclear as to why the reaction began to fail. Nonetheless, we found that fluoride mediated benzyne was key in allowing the formation of the ring in our hands and thus we began conceptualizing other mild methods for the creation of benzyne in our systems. We eventually arrived at phosphonium salts as a potential candidate for a novel way of creating benzyne which led us down a path to discover the chemistry outlined in the rest of the chapter.

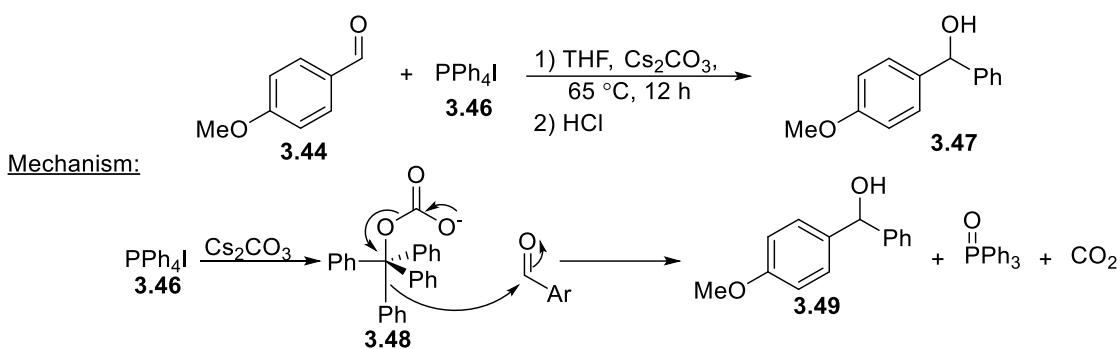


Scheme 3.10-A initial attempted synthesis of a 9-epoxycyclacene using an AB-cyclization triggered by a lithium halogen exchange with $n\text{-BuLi}$. **B-** First successful cyclization of a pyrene epoxycyclacene in our laboratory using a benzyne triggered by the addition of fluoride. **C-** Proposed monomer with orthogonal benzyne reactivity for the stepwise construction of a pyrene cyclacene.

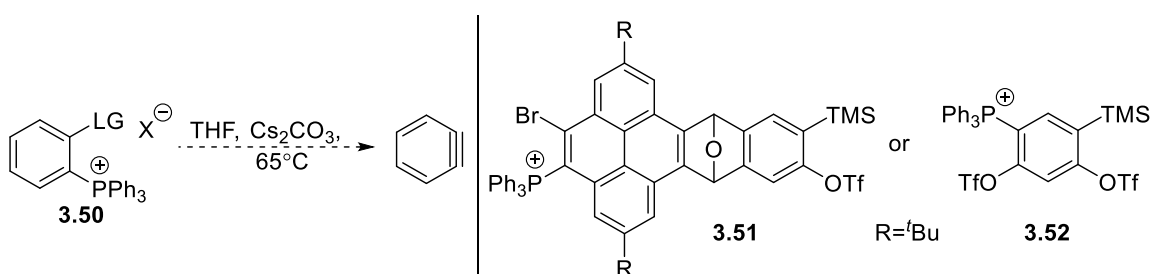
Although effective, the use of fluoride to trigger the benzyne formation did create unwanted side products leading to a low yield for the cyclic product (**Scheme 3.10B**). One potential solution was to perform the cyclization in a stepwise fashion. To achieve this, an orthogonal reactivity between the benzyne precursor was required to minimize the total number of unwanted products from the reaction. In other words, one side of the pyrene would be activated by fluoride which would lead to the creation of the *syn*- and *anti*-trimers. The diastereomers would then be separated and the *syn*-isomer would be cyclized by activating the remaining benzyne precursor (**Scheme**

3.10C). One potential candidate we sought as our new benzyne precursor was the creation of a phosphonium salt that would be stable to the desilylation conditions and in theory would allow for a mild benzyne formation.

Phosphonium salts have recently been shown to function as a mild arylating agents under the presence of Cs_2CO_3 . In the seminal publication by Xiao *et al.*, arylphosphonium salts were reacted with various aldehydes, imines and ketones to yield the corresponding alcohols in good yields.¹⁹⁷ The reaction works by having the Cs_2CO_3 attack the phosphorus center which in turn releases phosphine oxide and carbon dioxide driving the reaction forward. Upon the collapse of the phosphorus center an aryl nucleophile is created which then performs a nucleophilic attack on the carbonyl group (**Scheme 3.11**). In essence, we can think of the reaction of $^+\text{PPh}_4$ and Cs_2CO_3 to formally create an aryl anion. Therefore, if the phosphonium salt has a good leaving group nearby then it may be possible to use the creation of this formal aryl anion to force an elimination and form a benzyne using only Cs_2CO_3 (**Scheme 3.12**).



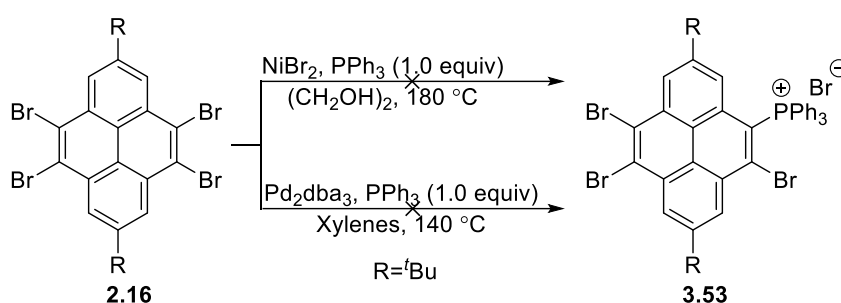
Scheme 3.11- Nucleophilic arylation with tetraarylphosphonium salts.¹⁹⁷



Scheme 3.12-(Left)Formation of benzyne through the elimination of a phosphonium salt. (Right) Target benzyne precursors for the stepwise formation of pyrene cyclacenes.

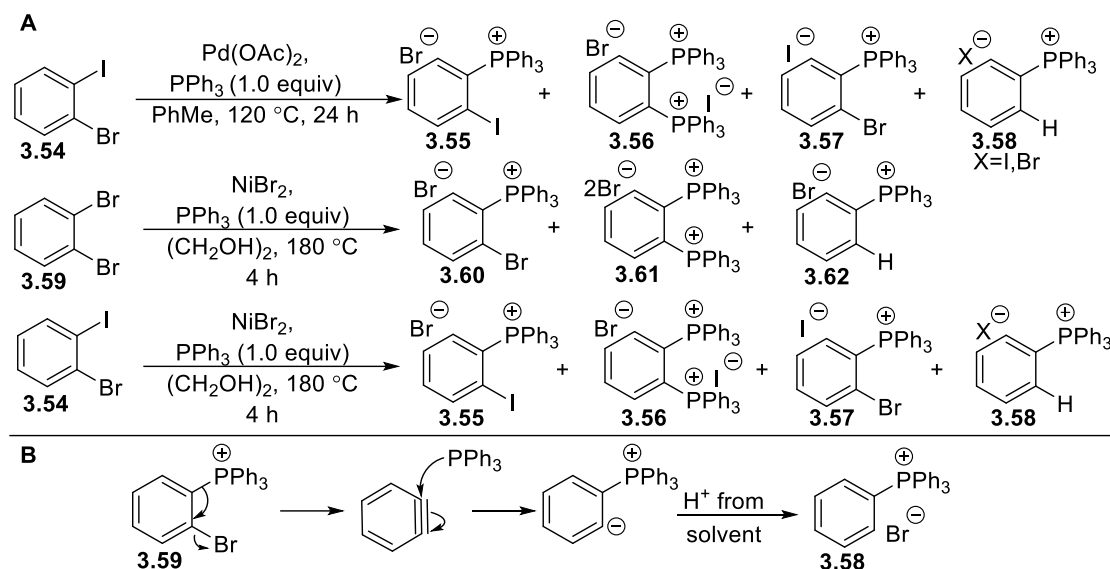
With this in mind, we began investigating the formation of arylphosphonium salts for creating benzyne for the purpose of aiding in our attempts to create a cyclacene. We envisioned a molecule such as **3.51** or **3.52** which could create benzyne orthogonally from either the addition of fluoride or Cs_2CO_3 . In order to synthesize these

molecules, we sought to perform a metal mediated coupling of tetrabromopyrene **2.16** with triphenylphosphine using either a Ni or Pd catalyst. Unfortunately, neither attempt resulted in the formation of the desired product and returned mostly unreacted starting material (**Scheme 3.13**). This is most likely due to the insolubility of the tetrabromopyrene **2.16** and potentially to a lesser extent the steric bulk in the *K*-regions of the pyrene. We encountered a similar problem when trying to attach TMS groups onto tetrabromopyrene **2.16** leading us to believe that the best approach was to perform a Diels-Alder reaction with another small molecule with the desired groups already attached.



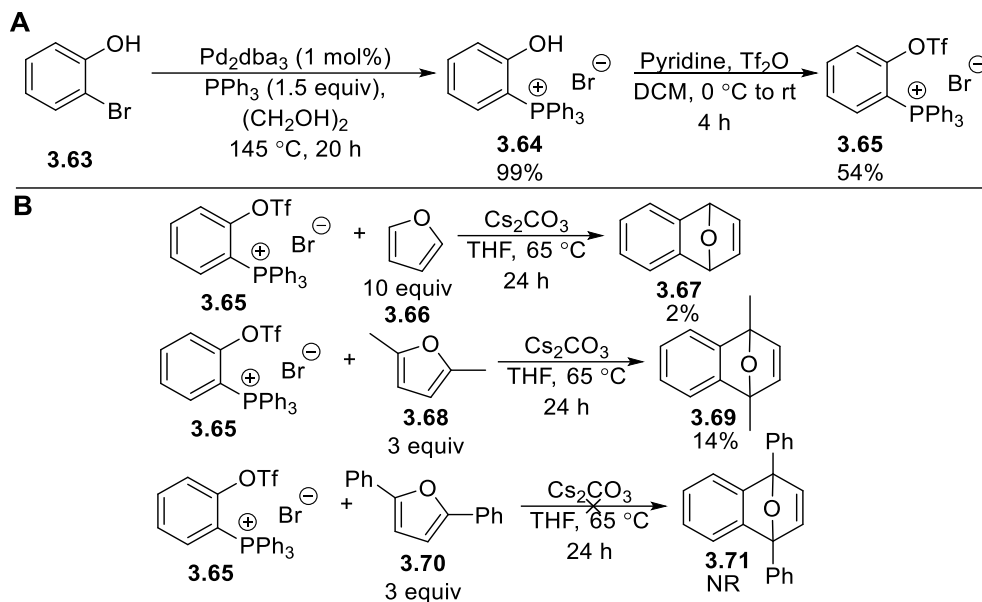
Scheme 3.13- Attempted synthesis of pyrene arylphosphonium salt through metal catalyzed cross-coupling.

We took a step back in our approach and decided to target compounds **3.55** or **3.56** as our test molecule for the benzyne precursor. 1,2-Dihalobenzenes were chosen as the model molecules as they resembled our available pyrene starting material the closest. Once again, we attempted to create this molecule using transition metal coupling and we were delighted to find that the reaction was able to proceed. Unfortunately, the high reactivity meant that some of the reactants coupled at both halogens creating a doubly charged molecule. Due to the high polarity exhibited by these salts any attempt at separating these compounds was unsuccessful and the different products were only able to be observed via mass spectrometry (**Scheme 3.14A**). This is consistent with previous reports as separating different phosphonium salts in the same mixture is often not possible by conventional chromatographic methods. In addition to the di coupled product, the formation of PPh_4^+ was also observed through mass spectrometry. The origin of this apparent reduction seems unclear, one possible hypothesis for its formation may be through the formation of benzyne which upon reacting with PPh_3 can abstract a proton from solvent or any residual water. The elimination may occur spontaneously at the high temperature the reaction is being conducted at or a nucleophile such as I^- or Br^- may attack the phosphorus center initiating the elimination (**Scheme 3.14B**).

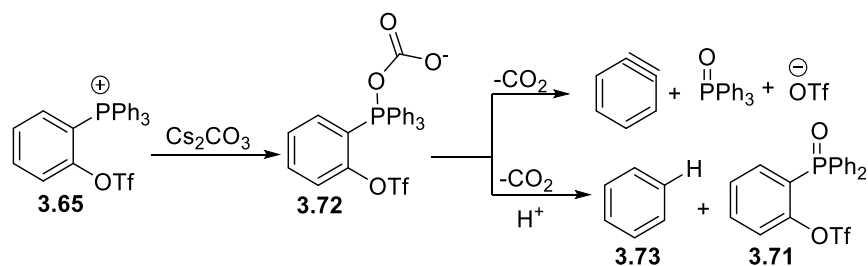


Scheme 3.14- **A**-Attempted synthesis of phosphonium benzyne precursor through metal catalyzed synthesis of tetraaryl phosphonium salts. **B**-Possible reduction mechanism for the metal cross coupling of 1,2-dihalobenzenes.

After observing the lack of selectivity when attempting to create arylphosphonium salts from 1,2-dihalobenzenes, we opted for a different route to create our benzyne precursor. Thus, we reacted PPh_3 with 2-bromophenol and were pleased to observe a quantitative yield for the cross-coupling reaction to obtain salt **3.13** (**Scheme 3.15A**). After obtaining our salt, we then converted the alcohol to the triflate using triflic anhydride and pyridine arriving at our phosphonium benzyne precursor **3.14** (**Scheme 3.15A**) in a 54% yield. With our benzyne candidate in hand, we tested our phosphonium salt to see if it could indeed function as a mild way to create benzyne. **3.14** Was reacted with Cs_2CO_3 and an excess of furan for 24 h in THF and the reaction was able to proceed to produce the epoxynaphthalene **3.15** (**Scheme 3.15B**) in a 2% yield. Having prior experience performing Diels-Alder reactions with furan made us suspect that the reaction may have failed due to the high volatility of the furan. Even though the reaction was carried out in a sealed vessel with an excess of the furan we would not be surprised if at the reaction temperature the furan was still able to escape the reaction vessel. We then performed the reaction with 2,5-dimethylfuran, a less volatile diene, and saw a 14% yield when the exact reaction conditions were repeated. We were still suspicious of that the volatility of the compound may be hindering the reaction, so we tested our reaction with 2,5-diphenylfuran and found that our reaction was not able to produce the epoxynaphthalene **3.17**.



Scheme 3.15-A-Synthesis of phosphonium benzyne precursor. **B**-Attempted Diels-Alder reaction with furan and Cs_2CO_3 generated benzyne.

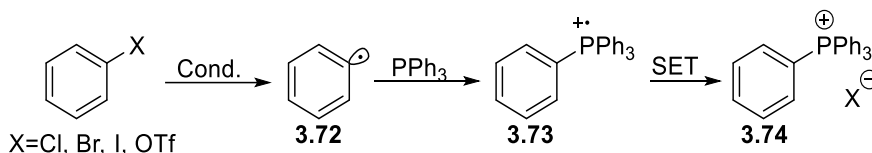


Scheme 3.16-Possible degradation pathway for **3.14** under Cs_2CO_3 .

When the reaction was scanned by ^{31}P NMR we saw roughly a 1:1 ratio between the phosphonium salt and the phosphine oxide. If our mechanism is true and 50% of the starting material converted to the oxide, then in theory we should expect a 50% yield back for the cycloaddition. The degradation of phosphonium salts when exposed to carbonate bases has been previously studied²¹¹⁻²¹³ and it is possible that rather than eliminating to produce a benzyne, the phosphonium salt was simply being transformed to the phosphine oxide or more likely the aryl anion may be being formed in one of the other aryl ligands which consequently would limit our yield to 25% if the degradation pathway is non-selective (**Scheme 3.16**). There are other experiments that could have been performed

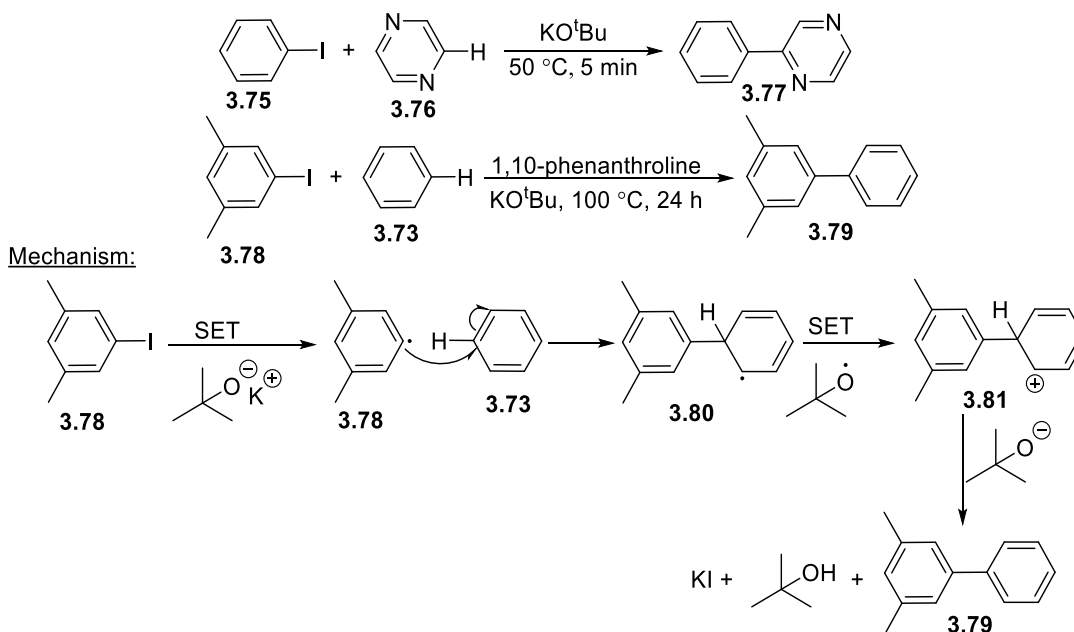
to check for the existence of the benzyne, such as introducing a nucleophile to attack the benzyne, however due to time constraints and the initial observed yields, this was not explored further.

3.4 SYNTHESIS OF ARYLPHOSPHONIUM SALTS THROUGH ALKALI BUTOXIDE ELECTRON TRANSFERS



Scheme 3.17- General scheme for the radical coupling of a phosphine to an aryl radical to form an arylphosphonium salt.

While trying to synthesize our benzyne precursor **3.14**, we became interested in ways of synthesizing phosphonium salts and wanted to create a new method that removed the need for harsh transition metal catalyzed conditions; as such, we set out to experiment and try to create new ways of creating arylphosphonium salts. Inspired by the photocatalytic synthesis of phosphonium salts outlined by Denton *et al.*, we set our sights on a radical based approach to creating phosphonium salts but aimed at improving the method by removing the diphenyl iodonium triflates required for the reaction to take place (**Scheme 3.17**).^{175,210}



Scheme 3.18- *tert*-Butoxide mediated radical coupling of aryl halides with aromatics and heteroaromatic groups.^{214,215}

We began by investigating the use of butoxide bases as a way of creating aryl radicals. Previous reports have highlighted that the use of alkali butoxide bases can be used to create aryl radicals from aryl halides that can go on to create bi-aryl systems.^{214–217} Potassium or sodium *tert*-butoxide are the reagents of choice and are theorized to react via a single electron transfer (SET) to the aryl halide creating a radical anion which then fragments into the aryl radical and corresponding halide anion. This new radical can then attack another aryl group which upon another SET yields an aryl cation that is then deprotonated to regain aromaticity creating the new bi-aryl molecule (**Scheme 3.18**). Often these reactions are carried out in the presence of a phenanthroline ligand whose function is to coordinate to the alkali metal as well as hold the aryl halide through π - π interactions to facilitate the SET (**Figure 3.3A**).²¹⁵ When dealing with nitrogen bearing heterocycles the ligand is no longer required as the heterocycle fulfills the role of the ligand by having the nitrogen coordinate to the alkali metal (**Figure 3.3B**), accelerating the reaction.²¹⁴ Consequently, when radical couplings are being performed with pyrazines the reaction proceeds at lower temperature and in a shorter time.

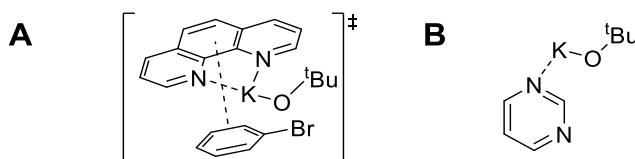
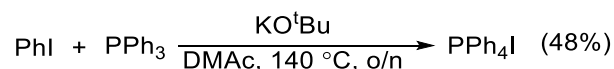


Figure 3.3-Coordination complexes between potassium *tert*-butoxide and nitrogen heteroaromatic molecules.^{214,215,217}

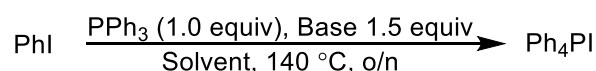
Having seen the potential of alkali *tert*-butoxides as a method for creating aryl radicals, we set out to create arylphosphonium salts by attempting to combine an aryl radical with a phosphine, starting with triphenylphosphine. Initially, we reacted iodobenzene with PPh_3 in DMAc with KO^tBu and were pleased to observe that after reacting overnight and allowing the reaction to cool we were presented with a clear precipitate (**Scheme 3.18**). This solid was in fact tetraphenylphosphonium iodide, which was confirmed by ^1H , ^{31}P and HRMS, and was obtained in a 48% yield after reacting overnight. The presence of a phosphorus atom in our chemistry allows for the facile screening of reactions as phosphorus is NMR active and provides a very simple spectrum. For most of the initial optimization, the reaction mixtures were aliquoted without any purification and were further diluted with deuterated chloroform to allow the NMR spectrometer to lock to the sample. The yields were determined using an internal standard (triphenyl phosphate). We observed the phosphonium salts appearing around ~ 25 ppm, the phosphine oxides around ~ 40 ppm

and the phosphines around ~5 ppm which allowed for the facile quantification of the individual components of the reaction. It should be noted that due to the crude nature of the NMR sample, the compound's NMR shifts would move slightly depending on the solvents present within the NMR tube. Additionally, an inverse gated NMR experiment was performed for all ³¹P NMR yields to negate any potential nuclear Overhauser effect (NOE) that may affect the outcome of the NMR yield.



Scheme 3.19-Optimized conditions for the synthesis of tetraarylphosphonium salts from aryl iodides and potassium *tert*-butoxide.

Following the initial success of the reaction it was quickly screened in a variety of solvents; however, DMAc, which was our initial choice, proved to be the ideal solvent for the reaction. The reaction time was also screened, and we were pleased to observe the yield was maximized after reaction for approximately one hour. Different alkali butoxides were also screened, in powdered form and from a standard solution, and we observed that the reaction yield improved by utilizing a 2 M solution of NaO^tBu (**Table 3.1**). The temperature and equivalents for the reaction were also screened leading us to the conditions outlined in **Scheme 3.19** with NaO^tBu as the base, DMAc as the solvent for 1 h at 145 °C. As a final attempt to boost the yield of the reaction, we performed the reaction in the presence of Cs₂CO₃ and Rb₂CO₃. The hope was to exchange the counter-ion in situ which would then further boost the reactivity of the base in a similar way as to how Schlosser's base is constructed.²¹⁸

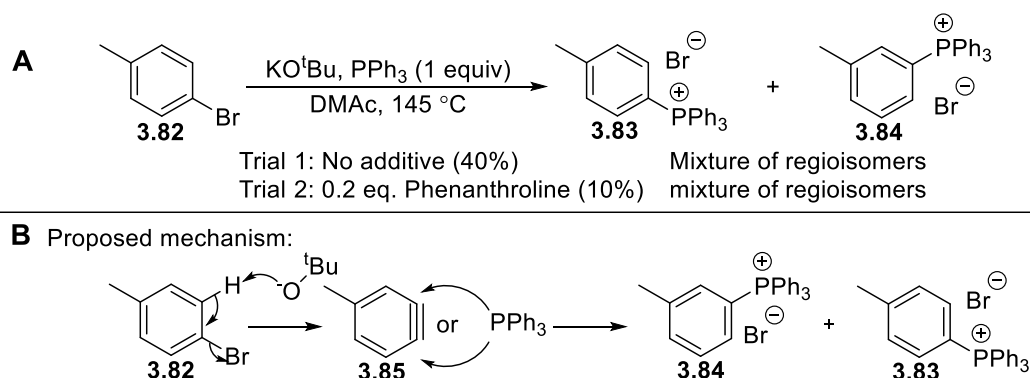


Entry	Base	Solvent	Yield (%)
1	NaO ^t Bu	DMAc	NR
2	NaO ^t Bu	THF	NR
3	NaO ^t Bu	neat	NR
4	NaO ^t Bu	MeCN	5
5	KO ^t Bu	MeCN	26
6	KO ^t Bu	DMAc	48
7 ^a	NaO ^t Bu	DMAc	nr
8 ^a	NaO ^t Bu	THF	49

Table 3.1-Reaction optimization for the metal free synthesis of arylphosphonium salts using *tert*-butoxide bases.

To ensure that the reaction was proceeding through a radical mechanism, we ran a trial with 4-bromotoluene to observe whether the radical was forming at the halide and were disappointed when we observed

a mixture of regioisomers resulting from the reaction (**Scheme 3.20A**). We therefore concluded that the most likely mechanism for the observed product was through a benzyne which formed through the elimination of the halide (**Scheme 3.20B**). This mechanism was further verified as previous reports have also observed the creation of a benzyne by an ortho elimination with a butoxide base.^{216,219,220} In a final attempt to create the radical, we re-ran the reaction using a phenanthroline ligand with the hope that ligand would force the reaction to a SET pathway rather than having the butoxide act as a base. Unfortunately, the ligand seemed to have little to no effect leading us to attempt and devise another method of creating our desired phosphonium salts. Finally, it should be highlighted that the previously described chemistry allows for the creation of phosphonium salts using only KO^tBu without requiring 2-(trimethylsilyl)aryl triflates. This is an improvement over the prior reports from Rémond *et al.*¹⁷⁶ and Neog *et al.*,²⁰⁷ however, our goal was to create a better synthetic route to construct arylphosphonium salts that proceeds via an SET pathway to limit the number of products from the reaction. Consequently, this was not investigated any further but may be worth revisiting in the future as a means to rapidly create arylphosphonium salts.

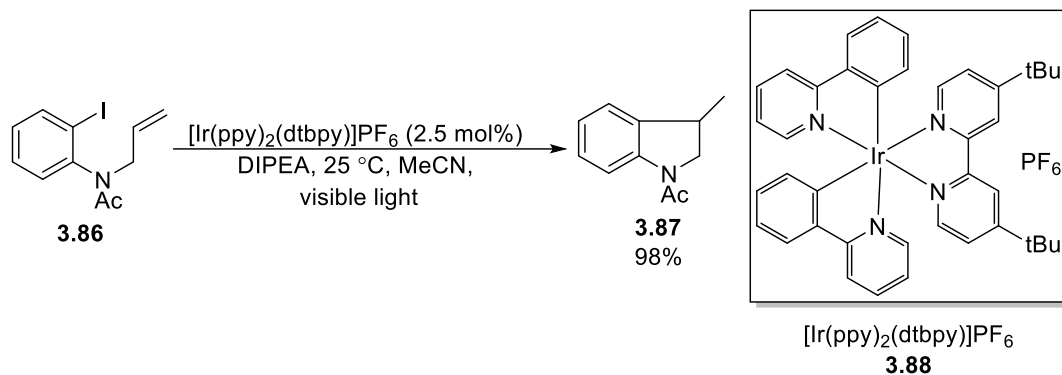


Scheme 3.20- A- Test reaction for the determination of a radical or benzyne mechanism. **B-** Mechanistic rationale for the formation of observed regioisomers.

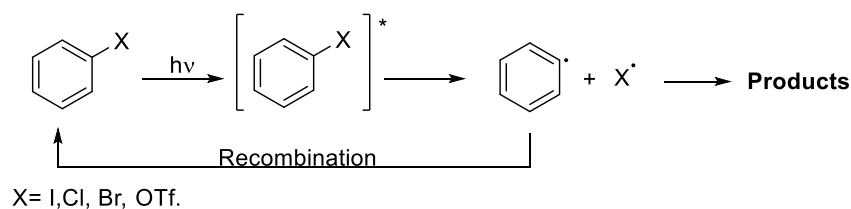
3.5 LIGHT AS A TOOL IN ORGANIC SYNTHESIS.

Light can be an extremely powerful tool in organic chemistry as the use of photons to drive chemistry can create unique reactivity without the need for additional reagents (**Scheme 3.21**). One of the more modern uses of light was pioneered by MacMillan and makes use of a metal or organic photocatalyst to mediate a wide variety of transformations under visible light. This type of photocatalysis can be further coupled with other metal catalysis to allow for a variety of unique transformations.²²¹ Unfortunately, there appears to be only a single report that utilizes

a photocatalyst for the formation of phosphonium salts.²¹⁰ As discussed previously, this method utilized aryl iodonium triflates which can be synthetically taxing and greatly reduce the applicability of the reaction. The wide appeal and promise of a light mediated formation of phosphonium salts made us set our sights on creating a new method for synthesizing phosphonium salts using ultraviolet light (UV) as it had been previously shown to promote a wide variety of reactions for creating carbon-carbon bonds as well as other transformations.



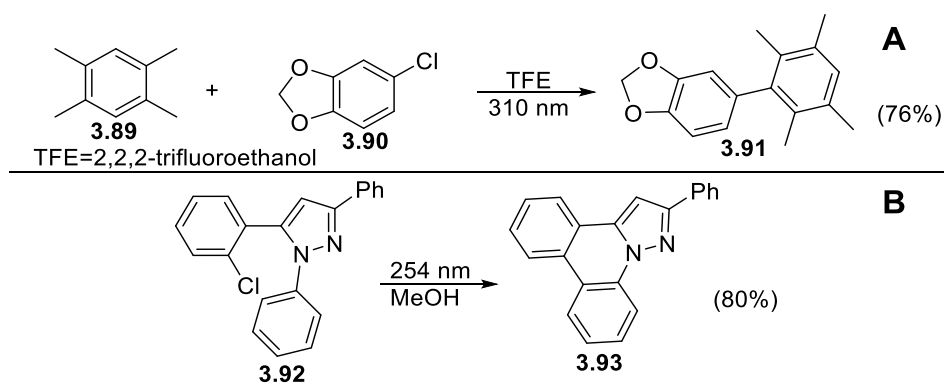
Scheme 3.21-Radical cyclization of aryl iodides using a $[\text{Ir}(\text{ppy})_2(\text{dtbbpy})]\text{PF}_6$ photocatalyst.²²²



Scheme 3.22- Homolytic dissociation of aryl halides under ultraviolet irradiation.

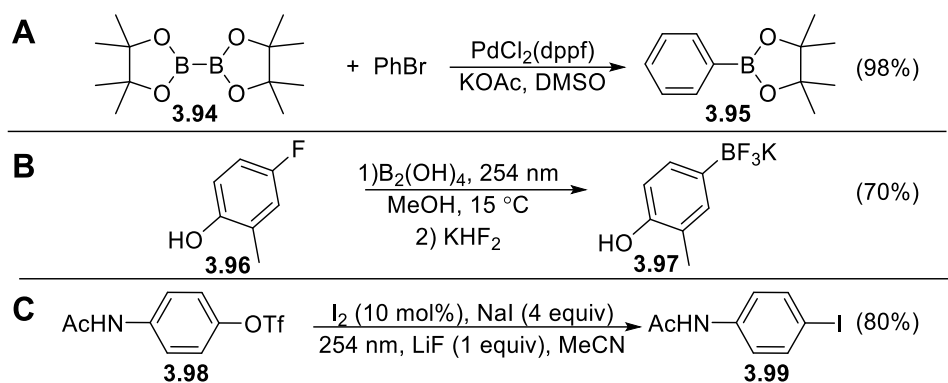
The irradiation of aryl halides under ultraviolet light can trigger a homolytic cleavage between the halide and the aryl group. This newly formed radical can then either recombine to return to the starting material or can proceed to form a wide variety of new bonds (**Scheme 3.22**).²²³ Although powerful, this reactivity is often overlooked despite allowing for unique transformations that would otherwise require additional reagents or simply do not occur. The simplest use of UV mediated transformation is for creating carbon-carbon bonds, this type of reactivity can occur either intermolecular or intramolecular and can often be observed in total synthesis as a way of creating rings. Two examples of this reactivity are highlighted in **Scheme 3.23**. In the top example, UV light is used in tandem with aryl chlorides as a way of creating biaryls following a similar mechanism as outlined in **Scheme 3.18**. The aryl

radical this time being created via homolysis of the C-Cl bond by UV light.²²⁴ By applying UV light to the reaction, the traditional methods by which biaryls are synthesized are bypassed thus removing the need for any transition metals or organometallic reagents. It is important to note that reaction can proceed under sterically hindered environments and can even be compatible with aryl fluorides which are usually inert to transition metals. The second example involves the intramolecular cyclization of an aryl halide under UV irradiation and can be seen in **Scheme 3.23-B**. For this example, the photocyclization of phenylpyrazoles was investigated and it was seen that irradiation at 254 nm was able to cyclize the product cleanly for aryl chlorides, bromides, iodides, and some ethers and esters.²²⁵ Additionally, the reaction was able to proceed at higher wavelengths when performed with benzophenone as a sensitizer but only with the aryl halides.



Scheme 3.23- A- Intermolecular photocyclization for the formation of biphenyls. **B-** Intramolecular photocyclization of phenyl pyrazoles

The application of UV light in organic synthesis applies well beyond the construction of carbon-carbon bonds, the method can also be used to construct bonds between aryl halides and other heteroatoms. One useful application of UV in synthesis is for the construction of boronate esters and acids from aryl halides. Typically, these substrates are constructed using a palladium-catalyzed coupling between either an alkyl boronates or tetrahydroxydiboron to yield the corresponding aryl boronate or aryl boronic acid (**Scheme 3.24A**).^{226,227} Although useful, alternatives to transition metal catalyzed couplings are always desired in order eliminate or reduce the use of expensive metal catalyst and ligands required to carry out these transformations.

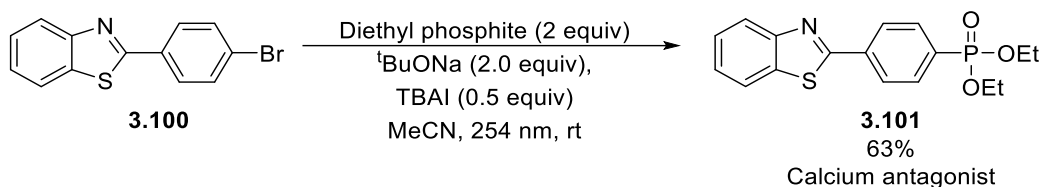


Scheme 3.24-A- Traditional Miyaura borylation of bromobenzene with pinacol borane.^{226,227} **B-** UV light synthesis of aryl boronates from aryl fluorides.²²⁸ **C-** Synthesis of aryl iodides from aryl triflates under UV conditions.²²⁹

Larionov *et al.* were able to demonstrate the coupling of aryl halides with boronic esters and acid by simply exposing the reagents to UV light (**Scheme 3.24A**).²²⁸ This methodology is powerful as it not only removes the need for transition metals but allows for the activation of previously inert bonds to Miyaura borylation conditions. Furthermore, since the reaction was being carried out with light it is amenable to be carried out in flow, thus allowing for a more efficient reaction that can be applied well to an industrial setting. Much like the other UV reactions listed in this chapter, the reaction operates by creating an aryl radical under UV light and then reacting with tetrahydroxydiboron or a diboronic ester to create the desired boronic acid or boronate. The reaction tolerates a wide range of substrates such as aryl chlorides, bromides and iodides and can even borylate aryl fluorides and aryl ammonium salts. Li *et al.* reported a similar finding in which aryl triflates are irradiated with UV light and subsequently transformed into aryl boronates or aryl iodides, both of which are highly desired substrates in synthesis (**Scheme 3.23C**).²²⁹ More importantly, since aryl triflates are synthesized from phenol this provides a pathway in which a phenol can somewhat function as a synthon for either an aryl boronate or iodide. The formation of aryl iodides from aryl triflates is a particularly interesting example as, on paper, the aryl iodide would be more reactive than the aryl triflate under UV conditions. Nonetheless, the authors were able to display that a wide array of compounds could be transformed from aryl triflates to aryl iodides under UV conditions.

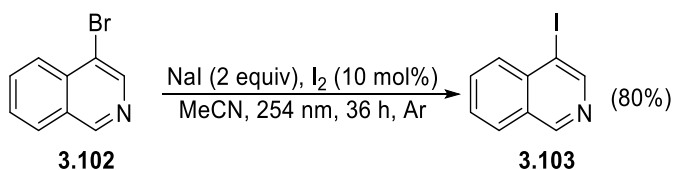
UV light can also be utilized as a way for constructing carbon-phosphorus bonds without the addition of additional reagents or catalysts. In 2019, Li *et al.* were able to demonstrate the use of UV light for constructing aromatic phosphonates without the need for transition metals (**Scheme 3.25**).²³⁰ In this example an aryl halide is irradiated in the presence of an H-phosphonate to create an aryl phosphonate. Once again, the versatility of UV light

in synthesis is put on display as the reaction proceeds with aryl chlorides, bromides and iodides and a variety of substrates containing electron withdrawing and donating groups, as well as heterocycles. The true value of the reaction comes in the form of providing a method to create these phosphonates, often found in pharmaceutical compounds, without ever introducing any metal compounds into the overall synthesis.



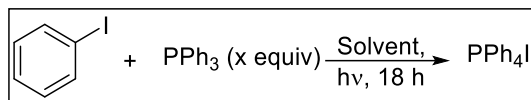
Scheme 3.25- Synthesis of a calcium antagonist via UV coupling of H-phosphonates.²³⁰

Finally, rather than creating bonds to other heteroatoms or carbon atoms, UV light can be used to effect an aromatic “Finkelstein” transformation in which either an aryl bromide or chloride can be switched for an iodine (**Scheme 3.26**).²³¹ This reaction is of great importance as aryl iodides can be more reactive and allow for reactions such as Suzuki, Heck and Buchwald-Hartwig reactions to proceed without any additional additives and under mild conditions.^{232–234} The reaction works by reacting an aryl radical, generated via UV, with NaI in the presence of 10 mol% I₂. Much like the classical Finkelstein, the reaction is carried out in MeCN causing the NaBr byproduct to precipitate out of solution driving the reaction forward. The iodine was introduced into the reaction to suppress any reduction of the aryl halide via hydrogen abstraction by creating an excess of aryl radicals.



Scheme 3.26- UV mediated aromatic “Finkelstein” of 4-bromoisoquinoline.²³¹

3.6 PHOTOPHOSPHORYLATION OF ARYL HALIDES WITH TRIPHENYLPHOSPHINE UNDER UV LIGHT

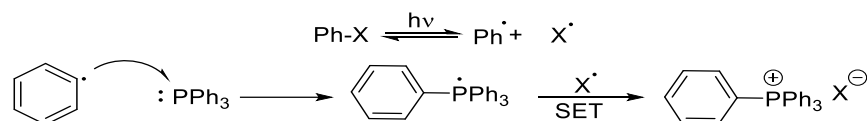


Entry	PPh ₃ (equiv.)	Solvent	λ (nm)	Yield (%)
1	2	MeCN	254 ^[a]	29
2	2	MeCN	350	30
3	2	Et ₂ O	350	4
4	2	Acetone	350	74
5	2	DMSO	350	70
6	2	EtOH	350	23
7	2	MeCN	300	58
8	2	Acetone	300	62
9	2	DMSO	300	71
10	3	DMSO	300	99
11	3	MeCN	254	49

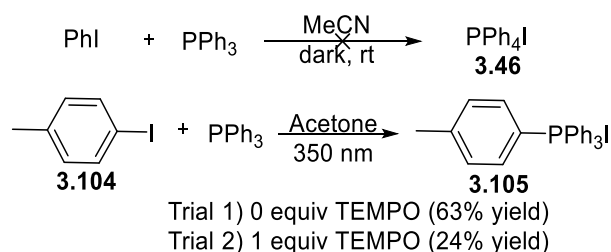
Table 3.2-Optimization for the UV synthesis of tetraphenyl phosphonium iodide from iodobenzene and triphenylphosphine. Reactions were performed in 0.2 M concentration for 18 h.[a]-reaction performed under UV light using a handheld TLC light for 4 h.

After observing all the potential synthetic possibilities that UV light can bring forth, we set out to construct arylphosphonium salts using UV light. To begin our investigation, we irradiated iodobenzene in MeCN at 254 nm using a handheld TLC lamp in the presence triphenylphosphine in a quartz cuvette. After 4 h we were pleased to observe a new polar spot by TLC which after isolation proved to be tetraarylphosphonium iodide in a 29% yield (**Table 3.2-Entry 1**). Iodobenzene was chosen as the dissociation for the carbon-halogen bond should be the weakest of all halogens and thus would be a good starting point for investigating the reaction. Following this result, we obtained a photoreactor (kindly borrowed from Dr. Scott Taylor's lab) and experimented with different conditions including the wavelength, solvent, and equivalents of phosphines. We began our condition scope by experimenting with the effect of solvent when the reaction is carried out at 350 nm, a summary of the results can be seen in **Table 3.2**. We observed that the best result for the reaction at 350 nm was observed in polar aprotic solvents such as DMSO and acetone, with the later providing a yield of 74% by ³¹P NMR (**Table 3.2-Entry 4-5**). Changing the light source to 300 nm resulted in a drop in yield when the reaction was carried out in acetone (**Table 3.2-Entry 8**), most likely due to the light source approaching the absorption threshold of acetone which in turn lowers the amount of UV photons that reach the reactants. Since acetone could no longer be utilized at this wavelength, we explored other polar aprotic solvents and observed that the reaction proceeded in a 71% yield when carried out in DMSO at 300 nm (**Table 3.2-Entry 9**). Finally, to try and boost the yield further the reaction was carried out with 3 equivalents of PPh₃

and to our delight we observe quantitative yield of the tetraarylphosphonium iodide (**Table 3.2-Entry 10**). To assess the validity of running our phosphorus reaction at higher energy wavelengths we also performed a trial in MeCN at 254 nm only to observe a yield of 49% by ^{31}P NMR. At 254 nm DMSO is no longer a viable solvent as it begins to absorb some of the light being shone on the sample, reducing the overall quantum yield, and causing the DMSO to begin to speciate.

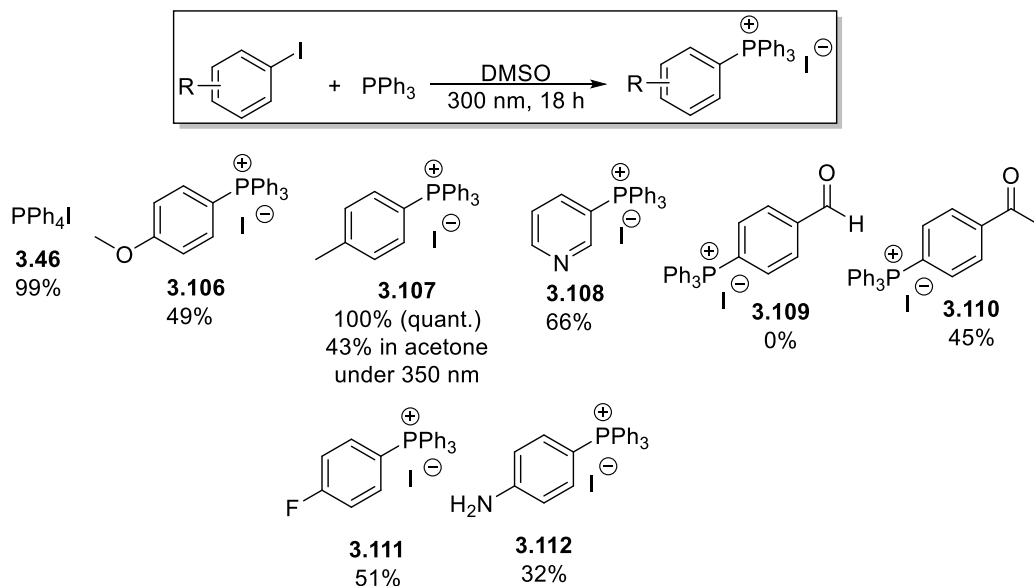


Scheme 3.27-Proposed mechanism for the synthesis of quaternary phosphonium salts via UV light.



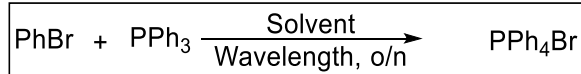
Scheme 3.28- Control reactions for the UV synthesis of tetraarylphosphonium iodides.

Our proposed mechanism is outlined in **Scheme 3.27**. The reaction is initiated through a homolytic C-X cleavage which is mediated by the UV light. Once the aryl-halide bond is fragmented, an aryl radical is created which can either recombine with the halide radical or proceed to attack a phosphine molecule creating a phosphine centered radical. This radical can then perform a SET with the halide radical to create the phosphonium salt. To further verify the importance of the UV light for the reaction, we performed a control experiment with PhI and PPh₃ under thermal conditions and observed that no reaction occurred, indicating that UV is indeed required for the reaction to proceed (**Scheme 3.28**). An additional control was performed with an equivalent of TEMPO to probe the nature of the reaction mechanism and we were pleased to observe that in the presence of TEMPO the reaction yield changed from 63% to 27%. This is significant as it provides evidence for the radical mechanism outlined in **Scheme 3.27**.



Scheme 3.29- Substrate scope for photophosphorylation of aryl iodides with triphenylphosphine. Reactions were carried out in DMSO [0.2 M] with 1 equiv of the aryl iodide and 3 equiv of triphenyl phosphite at 300 nm. Yields were determined by ^{31}P NMR using triphenyl phosphite as an internal standard.

Pleased with our optimized conditions we moved to examine the functional group tolerance of the reaction and thus performed the reaction with several substrates, which are outlined in **Scheme 3.29**. We screened alkyl (**3.107**), electron donating (**3.106**, **3.112**), withdrawing (**3.111**, **3.110**), and heterocyclic substrates (**3.108**) and quantified their yield by ^{31}P NMR. The reaction was able to tolerate most substrates in good to excellent yields except for aryl aldehydes (**3.109**). The lack of tolerance of aryl aldehydes may be due to reactivity that aldehydes exhibit when exposed to UV radiation, examples of this reactivity can be seen in transformations such as the Norrish reaction and the photo-Fries rearrangement.^{235–237} It should be stated that when dealing with stoichiometric amounts of phosphine, one detrimental side-product can be the formation of phosphine oxide, which often can be challenging to completely separate from a reaction mixture.²³⁸ The polar nature of the phosphonium salts allows for the facile removal of the phosphine oxide by selective precipitation of the phosphonium salt over the oxide in DCM/diethyl ether. To further boost the applicability of the reaction, no chromatography was needed to isolate the salts and any excess phosphine is also removed during the precipitation step. The reaction was also attempted using acetone as a solvent under 350 nm irradiation to observe if comparable yields could be obtained using the best conditions for both wavelengths, this however, proceeded at a much lower yield than when carried out at 300 nm with DMSO as the solvent.

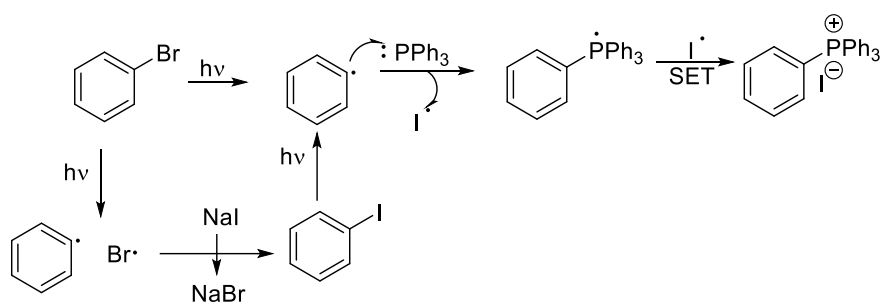


Entry	PPh ₃ (equiv)	Solvent	λ (nm)	Additives	Yield (%)
1	2	MeCN	350	-	2
2	2	MeCN	300	-	5
3	2	MeCN	254	-	1
4	3	DMSO	254	-	12
5	3	MeCN	350	NaI (2 equiv.)/I ₂ (0.1 equiv)	12
6	3	MeCN	254	NaI (2 equiv.)/I ₂ (0.1 equiv)	55
7	3	MeCN	254	I ₂ (0.1 equiv)	23
8	3	MeCN	254	NaI (2 equiv)	56
9 ^[a]	3	MeCN	254	NaI (2 equiv.)/I ₂ (0.1 equiv)	47

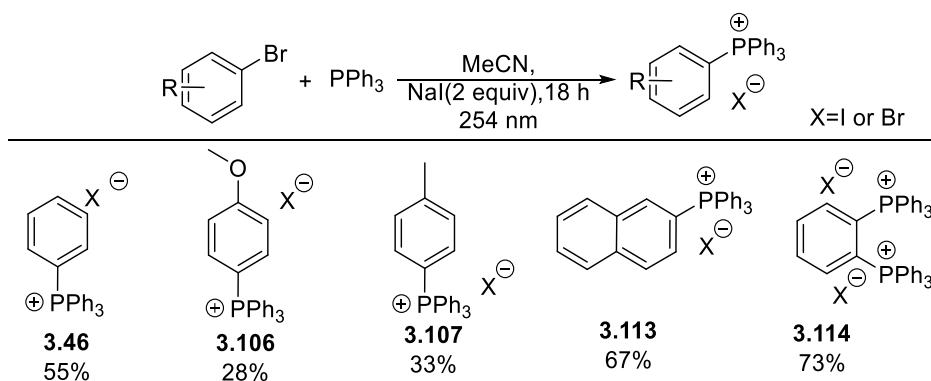
Table 3.3-Optimization of photophosphorylation of bromobenzene with triphenylphosphine. Reactions were carried out at 0.2 M for 18 h. Yields were determined by ³¹P NMR using triphenyl phosphate as an internal standard. [a]- Reaction was carried out for 36 h.

Our preliminary results looked promising, as already we had demonstrated how UV light can be used to create phosphonium salts from aryl iodides without using a metal or photocatalyst. Additionally, prior examples that utilized light to create phosphonium salts required pre-activation of the aryl component of the reaction by converting aryl iodides into iodoniums, whereas our photochemical method could create phosphonium salts solely from the aryl iodides.^{175,210} Having seen some success with the aryl iodides, we turned our attention towards aryl bromides as these compounds are typically easier to obtain and more likely to be commercially available. We began our investigation by irradiating bromobenzene in the presence of triphenylphosphine in MeCN at 350 nm (**Table 3.3-Entry 1**). MeCN was chosen as the initial solvent as we suspected that a higher energy wavelength would be required to break the C-Br bond thus the solvent needed to have a solvent threshold above 254 nm (MeCN λ_{max}=190 nm). The reaction was carried out at 350 nm, 300 nm and 254 nm only to reveal trace amounts of the phosphonium salt (**Table 3.3-Entry 1-3**). The experiment was repeated in DMSO at 254 nm however only a yield of 12% was observed (**Table 3.3-Entry 4**). The observed yields raised some concerns about the applicability of the reaction; if our proposed mechanism was correct, then irradiating the aryl bromides with UV light should create an aryl radical which would lead to the phosphonium salt. Thus, we sought inspiration in the previous works published by Li group.²³¹ From our previous experiments we understood that the reaction can proceed when conducted in the presence of an aryl iodide. Therefore, if we could transform our starting material from an aryl bromide to the aryl iodide *in situ* then the reaction should work (**Scheme 3.30**). To test our hypothesis, we conducted the experiment once more in MeCN.

However, this time, we introduced two equivalents of NaI to perform an aromatic “Finkelstein” to promote our reaction and were pleased to observe a dramatic increase in the yield to an acceptable 55% yield when performed at 254 nm (**Table 3.3, entry 6**). Running the reaction solely with NaI gave a slight increase in yield while performing the reaction with only 0.1 equiv of I₂ lowered the yield nearly in half (**Table 3.3- Entry 7-8**). The conditions for the aromatic Finkelstein are promoted by introducing an oxidant such as oxygen or iodine as outlined earlier in the chapter. In our case, however, the nature of the phosphine disallows the addition of an oxidant as either O₂ or I₂ will react with the phosphine to form the phosphine oxide or iodophosphonium salt, respectively. The iodination of phosphines with elemental iodine was something that initially did not become obvious to us, thus other experiments further in the chapter may contain trials with I₂ as at the time of the experiment the detrimental effect of the iodine was not clear. As a final trial the reaction was carried out for 36 h instead of 18 h however, no significant change in the yield was observed (**Table 3.3- Entry 9**).



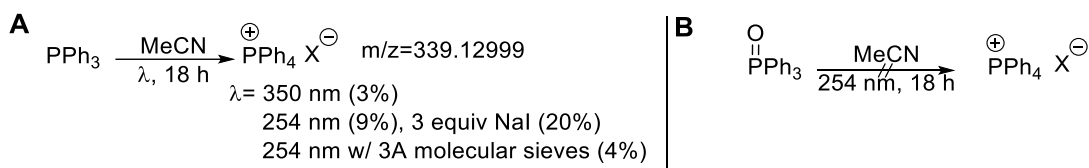
Scheme 3.30-Proposed mechanism for *in situ* aromatic “Finkelstein” followed by our photophosphorylation to form tetraphenyl phosphonium iodide.



Scheme 3.31- Substrate scope for the photophosphorylation of aryl bromides under UV irradiation. Reactions were performed with 1 equiv of aryl iodide, 3 equiv of PPh₃ in MeCN [0.2 M] for 18 h. Purity was determined by ³¹P NMR after isolation of the phosphonium salt.

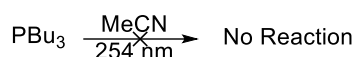
Although the yields for the reaction were not ideal, we decided to test the applicability of the reaction with the current optimized conditions (**Table 3.2, entry 8**) and began to scope a variety of aryl bromides (**Scheme 3.31**). One particularly interesting example was the di-cation obtained from subjecting 1,2-dibromobenzene to our reaction conditions which led to the formation of **3.114**. Regardless of the number of equivalents used the reaction always yielded the di-cation suggesting that the addition of one phosphonium group accelerated the subsequent phosphorylation. The reactions appeared to proceed with relative ease; however, when we began to characterize our salts by NMR, we began to observe that the integration for all our compounds appeared to be larger than expected which raised a couple of red flags. When isolated, these compounds displayed a single spot by TLC and behaved as crystalline solids. A more thorough look at the ^{31}P NMR revealed a small shoulder that coalesced with the signal for the product. When we then analyzed our compound by high resolution mass spectrometry (HRMS), we observed two main signals: One corresponded to our product while the other salt exhibited a m/z of 339.12999 corresponding to the tetraphenyl phosphonium cation. Upon discovering this, we re-analyzed our isolated phosphonium bromide salts and quantified the amount of impurity by ^{31}P NMR (**Scheme 3.32A**). The origin of this cation proved puzzling, thus, to confirm the origin of the compound we ran control experiments with triphenylphosphine and triphenylphosphine oxide under UV radiation in the absence of an aryl halide. To our displeasure, we observed that regardless of the wavelength, PPh_3 under UV exposure can generate the phosphonium cation albeit at low yields; the phosphine oxide on the other hand was completely inert to any degradation under UV light (**Scheme 3.32B**). As no additional salts were introduced to the reaction, the nature of the anion remains unclear. In an attempt to ascertain the identity of the anion, scanning in the negative mode in the HRMS was attempted, but revealed no new information and when the salt was isolated only one signal was observed in the ^{31}P NMR. We hypothesized that the most likely counter-ion could be an OH^- which may originate from any trace water in the reaction, thus we carried out the control once more with the addition of 3 Å molecular sieves and observed a drop in yield of PPh_4 which may indicate that OH^- may indeed be the counter-ion for the PPh_4^+ impurity. The control was also carried out with 3 equiv of NaI which saw a boost in the formation of the phosphonium impurity. This proved problematic as PPh_3 can solely create phosphoniums under UV, creating an impurity that is difficult to remove from our desired product. Several recrystallization solvents were attempted; however, the impurity was not able to be removed completely even under the best recrystallization conditions. Additionally, for substrates in which

the reaction proceeded in lower yields the amount of impurity matched the yield of the product closely thus recrystallization would prove ineffective.

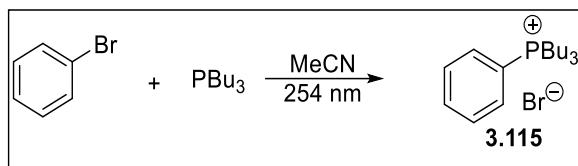


Scheme 3.32-Control reactions for photophosphorylation of aryl halides. **A**- 1 equiv of PPh₃ was irradiated at either 350 nm or 254 nm for 18 h in MeCN [0.2M]. **B**- 1equiv of triphenylphosphine oxide was irradiated at 254 nm for 18 h in MeCN [0.2 M]. Yields were determined via ³¹P NMR with triphenyl phosphate as an internal standard.

3.7 PHOTOPHOSPHORYLATION OF ARYL HALIDES WITH TRIBUTYLPHOSPHINE UNDER UV LIGHT



Scheme 3.33-Control reaction of PBu₃ under UV radiation. 1 equiv of PBu₃ was irradiated at 254 nm in MeCN [0.2 M] for 18 h. Yield was determined via ³¹P NMR with triphenyl phosphate as an internal standard.

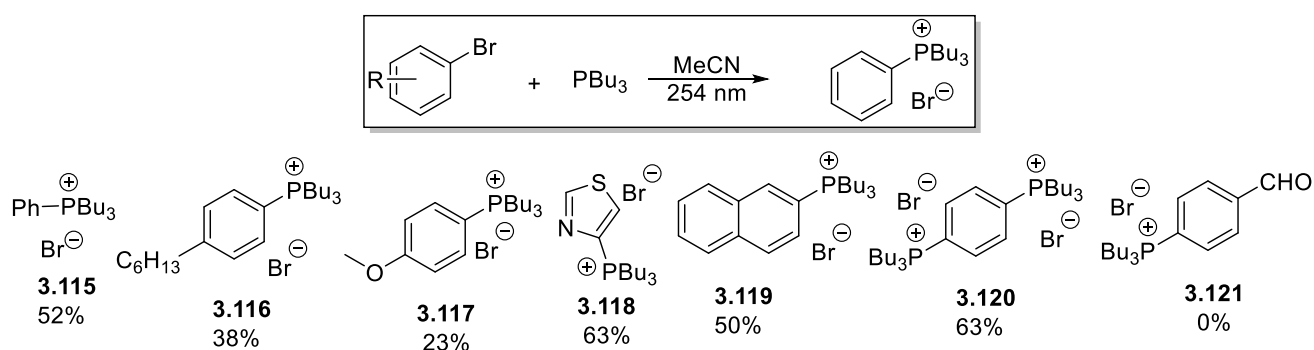


Entry	Additives	Yield (%)
1	-	50
2	NaI	36
3	NaI/I ₂ (0.1equiv)	47
4	Neat	8

Table 3.4- Optimization of photophosphorylation of bromobenzene with PBu₃. Reactions were performed at 254 nm with 1 equiv of bromobenzene, 3 equiv of PBu₃ in MeCN [0.2 M] for 18 h.

After discovering that PPh₃ can form ⁺PPh₄ under UV light it became apparent why the yields were low for the aryl bromides at 254 nm as the phenyl ligands on PPh₃ absorb a large part of the incoming light which not only speciates the phosphine but reduces the amount of light that reaches the aryl halides. We then theorized that if a different phosphine were used, with no aromatic groups, then the incoming radiation would only be absorbed solely by the aryl halides and consequently led to our desired product. We chose PBu₃ as a starting point for the new phosphine, due to its relative ease of use and commercial availability and exposed the PBu₃ to the same control as the PPh₃ (**Scheme 3.33**). To our delight we observed that no reaction occurred under UV radiation of the PBu₃ returning only starting material and some of the oxide. Next, we performed our phosphorylation reaction with bromobenzene in MeCN at 254 nm and observed a yield of 50% (**table 3.4-entry 1**). We then performed our initial

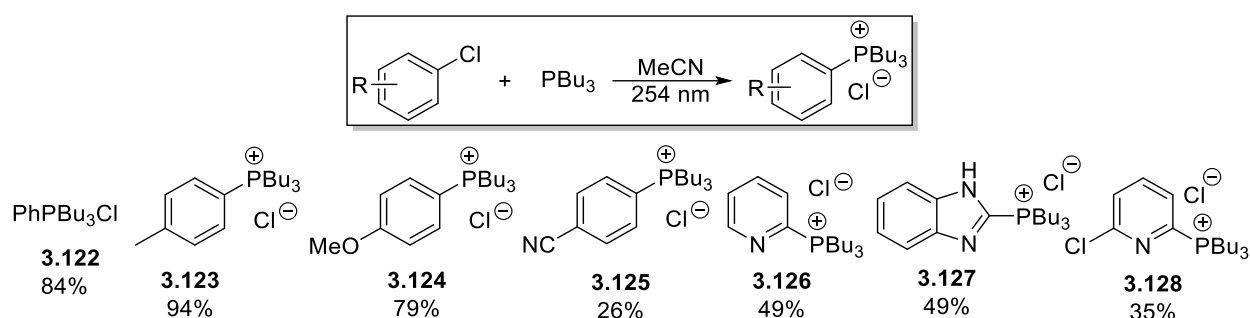
optimization of the reaction and attempted to boost the yield via the addition of NaI or NaI/I₂ (**Table 3.4-Entry 2-3**), however, no increase in yield was observed. Finally, since PBu₃ is a liquid, the reaction was carried out with the phosphine as the solvent which led to a drastic loss in yield (**Table 3.4-Entry 4**). Although not ideal we used these optimized conditions to perform a brief substrate scope for the reaction and were pleased to observe that the reaction conditions were amenable to a variety of substrates. Both electron donating (**3.117**) and withdrawing groups (**3.125**) were supported as well as heterocycles (**3.118**) and larger aromatics (**3.119**) (**Scheme 3.34**). Once again, aldehydes (**3.121**) were not able to be supported which aligned with our previous results for aryl iodides. Similarly to before, the introduction of a di-halobenzene to our reaction, in this case 1,4-bromobenzene led solely to the formation of the di-phosphorylated product.



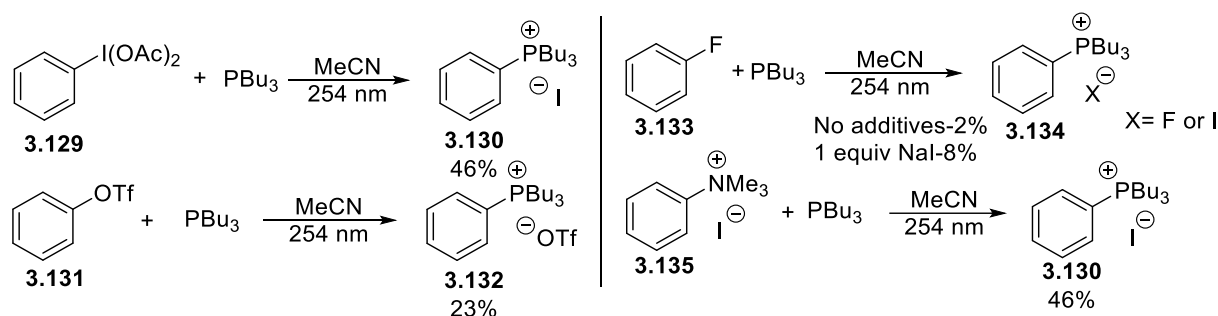
Scheme 3.34-Photophosphorylation of aryl bromides with PBu₃. Reactions were performed at 254 nm with 1 equiv of the aryl bromide, 3 equiv of PBu₃ in MeCN [0.2 M] for 18 h. Yields were determined by ³¹P NMR with triphenyl phosphate as an internal standard.

After observing the reactivity of aryl bromides, we were curious to see if aryl chlorides would be at all amenable to the reaction conditions. Thus, we attempted our UV reaction with chlorobenzene in MeCN with PBu₃ and were surprised to observe that the reaction proceeded in 84% yield (**Scheme 3.35**). At this point we simply continued with our previously optimized conditions (0.2 M MeCN, 3 equiv phosphine, 18 h) as these conditions provided the highest yields for the aryl iodides and bromides. We then set out to see if the aryl chlorides showed similar reactivity patterns to the other aryl halides by performing a quick substrate scope and were pleased to observe similar reactivity patterns as the other aryl halides, albeit with improved yields. The reaction was once again capable of transforming electron poor (**3.124**) and rich aryl chlorides (**3.125**) as well as some heterocycles (**3.126-3.128**). Given our unexpected success with aryl chlorides we decided to attempt to react less reactive substrates such as aryl fluorides, triflates and ammoniums (**Scheme 3.36**). Our method was able to functionalize the aryl triflates

and ammonium salts in respectable yields. Aryl fluorides on the other hand were able to be functionalized in trace amounts but we did notice that the addition of NaI was able to boost the yield from 2% to 8%. Although a lower reactivity is to be expected when dealing with aryl fluorides, part of the reason for the low yield may be due to the volatility of the fluorobenzene. In addition to the less reactive compounds, we also sought to investigate aryl iodoniums with our method as these compounds were previously displayed as the starting material for the photocatalytic synthesis of phosphonium salts.^{175,210} When exposed to our reaction conditions the phenyl iodonium was able to be converted to the phosphonium salt in a 46% yield.



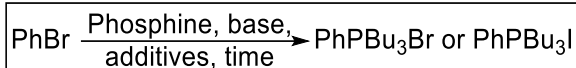
Scheme 3.35- Photophosphorylation of aryl chlorides with PBu_3 . Reactions were performed at 254 nm with 1 equiv of the aryl chloride, 3 equiv of PBu_3 in MeCN [0.2 M] for 18 h. Yields were determined by ^{31}P NMR with triphenyl phosphate as an internal standard.



Scheme 3.36- Reactions were performed at 254 nm with 1 equiv of the aryl halide/pseudohalide, 3 equiv of PBu_3 in MeCN [0.2 M] for 18 h. Yields were determined by ^{31}P NMR with triphenyl phosphate as an internal standard.

After observing the applicability of the reaction, we then set out to further optimize the reaction conditions in an attempt to boost the yields and facilitate the isolation of these salts. Additionally, we wanted, if possible, to reduce the amount of phosphine utilized in the reaction as the oxide generated from the excess PBu_3 could prove problematic at the isolation stage. Our optimization attempts began with the aryl bromides, as these compounds are usually easier to obtain and thus a wider library of aryl bromides is commercially available. Prior to this point all

photochemical reactions were carried out in the absence of stirring as the reactor lacked any stirring mechanism; we engineered a way to introduce stirring into the reactions by making use of an overhead stirrer. A summary of the attempted optimization conditions is highlighted in **Table 3.5**: We began by re-running our optimized conditions with the addition of stirring and were pleased to observe a slight increase in yield from 52% to 63% by ^{31}P NMR (**Table 3.5-Entry 1**). We then conducted the reaction over 36 h and we observed a near quantitative yield by NMR (**Table 3.5-Entry 2**); however, these conditions utilized a large amount of phosphine that proved problematic when trying to isolate the phosphonium salts. In an attempt to lower the equivalents of phosphine, the reaction was carried out with one equivalent of phosphine over 18 h and 36 h furnishing a yield of 45% and 63% respectively (**Table 3.5-Entry 3 and 4**). Once again, the reaction time seems to be an important factor towards the reaction reaching completion. We then carried out the reaction with 2 equiv of NaI over 18 h and 36 h and saw an increase of yield over 18 h but a decrease when carried out for 36 h (**Table 3.4-Entry 5-6**). To the best of our knowledge, these phosphonium salts should not degrade under UV light, and it remains unclear why the NaI would decrease the yield over a 36 h period when the reaction seems to proceed the best when carried out for that time period. Next, we attempted to use the HBF_4 salt of PBu_3 to reduce the amount of phosphine oxide generated as an impurity and to provide a phosphine which was easier to handle. BF_4HPBu_3 was made in quantitative yield from PBu_3 and HBF_4 following a procedure from Netherton and Fu.²³⁹ This type of phosphine has to be deprotonated *in situ* and for the base we chose diisopropylethylamine (DIPEA), using 1 equiv of BF_4HPBu_3 furnished a yield of 60% when conducted without stirring and 45% when stirring was introduced (**Table 3.4-Entry 7-8**). Extending the reaction time with BF_4HPBu_3 left the yield unchanged (**Table 3.4-Entry 9**). An excess of either the DIPEA or BF_4HPBu_3 was not able to improve the yield significantly (**Table 3.4-Entry 10-11**), only when the reaction was carried out with a 1:1 ratio of base to phosphine was the yield able to be increased (**Table 3.4-Entry 12**). Despite our extensive optimization studies the best results were obtained when the reaction was carried out with 3 equiv of PBu_3 for 36 h. Using the optimized conditions we set out to create a test our reaction on several aryl bromides but were met with a handful of obstacles when attempting to isolate these salts using our method.

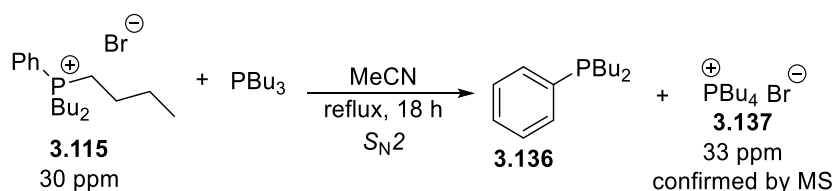


Entry	Phosphine	Base	Additives	Reaction time (h)	Yield (%)
1	P(nBu) ₃ (3 equiv)	-	-	18	63
2	P(nBu) ₃ (3 equiv)	-	-	36	99
3	P(nBu) ₃ (1 equiv)	-	-	18	45
4	P(nBu) ₃ (1 equiv)	-	-	36	63
5	P(nBu) ₃ (1 equiv)	-	NaI (2equiv)	18	67
6	P(nBu) ₃ (1 equiv)	-	NaI (2equiv)	36	28
7 ^[a]	HBF ₄ P(nBu) ₃ (1 equiv)	DIPEA (1 equiv)	-	18	60
8	HBF ₄ P(nBu) ₃ (1 equiv)	DIPEA (1 equiv)	-	18	41
9	HBF ₄ P(nBu) ₃ (1 equiv)	DIPEA (1 equiv)	-	36	45
10	HBF ₄ P(nBu) ₃ (3 equiv)	DIPEA (3 equiv)	-	18	46
11	HBF ₄ P(nBu) ₃ (3 equiv)	DIPEA (1.5 equiv)	-	18	47
12	HBF ₄ P(nBu) ₃ (3 equiv)	DIPEA (3 equiv)	-	36	86
13	HBF ₄ P(nBu) ₃ (1 equiv)	DIPEA (1 equiv)	NaI (2 equiv)	18	48

Table 3.5- Optimization of photophosphorylation of bromobenzene with PBU₃. Reactions were performed at 254 nm in MeCN [0.2 M]. Yields were determined by ³¹P NMR with triphenyl phosphate as an internal standard. a- reaction was carried out in the absence of stirring.

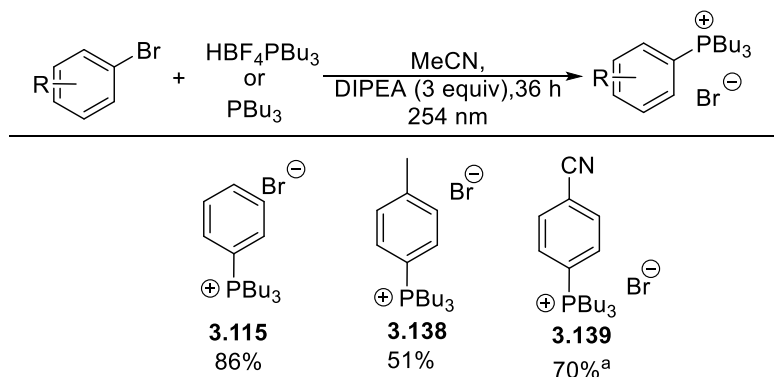
Unlike the tetraaryl phosphonium salts, the butyl phosphonium salts were not able to be precipitated because of the butyl groups that help solubilize the salt. Despite several efforts with a variety of solvent combinations, the salts could not be effectively isolated by precipitation but could potentially be isolated via column chromatography. We began isolating these compounds using column chromatography but began to notice an impurity by ³¹P NMR at ~33 ppm that was common in many of the substrates and would remain there despite multiple rounds of chromatography. In addition to this impurity, some of these compounds would also contain traces of phosphine oxide and would retain solvent, despite extended drying under vacuum, leading the compounds to appear as liquids when they are truly solids. Our main concern was the impurity present at 33 ppm as the other impurities present in the sample were accounted for and could be potentially removed. Thus, we introduced a sample which solely contained PhPBU₃Br plus the impurity into the HRMS and observed the mass corresponding to our product as well as an additional mass at 259.25408 g/mol. Based on the NMR shift we expected this compound to also be an alkyl phosphonium salt and indeed, we confirmed that the by-product of our reaction was PBU₄Br. The chemical shift of PBU₄Br matched literature and as an additional test we confirmed the nature of the impurity by TLC. Our prior controls showed that no reaction, aside from oxidation, occurs when PBU₃ was irradiated at 254 nm therefore the nature of the impurity must be from a thermal process. The most likely candidate seemed as an S_N2 reaction between the phosphonium and unreacted PBU₃ (**Scheme 3.37**). This conclusion was reached as it was

observed that when lower phosphine loadings were introduced in a reaction the amount of this impurity was lower. To confirm our hypothesis, we reacted PhPBu₃Br with PBu₃ in MeCN under reflux and observed a 14% yield of the PBu₄Br after 18 h, although the reaction is not high yielding it is still troublesome as the impurity cannot be removed through chromatography. Of the large number of aryl bromides that were reacted under our UV conditions only 4-bromobenzonitrile was able to be isolated cleanly in a 70% yield (**Scheme 3.37**) when using PBu₃, all other samples contained PBu₄Br or traces of the phosphine oxide which were not able to be removed from the product.



Scheme 3.37-Test reaction for the origin of PBu₄Br impurity. Reaction was carried out 1 equiv of PhPBu₃Br, 2 equiv of PBu₃ in MeCN [0.2 M] under reflux for 18 h. Yield was determined by ³¹P NMR using triphenyl phosphate as an internal standard.

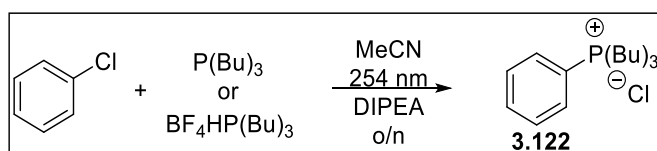
When trying to deal with the impurity our best approach was to prevent the formation of PBu₄Br as any attempt to remove the impurity proved ineffective. We were able to recrystallize PhPBu₃Br from ethyl acetate which successfully removed the impurity, but we were not able to translate this purification to other substrates. Any attempt at recrystallization was further complicated by the strong affinity these tributylphosphonium salts exhibited towards solvents. These molecules would often retain the prior solvent they were solvated in and thus would always remain in solution regardless of the recrystallization solvent.



Scheme 3.38- Isolatable tributyl phosphonium salts synthesized through UV phosphorylation. Reactions were carried out 3equiv of phosphine, 3 equiv of DIPEA and 1 equiv of the aryl bromide in MeCN [0.2 M] under 254 nm for 36 h. **a**-synthesized using 3 equiv of PBu₃.

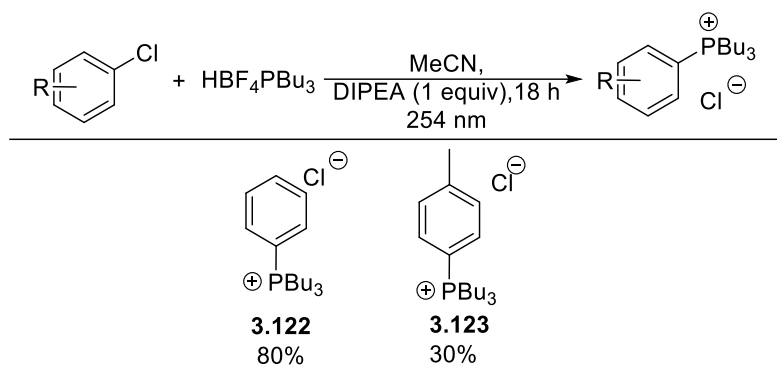
To attempt to minimize the unwanted side reaction we introduced a steady flow of air into the photoreactor which significantly brought the temperature down inside the reactor, but it was still elevated enough for the S_N2 to proceed. Looking back at our results, we observed by NMR that when the reaction was carried out with $BF_4HPBu_3/DIPEA$ the amount PBu_4Br was much lower than when it was carried out with the free phosphine, thus we attempted to create a substrate scope using $BF_4HPBu_3/DIPEA$ as the phosphine source. The scope for the aryl bromides synthesized with $BF_4HPBu_3/DIPEA$ is shown in **Scheme 3.38**. Although the use of the borate salt allowed for some of the aryl bromides to be functionalized with minimal impurities, several of the aryl bromides still contained PBu_4Br or the phosphine oxide.

At the same time, we were investigating the photophosphorylation of aryl bromides we also looked into the reactivity of aryl chlorides with PBu_3 under our UV conditions. The optimization for the aryl chlorides is highlighted in **Table 3.6**. Much like before, the aryl chlorides appear to be more susceptible towards our photochemical conditions allowing the reaction to proceed in high yield when only one equivalent of phosphine was used. Like the aryl bromides, the PBu_4Cl and phosphine oxide impurity were also present for the aryl chlorides thus we opted to use the BF_4HPBu_3 as the phosphine for the reaction. The lower phosphine loading would also ideally diminish any impurity as the contaminants from the reaction arise from excess phosphine.



Entry	Phosphine	equiv Phosphine	equiv DIPEA	Yield (%)
1	$P(nBu)_3$	3	-	54
2	$P(nBu)_3$	2	-	56
3	$P(nBu)_3$	1	-	75
4	$BF_4HP(nBu)_3$	3	3	50
5	$BF_4HP(nBu)_3$	2	2	58
6	$BF_4HP(nBu)_3$	1	1	80
7	$BF_4HP(nBu)_3$	3	1	64
8	$BF_4HP(nBu)_3$	2	1	65

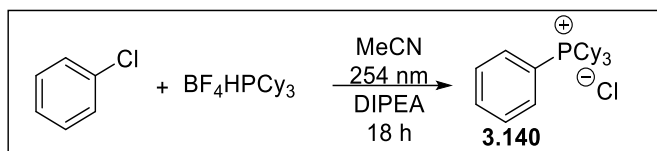
Table 3.6-Optimization for photophosphorylation of aryl chlorides with tributyl phosphine. Reactions were carried out with 1 equiv of the aryl chloride, 3 equiv of the phosphine in MeCN [0.2 M] for 18 h at 254 nm. Yields were determined by ^{31}P NMR using triphenyl phosphate as an internal standard.



Scheme 3.39- Isolatable tributyl phosphonium salts synthesized through UV phosphorylation. Reactions were carried out 1 equiv of phosphine, 1 equiv of DIPEA and 1 equiv of the aryl chloride in MeCN [0.2 M] under 254 nm for 18 h.

Investigations into the phosphorylation of aryl chlorides are still on going in the laboratory. So far, we have only been able to isolate two phosphonium salts using HBF_4PBu_3 (**Scheme 3.39**). Even though the equivalents of the phosphine are lower and the chlorides more reactive to our UV conditions, we still observe the oxide and PBu_4^+ in our reaction mixture. Ultimately, we chose to focus our attention on less nucleophilic and oxidation prone phosphines which are outlined in **Section 3.8**.

3.8 PHOSPHORYLATION OF ARYL HALIDES WITH TRIOCTYLPHOSPHINE AND TRICYCLOHEXYL PHOSPHINE UNDER UV LIGHT



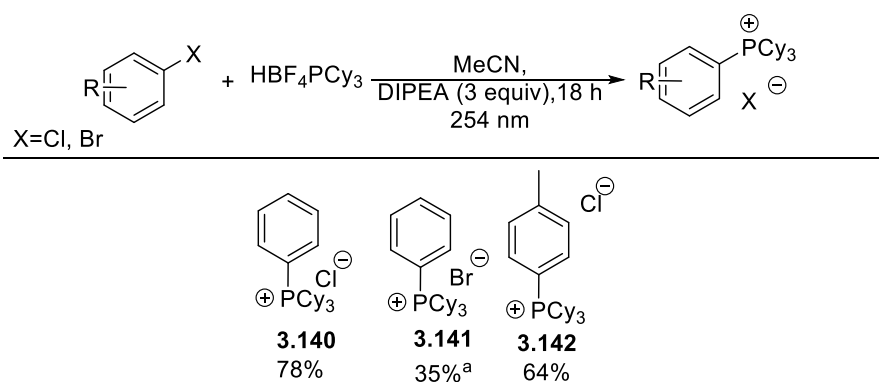
Entry	equiv. PCy_3HBF_4	Reaction Time (h)	Yield (%)
1	1	18	24
2	1	36	28
3	2	18	27
4	3	18	57
5^a	3	18	13
6	3	36	59
7^b	3	36	78

Table 3.7- Condition screening for the photophosphorylation of chlorobenzene with $\text{HBF}_4\text{PCy}_3/\text{DIPEA}$ (1:1ratio) under 254 nm. Reactions were carried out in MeCN [0.2 M]. **a**- 2 equiv of NaI was added to the reaction mixture. **b**- reaction was reacted at [0.1 M] concentration.

Having seen the ability of two different phosphines (PPh_3 and PBu_3) to be able to participate in the reaction we were interested to see what other phosphines could participate in our photochemistry. Initially, we wanted to move away from PBu_3 as this phosphine is particularly nucleophilic²⁴⁰ and as a consequence increases the presence

of PBu_4Br in the reaction mixture. Thus, we began experimenting with less nucleophilic phosphines and our first choice we tried PCy_3HBF_4 as the bulkiness of the Cy ligands should minimize any $\text{S}_{\text{N}}2$ byproducts.

We began our investigation with PCy_3HBF_4 by reacting the phosphine with chlorobenzene in MeCN under 254 nm irradiation for 18 h and were pleased to observe a 24% yield by ^{31}P NMR (**Table 3.7- Entry 1**). We decided to first optimize the reaction using chlorobenzene as aryl chlorides are more active under our reaction conditions. Due to the more rigid structure of the Cy ligands, we were able to precipitate the salt out of solution and when placed under high vacuum, the salt relinquished the solvent allowing the compound to exist as a solid. The optimization scope is summarized in **Table 3.6**. We experimented with different equivalents, reaction times, and additives but found that the ideal combination for this reaction was like before with 3 equiv of phosphine/base over 18 h providing the highest yield (**Table 3.7-Entry 4**). Compared to the reaction of PBu_3 with chlorobenzene the yield of the reaction is substantially lower; we believe this may be due to the increased bulk and rigidity of the system that prevents the aryl radical from reaching the phosphine. Following trials with trioctylphosphine (TOP) (see **Table 3.8**) we observed that the concentration had a significant effect on the reaction and observed that lowering the concentration to 0.1 M led to an increase in yield to 78%. Following this finding we performed the rest of our optimizations using the reduced concentrations.



Scheme 3.40-Reaction scope for the photophosphorylation of aryl halides with HBF_4PCy_3 . Reactions were carried out with 1 equiv of aryl halide, 3 equiv of HBF_4PCy_3 , 3 equiv of DIPEA in MeCN [0.2 M] under 254 nm for 18 h. [a]-Bromobenzene was irradiated for 36 h.

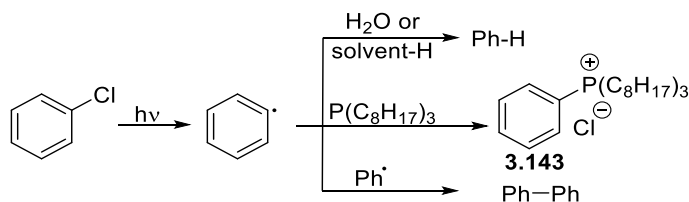
Due to the lessened reactivity of the PCy_3 towards our reaction we did not want to spend too much time testing an entire substrate scope for the reaction but still wanted to demonstrate the ability of the reaction to functionalize different types of arenes. The reaction scope for aryl chlorides with HBF_4PCy_3 is shown in **Scheme 3.40**.

Our reaction conditions so far have only been shown with alkyl aryl chlorides in good yields (**3.140-3.141**). Bromobenzene was also subjected to the UV conditions and was able to produce the phosphonium salt in a 35% under a 36 h reaction time.

Entry	Equiv TOP	Additives	Yield (%)
1	1	-	59
2	2	-	70
3	3	-	83
4	1 equiv HBF ₄ P(C ₈ H ₁₇) ₃	1 equiv DIPEA	59 ^a
5^b	1	-	58
6	1	2 equiv NaI	18
7	1	1 equiv DIPEA	26
8	1	1 equiv LiF	61
9	1	1 equiv Na ₂ SO ₄	68
10^c	1	-	79 ^a

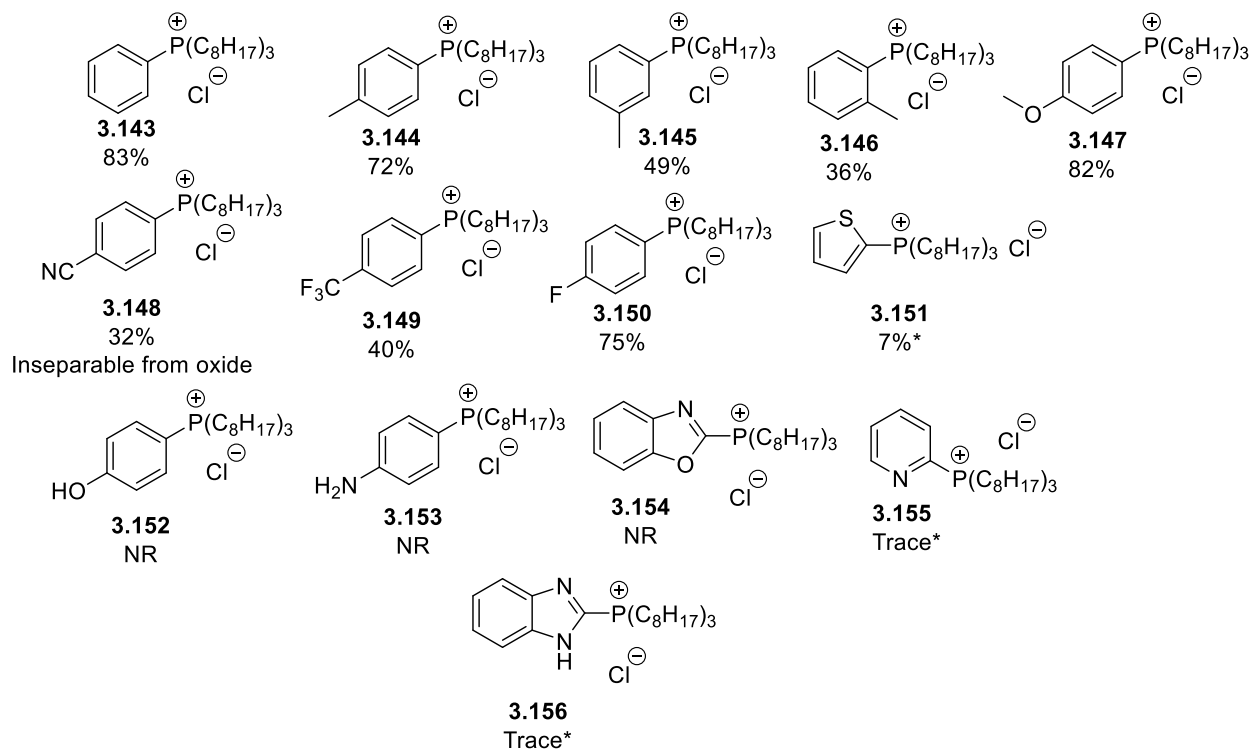
Table 3.8-Condition screening for the photophosphorylation of chlorobenzene with TOP. Reactions were carried out in MeCN [0.2 M] under 254 nm light. **A**-³¹P yield determined using triphenyl phosphate as an internal standard. **B**-reaction ran at [0.5 M] concentration. **C**- Reaction concentration changed to [0.1 M]

Slightly underwhelmed by the performance of PCy₃ for our reaction conditions we turned our attention towards TOP as a potential candidate for our UV reaction as this phosphine should behave similarly to PBU₃, which previously displayed good yields, but is less nucleophilic and less susceptible to oxidation thus should minimize the side products of the reaction. We began our investigation by attempting to react 1 equiv of TOP with chlorobenzene in MeCN at 254 nm for 18 h and were pleased to observe a 59% yield (**Table 3.9-Entry 1**), to boast the crude ³¹P NMR of the reaction was relatively clean when compared to the other phosphines mainly displaying the product signal alongside with a small amount of the TOP oxide. Seeing how by using TOP the reaction can proceed more cleanly, we set out to re-optimize the reactions as the TOP was the most likely candidate to yield isolatable phosphonium salts in a high yield.



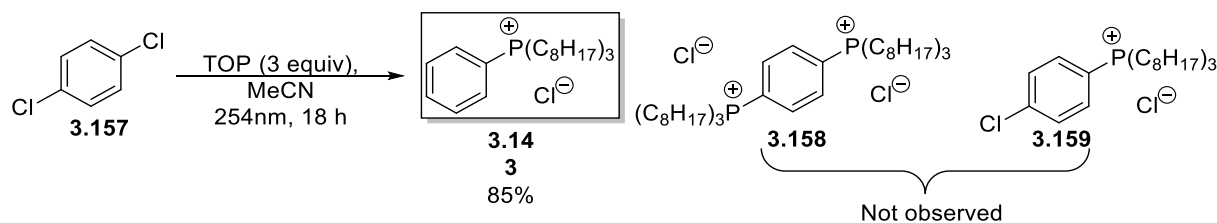
Scheme 3.41-Possible radical pathways during homolytic cleavage of chlorobenzene.

The optimization for the photophosphorylation of chlorobenzene with TOP is highlighted in **Table 3.8**. Following our initial success, we proceeded to experiment with the equivalents of TOP used in the reaction and observed that when 3 equiv of TOP were used the reaction proceeded in an 83% (**Table 3.8-entry 1-3**). Since using 1 equiv of TOP gave a surprisingly high yield, we investigated further to see if the yield could be increased using 1 equivalent as this would limit the number of TOP side products from the reaction. First, we changed the free TOP for the more oxygen tolerant $\text{HP}(\text{C}_8\text{H}_{17})_3\text{BF}_4$ to observe the effect of using this salt on the reaction, given the relative stability to air of TOP the yield of the reaction remained unchanged (**Table 3.8-entry 4**). The reaction was then performed at double the normal concentration, however, the yield once again remained roughly unchanged. Various additives such as DIPEA and NaI (**Table 3.8-entry 5-6**) were once again introduced but in both cases these compounds had a detrimental effect on the reaction. In particular, NaI seemed to accelerate the oxidation of the phosphine that in turn prevents the phosphines from participating in the reaction. DIPEA was added as a way of potentially aiding in the single electron transfer as some photochemistry is usually aided by the addition of a base, similarly LiF was added for a similar purpose but saw only a slight increase in yield (**Table 3.8- entry 8**).²²⁹ Na_2SO_4 was added to the reaction mixture as a drying agent as we hypothesized that water may be detrimental to the reaction as it can promote a reduction of the aryl halide (**Scheme 3.41**) and we were pleased to observe an increase in yield to 68% (**Table 3.8-entry 9**). 3 Å molecular sieves were also tried and gave a similar increase in yield to Na_2SO_4 . Although all our reactions are run under inert conditions, it is possible that during the course of the reaction water infiltrates the reaction vessel and negatively affects the reaction yield. Finally, we changed the concentration of the reaction and observed that a more dilute reaction was able to furnish a higher yield of 79% with only one equivalent of TOP (**Table 3.8-entry 10**).



Scheme 3.42- Reaction scope for the photophosphorylation of aryl chlorides with TOP. Reactions were carried out with 1 equiv of aryl chloride and 3 equiv of TOP in MeCN [0.1 M] under 254 nm light.* ³¹P yield determined using triphenyl phosphite as an internal standard.

Having now optimized the reaction conditions, we set out to examine the reaction's functional group tolerance (**Scheme 3.42**). As before, the reaction was found to proceed with a variety of electron rich (**3.147**) and electron poor (**3.148-3.150**) aryl chlorides. We were interested in observing how this reaction was affected by steric interactions and thus performed the reaction with chlorotoluenes with different substitution patterns. Given the large size of TOP, it comes as no surprise that the reaction proceeds best when the methyl group is at the *para* position; however, both the *meta* and chlorotoluenes (**3.145-3.146**) were also able to convert to the phosphonium salt albeit in a lower yield. Phenols and aryl amines were also attempted (**3.152-3.153**). Unfortunately, these compounds were not amenable to our reaction conditions suggesting that perhaps any exchangeable protons could be detrimental to the reaction. A series of heterocycles were also examined; however, little to no product was observed for these compounds. ³¹P NMR indicated that a small amount of the desired salt was formed for some of the heterocycles, but these proved difficult to isolate (**3.154-3.156**). Looking at the literature similar procedures heterocycles should be susceptible to our chemistry by the type of heterocycle and its substitution pattern may be critical for the reaction to proceed.²²⁸⁻²³¹



Scheme 3.43- UV photophosphorylation of 1,4-dichlorobenzene. Reaction was run with 1 equiv of the 1,4-dichlorobenzene. 3 equiv of TOP in MeCN [0.1 M] under 254 nm irradiation for 18 h.

We were also interested in functionalizing dichlorobenzenes to create diphosphonium cations as previously we were able to functionalize 1,4-dibromobenzene and 1,2-dibromobenzene with PPh_3 and PBU_3 to create the dication. Thus, we reacted 1,4-dichlorobenzene with 3 equiv of TOP in MeCN under 254 nm and to our surprise isolated back $\text{PhP}(\text{C}_8\text{H}_{17})_3\text{Cl}$ (**Scheme 3.43**). The exact mechanism behind this apparent reduction is unclear, either the dication forms and is cleaved photochemically or once the reaction proceeds the molecule can no longer be phosphorylated again and simply get reduced upon continual exposure to UV light. Neither the dication nor the *p*-chlorophosphonium salt were observed by ^{31}P NMR or mass spectrometry suggesting full conversion to the observed product.

3.9 CONCLUSIONS AND OUTLOOK

We were investigating methods of construction arylphosphonium salts to create a mild route towards benzyne with the sole addition of Cs_2CO_3 . The ultimate goal of this discovery was to provide a milder set of conditions to create benzyne for synthesizing macrocycles that may be sensitive to more forcing conditions that are usually required to create a benzyne.

To our dismay, our mild benzyne conditions from phosphonium salts were only able to generate Diels-Alder adducts in low yields that would not be beneficial if utilized for a complex synthetic pathway which may be due to a lack of selectivity upon decomposing the phosphonium salt. Gratifyingly, in our search for creating this salt we discovered two new methods of creating phosphonium salts. First, we were able to demonstrate how a butoxide base at elevated temperatures can create a benzyne without prior activation of the aryl iodide with the only drawback being regioselectivity. Secondly, we discovered how the use of ultraviolet light can be used to synthesize and create a variety of phosphonium salts under transition metal free conditions.

Seeing the potential importance of a metal free pathway for creating phosphonium salts we shifted our attention to this photochemical method and demonstrated how, by using UV light, it is possible to effectively couple aryl halides and alkyl phosphines under metal free conditions in good to high yields. The reaction is amenable to a wide range of substrates including electron poor and rich aryl halides and can be performed with different types of alkyl phosphines.

PART 2: CHAPTER 4

DEHYDRATION POLYMERIZATION OF CONJUGATED POLYMERS

4.1 CONJUGATED POLYMERS

Conjugated polymers are a class of organic conducting material with an extended π -system composed of alternating single and double bonds within the backbone of the molecule. This allows for π -electrons delocalization throughout the polymer leading to interesting optical and electronic properties. Conjugated polymers were officially recognized as a new class of conducting material following the findings by Heeger, MacDiarmid and Shirakawa wherein the researchers reported that polyacetylene could be made conductive if doped with iodine. This finding eventually led to these scientists winning the Nobel prize in chemistry in 2000 for “the discovery of conductive polymers”.²⁴¹

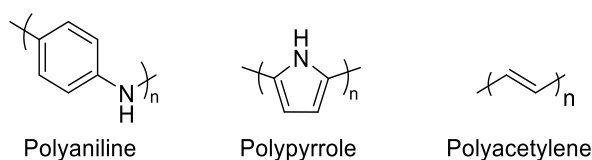


Figure 4.1-Early examples of conjugated polymers.

Although polyacetylene was the first recognized example of a conductive polymer, there were reports of electrochemical oxidation being used to make polyaniline and polypyrrole (**Figure 4.1**).²⁴² These findings were made long before the concept of polymers was accepted and although the structure of the material was not well understood, the original authors did observe that the substance was electrochemically active.²⁴² Soon after the discovery of conductive polyacetylene, the field of conjugated polymers saw renewed interest in these types of conjugated material and how they could supplant silicon in electronic applications.

4.2 PROPERTIES AND APPLICATION OF CONJUGATED POLYMERS

Conjugated polymers combine the semiconducting properties of silicon materials while possessing the physical and mechanical properties that organic polymers are known for. By virtue of being an organic polymer, the conjugated material is soluble in organic solvents which allows for facile processing and the development of thin

films using techniques such roll-to-roll printing, inkjet printing, and spray coating.^{243–245} Conjugated polymers are low-weight, flexible, and potentially low cost and have subsequently found use in applications such as photovoltaics,^{246,247} organic light-emitting diodes (OLEDs),^{248,249} chemical and biological sensors,²⁵⁰ and field effect transistors.^{251,252} The creation of thin films with conjugated polymers has enabled the possibility of flexible displays, which is the application that is most commonly associated with conjugated polymers.²⁵³

Although conjugated polymers offer several advantages over Si, such materials are not without their disadvantages. For example, conjugated polymers degrade quickly compared to their silicon counterparts making for shorter device lifetimes²⁵⁴ but more importantly, the performance of conjugated polymers has yet to approach that of Si in device applications. The theorized maximum power conversion efficiency (PCE), the ratio between input and output of useful energy, for a solar cell p-n junction is 32.33%²⁵⁵ and so far, researchers have been able to approach this value with reported PCEs of 26.7%.²⁵⁶ Some reports have stipulated that under the right conditions it may be possible to reach PCEs of 31%, approaching the theoretical limit.²⁵⁷ Conjugated polymers on the other hand have much lower PCE values with values of 7.7% being considered “high efficiency” while more recent examples have been able to reach PCEs of 13.1%.^{258,259} Conjugated polymers may, therefore, never supplant silicon, but may provide a cost-effective, tunable, and easy to process alternative that in the future may be able to compete with and work alongside with silicon.

4.3 GENERAL POLYMER TERMINOLOGY

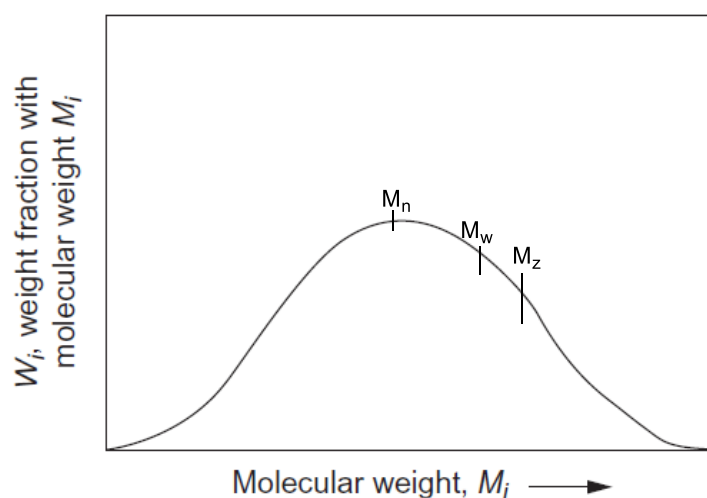


Figure 4.2-Molecular weight distribution in polymer science.

Important to the analysis of conjugated polymers are the inherent properties related to developing polymer materials. Of primary importance is the polymer's molecular weight: most polymerization reactions, with some exceptions, generate a range of molecular weights following a polymerization, thus, when referring to the molecular weights of polymers a statistical average of the masses is used. The two values most often referred when describing the molecular weight of a polymer are: M_n , which is the number average molecular weight and M_w , the weight average molecular weight. **Figure 4.2** provides a graphical representation of these mass averages on a normal distribution. M_n describes the weights of the polymers closest to the center of the distribution while M_w takes some of the larger weights into account. M_n and M_w are represented by the following equations: $\overline{M}_n = \frac{\sum n_i M_i}{\sum n_i}$ and $\overline{M}_w = \frac{\sum n_i M_i^2}{\sum M_i n_i}$, where n_i is the number of polymers per unit volume and M_i is the molecular weight. If this analysis is extended, then we can arrive at M_z and M_{z+1} which take more of the larger weight fraction into account. The last important value is the polydispersity index (PDI), that is defined as the ratio of M_w/M_n .²⁶⁰

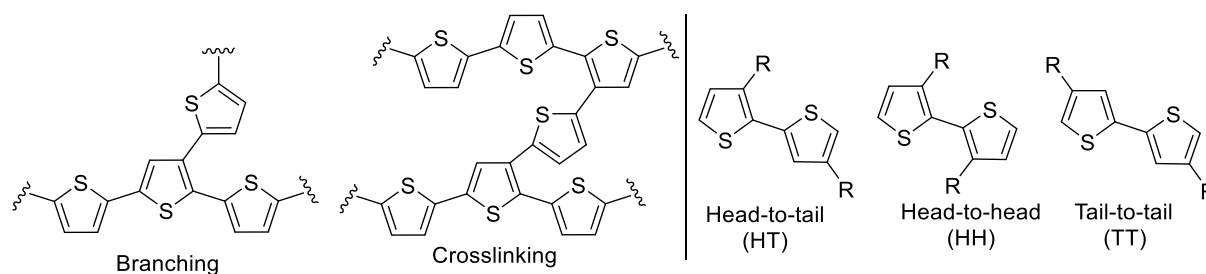


Figure 4.3-Branching and homocoupling defects (Left).; Possible diads in polyalkylthiophenes.

Another important facet of polymer synthesis is the potential defects that can occur during a polymerization. Some polymerization reactions can allow for the undesired propagation of the polymer chains resulting in either chain branching or crosslinking. Branching occurs when a non-desired site in the polymer chain is activated, and a secondary polymer chain is covalently bonded to the primary polymer chain (**Figure 4.3**). Crosslinking occurs when two polymer chains are bound together by a monomer or another polymer chain thus creating a 2D-polymer network (**Figure 4.3**). Usually, crosslinking and branching^{261,262} are not desired in conjugated polymers as these defects can negatively affect the optical and electronic properties as well as the processability of the polymer (See **Chapter 5**).

Lastly, polymers can have different stereochemical and regiochemical relationships upon polymerization; an example of this can be seen for in **Figure 4.3**, where polyalkylthiophenes can adopt three different types of diad configurations. The term regioregularity is used to describe the abundance of one type of relationship over another. For example, in **P3HT** the HT diad is desired over the other two dyads leading to several optimization studies on how to improve the regioregularity of HT diad within the polymer.^{263–266} Good polymerization reactions will not only proceed in good yield and with high molecular weights but will also display a high level of regioregularity. This value is important as it can affect the packing structure of the polymer in the solid state (See **Section 4.4.5**).²⁶⁷

4.4 CONJUGATED POLYMER DESIGN AND BANDGAP ENGINEERING

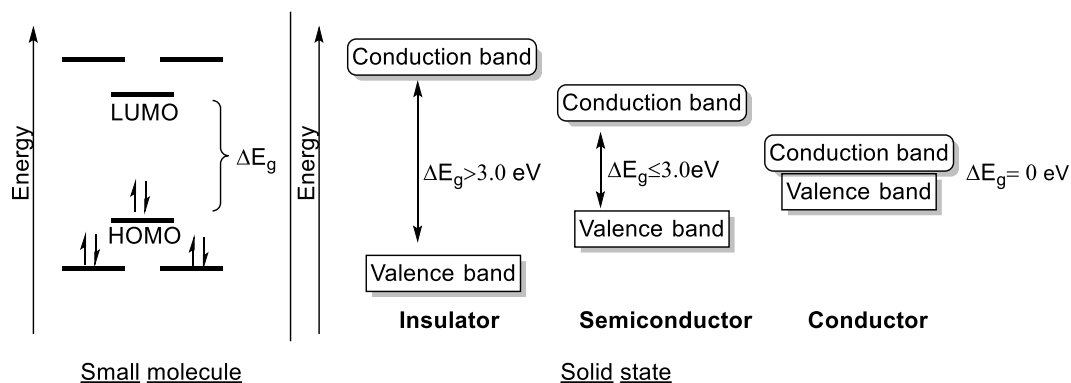


Figure 4.4-Band gap in small molecules versus the solid state.

Of fundamental importance to the electronic properties of conjugated polymers is the band gap. The HOMO-LUMO gap is the amount of energy required to promote an electron from the HOMO to the LUMO level in a single molecule.²⁶⁸ If this analysis is then extended to solid state materials, then we refer to this energy transition as the band gap; the amount of energy required to promote an electron from the conductance band to the valence band (**Figure 4.4**). The value of the bandgap determines if the material functions as an insulator ($\Delta E_g > 3.0$ eV), semiconductor ($\Delta E_g \leq 3.0$ eV) or conductor ($\Delta E_g = 0$).²⁶⁹ Different applications require different bandgaps and conjugated polymers comprise a variety of materials with different bandgaps that can be tailored towards the specific application.

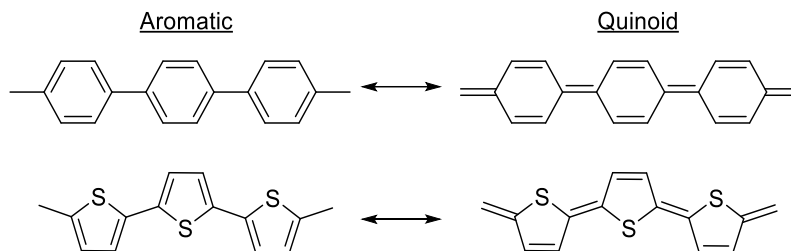


Figure 4.5-Aromatic vs quinoidal form in conjugated polymers.

When dealing with conjugated polymers there are several factors that can affect the band gap of the material. Firstly, conjugated polymers can be represented as either aromatic or quinoidal (**Figure 4.5**), this latter form is a consequence of the π -electrons traversing the polymer backbone which causes the conversion of single bonds to double bonds and *vice versa*.²⁷⁰ The aromatic form is more stable while the quinoid form is higher in energy but possesses a lower band gap.²⁷¹ The preference of the aromatic form over the quinoid form results in bond length alternation (BLA), which is an average of the C-C distance throughout the backbone of the polymer. Conjugated polymers with a higher quinoid character in the ground state will possess a lower BLA and, therefore a smaller band gap.²⁷⁰

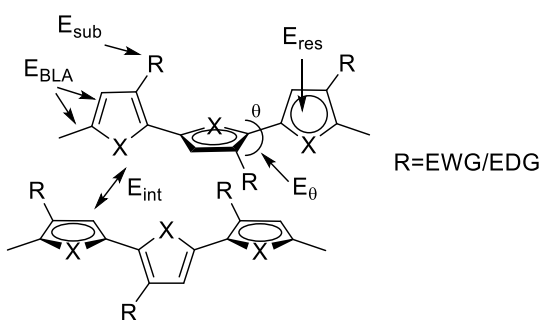


Figure 4.6-Schematic representation of all the contributions to the bandgap in conjugates polymers. X is a heteroatom such as O,N,S,Se, etc.²⁴⁷

Secondly, the energy required for the polymer to interconvert between aromatic and quinoid can affect the bandgap. This value is the dependent on the resonant stability of the molecule and its ability to confine the π -electrons away from the conducting backbone. Thirdly, the bandgap can be altered by including electron donating or withdrawing groups on the monomers and is the simplest way to modify the band gap. Fourthly, the dihedral angle between the monomers can affect the bandgap as disruptions in the planarity of the polymer will result in poor overlap in the polymer backbone and consequently higher BLA and a higher band gap. Lastly, the intermolecular

interaction between the polymers can affect charge transfer interactions between polymer chains which in turn can affect the band gap of the material. All the contributions to the band gap can be represented by the following equation: $E_g = E_{BLA} + E_{res} + E_{sub} + E_{\theta} + E_{int}$, where E_{BLA} is the BLA energy, E_{res} is the resonance energy, E_{sub} is the adjustment based on electron donation or withdrawing groups, E_{θ} is the rotational energy, and E_{int} is the intermolecular interaction contribution, a schematic representation of all these factors can be observed in **Figure 4.6**.²⁴⁷

4.4.1 BOND LENGTH ALTERNATION

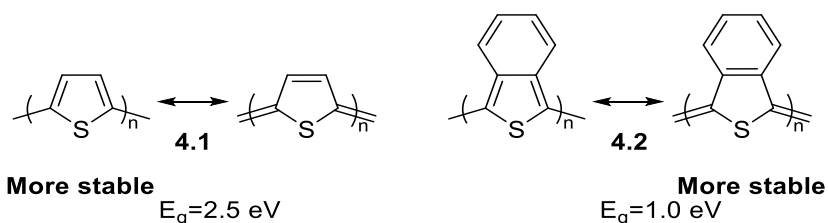


Figure 4.7-BLA in polythiophene (A) versus polyisothionaphthalene (B).

Modifying the bond length alternation is a useful way to control the bandgap of a conjugated polymer. Simply put, polymers with a lower BLA exhibit a higher quinoidal character in the ground state and lower band gaps, whereas polymers with a higher degree of BLA exist in a more aromatic ground state conformation and have wider band gaps. Since the quinoidal state is higher in energy most conjugated systems will favour the aromatic conformation in the ground state and must be modified to increase the quinoid character of the system. The most common example of decreasing the BLA is when fused heterocycles are used to stabilize the quinoid form. This can be seen when comparing polythiophene **4.1**, which preferentially lies in the aromatic form, and polyisothianaphthalene **4.2**, which possesses lower degree of BLA than the former (**Figure 4.7**).²⁷² The decreased BLA in polyisothianaphthalene is due to the additional resonance stabilization upon adopting the quinoid form which in this case is granted from the creation of a new Clar aromatic sextet.⁸⁴ The stabilization of the quinoid state has a profound effect on the bandgap with polythiophene having a bandgap of 2.5 eV while polyisothionaphthalene has a bandgap of 1.0 eV.

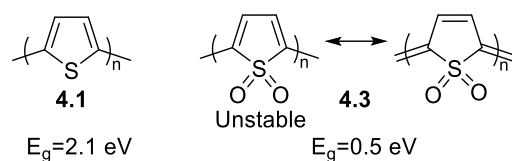


Figure 4.8-
Destabilization of aromatic resonance through oxidation of polythiophene to poly(thiophene-*S,S*-dioxide) (PTdO).²⁷³

The prior example showed a stabilization of the quinoid state to promote its adoption, however, the aromatic resonance form of the polymer can also be destabilized to force the polymer to adopt the less favourable quinoid form. An example of this can be seen in the oxidation of polythiophenes to poly(thiophene-*S,S*-dioxide) **4.3** (PTdO) (**Figure 4.8**).²⁷³ For this example, the aromaticity of the thiophenes is broken upon oxidation to the *S,S*-dioxides, with the aromatic resonance state now unstable the polymer has a lower energy gap to the quinoidal state. PTdO essentially behaves like polyacetylene and consequently the band gap of the system is drastically lowered from 2.1 eV to 0.5 eV.²⁷³

4.4.2-PLANIZATION AND RIGIDIFICATION

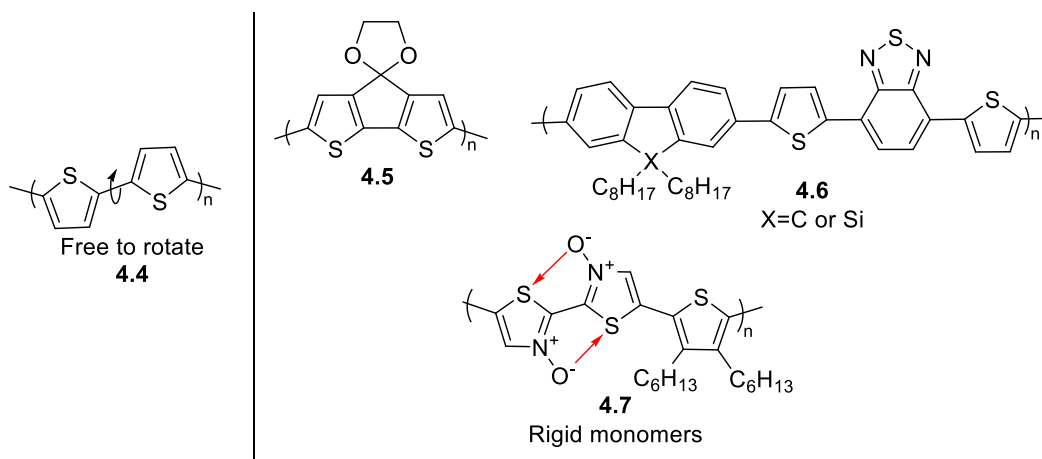


Figure 4.9-Covalent and non-covalent modifications to induce planarity in conjugated polymers.²⁷⁴

Reducing the dihedral angle between aromatic subunits can improve the π -electron delocalization and consequently reduce the band gap for the conjugated polymer. Often, conjugated polymers will have non-zero dihedral angles to attempt to reduce the number of steric interactions. Additions to the polymer chain such as bulky solubilizing chains or electron donating/withdrawing substituents can further add to the dihedral angle and have undesired effects towards the bandgap. Methods to eliminate the dihedral angle rely on the use of monomers where the aromatic groups have been tethered in a fixed position thus preventing the rotation of the aryl moieties. An example of this can be seen when polythiophene is tethered with a covalent sp^3 bridge, the resulting rigid polymer

now possesses better overlap with its partner leading to a drop in band gap of 0.9 eV (**Figure 4.9**).²⁷⁴ The nature of these bridging atoms can also influence the solid state structure of the polymer.^{275,276}

Covalent modification is a valid technique for planarizing the polymer backbone, however, the synthesis of the bridged monomers is not trivial and adds a significant number of steps for the materials synthesis. Non-covalent interactions can instead be used to induce planarization onto the polymer chain. The Schipper group very recently demonstrated how chalcogen bonding can induce a higher level of planarity within the polymer. This was done by the simple oxidation of the monomers to generate a thiazole *N*-oxide that upon polymerization would rigidify the polymer via S-O chalcogen bond.²⁷⁷

4.4.3-ELECTRON DONATING/WITHDRAWING EFFECTS

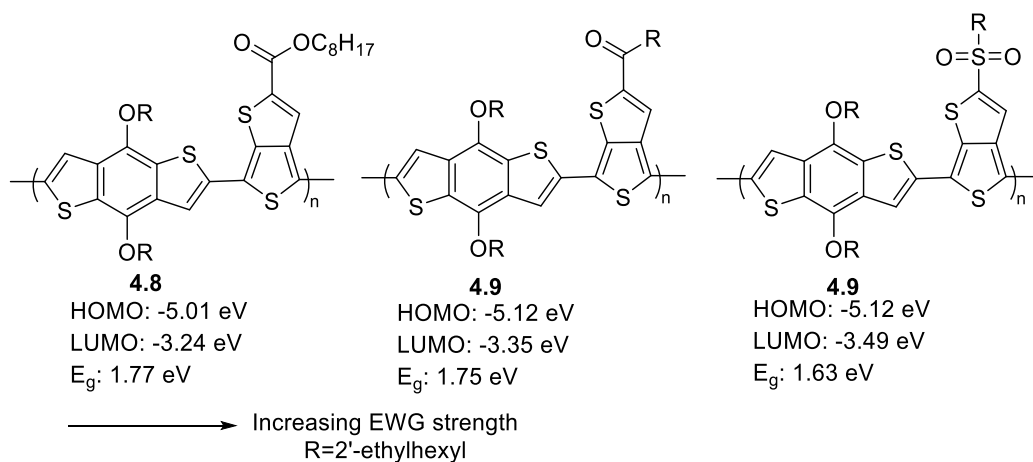


Figure 4.10-Effect of increasing electron withdrawing group strength on conjugated polymer band gap. ^{278,279}

The inclusion of electron donating (EDG) or withdrawing groups (EWG) is one of the oldest methods to tune conjugated polymer bandgaps. Early studies on poly(paraphenylene vinylenes) and polyparaphenylenes concluded that the addition of an EDG would raise both energy levels but would shift the HOMO level to a greater extent than the LUMO, while EWG would lower both energy levels but would downshift the LUMO farther than the HOMO levels.²⁸⁰ Consequently, both EDG and EWG are able to lower the bandgap of the material. The magnitude of the energy shift is dependent on the strength of the EWG/EDG (**Figure 4.10**). As the strength of the EWG increases the HOMO and LUMO levels become lower in energy, similarly, as the strength of the EWG increase the band gap decreases.^{278,279} The desired application may require bandgaps of a certain energy. The addition of EWG/EDG is a way to modify these energy levels while simultaneously lowering the band gap.

4.4.4 ACCEPTOR-DONOR MOTIFS.

One of the most powerful methods of lowering conjugated polymer bandgaps is by combining electron rich and poor monomers to create a donor and acceptor motif in the backbone of the molecule. **Figure 4.11** provides a molecular orbital diagram that describes the effect of donor-acceptor motifs in conjugated polymers; electron rich monomers (donors) will have higher lying orbitals, while electron poor monomers (acceptors) will have lower lying orbitals. When combined, a new set of orbitals will arise with a smaller bandgap than the individual monomers.^{281,282} This strategy has allowed for the realization of low bandgap conjugated polymers and offers a greater level of tunability as the HOMO is almost exclusively determined by the donor while the LUMO is exclusively dictated by the acceptor. This means that alterations to the donor will only affect the HOMO levels and leave the LUMO unchanged and *vice versa*. Furthermore, donor-acceptor motif facilitates electron transport and facilitate the conversion the quinoid for, thus reducing BLA and the band gap.²⁷¹

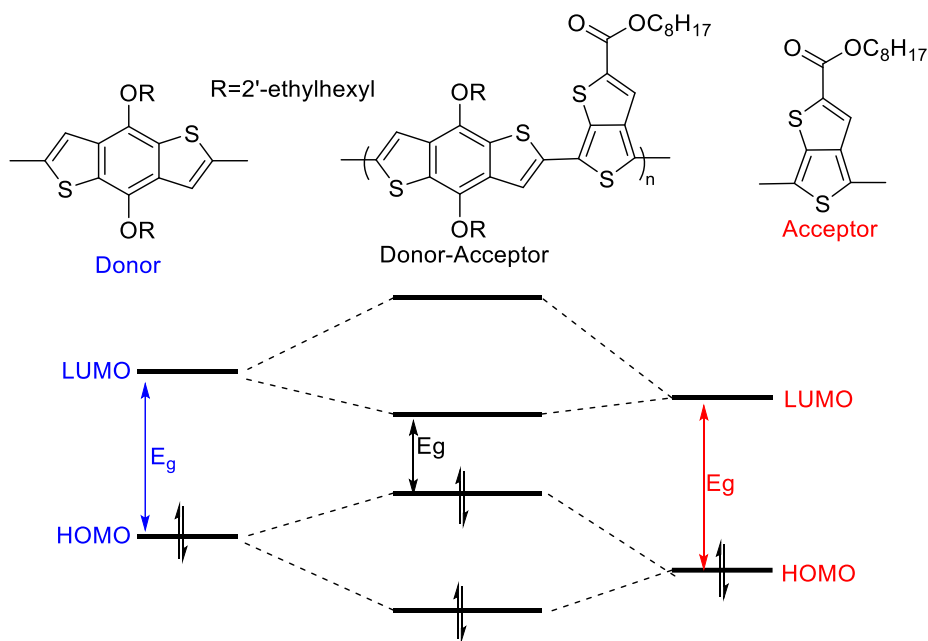


Figure 4.11- Molecular orbital diagram for donor-acceptor conjugated polymers.

4.4.5 INTRAMOLECULAR INTERACTIONS

So far, the discussed factors affect π -electron transport intramolecularly, however, the behavior of conjugated polymers in the solid state can also influence the electronic properties of the material. To begin, the way the polymer chains pack in the solid state is important for the transport properties of the material. A proper packing of the polymer chains ensures interactions between the π -systems of the polymers, which allows for good charge transport between polymer chains.²⁸³ The arrangement of the polymer chains in the solid state is often dictated by π -stacking interactions²⁸⁴ and through the organization of the polymer sidechains.²⁸⁵ π -Stacking interactions, i.e. attractive forces between aromatic rings, can be improved by utilizing small side chains or through the synthesis of regioregular polymers (**Figure 4.12A**).^{266,283} Other techniques include creating 2-dimensional polymers with aromatic moieties in the 2nd dimension that provide an additional layer of π -stacking thus increasing the order of the system in the solid state.²⁸⁶

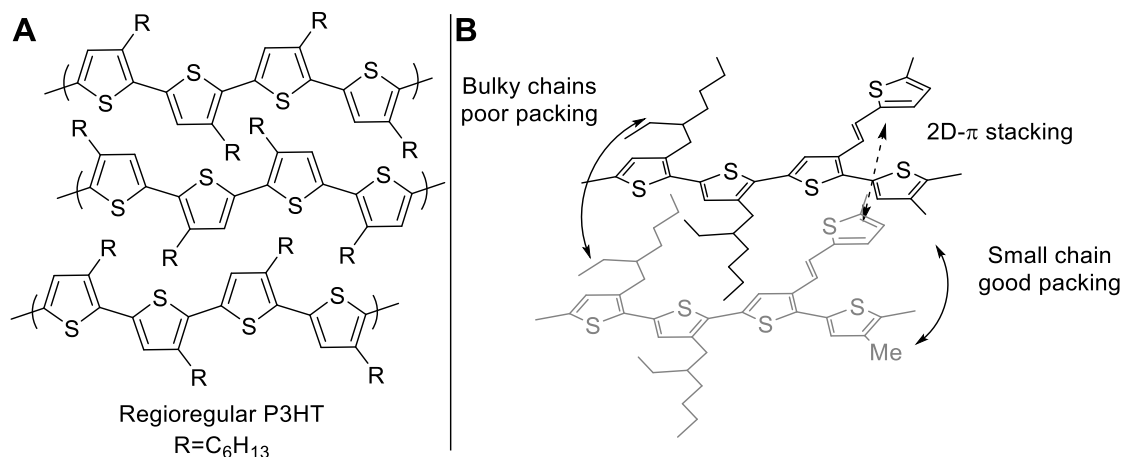
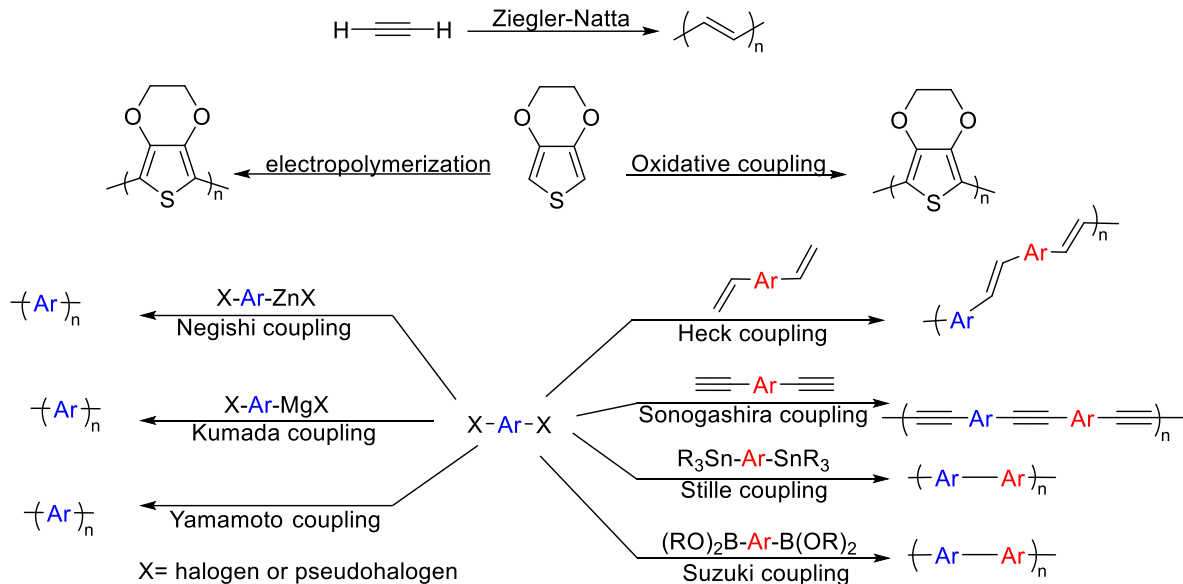


Figure 4.12-A- Lamellar structure of regioregular poly(3-hexylthiophene); **B-** Different effects on intermolecular interactions in the solid state.

Although π -stacking is critical to the transport properties of the material it can also be a detrimental factor as π -stacking can be responsible for poor solubility and aggregation.^{285,287,288} The introduction of bulky aliphatic sidechains are used to interfere with π -stacking and improve the solubility of the polymers. However, this consequently can have a negative effect on the intermolecular charge transport properties and increase the bandgap (**Figure 4.12B**).^{289,290} Thus, an intricate balance needs to be established between the solubilizing chains on the polymers and the degree by which the polymer chains can interact with one another.

4.5 SYNTHESIS OF CONJUGATED POLYMERS

The preparation of conjugated polymers requires the reliable construction of new carbon-carbon bonds between two sp^2 carbons. Not only do these reactions have to proceed continually to obtain high molecular weights but the polymerization must proceed in such a way as to minimize defects as much as possible. Since the electronic and optical properties are dependent on the conjugation within the polymer backbone, parameters such as molecular weight,²⁹¹ polydispersity²⁹² and structural defects^{261,293–295} can affect these properties. Thus, it is important to have access to reliable polymerization methods as, unlike small molecules, any defect or impurity becomes embedded within the polymer chain and cannot be removed.



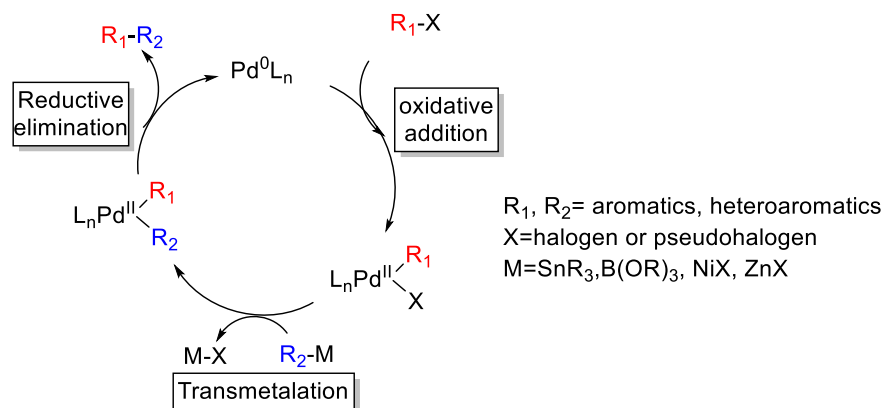
Scheme 4.1- Overview of traditional synthetic techniques for the preparation of conjugated polymers.²⁹⁶

Currently conjugated polymers are synthesized mainly through transition metal couplings (**Scheme 4.1**); however, other techniques are available but can be somewhat specific to a certain functional group. Prior to the advent of metal-catalyzed crossed couplings, conjugated polymers were mainly synthesized through oxidative coupling or electropolymerization with examples including polyphenylenes, polythiophenes, polypyrroles and polyanilines (**Scheme 4.1**).²⁹⁶ Other polymers such as the Nobel prize-winning polyacetylene could be synthesized using a Ziegler-Natta polymerization.²⁹⁷ Although oxidative coupling polymerizations still see some use, the reactions

do not offer the same level of control over the polymerization as transition metal catalyzed polymerizations. Herein, we will discuss some of the metal catalyzed polymerizations utilized to construct conjugated polymers as well as their advancements and drawbacks.

4.5.1 METAL CATALYZED POLYCONDENSATION OF CONJUGATED POLYMERS

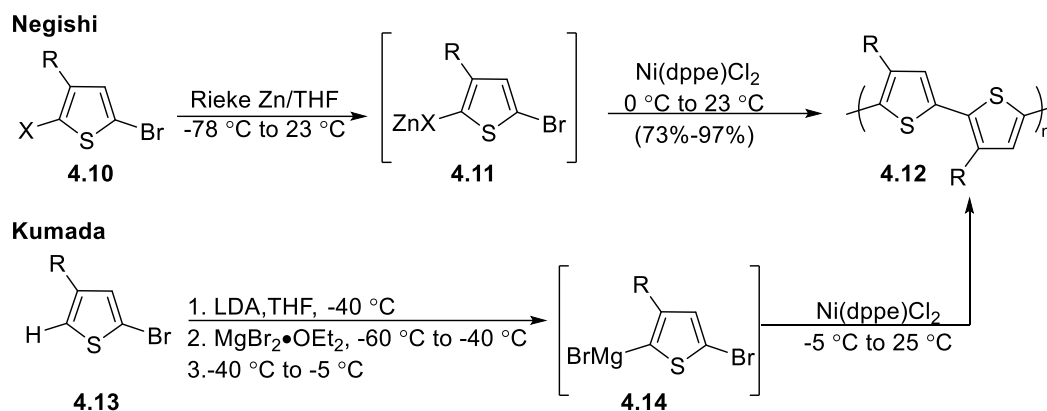
Transition metal (TM) catalyzed couplings were discovered in the early 1970s and expanded upon in the 1980s.^{298,299} Following their inception, TM couplings have become one of the most powerful ways of constructing C-C bonds. The general catalytic cycle for all metal catalyzed coupling follows the cycle outlined in **Scheme 4.2**. An oxidative addition occurs between an active catalyst and an aryl halide, with the catalyst inserting in between the aryl group and the halide. This is then followed by a transmetalation step, which exchanges the halide for another organic moiety. Finally, a reductive elimination takes place releasing the coupled product and regenerating the catalysts. The above example is showcased with palladium, but TM couplings are able to proceed with a variety of metals, with the most common being Ni and Pd.³⁰⁰



Scheme 4.2-Generic catalytic cycle for transition metal cross-couplings.

The preliminary reports concerning the synthesis of conjugated polymers via transition metal-catalyzed couplings made use of Ni catalysts (Kumada or Negishi couplings) to generate polythiophenes in high yield and high regioselectivity (**Scheme 4.3**).³⁰¹⁻³⁰³ These Ni catalyzed methods are still a reliable way to create conjugated polymers but suffer from some drawbacks as the high nucleophilicity of the monomers limits the substrate scope. Additionally, the reactions are air, temperature, and moisture sensitive due to the reactive intermediates and rapidly oxidizing

catalysts. Nonetheless, Ni catalyzed polymerizations have seen some further development and in some cases are able to proceed with step growth or living character.³⁰⁴



Scheme 4.3-Synthesis of polyalkylthiophene via Negishi and Kumada cross-couplings.

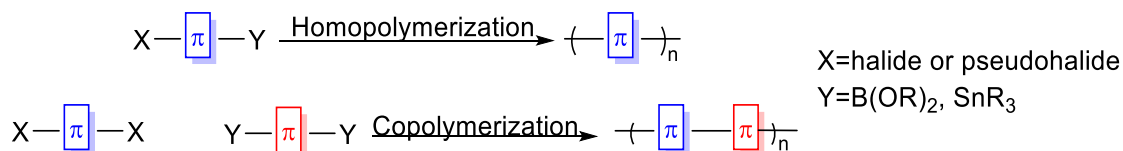
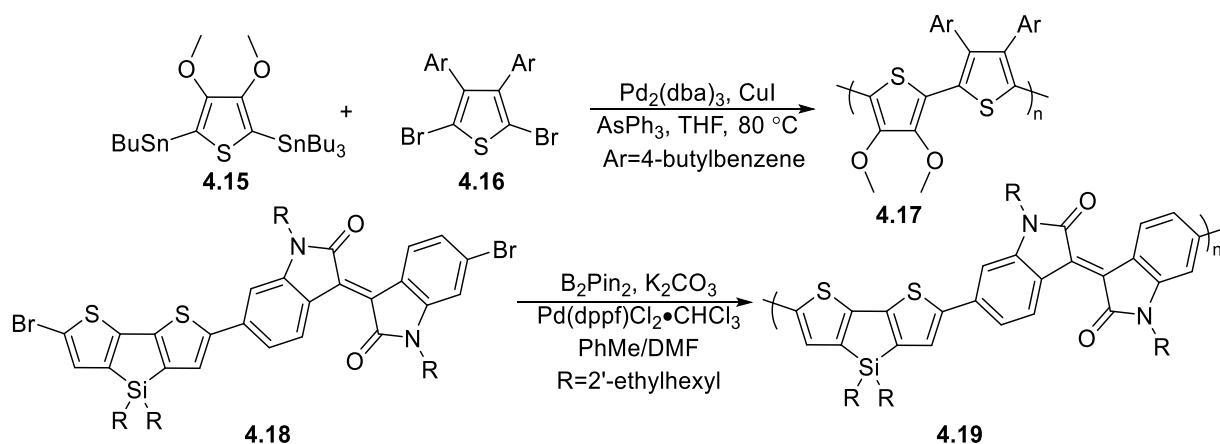


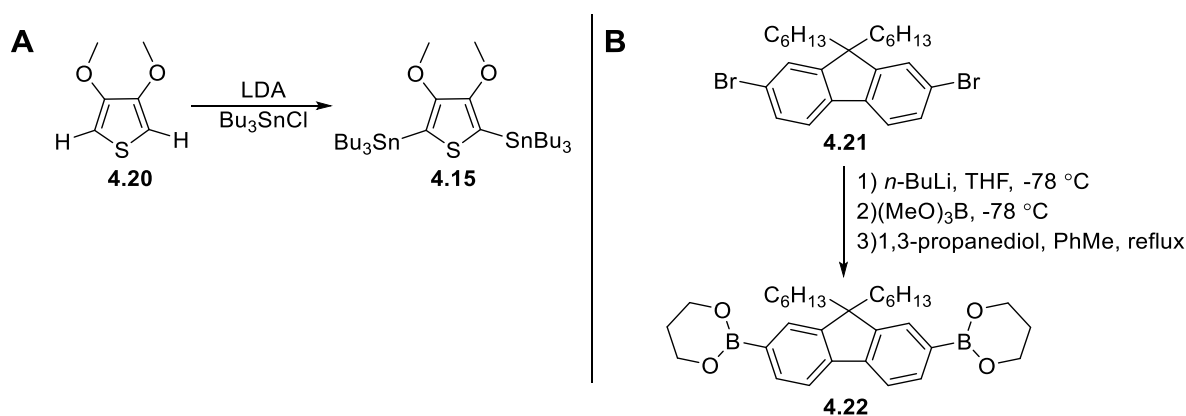
Figure 4.13- Schematic representation of homopolymerization and copolymerization for Stille and Suzuki cross coupling

Palladium catalyzed cross-coupling reactions, such as Stille and Suzuki cross-couplings, are the most popular methods by which conjugated polymers are synthesized. These reactions offer a greater range of functional group tolerance and can be carried out with stable organometallic intermediates, such as organoboranes and organostannanes. In comparison to Ni catalysts, Pd catalysts are more stable and less prone to side reactions such as homocouplings.³⁰⁵ Polymerizations with Pd catalysts can be performed in one of two ways. In an AB polymerization or homopolymerization, both the aryl halide and organometallic group lie on the same monomer. In an AA-BB polymerization, one monomer contains two aryl halides and a different monomer contains the organometallic components. The latter is usually preferred as it is easier to synthesize and offers in wider library of building blocks for conjugated copolymers.²⁹⁶

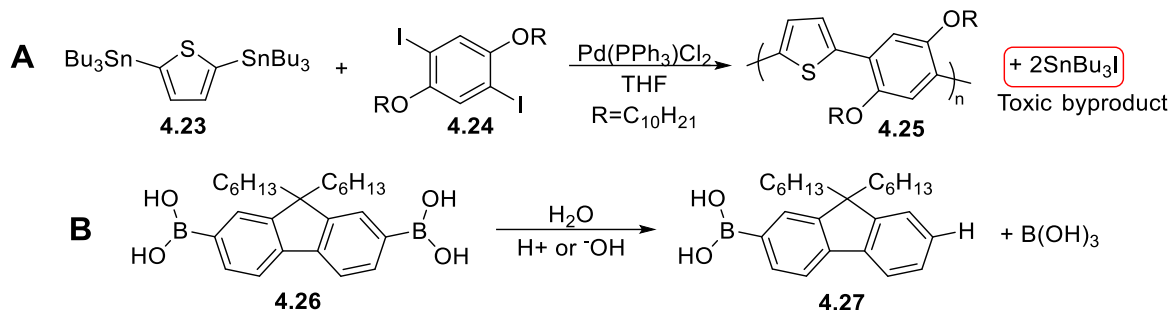


Scheme 4.4-Example of a Stille homopolymerization (top) and a Suzuki one-pot homopolymerization (bottom).²⁸²

Two examples of palladium catalyzed polycondensations are highlighted in **Scheme 4.4**. The first example is by Zhang and Tour, where the authors used a Stille-copolymerization to create a series of polythiophenes with narrow bandgaps.²⁸² Stille cross-coupling has a high functional group tolerance and thus allowed for the synthesis of polythiophene copolymers with functional groups including nitro, ketone, amine and quinone.^{282,306} A copper(I) salt was utilized to accelerate the rate of reaction by transmetalating with the organostannane creating a more reactive organocuprate.³⁰⁷ The second example is by Hummelen and coworkers, wherein the authors utilized a Suzuki polymerization on an acceptor-donor macromonomer but performed the reaction in one pot by synthesizing the organoborane *in situ*.³⁰⁸ This polymerization is unique as the monomer is both pre-functionalized and polymerized all in a single step.



Scheme 4.5- Pre-functionalization of Pd catalyzed cross coupling monomers for Stille (**A**) and Suzuki (**B**).^{282,309}



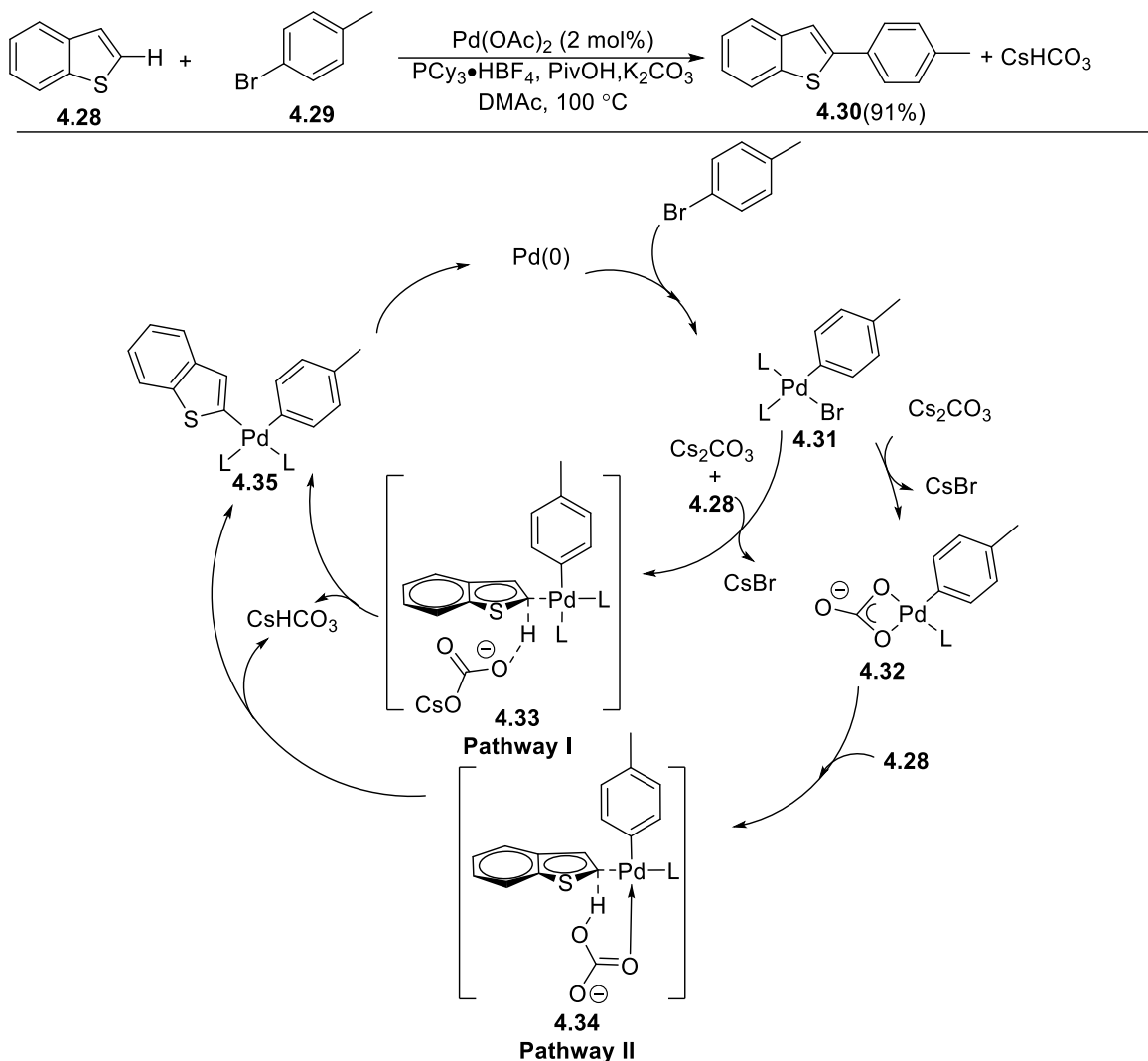
Scheme 4.6-Drawbacks of Pd catalyzed polycondensations; Stille copolymerization resulting in the formation of stoichiometric amount of toxic organotin waste (**A**).³¹⁰ Protodeboronation of a bifunctional Suzuki monomer (**B**).³¹¹

Although Suzuki and Stille cross-couplings have allowed for the construction of a wide library of conjugated polymers, the reactions are not without drawbacks. To begin, both Suzuki and Stille condensations require pre-functionalization of the monomers to the organometallic reagents (**Scheme 4.5**), which can be costly and often requires further purification. The reactions both produce a stoichiometric amount of organometallic waste, which in the case of a Stille condensation can lead to toxic organotin byproducts (**Scheme 4.6A**). Organoboranes used in Suzuki couplings can be subject to protodeboronations, a process wherein an organoborane is replaced by a proton, leading to the loss of functionality that can ultimately result in premature termination of the polymer chain (**Scheme 4.6B**).³¹¹ Finally, the Pd catalysts used for the polymerizations leave behind trace metal impurities that in most cases are detrimental to the electronic properties of the polymer.³¹²

4.5.2 DIRECT ARYLATION

Direct arylation is a relatively new Pd catalyzed cross coupling where an aryl halide can be coupled with an (hetero)arene without the need for an organometallic reagent.^{296,313–316} In contrast to previous methods (Suzuki, Stille, etc.) the reaction does not require any pre-functionalization steps and the only byproduct is a small molecule such as HBr or CsHCO₃. The reaction can proceed through several pathways with the most commonly accepted mechanism following a concerted metalation deprotonation (CMD) transition state, whereby the heteroaryl group is simultaneously deprotonated and metalated in a concerted process.³¹⁷ The catalytic cycle for direct arylation is shown in **Scheme 4.7**. Similarly to previous metal catalyzed couplings, the first step is an oxidative addition between the catalyst and aryl halide. Following this step, the reaction can take two possible pathways. Pathway I involves the carbonate aiding CMD without being bound to the catalysts, while pathway II sees the carbonate directly ligating

the metal center while deprotonating the heteroaryl.³¹⁷ Following the CMD step, a reductive elimination occurs releasing the coupled biaryl alongside the protonated carbonate.

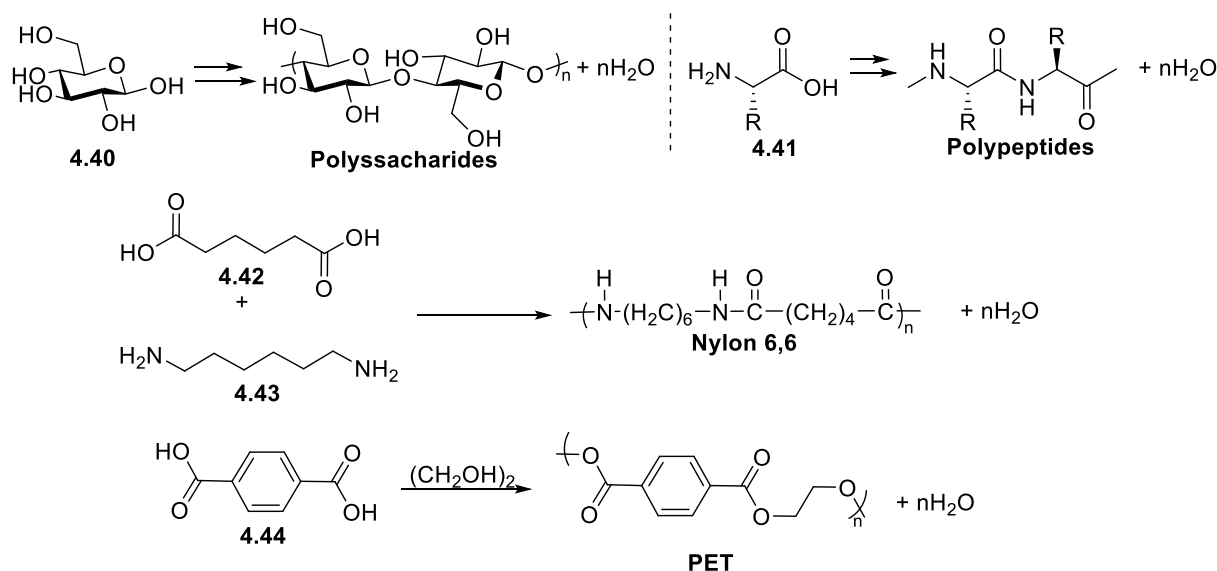


Scheme 4.7–Direct arylation of benzothiazole with 4-bromotoluene and catalytic cycle for direct arylation.³¹⁴

The impact of direct arylation on transition metal couplings cannot be overstated. The reaction allows for the simplification of synthesis and removes any toxic byproducts typically associated with metal catalyzed coupling reactions. Of particular interest is the use of direct arylation to create biaryl motifs, which are common in drugs, aromatic ligands, and in conjugated aromatic materials.³¹⁴ Soon after the discovery of direct arylation, the method saw use in the synthesis of conjugated polymers and thus far has allowed for the preparation of conjugated polymers with properties that match or surpass polymers previously synthesized with Suzuki or Stille cross-couplings couplings.^{296,313,315} An example of the performance of direct arylation polymerization can be seen in Leclerc and

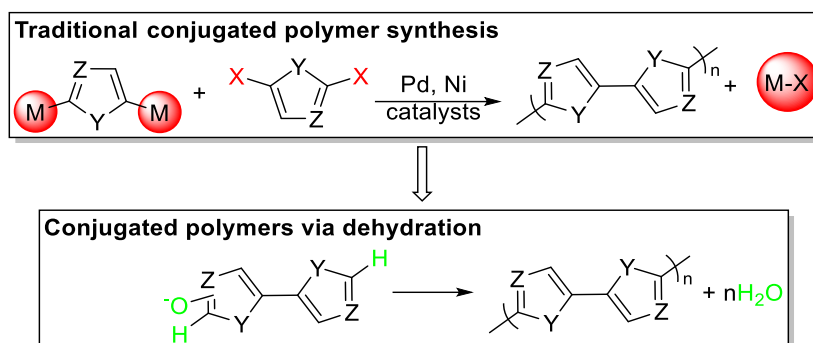
4.6 CONDENSATION POLYMERIZATION OF COMMODITY POLYMERS

There are two main drawbacks surrounding metal catalyzed polymerizations: Firstly, the polymerization requires the use of a transition metal catalyst (typically Pd) which can be costly and leaves metallic residues within the polymer. Secondly, traditional coupling techniques require the use of complex organometallic reagents that can generate a stoichiometric amount of potentially toxic waste following the polymerization. In contrast, many of the commodity polymers we enjoy today are synthesized at industrial scales and leave behind no byproducts. Of particular interest is dehydration polymerization, whereby two monomers react leaving a molecule of water behind as the sole byproduct. Glycosidic and peptide bonds found in nature are the most common iterations of these reactions and are responsible for biopolymers such as polysaccharides, polyamides, polypeptides, and the highly abundant cellulose.³²⁰ Moreover, dehydration polymerizations are employed for the large-scale manufacturing of polymers such as nylon 6,6, and polyesters including polyethylene terephthalate (PET).³²¹ Even though dehydration polymerization had been a historically important reaction with vast applicability and conjugated polymers are in high demand, there have not been any prior reports regards the dehydration polymerization for the synthesis of poly(hetero)aromatics.



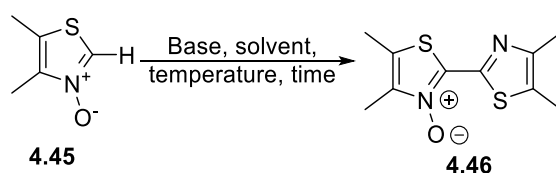
Scheme 4.9- Synthesis of biopolymers and commodity polymers through dehydration polymerization.

4.7-DEHYDRATION POLYMERIZATION OF POLY(HETERO)ARENES³²²



Scheme 4.10-Traditional synthesis of conjugated polymers versus dehydration polymerization for the preparation of conjugated polymers. Z is a carbon or heteroatom, Y is a heteroatom, X is a halide.

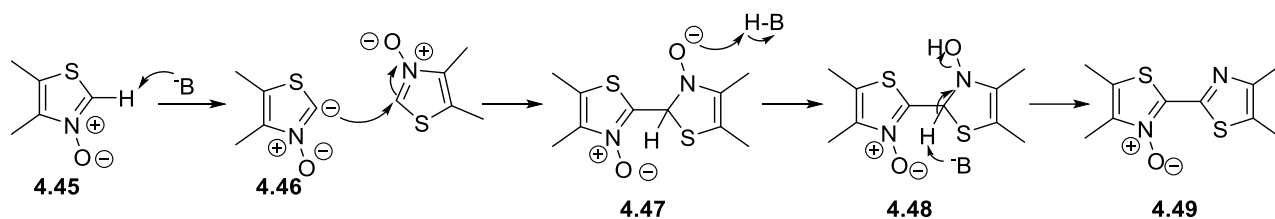
An initial goal was to develop a new set of conditions that allowed for a dehydrative polymerization to form poly(hetero)arenes, thus negating the need for a catalyst and providing only water as the byproduct. Our preliminary finding was observed while investigating the reactivities of thiazole *N*-oxides which in contrast to other direct arylation reactions are able to proceed under mild conditions.^{323,324} While experimenting with different conditions, 2,5-dimethylthiazole *N*-oxide **4.45** was reacted in the absence of a metal catalyst under basic conditions and gratifyingly was able to produce a bithiazole dimer **4.46** in 25% yield. Although not a dehydration, the formation of the thiazole dimer proceeds through the loss of an oxygen and two hydrogens, meaning formally, one water molecule has been lost. This ensuing reactivity opened the door towards the dehydrative polymerization of thiazole and would finally give rise to a long-sought technique to synthesize poly(hetero)arene conjugated material.



Entry	Solvent	Base	Temperature (°C)	Time (min)	Yield (%)
1	PhMe	NaO ^t Bu	90	30	25
2	PhMe	NaO ^t Bu	50	30	63
3	PhMe	NaO ^t Bu	rt	30	25
4	PhMe	LiO ^t Bu	rt	30	83
5	Et ₂ O	NaO ^t Bu	rt	30	70
6	THF	LiO ^t Bu	0	30	77
7	THF	LiO ^t Bu	0 to rt	5	89

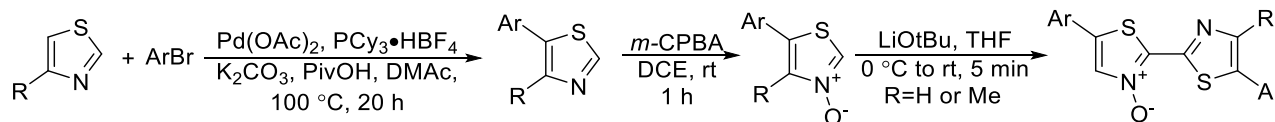
Table 4.1-Optimization of thiazole dimerization. 1 equiv of 4,5-dimethylthiazole *N*-oxide was reacted with 1.5 equiv of base in 0.25 M solvent. Initial optimization carried out by Dr. Michael R. Emmett.

Following our initial result, we set out to optimize the reaction towards an increased yield (**Table 4.1**). Our first step was to reduce the reaction temperature, which led to an increase in yield to 63% (**Table 4.1-Entry 2**). Further cooling the reaction led to a decrease in yield (**Table 4.1-Entry 3**), however, when the base was swapped for LiO^tBu the yield was substantially increased to 83% (**Table 4.1-Entry 4**). Switching to ethereal solvent resulted in an improved yield but our best results were obtained when the reaction was conducted in THF with LiO^tBu from 0 °C to room temperature over a 5-min period resulting in an 89% yield (**Table 4.1-Entry 7**).



Scheme 4.11- Proposed mechanism for dehydrative dimerization of 4,5-dimethylthiazole.

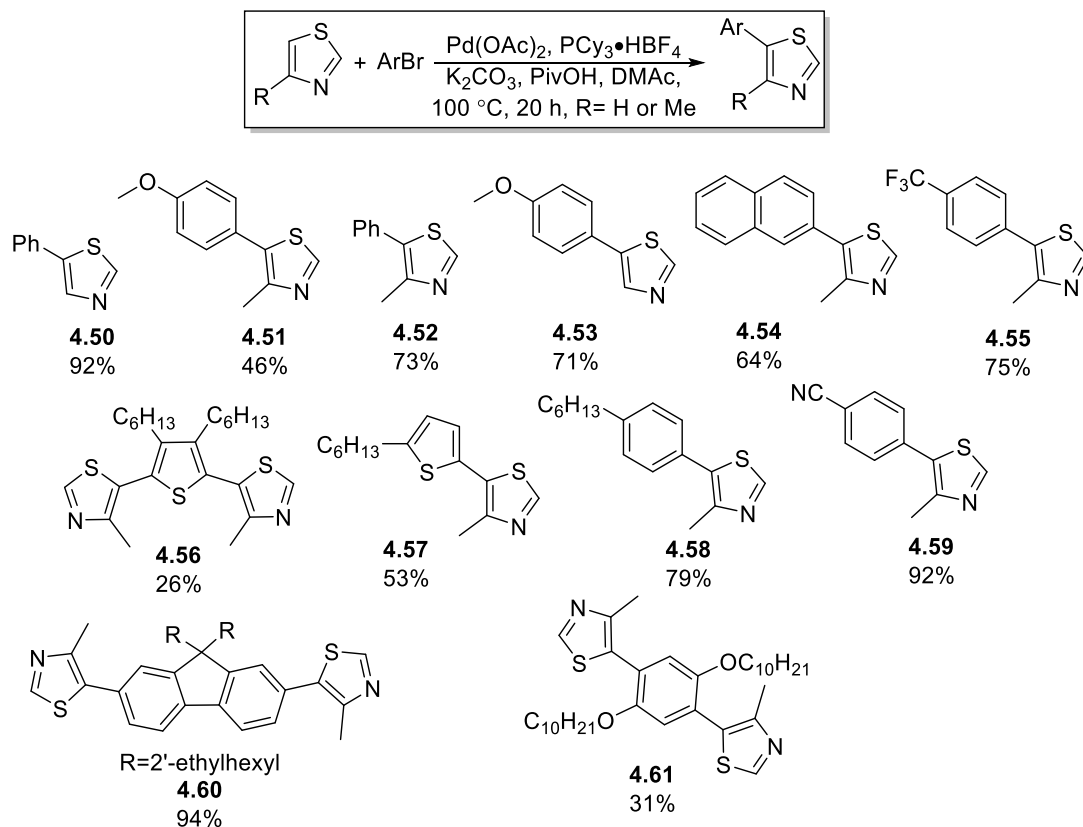
A proposed mechanism based on known reactivity is outlined in **Scheme 4.11**. First a deprotonation occurs at the 2-position of the thiazole *N*-oxide making that carbon nucleophilic. The newly formed anion then proceeds to attack another equivalent of *N*-oxide leading to intermediate **4.47**. The *N*-oxide proceeds to abstract a proton from the conjugate acid leading to intermediate **4.48**. An equivalent of base then deprotonates the thiazole to restore aromaticity expelling hydroxide in the process and arriving at the thiazole dimer **4.49**. It is also possible that the reaction is proceeding through a carbene intermediate as thiazoles can form persistent carbenes,³²⁵ however, no further studies were performed to confirm the nature of the mechanism.



Scheme 4.12- Thiazole dehydration substrate scope general outline.

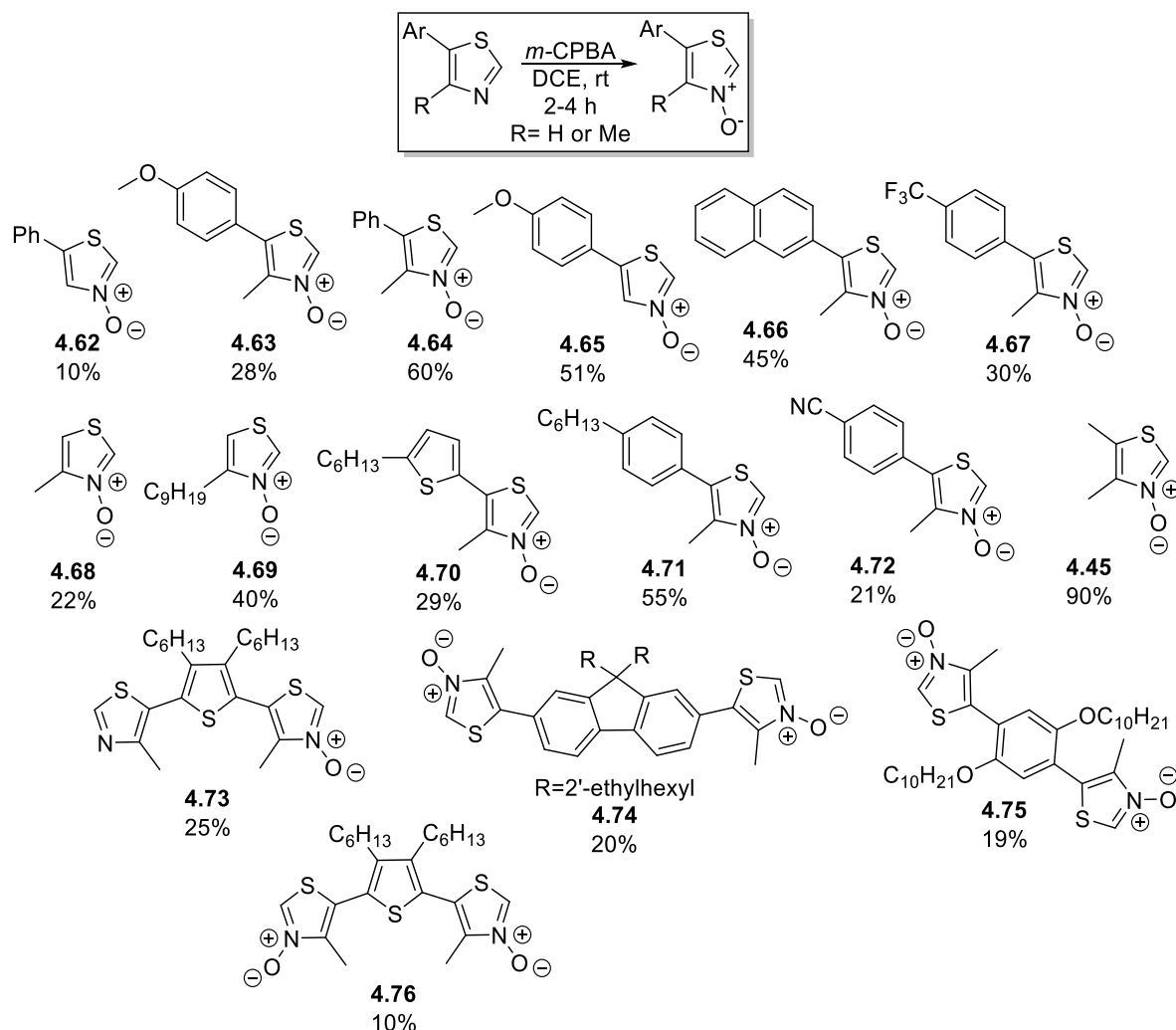
With the optimized conditions in hand, we set out to determine the functional group tolerance of our newly developed reaction, however, prior to synthesizing our dehydration dimers, we needed to synthesize the corresponding thiazole *N*-oxides. The synthetic route to the *N*-oxide precursors is outlined in **Scheme 4.12**. Starting

with thiazole, we performed a direct arylation to introduce different groups onto the thiazole (**Scheme 4.13**). Following the direct arylation, the thiazoles were oxidized to the thiazole *N*-oxide with *m*CPBA which was then followed by our dehydration conditions to yield the thiazole dimers.



Scheme 4.13-Synthesis of thiazole *N*-oxide precursors by direct arylation. Reactions were carried out with 1.5 equiv of thiazole, 1 equiv of aryl bromide, 1.5 equiv of K_2CO_3 , $Pd(OAc)_2$ (2 mol%), PCy_3HBF_4 (4 mol%), 0.3 equiv of *PivOH* in *DMAc* [0.5 M] for 20 h at 100 °C.

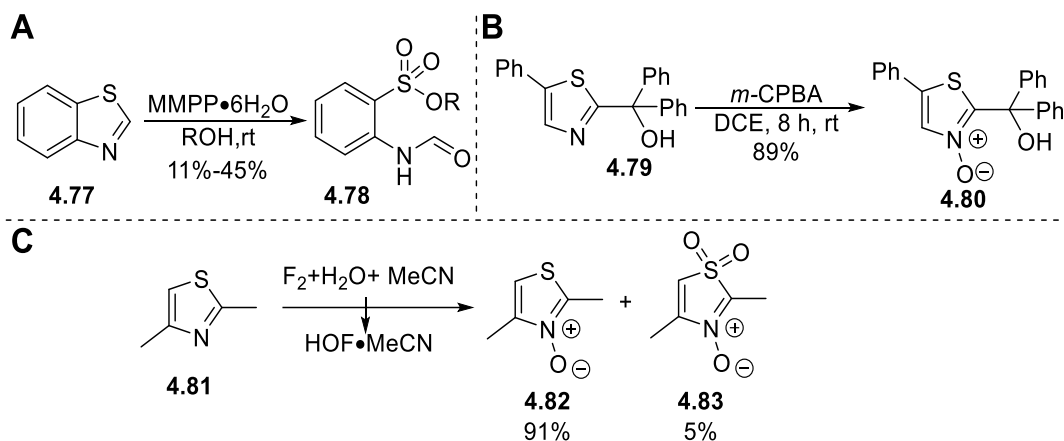
We began by synthesizing a variety of aryl thiophenes through direct arylation which proceeded in good yields. Through direct arylation we were able to create electron rich (**4.51**, **4.54**) and poor thiazoles (**4.55**, **4.59**) and we were also able to access heteroaryls (**4.57**, **4.56**) to create oligomers further down the line. We also synthesized bifunctional monomers (**4.56**, **4.60**, **4.61**) that served as our starting material for the polymerization. The fluorene monomer proceeded in good yield while the thiophene and 1,4-alkoxybenzenes gave lower yields.



Scheme 4.14—Oxidation of thiazole with *m*CPBA. Oxidations were carried out with 1 equiv of thiazole, 1.5 equiv of *m*-CPBA in DCE [0.33 M] for 2–4 h.

Following the direct arylation, we proceeded with the thiazole oxidation with our recently made compounds as well as some other commercially available thiazoles. The oxidation of thiazole was one of the major hurdles of the project as it proved quite difficult to raise the yield of the oxidation above 50% for most substrates, with the only exception being 4,5-dimethylthiazole **4.45**. Critical to the success of the oxidation was the substitution of the thiazole at the 4-position. Thiazoles that were not substituted were difficult to oxidize (**4.62**) and as a consequence we were not able to show the dehydration reaction on unsubstituted thiazoles. *m*-CPBA was the only oxidant able to provide decent yields, we did however screen other oxidants including Koser's reagent, MMPP, ClO₂, H₂O₂, Mo(CO)₆/*t*-BuOOH, DMDO, and PhIO but these oxidants gave lower yields or no reaction. In addition to the low yields, the thiazole *N*-oxides were heat sensitive, thus the purification of these compounds was tedious as the

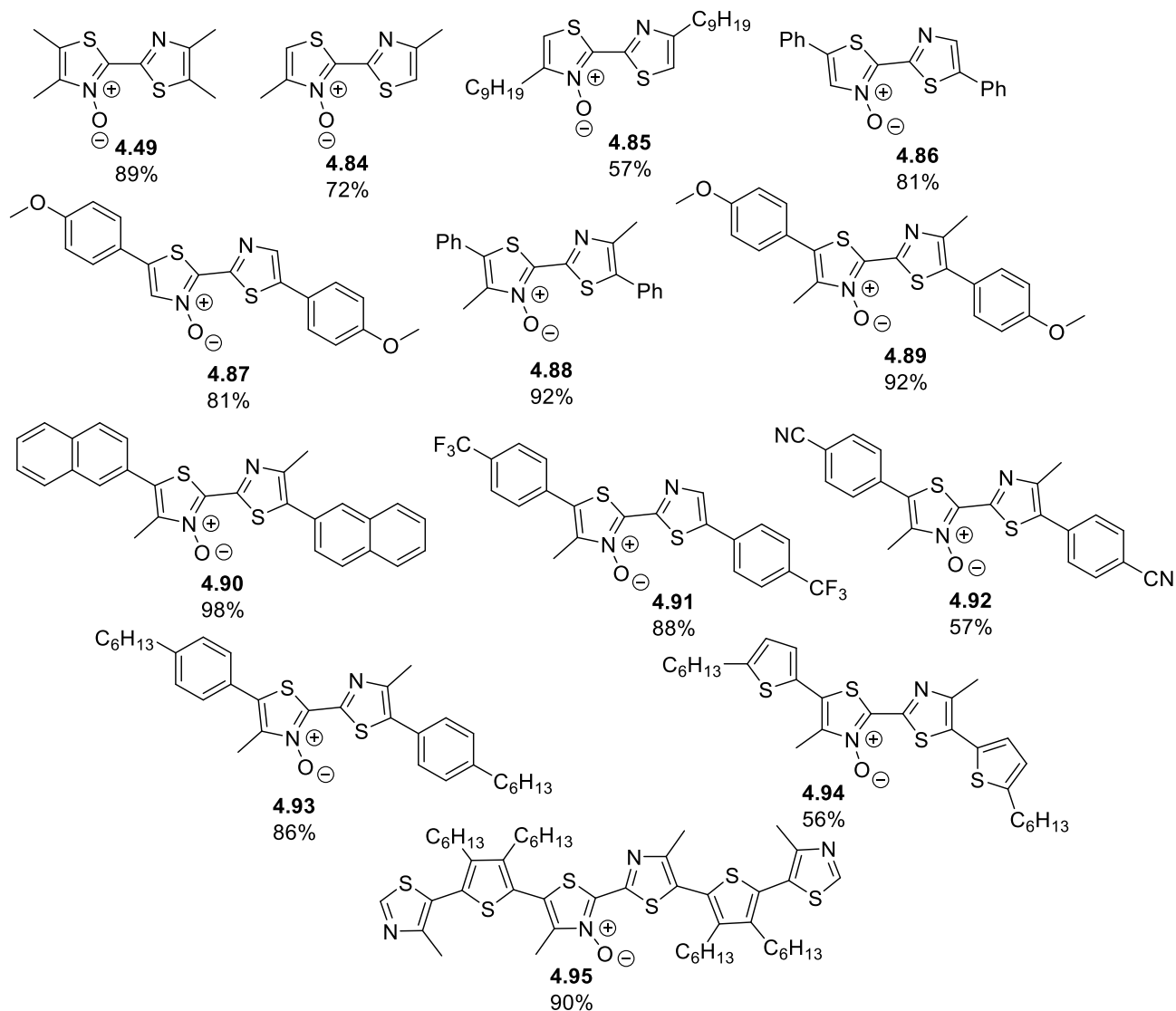
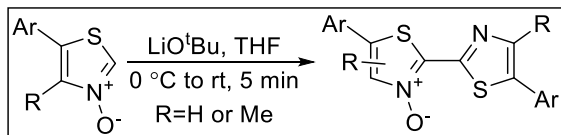
temperature could not be raised above 30 °C without risking decomposition. Even though the oxidation conditions proved less than ideal we proceeded to oxidize our thiazole with yields ranging from 10%-90%. Bisthiazole-N,N,-dioxides (**4.74-4.76**) were also synthesized using this method. The oxidation was somewhat challenging due to the high polarity of the product and due to the tendency for the sulfur to oxidize if an excess of oxidant was utilized.



Scheme

4.15-A-Oxidative ring opening of benzothiazoles.³²⁶ **B**-Directed oxidation of thiazoles through a diphenyl carbinol.³²⁷ **C**-Oxidation of thiazoles with Rozen's reagent.³²⁸

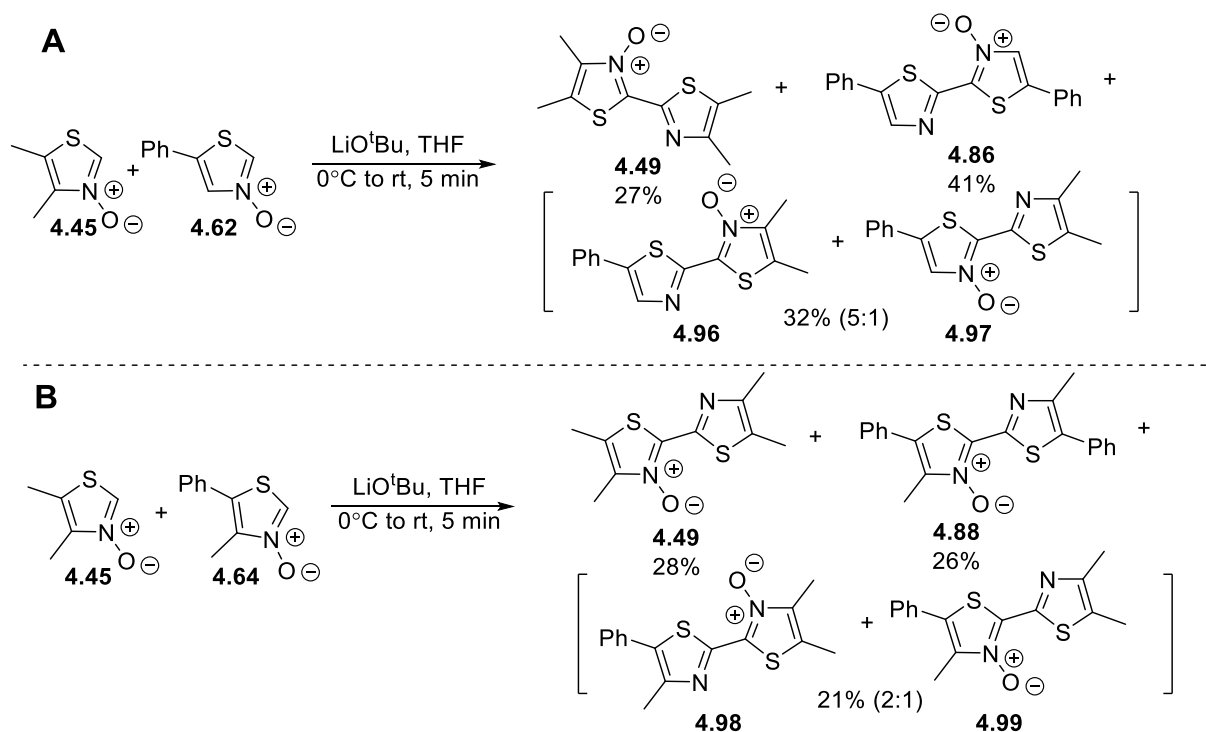
The temperature instability of thiazole *N*-oxides was thoroughly investigated, although it is inconclusive as to how thiazole *N*-oxides decompose. Our best hypothesis proposes that under heat thiazole *N*-oxides undergo a ring opening reaction. We did collect some evidence on this mechanism when our group observed that if benzothiazole was oxidized with MMPP then a ring opening product was isolated rather than benzothiazole *N*-oxide (**Scheme 4.15A**).³²⁶ To combat the *N*-oxide decomposition and improve the yield of the oxidation, our group developed a new technique to oxidize thiazoles which relied on the instalment of a diphenyl carbinol that helped direct the oxidation (**Scheme 4.15C**).³²⁷ This new method allowed for much higher oxidation yields and prevented the decomposition of the thiazole *N*-oxides, thus allowing for a less tedious isolation. Following the preparation of the *N*-oxide, the compound was subject to the similar dehydration conditions following the addition of base. This new method provides a good alternative to more forcing methods such as Rozen's reagent (**Scheme 4.15C**), an electrophilic oxidant generated from the reaction of fluorine gas, water and acetonitrile.³²⁸



Scheme 4.16-Reaction scope for the dehydrative coupling of thiazole *N*-oxides. Reactions were run with 1 equiv of *N*-oxide and 1.5 equiv of LiOtBu in THF[0.25 M].

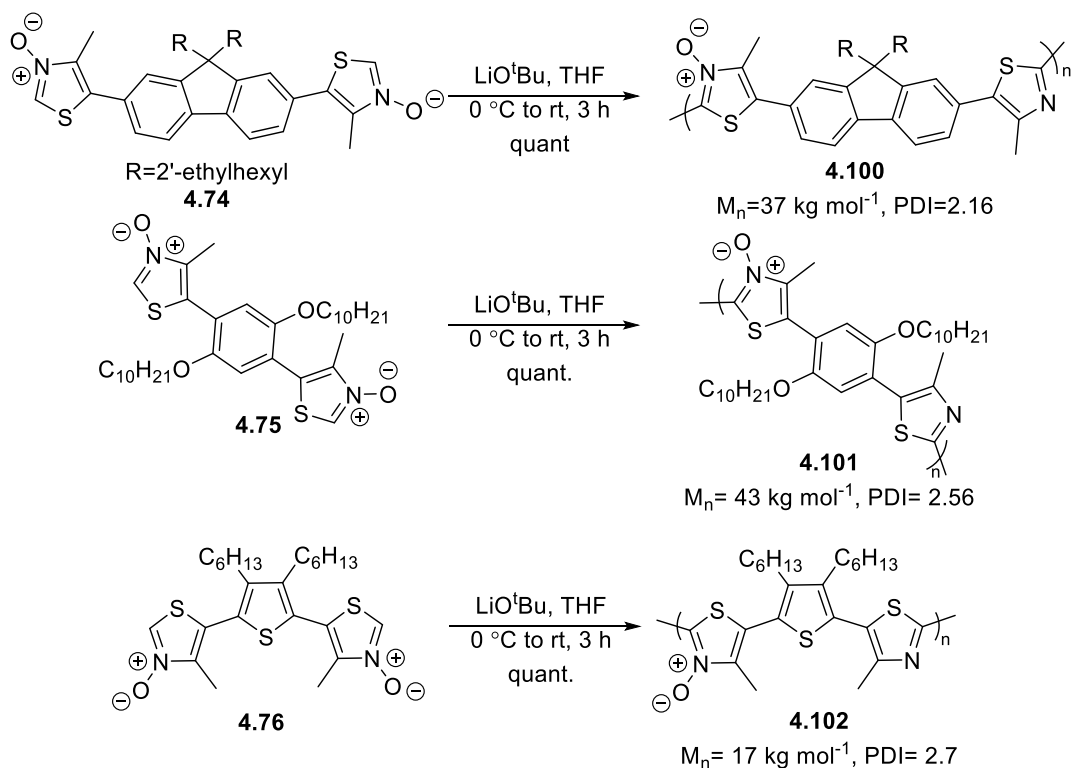
With the *N*-oxides in hand, we proceeded to perform the dehydrative coupling of a variety of thiazole *N*-oxides. The reaction was found to proceed well with alkyl (**4.49-4.85**), aryl (**4.86**, **4.88**, **4.90**, **4.93**) and heteroaryl substituents (**4.94-4.95**) as well as electron poor (**4.91-4.92**) and electron rich substituents (**4.87**, **4.89**). Additionally, the reaction was able to couple heteroarenes to construct small heteroaryl conjugated oligomers (**4.94-4.95**). Of particular interest in compound **4.95**, that in theory could be oxidized further and propagated via an iterative-

convergent/divergent (IDC) approach to yield molecularly defined conjugated heteroaryls.³²⁹ This was attempted by our group with some level of success; however, we were met with several regioselectivity issues when faced with the oxidation and our choices of oxidant were limited as only *m*CPBA yielded good results.³³⁰ Consequently, the approach has not been explored further but it may be worth revisiting using our newly developed chemistry.



Scheme 4.17- Dehydrative cross couplings of thiazoles. Reactions were run with 1 equiv each of *N*-oxide and 3.0 equiv of LiOtBu in THF [0.25 M].

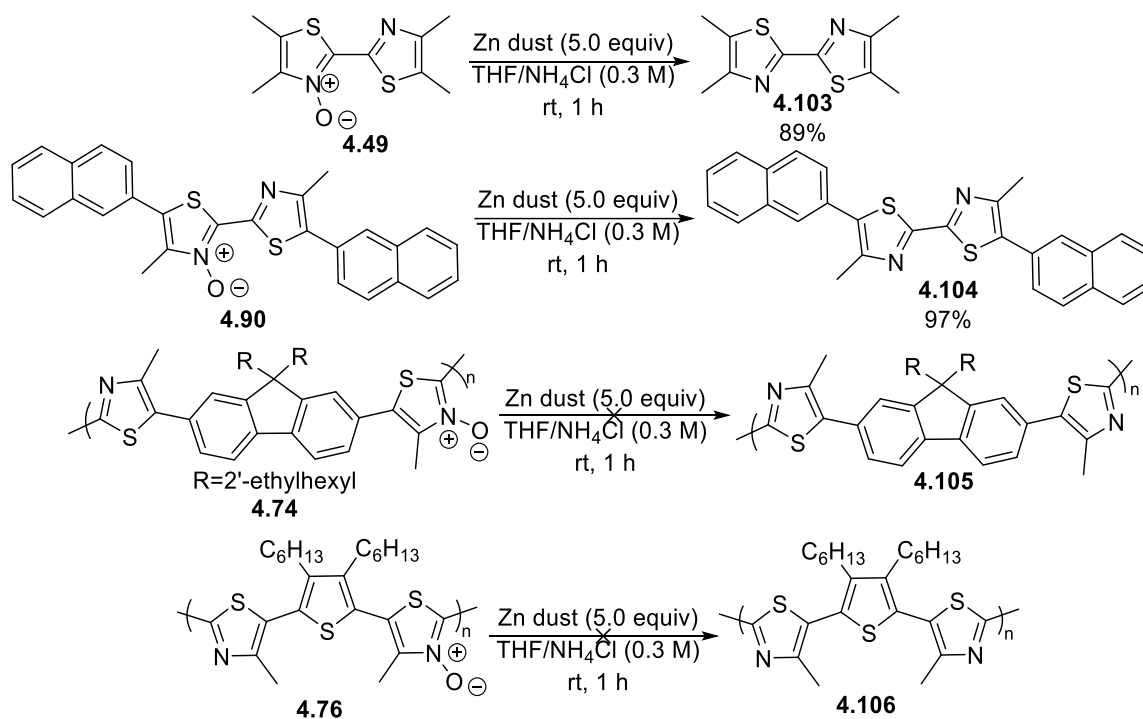
We were also able to display the mixed dehydrative cross coupling of thiazoles (**Scheme 4.17**). The reaction was able to yield the cross dimerized products as well as the respective homodimers in good yield. In terms of regioselectivity, the only observation we can make is that the *N*-oxide remaining from the dehydration prefers to lie with the less hindered thiazole, however, we have not collected enough data to support this claim. For **Scheme 4.16A** we were able to isolate each individual component of the reaction while for **Scheme 4.17 B** we observed the two cross-dimer regioisomers by ¹H NMR.



Scheme 4.18-Dehydration polymerization of thiazole *N*-oxides.

Following the successful demonstration of our dehydration dimerizations on small molecules, we proceeded to attempt the dehydration for the synthesis of poly(hetero)arenes (**Scheme 4.18**). We exposed the bifunctional monomer **4.74** to LiOtBu and were pleased to see the immediate formation of polymer characterized by the precipitation of red fibers upon introduction of the base to the reaction mixture. This methodology was repeated for monomers **4.75** and **4.76** to yield conjugated polymers in quantitative yield and with high molecular weight. To our knowledge, this was the first example of a poly(heteroarene) synthesized through dehydrative polymerization; similar polymers had to be synthesized with transition metal catalysts.³³¹ It should be noted that since our polycondensation is metal free then the polymerization should follow Carothers' condensation kinetics (i.e. $\text{PDI} \leq 2$);³³² though this discrepancy in the PDI is likely due to side reactions that occur during the polymerization that we are currently not aware of but may be able to track through a more thorough analysis of the polymers by ^1H NMR.

The level of oxidation within a conjugated small molecule or polymer can affect the optical and electronic properties of the material,³³³ we therefore were interested in whether it was possible to remove *N*-oxides remaining from the dehydration. We exposed dimer **4.49** and **4.90** to reducing conditions using zinc dust and were able to successfully deoxygenate the dimers in good yield (**Scheme 4.19**). This procedure was extended onto our dehydration polymers, but we suspect that we were unable to deoxygenate the polymers as analysis by UV-VIS and GPC revealed no change in the polymer's properties. This lack of reactivity is most likely due to the compounds' solubility and the difficulty associated with performing chemical transformations on polymers. Although we were unable to remove the oxide from our polymers, further studies in our lab revealed that *N*-oxides can form chalcogen bonds with the neighboring sulfur thus planarizing the molecule and lowering the bandgap.²⁷⁷



Scheme 4.19-Deoxygenation of thiazole dehydration dimers and polymers.

4.8 CONCLUSIONS

Drawing inspiration from historically important dehydration reactions we were able to create a new polymerization method for the synthesis of poly(heteroarenes) that can produce conjugated polymers in high yield and high molecular weight. The reaction is able to yield coupled products in high yield without the aid of a transition metal

and with the only byproduct being the formal loss of water. Our dehydrative methodology is also amenable to a wide variety of substrates including alkyl, aryl, and heteroaromatics as well as electron rich and poor arenes with yields up to 98%.

This new methodology has inspired other studies in our laboratory that have improved upon our initial reports with higher oxidation yields and a larger scope of compounds.^{277,327} The polymers and dehydration adducts were all examined by UV-VIS, fluorescence, and cyclic voltammetry to examine their optoelectronic properties (See supporting information); however, the materials themselves did not display properties worthy of further evaluation in device applications. In the future, dehydrative polymerization may be combined with bandgap engineering techniques to create low bandgap polymers rapidly with the only major byproduct being the formal loss of water.

PART 2: CHAPTER 5

DESIGN OF A NEW PALLADIUM PRECATALYST FOR DIRECT (HETERO)ARYLATION POLYMERIZATION

5.1 DIRECT (HETERO)ARYLATION POLYMERIZATION

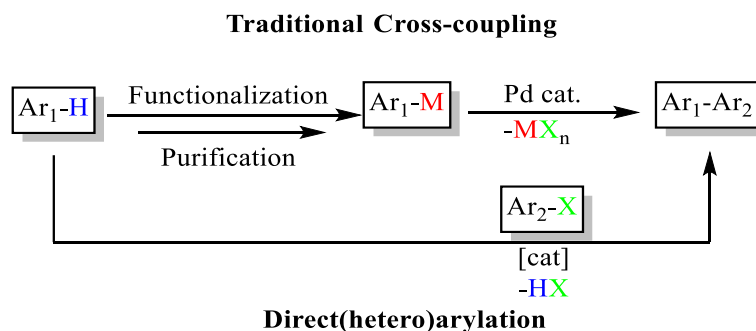
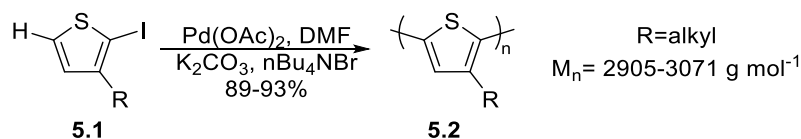


Figure 5.1-Comparison between traditional cross coupling reactions and direct(hetero)arylation.³¹³

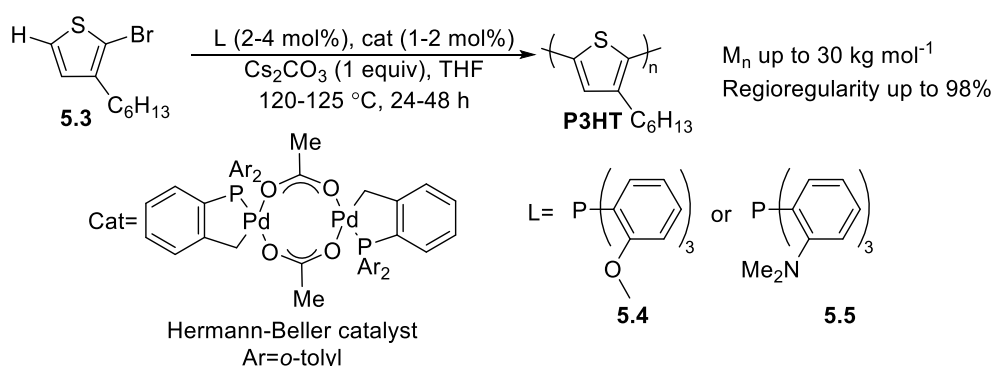
As discussed in **Chapter 4**, direct arylation is a new way of synthesizing conjugated polymers that bypasses the traditional requirement for pre-functionalization and instead proceeds solely from an aryl halide and a heteroaryl generating only a small molecule, such as HBr, as a byproduct.^{296,313,315} The mechanism of the reaction was discussed in **Chapter 4**, but in summary, the reaction follows a similar catalytic cycle to traditional metal catalyzed couplings with the key step in the catalytic cycle being the CMD transition state.³¹⁷ While most conjugated polymers are still synthesized by traditional methods, in particular by Stille coupling, direct arylation is beginning to emerge as a powerful alternative from which conjugated material can be accessed.



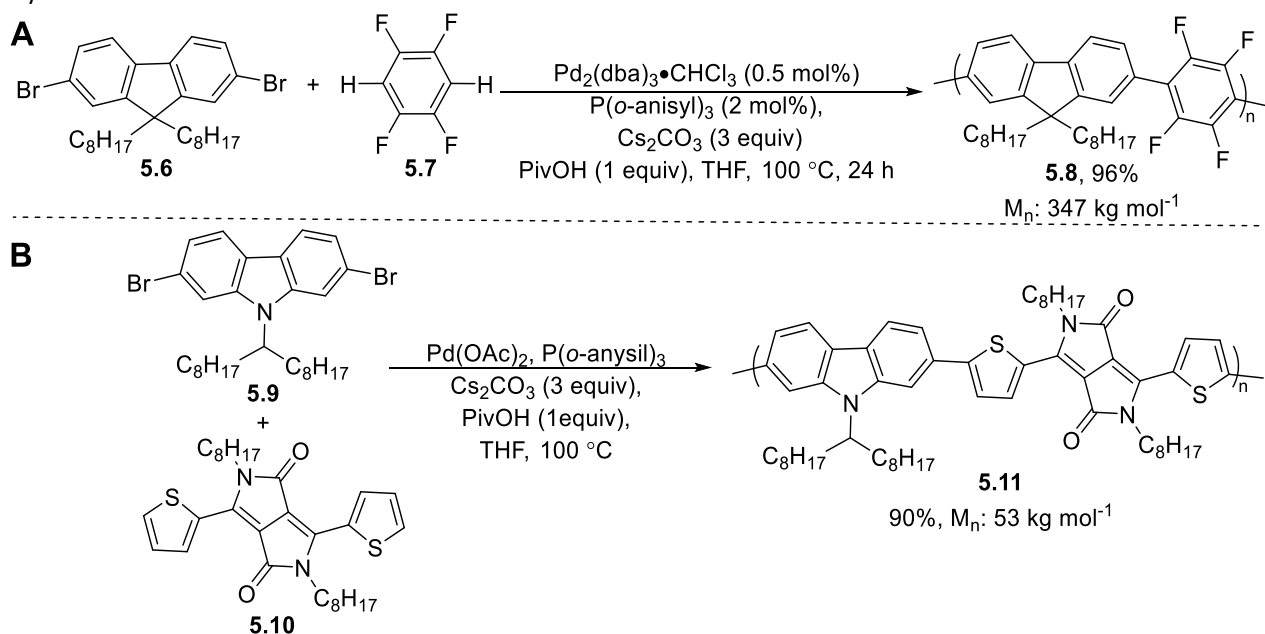
Scheme 5.1- Lemaire and coworkers synthesis of polyalkylthiophenes.³³⁴

C-H activation reactions have been known since the 1960s³³⁵ yet their application towards the synthesis of conjugated polymers was not reported until recently. The first example of a direct arylation polymerization was described by Lemaire and coworkers in 1999, where the authors polymerized **5.1** to create polyalkylthiophenes with number average molecular weights around 3 kg mol^{-1} in good yield.³³⁴ Since direct arylation was not an established

method at the time, the authors hypothesized that the reaction proceeded through a Heck-like mechanism.³³⁴ Following Lemaire's report, direct arylation polymerization did not see much use until 2010 when Ozawa and coworkers were able to demonstrate the efficient synthesis of highly regioregular polythiophene using a palladium catalyzed dehydrohalogenative polycondensation.³¹⁹ For this seminal report, the authors utilized the highly stable Herrmann-Beller catalyst in tandem with the ligands $P(o\text{-anisyl})_3$ **5.4** or $P(o\text{-aniline})_3$ **5.5** to yield polyalkylthiophenes with regioregularities as high as 98% as well as number average molecular weights ranging from 24 kg mol⁻¹ to 30 kg mol⁻¹.



Scheme 5.2- Ozawa and coworkers' synthesis of highly regioregular poly(3-hexylthiophene) through direct arylation.³¹⁹



Scheme 5.3-A- Ozawa and coworkers' synthesis of PDOF-TP **5.8**.³³⁶ **B-** Leclerc and coworkers' synthesis of PCDDP **5.11**.¹⁷⁴

Ozawa's synthesis of **P3HT** renewed interest in direct arylation, which resulted in a growing number of publications in the following years that utilized the new polymerization technique. The reaction has since been utilized to construct a variety of conjugated polymers with electron-rich and electron poor monomers and in some cases, the polymers synthesized through direct arylation display similar or better properties than polymers synthesized with traditional coupling reactions.^{296,313,315} Two examples of direct (hetero)arylation polymerization (DHAP) are highlighted in **Scheme 5.3**. The first example is once again by Ozawa and coworkers, for this report the authors were able to construct PDOF-TP **5.8** in high molecular weight (up to 346 kg mol⁻¹!) via DHAP using Pd₂dba₃·CHCl₃ as the catalyst and P(*o*-anisyl)₃ **5.4** as the ligand.³³⁶ With a few exceptions, most polymerizations up to that point were carried out in highly polar solvents, such as DMF or DMAc,^{337,338} where the catalysis seemed most efficient; however, these solvents are not ideal for polymer solubility.³³⁶ By carefully screening conditions including the catalyst, ligand, carboxylate additives, and solvent, Ozawa and coworkers were able to show how DHAP can be tuned to yield high molecular weight conjugated polymers. The second example is by Leclerc and coworkers (**Scheme 5.3B**),¹⁷⁴ herein, the authors developed a set of conditions that was applicable towards several monomers and allowed for the construction of high weight molecular weight conjugated polymers in good yield with minimal defects. **Scheme 5.3B** highlights the use of these optimized conditions to synthesize the push/pull co-polymer PCDDP **5.11**.

5.2 EFFECT OF THE LIGAND ON DIRECT (HETERO)ARYLATION POLYMERIZATION

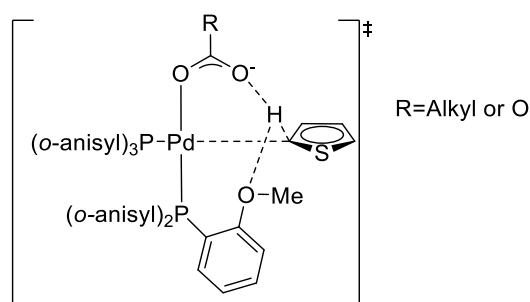
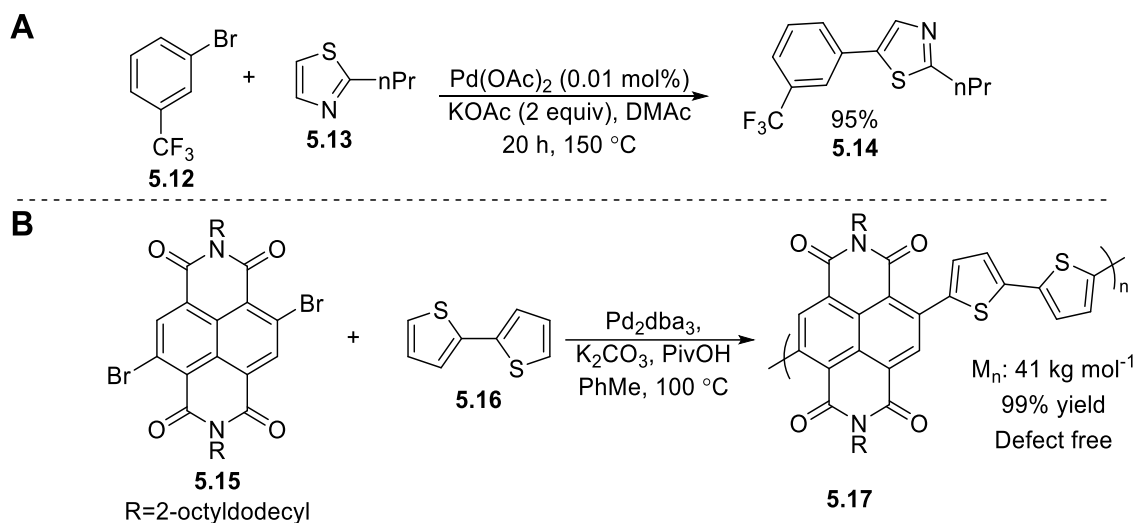


Figure 5.2- Effect of coordinating ligands on CMD transition state.

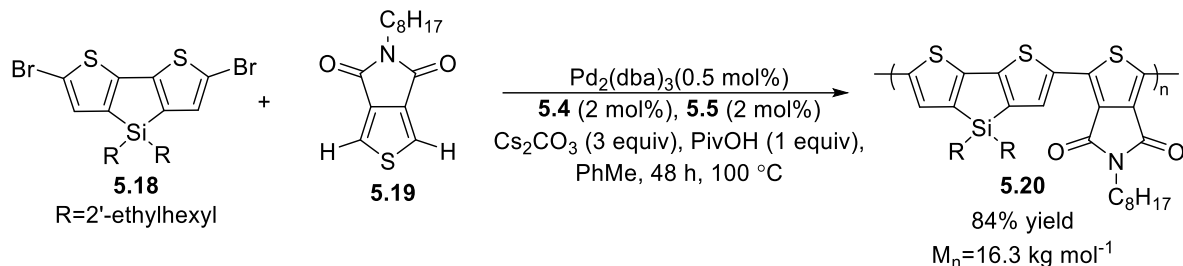
Most direct arylation polymerizations are carried in the presence of the ligands P(*o*-anisyl)₃ **5.4** or P(*o*-aniline)₃ **5.5**. Although the exact mechanism by which the ligands aid DHAP has not been fully elucidated, it is believed that the coordinating ability of the ligands aids in the CMD step by elongating the reactive C-H bonds (**Figure 5.2**).³³⁶ The power of these ligands was first displayed in Ozawa's synthesis of regioregular P3HT³³⁶ and was later

built upon by Leclerc and coworkers, who demonstrated that the use of these coordinating ligands can lead to conjugated polymers with optoelectronic properties that were identical to the conjugated polymers made via Stille coupling.³¹⁸ The Ozawa report is of particular importance as it suggests that the ligand used in DHAP could affect the regioregularity of the ensuing polymer.



Scheme 5.4- Examples of ligand free direct arylation in small molecules (**A**)³³⁹ and in conjugated polymers (**B**).³⁴⁰

Direct arylation is also able to proceed in the absence of a ligand although this is typically reserved for small molecule couplings (**Scheme 5.4A**).³³⁹ The CMD transition state necessitates the use of a bidentate ligand such as carbonate to aid in the deprotonation; therefore phosphine ligands are not necessarily required as long as the role of a carbonate is fulfilled. All direct arylations are carried out in the presence of carbonates and carboxylic acids which can act as ligands to aid in the CMD step.^{317,341} The solvent can also fulfil the role of the ligands, the very first examples of direct arylation featured high catalytic activity when conducted in DMF or DMAc, it was later discovered that the solvent coordinated to the catalyst and aided in the CMD.³⁴² Few examples are present in the literature that utilize ligand free DHAP, for example, **P3HT** has been previously synthesized under ligand free conditions but the molecular weights and yields failed to approach similar values to Ozawa and coworkers' report.^{343,344} Other studies suggest that the inclusion of phosphine ligands could be detrimental to the reactivity as seen in Sommer and coworkers' study on the synthesis of **5.17**.³⁴⁰ In this report, the reactivity shut down when carried out in the presence of phosphine ligands but proceeded to give high yields and molecular weights under ligand free conditions.



Scheme 5.5- Mixed ligand polymerization of **5.20**.^{345–347}

Mixed ligand catalysis has also been used in DHAP and was shown to decrease the total number of defects within the conjugated polymers. Ozawa and coworkers published several reports using mixed ligand catalysis and showed that the inclusion of two different ligands could allow for the synthesis of high weight conjugated polymers previously inaccessible through DHAP.^{345–347} **Scheme 5.5** outlines the mixed ligand polymerization that produces **5.20**. Previous attempts to synthesize **5.20** were met with no reaction when **5.5** was employed as a ligand or led to solely insoluble materials when **5.4** was used. The mixture of the two ligands provided the right amount of reactivity for the polymerization to proceed while minimizing side reactions that consequently allowed for the isolation of polymer **5.20** in an 84% yield.

5.3-SIDE REACTIONS AND DEFECTS OF DIRECT (HETERO)ARYLATION POLYMERIZATION

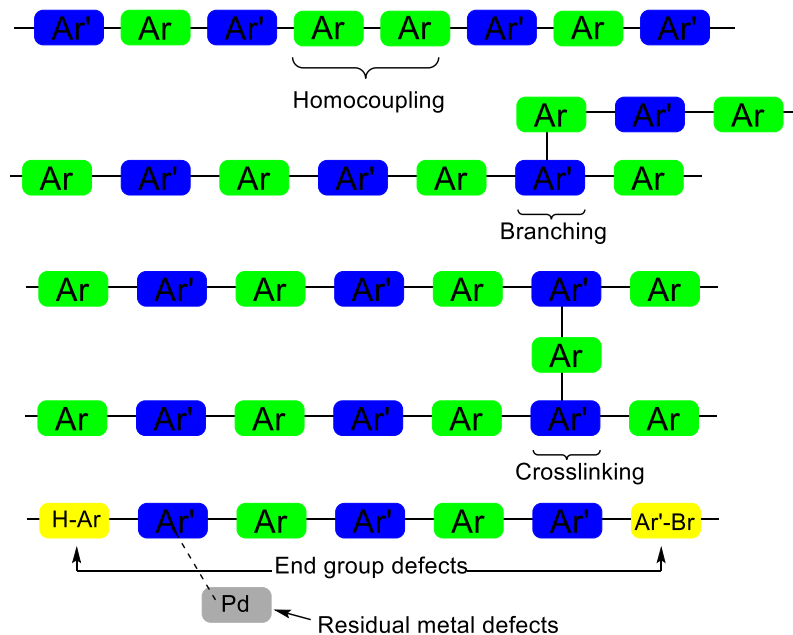
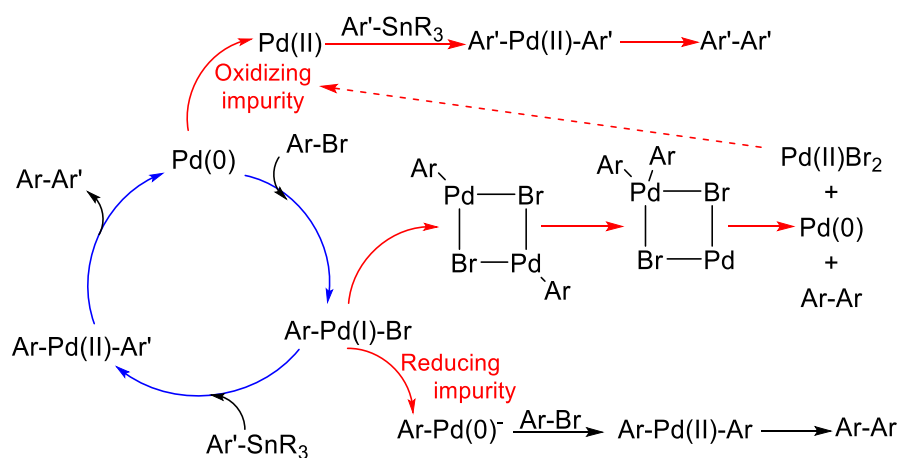


Figure 5.3- Defects associated with conjugated polymers synthesized through DHAP.²⁹³

Direct arylation polymerization is a new and emerging technique for creating conjugated polymers that possesses several advantages over traditional coupling techniques; however, DHAP is notorious for the high number of defects present within the synthesized polymers.²⁹³ The possible defects within conjugated polymers are highlighted in **Figure 5.3** and include homocoupling, branching, crosslinking, end-group defects, residual metal defects.²⁹³ Since the optical and electronic properties of conjugated polymers are dependent on their structure (see **Chapter 4**), these defects can negatively affect performance of a polymer in device applications. Herein, the side reactions that bring about defects in conjugated polymers will be discussed. Additionally, the solutions that different research groups have used to limit or prevent unwanted reactions will be examined.

5.3.1 HOMOCOUPLING



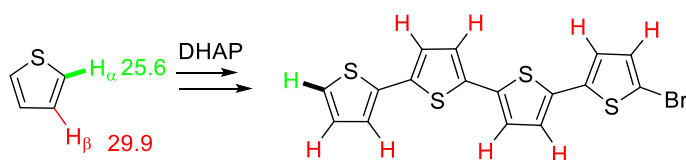
Scheme 5.6-Homocoupling pathways in transition metal catalyzed couplings as exemplified by Stille coupling.²⁹³

Homocoupling occurs when two monomers with the exact same functionality are coupled together. This process is a consequence of transition metal catalyzed couplings and is also observed in traditional couplings (Suzuki or Stille). There are several pathways by which homocouplings can occur, for example, oxidative or reductive impurities within the reaction mixture may change the oxidation state of the metal. Consequently, this can lead to homocoupling³⁴⁸ or a disproportionation reaction may occur³⁴⁹ enabling the coupling of two identical groups (**Scheme 5.6**). Since homocouplings still occur even under strictly regulated conditions and aryl palladium groups have been previously documented to undergo aryl exchange reactions,³⁴⁹⁻³⁵² it is most likely that the active homocoupling mechanism is a disproportionation.

Homocoupling can have negative effects on the properties of conjugated polymers, for example, homocoupling defects in **P3HT** have been shown to kink the polymer backbone leading to a decrease in order within the polymer. This loss in order has a negative influence on properties including crystallinity,³⁵³ optical properties,³⁵⁴ thermal properties,³⁵⁵ charge transport,³⁵⁶ specific capacitance,³⁵⁷ and performance in organic photovoltaic devices (OPV).^{355,358} In the realm of DHAP, homocoupling has been identified as one of the critical side reactions, defects of this nature usually result in a widening of the bandgap for the material.^{359,360}

Even though homocoupling is an inherent consequence of transition metal couplings, techniques do exist to limit the number of homocoupling defects within a polymer. The ligands may play an important role in limiting disproportionation, which was made evident by Ozawa and coworkers' synthesis of highly regioregular P3HT where the authors utilized ligands **5.6** and **5.7** to achieve regioregularities of 93% and 96%, respectively.³¹⁹ Since homocouplings affect regioregularity, then it can be concluded that high regioregularities are indicative of minimal side reactions, including homocouplings. A study by Sommer and coworkers further highlighted the importance of phosphine ligands, as the authors observed that homocouplings were significantly reduced when polymerizations were carried out in the presence of phosphine ligands.³⁶⁰ Additionally, the temperature of the reaction can affect the occurrence of homocouplings with higher temperatures being more prone to disproportionation reactions leading to homocouplings.^{264,360}

5.3.2- BRANCHING AND CROSS-LINKING

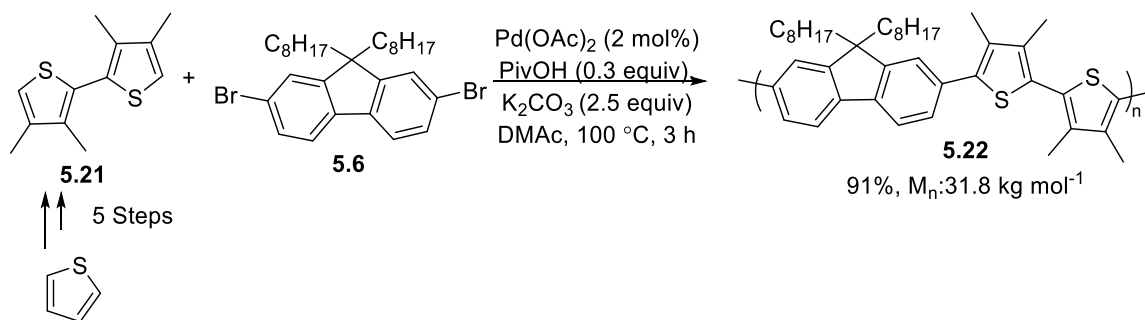


Scheme 5.7- Free energy of activation (ΔG_{298} , kcal mol⁻¹) for C-H activation via CMD for thiophene.³¹⁷

Branching and cross-linking are defects that are unique to DHAP and are considered one of the main deterrents stopping direct arylation from becoming the main way by which conjugated polymers are made. Branching occurs when a secondary polymer chain forms on an already growing chain while crosslinking occurs when two polymer chains are covalently bonded by a monomer or oligomer forming a 2-dimensional polymer network. Since hydrogens are the propagating species in DHAP then the reaction is very amenable to cross-linking and branching due to the potentially high number of reactive hydrogens present on the monomer. To illustrate this

problem, we can look at polythiophene (**Scheme 5.7**) which possesses two reactive hydrogens. The α -alpha hydrogen is lower in energy and is thus preferentially activated during the polymerization;³¹⁷ however, as the reaction continues the concentration of α -hydrogens decreases leaving an abundance of potentially reactive β -hydrogens available to branch or crosslink.^{174,293} Therefore, as the polymerization begins to reach high conversions it becomes more prone to unwanted branching and crosslinking.

Branching and crosslinking is a particularly detrimental defect as heavily branched polymers will often suffer from poor solubility leading to tedious extraction procedures that lower the overall yield.^{264,343,361} In some cases, branching is so abundant that it leads to the formation of insoluble gels that cannot be processed further, which causes some polymers to be inaccessible through DHAP or only isolatable at low conversions.³⁶² Additionally, branching defects can have a negative impact on the thermal and optoelectronic properties of the electronic of the polymer.^{262,355,363} The charge transfer properties are also affected by branching leading to poor OPV performance.²⁶¹



Scheme 5.8- Copolymerization of fluorene and bithiophene using β -protected monomers.^{362,364}

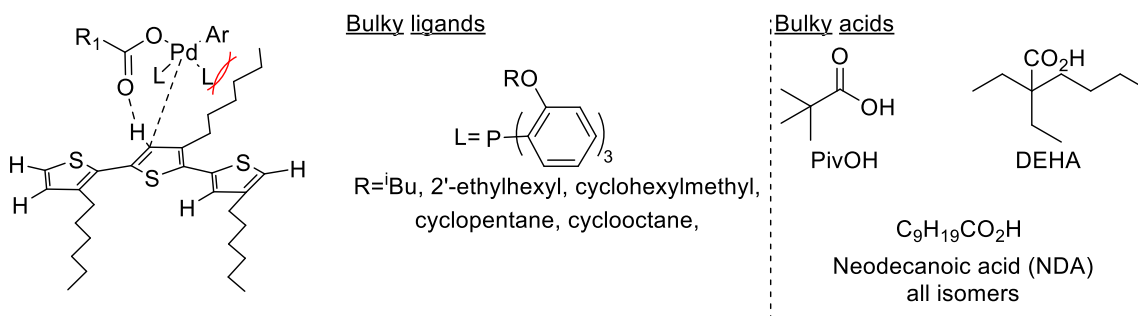


Figure 5.4- β -branching prevention by bulky ligands and carboxylic acids.^{264,365,366}

Several methods for controlling branching and cross-linking defects have been reported previously. The simplest solution to negate any branching is to utilize monomers that have all unwanted positions blocked or feature a directing group to prevent functionalization at unwanted positions (**Scheme 5.8**).^{362,364,367,368} This, however, requires additional synthetic steps and severely limits the number of monomers available for DHAP while not addressing the core reactivity problem. Other solutions tackle the problem from the catalysts' side by introducing bulky carboxylic acids,^{264,365} such as neodecanoic acid, or bulky phosphine ligands.³⁶⁶ The addition of these sterically hindered groups to the catalyst makes the functionalization of the undesired β -hydrogens less favourable; however, this approach is substrate dependent and requires bulky sidechains to be present on the growing polymer chain to clash sterically with the incoming catalyst (**Figure 5.4**). Finally, it has been noted that milder conditions, such as lower temperatures, will result in less branching/cross-linking; however, changing the reaction parameters will lower the number of unwanted functionalization but not remove them completely.²⁶⁴

5.3.3 END GROUP DEFECTS

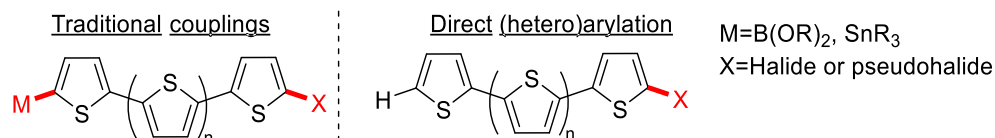
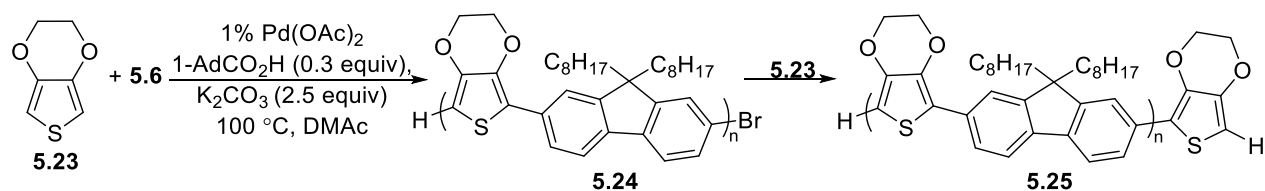


Figure 5.5-End group defects in traditional couplings and direct(hetero)arylation.



Scheme 5.9- Removal of end group defects by end capping Br-terminus.³⁶⁹ 1-AdCOOH- 1-adamantanecarboxylic acid.

End group defects consists of the left-over groups from the monomers following polymerization. This is more so a problem for traditional couplings as two end group defects are created and must be dealt with individually whereas DHAP only leaves behind aryl halides as end groups (**Figure 5.5**). Nonetheless, the presence of end group defects can have negative effects on the polymer's properties and must thus be removed if possible.³⁷⁰ Most solutions to end group defects in DHAP are quite simple, for example, Kanbara and coworkers introduced more EDOT **5.23** monomer at the end of the copolymerization of EDOT **5.23** and fluorene **5.6** and observed the disappearance of Br end groups by ¹H-NMR and MALDI-TOF MS (**Scheme 5.9**).³⁶⁹ A similar end capping procedure was reported by

Ozawa and coworkers for the polymerization of thienopyrrolodione (TPD) and dibromothiophene, where the authors introduced more of TPD monomer at the end of the polymerization and observed the depletion of Br end groups by ^1H NMR.³⁷¹

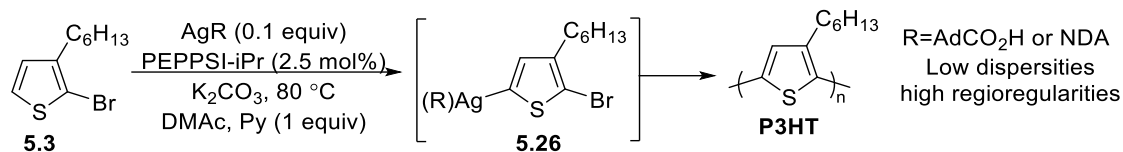
5.3.4 RESIDUAL METAL DEFECTS

Unlike the previously mentioned defects, residual metal defects are not covalently bound to the polymer chain. It is believed that the left-over metal particles become physically entrapped by, or bound to, the polymer which renders any purification method ineffective.³⁷² Consequently, the residual metal particles are thought of as defects rather than impurities. In terms of the number of metal defects, DHAP stacks quite well against traditional polymerization reaction with lower residual metal and phosphine concentrations when analyzed by methods like inductively coupled plasma (ICP)-MS.^{373,374} These findings further highlight the attractiveness of DHAP as a polymerization method as a result of the lower number of residual metal defects.

Reducing the overall number of metal defects is problematic. Put simply, lower catalytic loadings led to a lower number of residual metal defects within the polymer which in turn yield better material properties.³¹² Thus, more active catalysts are required to minimize the loadings while still being able to achieve high molecular weights.

5.4 CATALYST DESIGN IN DIRECT (HETERO)ARYLATION POLYMERIZATION.

Catalyst design is an often-overlooked aspect of DHAP, with most of the focus lying on the construction and polymerization of new monomers to create low bandgap materials.^{296,313,375} Much of the progress in traditional cross couplings is owed to a more thorough understanding on how the ligands and the metal center affect the reaction. Consequently, this has led to the design of new catalysts that throughout the years have greatly improved cross-coupling reactions and allowed for the functionalization of previously unreactive substrates.^{376,377} The most famous example of catalyst design for DHAP is Ozawa's synthesis of **P3HT** in which the tailored DHAP catalyst allowed for high molecular weights and regioregularities.³¹⁹ Other examples include the previously discussed composite catalysts that feature carefully selected combinations of ligands and carboxylic acids that minimize branching and homocouplings.^{264,345,347,366,378}

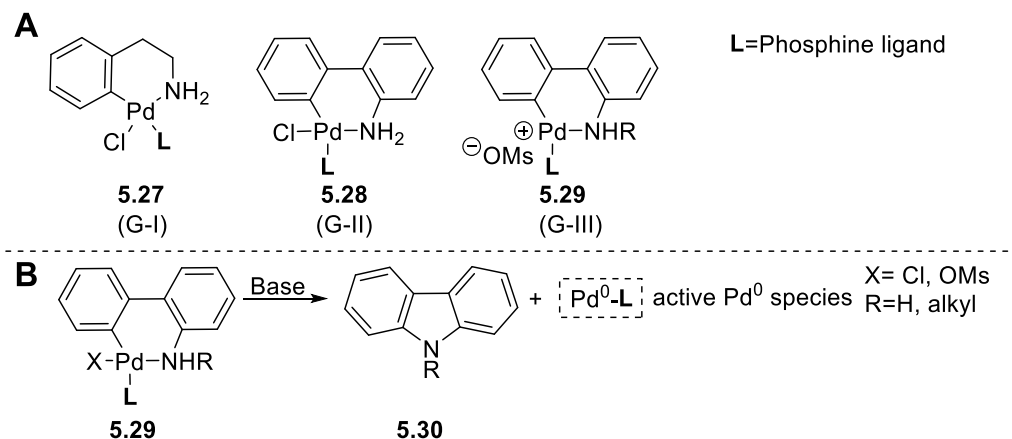


Scheme 5.10-Dual catalytic direct arylation polymerization of P3HT. ^{379,380}

Other attempts at catalyst design seek to create living direct arylation polymerizations, a highly sought-after polymerization reaction that could allow for the synthesis of conjugated block copolymers.³⁸¹ Living polymerizations have been previously reached using Kumada or Negishi couplings but the high nucleophilicity of the organometallics reagents severely limits the applicability of the reactions.³⁰⁴ In an attempt to create a living direct arylation polymerization, Luscombe and coworkers employed a dual catalytic system, using silver and palladium, that displayed step growth kinetics (**Scheme 5.10**).^{379,380} The purpose of the silver carboxylate was to perform an oxidative addition on the thiophene C-H bond creating a new organometallic reagent that is more reactive towards transmetalation with the Pd catalyst. Although not a traditional direct arylation, since the reaction avoids the CMD mechanism, the reaction proceeds without the need for prior functionalization. It should be noted that Luscombe and coworkers method displayed low molecular weights and high polydispersities for a living polymerization, thus more work needs to be carried out to properly elucidate a living DHAP. ^{379,380}

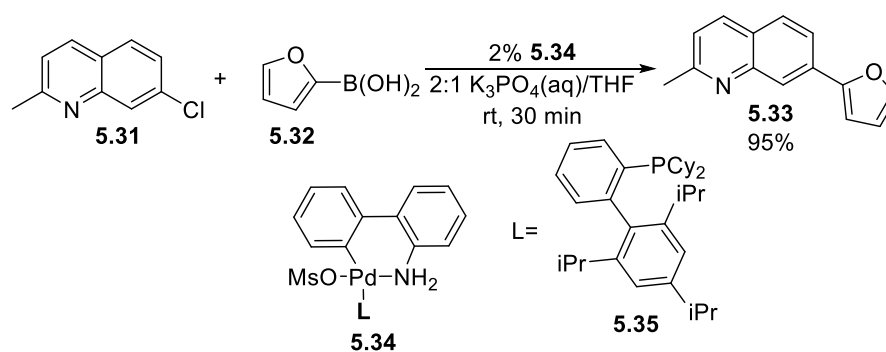
5.5 BUCHWALD PRECATALYSTS

Most transition metal catalyzed reactions are carried out with palladium sources such as Pd(OAc)₂ or Pd₂(dba)₃ alongside a ligand with the intention of forming the active L_nPd⁰ species in situ. Often times however, the transformation from the Pd(II) species to the active Pd(0) is not straight forward. Firstly, the ligands that come prebound to commercially available Pd sources, such as dba, have been known to interfere with the added ligands thus lowering the catalytic activity.^{382,383} Secondly, the quality of commercially available Pd(0) precursors is highly dependent on the supplier and synthetic method.^{384,385} Lastly, as discussed in **Section 5.31**, transition metal catalyzed reactions are vulnerable to off cycle species that can lead to unwanted reactivities.



Scheme 5.11-A-Buchwald precatalyst generations I, II, III.; **B**- Mode of activation for Buchwald precatalyst.^{382,386}

Some of the aforementioned issues can be bypassed by using Pd(0) catalyst such as Pd(PPh₃)₄ or Pd[P^tBu₃]₂. Unfortunately, these Pd(0) catalysts are often not stable and in the case of the commercially available Pd(PPh₃)₄, come prebound with ligands that are less than ideal for catalysis.³⁷⁶ To address these issues, Buchwald and coworkers designed a series of pre-catalysts that upon the addition of base release an active palladium (0) species thus ensuring the molecularly defined reduction of Pd(II) to Pd(0) (**Scheme 5.11A**).^{382,386} The mechanism by which Buchwald catalysts are activated is outlined in **Scheme 5.11B**. When base is introduced to the system, the amine on the precatalyst is deprotonated leading to a reductive elimination that releases carbazole **5.30** and Pd(0) with the ligand already bound to the metal center.^{382,386}

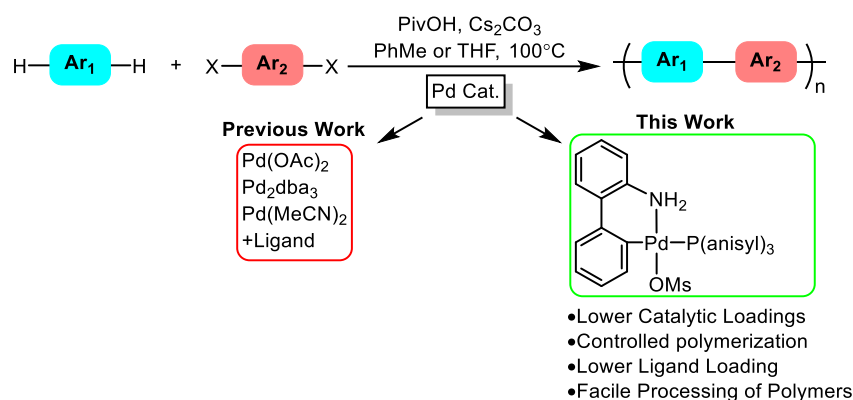


Scheme 5.12- Suzuki coupling of unstable boronic acids with Buchwald precatalysts.³⁸²

So far, Buchwald precatalysts have allowed for the improved synthesis for a variety of carbon-carbon and carbon-heteroatom bonds.³⁸⁶ Additionally, the precatalysts have also seen some use, although limited, for direct

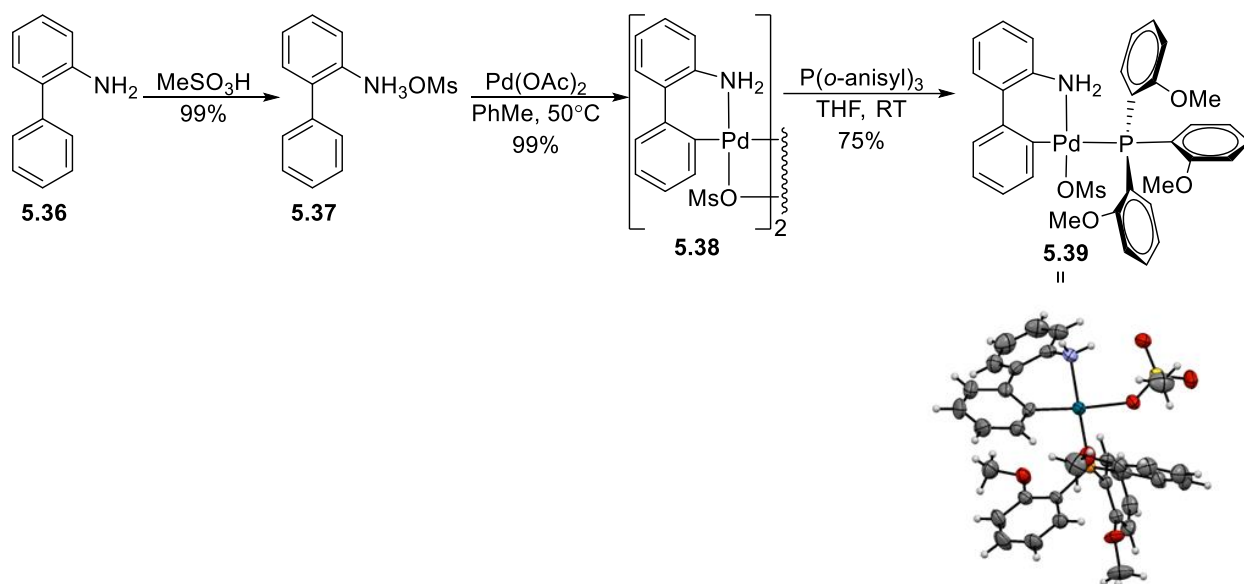
arylation and DHAP.^{387,388} An example of a reaction improved by the use of a Buchwald precatalyst is highlighted in **Scheme 5.12**. Here, the Suzuki coupling between unstable heteroaryl boronic acids and aryl chlorides was demonstrated. Given the fast rate of protodeboronation for **5.32**, the catalyst needs to activate quickly for the reaction to be successful. Nonetheless, it was demonstrated that the rapid activation of the Buchwald precatalysts allowed for the reaction to proceed in high yield.³⁸²

5.6 DESIGN OF A PALLADIUM PRECATALYST FOR DIRECT (HETERO)ARYLATION POLYMERIZATIONS³⁸⁹



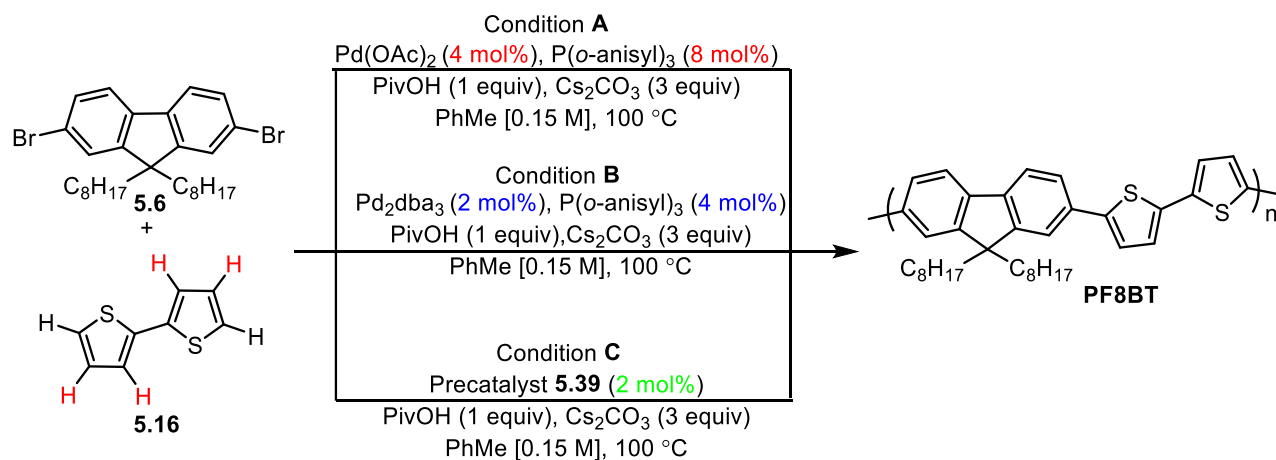
Scheme 5.13- Buchwald precatalyst for direct (hetero)arylation polymerization.

There are several problems at the center of DHAP arylation that prevent the method from becoming the main route towards the synthesis of conjugated polymers. We believe that catalyst design may be key in the betterment of DHAP as a synthetic method, so we endeavored to create a new catalytic species that displays a high level of activity while minimizing unwanted side reactions and defects. Herein, we outline the development of a new Buchwald precatalyst fitted with **5.4** as the ligand that can proceed at lower catalytic and phosphine loadings and yield easily processable polymers at high yields with a minimum number of defects (**Scheme 5.13**).



Scheme 5.14- Synthesis of direct arylation Buchwald precatalyst **5.39** and crystal structure.³⁸²

We began our investigation by synthesizing the direct arylation Buchwald precatalyst **5.39** following the procedure outlined by Buchwald and coworkers.³⁸² The synthetic scheme for the precatalysts is outlined in **Scheme 5.14**. 2-Aminobiphenyl **5.36** was first protonated with MeSO₃H to form the mesylate salt **5.37** in quantitative yield. **5.37** was then introduced to Pd(OAc)₂ in PhMe leading to a cyclopalladation generating the dimeric palladacycle **5.38**, also in quantitative yield. Dimer **5.38** was then reacted with P(*o*-anisyl)₃ **5.7** in THF and gave the corresponding precatalyst **5.39** in a 75% yield. A crystal structure of **5.39** was obtained and revealed a similar geometry to other Buchwald precatalysts with the OMs moiety still bound to the Pd center.



Scheme 5.15- Synthesis of **PF8BT**.

With precatalyst **5.39** in hand, we proceeded to test the new catalytic species in a series of polymerizations. The first polymer we wanted to tackle was poly(dioctylfluorenebithiophene) **PF8BT**. We chose **PF8BT** as our test polymer due to its inclusion of the bithiophene (**5.16**) monomer which is one of the worst examples with regard to branching and has been well documented to yield insoluble materials when exposed to DHAP conditions.^{174,362} To properly assess the catalytic activity, we wanted to get a real-time assessment of the reaction kinetics. To do so we constructed a time vs. molecular weight plot following a procedure previously outlined by Leclerc and coworkers.¹⁷⁴ The kinetic plot was constructed by performing the **PF8BT** polymerization and at set time intervals, an aliquot from the reaction mixture was removed and analyzed by gel permeation chromatography (GPC) without any further purification. This analysis was repeated periodically until no further growth in the molecular weight was observed. Three sets of conditions were used for the **PF8BT** polymerization (**Scheme 5.15**). Condition A was utilized as a control and followed Leclerc and coworkers' original conditions using Pd(OAc)₂/**5.4**. Condition B utilized Pd₂dba₃/**5.4** and served as a means of evaluating the effect of another Pd(0) source on the polymerization. Finally, condition C used our new precatalyst **5.39** for the **PF8BT** polymerization.

The time vs. molecular weight plot can be seen in **Figure 5.6** and a summary of the yields, molecular weights and dispersities can be seen in **Table 5.1**. In regard to conditions A and B – from the kinetic plot we can see that both these conditions led to a rapid development in molecular weight that levels out around 3 h. The drop in molecular weight seen for conditions A and B is due to the higher molecular weight polymers joining the insoluble fraction – since we can only assess what is in solution then we observe what appears to be a decrease in molecular weight as the reaction progresses. The insolubility of **PF8BT** synthesized through conditions A or B may be due to the higher weight polymers displaying poor solubility or due to branching/crosslinking.

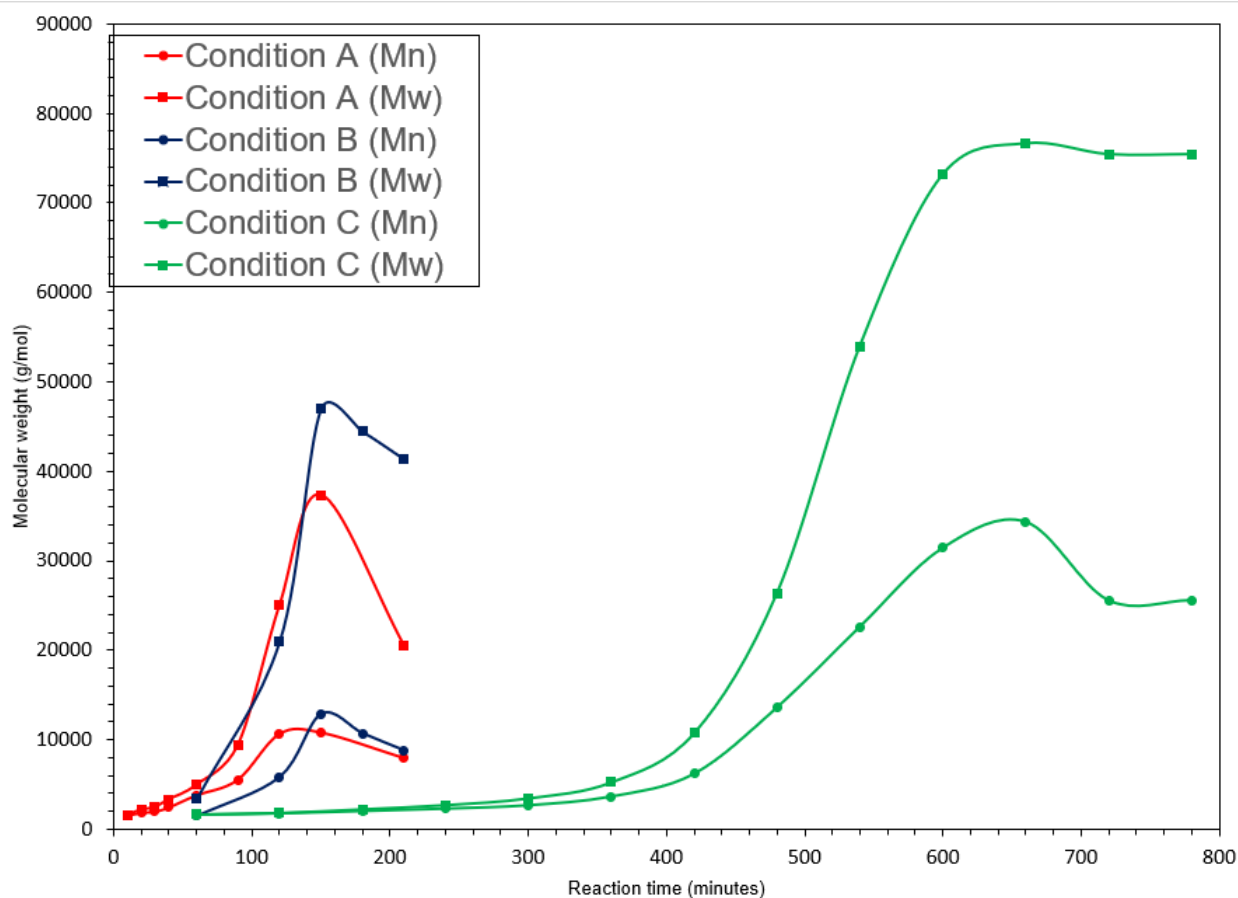


Figure 5.6-Time vs. molecular weight plots for **PF8BT** synthesized under conditions A, B and C.

Condition	Catalytic system	%Yield	M_n (kg mol ⁻¹)	M_w (kg mol ⁻¹)	\bar{D}
A	Pd(OAc) ₂ /P(<i>o</i> -anisyl) ₃	89%	10.7	37.4	3.5
B	Pd ₂ dba ₃ /P(<i>o</i> -anisyl) ₃	93%	12.8	47.0	3.7
C	Precatalyst (5.39)	96%	32.0	73.6	2.3

Table 5.1- Summary of results for **PF8BT** polymerization under different conditions. Molecular weights were estimated by GPC with THF at 35 °C against polystyrene standards.

In contrast, **PF8BT** was synthesized using condition **C** displayed a much longer reaction time but was able to achieve a higher molecular weight and lower PDI than conditions A and B. Given that Buchwald precatalysts have been known to be more catalytically active than traditional Pd sources the slow reaction rate of condition C gave us some clues as to the behaviour of **PF8BT** when synthesized through DHAP. Based on condition C, we believe that the rapid growth in molecular weight for conditions A and B might be indicative of unwanted β -functionalization on the bithiophene **5.16** monomer while the slower reaction time of condition **C** indicates preferential activation of α -hydrogens. This claim is further supported by the observed solubilities of **PF8BT**. When synthesized using conditions A and B, the resulting polymer was sparingly soluble and could only be dissolved in high boiling solvents like

trichlorobenzene (TCB). Whereas **PF8BT** made using condition C gave polymer that was soluble in THF at room temperature. Additionally, conditions A and B were prone to gelation if the reaction time was not carefully monitored. The precatalyst conditions on the other hand were less sensitive and often times the polymerization could be carried out overnight without running the risk of gelation.

It should be noted that Leclerc and coworkers recorded a similar M_n in a shorter time, however, the **PF8BT** was analyzed in TCB at 135 °C, whereas **PF8BT** made with our precatalysts was able to yield a higher M_n in THF at 35 °C. GPC conducted at higher temperature can eliminate polymer aggregates which consequently raise the molecular weights and lower PDI.³⁹⁰ Therefore, the values that we obtained with our catalyst appear to improve on previous methods despite being analyzed with conditions that may limit the incorporation of higher weight polymers and allow for polymer aggregation. Lastly, the use of conditions C allowed for the synthesis of **PF8BT** with only a 2% catalytic loading thus lowering the cost of the polymerization as well as limiting metal defects within the polymer.

Condition	Catalytic System	T_m (°C)	ΔH_m (J/g)
A	Pd(OAc) ₂ /P(<i>o</i> -anisyl) ₃	267.79	1.3967
B	Pd ₂ dba ₃ /P(<i>o</i> -anisyl) ₃	239.12	0.5483
C	Precatalyst (5.39)	271.65	1.3770

Table 5.2- Differential calorimetry data for **PF8BT** synthesized through conditions A, B, and C.

So far, we believe that our direct arylation precatalyst **5.39** was able to limit unwanted reactions that led to branching and crosslinking to produce a polymer with better optoelectronic properties. To quantify the level of branching or crosslinking for the different catalytic system we attempted to observe the change in melting temperature (T_m) between **PF8BT** synthesis with conditions A, B, and C. Due to the decreased mobility cause by branching or crosslinking the T_m for the polymers will be suppressed.^{353,355,391} The differential scanning calorimetry (DSC) data is summarized in **Table 5.2**. We were pleased to observe that our precatalyst (Condition **C**) displayed the highest T_m and a similar melting enthalpy (ΔH_m) to the **PF8BT** generated using Pd(OAc)₂/P(*o*-anisyl)₃. To our surprise the **PF8BT** synthesized with Pd₂dba₃/P(*o*-anisyl)₃ displayed the lowest T_m out of all three polymers. This provides some evidence that precatalyst **5.39** leads to a decreased level of branching/crosslinking for **PF8BT**. Furthermore, the low T_m for condition **B** serves to further illustrate the negative effect of ligands that come prebound to commercial Pd(0) sources.

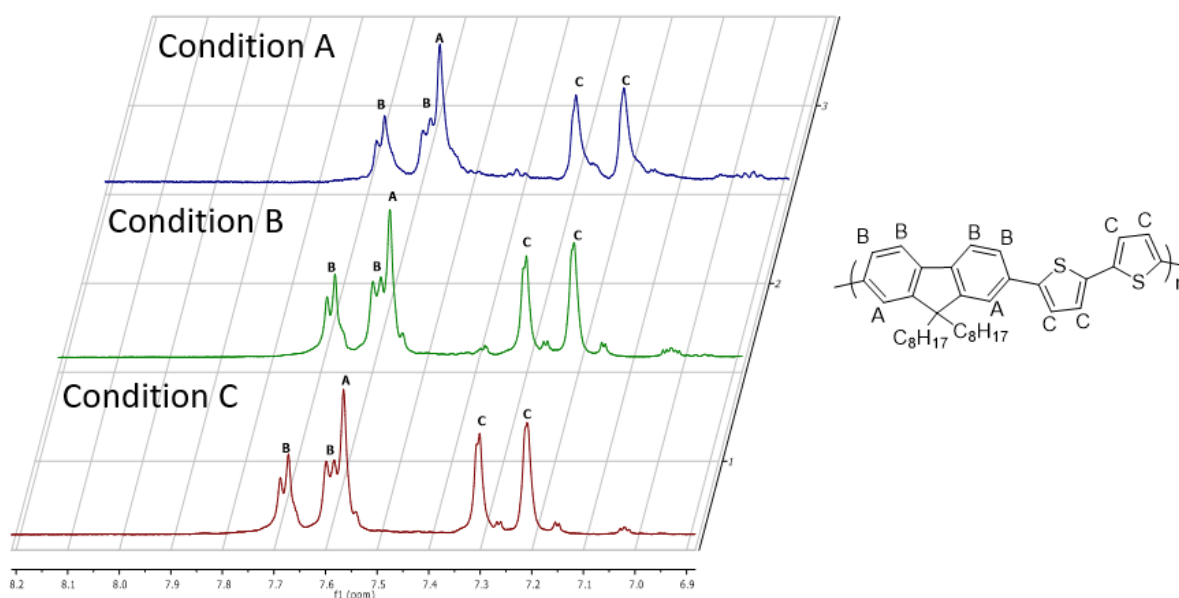


Figure 5.7- ^1H NMR of the aromatic region of **PF8BT** at 80 °C in deuterated 1,1,2,2-tetrachloroethane (TCE).

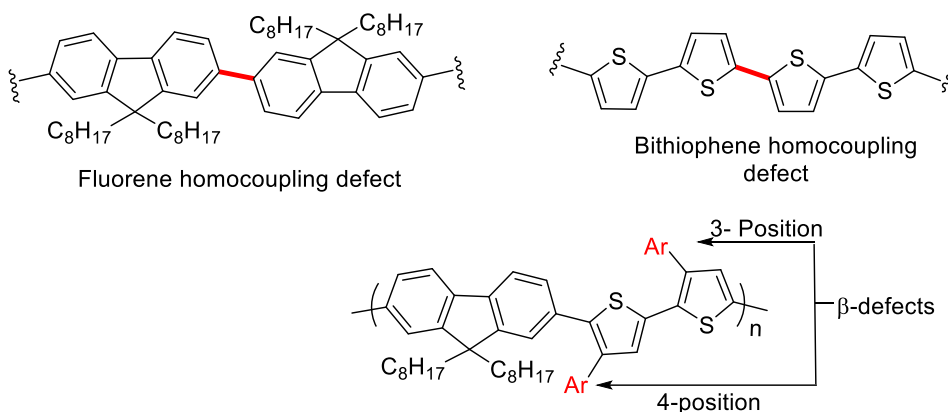


Figure 5.8- Possible defects present in **PF8BT**.

To further characterize the polymers, we performed ^1H -NMR analysis of the polymers in deuterated TCE at 80 °C and were pleased to observe that the spectra of the **PF8BT** synthesized with our precatalyst matched the spectra of similar reports.¹⁷⁴ Next, we wanted to characterize the extent of β -functionalization between all three polymers, however, the NMR analysis proved challenging due to the complex spectra of **PF8BT**. **Figure 5.7** shows the spectra of **PF8BT** synthesized through conditions A, B, C – the spectra of **PF8BT** is consistent throughout all three methods – the only difference between the polymers is the appearance of smaller peaks around the assigned signals.

At the present time, we do not have enough information to properly assign the remaining peaks, but we can speculate as to what they may correspond. Within this polymerization we can hypothesize four possible types of defects (**Figure 5.8**): a homocoupling defect with either the fluorene or bithiophene and β -branching defects at either the 3 or 4 positions of the bithiophene. Additionally, end group defects will also be present but should be minimal compared to the main polymer NMR signals.

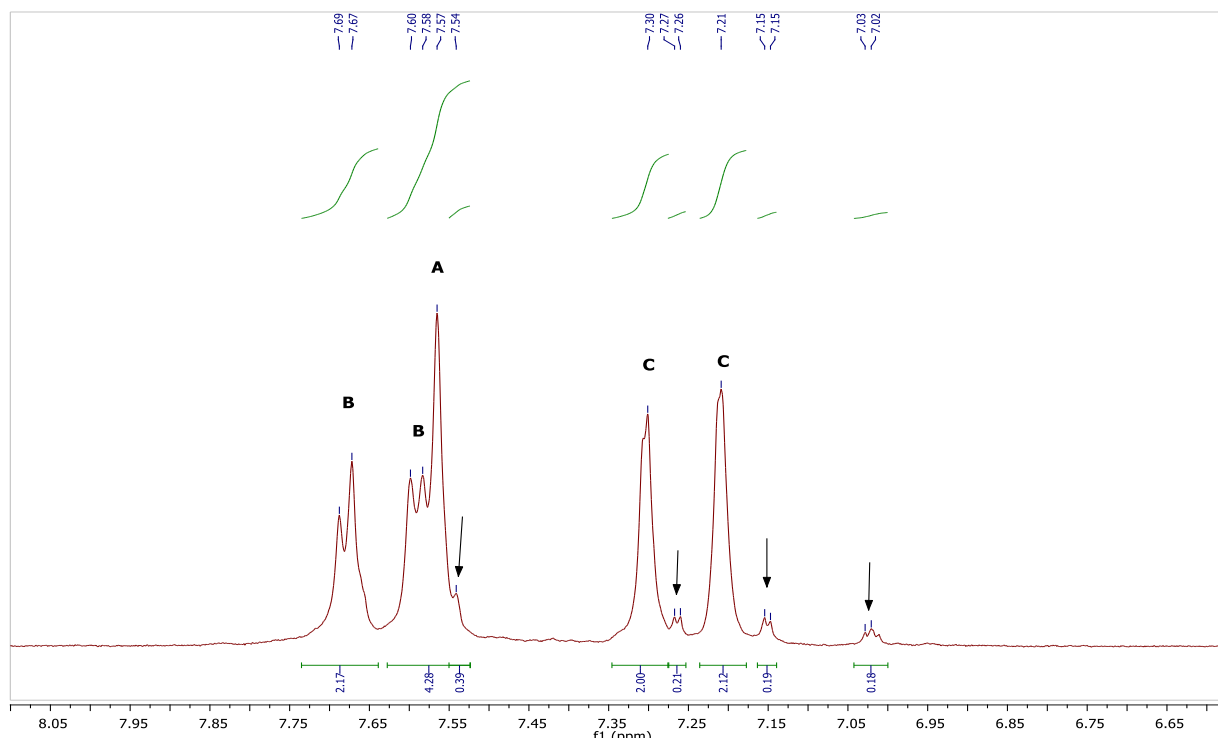


Figure 5.9- ^1H NMR of the aromatic region of **PF8BT** made using condition **C** at 80 °C in deuterated 1,1,2,2-tetrachloroethane (TCE). Arrows indicate defect NMR signals.

Cond.	$\delta 7.54$ (%)	$\delta 7.39$ (%)	$\delta 7.27$ (%)	$\delta 7.15$ (%)	$\delta 7.03$ (%)	Other	Total defects (%)
A	4.50	2.10	4.12	1.20	1.05	2.92	15.89
B	3.05	2.57	2.17	2.17	2.57	0	12.54
C	3.38	-	1.82	1.65	1.56	0	8.41

Table 5.3- Percentage of impurities present in **PF8BT** synthesized through conditions A, B, and C.

If we assume that the smaller peaks present in the ^1H NMR spectra corresponds to prior mentioned defects, then we can assign a percent composition based on the peak integration. **Figure 5.9** shows the ^1H -NMR spectra of **PF8BT** synthesized through condition C; the arrows indicate the defect signals. A summary of the percent defects for **PF8BT** is given in **Table 5.3**. Looking at the results from the NMR analysis we can see that the precatalyst conditions minimize the number of defects present within the polymer, although it does not fully eliminate them. The only

signal we can somewhat confidently assign is the shoulder at 7.54 ppm, which likely corresponds to fluorene homocoupling defect. Similar analysis in the literature will Soxhlet the polymers before performing the NMR analysis, thus removing any unwanted defects from the polymer. We, however, wanted a real picture of the **PF8BT** following the polymerization, and therefore opted to forgo this procedure to obtain a clearer picture of the catalysis. To that end, previous literature procedures stated that the use of condition A led to a defect free polymer, yet if our analysis is correct then this condition (A) gave the highest percentage of defects within **PF8BT**.¹⁷⁴

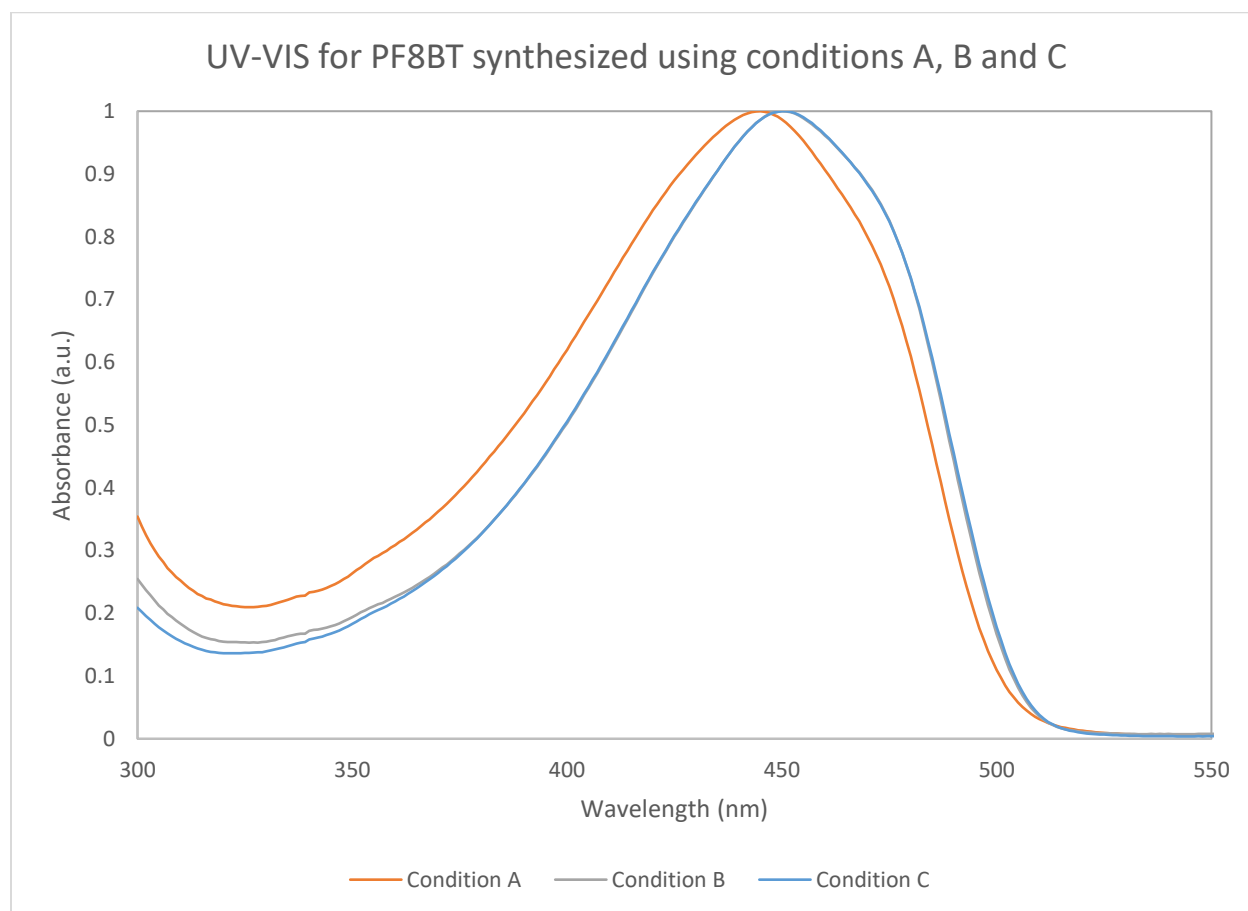


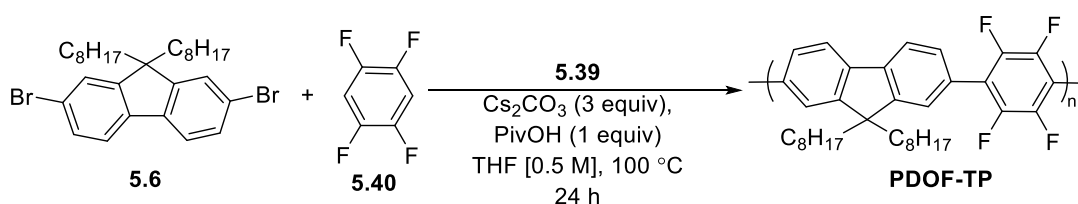
Figure 5.10- UV-VIS spectrum of PF8BT synthesized through conditions A, B, and C.

	Condition A	Condition B	Condition C
$\lambda_{\max}(\text{nm})$	445	450	451

Table 5.4- Maximum absorption wavelengths for PF8BT synthesized with conditions A, B, and C

We also performed a UV-VIS analysis on the **PF8BT** to observe if the lower level of defects from condition **C** change the optical properties. If the **PF8BT** is more linear/ has fewer defects then we expect a smaller bandgap and a redshift in the UV – ²⁶² **Figure 5.10** shows the UV-VIS spectrum for the **PF8BT**. From the UV spectrum we can

D). LiO^tBu was chosen as the base as it outperformed other alkoxide bases in terms of M_n and PDI of the resulting polymer. The use of a strong base greatly reduced the reaction time from 13 h to 6 h and allowed for the generation of **PF8BT** with similar M_n and a lower PDI than when **PF8BT** was generated under condition A. The other bases screened for the reaction provided a similar reduction in reaction time but were ultimately discarded as the PDI of the polymerization was larger than the **PF8BT** synthesized with the aid of LiO^tBu. In comparison to the catalytic system using condition C (**Figure 5.8**), the utilization of the stronger base produced a similar M_n of 20.4 kg mol⁻¹ and M_w of 54.8 kg mol⁻¹ and a yield of 87% with the only drawback being a slight increase in PDI.



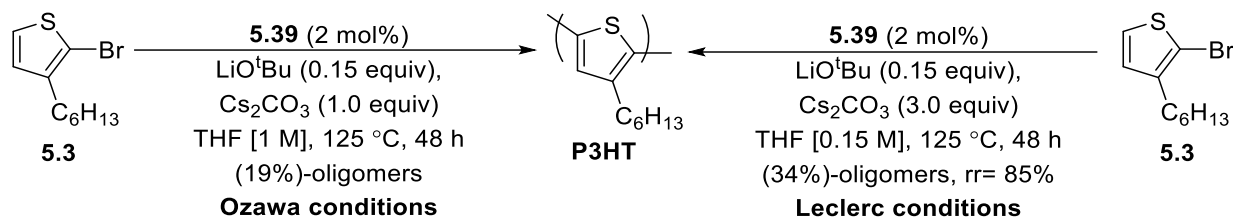
Scheme 5.16-Synthesis of PDOF-TP using precatalyst **5.41**.

Entry	Catalytic loading (mol %)	Reaction time (h)	M _n /M _w (kg mol ⁻¹)	Yield (%)
1	1	24	15.0/53.3	79
2	2	24	21.9/57.6	>100
3	2	127	12.4/31.4	74
4	2	24	15.7/40.0	80
5 ^a	2	24	15.0/42.8	>100
6	5	24	16.1/41.7	>100
7	0.05	24	12.9/32.4	>100

Table 5.5- Molecular weights and yields for polymerization of PDOF-TP with precatalyst **5.39**.

Following our synthesis of PF8BT we wanted to test our catalyst's activity with a system that is not subject to branching and crosslinking defects. We settled on **PDOF-TP** as the test polymer as it had been previously synthesized in high molecular weights and lacked any branching hydrogens.^{336,337} A variety of different conditions based on Ozawa and coworkers' previous report were attempted on the polymerization of **PDOF-TP** and the results are summarized in **Table 5.5**.³³⁶ We were expecting that the lack of branching hydrogen would propel the catalyst to yield high molecular weights that matched those previously reported by Ozawa and coworkers. Unfortunately, the molecular weights with **5.39** were relatively low with the best results arising when the polymerization was carried out at a 2% catalytic loading (**Table 5.5-entry 2**). Once again, we opted to forgo Soxhlet extractions in favour of

analyzing the material post polymerization. Our hope was that the precatalyst would conduct the polymerization more cleanly, negating the need for purification following the polymerization. Several of the trials featured yields surpassing 100% – this is due to impurities still present in the polymer that are usually removed through Soxhlet extractions. Ultimately, we were not able to abstract any useful information from this polymerization and opted to move on to a different polymer.



Scheme 5.17-Synthesis of **P3HT** with precatalyst **5.39**.

The last reaction we wanted to attempt was the polymerization of 2-bromo-3-hexylthiophene **5.3** to create the well know **P3HT**. Since **P3HT** has been so thoroughly studied, all the chemical shifts of the different regioisomers and defects have been assigned and can thus be easily quantified by NMR. As such, **P3HT** offers a useful platform to investigate how well a catalyst can perform the polymerization. We carried out the polymerization under two sets of conditions – the first closely followed Ozawa’s procedure while the second method closely followed Leclerc’s method. Using what we have previously learned from our polymerization we added 0.15 equiv of LiO^tBu to ensure the activation of our catalyst (**Scheme 5.17**).

Both polymerization methods gave less than satisfactory results, with the Leclerc method outperforming the Ozawa conditions with a yield of 34% compared to 19% with the Ozawa method. The molecular weight was difficult to estimate by GPC due to the low weight of the oligomers and our lack of standards in the 3000-100 g mol⁻¹ range. We estimate that the M_n of the oligomers for the Leclerc conditions lies around 3000 g mol⁻¹, which if true, is rather low when compared to other literature preparations for **P3HT**. By ¹H-NMR the regioregularity is 85% for the head to tail diad. This value is in the range of some methods to construct **P3HT** but given the low molecular weight it is difficult to tell if this value is representative of the catalytic activity.

We are currently investigating different conditions to synthesize **P3HT** using our precatalyst. The polymerization of **5.3** is particularly challenging, thus far no other research group has been able to obtain molecular weights and regioregularities by DHAP that approach the values reported by Ozawa and coworkers. Our best attempts to try and replicate Ozawa's exact conditions yielded an M_n 24 kg mol⁻¹ with a PDI of 2.5 which fall short compared to the M_n of 32 kg mol⁻¹ Ozawa reported.^{264,319} The polymerization of **P3HT** therefore seems to be quite sensitive to the conditions and may require a more thorough optimization to give high molecular yields.

5.7 CONCLUSIONS AND OUTLOOK

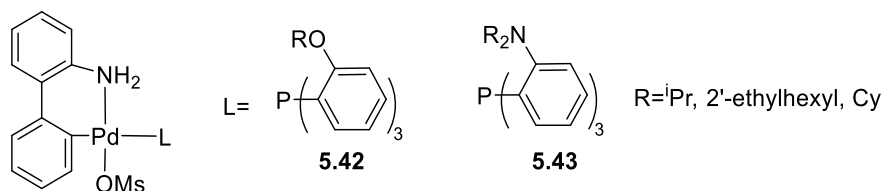


Figure 5.12- Candidates for new series of DHAP precatalysts.

By utilizing rational design, we have constructed a new palladium precatalyst specifically designed for DHAP. We believe that this new catalytic species was able to reduce the number of unwanted side reactions including homocoupling and branching as evidenced by the high molecular weights, good processability, lower PDIs than previously established methods, higher melting temperatures, and more red shifted UV absorption. Furthermore, the pre-catalyst species allows for a lower catalytic and ligand loading while still being able to maintain high molecular weights. We have shown that through catalyst design DHAP can be improved without the need for additional synthetic steps to block potentially reactive C-H bonds.

Research is ongoing in our laboratory to improve the scope of this catalyst to other polymers, in particular P3HT which will provide a more concise analysis of the defects within the polymer. In the future, catalyst design can be expanded further by constructing precatalysts with bulky coordinating ligands that have been demonstrated to help DHAP (**figure 5.12**). This can be further coupled with other side-reaction limiting techniques, such as the addition of bulky carboxylic additives, to prevent defects and improve catalytic activity.

SUPPORTING INFORMATION

6.0 GENERAL CONSIDERATIONS

All reactions were performed under a protective argon atmosphere unless otherwise stated. Solvents used in reactions were either HPLC or reagent grade. Tetrahydrofuran, toluene, dichloromethane, acetonitrile, and triethylamine were obtained from a JC Meyer solvent-purification system and dispensed under a protective atmosphere. Chemical reagents were purchased from Millipore-Sigma or Oakwood Chemicals. Thin layer chromatography (TLC) was performed on aluminum backed TLC plates (Kieselgel 60 F₂₅₄, Merck) and examined under UV light or with a stain. Flash chromatography was performed using a Teledyne-isco Combiflash automated chromatography system with either 230-400 mesh silica gel or 15-40 mesh silica gel.

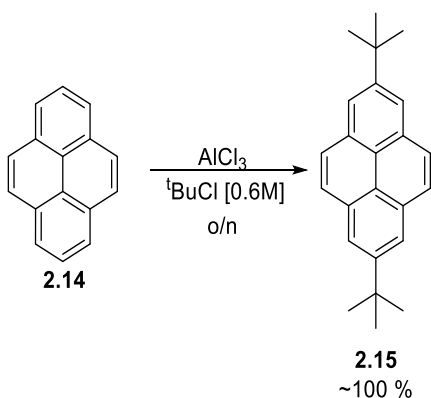
¹H, ¹³C, and ³¹P NMR spectra was recorded on a Bruker Avance 300 or Bruker AC300 NMR spectrometer. ¹⁹F-NMR spectra were recorded on a Bruker AVANCE300 NMR spectrometer. Chemical shifts are reported in parts per million (ppm) relative to chloroform (7.26 ppm for ¹H, 77.00 ppm for ¹³C), phosphoric acid for ³¹P and CFC₃ for ¹⁹F NMR. The following abbreviations are used for NMR peak multiplicities: singlet (s), doublet (d), triplet (t), multiplet (m), broad singlet (bs). High resolution mass spectrometry was conducted via electrospray ionization on a Thermo Scientific Q exactive™ Plus Hybrid Quadrupole-Orbitrap™ at the University of Waterloo Mass Spectrometry Facility. MALDI-TOF MS was conducted on a Bruker Autoflex Speed MALDI using *trans*-2-[3-(4-*tert*-butylphenyl)-2-methyl-2-propenylidene]malononitrile (DCTB) as the matrix at the University of Waterloo Mass Spectrometry Facility. The MALDI-TOF MS was carried out in Reflectron mode and was calibrated using red phosphorus as the standard. X-ray crystal structures were determined by Dr. Jalil Assoud and generated using the Mercury software package. Ultraviolet-visible (UV-Vis) spectra were carried out with a Cary-4000 spectrophotometer and corrected with a solvent filled cuvette. Fluorescence spectra was measured with a Photon Technology International Steady State spectrometer with a xenon arc lamp. All electrochemical measurements were carried out with a WaveNano potentiostat (Pine Research Instrumentation) in a conventional three-electrode configuration system: a platinum button working electrode (1.6 mm diameter), a platinum wire counter electrode and a platinum wire as a reference

electrode with ferrocene added after every run as the internal standard. Dichloromethane or chloroform were employed as the solvent with 0.1 mM $n\text{Bu}_4\text{NPF}_6$ as electrolyte and the experiments were performed under ambient condition with scan rate of 0.1 V/s. Electrochemical measurements for the polymers were carried out by drop-casting a sample onto the working electrode and performing the experiment in acetonitrile with 0.1mM $n\text{Bu}_4\text{NPF}_6$ as the electrolyte with the experimental setup described above.

Number-average (M_n) and weight-average (M_w) molecular weights are relative to polystyrene standards and were determined by size exclusion chromatography with a Viscotek GPC MAX VE2001 at 35 °C equipped with a VE 3580 RI detector and two PAS-104 styrene-divinylbenzene gel columns. The flow rate was fixed at 1.0 mL/min using tetrahydrofuran (THF) as the eluent. All GPC samples were prepared nominally at 2 mg/mL in THF and filtered through a 0.22 μM PTFE filter into a 1 mL chromatography vial. Differential scanning calorimetry (DSC) was performed on q2000 DSC from TA instruments using a rate of 10 °C/min under N_2 . Photochemistry was carried out in 10 mL quartz test tubes inside a Rayonette photoreactor under either 254 nm, 300 nm or 350 nm.

6.1 SYNTHETIC PROCEDURES-CHAPTER 2

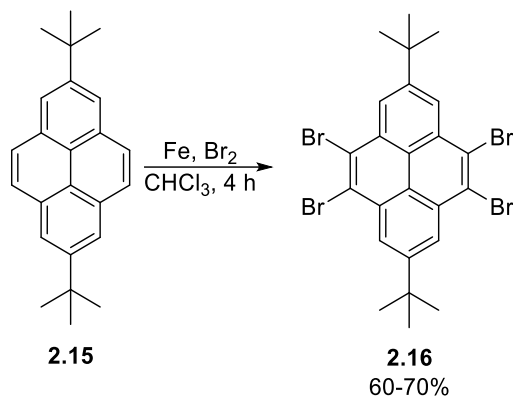
2,7-Di-*tert*-butylpyrene (2.15)



2,7-Di-*tert*-butylpyrene **2.15** was synthesized according to a previously reported procedure to give **2.15** in quantitative yield and exhibited identical data to previously reported.¹²⁴

$^1\text{H NMR}$ (300 MHz, CDCl_3): δ 8.18 (s, 4H), 8.02 (s, 4H), 1.58 (s, 18H).

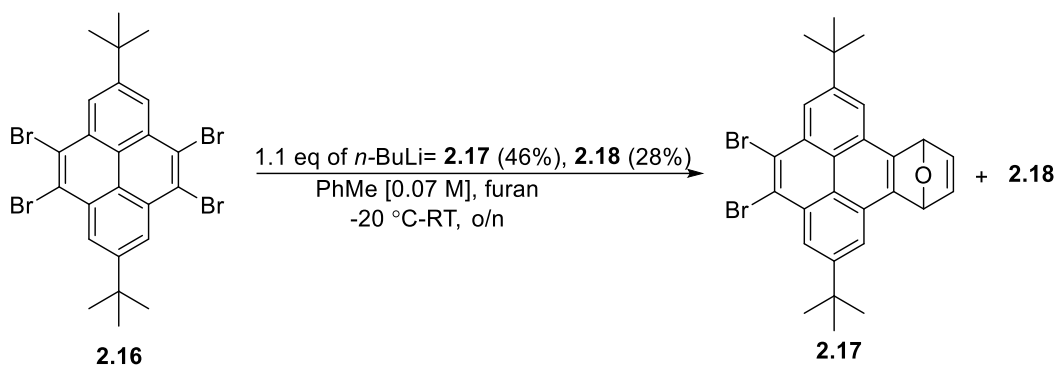
4,5,9,10-Tetrabromo-2,7-di-*tert*-butylpyrene (**2.16**)



Tetrabromopyrene **2.16** was synthesized following a modified previously reported procedure.¹²⁸ In a 2 L round bottom flask with a stir bar compound **2.15** (20.0 g, 63.6 mmol, 1 equiv) was charged and dissolved in 1 L of CHCl₃. The solution was set to stir at which point iron powder (21.3 g, 0.382 mol, 6 equiv) was added. A 250 mL addition funnel was then added to the flask and a solution of bromine (62.0 g, 0.388 mol, 6.1 equiv) in 194 mL CHCl₃ was charged to the addition funnel. The flask was placed in an ice water bath and the bromine solution was then added dropwise over 20-min. After the addition of the bromine the reaction was left to stir at room temperature for 4 h. The reaction mixture was transferred to an Erlenmeyer flask and ice water was added to the mixture followed by a saturated solution of Na₂S₂O₃. The contents of the flask were then transferred to a separatory funnel and the organic layer was washed 3 times with a saturated NaCl solution. The organic layer was then dried with MgSO₄, and solvent was removed via rotary evaporation. The crude solid was then recrystallized with hexanes/chloroform to yield tetrabromopyrene **2.16** as a pink solid in (24.0-28.0 g) 60-70% yield and exhibited identical data to previously reported.¹²⁸

¹H NMR (300 MHz, CDCl₃): δ 8.88 (s, 4H), 1.62 (s, 18H).

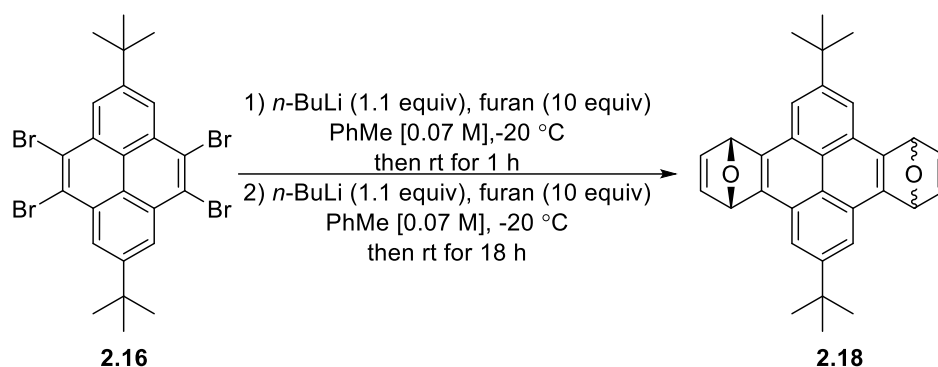
4,5-Dibromo-2,7-di-*tert*-butyl-9,12-dihydro-9,12-epoxybenzo[*e*]pyrene (2.17)



To a RB flask with a stir bar 1.0 g of tetrabromopyrene **2.13** (1.6 mmol, 1 equiv) was added. The flask was then sealed and purged with argon gas followed by the addition of dry PhMe (23 mL, 0.07 M). The flask was then placed in a -20 °C cold bath (3:1 ice to NaCl) and allowed to stir. Once the reaction mixture cooled, freshly distilled furan (1.2 mL, 15.9 mmol, 10 equiv) was added via syringe to the reaction mixture. *n*-BuLi (1.1 mL, 1.6 M, 1.1 equiv) was then added dropwise at -20 °C over a 20-min period. After the addition of *n*-BuLi the reaction was left in the cold bath for 10 min and was then allowed to react at room temperature overnight. After the reaction time any remain *n*-BuLi was quenched using a small amount of IPA (1-2 mL). The reaction mixture was then transferred to a separatory funnel and washed with brine (x3). The reaction mixture was then dried with MgSO₄, and the solvent was removed via rotary evaporation. The crude product was then purified via column chromatography (95% hexanes/ 5% EtOAc, slow gradient) to yield the mono-pyrenoendoxide (**2.17**) in 46% yield (0.39 g) and the di-pyrenoendoxide (**2.18**) in 28% yield (0.20 g) and exhibited identical data to previous reported.^{80,124}

¹H NMR (300 MHz, CDCl₃): δ 8.78 (s, 2H), 8.27 (s, 2H), 7.40 (s, 2H), 6.57 (s, 2H), 1.63 (s, 18H).

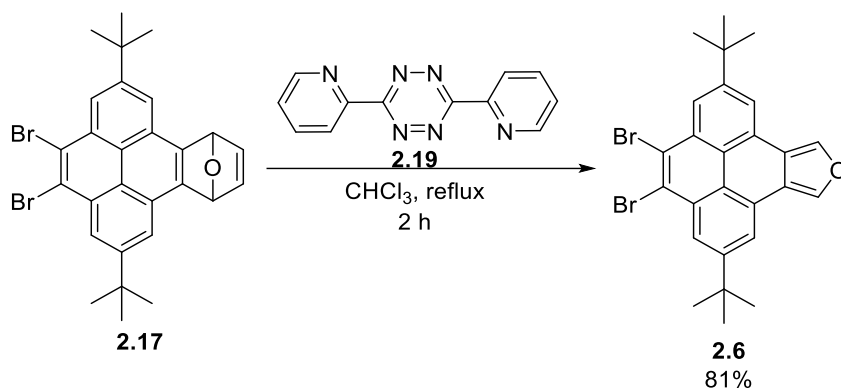
(4R,7S)-2,9-Di-*tert*-butyl-4,7,11,14-tetrahydro-4,7:11,14-diepoxydibenzo[fg,op]tetracene (2.18)



To a RB flask with a stir bar 1 g of tetrabromopyrene **3** (1.6 mmol, 1 equiv) was added. The flask was then sealed and purged with argon gas followed by the addition of dry toluene (23 mL, 0.07 M). The flask was then placed in a -20 °C cold bath (3:1 ice to NaCl) and allowed to stir. Once the reaction mixture cooled, freshly distilled furan (1.2 mL, 15.9 mmol, 10 eq) was added via syringe to the reaction mixture. *n*-BuLi (1.1 mL, 1.6 M, 1.1 equiv) was then added dropwise at -20°C over a 20-min period. After the addition of *n*-BuLi the reaction was left in the cold bath for 10 min and then allowed to react at room temperature for 1 h. After the reaction time the flask was brought to -20 °C at which point furan (1.2 mL, 15.9 mmol, 10 equiv) was added followed by the dropwise addition of *n*-BuLi (1.1 mL, 1.6 M, 1.1 equiv) over a 20 min period. The reaction was then allowed to warm to room temperature and react overnight. After the reaction time any remain *n*-BuLi was quenched using a small amount of IPA (approx. 1 mL). The reaction mixture was then transferred to a separatory funnel and washed with brine (x3). The reaction mixture was then dried with MgSO₄, and solvent removed via rotary evaporation. The crude product was then purified via column chromatography (100% hexanes to 95% hexanes/ 5% EtOAc, slow gradient) to yield the di-pyrenoendoxide **2.18** in a 67% yield (0.48 g) as a mixture of diastereomers. The mono-furan adduct was also observed in small quantities alongside an unidentified impurity. Compound **2.18** is the last compound to elute once the gradient has reached 5% ethyl acetate. The di-pyrenoendoxide **2.18** exhibited identical data to previous reports.¹²⁴

¹H NMR (300 MHz, CDCl₃): δ 8.20 (s, 4H), 7.40 (s, 2H), 7.39 (s, 2H), 6.58 (s, 4H), 1.65 (s, 18H).

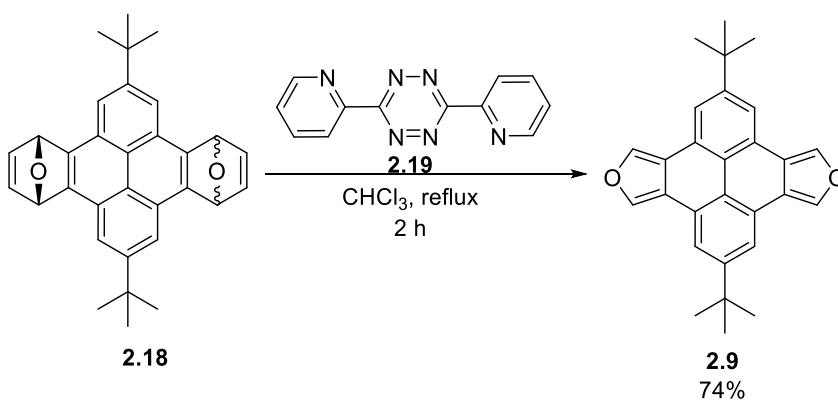
4,5-Dibromo-2,7-di-*tert*-butylpyreno[4,5-*c*]furan (**2.6**)



In a RB flask with a stir bar 1.54 g of the pyrenoendoxide (**2.17**) (2.86 mmol, 1 equiv), alongside 1.01 g of dipytet (**2.19**) (4.30 mmol, 1.5 equiv) were charged. The RB flask was then attached to a reflux condenser and placed under a steady stream of nitrogen gas. After purging, CHCl_3 was added (29 mL, 0.1 M) resulting in the immediate evolution of nitrogen gas (Care must be taken to not build pressure at large scales). The reaction mixture was then set to reflux for two hours. After the reaction time the furan **2.6** was isolated by column chromatography (100% hexanes) in an 81% yield (1.2 g) and exhibited identical spectra to previously reported.⁸⁰

$^1\text{H NMR}$ (300 MHz, CDCl_3): δ 8.57 (s, 2H), 8.45 (s, 2H), 8.30 (s, 2H), 1.56 (s, 18H)

2,8-Di-*tert*-butylpyreno[4,5-*c*:9,10-*c'*]difuran (**2.9**)

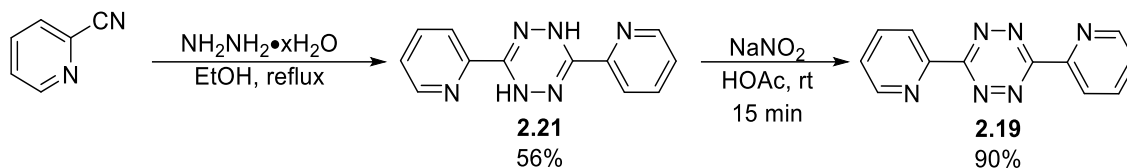


In a microwave vial with a stir bar 0.73 g of the dipyrnoendoxide (**2.18**) (1.7 mmol, 1 equiv), alongside 1.17 g of dipytet (**2.19**) (4.93 mmol, 3 equiv) were charged. The vial was then sealed and purged with argon gas. After purging, CHCl_3 was added (16.5 mL, 0.1 M) resulting in the immediate evolution of nitrogen gas (Care must be taken

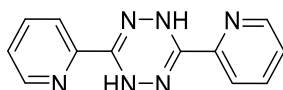
to not build pressure at larger scales). The reaction mixture was then set to reflux for two hours. After the reaction time the reaction was purified by column chromatography using 100% hexanes (0.50 g, 74% yield). The di-pyrenofuran **2.9** exhibited identical data to previous reports.¹²⁴

¹H NMR (300 MHz, CDCl₃): 8.35 (s, 4H), 8.02 (s, 4H), 1.51 (s, 18H).

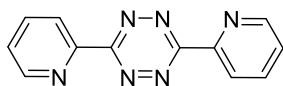
3,6-Di-2-pyridyl-1,2,4,5-tetrazine (**2.19**)



Tetrazine **2.19** was synthesized according to literature procedures and exhibited identical spectra as previous reports.³⁹²

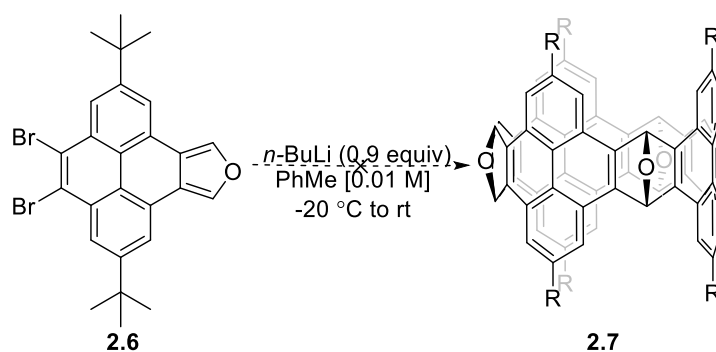


¹H NMR (300 MHz, CDCl₃): δ 8.57 (m, 4H), 8.04 (d, *J* = 8.0 Hz, 2H), 7.75 (t, *J* = 7.7 Hz, 2H), 7.43 – 7.27 (m, 2H).



¹H NMR (300 MHz, CDCl₃): δ 9.08 – 8.96 (m, 2H), 8.76 (dd, *J* = 7.9, 0.9 Hz, 2H), 8.02 (dd, *J* = 7.8, 1.8 Hz, 2H), 7.59 (ddd, *J* = 7.6, 4.7, 1.1 Hz, 2H).

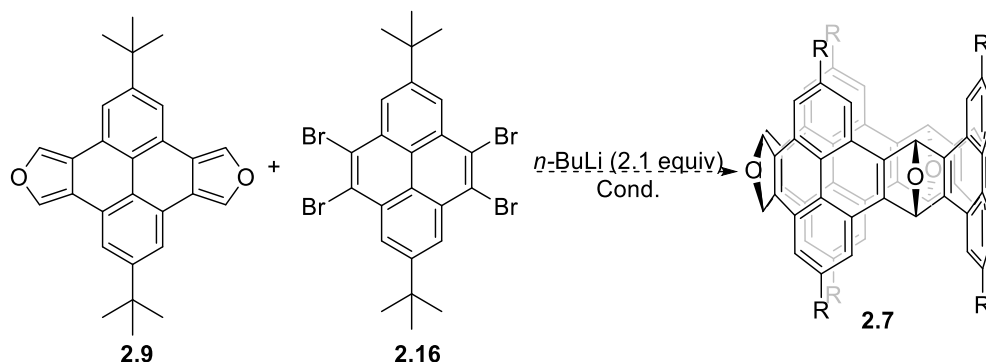
General procedure for “Shotgun” AB- cyclization



A flame dried MW vial with a stir bar was charged with **2.6** (26.9 mg, 0.0530 mmol, 1 equiv), sealed and purged with Ar gas. After purging, dry PhMe (0.010 M, 5.3 mL) was added via syringe and the reaction mixture was cooled to -20 °C. Once the reaction reached temperature *n*-BuLi (30 μL, 1.6 M, 0.9 equiv) was added dropwise and

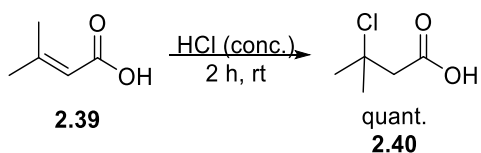
the reaction was set to stir overnight. The addition of *n*-BuLi was marked by a colour change from yellow to a dark brown colour. Following the reaction time, a complex mixture of products was retrieved, the starting material was successfully recovered indicating a 40% consumption of **2.6**.

General procedure for "Shotgun" AA-BB- cyclization



A flame dried MW was charged with **2.9** (101.0 mg, 0.256 mmol, 1 equiv) and **2.16** (161.3 mg, 0.256 mmol, 1 equiv), sealed, and purged with Ar gas. After purging, dry PhMe (0.07 M, 3.7 mL) was added via syringe and the reaction mixture was cooled to -20 °C. Once the reaction reached temperature *n*-BuLi (0.35 mL, 1.6 M, 2.2 equiv) was added slowly and the reaction was set to stir overnight. The addition of *n*-BuLi was marked by a colour change from yellow to a dark brown colour. Following the reaction time, a complex mixture of products was retrieved, the starting material was successfully recovered indicating a 38% consumption of **2.6** and 61% conversion of **2.16**.

3-Chloro-3-methylbutanoic acid (**2.40**)



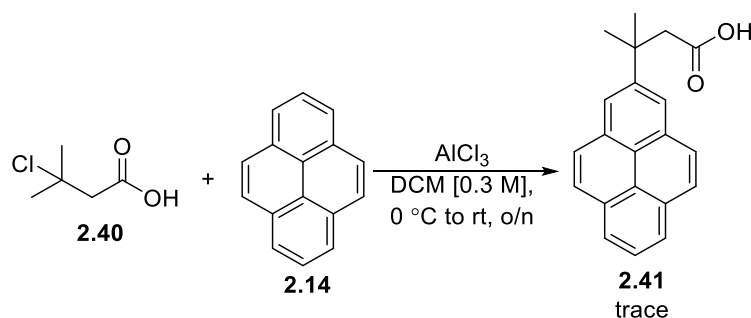
A 10 mL RB flask with a stir bar was charged with senecioic acid **2.39** (100 mg, 0.949 mmol, 1 equiv) and concentrated HCl (3.2 mL) and set to stir for 2 h. After the reaction time the reaction mixture was transferred to a separatory funnel with the aid of water and was diluted with DCM. The aqueous layer was removed, and the organic layer was neutralized with NaHCO₃. Following the neutralization, the organic phase was washed 2 more times with

water, dried and the solvent was removed via rotatory evaporation revealing **2.40** as a dark coloured solid in quantitative yield (130 mg).

$^1\text{H NMR}$ (300 MHz, CDCl_3): δ 2.88 (s, 2H), 1.75 (s, 6H).

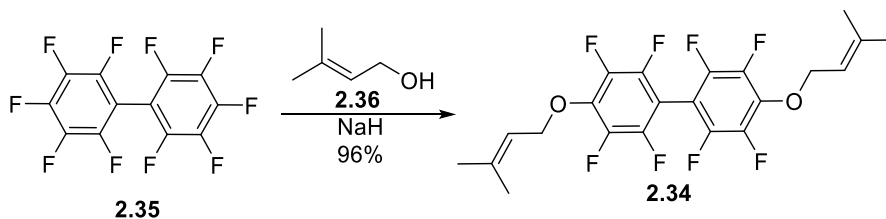
$^{13}\text{C NMR}$ (75 MHz, CDCl_3): δ 176.0, 65.4, 49.6, 32.4.

3-Methyl-3-(pyren-2-yl)butanoic acid (**2.41**)



In a flame dried MW vial with a stir bar, **2.14** (18.5 mg, 0.0920 mmol, 1 equiv) and **2.40** (50 mg, 0.37 mmol, 4 equiv) were added followed by DCM (0.31 mL, 0.3 M). Once solvated, the reaction was brought to $0\text{ }^\circ\text{C}$ and the AlCl_3 (24.4 mg, 0.183 mmol, 2 equiv) was added changing the colour of the reaction mixture to a reddish-brown colour. The reaction was then allowed to react overnight. Following the reaction time, the reaction mixture was transferred to a separatory funnel and the organic layer was washed twice with a brine solution. The organic layer was then collected, dried and the solvent was removed via rotatory evaporation. **2.41** was observed by TLC-MS but was not successfully isolated.

2,2',3,3',5,5',6,6'-Octafluoro-4,4'-bis((3-methylbut-2-en-1-yl)oxy)-1,1'-biphenyl (**2.34**)



A flame dried RB flask with a stir bar was charged with NaH (60% w/w, 0.13 g, 3.2 mmol, 2.1 equiv). Prenol **2.36** (2.15 mL, 1.50 mmol, 2 equiv) was then carefully added to the flask and the solution was allowed to stir for 15

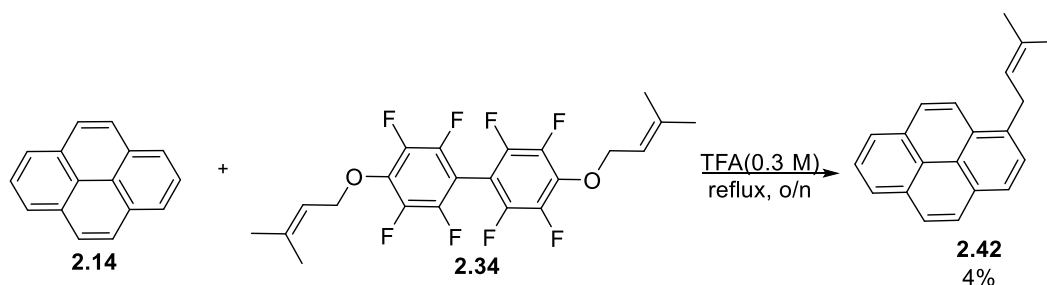
min at room temperature. **2.35** (250 mg, 0.75 mmol, 1 equiv) was then added to the flask at room temperature and the reaction mixture was allowed to stir for 30 min. After the reaction time the reaction mixture was diluted with DCM and transferred to a separatory funnel where the organic layer was washed with 1 M HCl, then 2 more times with DI water. The organic layer was then dried, and the solvent was removed via rotatory evaporation. **2.34** was isolated in 96% (0.34 g) yield following column chromatography (80% hexanes/20% EtOAc).

¹H NMR (300 MHz, CDCl₃): δ 5.52 (m, 2H), 4.81 (d, *J* = 7.3 Hz, 4H), 1.80 (s, 3H), 1.73 (s, 3H).

¹³C NMR (75 MHz, CDCl₃): δ 146.4 (m), 143.2 (m), 141.68, 139.8 (m), 138.6 (m), 118.5, 71.2 (t, *J* = 3.5 Hz), 25.7, 17.9.

¹⁹F NMR (282 MHz, CDCl₃): δ -140.3 (m), -156.2 (dd, *J*=15.1 Hz, 5.60 Hz).

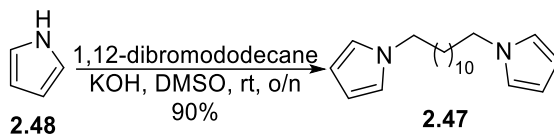
2-(3-Methylbut-2-en-1-yl)pyrene (2.42)



A flame dried RB flask with a stir bar was charged with **2.14** (43.5 mg, 0.215 mmol, 1.02 equiv) and **2.34** (95.6 mg, 0.212 mmol, 1 equiv). The flask was fitted with a reflux condenser and the apparatus was sealed with a rubber setup and purged with argon. TFA was then added, and the reaction was allowed to reflux overnight. Following the reaction time, the reaction mixture was diluted with DCM and transferred to a separatory funnel. The organic layer was then washed with water 3 times. The organic layer was then dried, and the solvent was removed via rotatory evaporation. **2.42** was isolated through column chromatography (100% hexanes) in a 4% yield (2.3 mg).

¹H NMR (300 Hz, CDCl₃): δ 8.27 (d, *J* = 9.3 Hz, 1H), 8.19 – 8.07 (m, 4H), 8.04 – 7.94 (m, 3H), 7.88 (d, *J* = 7.8 Hz, 1H), 5.48 (t, *J* = 6.9 Hz, 1H), 4.05 (d, *J* = 6.9 Hz, 2H), 1.89 (s, 3H), 1.77 (s, 3H).

1,10-Di(1*H*-pyrrol-1-yl)undecane (**2.47**)

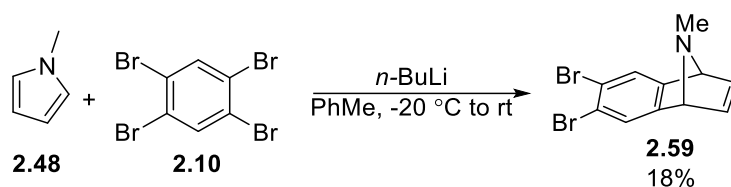


A flame dried RB flask with a stir bar was charged with KOH (453 mg, 8.08 mmol, 8 equiv) and 1,12-dibromododecane (335.5 mg, 1.02 mmol, 1 equiv). The flask was then capped with a rubber septum and purged with Ar. After the pyrrole **2.48** (542 mg, 8.08 mmol, 8 equiv) and DMSO (41 mL, 0.025 M) were added. The reaction was then allowed to stir at room temperature overnight. After the reaction time the mixture was transferred to a separatory funnel and diluted with ethyl ether. The organic phase was then washed 3x with a saturated brine solution. The organic layer was then dried, and the solvent was removed via rotatory evaporation. **2.47** Was then isolated in a 90% yield (278 mg) following column chromatography (80% hexanes/20% EtOAc) and exhibited identical spectra to previous reports.³⁹³

¹H NMR (300 MHz, CDCl₃): δ 6.64 (s, 4H), 6.13 (s, 4H), 3.86 (t, *J* = 7.2 Hz, 4H), 1.75 (m, 4H), 1.23 (m, 16H).

¹³C NMR (75 MHz, CDCl₃): δ 120.34, 107.65, 49.52, 31.49, 29.41, 29.37, 29.11, 26.67.

6,7-Dibromo-9-methyl-1,4-dihydro-1,4-epiminonaphthalene (**2.59**)

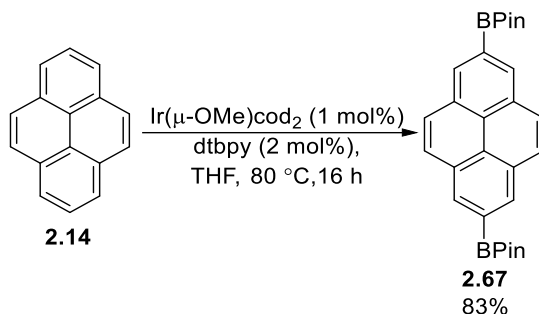


A flame dried MW vial with a stir bar was charged with **2.10** (26 mg, 0.067 mmol, 1 equiv) and sealed. The vial was then purged with Ar. After purging, **2.48** (54 mg, 0.67 mmol, 10 equiv) and PhMe (1 mL, 0.07 M) were added, and the reaction mixture was set to stir at -20 °C. *n*-BuLi (83 μL, 1.6 M) was then added over a 1 h period. After the addition period the reaction was brought to room temperature and then allowed to stir overnight. Following the reaction time, the mixture was transferred to a separatory funnel and diluted with DCM. The organic phase was then washed 3x with a saturated brine solution. The organic layer was dried, and the solvent was removed via rotatory

evaporation. **2.59** was then isolated in a 18% yield (3.8 mg) following column chromatography (60% hexanes/40% EtOAc).

HRMS [M+H]⁺: Calculated C₁₁H₁₀Br₂N (M+H)⁺=313.91745; found= 313.91755

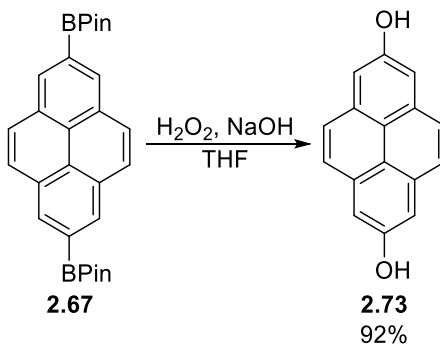
2,7-Bis(4,4,5,5-tetramethyl-1,3,2-dioxaborolan-2-yl)pyrene (2.67)



2.67 was synthesized according to previous literature procedure in a 83% yield and exhibited identical spectra to previously reported.¹⁵³

¹H NMR (300 MHz, CDCl₃): δ 8.64 (s, 4H), 8.10 (s, 4H), 1.48 (s, 24H).

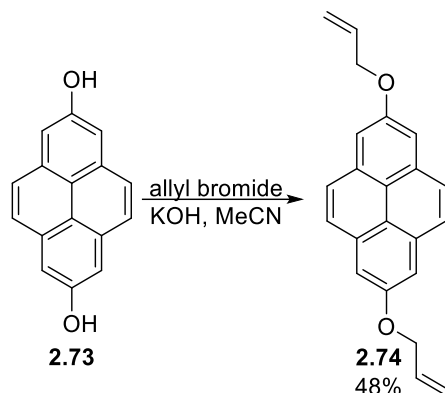
Pyrene-2,7-diol (2.73)



2.73 was synthesized according to a previous literature procedure in a 92% yield and exhibited identical spectra to previously reported.¹⁵³

¹H NMR (300 MHz, D₆-DMSO): δ 9.87(s, 2H), 7.94 (s, 4H), 7.60 (s, 4H).

2,7-Bis(allyloxy)pyrene (2.74)



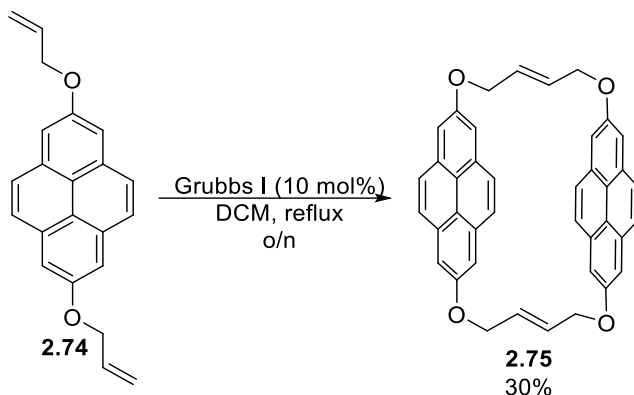
Procedure was adapted from a prior report.³⁹⁴ A flame dried MW vial with a stir bar was charged with **2.73** (100 mg, 0.427 mmol, 1 equiv) and was followed by MeCN (1.7 mL, 0.25 M). KOH (53 mg, 0.939 mmol, 2.2 equiv) was then added to the vial and the reaction was set to stir at room temperature for 20 min. Allyl bromide (124 mg, 1.025 mmol, 2.4 equiv) was then added and the reaction was then allowed to stir at room temperature for 24 h. The reaction was then filtered with the aid of MeCN, diluted with DCM, and then transferred to a separatory funnel where the organic layer was washed 3 times with DI water. The organic layer was dried, and the solvent was removed via rotatory evaporation. **2.74** was then isolated in a 48% (64 mg) yield following column chromatography (80% hexanes/ 20% EtOAc).

¹H NMR (500 MHz, CDCl₃): δ 7.96 (s, 4H), 7.71 (s, 4H), 6.21 (ddd, *J* = 16.7, 10.5, 4.9 Hz, 2H), 5.54 (d, *J* = 17.4 Hz, 2H), 5.36 (d, *J* = 10.7 Hz, 2H), 4.83 (d, *J* = 4.4 Hz, 4H).

¹³C NMR (75 MHz, CDCl₃): δ 156.18, 133.47, 131.59, 127.48, 120.18, 117.77, 111.51, 69.36.

HRMS[M+H]⁺: Calculated for C₂₂H₁₉O₂(M+H)⁺=315.13751; found=315.13751

(4E,11E)-2,7,9,14-Tetraoxa-1,8(2,7)-dipyrenacyclotetradecaphane-4,11-diene (2.75)

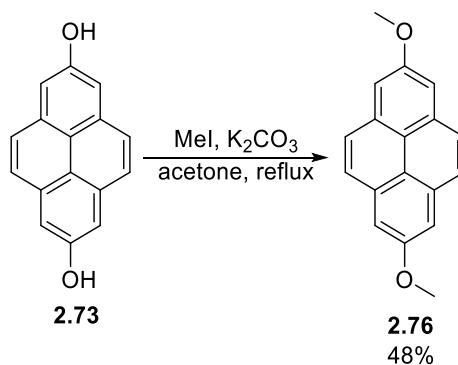


Procedure was adapted from a prior report.¹³² Grubbs I catalyst (20 mg, 0.023 mmol, 0.1 equiv) was added to a flame dried RB flask with a stir bar. The flask was then sealed with a rubber septum and purged with Ar. Dry DCM (12 mL) was then added via syringe and the reaction was set to reflux at 45 °C. A solution of **2.74** (75 mg, 0.24 mmol, 1 equiv) in DCM (63 mL) was made in a separate flask and added over a 1 h period to the catalyst solution. After the addition of **2.74** the reaction was allowed to reflux for overnight. After the reaction time, the solvent was removed and **2.75** was isolated in 30% (41 mg) yield following column chromatography (85% hexanes/15% EtOAc to 50% hexane/50% EtOAc).

¹H NMR (300 MHz, CDCl₃): δ 7.36 (s, 8H), 6.91 (s, 8H), 6.25 (m, 4H), 4.99 (app s, 8H).

¹³C NMR (75 MHz, CDCl₃): δ 154.7, 131.7, 131.18, 126.6, 119.6, 111.5, 67.2.

2,7-Dimethoxyppyrene (2.76)



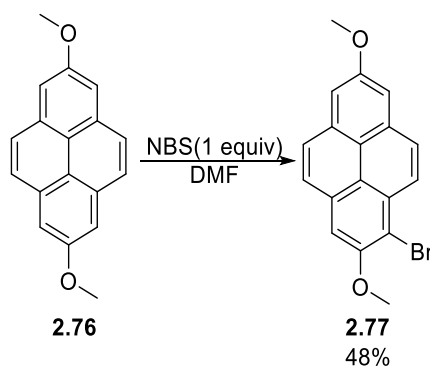
Procedure was adapted from a previous report.³⁹⁵ A flame dried MW vial with a stir bar was charged with **2.73** (100 mg, 0.427 mmol, 1 equiv) and K₂CO₃ (295 mg, 2.13 mmol, 5 equiv), sealed, and purged with Ar. Acetone (1.4 mL, 0.31 M) was then added via syringe followed by MeI (242 mg, 1.71 mmol, 4 equiv) and the reaction was set to stir at reflux for 24 h. After the reaction time the reaction mixture was cooled to room temperature and neutralized with 1 M HCl (approx. 2 mL). The reaction mixture was then diluted in DCM and transferred to a separatory funnel where it was washed twice with DI water. The organic layer was dried, and the solvent was removed via rotatory evaporation. **2.76** was then isolated in a 48% (54 mg) yield following column chromatography (80% hexanes/20% EtOAc).

¹H NMR (300 MHz, CDCl₃): δ 7.98 (s, 4H), 7.71 (s, 4H), 4.10 (s, 6H).

¹³C NMR (75 MHz, CDCl₃): δ 157.2, 131.6, 127.5, 120.1, 110.7, 55.8.

HRMS[M+H]⁺: Calculated for C₁₈H₁₅O₂(M+H)⁺=263.10666; found 263.10654

1-Bromo-2,7-dimethoxy pyrene (2.77)

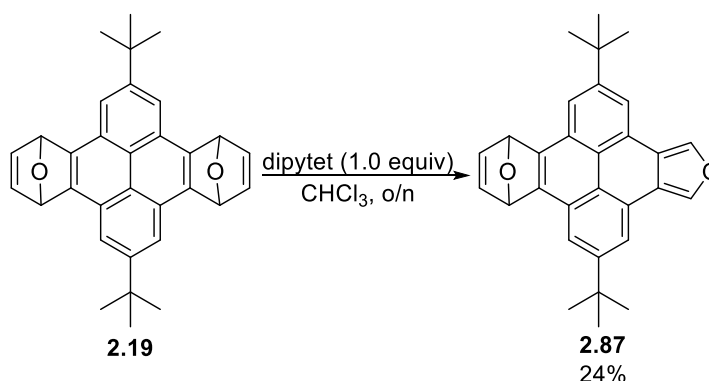


A flame dried MW vial with a stir bar was charged with **2.76** (40 mg, 0.15 mmol, 1 equiv) and NBS (27 mg, 0.15 mmol, 1 equiv), sealed and purged with Ar. The reaction vessel was brought to 0 °C and DMF (0.76 mL, 0.2 M) was added to the mixture. The reaction was then allowed to stir overnight. After the reaction time, the mixture was filtered with the aid of toluene and the filtrate was then transferred to a separatory funnel. The organic layer was then washed 3 times with DI water. The organic layer was then dried, and the solvent was removed via rotatory

evaporation. **2.77** was then isolated in a 48% yield (25 mg) following column chromatography (80% hexanes/20% EtOAc).

$^1\text{H NMR}$ (300 MHz, CDCl_3): δ 8.47 (d, $J = 9.4$ Hz, 1H), 8.10 (d, $J = 9.3$ Hz, 1H), 8.06 – 7.98 (m, 2H), 7.76 (m, 2H), 7.73 (s, 1H), 4.20 (s, 3H), 4.11 (s, 3H).

2,8-Di-*tert*-butyl-10,13-dihydro-10,13-epoxybenzo[9,10]pyreno[4,5-*c'*]furan (**2.87**)

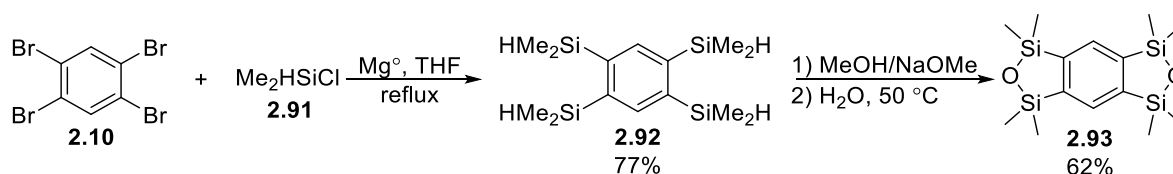


A flame dried MW vial with a stir bar was charged with **2.19** (264 mg, 0.592 mmol, 1 equiv) and dipytet **2.19** (140 mg, 0.592 mmol, 1 equiv). The vial was then sealed and purged with Ar at which point CHCl_3 (12 mL, 0.05 M) was added via syringe. The reaction was then set to stir at room temperature overnight. After the reaction time the solvent was removed via rotatory evaporation and **2.87** was isolated in a 24% yield (60 mg) following column chromatography (100% hexanes).

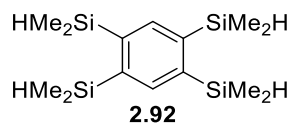
$^1\text{H NMR}$ (300 MHz, CDCl_3): δ 8.43 (s, 2H), 8.22 (s, 2H), 7.96 (s, 2H), 7.37 (s, 2H), 6.49 (s, 2H), 1.54 (s, 18H).

$^{13}\text{C NMR}$ (75 MHz, CDCl_3): δ 149.2, 147.7, 144.2, 136.7, 126.9, 125.5, 121.9, 118.8, 117.1, 82.2, 35.2, 31.7.* Signal missing due to overlapping peaks.

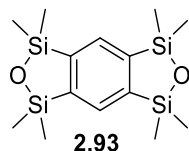
1,1,3,3,5,5,7,7-Octamethyl-5,7-dihydro-1*H*,3*H*-benzo[1,2-*c*:4,5-*c'*]bis[1,2,5]oxadisilole (**2.93**)



Benzobisoxadisilole **2.19** was synthesized according to literature procedures and exhibited identical spectra as previous reports.¹⁴¹

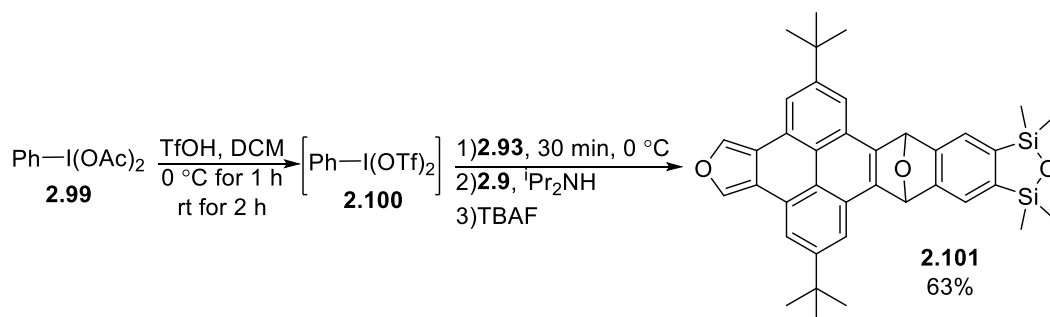


¹H NMR (300 MHz, CDCl₃): δ 7.75 (s, 2H), 4.65 (sept, *J* = 6.0 Hz, 4H), 0.37 (d, *J* = 6.0 Hz, 24H).



¹H NMR (300 MHz, CDCl₃): δ 7.79 (s, 2H), 0.38 (s, 24H).

2,8-Di-*tert*-butyl-12,12,14,14-tetramethyl-10,12,14,16-tetrahydro-10,16-epoxydibenzo[6,7:10,11]-furo[3',4':8,9]-tetraceno[2,3-c][1,2,5]oxadisilole (2.101)

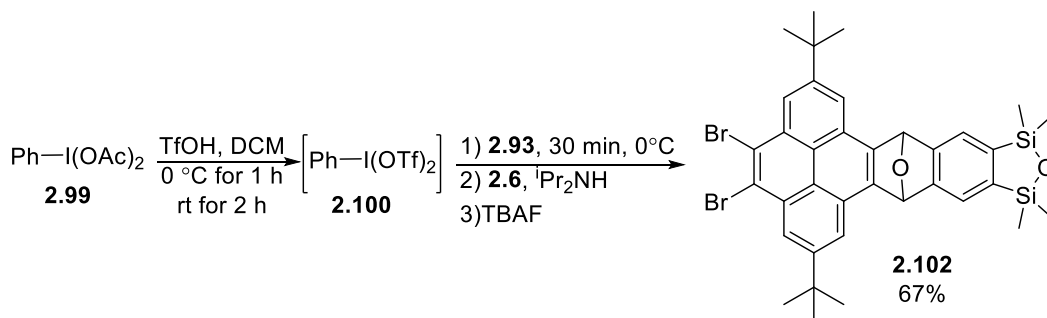


Procedure was adapted from a prior report.¹⁴¹ A flame dried MW vial with a stir bar was charged with **2.99** (39.1 mg, 0.122 mmol, 1.5 equiv) and the vial was then sealed and purged with Ar. The reaction vessel was brought down to 0 °C at which point DCM (0.81 mL, 0.15 M) was added via syringe followed by TfOH (36.5 mg, 0.243 mmol, 3 equiv). The solution was then allowed to stir for 1 h at 0 °C then 2 h at room temperature. A solution of **2.93** (25 mg, 0.081 mmol, 1 equiv) in DCM (0.41 mL, 0.2 M) was then added to the reaction mixture and was allowed to stir for 30 min at room temperature. A solution of **2.9** (64.4 mg, 0.161 mmol, 2 equiv) in DCM (0.8 mL, 0.2 M) was then added followed by ⁱPr₂NH (20.5 mg, 0.203 mmol, 2.5 equiv) and lastly TBAF (0.2 mL, 1.0 M in THF). After all the reagents were added to the reaction, the mixture was allowed to stir overnight. Following the reaction time, the mixture was diluted in DCM and transferred to a separatory funnel where the organic layer was washed 3x with DI

water. The organic layer was then dried, and the solvent was removed via rotatory evaporation. **2.101** was then isolated in a crude 63% yield (31 mg) following column chromatography (90% hexanes/ 10% EtOAc).

¹H NMR (300 MHz, CDCl₃) δ 8.41 (s, 2H), 8.23 (s, 2H), 8.05 (s, 2H), 7.61(s, 2H), 6.76 (s, 2H), 1.59 (s, 18 H), 0.35 (s, 6H), 0.20 (s, 6H).

4,5-Dibromo-2,7-di-tert-butyl-11,11,13,13-tetramethyl-9,11,13,15-tetrahydro-9,15-epoxydibenzo[6,7:10,11]-tetraceno[2,3-c][1,2,5]oxadisilole (2.102)

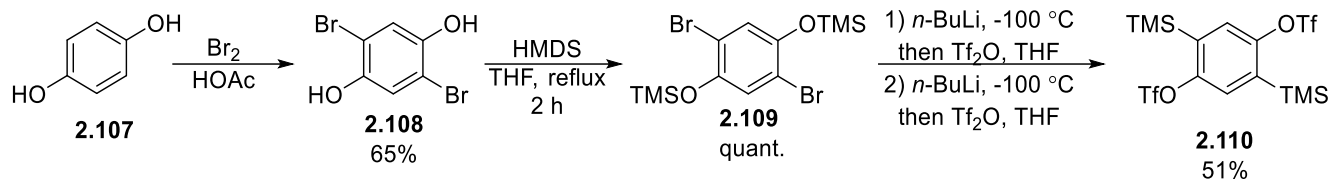


Procedure was adapted from a prior report.¹⁴¹ A flame dried MW vial with a stir bar was charged with **2.99** (78.8 mg, 0.245 mmol, 1.5 equiv) and the vial was then sealed and purged with Ar. The reaction vessel was brought down to 0 °C at which point DCM (1.6 mL, 0.15 M) was added via syringe followed by TfOH (73.4 mg, 0.489 mmol, 3 equiv). The solution was then allowed to stir for 1 h at 0 °C then 2 h at room temperature. A solution of **2.93** (50.0 mg, 0.163 mmol, 1 equiv) in DCM (0.8 mL, 0.2 M) was then added to the reaction mixture and allowed to stir for 30 min at room temperature. A solution of **2.6** (100 mg, 0.2 mmol, 1.2 equiv) in DCM (1 mL, 0.2 M) was then added followed by ⁱPr₂NH (41.2 mg, 0.408 mmol, 2.5 equiv) and lastly TBAF (0.41 mL, 1.0 M in THF). After all the reagents were added to the reaction, the mixture was allowed to stir overnight. Following the reaction time, the mixture was diluted in DCM and transferred to a separatory funnel where the organic layer was washed 3x with DI water. The organic layer was then dried, and the solvent was removed via rotatory evaporation. **2.102** was then isolated in a crude 67% yield (78 mg) following column chromatography (90% Hexanes/ 10% EtOAc).

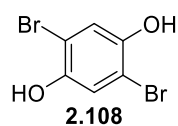
¹H NMR (300 MHz, CDCl₃) δ 8.78 (s, 2H), 8.36 (s, 2H), 7.63 (s, 2H), 6.84 (s, 2H), 1.65 (s, 18H), 0.35 (s, 6H), 0.18 (s, 6H).

^{13}C NMR (300MHz, CDCl_3): δ 150.3, 149.8, 146.7, 146.2, 130.7, 127.4, 125.7, 124.8, 122.0, 121.4, 118.8, 82.4, 35.7, 32.0, 1.1, 0.92

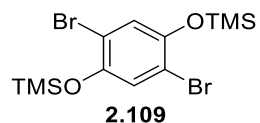
2,5-Bis(trimethylsilyl)-1,4-phenylene bis(trifluoromethanesulfonate) (2.110)



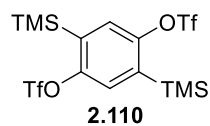
2.110 was synthesized according to literature procedures and exhibited identical spectra as previous reports.³⁹⁶



^1H NMR (300 MHz, CDCl_3): δ 7.17 (s, 2H), 5.14 (s, 2H).

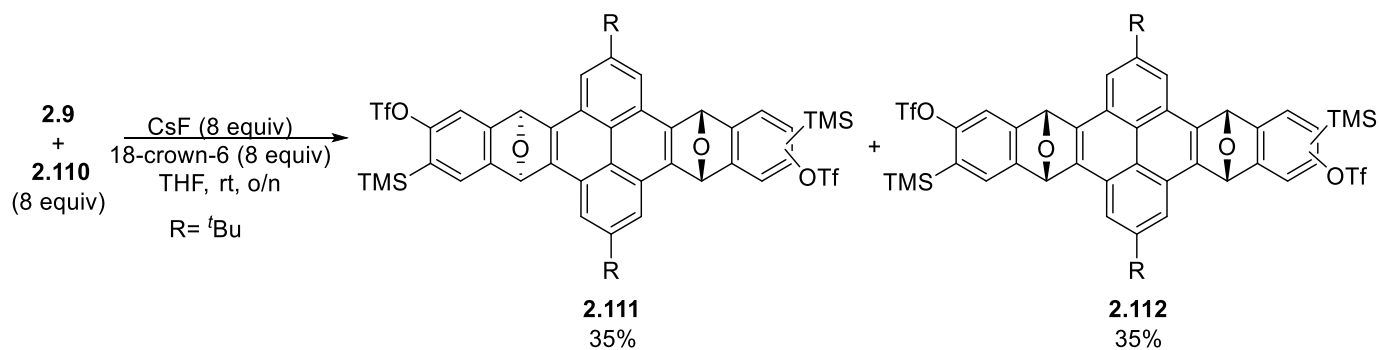


^1H NMR (300 MHz, CDCl_3): δ 7.04 (s, 2H), 0.29 (s, 18H).

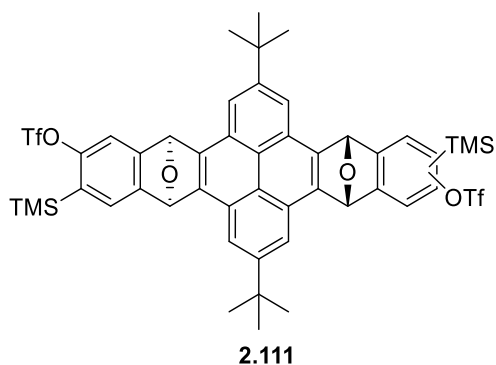


^1H NMR (300 MHz, CDCl_3): δ 7.45 (s, 2H), 0.38 (s, 18H).

2,11-Di-*tert*-butyl-7,16-bis(trimethylsilyl)-4,9,13,18-tetrahydro-4,9:13,18-diepoxydibenzo[*hi,uv*]hexacene-6,15-diyl bis(trifluoromethanesulfonate) (2.111 and 2.112)



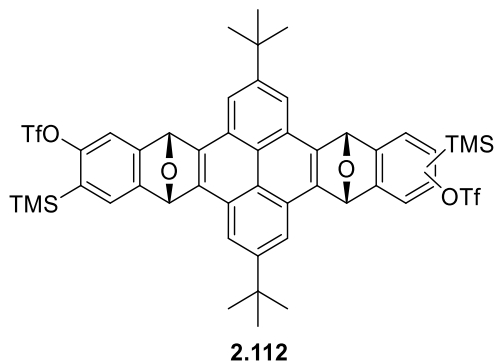
To a microwave vial with a stir bar difuran **2.9** (50.0 mg, 0.127 mmol, 1 equiv), bistriflate **2.110** (523 mg, 1.02 mmol, 8 equiv), 18-crown-6 (269 mg, 1.02 mmol, 8 equiv) and CsF (163 mg, 1.02 mmol, 8 equiv) were charged. The vial was then sealed and purged with Ar at which point THF (2.5 mL, 0.07 M) was added. The reaction was then left to stir at room temperature overnight. As the reaction progressed the yellow solution slowly converted to a dark brown-red colour. After the reaction time, the reaction mixture was worked up with DCM/water. The mixture was then dried, followed by the removal of the solvent through rotatory evaporation. The mixture was then purified via column chromatography with 95% hexanes/ 5% EtOAc (slow gradient). The order of elution is as follows: First any unreacted starting material elutes while only hexane is present. As the gradient is raised some monoadduct **2.115** co-elutes with an unidentified impurity followed by the *anti*-adduct **2.111** (44 mg, 35% yield) and finally the *syn*-adduct **2.112** (44 mg, 35% yield). Both products exhibited identical spectra as previous reports.¹²²



¹H NMR (300 MHz, CDCl₃): δ 8.29 (s, 2H), 8.26 (s, 2H), 7.51 (s, 2H), 7.44 (s, 2H), 6.82 (s, 4H), 1.66 (s, 18H), 0.26 (s, 18H).

¹³C NMR (300 MHz, CDCl₃): δ 153.3, 152.5, 148.0, 126.1, 117.9, 112.6, 82.0, 35.5, 32.0, -0.9.

MALDI-TOF MS: Calculated for C₄₈H₄₈F₆O₈S₂Si₂(M⁺)=986.223; Found= 986.190

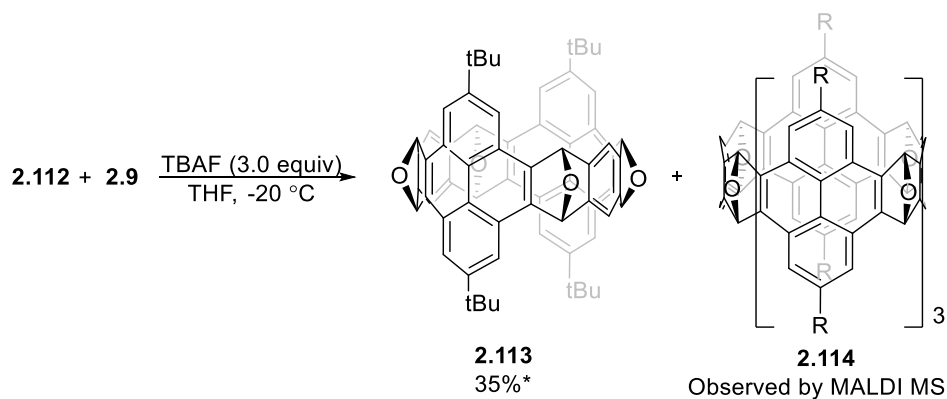


^1H NMR (300 MHz, CDCl_3): δ 8.28 (s, 2H), 8.26 (s, 2H), 7.42 (s, 2H), 7.35 (s, 2H), 6.84 (s, 4H) 1.66 (s, 18H), 0.30 (s, 18H).

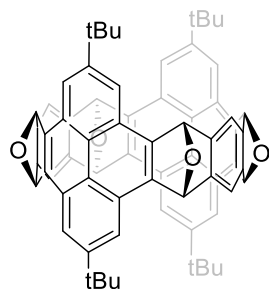
^{13}C NMR (300 MHz, CDCl_3): δ 153.2, 152.4, 149.5, 147.9, 146.5, 146.4, 146.0, 129.1, 126.1, 125.7, 120.8, 117.8, 117.7, 112.3, 82.2, 82.0, 35.5, 32.0, -1.0

MALDI-TOF MS: Calculated for $\text{C}_{48}\text{H}_{48}\text{F}_6\text{O}_8\text{S}_2\text{Si}_2(\text{M}^+)=986.223$; Found=986.218

[10]Tetraepoxyppyrenecyclacene (**2.113**) and [20]octoepoxyppyrenecyclacene (**2.114**)



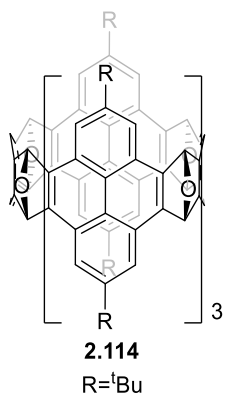
In a MW vial with a stir bar adduct **2.112** (30.5 mg, 0.0310 mmol, 1 equiv) was charged alongside the difuran **2.9** (12.9 mg, 0.0310 mmol, 1 equiv). The vial was sealed and purged with Ar, at which point it was placed in a $-20\text{ }^\circ\text{C}$ cold bath and allowed to stir. TBAF (93 μL , 1 M, 0.093 mmol) was added over a 10-min period. As the TBAF was introduced to the reaction mixture the solution changed from a yellow to a dark brown/red colour. The reaction mixture was slowly warmed to room temperature and then left to react overnight at room temperature. After the reaction time, the mixture was a dark brown/red colour with some precipitate present in solution. The solvent was then removed, and the solids were re-dissolved in CHCl_3 and washed twice with deionized water. The organic layer was dried and then the solvent was then removed through rotatory evaporation. Cycle **2.113** was isolated following column chromatography (9:1 DCM/Ether) in a 35% (10 mg) crude yield. Samples for NMR were made by subjecting the crude product to several rounds of chromatography (6% yield). Cycle **2.113** exhibited identical spectra to previously reported.¹²²



2.113

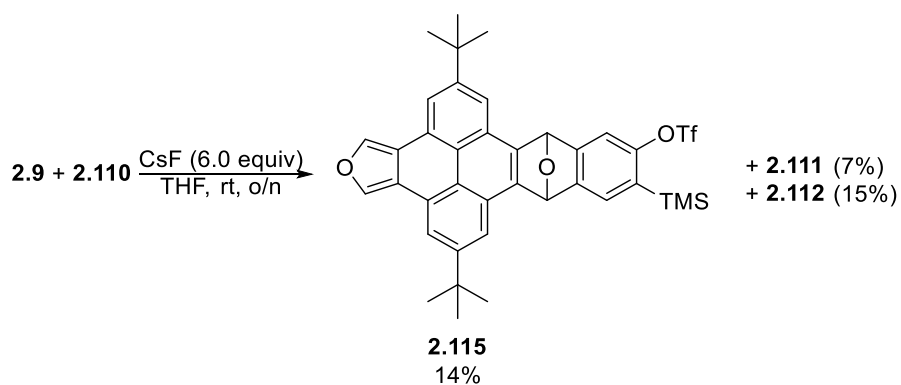
$^1\text{H NMR}$ (300 MHz, CDCl_3): 8.26 (s, 8H), 7.80 (s, 4H), 6.57 (s, 8H)

MALDI-TOF MS: Calculated for $\text{C}_{68}\text{H}_{56}\text{O}_4[\text{M}^+]=936.418$; Found= 936.526



MALDI-TOF MS: Calculated for $\text{C}_{136}\text{H}_{112}\text{O}_8[\text{M}^+]=1872.836$; Found= 1873.963

2,8-Di-*tert*-butyl-13-(trimethylsilyl)-10,15-dihydro-10,15-epoxydibenzo[4,5:12,1]tetraceno[2,3-*c*]furan-12-yl trifluoromethanesulfonate (2.115)



A microwave vial with a stir bar was charged with **2.9** (30 mg, 0.076 mmol, 1 equiv), **2.109** (40.4 mg, 0.076 mmol, 1 equiv), and CsF (69.3 mg, 0.456 mmol, 6 equiv). The vial was then sealed and purged with Ar, at which point THF (2.5 mL, 0.07 M) was added. The reaction was then left to stir at room temperature overnight. As the reaction

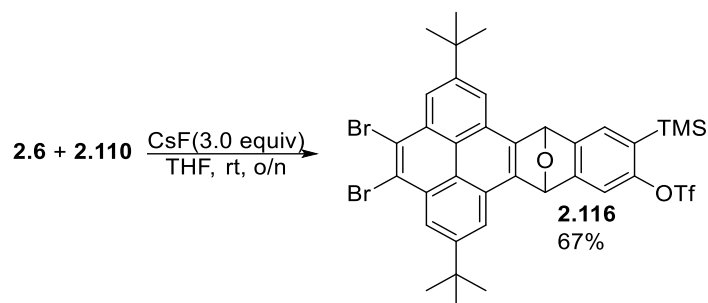
progressed the yellow solution slowly converted to a dark brown-red colour. After the reaction time the reaction mixture was worked up with DCM/water. The mixture was then dried followed by the removal of the solvent through rotatory evaporation. **2.114** was then isolated in a 14% yield (7.4 mg) following column chromatography (95% hexanes/5% EtOAc).

¹H NMR (300 MHz, CDCl₃): δ 8.42 (s, 2H), 8.24 (s, 2H), 8.03 (s, 1H), 8.00 (s, 1H), 7.49 (s, 1H), 7.42 (s, 2H), 6.77 (s, 2H), 1.59 (s, 9H), 1.58 (s, 9H), 0.28 (s, 9H).

¹³C NMR (75 MHz, CDCl₃): δ 153.5, 152.5, 149.8, 149.6, 148.1, 145.8, 145.5, 136.8, 129.1, 126.2, 125.9, 125.8, 125.8, 122.3, 122.2, 121.7, 119.5, 119.4, 117.3, 117.2, 112.6, 82.3, 82.1, 31.8, 31.7, -0.86. *Missing signals due to overlapping peaks.

MALDI-TOF MS: Calculated for C₃₈H₃₇F₃O₅SSi[M⁺]=690.208; Found= 690.124

4,5-Dibromo-2,7-di-*tert*-butyl-12-(trimethylsilyl)-9,14-dihydro-9,14-epoxydibenzo[de,qr]tetracen-11-yl trifluoromethanesulfonate (2.116)

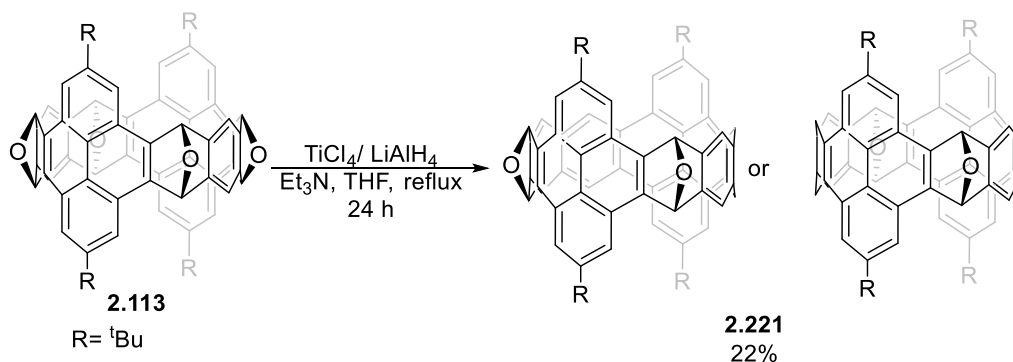


A microwave vial with a stir bar was charged with **2.6** (50.0 mg, 0.098 mmol, 1 equiv), **2.109** (52 mg, 0.098 mmol, 1 equiv), and CsF (44.5mg, 0.293mg, 3 equiv). The vial was then sealed and purged with Ar at which point THF (2.5 mL, 0.07 M) was added. The reaction was then left to stir at room temperature overnight. As the reaction progressed the yellow solution slowly converted to a dark brown-red colour. The reaction mixture was worked up with DCM/water. The organic layer was then dried followed by the removal of the solvent through rotatory evaporation. **2.114** was then isolated in a 67% yield (53 mg) following column chromatography (95% hexanes/5% EtOAc).

$^1\text{H NMR}$ (300 MHz, CDCl_3): δ 8.80 (s, 2H), 8.34 (s, 1H), 8.31 (s, 1H), 7.51 (s, 1H), 7.44 (s, 1H), 6.86 (s, 2H), 1.65 (s, 9H), 1.64 (s, 9H), 0.26 (s, 9H).

$^{13}\text{C NMR}$ (75 MHz, CDCl_3): δ 153.2, 152.5, 150.5, 150.4, 147.9, 146.01, 145.6, 130.8, 130.7, 129.4, 126.0, 125.5, 125.1, 125.1, 118.7, 82.4, 82.2, 35.7, 31.9, 31.9, -0.90.

[10]Di-epoxycyclacene (**2.221**)



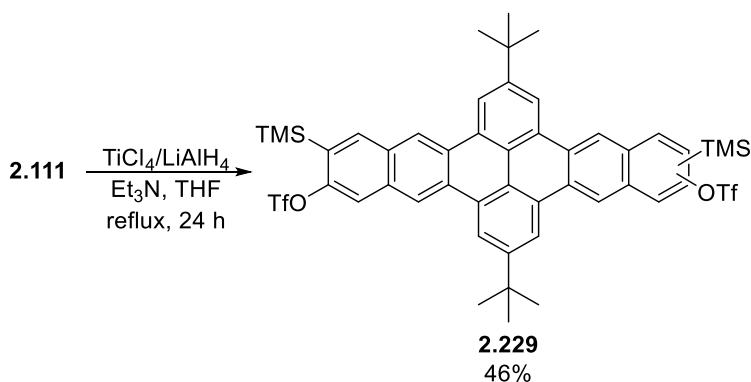
Reduction was carried out by adapting a previously reported procedure.³⁹⁷ First, an approximately 1 M solution of Ti “0” was created. In a sealed flame dried MW vial with a stir bar previously purged with argon, TiCl_4 (0.11 mL, 190 mg, 1.02 mmol) was added followed by 0.42 mL of THF (2.4 M). Upon adding the THF, the clear solution transformed to a yellow solid due to the complexation of the THF with TiCl_4 . The reaction vessel was then brought to 0 °C at which point a suspension of LiAlH_4 in THF (0.38 mL, 1 M) was added carefully to the reaction vessel followed by Et_3N in THF (0.42 mL, 0.55 M). At this point the reaction mixture was allowed to warm to 65 °C and set to stir for 0.5 h. As the reaction stirred, the mixture slowly turned to a black colour. Compound **2.113** (41 mg, 65 μmol , 1 equiv) was charged to a separate vial with a stir bar and the vessel was sealed and purged with argon gas. **2.113** was then dissolved in a minimal amount of dry THF and 0.26 mL of the 1 M solution of Ti “0” solution (0.26 mmol, 4 equiv) was added to reaction vessel with the aid of a syringe. The reaction was then set to reflux for 24 h. After the reaction time the mixture was diluted with DCM and quenched with saturated NaHCO_3 . The mixture was then passed through a Celite plug to remove any metals and washed 3 times with deionized water. The filtrate was then transferred to a separatory funnel and the organic layer was washed 3x with brine. The mixture was then dried with

MgSO₄, followed by the removal of the solvent. Cyclacene **2.221** was then isolated in a 22% crude yield (18 mg) following column chromatography (90% hexanes/10% EtOAc-slow gradient).

¹H NMR (300 MHz, CDCl₃): δ 8.25 (s, 4H), 8.02 (s, 4H), 7.58 (s, 4H), 6.86 (s, 4H), 6.79 (s, 4H), 1.57 (s, 36H).

MALDI-TOF MS: Calculated for C₆₈H₅₆O₂[M⁺]= 904.428; Found= 904.395

2,11-Di-*tert*-butyl-7,16-bis(trimethylsilyl)dibenzo[hi,uv]hexacene-6,15-diyl-bis(trifluoromethanesulfonate)
(**2.229**)



Reduction was carried out by adapting a previously reported procedure.³⁹⁷ In a sealed flame dried MW vial with a stir bar previously purged with argon, TiCl₄ (1.38 g, 7.37 mmol, 8 equiv) was added followed by 3.0 mL of THF (2.4 M). Upon adding the THF clear solution transforms to a yellow solid due to the complexation of the THF with TiCl₄. The reaction vessel was then brought to 0 °C at which point a suspension of LiAlH₄ in THF (2.8 mL, ~1 M) was added carefully to the reaction vessel followed by Et₃N in THF (2.5 mL, 0.55 M). At this point the reaction mixture was allowed to warm to 65 °C and set to stir for 0.5 h. As the reaction stirred, the mixture slowly turned to a black colour. **2.111** (0.896 g, 0.908 mmol, 1 equiv) was then dissolved in a minimal amount of THF and transferred into the Ti solution, at which point the reaction was set to reflux for 24 h. After the reaction time, the mixture was diluted with DCM and quenched with saturated NaHCO₃. The mixture was then passed through a Celite plug to remove any metals and washed 3 times with deionized water. The filtrate was then transferred to a separatory funnel and the organic layer was washed 3x with brine. The mixture was then dried with MgSO₄, followed by the removal of the

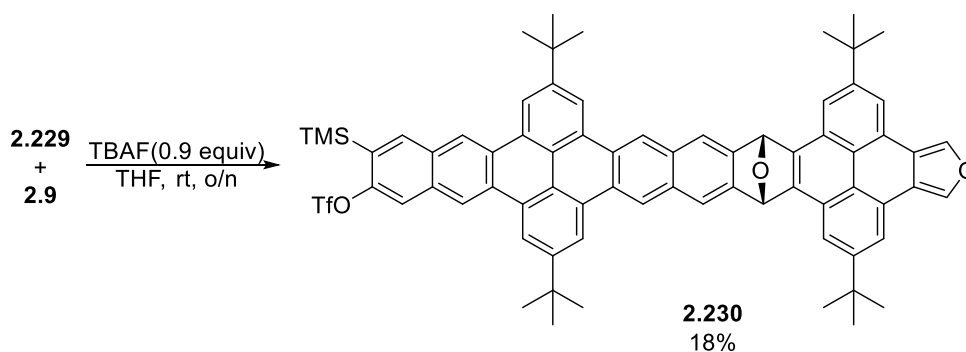
solvent. Cyclacene **2.229** was then isolated in a 22% yield following column chromatography (90% hexanes/10% EtOAc-slow gradient).

¹H NMR (300 MHz, CDCl₃): δ 9.24 (s, 2H), 9.19 (s, 2H), 9.05 (s, 4H), 8.36 (s, 2H), 8.15 (s, 2H), 1.77 (s, 18H), 0.54 (s, 18H).

¹³C NMR (75 MHz, CDCl₃): δ 152.7, 149.5, 138.1, 132.6, 131.6, 130.6, 130.4, 129.9, 129.1, 129.1, 128.8, 128.8, 122.5, 122.3, 120.4, 120.1, 120.1, 119.9, 116.1, 35.7, 32.0, -0.59.

MALDI-TOF MS: Calculated for C₄₈H₄₈F₆O₆S₂Si₂[M⁺]=954.234; Found= 954.130

Tetra-*tert*-butyl-trimethylsilyl-epoxytetrabenzododecapyren[4,5-*c*]acene-trifluoromethanesulfonate (2.230)

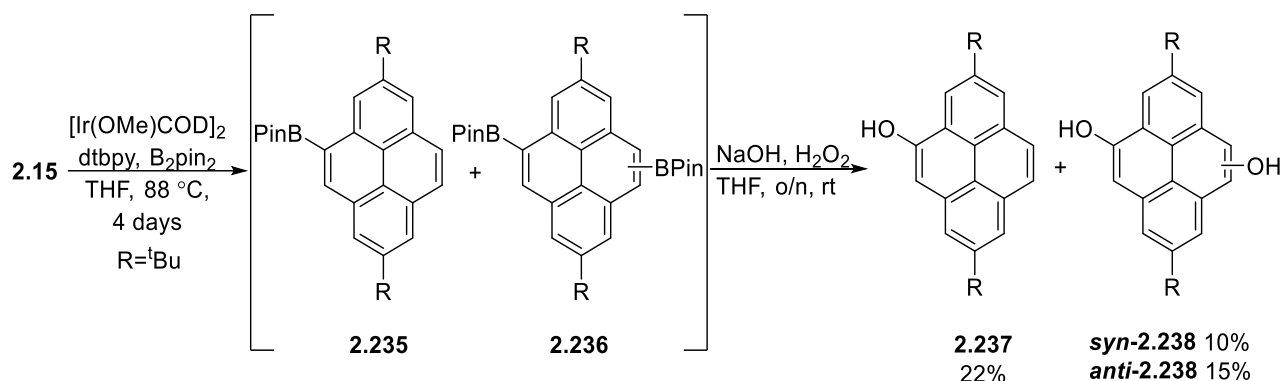


A microwave vial with a stir bar was charged with **2.229** (50 mg, 0.052 mmol, 1 equiv), and **2.9** (41.4 mg, 0.105 mmol, 2 equiv). The vial was then sealed and purged with argon gas at which point THF (2.5 mL, 0.07 M) was added followed by TBAF (47 μL, 1 M, 0.9 equiv). The reaction was then left to stir at room temperature overnight. As the reaction progressed the yellow solution slowly converted to a dark brown-red colour. After the reaction time the mixture was worked up with DCM/water. the organic layer was then dried followed by the removal of the solvent through rotatory evaporation. **2.230** was then isolated in an 18% crude yield (11 mg) following column chromatography (95% hexanes/5% EtOAc).

¹H NMR (300 MHz, CDCl₃): δ 9.24 (s, 1H), 9.20 (s, 1H), 9.11 (s, 2H), 9.01 (s, 4H), 8.42 (s, 2H), 8.36 (s, 2H), 8.27 (s, 2H), 8.21 (s, 2H), 8.15 (s, 2H), 7.01 (s, 2H), 1.72 (s, 18H), 1.65 (s, 18H), 0.55 (s, 9H).

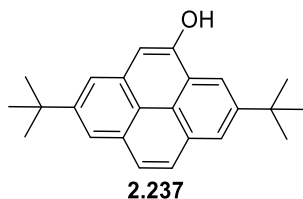
MALDI-TOF MS: Calculated for C₇₂H₆₅F₃O₅SSi[M⁺]=1126.427; Found= 1127.284

2,7-Di-*tert*-butylpyren-4-ol (2.237) and 2,7-di-*tert*-butylpyrene-4,8/9-diol (2.238)



Reaction was carried out by adapting a previously reported procedure.¹⁵³ To a MW with stir bar was added **2.15** (3.0 g, 9.5 mmol, 1 equiv), B_2Pin_2 (7.3 g, 29 mmol, 3 equiv), 4,4'-di(*tert*-butyl)-2,2'-bipyridine (dtbpy) (256 mg, 0.950 mmol, 10 mol%), and $\text{Ir}[(\text{COD})(\text{MeO})]_2$ (318 mg, 0.480 mmol, 5 mol%). The vial was sealed and purged with Ar. Next 12 mL of dry THF (0.8 M) was added. The reaction was then heated at 88 °C for 4 d. After reaction time the mixture was diluted with THF and filtered. The filtrate was collected, the solvent was removed, and the crude reaction mixture was used without further purification in the next step.

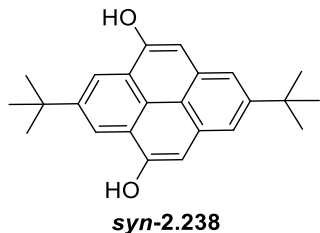
To a 1000 mL RB flask was added the crude reaction mixture (9.5 mmol, 1 equiv). 430 mL of THF was added followed by the addition of NaOH (2.3 g, 57 mmol, 6 equiv) and 4.54 mL of 35% H_2O_2 (57.2 mmol, 6 equiv). The reaction was then allowed to stir overnight. After reaction time, the mixture was acidified with HCl and diluted with diethyl ether. The organic layer was then washed with DI water (x2), dried with MgSO_4 , and the solvent was removed through rotatory evaporation. **2.237** and **2.238** were isolated following column chromatography (80% hexanes/ 20% EtOAc) in 22% (0.69 g) and 25% yields (0.82 g), respectively.



$^1\text{H NMR}$ (300 MHz, CDCl_3): δ 8.53 (d, J = 1.3 Hz, 1H), 8.22 (d, J = 1.5 Hz, 1H), 8.05 (d, J = 3.0 Hz, 1H), 8.02 (d, J = 3Hz, 1H), 8.00 (bs, 2H), 7.32 (s, 1H), 5.49 (s, 1H), 1.60 (s, 9H), 1.56 (s, 9H).

^{13}C NMR (300 MHz, CDCl_3): δ 150.4, 149.0, 148.4, 131.3, 130.9, 130.7, 127.6, 127.2, 124.4, 123.8, 122.8, 120.4, 120.0, 119.6, 116.3, 106.5, 35.4, 35.2, 32.0, 31.9.

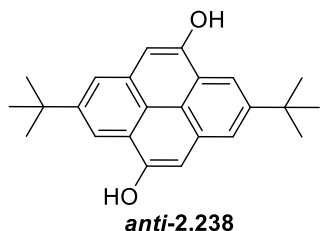
HRMS $[\text{M}+\text{H}]^+$: Calculated for $\text{C}_{24}\text{H}_{27}\text{O}$ $(\text{M}+\text{H})^+=331.20654$; found 331.28445



^1H NMR (300 MHz, D_6 -acetone): δ 8.19 (d, $J = 2.2$ Hz, 2H), 8.07 (d, $J = 2.2$ Hz, 2H), 7.85 (s, 2H), 1.48 (s, 18H).

^{13}C NMR (300 MHz, D_6 -acetone): δ 170.2, 149.4, 135.3, 134.2, 128.6, 128.3, 127.5, 126.7, 35.3, 31.6. * Missing signals due to overlapping peaks.

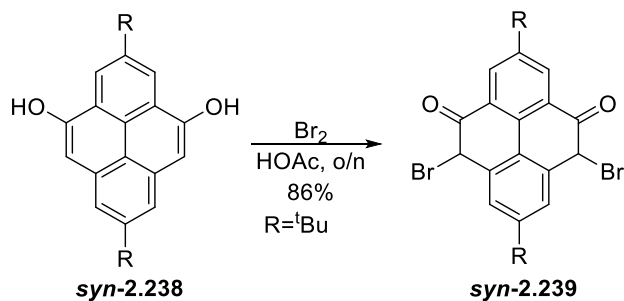
HRMS $[\text{M}]^-$: calculated for $\text{C}_{24}\text{H}_{25}\text{O}_2$ $(\text{M}-\text{H})^-=345.18600$; found= 345.18514



^1H NMR (300 MHz, CDCl_3) δ 8.55 (d, $J = 1.9$ Hz, 2H), 8.12 (d, $J = 1.9$ Hz, 2H), 7.80 (s, 2H), 1.49 (s, 18H).

^{13}C NMR (75 MHz, CDCl_3) δ 180.8, 150.9, 131.7, 131.7, 129.6, 128.2, 127.1, 126.3, 35.1, 31.2.

Dibromo-2,7-di-tert-butylpyrene-syn-diol (**syn-2.239**)

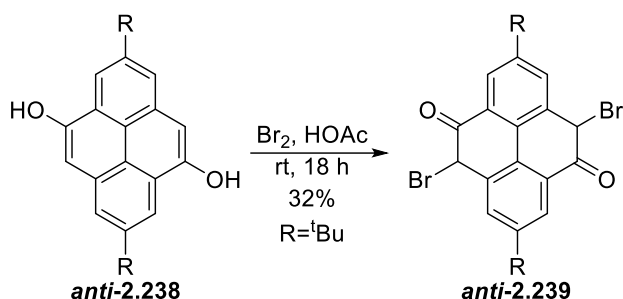


Reaction was carried out by adapting a previously reported procedure.³⁹⁶ **syn-2.237** (50.0 mg, 0.188 mmol, 1 equiv) was charged to a MW vial with a stir bar. AcOH (0.16 mL, 0.9 M) was then added to the flask and the reaction was set to stir. Br_2 (48.4 mg, 0.303 mmol, 2.1 equiv) was then added dropwise to the reaction mixture. The reaction

was then set to stir overnight. After the reaction time the mixture was transferred to a separatory funnel and diluted with DCM and water. The aqueous layer was removed and quenched with saturated $\text{Na}_2\text{S}_2\text{O}_4$. The organic layer was then washed with sat. $\text{Na}_2\text{S}_2\text{O}_4$, brine, and DI water. The organic layer was then dried, and the solvent was removed via rotatory evaporation. **syn-2.239** Was then isolated following column chromatography (80% hexanes/ 20% EtOAc) in an 86% yield (82 mg).

$^1\text{H NMR}$ (300 MHz, CDCl_3): δ 8.22 (s, 2H), 7.61 (s, 2H), 5.55 (s, 2H), 1.43 (s, 18H).

5,10-Dibromo-2,7-di-tert-butyl-5,10-dihydropyrene-4,9-dione (*anti*-2.239)

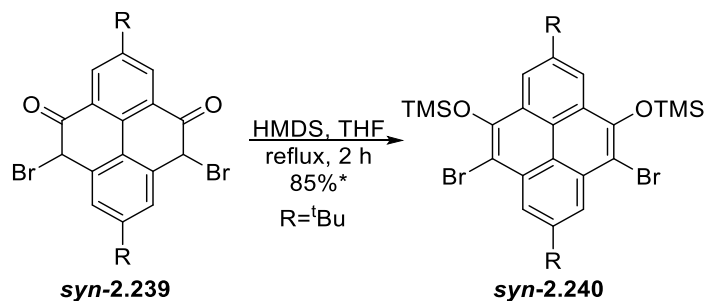


anti-2.239 was synthesized in a 32% yield following the procedure outlined for **syn-2.239**.

$^1\text{H NMR}$ (300 MHz, CDCl_3) δ 8.22 (d, $J = 2.0$ Hz, 2H), 7.70 (d, $J = 2.0$ Hz, 2H), 5.76 (s, 2H), 1.41 (s, 18H).

$^{13}\text{C NMR}$ (300MHz, CDCl_3): δ 173.7, 151.6, 136.0, 130.6, 130.4, 129.1, 34.9, 31.9.* Missing signal due to overlapping peak.

((Dibromo-2,7-di-tert-butylpyrene-diyl)bis(oxy))bis(trimethylsilane) (*syn*-2.240)

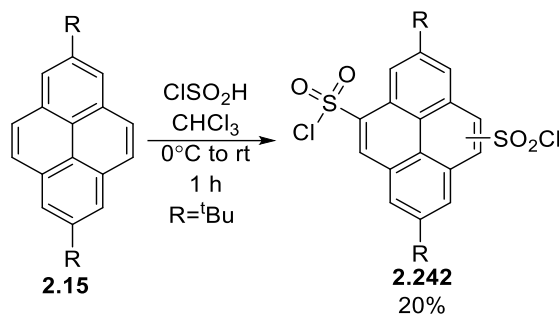


Reaction was carried out by adapting a previously reported procedure.³⁹⁶ **syn-2.239** (40 mg, 0.079 mmol, 1 equiv) was charged to a MW vial with a stir bar and the vial was sealed and purged with Ar. THF (0.04 mL, 2 M) was then added to the vial followed by the dropwise addition of HMDS (26.9 mg, 0.167 mmol, 2.1 equiv). The reaction

was then set to reflux for 2 h. Following the reaction time, the solvent was removed under vacuum and **syn-2.240** was isolated in a 85% yield (44 mg) without any further purification.

$^1\text{H NMR}$ (300 MHz, CDCl_3): δ 8.04 (s, 2H), 7.53 (s, 2H), 1.40 (s, 18H), 0.13 (s, 18H).

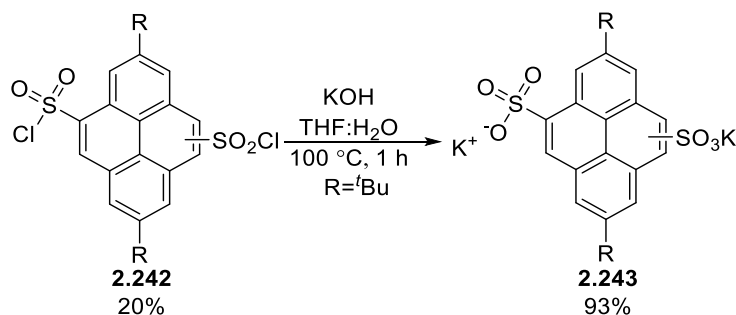
2,7-Di-*tert*-butylpyrene-disulfonyl dichloride (**2.242**)



2.15 (2.0 g, 6.4 mmol, 1 equiv) was added to a flame dried MW vial with a stir bar. The vial was sealed and brought to 0 °C at which point chlorosulfonic acid (3.70 g, 31.8 mmol, 5 equiv) was added dropwise forming a black-coloured solution. The reaction was the allowed to stir for 1 h at room temperature. The reaction mixture was then poured into a separatory funnel containing ice water and was diluted further with chloroform. The organic layer was then washed 3x with DI water. The organic layer was then dried, and the solvent was removed via rotatory evaporation. The mixture was then redissolved in DCM and filtered through a silica plug with the aid of DCM and EtOAc. The filtrate was discarded, and the plug was then washed with 10% MeOH/DCM. The solvent was then report and compound **2.242** was isolated in a 20% crude yield (0.65 g) following column chromatography (9:1 DCM:MeOH). **2.242** slowly converts to **2.242** due to ambient moisture. Compound **2.242** was used as a crude mixture for the next step without any further purification.

$^1\text{H NMR}$ (300 MHz, CDCl_3): δ 9.12 (s, 2H), 8.93 (s, 2H), 8.35 (s, 2H), 1.41 (s, 18H).

Potassium 2,7-di-*tert*-butylpyrene-disulfonate (**2.243**)

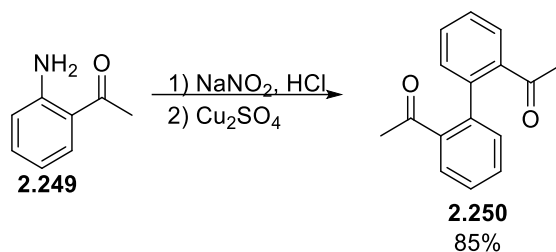


2.242 (50 mg, 0.096 mmol, 1 equiv) and KOH (16.2 mg, 0.289 mmol, 3 equiv) were charged into a MW vial with a stir bar. The vial was sealed and the solvent [1:1 THF:H₂O (0.1 M)] was added to the reaction vessel. The reaction was then set to stir at 100 °C for 1 h. Following the reaction time, the mixture was transferred to a separatory funnel and the aqueous layer was washed 3x with DCM. The aqueous layer was then collected, and the solvent was removed with a stream of air revealing **2.243** in a 93% yield (43 mg) as mixture of regioisomers.

¹H NMR (300 MHz, D₂O): δ 9.23 (s, 2H), 8.84 (s, 2H), 8.65 (s, 2H), 1.62 (s, 9H), 1.58 (s, 9H).

HRMS [M/2]= Calculated for C₂₄H₂₄O₆S (M-2H)²⁻=236.05017; found: 236.04924

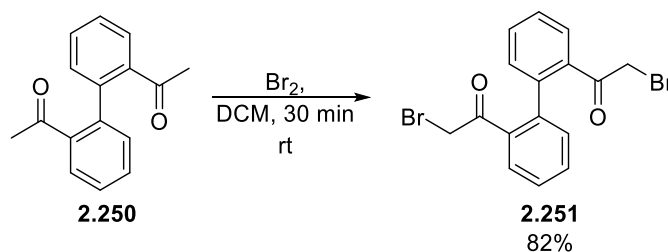
1,1'-([1,1'-Biphenyl]-2,2'-diyl)bis(ethan-1-one) (**2.250**)



2.250 was synthesized according to literature procedures in an 85% yield and exhibited identical spectra as previous reports.^{398,399}

¹H NMR (300 MHz, CDCl₃): δ 7.74 (d, J=7.2Hz, 2H), 7.52-7.42(m, 4H), 7.17 (d, J=7.5Hz, 2H), 2.26 (s, 6H).

1,1'-([1,1'-Biphenyl]-2,2'-diyl)bis(2-bromoethan-1-one) (**2.251**)

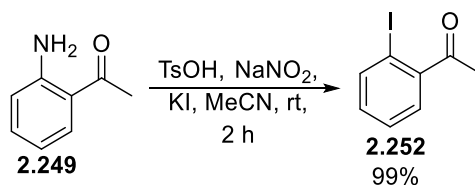


2.251 was synthesized by adapting a previously reported procedure⁴⁰⁰ and exhibited identical spectra to previously reported.⁴⁰¹ A flame dried MW vial with a stir bar was sealed and **2.250** (1.0 g, 4.2 mmol, 1 equiv) was then added to the reaction vessel. DCM (8.4 mL, 0.5 M) was then added, and the reaction was brought to 0 °C. Using a syringe pump, bromine (0.43 mL, 8.4 mmol, 2 equiv) was added over a 15-min period. After the addition period, the reaction was allowed to warm up to room temperature and react for 30 min. Following the reaction time, the mixture was diluted with DCM and transferred to a separatory funnel. The organic layer was then washed with

saturated $\text{Na}_2\text{S}_2\text{O}_3$ followed by two more washes with deionized water. The organic layer was then dried, filtered, and concentrated using rotatory evaporation. **2.251** was then isolated in 82% yield (1.4 g) following column chromatography (95% hexanes/5% EtOAc) and recrystallization with ethyl acetate/hexanes and exhibited identical spectra to previously reported.⁴⁰¹

^1H NMR (300MHz, CDCl_3): δ 7.76-7.74 (m, 2H), 7.58-7.47 (m, 4H), 7.23 (m, 2H), 4.27 (d, $J=11.2\text{Hz}$, 2H), 4.01 (d, $J=11.2\text{Hz}$, 2H).

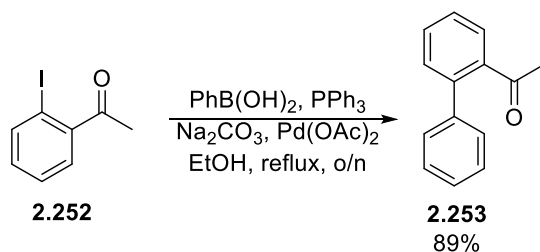
2'-Iodoacetophenone (**2.252**)



2'-Iodoacetophenone was synthesized according to a previous procedure⁴⁰² and exhibited identical spectra to previously reported.⁴⁰³

^1H NMR (300 MHz, CDCl_3): δ 7.94 (d, $J = 7.9$ Hz, 1H), 7.43 (m, 2H), 7.18 – 7.06 (m, 1H), 2.61 (s, 3H).

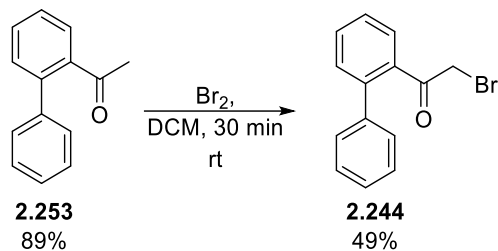
1-([1,1'-Biphenyl]-2-yl)ethan-1-one (**2.253**)



2.253 was synthesized according to a previous procedure⁴⁰⁴ and exhibited identical data to previously reported.⁴⁰⁵

^1H NMR (300 MHz, CDCl_3): δ 7.56 (dd, $J = 1.6, 7.6$ Hz, 1H), 7.50 (dt, $J = 1.6, 7.6$ Hz, 1H), 7.45–7.33 (m, 7H), 2.01 (s, 3H).

1-([1,1'-Biphenyl]-2-yl)-2-bromoethan-1-one (2.244)



2.244 was synthesized by adapting a previously reported procedure⁴⁰⁰. A flame dried MW vial with a stir bar was sealed and **2.253** (0.5 g, 2.6 mmol, 1 equiv) was then added to the reaction vessel. CHCl_3 (5.1 mL, 0.5 M) was then added, and the reaction was brought to 0 °C. Using a syringe pump, bromine (0.14 mL, 2.8 mmol, 1.1 equiv) was added over a 30-min period. After the addition period, the reaction was allowed to warm up to room temperature and react for 1 h. Following the reaction time, the mixture was diluted with DCM and transferred to a separatory funnel, the organic layer was then washed with saturated $\text{Na}_2\text{S}_2\text{O}_3$ followed by two more washes with deionized water. The organic layer was then dried, filtered, and concentrated using rotatory evaporation. **2.244** was then isolated in a 59% yield (0.42 g) following column chromatography (95% hexanes/5%EtOAc).

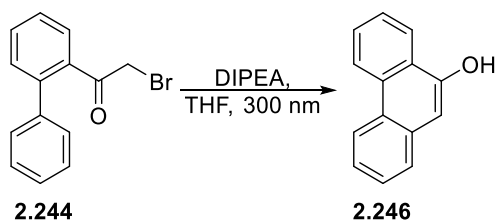
$^1\text{H NMR}$ (300 MHz, CDCl_3): δ 7.60 (m, 2H), 7.49 (m, 5H), 7.38 (m, 2H), 3.70 (s, 2H)

$^{13}\text{C NMR}$ (75 MHz, CDCl_3): δ 198.4, 140.6, 140.1, 137.5, 131.7, 130.3, 129.2, 129.2, 128.8, 128.5, 127.8, 34.6.

HRMS $[\text{M}+\text{H}]^+$: Calculated for $\text{C}_{14}\text{H}_{12}\text{BrO}$ ($\text{M}+\text{H}$)⁺ = 275.0060; found = 275.007262.

Photocyclization procedures

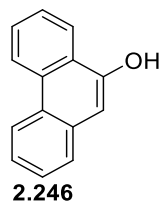
Synthetic procedure 2A:



In a 10 mL quartz test tube **2.244** was charged (30.0 mg, 0.109 mmol, 1 equiv) and the vial was then sealed with a rubber septum and purged twice with Ar. THF (0.55 mL, 0.2 M) was then added to the test tube followed by DIPEA (38 μL , 0.22 mmol, 2 equiv) and the test tube was mixed on a vortex mixer. The reaction mixture was then

allowed to react under 300 nm irradiation overnight. After the reaction time the reaction mixture was diluted in EtOAc and washed twice with deionized water, the organic layer was then dried and concentrated under rotatory evaporation. 9-Phenanthrol (**2.246**) was then isolated in 53% yield (11 mg) following column chromatography (90% hexanes/10% EtOAc).

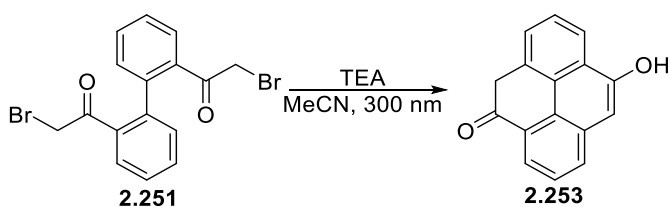
9-Phenanthrol (**2.246**)



9-phenanthrol was synthesized according to synthetic procedure A in a 53% yield and exhibited identical spectra to previously reported.⁴⁰⁶

¹H NMR (300 MHz, CDCl₃): δ 8.71–8.62 (m, 1H), 8.63–8.55 (m, 1H), 8.32–8.30 (m, 1H), 7.73–7.67 (m, 2H), 7.64 (ddd, $J = 8.0, 7.0, 1.3$ Hz, 1H), 7.57–7.45 (m, 2H), 7.01 (s, 1H), 5.43 (s, 1H).

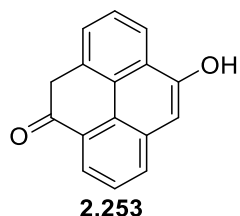
Synthetic procedure 2B:



In a 10 mL quartz test tube **2.250** was charged (50.0 mg, 0.127 mmol, 1 equiv) and the vial was then sealed with a rubber septum and purged twice with Ar. MeCN (0.64 mL, 0.2 M) was then added to the test tube followed by TEA (71 μ L, 0.51 mmol, 4 equiv) and the test tube was mixed on a vortex mixer. The reaction mixture was then allowed to react under 300 nm irradiation overnight. After the reaction time the reaction mixture was diluted in EtOAc and washed twice with deionized water, the organic layer was then dried and concentrated under rotatory

evaporation. 9-hydroxypyren-4(5H)-one **2.253** was then isolated in 26% yield (7.7 mg) following column chromatography (80% hexanes/20% EtOAc).

9-Hydroxypyren-4(5H)-one (**2.253**)

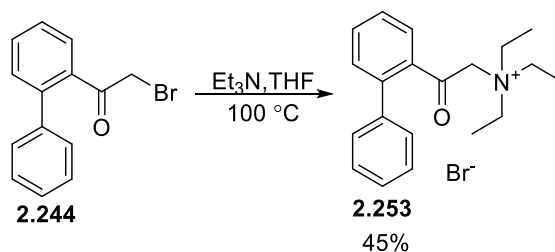


9-Hydroxypyren-4(5H)-one was synthesized according to synthetic procedure B in a 26% yield.

¹H NMR (300MHz, CDCl₃): δ 7.81 (m, 3H), 7.67 (m, 2H), 7.55 (m, 4H), 6.87 (s, 1H), 4.84 (s, 2H). * Impurities raised integration values

HRMS [M⁺]: Calculated C₁₆H₁₁O₂(M+H)⁺=235.07536; found= 235.07410

2-([1,1'-Biphenyl]-2-yl)-N,N,N-triethyl-2-oxoethan-1-aminium bromide (**2.253**)



2.244 (35.6 mg, 0.129 mmol, 1 equiv) was charged to a flame dried MW vial with stir bar. The vial was sealed and purged twice with Ar. THF (0.65 mL, 0.2 M) was then added followed by Et₃N (26.2 mg, 0.256 mmol, 2 equiv) and the reaction was set to stir overnight at 100 °C. After the reaction time, white precipitate (**2.253**) appeared and was isolated via suction filtration and washed with minimal amount of cold THF. (22 mg, 45%)

¹H NMR (300 MHz, CDCl₃) δ 8.05 (d, *J* = 7.4 Hz, 1H), 7.58 (m, 2H), 7.40 (m, 6H), 4.86 (s, 2H), 3.68 (q, *J* = 7.2 Hz, 6H), 1.26 (t, *J* = 7.3 Hz, 9H).

HRMS [M⁺]: Calculated for C₂₀H₂₆NO(M⁺)= 296.20089; found= 296.20091

Computational details:

The Gaussian 16 program was used for optimization with DFT at the UB3LYP/6-31G(d) level of theory. All structures were optimized without any symmetry assumptions. Zero-point energy, enthalpy, and Gibbs free energy at 298.15 K and 1 atm were estimated from the gas-phase. Harmonic vibration frequency calculations at the same level were performed to verify all stationary points as local minima (with no imaginary frequency). Gd3 empirical dispersion was used on all calculations.

Optimized Structures for [10]pyrenecyclacene (2.117)

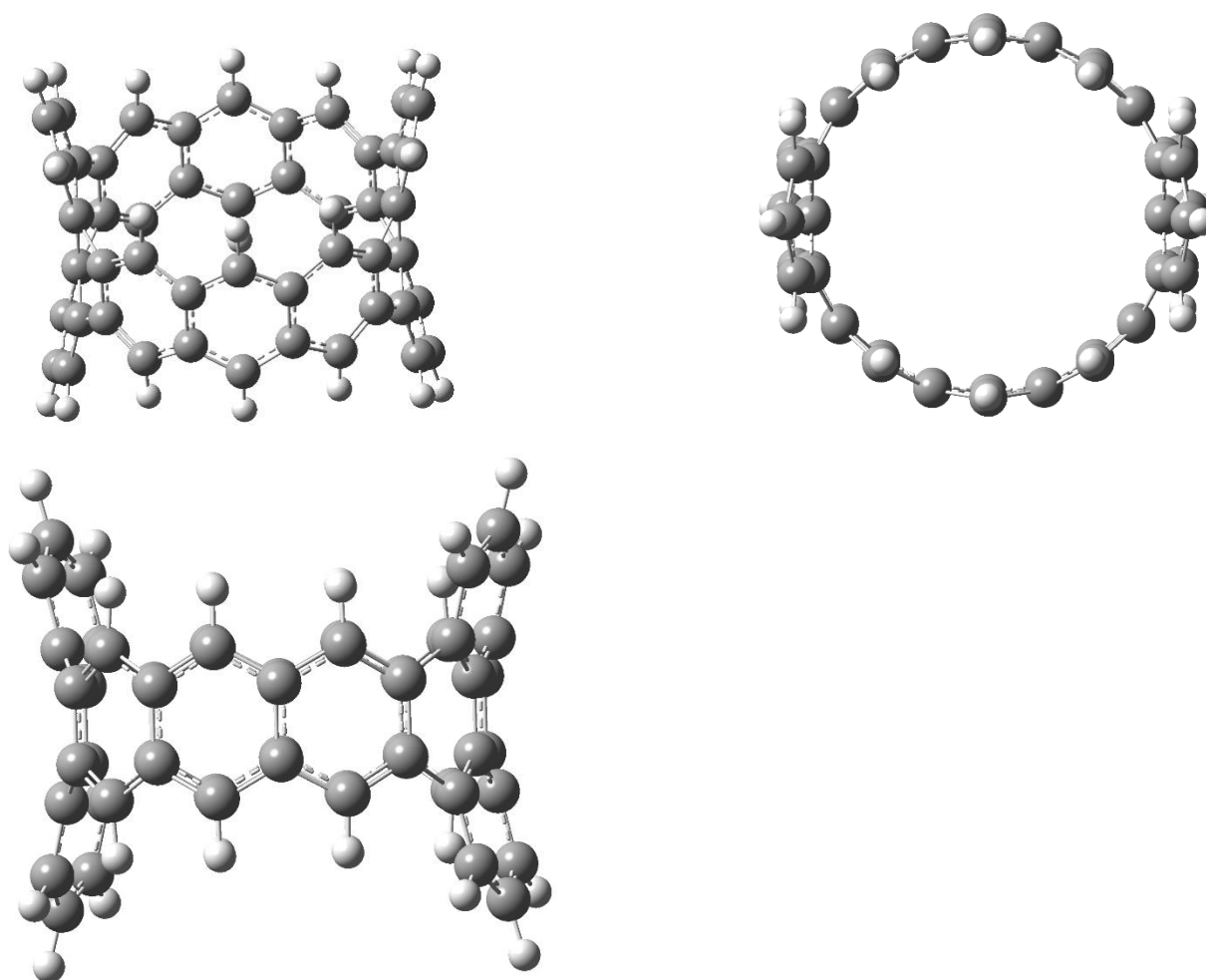


Figure S1- Geometry optimized structure for [10]pyrenecyclacene (**2.117**)

Bond Lengths

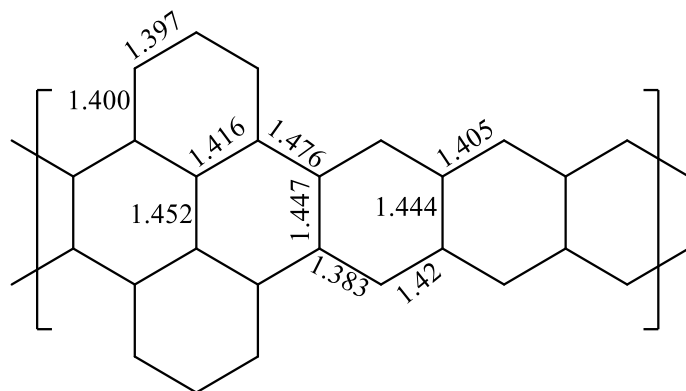


Figure S2- Bond lengths in **2.117**

Bond Lengths given in angstroms (Å), non labelled bond lengths are connected by symmetry.

Cavity Size	7.65 Å
Wagging Bend	101.65°

Table S1- Cavity size and wagging bend angle for **2.117**

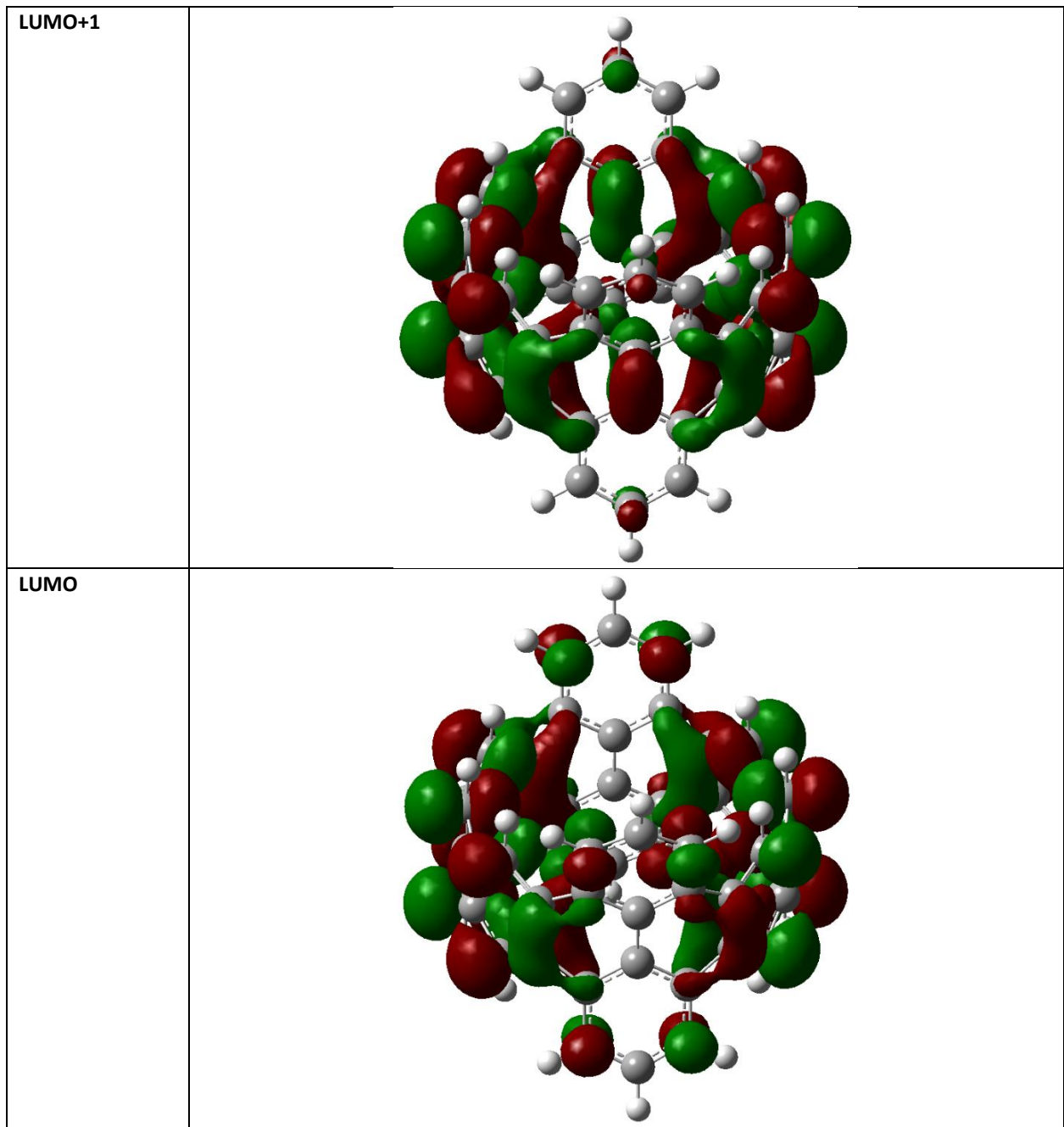
Thermochemistry

10-Pyrenecyclacene (2.117)	Energy Summary (Hartrees)
Electronic Energies (EE)	-1996.08
ZPE	0.5860
EE+ZPE	-1995.49
H	-1994.87
G	-1994.96

Table S2- Thermochemistry for [10]Cyclacene.

Orbital	Energy (Hartrees)	Energy (eV)	Band Gap (eV)
LUMO+1	-0.0687	-1.87	2.67
LUMO	-0.0751	-2.05	
HOMO	-0.1734	-4.72	
HOMO-1	-0.1799	-4.89	

Table S3- FMOs for [10]Cycloacene.



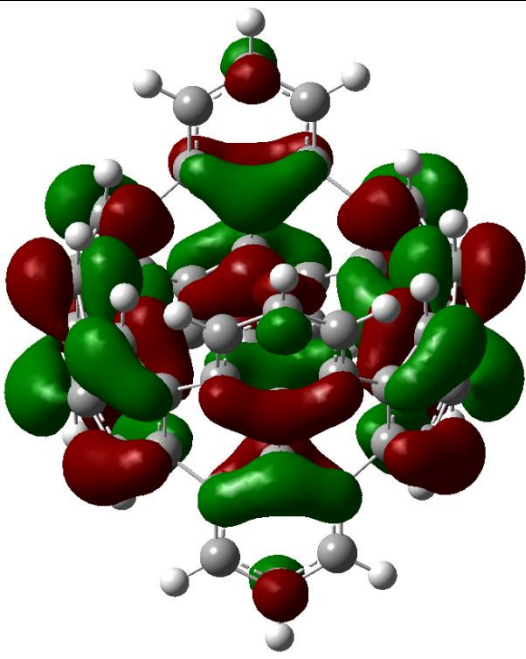
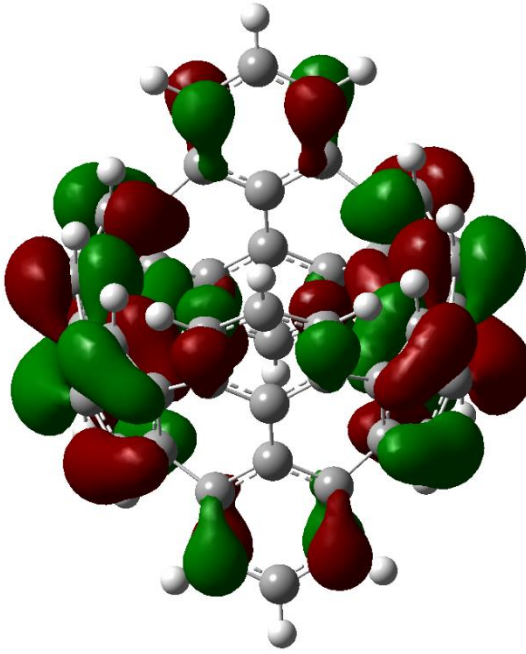
<p>HOMO</p>	
<p>HOMO-1</p>	

Table S4-FMOs for 10-pyrenecyclacene **2.112**

10-Pyrenecyclacene Triplet (2.117)

Imaginary Freq	0
EE (Hartrees)	-1996.01
ZPE (Hartrees)	0.5832
E+ ZPE (Hartrees)	-1995.43
H (Hartrees)	-1994.81
S (Kcal/Mol*K)	0.1849
G (Hartrees)	-1994.90

Table S5- Thermochemical data for **2.117** triplet.

Label	Population	Orbital #	Energy (eV)	Singlet triplet Gap (eV)
		172	-1.17	
LUMO		171	-1.44	
SOMO+1	↑	170	-2.46	
SOMO	↑	169	-3.01	0.0203
HOMO	↑↓	168	-4.92	
	↑↓	167	-5.07	
	↑↓	166	-6.39	

Table S6-FMOs for **2.117** triplet.**Strain Analysis**

	<i>EE (Hartrees)</i>	<i>EE+ZPE (Hartrees)</i>	<i>H</i>	<i>G</i>
10-Pyrenecyclacene	-1996.07	-1995.49	-1994.87	-1994.96
15-Pyrenecyclacene	-2994.28	-2993.40	-2992.46	-2992.58
20-Pyrenecyclacene	-3992.44	-3991.27	-3990.03	-3990.19
25-Pyrenecyclacene	-4990.59	-4987.13	-4987.57	-4987.77

Table S7-Thermochemical data for cyclacene species used in strain analysis.

Pyrene Cyclacene	HOMO (eV)	LUMO (eV)	Band Gap (eV)
10	-4.72	-2.05	2.67
15	-4.81	-2.11	2.70
20	-4.85	-2.19	2.67
25	-4.87	-2.20	2.67

Table S8-FMO comparison for pyrenecyclacenes of varying sizes.

Compound	Strain Energy (kCal/Mol)	Orbital Energy (eV)		
		HOMO	LUMO	Band Gap
10-Pyrenecyclacene	121.26	-4.72	-2.05	2.67
10-Cyclacene	132.43	-3.92	-2.92	1.00
20-Pyrenecyclacene	60.63	-4.85	-2.19	2.67
20-Cyclacene	66.22	-3.90	-3.23	0.67

Table S9- Strain and thermochemical comparison between cyclacenes and pyrenecyclacenes of varying sizes.

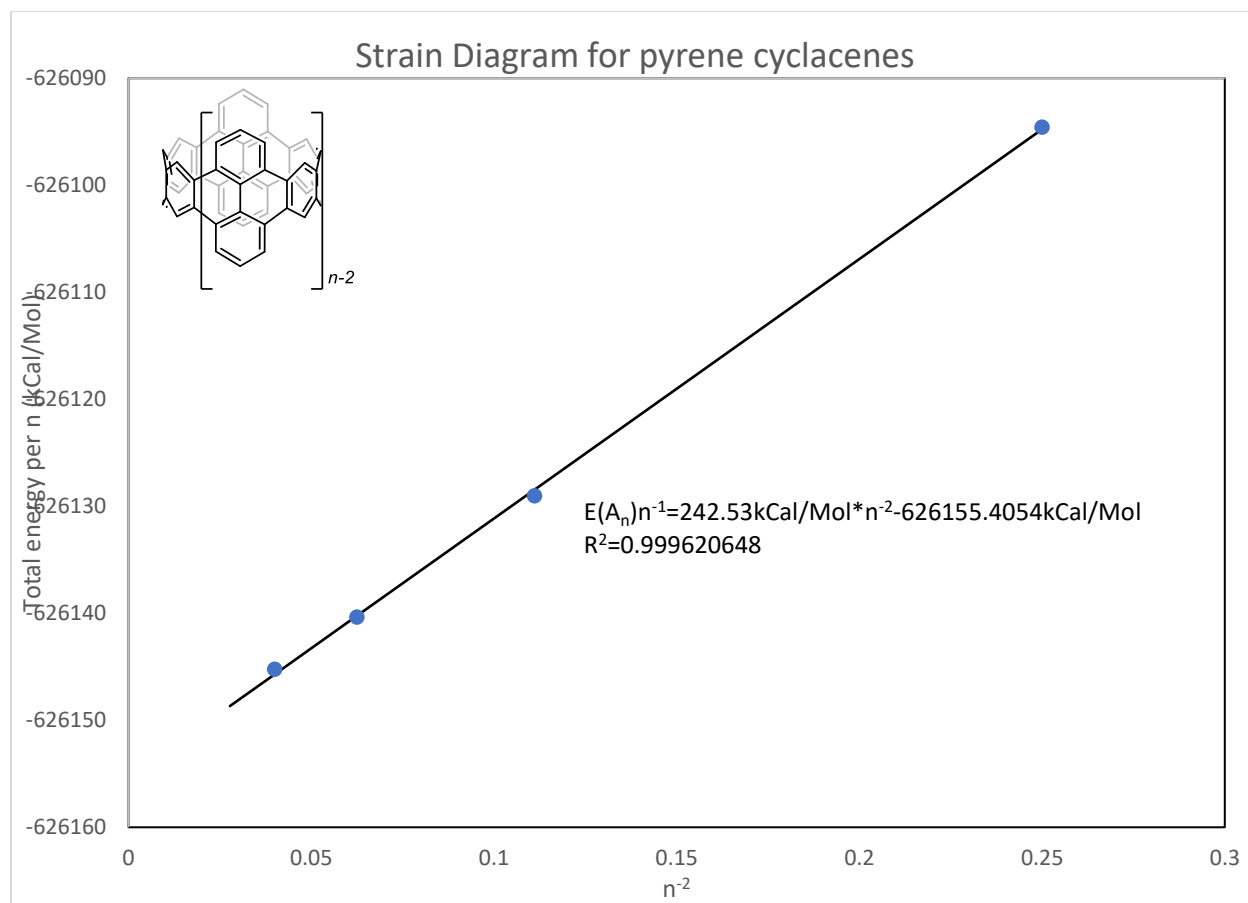
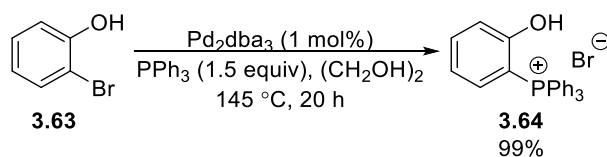


Figure S3- Strain analysis for pyrene cyclacenes.⁴⁰⁷

6.2 SYNTHETIC PROCEDURES- CHAPTER 3

(2-Hydroxyphenyl)triphenylphosphonium bromide (**3.64**)



3.64 was synthesized by adapting a previously reported procedure.⁴⁰⁸ PPh_3 (2.27 g, 8.67 mmol, 1.5 equiv) and Pd_2dba_3 (53 mg, 0.058 mmol, 1 mol%) were charged to a flame dried MW vial. The vial was sealed and purged with Ar, at which point previously degassed ethylene glycol (1.2 mL, 5 M) and 2-bromophenol (1.0 g, 5.8 mmol, 1 equiv) were added to the reaction mixture via syringe. The reaction was then set to stir at $145\text{ }^\circ\text{C}$ for 24 h. After the reaction time, the mixture was dissolved in DCM and washed with DI water. The organic layer was then dried, and the solvent was removed through rotatory evaporation. The solids were then redissolved in a minimal amount of

DCM and added dropwise to stirring diethyl ether forcing the phosphonium to precipitate. **3.13** was then isolated after suction filtration in a 99% yield (2.5 g).

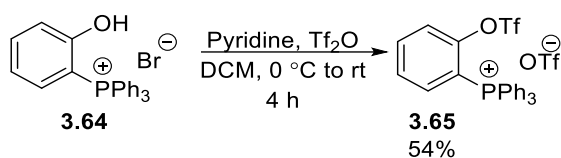
$^1\text{H NMR}$ (300MHz, CDCl_3): δ 7.91 (br s, 1H), 7.61-7.54 (m, 19H)

$^{31}\text{P NMR}$ (121 MHz, CDCl_3): δ 22.4.

$^{13}\text{C NMR}$ (75 Hz, CDCl_3): 137.8, 134.5, 134.4, 134.3, 134.1 (d, $J = 10.4$ Hz), 129.9 (d, $J = 13.0$ Hz), 120.0, 119.5 (d, $J = 7.5$ Hz), 118.7, 101.5 (d, $J = 93.8$ Hz).

HRMS [M^+]: Calculated $\text{C}_{24}\text{H}_{20}\text{OP}$ =355.12463; found= 355.12437

Triphenyl(2(((trifluoromethyl)sulfonyl)oxy)phenyl)phosphonium bromide(**3.65**)



3.65 was synthesized by adapting a previously reported procedure.⁴⁰⁹ In a flame dried MW vial with a stir bar **3.64** (0.5 g, 1.41 mmol, 1 equiv) was charged and the vial was sealed and purged with Ar. DCM (4.7 mL, 0.3 M) and pyridine (445 mg, 5.64 mmol, 4 equiv) were then added and the reaction mixture was brought to 0°C. Once cooled, Tf_2O (437 mg, 1.85mmol, 1.1) was added dropwise and the reaction was then allowed to slowly warm to room temperature. The reaction was then allowed to stir for an additional 4 h at room temperature. After the reaction time, the mixture was transferred to a separatory funnel and the organic layer was washed with DI water. The organic layer was then dried, and the solvent was removed through rotatory evaporation. The solids were then redissolved in a minimal amount of DCM and added dropwise to stirring diethyl ether forcing the phosphonium to precipitate. **3.14** was then isolated after suction filtration in a 54% yield (0.37 g).

$^1\text{H NMR}$ (300MHz, CDCl_3): δ 7.90-7.63 (m, 19H)

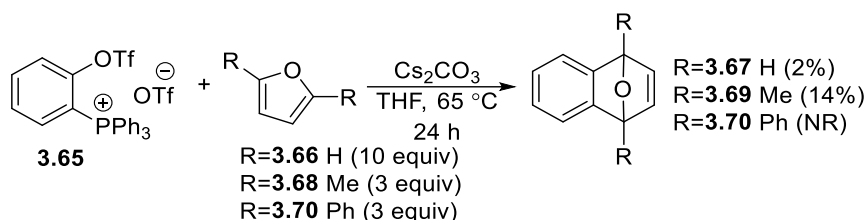
$^{31}\text{P NMR}$ (121 MHz, CDCl_3): δ 22.7.

^{13}C NMR (75 MHz, CDCl_3): δ 151.3, 139.0 (d, $J = 1.5$ Hz), 137.9 (d, $J = 8.2$ Hz), 135.8 (d, $J = 2.8$ Hz), 134.5 (d, $J = 2.7$ Hz), 133.8 (d, $J = 10.7$ Hz), 130.7 (d, $J = 13.3$ Hz), 129.9 (m), 129.7 (m), 121.1 (d, $J = 4.1$ Hz), 116.1 (d, $J = 91.1$ Hz), 110.3 (d, $J = 91.5$ Hz).

^{19}F NMR (283 MHz, CDCl_3): δ -73.9, -78.2.

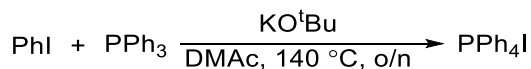
HRMS [M^+]: Calculated $\text{C}_{25}\text{H}_{19}\text{F}_3\text{O}_3\text{PS}$ (M^+) = 487.07391; found = 487.07333

General procedure for phosphonium generated benzyne



Procedure adapted from previous report.¹⁹⁷ In a flame dried MW vial **3.14** (50 mg, 0.08 mmol, 1 equiv) and Cs_2CO_3 (116 mg, 0.360 mmol, 4.5 equiv) were charged, the vial was then sealed and purged with Ar. THF (0.8 mL, 0.1 M) was then added followed furan (53.8 mg, 0.790 mmol, 10 equiv), The reaction was then set to stir at 65 °C for 24h. After the reaction time, the solvent was removed under vacuum and the yield was determined using 1,3,5-trimethoxy benzene as an internal standard.

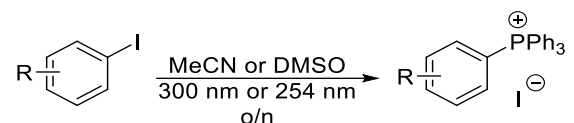
General procedure for *tert*-butoxide mediated synthesis of phosphonium salts



In a flame dried MW vial PPh_3 (256 mg, 0.980 mmol, 1 equiv) was charged, the vial was then sealed and purged with Ar. Previously degassed DMAc (0.07 mL, 15 M) was then added to the reaction mixture followed by PhI (200 mg, 1 mmol, 1 equiv). The reaction was then set to stir at 140 °C overnight. If the salt was to be isolated, first the reaction mixture was dissolved in DCM and washed multiple times with water. The organic layer was then dried, and the solvent was removed via rotatory evaporation. The solids were then redissolved in a minimal amount of DCM and added dropwise to stirring diethyl ether forcing the phosphonium to precipitate. If the yields were to be

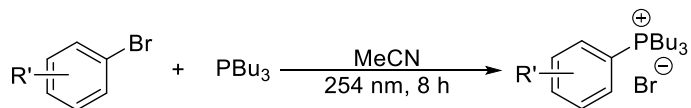
determined by ^{31}P NMR then the mixture was diluted with CHCl_3 and a known amount of triphenyl phosphate was added to the reaction mixture. An aliquot of the reaction mixture was then transferred to an NMR tube and diluted further with CDCl_3 .

General Procedure 3A: Aryl Iodides



To a 10 mL quartz test tube PPh_3 (386 mg, 1.47 mmol, 3 equiv) was added. If the aryl iodide (0.49 mmol, 1 equiv) is a solid it was charged alongside the PPh_3 . This was then followed by sealing the vessel with a rubber septum and purging with argon. Once the vessel was purged the solvent (2.45 mL, 0.2 M) was added and the reaction mixture was briefly stirred using a vortex mixer. If the aryl iodide is a liquid, the vessel was sealed with a rubber septum and purged with argon. After purging the aryl iodide (0.49 mmol, 1 equiv), and solvent (2.5 mL, 0.2 M) were added via syringe and the mixture was then stirred using a vortex mixer. The test tube was placed inside the photoreactor and allowed to be irradiated for 8 h or overnight. After the reaction time the solvent was removed, and the solids were re-dissolved in a small amount of DCM. Diethyl ether was then used to precipitate the phosphonium salts which were subsequently isolated via suction filtration and washed with the addition of cold ether.

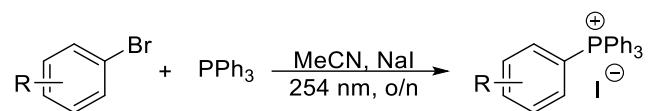
General Procedure 3B: Aryl Bromides



A 10 mL quartz test tube was sealed with a rubber septum and purged with argon. If the aryl bromide (0.49 mmol, 1 equiv) were solids then they were added to the test tube prior to purging the vessel. PBu_3 (297 mg, 1.47 mmol, 3 equiv.), the aryl bromide (0.49 mmol, 1 equiv) and MeCN (2.5 mL, 0.2 M) were then added via syringe to the test tube. The reaction mixture was then briefly mixed using a vortex mixer and was then irradiated at 254 nm for 8 h or overnight. After the reaction time, the reaction mixture was transferred to a separatory funnel and worked

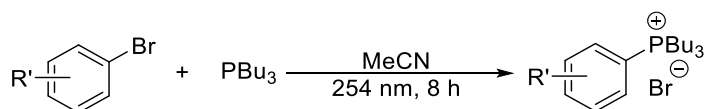
up with MeCN/hexanes to remove the excess PBu_3 . The MeCN layer was collected, and the solvent was removed through rotatory evaporation. The phosphonium salt was then isolated through column chromatography using 9:1 DCM/MeOH as the eluent.

General Procedure 3C: Aryl Bromide/Aromatic Finkelstein reaction



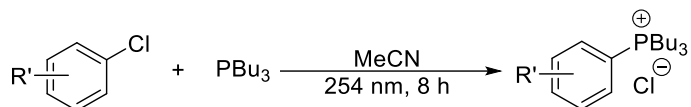
A 10 mL quartz test tube was charged with NaI (220 mg, 1.5 mmol, 3 equiv), sealed with a rubber septum and purged with argon. PPh_3 (297 mg, 1.47 mmol, 3 equiv.), the aryl bromide (0.49 mmol, 1 equiv) and MeCN (2.5 mL, 0.2 M) were then added via syringe to the test tube. The reaction mixture was then briefly mixed using a vortex mixer and was then irradiated at 254 nm for 8 h or overnight. After the reaction, time the solvent was removed, and the solids were re-dissolved in a small amount of DCM. Diethyl ether was then used to precipitate the phosphonium salts which were subsequently isolated via suction filtration and washed with the addition of cold ether. The yield was determined through ^{31}P quantitative NMR with triphenyl phosphate as an internal standard.

General Procedure 3D: Aryl Bromides/ PBu_3



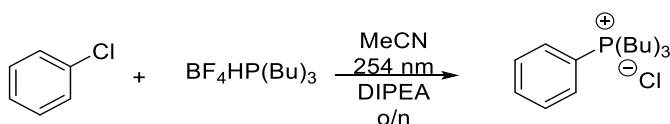
A 10 mL quartz test tube was sealed with a rubber septum and purged with argon. If the aryl bromides (0.49 mmol, 1 equiv) were solids then they were added to the test tube prior to purging the vessel. PBu_3 (297 mg, 1.47 mmol, 3 equiv), the aryl bromide (0.49 mmol, 1 equiv) and MeCN (2.5 mL, 0.2 M) were then added via syringe to the test tube. The reaction mixture was then briefly mixed using a vortex mixer and was then irradiated at 254 nm for 8 h or overnight. After the reaction time, the reaction mixture was transferred to a separatory funnel and worked up with MeCN/hexanes to remove the excess PBu_3 . The MeCN layer was collected, and the solvent was removed through rotatory evaporation. The phosphonium salt was then isolated through column chromatography using 9:1 DCM/MeOH as the eluent. The yield was determined through ^{31}P quantitative NMR with triphenyl phosphate as an internal standard.

General Procedure 3E: Aryl Chlorides/PBu₃



A 10 mL quartz test tube was sealed with a rubber septum and purged with argon. If the aryl chlorides (0.49 mmol, 1 equiv) were solids then they were added to the test tube prior to purging the vessel. PBu_3 (297 mg, 1.47 mmol, 3 equiv.), the aryl chloride (0.49 mmol, 1 equiv) and MeCN (2.5 mL, 0.2 M) were then added via syringe to the test tube. The reaction mixture was then briefly mixed using a vortex mixer and was then irradiated at 254 nm for 8 h or overnight. After the reaction time the reaction mixture was transferred to a separatory funnel and worked up with MeCN /hexanes to remove the excess PBu_3 . The MeCN layer was collected, and the solvent was removed through rotatory evaporation. The phosphonium salt was then isolated through column chromatography using 9:1 DCM/MeOH as the eluent the yield was determined through ^{31}P quantitative NMR with triphenyl phosphate as an internal standard.

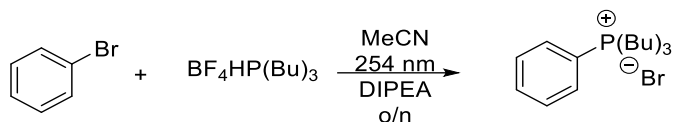
General Procedure 3F: Aryl Chlorides/ BF_4HPBu_3



A 10 mL quartz test tube was charged with BF_4HPBu_3 (0.49 mmol, 1 equiv), sealed with a rubber septum and purged with argon. If the aryl chlorides (0.49 mmol, 1 equiv) were solids, then they were added to the test tube prior to purging the vessel. DIPEA (0.49 mmol, 1 equiv), the aryl chloride (0.49 mmol, 1 equiv) and MeCN (2.5 mL, 0.2 M) were then added via syringe to the test tube. The reaction mixture was then briefly mixed using a vortex mixer and was then irradiated at 254 nm for 8 h or overnight. After the reaction time, the reaction mixture was transferred to a separatory funnel and worked up with MeCN /hexanes to remove any excess PBu_3 . The MeCN layer was collected, and the solvent was removed through rotatory evaporation. The reaction mixture was then dissolved in DCM , washed with NaHCO_3 , then DI water. The organic layer was then dried, and the solvent was removed through rotatory evaporation. The phosphonium salt was then isolated through column chromatography using 9:1

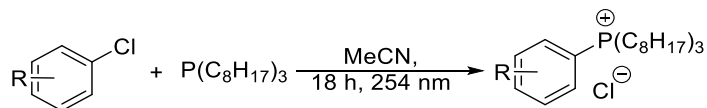
DCM/MeOH as the eluent or the yield was determined through ^{31}P quantitative NMR with triphenyl phosphate as an internal standard.

General Procedure 3G: Aryl Bromides/ HBF_4PBU_3



A 10 mL quartz test tube was charged with BF_4HPBU_3 (1.47 mmol, 3 equiv), sealed with a rubber septum and purged with argon. If the aryl bromides (0.49 mmol, 1 equiv) were solids then they were added to the test tube prior to purging the vessel. DIPEA (1.47 mmol, 3 equiv), the aryl chloride (0.49 mmol, 1 equiv) and MeCN (2.45 mL, 0.2 M) were then added via syringe to the test tube. The reaction mixture was then briefly mixed using a vortex mixer and was then irradiated at 254 nm for 8 h or overnight. After the reaction time the reaction mixture was transferred to a separatory funnel and worked up with MeCN/hexanes to remove the excess PBU_3 . The MeCN layer was collected, and the solvent was removed through rotatory evaporation. The reaction mixture was then dissolved in DCM and washed with NaHCO_3 , followed by DI water. The organic layer was dried, and the solvent was removed through rotatory evaporation. The phosphonium salt was then isolated through column chromatography using 9:1 DCM/MeOH as the eluent the yield was determined through ^{31}P quantitative NMR with triphenyl phosphate as an internal standard.

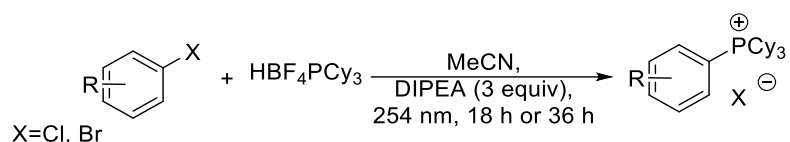
General Procedure 3H: Aryl Chlorides/TOP



A 10 mL quartz test tube was sealed with a rubber septum and purged with argon. If the aryl chlorides (0.490 mmol, 1 equiv) were solids then they were added to the test tube prior to purging the vessel. TOP (182 mg, 0.490 mmol, 1 equiv), the aryl chloride (0.49 mmol, 1 equiv) and MeCN (2.45 mL, 0.2 M) were then added via syringe to the test tube. The reaction mixture was then briefly mixed using a vortex mixer and was then irradiated at 254 nm for 8 h or overnight. After the reaction time, the reaction mixture was transferred to a separatory funnel and

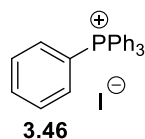
worked up with DCM/water. The organic layer was then dried, and the solvent was removed through rotatory evaporation. The phosphonium salt was then isolated through column chromatography using 9:1 DCM/MeOH as the eluent.

General Procedure 3I: Aryl halides/ HBF_4PCy_3



A 10 mL quartz test tube was charged with BF_4HPCy_3 (0.49 mmol, 1 equiv), sealed with a rubber septum and purged with Ar. If the aryl halides (0.49 mmol, 1 equiv) were solids, then they were added to the test tube prior to purging the vessel. DIPEA (0.49 mmol, 1 equiv), the aryl halides (0.49 mmol, 1 equiv) and MeCN (2.45 mL, 0.2 M) were then added via syringe to the test tube. The reaction mixture was then briefly mixed using a vortex mixer and was then irradiated at 254 nm for 18 h for aryl chlorides and 36 h for aryl bromides. After the reaction time, the reaction mixture was then diluted in DCM and washed with NaHCO_3 , then DI water. The organic layer was then dried, and the solvent was removed through rotatory evaporation. The phosphonium salt was then isolated through column chromatography using 9:1 DCM/MeOH as the eluent or the yield was determined through ^{31}P quantitative NMR with triphenyl phosphate as an internal standard.

Tetraphenylphosphonium iodide (3.46)

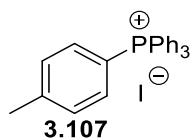


Tetraphenyl phosphonium iodide was synthesized according to general procedure 3A in 99% yield and displayed identical spectra to previously reported.²⁰⁵ Tetraphenyl phosphonium iodide was also synthesized following procedure 3C in a 55% yield and displayed identical spectra to previously reported.²⁰⁵

^1H NMR (300 MHz, CDCl_3): δ 7.91 (m, 4H), 7.81 (m, 8H), 7.68 (m, 8H).

^{31}P NMR (121 MHz, CDCl_3): δ 22.9

(4-Toluene)triphenylphosphonium iodide (3.107)

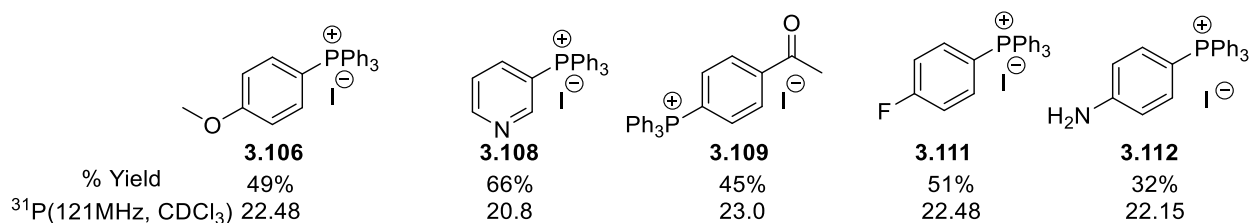


Tetraaryl phosphonium iodide was synthesized according to general procedure 3A in quantitative yield and displayed identical spectra to previously reported.²⁰⁵

¹H NMR (300 Hz, CDCl₃): δ 7.87-7.81 (m, 3H), 7.76-7.69 (m, 6H), 7.57-7.49 (m, 8H), 7.45-7.38 (m, 2H), 2.54 (s, 2H).

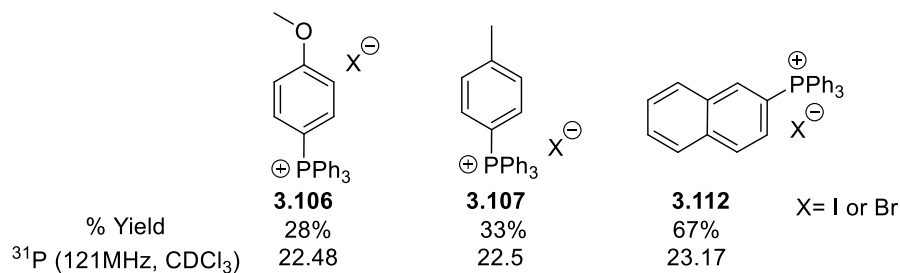
³¹P NMR (121 Hz, CDCl₃): δ 22.5

Tetraarylphosphonium salts (3.106, 3.108-3.111)



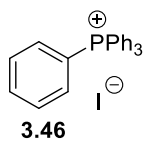
Tetraaryl phosphonium salts **3.106**, **3.108-3.111** were synthesized through general procedure 3A but could not be separated from PPh₄⁺ impurity; yields were determined through ³¹P quantitative NMR with triphenyl phosphate as an internal standard.

Tetraarylphosphonium salts-Finkelstein conditions



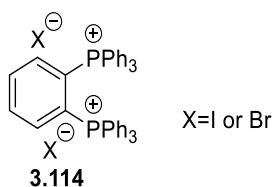
Compounds **3.106-3.112** were synthesized through general procedure 3C but were not successfully isolated, yields were determined through ³¹P quantitative NMR with triphenyl phosphate as an internal standard.

Tetraphenylphosphonium iodide (3.46)



Tetraphenyl phosphonium iodide was synthesized according to general procedure 3C in 55% yield and displayed identical spectra as previously **3.46** synthesized using condition 3A.

1,2-Phenylenebis(triphenylphosphonium) (3.114)



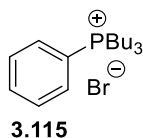
1,2-phenylenebis(triphenylphosphonium) diiodide was synthesized according to general procedure 3C in 73% yield.

¹H NMR (300 MHz, CDCl₃): δ 8.26 (m, 1H), 7.93 (m, 3H), 7.77 (m, 9H), 7.60 (m, 21H).

³¹P NMR (121 MHz, CDCl₃): δ 26.5

HRMS [M⁺/2]: Calculated C₄₂H₃₄P₂(M²⁺)=300.10624; found= 300.10632

Tributyl(phenyl)phosphonium bromide (3.115)



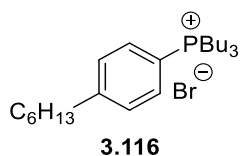
Tributyl(phenyl)phosphonium bromide was synthesized according to general procedure 3B in a 50% yield and displayed identical spectra as previously reported.²⁰⁸

¹H NMR (300 MHz, CDCl₃): δ 8.05 – 7.90 (m, 2H), 7.69 (m, 3H), 3.04 – 2.74 (m, 6H), 1.62 – 1.34 (m, 12H), 0.94 (t, J = 6.9 Hz, 9H).

³¹P NMR (121 MHz, CDCl₃): δ 29.7

HRMS: Calculated C₁₈H₃₂P (M⁺)=279.22361; found=279.22593

Tributyl(4-hexylphenyl)phosphonium bromide (3.116)

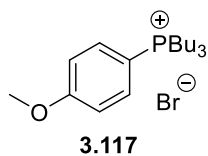


Tributyl(4-hexylphenyl)phosphonium bromide was synthesized according to general procedure 3B in a 38% yield. Product contained inseparable impurities (PBu₄⁺) thus yield was determined through ³¹P quantitative NMR with triphenyl phosphate as an internal standard.

³¹P NMR (300 MHz, CDCl₃): δ 29.1

HRMS [M⁺]: Calculated for C₂₄H₄₄P (M⁺)=363.31751; found= 363.31716

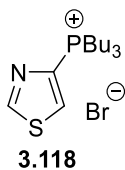
Tributyl(4-methoxyphenyl)phosphonium bromide (3.117)



Tributyl(4-methoxyphenyl)phosphonium bromide was synthesized according to general procedure 3B in a 23%. Product contained inseparable impurities (PBu₄⁺) thus yield was determined through ³¹P quantitative NMR with triphenyl phosphate as an internal standard.

³¹P NMR (121 Hz, CDCl₃): δ 28.6

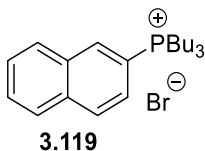
Tributyl(thiazol-4-yl)phosphonium bromide (3.118)



Tributyl(thiazol-4-yl)phosphonium bromide was synthesized according to general procedure 3B in 63% yield. Product contained inseparable impurities (PBu_4^+) thus yield was determined through ^{31}P quantitative NMR with triphenyl phosphate as an internal standard.

^{31}P NMR (121 MHz, CDCl_3): δ 30.1

Tributyl(naphthalen-2-yl)phosphonium bromide (3.119)



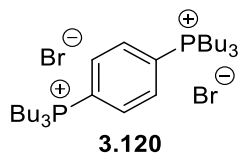
Tributyl(naphthalen-2-yl)phosphonium bromide was synthesized according to general procedure 3B in 50% yield. Product contained inseparable impurities (PBu_4^+) thus yield was determined through ^{31}P quantitative NMR with triphenyl phosphate as an internal standard.

^1H NMR (300 MHz, CDCl_3): δ 8.64 (d, $J = 13.5$ Hz, 1H), 8.13 (m, 2H), 7.99 – 7.83 (m, 2H), 7.72 (m, 2H), 2.96 (s, 6H), 1.53 (m, 12H), 0.94 (t, $J = 6.5$ Hz, 9H).

^{31}P NMR (121 MHz, CDCl_3): δ 30.5

HRMS [M^+]: Calculated for $\text{C}_{22}\text{H}_{34}\text{P}$ (M^+)=329.23926; found= 329.23964

1,4-Phenylenebis(tributylphosphonium) bromide (3.120)

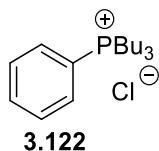


1,4-Phenylenebis(tributylphosphonium) bromide was synthesized according to general procedure 3B in 63% yield.

¹H NMR (300 MHz, CDCl₃) δ 8.85 (m, 4H), 2.84 (m, 12H), 1.47 (m, 24H), 0.97 (t, *J* = 7.0 Hz, 18H).

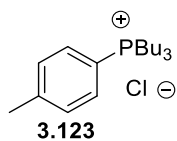
³¹P NMR (121 MHz, CDCl₃) δ 31.9.

Tributyl(phenyl)phosphonium chloride (3.122)



Tributyl(phenyl)phosphonium chloride was synthesized according to general procedure 3D in 84% yield. The compound exhibited identical spectra as the bromide salt **3.115**.

Tributyl(*p*-tolyl)phosphonium chloride (3.123)



Tributyl(*p*-tolyl)phosphonium chloride was synthesized according to general procedure 3D in 94% yield.

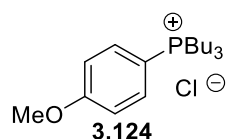
¹H NMR (300 MHz, CDCl₃): δ 7.88 – 7.77 (m, 2H), 7.48 (dd, *J* = 7.6, 2.1 Hz, 2H), 2.88 (m, 6H), 2.47 (s, 3H), 1.59 – 1.33 (m, 12H), 0.93 (t, *J* = 6.8 Hz, 9H).

³¹P NMR (121 MHz, CDCl₃): δ 29.6

¹³C NMR (75 MHz, CDCl₃): δ 145.6 (d, *J* = 3.0 Hz), 131.4 (d, *J* = 30.8 Hz), 131.2 (d, *J* = 33.8 Hz), 113.7 (d, *J* = 81.8 Hz), 23.6 (d, *J* = 20.3 Hz), 23.5, 21.7, 19.1 (d, *J* = 48.8 Hz), 13.3

HRMS [M⁺]: Calculated for C₁₉H₃₄ClP (M⁺)=293.23926 found=293.23901

Tributyl(4-methoxyphenyl)phosphonium chloride (3.124)

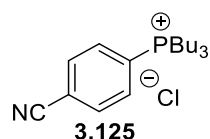


Tributyl(4-methoxyphenyl)phosphonium chloride was synthesized according to general procedure 3D in 79% yield.

The compound exhibited identical spectra as the bromide salt **3.117**. Product contained inseparable impurities (PBu₄⁺) thus yield was determined through ³¹P quantitative NMR with triphenyl phosphate as an internal standard.

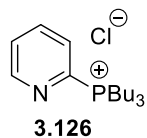
³¹P NMR (121 Hz, CDCl₃): 28.6

Tributyl(4-cyanophenyl)phosphonium chloride (3.125)



Tributyl(4-cyanophenyl)phosphonium chloride was synthesized according to general procedure 3D in 25% yield. The compound exhibited identical spectra as the bromide salt **3.138**.

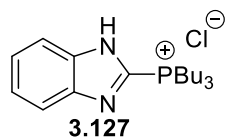
Tributyl(pyridin-2-yl)phosphonium chloride (3.126)



Tributyl(pyridin-2-yl)phosphonium chloride was synthesized according to general procedure 3D in 49% yield by ³¹P quantitative NMR with triphenyl phosphate as an internal standard.

³¹P NMR (121 MHz, CDCl₃): δ 30.6

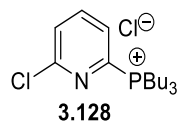
(1H-Benzo[d]imidazol-2-yl)tributylphosphonium chloride (3.127)



(1H-*Benzo[d]*imidazol-2-yl)tributylphosphonium chloride was synthesized according to general procedure C in 49% yield by ^{31}P quantitative NMR with triphenyl phosphate as an internal standard.

^{31}P NMR (121 MHz, CDCl_3): δ 31.8

Tributyl(6-chloropyridin-2-yl)phosphonium chloride (3.128)

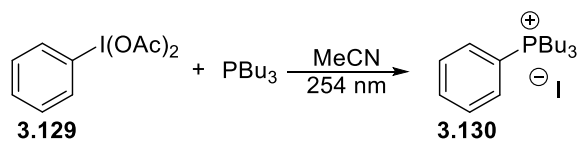


Tributyl(6-chloropyridin-2-yl)phosphonium chloride was synthesized according to general procedure 3D in 35% yield by ^{31}P quantitative NMR with triphenyl phosphate as an internal standard. PBU_4^+ impurity was present alongside arylphosphonium salt.

^1H NMR (300 MHz, CDCl_3): δ 9.33 – 9.18 (m, 1H), 8.05 (d, $J = 4.3$ Hz, 1H), 7.60 (d, $J = 7.7$ Hz, 1H), 3.10 – 2.79 (m, 6H), 1.52 (m, 12H), 0.96 (t, $J = 6.7$ Hz, 9H).

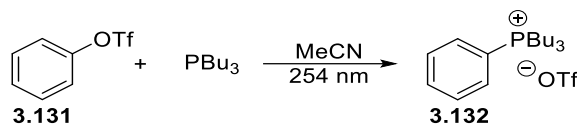
^{31}P NMR (121 MHz, CDCl_3): δ 32.4

Tributyl(phenyl)phosphonium iodide from phenyl-*I*-iodanediyl diacetate (3.130)



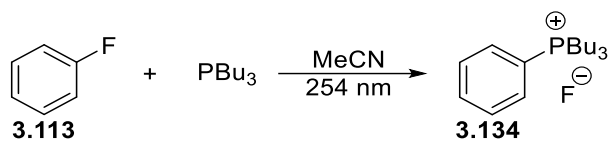
Tributyl(phenyl)phosphonium chloride was synthesized according to general procedure 3E in a 46% yield and displayed identical spectra to **3.115** and **3.122**.

Tributyl(phenyl)phosphonium iodide from phenyl triflate (3.132)



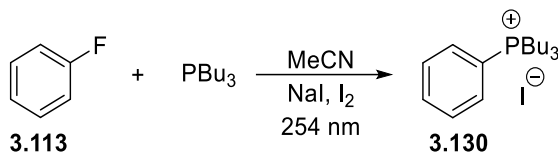
Tributyl(phenyl)phosphonium chloride was synthesized according to general procedure 3E in a 23% yield and displayed identical spectra to **3.115** and **3.122**.

Tributyl(phenyl)phosphonium iodide from fluorobenzene (3.134)



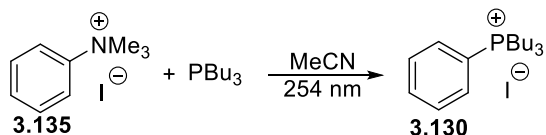
Tributyl(phenyl)phosphonium fluoride was synthesized according to general procedure 3E in a 2% yield by ^{31}P quantitative NMR with triphenyl phosphate as an internal standard.

Tributyl(phenyl)phosphonium iodide from fluorobenzene with NaI/I₂ (3.130)



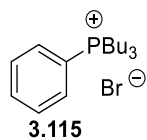
Tributyl(phenyl)phosphonium iodide was synthesized according to general procedure 3E in a 8% yield by ^{31}P quantitative NMR with triphenyl phosphate as an internal standard.

Tributyl(phenyl)phosphonium iodide from N,N,N-trimethylbenzenaminium (3.130)



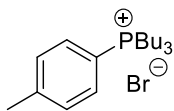
Tributyl(phenyl)phosphonium iodide was synthesized according to general procedure 3E in 46% yield and displayed identical spectra to **3.115** and **3.122**.

Tributyl(phenyl)phosphonium chloride (3.115)



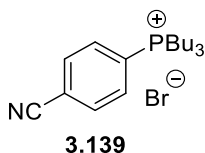
Tributyl(phenyl)phosphonium bromide was synthesized according to general procedure 3G in 86% yield. The compound exhibited identical spectra as the **3.122** and previously reported.²⁰⁸

Tributyl(*p*-tolyl)phosponium chloride (3.138)



Tributyl(*p*-tolyl)phosponium bromide was synthesized according to general procedure 3G in 51% yield. The compound exhibited identical spectra as **3.123** synthesized through condition 3D.

Tributyl(*p*-cyano)phosponium bromide (3.139)



Tributyl(*p*-cyano)phosponium bromide was synthesized according to general procedure 3B in 70% yield.

¹H NMR (300 MHz, CDCl₃): δ 8.49 (dd, *J* = 11.1, 8.4 Hz, 2H), 7.92 (m, 2H), 2.87 (m, 6H), 1.45 (m, 12H), 0.87 (t, *J* = 6.7 Hz, 9H).

³¹P NMR (121M Hz, CDCl₃): δ 30.0

¹³C NMR (75 MHz, CDCl₃) δ 133.9 (d, *J* = 9.4 Hz), 133.3 (d, *J* = 11.9 Hz), 123.6 (d, *J* = 77.4 Hz), 117.7 (d, *J* = 3.3 Hz), 117.1 (d, *J* = 1.7 Hz), 23.8 (d, *J* = 3.2 Hz), 23.6 (d, *J* = 8.2 Hz), 19.5 (d, *J* = 47.1 Hz), 13.5.

HRMS[M⁺]: Calculated for C₁₉H₃₁NP (M⁺)=304.21886; found=304.21979.

Tricyclohexyl(phenyl)phosponium bromide (3.141)



Tricyclohexylphosponium bromide was synthesized according to procedure 3I in 35% yield.

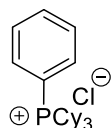
¹H NMR (300 MHz, CDCl₃) δ 7.78 (m, 5H), 2.98-2.86 (m, 3H), 2.02 – 1.94 (m, 13H*), 1.87 – 1.82 (m, 6H), 1.51-1.43 (m, 13H[#]), 1.28-1.14 (m, 6H). (*) Coalescence with adjacent peak raises integration value. (#) Coalescence with water/grease signals raises integration values.

³¹P NMR (121 MHz, CDCl₃) δ 29.6

¹³C NMR (75 MHz, CDCl₃) δ 134.2, 133.0 (d, *J* = 6.4 Hz), 130.5 (d, *J* = 10.7 Hz), 113.2 (d, *J* = 73.1 Hz), 30.8 (d, *J* = 37.7 Hz), 29.5 (d, *J* = 41.3 Hz), 26.7 (d, *J* = 3.4 Hz), 26.3 (d, *J* = 12.1 Hz), 25.4.

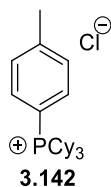
HRMS [M⁺]: Calculated for C₂₄H₃₈P (M⁺)=357.27056; found= 357.27009

Tricyclohexyl(phenyl)phosphonium chloride (3.140)



Tricyclohexyl phosphonium chloride was synthesized according to procedure 3I in 78% yield and displayed identical spectra to compound **3.141**.

Tricyclohexyl(*p*-tolyl)phosphonium chloride (3.142)



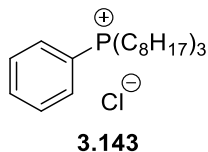
Tricyclohexyl(*p*-tolyl)phosphonium was synthesized according to procedure 3I in 64% yield.

¹H NMR (300 MHz, CDCl₃): δ 7.61 (m, 4H), 2.92-2.80 (m, 3H), 2.47 (s, 3H), 2.00 – 1.91 (m, 16H*), 1.84 – 1.81 (m, 16H), 1.49-1.42 (m, 13H[#]), 1.29-1.21 (m, 6H). (*) Coalescence with adjacent peak raises integration value. (#) Coalescence with water/grease signals raises integration values.

³¹P NMR (121 MHz, CDCl₃) δ 29.3

HRMS [M⁺]: Calculated for C₂₅H₄₀P (M⁺)=371.28621; found= 371.28668

Trioctyl(phenyl)phosphonium chloride (3.143)



Trioctyl(phenyl)phosphonium chloride was synthesized according to general procedure 3H in 83% yield as a light-yellow oil. Mass of the residual solvent was subtracted from the isolated yield through ¹H NMR analysis.

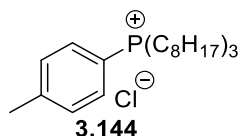
¹H NMR (300 MHz, CDCl₃) δ 7.98 (dd, *J* = 10.9, 7.5 Hz, 2H), 7.69 (m, 3H), 2.90 (m, 6H), 1.48 (m, 12H), 1.24 (m, 24H), 0.86 (t, *J* = 6.5 Hz, 9H).

³¹P NMR (121 MHz, CDCl₃) δ 30.1

¹³C NMR (75 MHz, CDCl₃) δ 134.0 (d, *J* = 2.8 Hz), 131.8 (d, *J* = 8.8 Hz), 130.0 (d, *J* = 11.7 Hz), 118.0, 116.9, 31.3, 30.2 (d, *J* = 14.9 Hz), 28.5, 22.2, 21.5 (d, *J* = 4.4 Hz), 19.8, 19.2, 13.7.

HRMS [M⁺]: Calculated for C₃₀H₅₆P (M⁺)= 447.41141; found= 447.41010

Trioctyl(*p*-tolyl)phosphonium chloride (3.144)



Trioctyl(*p*-tolyl)phosphonium chloride was synthesized according to general procedure 3H in 72% yield as a light yellow oil. Mass of the residual solvent was subtracted from the isolated yield through ¹H NMR analysis.

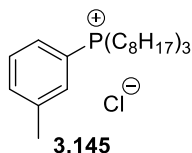
¹H NMR (300 MHz, CDCl₃) δ 7.82 (dd, *J* = 11.5, 8.2 Hz, 2H), 7.47 (dd, *J* = 8.0, 2.6 Hz, 2H), 2.98 – 2.72 (m, 6H), 2.46 (s, 3H), 1.53 – 1.40 (m, 12H), 1.25 (m, 24H), 0.86 (t, *J* = 6.7 Hz, 9H).

^{13}C NMR (75 MHz, CDCl_3) δ 145.5 (d, $J = 2.9$ Hz), 131.9 (d, $J = 9.0$ Hz), 131.0 (d, $J = 12.1$ Hz), 114.1 (d, $J = 81.0$ Hz), 31.6, 30.5 (d, $J = 14.9$ Hz), 28.9 (d, $J = 2.2$ Hz), 22.5, 21.8 (d, $J = 4.4$ Hz), 21.7, 19.9 (d, $J = 48.5$ Hz), 14.0.

^{31}P NMR (122 MHz, CDCl_3) δ 29.6

HRMS [M^+]: Calculated for $\text{C}_{31}\text{H}_{58}\text{P}$ (M^+) = 461.42706; found = 461.42598

Trioctyl(*m*-tolyl)phosphonium chloride (3.145)



Trioctyl(*m*-tolyl)phosphonium chloride was synthesized according to general procedure 3H in 49% yield as a light yellow oil. Mass of the residual solvent was subtracted from the isolated yield through ^1H NMR analysis.

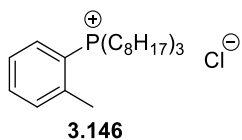
^1H NMR (300 MHz, CDCl_3) δ 7.70 (m, 2H), 7.56 – 7.44 (m, 2H), 2.77 (m, 6H), 2.44 (s, 2H), 1.42 (m, 12H), 1.17 (s, 24H), 0.79 (t, $J = 6.5$ Hz, 9H).

^{13}C NMR (75 MHz, CDCl_3) δ 140.4 (d, $J = 11.6$ Hz), 135.0 (d, $J = 3.0$ Hz), 131.9 (d, $J = 8.7$ Hz), 130.0 (d, $J = 12.4$ Hz), 128.9 (d, $J = 8.6$ Hz), 117.5 (d, $J = 78.4$ Hz), 31.4, 30.4 (d, $J = 14.9$ Hz), 28.7, 22.4, 21.7 (d, $J = 4.5$ Hz), 21.3, 19.8 (d, $J = 48.1$ Hz), 13.8.

^{31}P NMR (122 MHz, CDCl_3) δ 29.8

HRMS [M^+]: Calculated for $\text{C}_{31}\text{H}_{58}\text{P}$ (M^+) = 461.42706; found = 461.42507

Trioctyl(*o*-tolyl)phosphonium chloride (3.146)

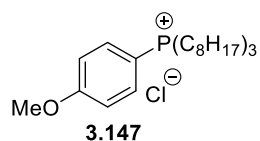


Trioctyl(*o*-tolyl)phosphonium chloride was synthesized according to general procedure 3H in 36% yield as a light yellow oil. Mass of the residual solvent was subtracted from the isolated yield through ^1H NMR analysis. Impurities present by ^{31}P NMR, Integrations not accurate.

^1H NMR (300 MHz, CDCl_3) δ 7.90 (dd, $J = 11.1, 8.5$ Hz, 2H), 7.50 – 7.38 (m, 2H), 2.81 (m, 6H), 2.52 (s, 3H), 1.46 (m, 12H), 1.23 (s, 24H), 0.85 (t, $J = 6.3$ Hz, 9H).

^{31}P NMR (122 MHz, CDCl_3) δ 29.6

Trioctyl(*p*-anisole)phosphonium chloride (3.147)



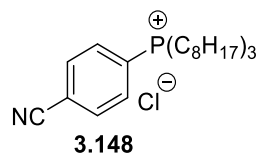
Trioctyl(*p*-anisole)phosphonium chloride was synthesized according to general procedure 3H in 82% yield as a light yellow oil. Mass of the residual solvent was subtracted from the isolated yield through ^1H NMR analysis.

^1H NMR (300 MHz, CDCl_3) δ 7.86 (dd, $J = 10.8, 8.9$ Hz, 2H), 7.12 – 7.01 (m, 2H), 3.77 (s, 3H), 2.64 (m, 6H), 1.35 (m, 12H), 1.11 (m, 24H), 0.73 (t, $J = 6.2$ Hz, 9H).

^{13}C NMR (75 MHz, CDCl_3) δ 164.2 (d, $J = 2.9$ Hz), 134.1 (d, $J = 10.2$ Hz), 116.0 (d, $J = 12.8$ Hz), 107.3 (d, $J = 85.9$ Hz), 55.7, 31.5, 30.5 (d, $J = 14.8$ Hz), 28.9, 28.8, 22.5, 21.7 (d, $J = 4.3$ Hz), 20.0 (d, $J = 48.9$ Hz), 13.9.

^{31}P NMR (122 MHz, CDCl_3) δ 29.0

(4-Cyanophenyl)trioctylphosphonium chloride (3.148)

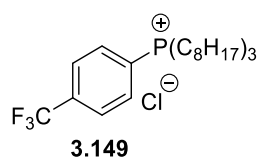


(4-Cyanophenyl)trioctylphosphonium chloride was synthesized according to general procedure 3H in 32% yield as a light yellow oil.

$^1\text{H NMR}$ (300 MHz, CDCl_3) δ 8.39 (dd, $J = 11.2, 8.4$ Hz, 2H), 8.04 – 7.93 (m, 2H), 2.99 (m, 6H), 1.49 (m, 12H), 1.26 (m, 24H), 0.87 (t, $J = 5.6$ Hz, 9H).

$^{31}\text{P NMR}$ (122 MHz, CDCl_3) δ 31.9

Trioctyl(4-(trifluoromethyl)phenyl)phosphonium chloride (3.149)

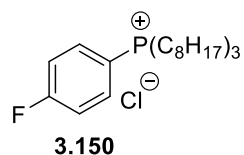


Trioctyl(4-(trifluoromethyl)phenyl)phosphonium chloride was synthesized according to general procedure 3H in 40% yield as a light yellow oil. Mass of the residual solvent was subtracted from the isolated yield through $^1\text{H NMR}$ analysis.

$^1\text{H NMR}$ (300 MHz, CDCl_3): δ 8.31 (m, 2H), 7.96 (m, 2H), 2.95 (m, 6H), 1.49 (m, 12H), 1.25 (s, 24H), 0.86 (t, $J = 6.2$ Hz, 9H).

$^{31}\text{P NMR}$ (122 MHz, CDCl_3) δ 31.4

(4-Fluorophenyl)trioctylphosphonium chloride (3.150)



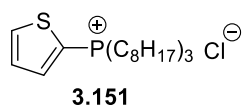
(4-Fluorophenyl)trioctylphosphonium chloride was synthesized according to general procedure 3H in 75% yield as a light yellow oil. Mass of the residual solvent was subtracted from the isolated yield through $^1\text{H NMR}$ analysis.

¹H NMR (300 MHz, CDCl₃): δ 8.13 (ddd, *J* = 11.3, 8.7, 5.1 Hz, 2H), 7.32 (m, 2H), 2.82 – 2.66 (m, 6H), 1.39 (m, 12H), 1.14 (m, 24H), 0.76 (t, *J* = 8.3, 9H).

³¹P NMR (122 MHz, CDCl₃) δ 30.3

¹³C NMR (75 MHz, CDCl₃) δ 166.3 (dd, *J* = 258.4, 3.4 Hz), 135.3 (dd, *J* = 9.8, 14Hz), 118.0 (dd, *J* = 21.9, 13.0 Hz), 113.4 (dd, *J* = 82.7, 3.5 Hz), 31.6, 30.5 (d, *J* = 15.0 Hz), 28.9, 28.8, 22.5, 21.7 (d, *J* = 4.4 Hz), 19.8 (d, *J* = 48.0 Hz), 13.9.

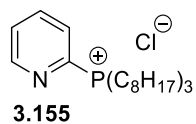
Trioctyl(thiophen-2-yl)phosphonium chloride (3.151)



Trioctyl(thiophen-2-yl)phosphonium chloride was synthesized according to general procedure 3H in 7% yield by ³¹P quantitative NMR with triphenyl phosphate as an internal standard.

³¹P NMR (122 MHz, CDCl₃): δ 27.8

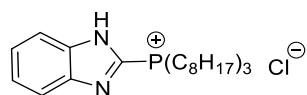
Trioctyl(pyridin-2-yl)phosphonium chloride (3.155)



Trioctyl(pyridin-2-yl)phosphonium chloride was synthesized according to general procedure 3H in a 11% crude yield. TOP oxide and other unidentified impurities were present with the desired compound.

³¹P NMR (122 MHz, CDCl₃): δ 25.0

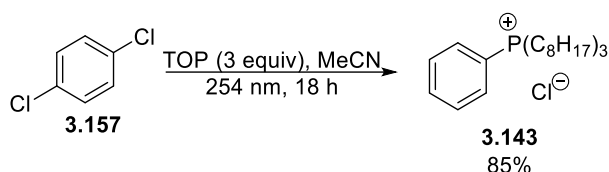
(1H-Benzo[d]imidazol-2-yl)trioctylphosphonium chloride (3.156)



(1H-Benzo[d]imidazol-2-yl)trioctylphosphonium chloride was synthesized according to general procedure 3H in a 24% by ^{31}P quantitative NMR with triphenyl phosphate as an internal standard. TOP oxide and other unidentified impurities were present with the desired compound.

^{31}P NMR (122 MHz, CDCl_3): δ 35.3

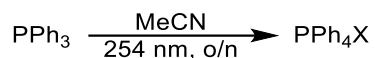
Synthesis of 3.143 from 1,4-dichlorobenzene.



1,4-Dichlorobenzene was reacted according to procedure 3H and furnished **3.143** in 85% yield. Compound displayed identical spectra to **3.143** synthesized from chlorobenzene through procedure 3H.

Control Experiments

Irradiation of PPh_3



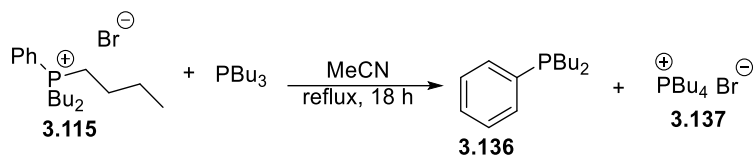
A 10 mL quartz test tube was charged with PPh_3 (386 mg, 1.47 mmol, 3 equiv), sealed with a rubber septum and purged with argon gas. MeCN was then added via a syringe and the tube was briefly stirred with a vortex mixer. The tube was then placed in the photoreactor and irradiated at 254 nm overnight. After the reaction time the solvent was removed, and the solids were re-dissolved in a small amount of DCM. Diethyl ether was then used to precipitate the phosphonium salts which were subsequently isolated via suction filtration and washed with the addition of cold ether.

^1H NMR (300 Hz, CDCl_3): δ 7.83-7.23 (m, 20H)

^{31}P NMR (121 Hz, CDCl_3): δ 23.0

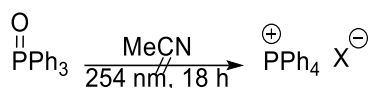
HRMS [M^+]: Calculated for $\text{C}_{24}\text{H}_{20}\text{P}$ (M^+)=339.12971; found= 339.12999

S_N2 of 3.115



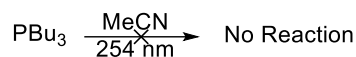
3.115 (14.5 mg, 0.041 mmol, 1 equiv) was added to a flame dried MW vial with a stir bar. The vial was then sealed and purged with Ar. MeCN (0.2 mL, 0.2 M) was then added followed by PBU₃ (16.7 mg, 0.082 mmol, 2 equiv) and the reaction was set to reflux overnight. After the reaction time an aliquot of the reaction mixture was transferred to an NMR tube and diluted with CDCl₃. The formation of PBU₄Br was then observed by ³¹P NMR.

Irradiation of triphenylphosphine oxide



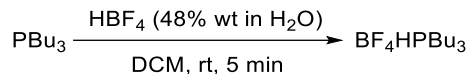
Triphenylphosphine oxide (50 mg, 0.2 mmol, 1 equiv) was added to a flame dried MW vial with a stir bar. The vial was then sealed and purged with Ar. MeCN (0.9 mL, 0.2 M) was then added and the reaction was irradiated at 254 nm for 18 h. Following the reaction time, the solution was analyzed by ³¹P and revealed only triphenylphosphine oxide.

Irradiation of PBU₃



Tributyl phosphine (50.0 mg, 0.250 mmol, 1equiv) was added to a flame dried MW vial with a stir bar that was previously purged with Ar. MeCN (1.24 mL, 0.2 M) was then added and the reaction was irradiated at 254 nm for 18 h. Following the reaction time, the solution was analyzed by ³¹P NMR revealing PBU₃ with some tributylphosphine oxide.

Synthesis of HBF₄PBu₃



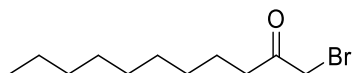
HBf₄PBu₃ was synthesized in 92% yield according to a previously outlined procedure and displayed identical data to previously reported.²³⁹

¹H NMR (300 MHz, CDCl₃): δ 6.08 (dq, *J* = 486, 5.3 Hz, 1H), 2.32-2.20 (m, 6H), 1.66-1.47 (m, 12H), 0.96 (t, *J* = 7.5 Hz, 9H)

³¹P NMR (121 MHz, CDCl₃): δ 13.4

6.3 SYNTHETIC PROCEDURES- CHAPTER 4

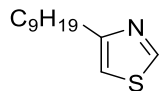
1-Bromoundecan-2-one (S4-1)



1-Bromoundecan-2-one was prepared according to a previously reported procedure to give the product in 32% yield.⁴¹⁰

¹H NMR (300 MHz, CDCl₃): δ 3.88 (s, 2H), 2.65 (t, *J* = 7.3 Hz, 2H), 1.62 (tt, *J* = 7.3, 7.0 Hz, 2H), 1.26 (m, 12H), 0.88 (t, *J* = 6.9 Hz, 3H).

4-Nonyl-thiazole (S4-2)



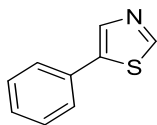
4-Nonyl-5-phenylthiazole was synthesized according to a previously reported procedure to give the product in 62% yield.⁴¹¹

¹H NMR (300 MHz, CDCl₃): δ 8.73 (s, 1H), 6.91 (s, 1H), 2.81 (t, *J* = 7.6 Hz, 2H), 1.72 (tt, *J* = 7.6, 7.6 Hz, 2H), 1.40-1.20 (m, 12H), 0.86 (t, *J* = 7.0 Hz, 3H).

General Direct Arylation Procedure:

The 5-aryl thiazoles were synthesized following literature procedure.⁴¹² K_2CO_3 (4.14 g, 30.0 mmol, 1.5 equiv.), $Pd(OAc)_2$ (89.8 mg, 0.400 mmol, 0.02 equiv.), $PCy_3 \cdot HBF_4$ (294 mg, 0.800 mmol, 0.04 equiv.), and PivOH (612 mg, 6.00 mmol, 0.30 equiv.) were weighed to air and placed in a screw-cap vial equipped with a magnetic stir bar. The thiazole (30.0 mmol, 1.5 equiv.) and the aryl bromide (20.0 mmol, 1 equiv.) were added at this point if solids. The vial was purged with argon, and DMA (65 mL) was added. The thiazole (30.0 mmol, 1.5 equiv.) and the aryl bromide (20.0 mmol, 1 equiv.) were added at this point if liquids. The reaction mixture was then vigorously stirred at 100 °C for 20 hours. The solution was cooled to room temperature, diluted with 200 mL of EtOAc, washed (3 x 200 mL) with saturated aqueous NH_4Cl , dried over $MgSO_4$, filtered, and evaporated under reduced pressure. The mixtures were then purified via silica gel column chromatography to afford the corresponding product in 40-95% yield.

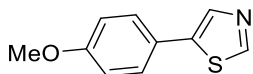
5-Phenylthiazole (4.50)



5-Phenylthiazole was synthesized according to general thiazole direct arylation procedure to give the product in 92% yield and exhibited identical data to previously reported.⁴¹³

1H NMR (300 MHz, $CDCl_3$): δ 8.76 (s, 1H), 8.09 (s, 1H), 7.59 (dd, $J = 7.1, 1.6$ Hz, 2H), 7.50-7.30 (m, 3H).

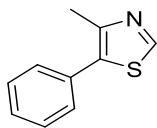
5-(4-Methoxyphenyl)-thiazole (4.51)



5-(4-Methoxyphenyl)-thiazole was synthesized according to the general thiazole direct arylation procedure to give the product in 46% yield and exhibited identical data to previously reported.⁴¹³

1H NMR (300 MHz, $CDCl_3$): δ 8.70 (s, 1H), 7.98 (s, 1H), 7.51 (d, $J = 8.8$ Hz, 2H), 6.95 (d, $J = 8.8$ Hz, 2H), 3.85 (s, 3H).

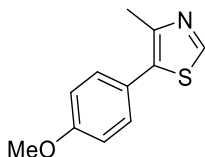
4-Methyl-5-phenylthiazole (4.52)



4-Methyl-5-phenylthiazole was synthesized according to general thiazole direct arylation procedure to give the product in 73% yield and exhibited identical data to previously reported.⁴¹⁴

¹H NMR (300 MHz, CDCl₃): δ 8.50 (s, 1H), 7.48-7.23 (m, 5H), 2.49 (s, 3H).

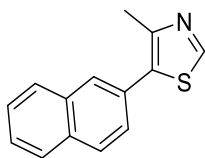
5-(4-Methoxyphenyl)-4-methylthiazole (4.53)



5-(4-Methoxyphenyl)-4-methylthiazole was synthesized according to the general thiazole direct arylation procedure to give the product in 71% yield and exhibited identical data to previously reported.⁴¹⁴

¹H NMR (300 MHz, CDCl₃): δ 8.74 (s, 1H), 7.34 (d, J = 8.4 Hz, 2H), 6.94 (d, J = 8.3 Hz, 2H), 3.82 (s, 3H), 2.52 (s, 3H).

4-Methyl-5-(naphthalen-2-yl)thiazole (4.54)



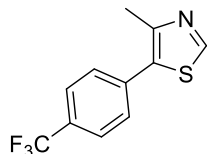
4-Methyl-5-(naphthalen-2-yl)thiazole was synthesized according to the general thiazole direct arylation procedure to give the product in 64% yield.

¹H NMR (300 MHz, CDCl₃): δ 8.72 (s, 1H), 7.95-7.79 (m, 4H), 7.60-7.45 (m, 3H), 2.60 (s, 3H).

^{13}C NMR (300 MHz, CDCl_3): δ 150.5, 148.9, 133.3, 132.7, 132.1, 129.4, 128.5, 128.4, 128.1, 127.8, 127.2, 126.7, 126.6, 16.3.

HRMS $[\text{M}+\text{H}]^+$: calculated for $\text{C}_{14}\text{H}_{12}\text{NS}$ ($\text{M}+\text{H}$) $^+$ = 225.0685; found = 226.0674.

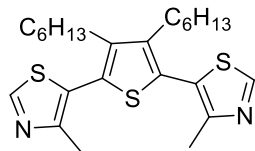
4-Methyl-5-(4-trifluoromethylphenyl)thiazole (4.55)



4-Methyl-5-(4-trifluoromethylphenyl)thiazole was synthesized according to the general thiazole direct arylation procedure to give the product in 75% yield and exhibited identical data to previously reported.⁴¹⁵

^1H NMR (300 MHz, CDCl_3): δ 8.65 (s, 1H), 7.61 (d, J = 8.1 Hz, 2H), 7.48 (d, 8.0 Hz, 2H), 2.48 (s, 3H).

5,5'-(3,4-Dihexylthiophene-2,5-diyl)bis(4-methylthiazole) (4.56)



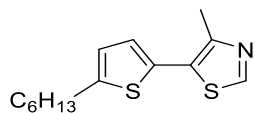
5,5'-(3,4-Dihexylthiophene-2,5-diyl)bis(4-methylthiazole) was synthesized in 26% yield according to the general direct arylation procedure with the exception of employing only 0.5 equivalents (10 mmol) of the dibromothiophene instead 1 equivalent of the aryl bromide.

^1H NMR (300 MHz, CDCl_3): δ 8.78 (s, 2H), 2.50-2.40 (m, 10H), 1.70-1.20 (m, 16H), 0.85 (t, J = 6.8 Hz, 6H).

^{13}C NMR (75 MHz, CDCl_3): δ 152.3, 152.2, 143.1, 127.1, 123.5, 31.5, 30.6, 29.5, 28.1, 22.6, 16.1, 14.1.

HRMS $[\text{M}+\text{H}]^+$: calculated for $\text{C}_{24}\text{H}_{35}\text{N}_2\text{S}_3$ ($\text{M}+\text{H}$) $^+$ = 447.1957; found = 447.1956.

5-(5-Hexylthiophen-2-yl)-4-methylthiazole (4.57)



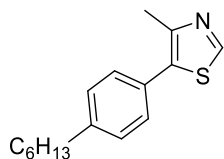
5-(5-Hexylthiophen-2-yl)-4-methylthiazole was synthesized according to the general thiazole direct arylation procedure to give the product in 53% yield.

¹H NMR (300 MHz, CDCl₃): δ 8.51 (s, 1H), 6.90 (d, *J* = 3.3 Hz, 1H), 6.69 (d, *J* = 2.9 Hz, 1H), 2.77 (t, *J* = 7.6 Hz, 2H), 2.56 (s, 3H), 1.75-1.56 (m, 2H), 1.44-1.20 (m, 6H), 0.86 (t, *J* = 6.3 Hz, 3H).

¹³C NMR (75 MHz, CDCl₃): δ 149.2, 148.2, 147.0, 130.4, 126.7, 126.0, 124.5, 31.4, 30.0, 28.9, 23.6, 22.5, 16.4, 14.0.

HRMS [M+H]⁺: calculated for C₁₄H₂₀NS₂ (M+H)⁺ = 266.1032; found = 266.1033.

5-(4-Hexylphenyl)-4-methylthiazole (4.58)



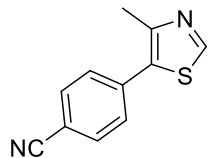
5-(4-Hexylphenyl)-4-methylthiazole was synthesized according to the general thiazole direct arylation procedure to give the product in 79% yield.

¹H NMR (300 MHz, CDCl₃): δ 8.63 (s, 1H), 7.33 (d, *J* = 7.9 Hz, 2H), 7.21 (d, *J* = 7.8 Hz, 2H), 2.62 (t, *J* = 7.7 Hz, 2H), 2.52 (s, 3H), 1.71-1.55 (m, 2H), 1.43-1.23 (m, 6H), 0.88 (t, *J* = 6.3 Hz, 3H).

¹³C NMR (75 MHz, CDCl₃): δ 149.8, 148.1, 142.8, 131.9, 129.0, 128.6, 35.6, 31.6, 31.2, 28.9, 22.5, 16.0, 14.0, one overlapping signal as one peak is missing even with prolonged scans.

HRMS [M+H]⁺: calculated for C₁₆H₂₂NS (M+H)⁺ = 260.1467; found = 260.1460.

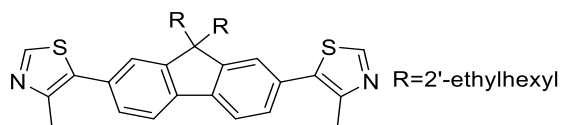
4-(4-methylthiazol-5-yl)benzotrile (4.59)



4-(4-methylthiazol-5-yl)benzonitrile was synthesized according to the direct arylation procedure in a 92% yield and exhibited identical data to previously reported.³³⁹

¹H NMR (300MHz, CDCl₃): δ 8.76 (s, 1H), 7.80 (d, *J* = 8.31 Hz, 2H), 7.57 (d, *J* = 8.23 Hz, 2H), 2.57 (s, 3H).

5,5'-(9,9-Bis(2-ethylhexyl)-9H-fluorene-2,7-diyl)bis(4-methylthiazole) (4.60)



5,5'-(9,9-Bis(2-ethylhexyl)-9H-fluorene-2,7-diyl)bis(4-methylthiazole) was synthesized in 94% yield according to the general direct arylation procedure with the exception of employing only 0.5 equivalents (10 mmol) of the dibromofluorene instead 1 equivalent of the aryl bromide.

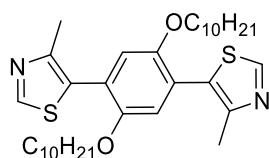
¹H NMR (300 MHz, CDCl₃): δ 8.65 (s, 2H), 7.71 (d, *J* = 7.8 Hz, 2H), 7.48-7.32 (m, 4H), 2.54 (s, 6H), 2.11-1.91 (m, 4H), 0.90-0.44 (m, 30H).

¹³C NMR (75 MHz, CDCl₃): δ 151.0*, 149.9, 148.2*, 140.3, 132.4, 130.2*, 128.2*, 124.9*, 119.8, 55.1, 44.4, 34.6, 33.7*, 28.1*, 26.9*, 22.5, 16.0*, 13.8, 10.2*.

* denotes peaks that appear as multiplets due to the presence of diastereomers.

HRMS [M+H]⁺: calculated for C₃₇H₄₉N₂S₂ (M+H)⁺ = 585.3332; found = 585.3329.

5,5'-(2,5-Bis(decyloxy)-1,4-phenylene)bis(4-methylthiazole) (4.61)



5,5'-(2,5-Bis(decyloxy)-1,4-phenylene)bis(4-methylthiazole) was synthesized in 31% yield according to the general direct arylation procedure with the exception of employing only 0.5 equivalents (10 mmol) of dibromobenzene derivative instead 1 equivalent of the aryl bromide.

¹H NMR (300 MHz, CDCl₃): δ 8.73 (s, 2H), 6.91 (s, 2H), 3.89 (t, *J* = 6.5 Hz, 4H), 2.47 (s, 6H), 1.68 (tt, *J* = 6.9, 6.7 Hz, 4H), 1.23 (m, 28H), 0.85 (t, *J* = 6.8 Hz, 6H).

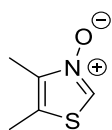
¹³C NMR (75 MHz, CDCl₃): δ 151.2, 150.2, 150.0, 126.8, 121.7, 116.2, 69.5, 31.8, 29.4, 29.2, 29.1, 29.0, 25.9, 22.6, 16.4, 14.0, one overlapping signal as one peak is missing even with prolonged scans.

HRMS [M+H]⁺: calculated for C₃₄H₅₃N₂O₂S₂ (M+H)⁺ = 585.3554; found = 585.3541.

General Oxidation Procedure:

The thiazole (5.00 mmol, 1 equiv.) was dissolved in reagent grade dichloroethane (15 mL). To this solution was added *m*CPBA (77% w/w, 1.68 g, 7.50 mmol, 1.5 equiv.) portion-wise. Once all of the *m*CPBA had been added, the reaction was stirred for 2-4 h. The *N*-oxides were then purified via silica gel column chromatography using a gradient of 0-15% MeOH/EtOAc as the eluent to afford the corresponding product in 10-90% yield.

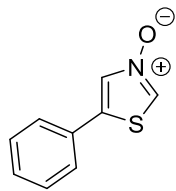
4,5-Dimethylthiazole 3-oxide (4.45)



4,5-Dimethylthiazole 3-oxide was synthesized according to the general thiazole oxidation procedure in 90% yield and exhibited identical data to previously reported.³²⁴

¹H NMR (300 MHz, CDCl₃): δ 8.06 (s, 1H), 2.39 (s, 3H), 2.30 (s, 3H).

5-Phenylthiazole 3-oxide (4.62)



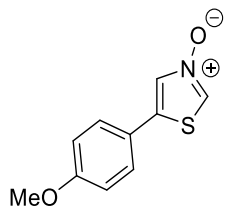
5-Phenylthiazole 3-oxide was synthesized according to the general thiazole oxidation procedure in 10% yield.

¹H NMR (300 MHz, CDCl₃): δ 8.22 (s, 1H), 7.89 (s, 1H), 7.45 (m, 5H).

¹³C NMR (300 MHz, CDCl₃): δ 139.2, 134.1, 131.6, 130.8, 129.8, 128.3, 126.4.

HRMS [M+H]⁺: calculated for C₉H₈NOS (M+H)⁺ = 178.0321; found = 178.0321.

5-(4-Methoxyphenyl)thiazole 3-oxide (4.63)



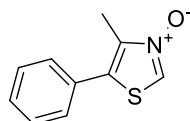
5-(4-Methoxyphenyl)thiazole 3-oxide was synthesized according to the general thiazole oxidation procedure in 28% yield.

¹H NMR (300 MHz, CDCl₃): δ 8.15 (s, 1H), 7.80 (s, 1H), 7.35 (d, *J* = 6.5 Hz, 2H), 6.88 (d, *J* = 6.8 Hz, 2H), 3.80 (s, 3H).

¹³C NMR (75 MHz, CDCl₃): δ 161.0, 137.6, 131.4, 129.2, 127.4, 121.2, 114.7, 55.3.

HRMS [M+H]⁺: calculated for C₁₀H₁₀NO₂S (M+H)⁺ = 208.0427; found = 208.0427.

4-Methyl-5-phenylthiazole 3-oxide (4.64)



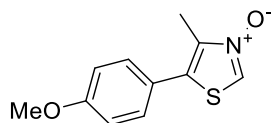
4-Methyl-5-phenylthiazole 3-oxide was synthesized according to the general thiazole oxidation procedure in 60% yield.

¹H NMR (300 MHz, CDCl₃): δ 8.24 (s, 1H), 7.54-7.40 (m, 5H), 2.46 (s, 3H).

¹³C NMR (75 MHz, CDCl₃): δ 141.4, 130.9, 130.6, 129.4, 129.2, 128.6, 128.4, 11.8.

HRMS [M+H]⁺: calculated for C₁₀H₁₀NOS (M+H)⁺ = 192.0478; found = 192.0477.

5-(4-Methoxyphenyl)-4-methylthiazole 3-oxide (4.65)



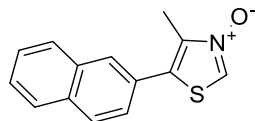
5-(4-Methoxyphenyl)-4-methylthiazole 3-oxide was synthesized according to the general thiazole oxidation procedure in 51% yield.

¹H NMR (300 MHz, CDCl₃): δ 8.19 (s, 1H), 7.35 (d, *J* = 8.7 Hz, 2H), 6.99 (d, *J* = 8.7 Hz, 2H), 3.85 (s, 3H), 2.42 (s, 3H).

¹³C NMR (75 MHz, CDCl₃): δ 160.5, 140.7, 130.8, 129.9, 127.9, 122.8, 114.6, 55.4, 11.7.

HRMS [M+H]⁺: calculated for C₁₁H₁₂NO₂S (M+H)⁺ = 222.0583; found = 222.0583.

4-Methyl-5-(naphthalen-2-yl)thiazole 3-oxide (4.66)



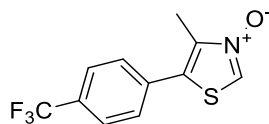
4-Methyl-5-(naphthalen-2-yl)thiazole 3-oxide was synthesized according to the general thiazole oxidation procedure in 45% yield.

¹H NMR (300 MHz, CDCl₃): δ 8.29 (s, 1H), 7.99-7.87 (m, 4H), 7.62 (m, 3H), 2.54 (s, 3H).

¹³C NMR (75 MHz, CDCl₃): δ 141.7, 133.3, 133.1, 131.1, 129.2, 129.0, 128.3, 128.2, 127.9, 127.4, 127.2, 125.6, 12.0, one overlapping signal as one peak is missing even with prolonged scans.

HRMS [M+H]⁺: calculated for C₁₄H₁₂NOS (M+H)⁺ = 242.0634; found = 242.0634.

4-Methyl-5-(4-trifluoromethylphenyl)thiazole 3-oxide (4.67)



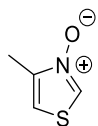
4-Methyl-5-(4-trifluoromethylphenyl)thiazole 3-oxide was synthesized according to the general thiazole oxidation procedure in 30% yield.

¹H NMR (300 MHz, CDCl₃): δ 8.27 (s, 1H), 7.76 (d, *J* = 8.2 Hz, 2H), 7.58 (d, *J* = 8.2 Hz, 2H), 2.28 (s, 3H).

¹³C NMR (75 MHz, CDCl₃): δ 142.5, 134.1, 131.4 (q, *J* = 33.2 Hz), 129.1, 129.0, 128.9, 126.2 (q, *J* = 3.6 Hz), 123.5 (q, *J* = 272.3 Hz), 11.8.

HRMS [M+H]⁺: calculated for C₁₁H₉F₃NOS (M+H)⁺ = 260.0351; found = 260.0351.

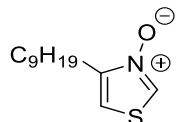
4-Methylthiazole 3-oxide (4.68)



4-Methylthiazole 3-oxide was synthesized according to the general thiazole oxidation procedure in 22% yield and exhibited identical data to previously reported.³²⁴

¹H NMR (300 MHz, CDCl₃): δ 8.20 (d, *J* = 3.1 Hz, 1H), 7.05 (d, *J* = 2.1 Hz, 1H), 2.38 (s, 3H).

4-Nonylthiazole 3-oxide (4.69)



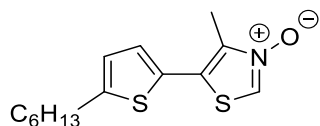
4-Nonylthiazole 3-oxide was synthesized according to the general thiazole oxidation procedure in 40% yield.

¹H NMR (300 MHz, CDCl₃): δ 8.24 (d, *J* = 3.1 Hz, 1H), 6.96 (d, *J* = 3.1 Hz, 1H), 2.70 (t, *J* = 7.7 Hz, 2H), 1.64 (tt, *J* = 7.7, 7.3 Hz, 2H), 1.25-1.00 (m, 12H), 0.81 (t, *J* = 6.9 Hz, 3H).

¹³C NMR (75 MHz, CDCl₃): δ 149.8, 130.2, 112.5, 31.7, 29.3, 29.2, 29.1, 29.0, 26.5, 22.5, 14.0, one overlapping signal as one peak is missing even with prolonged scans.

HRMS [M+H]⁺: calculated for C₁₂H₂₂NOS (M+H)⁺ = 228.1422; found = 228.1417.

5-(5-Hexylthiophen-2-yl)-4-methylthiazole 3-oxide (4.70)



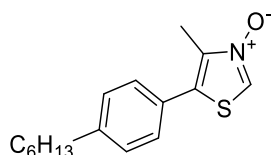
5-(5-Hexylthiophen-2-yl)-4-methylthiazole 3-oxide was synthesized according to the general thiazole oxidation procedure in 29% yield.

¹H NMR (300 MHz, CDCl₃): δ 8.21 (s, 1H), 7.04 (d, *J* = 3.6 Hz, 1H), 6.78 (d, *J* = 3.6 Hz, 1H), 2.82 (t, *J* = 7.7 Hz, 2H), 2.513 (s, 3H), 1.68 (tt, *J* = 7.6, 7.1 Hz, 2H), 1.32 (m, 6H), 0.88 (t, *J* = 6.7 Hz, 3H).

¹³C NMR (75 MHz, CDCl₃): δ 149.0, 140.4, 128.8, 127.9, 127.3, 125.3, 124.9, 31.4, 30.0, 28.6, 22.4, 13.9, 11.9.

HRMS [M+H]⁺: calculated for C₁₄H₂₀NOS₂ (M+H)⁺ = 282.0981; found = 282.0981.

5-(4-Hexylphenyl)-4-methylthiazole-3-oxide (4.71)



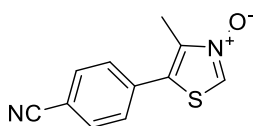
5-(4-Hexylphenyl)-4-methylthiazole-3-oxide was synthesized according to the general thiazole oxidation procedure in 55% yield.

¹H NMR (300 MHz, CDCl₃): δ 8.26 (s, 1H), 7.30-7.20 (m, 4H), 2.57 (t, *J* = 7.7 Hz, 2H), 2.37 (s, 3H), 1.56 (tt, *J* = 7.6, 7.1 Hz, 2H), 1.24(m, 6H), 0.80 (t, *J* = 6.7 Hz, 3H).

¹³C NMR (75 MHz, CDCl₃): δ 150.3, 149.2, 148.0, 143.0, 130.2, 129.2, 128.8, 35.7, 31.7, 31.4, 29.0, 22.6, 16.0, 14.1.

HRMS [M+H]⁺: calculated for C₁₆H₂₂NOS (M+H)⁺= 276.1417; found = 276.1406.

5-(4-Cyanophenyl)-4-methylthiazole 3-oxide (4.72)



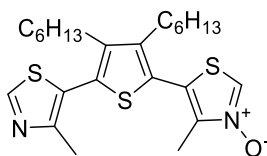
5-(4-cyanophenyl)-4-methylthiazole 3-oxide was synthesized according to the general oxidation procedure in a 21% yield.

¹H NMR (300 MHz, CDCl₃): δ 8.33 (s, 1H), 7.73 (d, *J* = 8.38 Hz, 2H), 7.58 (d, *J* = 8.34 Hz, 2H), 2.49 (s, 3H)

¹³C NMR (75 MHz, CDCl₃): δ 143.0, 135.1, 133.1, 129.6, 129.3, 128.8, 117.9, 113.3, 12.0.

HRMS [M+H]⁺: calculated for C₁₁H₉N₂OS (M+H)⁺= 217.0430; found= 217.0432.

4-Methyl-5-(5-(4-methylthiazol-5-yl)thiophen-2-yl)thiazole 3-oxide (4.73)



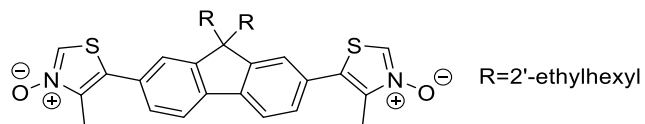
4-Methyl-5-(5-(4-methylthiazol-5-yl)thiophen-2-yl)thiazole 3-oxide was synthesized according to the general oxidation procedure, with the exception of employing 3 equivalents of *m*CPBA. The product was obtained in 25% yield. Note: the di-*N*-oxide (**4.74**) that was also produced and isolated from this reaction.

¹H NMR (300 MHz, CDCl₃): δ 8.80 (s, 1H), 8.44 (s, 1H), 2.50-2.40 (m, 7H), 2.35 (s, 3H), 1.50-1.10 (m, 16H), 0.85 (t, *J* = 5.5 Hz, 6H).

¹³C NMR (75 MHz, CDCl₃): δ 152.5, 152.2, 144.1, 143.3, 130.9, 128.7, 127.8, 124.7, 123.1, 122.5, 31.3, 30.6, 30.2, 29.3, 29.2, 28.0, 27.8, 22.4, 15.8, 13.9, 12.0.

HRMS [M+H]⁺: calculated for C₂₄H₃₅N₂OS₃ (M+H)⁺ = 463.1906; found = 463.1906.

5,5'-(9,9-Bis(2-ethylhexyl)-9H-fluorene-2,7-diyl)bis(4-methylthiazole 3-oxide) (**4.74**)



The general thiazole oxidation procedure was followed with the following deviations: 3 equiv of *m*CPBA was added instead of 1.5 equiv. Additionally, after 2 hours of stirring, another 3 equiv of *m*CPBA was added to the reaction. The product (**4.74**) was afforded in 28% yield.

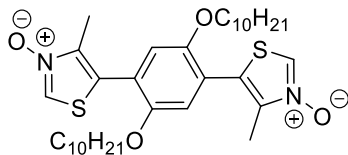
¹H NMR (300 MHz, CDCl₃): δ 8.26 (s, 2H), 7.85 (d, *J* = 8.1, 2H), 7.47-7.43 (m, 4H), 2.46 (s, 6H), 2.05 (m, 4H), 0.90-0.40 (m, 30H).

¹³C NMR (75 MHz, CDCl₃): δ 151.8*, 141.4, 141.3, 131.2, 129.3*, 128.3, 127.8*, 124.3, 120.8*, 55.5, 44.4, 34.8, 33.9*, 28.2*, 27.0*, 22.6, 13.9, 11.8*, 10.2*.

* denotes peaks that appear as multiplets due to the presence of diastereomers;

HRMS [M+H]⁺: calculated for C₃₇H₄₉N₂O₂S₂ (M+H)⁺ = 617.3230; found = 617.3227.

5,5'-(2,5-Bis(decyloxy)-1,4-phenylene)bis(4-methylthiazole 3-oxide) (4.75)



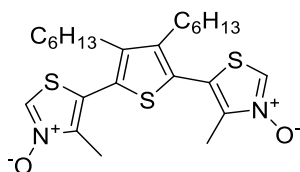
The general thiazole oxidation procedure was followed with the following deviations: 3 equiv of *m*CPBA was added instead of 1.5 equiv. Additionally, after 2 hours of stirring, another 3 equiv of *m*CPBA was added to the reaction. The product (**4.75**) was afforded in 19% yield.

¹H NMR (300 MHz, CDCl₃): δ 8.43 (s, br, 2H), 6.90 (s, 2H), 3.93 (t, *J* = 6.5 Hz, 4H), 2.39 (s, 6H), 1.71 (tt, *J* = 6.9, 6.7 Hz, 4H), 1.23 (m, 28H), 0.85 (t, *J* = 6.8 Hz, 6H).

¹³C NMR (75 MHz, CDCl₃): δ 150.1, 150.1, 126.8, 120.9, 115.4, 69.6, 31.8, 29.6, 29.4, 29.2, 29.1, 29.0, 25.9, 22.6, 14.0, 12.4, one overlapping signal as one peak is missing even with prolonged scans.

HRMS [M+H]⁺: calculated for C₃₄H₅₃N₂O₄S₂ (M+H)⁺ = 617.3441; found = 617.3441.

5,5'-(3,4-Dihexylthiophene-2,5-diyl)bis(4-methylthiazole-3-oxide) (4.76)



5,5'-(3,4-Dihexylthiophene-2,5-diyl)bis(4-methylthiazole 3-oxide) was synthesized according to the general thiazole oxidation procedure, with the exception of employing 3 equivalents of *m*CPBA. The product was obtained in 10% yield. Note the mono-*N*-oxide (**4.73**) was also produced and isolated from this reaction.

¹H NMR (300 MHz, CDCl₃): δ 8.37 (s, 2H), 2.48 (tt, *J* = 8.1, 7.7 Hz, 4H), 2.33 (s, 6H), 1.50-1.10 (m, 16H), 0.84 (t, *J* = 6.7 Hz, 6H).

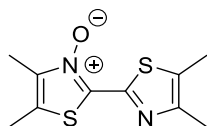
¹³C NMR (75 MHz, CDCl₃): δ 144.6, 144.5, 130.1, 126.4, 122.3, 31.3, 30.6, 29.3, 27.9, 22.4, 13.9, 12.0.

HRMS [M+H]⁺: calculated for C₂₄H₃₅N₂O₂S₃ (M+H)⁺ = 479.1855; found = 479.1855.

General Dehydration Procedure:

The *N*-oxide (0.1 mmol, 1 equiv.) was dissolved in reagent grade THF (0.4 mL) and the solution was cooled in an ice bath. To this cold solution was added 1.0 M LiOtBu in THF (150 μL, 0.15 mmol, 1.5 equiv.) dropwise which usually resulted in a significant color change. After consumption of starting material (5-15 min), the mixture was poured into an extraction funnel containing CH₂Cl₂ and saturated NH₄Cl. The aqueous phase is washed with CH₂Cl₂ (2 x 15 mL) and the organics are combined, dried with MgSO₄, filtered and concentrated under reduced pressure. The products were generally analytically pure after work up and did not need further purification in 55-98% yield.

4,4',5,5'-Tetramethyl-[2,2'-bithiazole] 3-oxide (4.49)



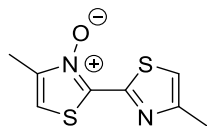
4,4',5,5'-Tetramethyl-[2,2'-bithiazole] 3-oxide was synthesized according to the general dehydration procedure in 89% yield.

¹H NMR (300 MHz, CDCl₃): δ 2.38 (m, 6H), 2.35 (s, 3H), 2.30 (s, 3H).

¹³C NMR (75 MHz, CDCl₃): δ 149.1, 148.4, 140.9, 137.8, 128.1, 123.5, 14.7, 13.0, 11.2, 10.4.

HRMS [M+H]⁺: calculated for C₁₀H₁₃N₂OS₂ (M+H)⁺ = 241.0464; found = 241.0463.

4,4'-Dimethyl-[2,2'-bithiazole] 3-oxide (4.84)



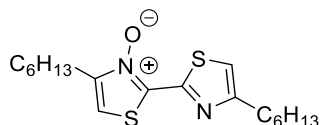
4,4'-Dimethyl-[2,2'-bithiazole] 3-oxide was synthesized according to the general dehydration procedure in 72% yield.

¹H NMR (300 MHz, CDCl₃): δ 7.07 (s, 1H), 7.06 (s, 1H), 2.50 (s, 3H), 2.42 (s, 3H).

¹³C NMR (75 MHz, CDCl₃): δ 153.6, 152.7, 145.4, 140.1, 115.8, 111.7, 17.2, 12.7.

HRMS [M+H]⁺: calculated for C₈H₉N₂OS₂ (M+H)⁺ = 213.0151; found = 213.0142.

4,4'-Dinonyl-[2,2'-bithiazole] 3-oxide (4.85)



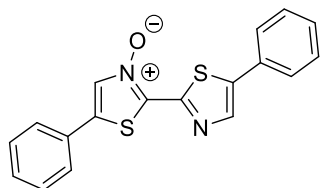
4,4'-Dinonyl-[2,2'-bithiazole] 3-oxide was synthesized according to the general dehydration procedure in 57% yield.

¹H NMR (300 MHz, CDCl₃): δ 7.08 (s, 1H), 7.01 (s, 1H), 2.83 (m, 4H), 1.74 (m, 4H), 1.26 (m, 24H), 0.87 (m, 6H).

¹³C NMR (75 MHz, CDCl₃): δ 158.6, 152.5, 149.7, 140.5, 115.0, 111.0, 31.9, 31.9, 31.5, 29.6, 29.5, 29.5, 29.3, 29.3, 29.3, 26.8, 26.6, 22.7, 22.7, 14.1, overlapping signals as multiple peaks are missing even with prolonged scans.

HRMS [M+H]⁺: calculated for C₂₄H₄₁N₂OS₂ (M+H)⁺ = 437.2655; found = 437.2655.

5,5'-Diphenyl-[2,2'-bithiazole] 3-oxide (4.86)



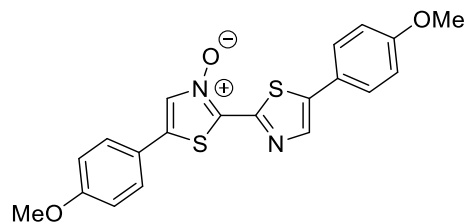
5,5'-Diphenyl-[2,2'-bithiazole] 3-oxide was synthesized according to the general dehydration procedure but required flash column chromatography to purify using 40% EtOAc/Hexanes to afford the product in 81% yield.

¹H NMR (300 MHz, CDCl₃): δ 8.19 (s, 1H), 8.01 (s, 1H), 7.70-7.30 (m, 10H).

¹³C NMR (75 MHz, CDCl₃): δ 151.1, 140.6, 139.6, 139.2, 135.7, 131.9, 131.0, 130.4, 129.5, 129.2, 128.7, 128.7, 126.9, 126.0.

HRMS [M+H]⁺: calculated for C₁₈H₁₃N₂OS₄ (M+H)⁺= 337.0464; found = 337.0463.

5,5'-Bis(4-methoxyphenyl)-[2,2'-bithiazole] 3-oxide (4.87)



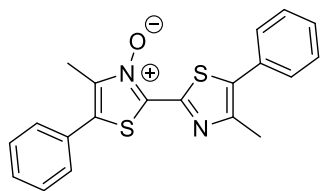
5,5'-Bis(4-methoxyphenyl)-[2,2'-bithiazole] 3-oxide was synthesized according to the general dehydration procedure in 81% yield.

¹H NMR (300 MHz, CDCl₃): δ 8.08 (s, 1H), 7.91 (s, 1H), 7.62 (d, *J* = 7.5 Hz, 2H), 7.52 (d, *J* = 7.5 Hz, 2H), 7.01 (d, *J* = 7.0 Hz, 2H), 6.97 (d, *J* = 7.0 Hz, 2H), 3.85 (s, 3H), 3.84 (s, 3H).

¹³C NMR (75 MHz, CDCl₃): δ 161.4, 160.1, 140.7, 139.15, 138.2, 132.2, 130.9, 128.3, 127.5, 123.7, 121.3, 115.0, 114.8, 113.6, 55.5, 55.4.

HRMS [M+H]⁺: calculated for C₂₀H₁₇N₂O₃S₂ (M+H)⁺= 397.0675; found = 397.0676.

4,4'-Dimethyl-5,5'-diphenyl-[2,2'-bithiazole] 3-oxide (4.88)



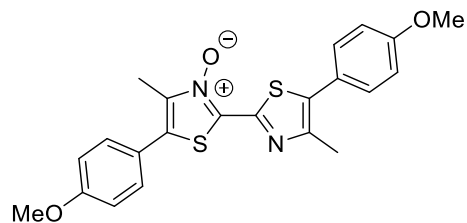
4,4'-Dimethyl-5,5'-diphenyl-[2,2'-bithiazole] 3-oxide was synthesized according to the general dehydration procedure in 92% yield.

¹H NMR (300 MHz, CDCl₃): δ 7.60-7.30 (m, 10H), 2.59 (s, 3H), 2.55 (s, 3H).

¹³C NMR (75 MHz, CDCl₃): δ 149.9, 148.8, 140.9, 139.2, 133.8, 131.9, 130.4, 129.5, 129.3, 129.2, 129.1, 128.7, 128.5, 127.9, 16.4, 11.8.

HRMS [M+H]⁺: calculated for C₂₀H₁₇N₂O₂S₂ (M+H)⁺= 365.0777; found = 365.0777.

5,5'-Bis(4-methoxyphenyl)-4,4'-dimethyl-[2,2'-bithiazole] 3-oxide (4.89)



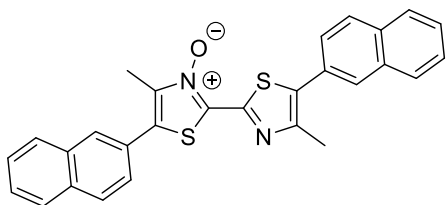
5,5'-Bis(4-methoxyphenyl)-4,4'-dimethyl-[2,2'-bithiazole] 3-oxide was synthesized according to the general dehydration procedure in 92% yield.

¹H NMR (300 MHz, CDCl₃): δ 7.50-7.40 (m, 4H), 7.10-6.95 (m, 4H), 3.88 (s, 3H), 3.87 (s, 3H), 2.58 (s, 3H), 2.53 (s, 3H).

¹³C NMR (75 MHz, CDCl₃): δ 160.7, 159.6, 149.5, 148.3, 140.2, 138.9, 133.7, 130.5, 130.0, 129.1, 124.3, 122.8, 114.9, 114.4, 55.5, 55.4, 16.5, 11.9.

HRMS [M+H]⁺: calculated for C₂₂H₂₁N₂O₃S₂ (M+H)⁺= 425.0988; found = 425.0986.

4,4'-Dimethyl-5,5'-di(naphthalen-2-yl)-[2,2'-bithiazole] 3-oxide (4.90)



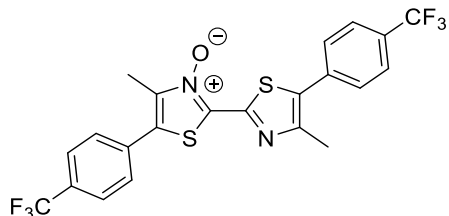
4,4'-Dimethyl-5,5'-di(naphthalen-2-yl)-[2,2'-bithiazole] 3-oxide was synthesized according to the general dehydration procedure in 98% yield.

¹H NMR (300 MHz, CDCl₃): δ 8.02-7.87 (m, 8H), 7.69-7.52 (m, 6H), 2.70 (s, 3H), 2.66 (s, 3H).

^{13}C NMR (75 MHz, CDCl_3): δ 150.3, 149.3, 141.3, 139.5, 134.1, 133.5, 133.4, 133.3, 132.8, 129.5, 129.5, 129.4, 128.7, 128.5, 128.4, 128.4, 128.3, 128.0, 127.9, 127.9, 127.6, 127.4, 127.0, 126.9, 126.7, 125.7, 16.8, 12.2.

HRMS $[\text{M}+\text{H}]^+$: calculated for $\text{C}_{28}\text{H}_{21}\text{N}_2\text{OS}_2$ $(\text{M}+\text{H})^+ = 465.1090$; found = 465.1090.

4,4'-Dimethyl-5,5'-bis(4-(trifluoromethyl)phenyl)-[2,2'-bithiazole] 3-oxide (4.91)



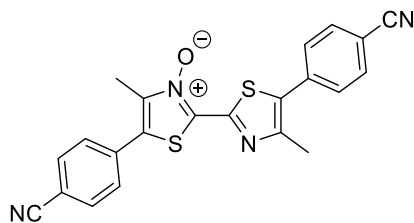
4,4'-Dimethyl-5,5'-bis(4-(trifluoromethyl)phenyl)-[2,2'-bithiazole] 3-oxide was synthesized according to the general dehydration procedure in 88% yield.

^1H NMR (300 MHz, CDCl_3): δ 7.80 (s, 2H), 7.72 (m, 2H), 7.66 (s, 4H), 2.62 (s, 3H), 2.59 (s, 3H).

^{13}C NMR (75 MHz, CDCl_3): δ 150.5, 150.0, 142.1, 139.6, 135.6, 134.0, 132.3, 131.6 (q, $J = 32.6$ Hz), 130.0 (q, $J = 33.5$ Hz), 129.4, 129.0, 127.8, 126.4 (q, $J = 3.5$ Hz), 125.8 (q, $J = 3.5$ Hz), 123.9 (q, $J = 272.1$ Hz), 123.6 (q, $J = 272.2$ Hz), 16.5, 12.0.

HRMS $[\text{M}+\text{H}]^+$: calculated for $\text{C}_{22}\text{H}_{15}\text{F}_6\text{N}_2\text{OS}_2$ $(\text{M}+\text{H})^+ = 501.0525$; found = 501.0524.

5,5'-Bis(4-cyanophenyl)-4,4'-dimethyl-[2,2'-bithiazole] 3-oxide (4.92)



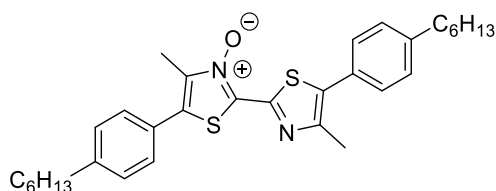
5,5'-bis(4-cyanophenyl)-4,4'-dimethyl-[2,2'-bithiazole] 3-oxide was synthesized according to the general dehydration procedure in a 57% yield.

¹H NMR (300 MHz, CDCl₃): δ 7.87-7.86 (d, *J* = 8.42 Hz, 2H), 7.80-7.78 (d, *J* = 8.07 Hz, 3H), 7.70-7.68 (d, *J* = 8.57 Hz, 3H), 7.69-7.68 (d, *J* = 8.4 Hz, 2H), 2.66 (s, 3H), 2.63 (s, 3H).

¹³C NMR (75 MHz, CDCl₃): Due to poor solubility in a variety of solvents a ¹³C for the compound could not be obtained.

HRMS [M+H]⁺: calculated for C₂₂H₁₅ON₄S₂ (M+H)⁺ = 415.0682; found = 415.0683.

5,5'-Bis(4-hexylphenyl)-4,4'-dimethyl-[2,2'-bithiazole] 3-oxide (4.93)



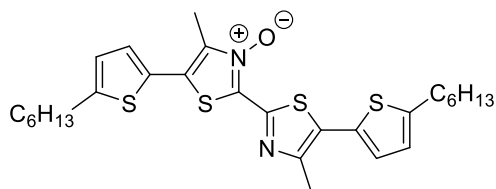
5,5'-Bis(4-hexylphenyl)-4,4'-dimethyl-[2,2'-bithiazole] 3-oxide was synthesized according to the general dehydration procedure in 86% yield.

¹H NMR (300 MHz, CDCl₃): δ 7.50-7.40 (m, 4H), 7.35-7.20 (m, 4H), 2.75-2.40 (m, 10H), 1.66 (m, 4H), 1.34 (m, 12H), 0.90 (m, 6H).

¹³C NMR (75 MHz, CDCl₃): δ 148.5, 144.8, 143.1, 140.6, 134.0, 129.4, 129.3, 129.2, 129.1, 129.1, 128.9, 128.6, 128.4, 127.8, 35.8, 35.7, 31.7, 31.7, 31.3, 31.2, 29.0, 29.0, 22.6, 16.5, 14.1, 11.9, overlapping signals as multiple peaks are missing even with prolonged scans.

HRMS [M+H]⁺: calculated for C₃₂H₄₁N₂OS₂ (M+H)⁺ = 533.2655; found = 533.2655.

5,5'-Bis(5-hexylthiophen-2-yl)-4,4'-dimethyl-[2,2'-bithiazole] 3-oxide (4.94)



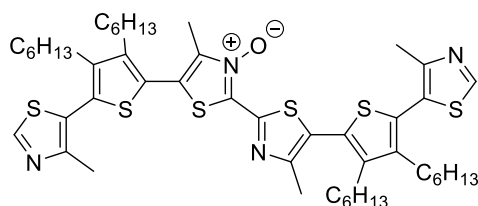
5,5'-Bis(5-hexylthiophen-2-yl)-4,4'-dimethyl-[2,2'-bithiazole] 3-oxide was synthesized according to the general dehydration procedure in 56% yield.

¹H NMR (300 MHz, CDCl₃): δ 7.13 (d, *J* = 3.5 Hz, 1H), 7.07 (d, *J* = 3.5 Hz, 1H), 6.82 (d, *J* = 3.5 Hz, 1H), 6.78 (d, *J* = 3.5 Hz, 1H), 2.84 (m, 4H), 2.66 (s, 3H), 2.62 (s, 3H), 1.71 (m, 4H), 1.45-1.20 (12H, m), 0.90 (6H, m).

¹³C NMR (75 MHz, CDCl₃): δ 149.4, 148.5, 148.5, 147.7, 139.7, 137.8, 130.9, 129.2, 128.3, 127.4, 126.9, 125.2, 125.0, 123.8, 31.6, 31.5, 30.2, 30.2, 29.7, 28.8, 28.8, 22.7, 22.6, 22.6, 17.0, 14.2, 14.1, 12.1.

HRMS [M+H]⁺: calculated for C₂₈H₃₇N₂OS₄ (M+H)⁺ = 545.1783; found = 545.1782.

5,5'-Bis(3,4-dihexyl-5-(4-methylthiazol-5-yl)thiophen-2-yl)-4,4'-dimethyl-[2,2'-bithiazole] 3-oxide (4.95)



5,5'-Bis(3,4-dihexyl-5-(4-methylthiazol-5-yl)thiophen-2-yl)-4,4'-dimethyl-[2,2'-bithiazole] 3-oxide was synthesized according to the general dehydration procedure in 90% yield.

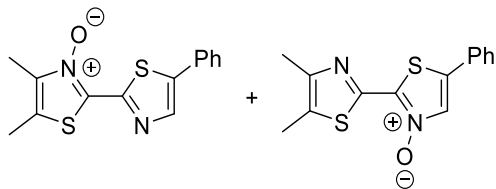
¹H NMR (300 MHz, CDCl₃): δ 8.81-8.75 (m, 2H), 2.65-2.30 (m, 20H), 1.42 (m, 8H), 1.23 (m, 24H), 0.85 (m, 12H).

¹³C NMR (75 MHz, CDCl₃): δ 152.5, 152.1, 151.3, 144.2, 143.6, 143.5, 143.1, 143.0, 140.1, 128.9, 127.3, 127.0, 125.8, 124.7, 121.6, 31.4, 31.3, 31.3, 30.7, 30.4, 30.3, 30.3, 29.3, 29.2, 29.2, 27.9, 27.9, 22.4, 22.4, 16.1, 15.9, 13.9, 12.0, overlapping signals as multiple peaks are missing even with prolonged scans.

HRMS [M+H]⁺: calculated for C₄₈H₆₇N₄OS₆ (M+H)⁺ = 907.3634; found = 907.3623.

Cross Dimerization Dehydration:

4',5'-Dimethyl-5-phenyl-[2,2'-bithiazole] 3-oxide (4.96) and 4,5-dimethyl-5'-phenyl-[2,2'-bithiazole] 3-oxide (4.97)



5-Phenylthiazole-3-oxide (49.0 mg, 0.258 mmol, 1.0 equiv) and 4,5-dimethylthiazole-3-oxide (32.2 mg, 0.250 mmol, 1.0 equiv) were charged into a microwave vial with a stir bar. The *N*-oxides were dissolved in reagent grade THF (0.83 mL, 0.3 M) and the solution was brought to 0 °C. To this cold solution was added 1.0 M LiOtBu in THF (0.38 mL, 2.5 equiv), which resulted in a significant color change. After consumption of starting material (5-15 min), the mixture was poured into an extraction funnel containing CH₂Cl₂ and saturated NH₄Cl. The aqueous phase is washed with two volumes of CH₂Cl₂ and the organics are combined, dried with MgSO₄, filtered and concentrated under reduced pressure. The mixture was then dry loaded onto silica and separated via column chromatography using 50% Hexanes/50% Ethyl Acetate to 100% Ethyl Acetate. 4',5'-dimethyl-5-phenyl-[2,2'-bithiazole] 3-oxide (**4.97**) was obtained as a mixture of 4,5-dimethyl-5'-phenyl-[2,2'-bithiazole] 3-oxide (**4.97**) and 4',5'-dimethyl-5-phenyl-[2,2'-bithiazole] 3-oxide (**4.98**) in 32% yield with the isomers existing in a 5:1 ratio by ¹H NMR. The respective homodimers were also observed with 4,4',5,5'-Tetramethyl-[2,2'-bithiazole] 3-oxide (**4.49**) isolated in 28% yield and 5,5'-diphenyl-[2,2'-bithiazole] 3-oxide (**4.86**) isolated in 26% yield.

Major Isomer Spectra:

¹H NMR (300 MHz, CDCl₃): δ 8.14 (s, 1H), 7.67 (d, 2H, *J* = 7.4 Hz), 7.46 (t, 1H, *J* = 6.0 Hz), 7.42 (d, 2H, *J* = 7.5 Hz), 2.47 (s, 3H), 2.39 (s, 3H).

¹³C NMR (75 MHz, CDCl₃): δ 141.39, 138.95, 133.31, 130.2, 129.6, 129.25, 128.3, 126.9, 125.9, 124.9, 13.3, 10.6.

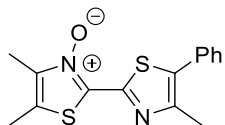
HRMS [M+H]⁺: Calculated for C₁₄H₁₃ON₂S₂ (M+H)⁺ = 289.0464; Found = 289.0463

Minor Isomer Spectra

¹H NMR (300 MHz, CDCl₃): δ 7.95 (s, 1H), 7.55 (d, 2H, *J* = 8.0Hz), 7.37 (m, 1H), 7.34 (d, 2H, *J* = 7.0Hz), 2.46(s, 3H), 2.43 (s, 3H)

¹³C NMR (75 MHz, CDCl₃): Not observed

4,4',5'-Trimethyl-5'-phenyl-[2,2'-bithiazole] 3-oxide (4.98)



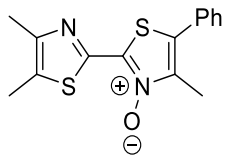
A microwave vial was charged with 4-methyl-5-phenylthiazole-3-oxide (21.6 mg, 0.17 mmol, 1.0 equiv) and 4,5-dimethylthiazole-3-oxide (31.7 mg, 0.17 mmol, 1.0 equiv) with a stir bar. The *N*-oxides were dissolved in reagent grade THF (0.56 ml, 0.3 M) and the solution was cooled to 0 °C. To this cold solution was added 1.0 M LiOtBu in THF (0.5 mL, 3.0 equiv), which resulted in a significant color change. After consumption of starting material (5-15 min), the mixture was poured into an extraction funnel containing CH₂Cl₂ and saturated NH₄Cl. The aqueous phase is washed with two volumes of CH₂Cl₂ and the organics are combined, dried with MgSO₄, filtered and concentrated under reduced pressure. The mixture was then dry loaded onto silica and separated via column chromatography using 50% Hexanes/50% Ethyl Acetate to 100% Ethyl Acetate. 4,4',5'-trimethyl-5'-phenyl-[2,2'-bithiazole] 3-oxide (**4.102**) was synthesized in 14% yield alongside 4,4',5'-trimethyl-5-phenyl-[2,2'-bithiazole] 3-oxide (**4.101**) in 7% yield, 4,4',5,5'-Tetramethyl-[2,2'-bithiazole] 3-oxide (**4.99**) in 27% yield and 4,4'-Dimethyl-5,5'-diphenyl-[2,2'-bithiazole] 3-oxide (**4.100**) in 41% yield.

¹H NMR (300 MHz, CDCl₃): δ 7.50 (m, 5H), 2.55 (s, 3H), 2.47 (s, 3H), 2.43 (s, 3H).

¹³C NMR (75 MHz, CDCl₃): δ 149.6, 148.4, 140.8, 130.5, 129.4, 129.3, 128.6, 128.5, 14.9, 11.9, 11.4; Overlapping signal as one peak is missing even with prolonged scans.

HRMS [M+H]⁺: calculated for C₁₅H₁₅O₄N₂S₂ (M+H)⁺ =303.0620; found =303.0620

4,4',5'-Trimethyl-5-phenyl-[2,2'-bithiazole] 3-oxide (4.99)



4,4',5'-trimethyl-5-phenyl-[2,2'-bithiazole] 3-oxide (**4.102**) was synthesized in 7% yield. Note: 4,4',5-trimethyl-5'-phenyl-[2,2'-bithiazole] 3-oxide (**4.101**) was also produced.

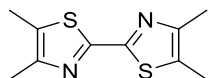
¹H NMR (300 MHz, CDCl₃): δ 7.53-7.37(m, 5H), 2.58 (s,3H), 2.46 (s, 3H), 2.38 (s, 3H).

¹³C NMR (75 MHz, CDCl₃): δ 150.3, 148.8, 141.5, 133.6, 132.1, 129.4, 129.0, 128.1, 128.1, 124.4, 16.6, 13.4, 10.8.

HRMS [M+H]⁺: Calculated for C₁₅H₁₅O₄N₂S₂ (M+H) =303.0620; found =303.0617

***N*-Oxide Reduction:**

4,4',5,5'-Tetramethyl-2,2'-bithiazole (4.103)



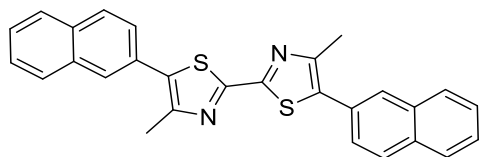
4,4',5,5'-tetramethyl-2,2'-bithiazole was synthesized according to a previously reported procedure to give the product in an 89% yield.³²³

¹H NMR (300 MHz, CDCl₃): δ 2.39 (s, 6H), 2.36 (s, 6H)

¹³C NMR (75 MHz, CDCl₃): δ 157.3, 149.8, 128.4, 15.1, 11.9.

HRMS [M+H]⁺: Calculated for C₁₀H₁₃N₂S₂ (M+H)⁺ =255.0515; found =225.0515

4,4'-Dimethyl-5,5'-di(naphthalen-2-yl)-2,2'-bithiazole (4.104)



4,4'-dimethyl-5,5'-di(naphthalen-2-yl)-2,2'-bithiazole was synthesized according to a previously reported procedure to give the product in an 97% yield.³²³

¹H NMR (300 MHz, CDCl₃): δ 7.96-7.93 (m, 8H), 7.62-7.54 (m, 6H), 2.64 (s, 6H).

¹³C NMR (75 MHz, CDCl₃): δ 158.6, 149.7, 134.5, 133.4, 132.9, 129.3, 128.7, 128.4, 128.3, 127.9, 127.0, 126.9, 126.8, 16.7.

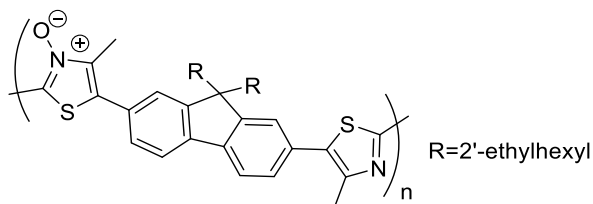
HRMS [M+H]⁺: Calculated for C₂₈H₂₁N₂S₂ (M+H)⁺ =449.1141; found =449.1140

General Dehydration Polymerization Procedure:

The di-*N*-oxide (0.20 mmol, 1 equiv) was dissolved in reagent grade THF (0.03 M) and the solution was placed in an ice bath. To this cold solution was added 1.0M LiOtBu in THF (300 μL, 0.30 mmol, 1.5 equiv) which usually resulted in a significant color change. The mixture was allowed to warm to room temperature and was stirred for 3 hours. The solution was then concentrated and precipitated in methanol and isolated through filtration.

Poly[5-(9,9-bis(2-ethylhexyl)-7-(4-methylthiazol-5-yl)-9H-fluoren-2-yl)-4-methyl-3-(λ¹-oxidaneyl)-3λ⁴-thiazole]

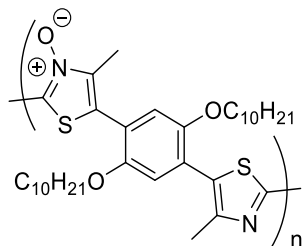
(4.100)



4.101 was synthesized according to the general polymerization procedure in quantitative yield, $M_n = 37$, $M_w = 80$ kg mol⁻¹.

$^1\text{H NMR}$ (300 MHz, CDCl_3): δ 7.84 (br, 2H), 7.59 (m, 4H), 2.75-2.50 (m, 6H), 2.20-1.90 (m, 4H), 0.90-0.40 (m, 30H).

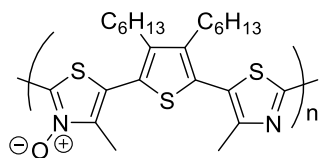
Poly[5-(2,5-bis(decyloxy)-4-(2,4-dimethylthiazol-5-yl)phenyl)-4-methylthiazole 3-oxide] (4.101)



4.102 was synthesized according to the general polymerization procedure in quantitative yield, $M_n = 43$, $M_w = 110$ kg mol⁻¹.

$^1\text{H NMR}$ (300 MHz, CDCl_3): δ 6.96 (br, 2H), 3.93 (br, 4H), 2.25 (br, 6H), 1.80 (br, 4H), 1.24 (m, 28H), 0.85 (br, 6H).

Poly[5-(3,4-dihexanoyl-5-(4-methylthiazol-5-yl)thiophen-2-yl)-4-methylthiazole 3-oxide] (4.102)

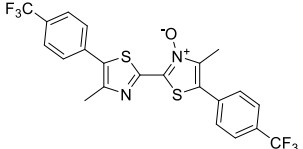
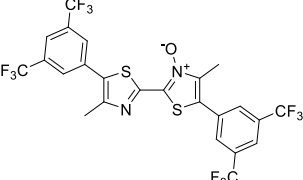
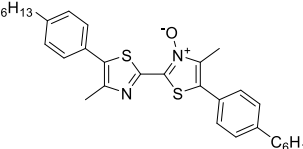
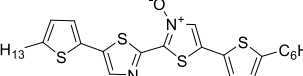
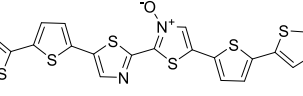
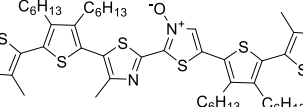


22 was synthesized according to the general polymerization procedure in quantitative yield, $M_n = 17$, $M_w = 46$ kg mol⁻¹.

$^1\text{H NMR}$ (300 MHz, CDCl_3): δ 2.65-2.30 (br, 10H), 1.50-1.10 (m, 16H), 0.85 (br, 6H).

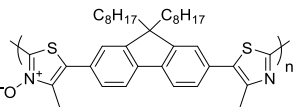
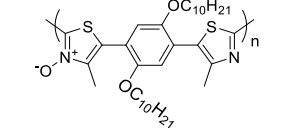
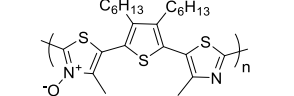
PHOTO/ELECTROCHEMICAL PROPERTIES – SMALL MOLECULES

Compound	λ_{max} (nm) ^[a]	λ_{max} Emission (nm) ^[a]	$E_{\text{ox. onset}}$ (V) ^[b]	$E_{\text{g,opt}}$ (eV) ^[c]	HOMO/LUMO (eV) ^[d]
	355	n/a	0.99	3.2	-5.8/-2.6
	346	n/a	0.54, 1.0 ^e	3.2	-5.4/-2.2
	346	n/a	1.2	3.3	-6.0/-2.7
	397	446, 467	0.94	2.8	-5.7/-3.0
	410	469, 489	0.96	2.7	5.8/-3.1
	386	468	0.95	2.8	-5.7/-2.9
	419	466, 481	0.86, 1.1	2.5	-5.7/-3.1
	400	469	0.75	2.7	-5.6/-2.8
	396	461, 475	n/a	2.8	n/a

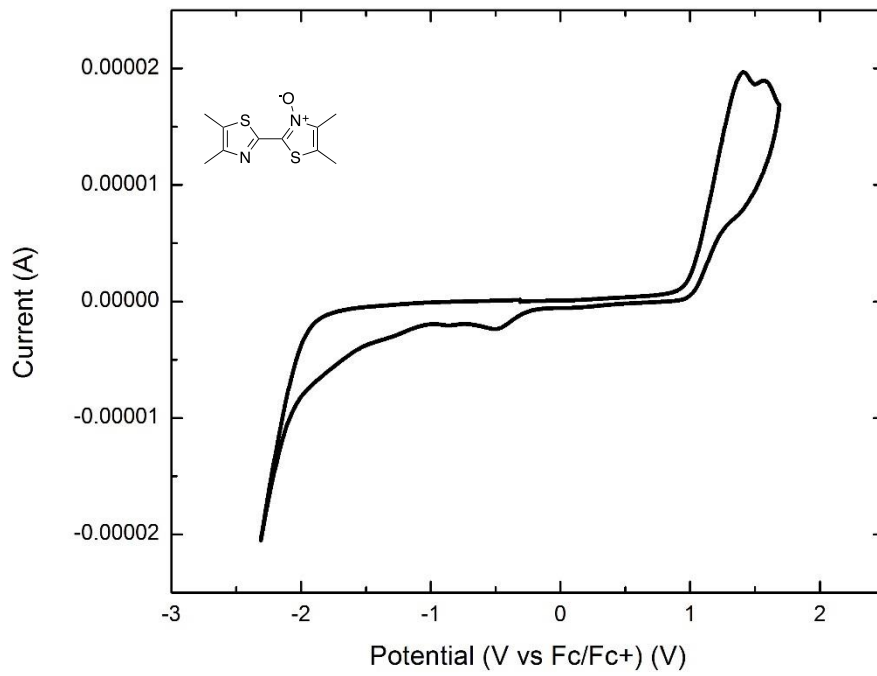
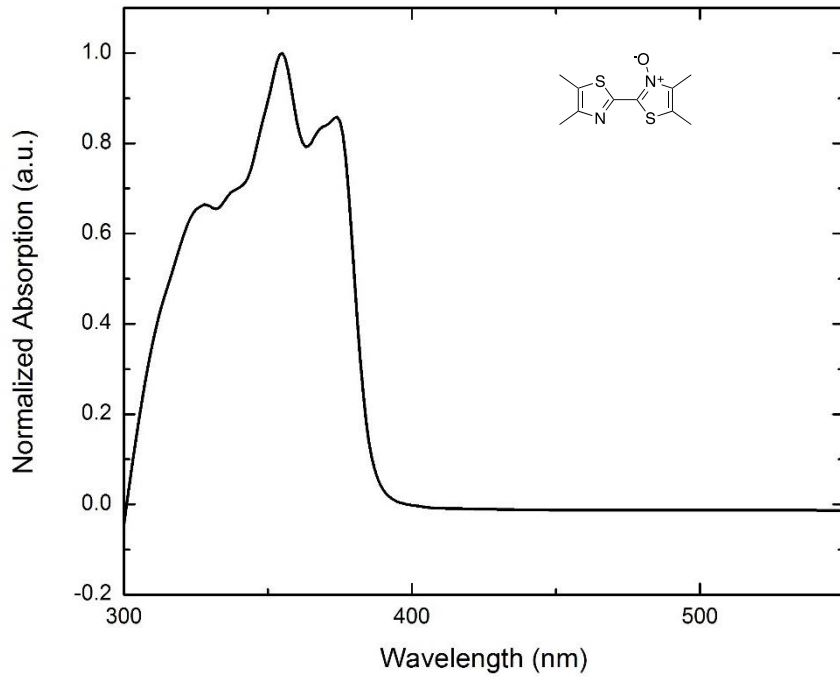
Compound	λ_{\max} (nm) ^[a]	λ_{\max} Emission (nm) ^[a]	$E_{\text{ox. onset}}$ (V) ^[b]	$E_{\text{g opt}}$ (eV) ^[c]	HOMO/LUMO (eV) ^[d]
	386	451, 461	1.1	2.9	-5.9/-3.0
	355	466	0.63, 1.2	3.2	-5.4/-2.2
	392	467	0.96	2.9	-5.8/-2.9
	441	500, 512	0.75	2.3	-5.6/-3.2
	431	556	0.63	2.5	-5.4/-2.9
	326	513	0.77, 1.0	2.6	-5.6/-2.9

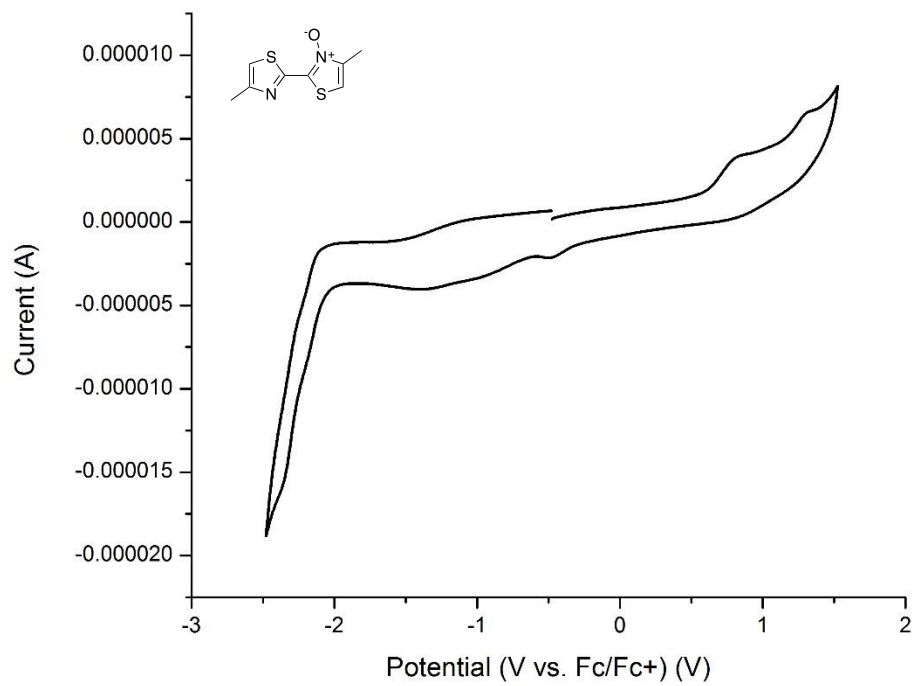
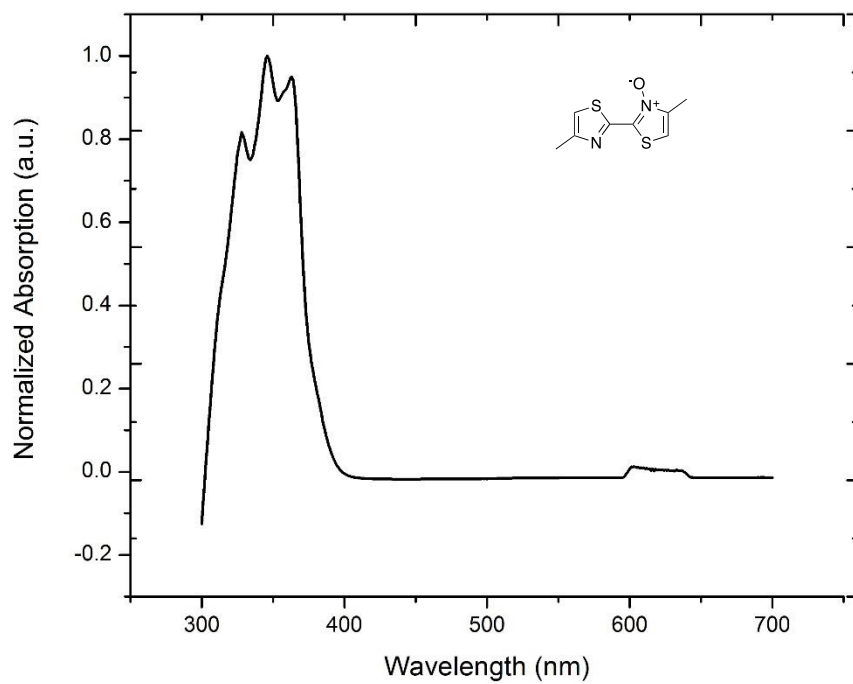
[a] Measured in CHCl_3 . [b] CV measured in CHCl_3 with 0.1M $n\text{Bu}_4\text{NPF}_6$ as the supporting electrolyte using a Pt button working electrode, Pt counter electrode, and Pt reference electrode with Fc/Fc^+ as an internal standard. [c] Estimated from the absorption onset: $E_{\text{g}} = 1240/\lambda_{\text{onset}}$. [d] HOMO estimated from first oxidation potential $E_{1/2}$: $\text{HOMO} = -(E_{1/2}^{\text{ox}} + 4.8)$; $\text{LUMO} = \text{HOMO} - E_{\text{g}}$. [e] CV measured in CH_2Cl_2 .

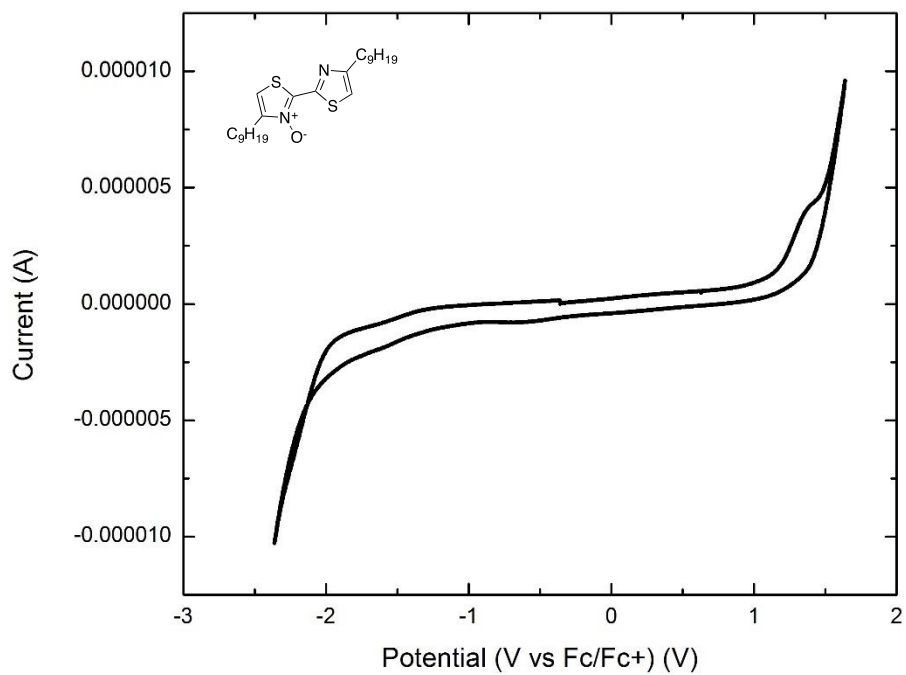
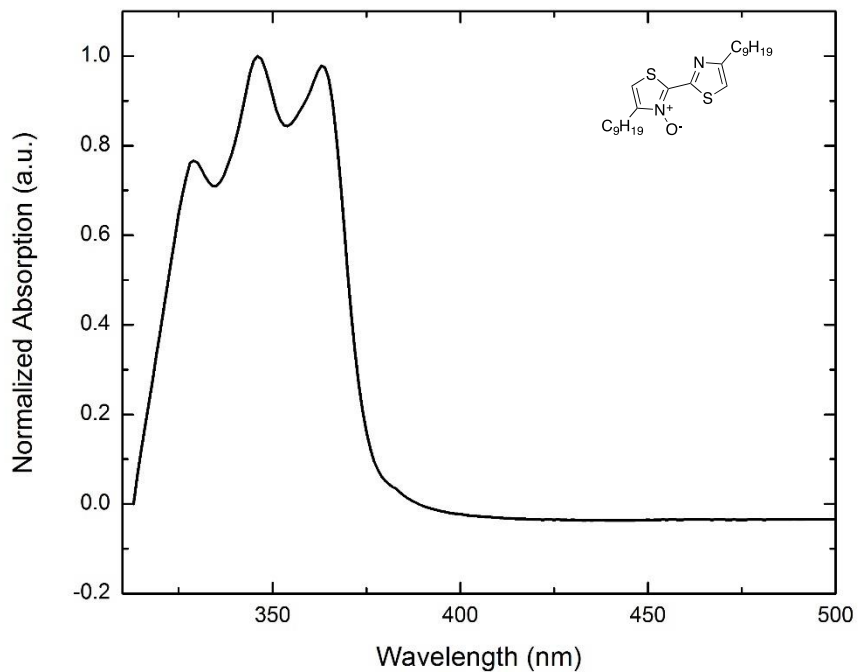
PHOTO/ELECTROCHEMICAL PROPERTIES - POLYMERS

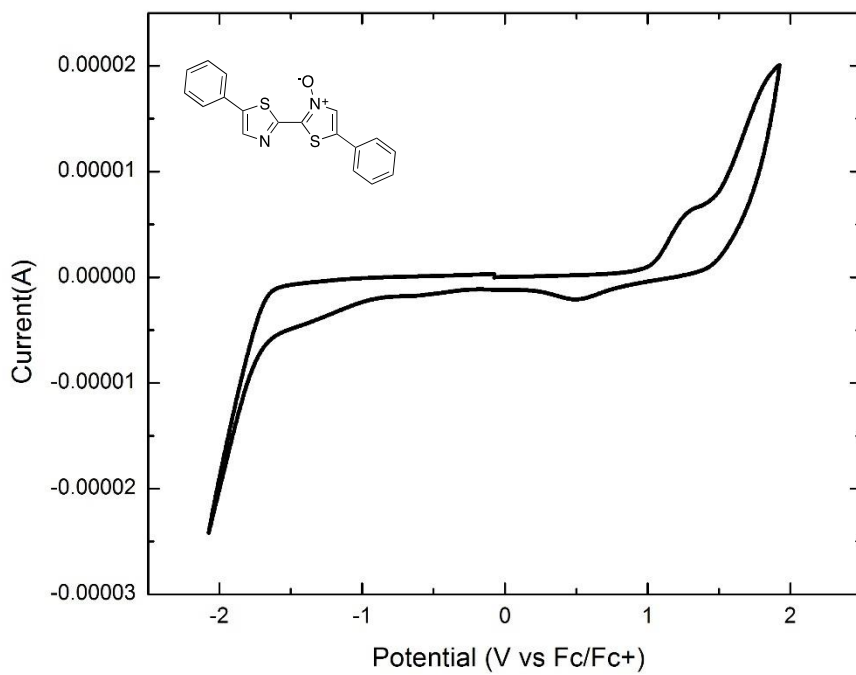
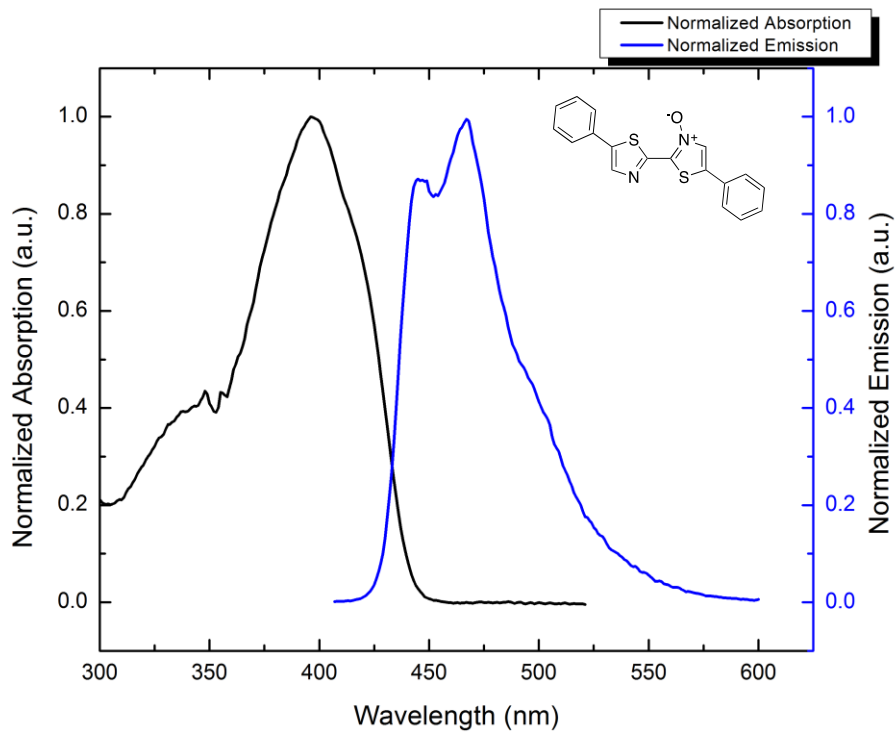
Compound	λ_{\max} (nm) ^[a]	λ_{\max} Em. (nm) ^[a]	$E_{\text{ox. onset}}$ (V) ^[b]	$E_{\text{red. onset}}$ (V) ^[b]	$E_{\text{g opt}}$ (eV) ^[c]	$E_{\text{g ec}}$ (eV) ^[d]	HOMO/LUMO _{ec} (eV) ^[e]
	434	497	1.2	-1.2, -1.7	2.6	2.9	-6.0/-3.1
	348	397, 483	0.82	n/a	2.7	n/a	-5.6/-2.9*
	406	539	1.2	-1.4	2.6	2.6	-6.0/-3.4

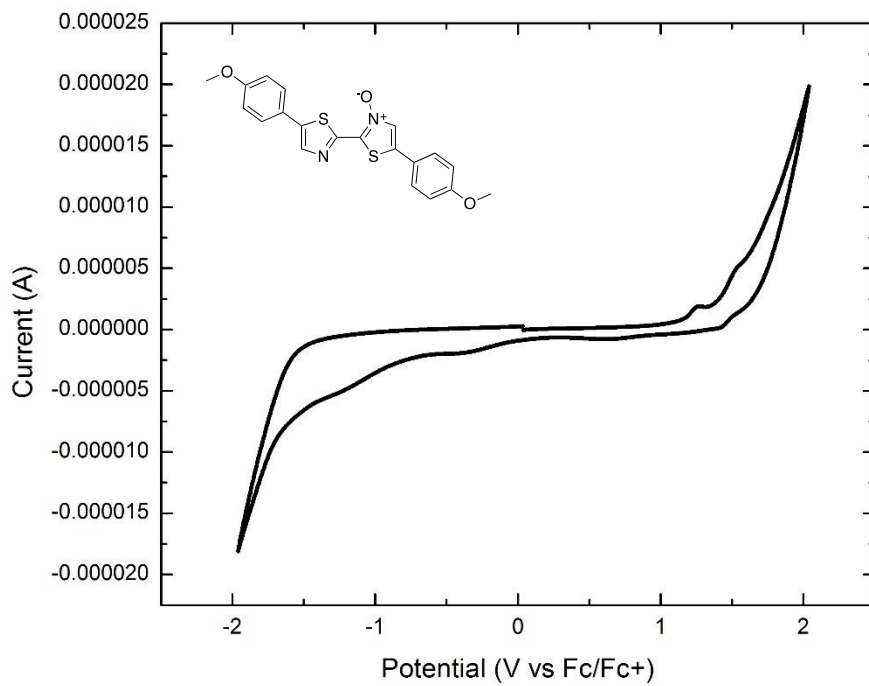
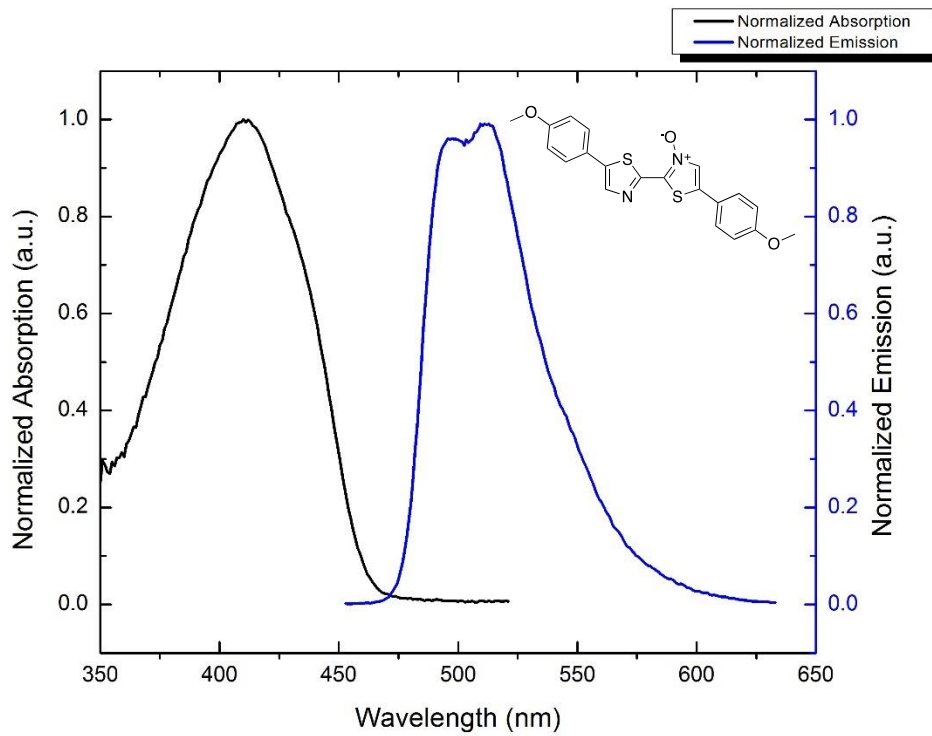
[a] Measured in CHCl_3 . [b] CV performed by dropcasting polymer onto Pt button working electrode. Measured in MeCN with 0.1M $n\text{Bu}_4\text{NPF}_6$ as the supporting electrolyte, using a Pt counter electrode, and Pt reference electrode with Fc/Fc^+ as an internal standard. [c] Estimated from the absorption onset: $E_{\text{g}} = 1240/\lambda_{\text{onset}}$. [d] Electrochemical bandgap determined by difference between HOMO and LUMO levels. $E_{\text{g ec}} = \text{LUMO} - \text{HOMO}$. [e] HOMO estimated from first oxidation potential $E_{1/2}$: $\text{HOMO} = -(E_{1/2}^{\text{ox}} + 4.8)$; $\text{LUMO} = -(E_{1/2}^{\text{red}} + 4.8)$. *LUMO was estimated using optical bandgap. $\text{LUMO} = \text{HOMO} - E_{\text{g}}$

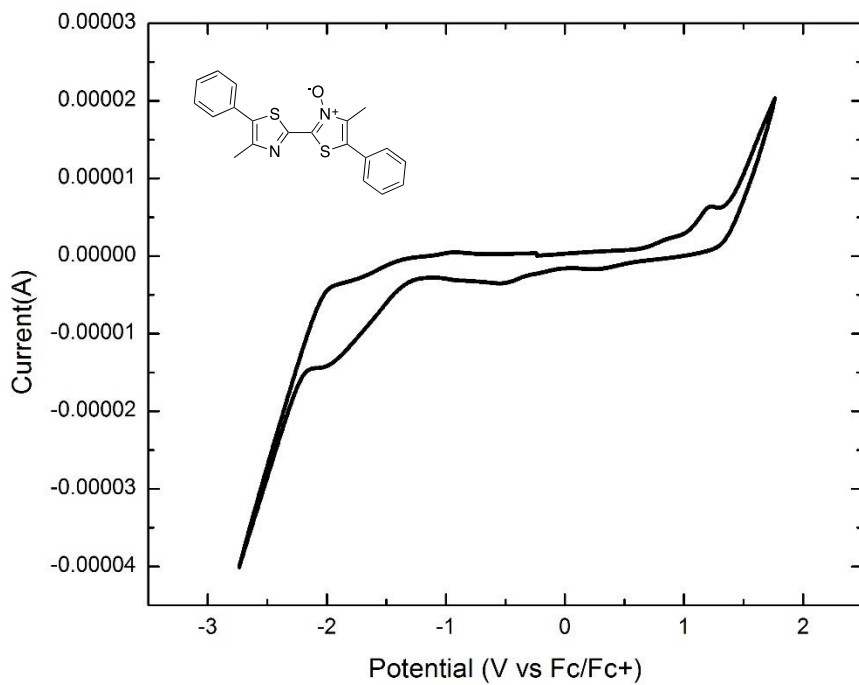
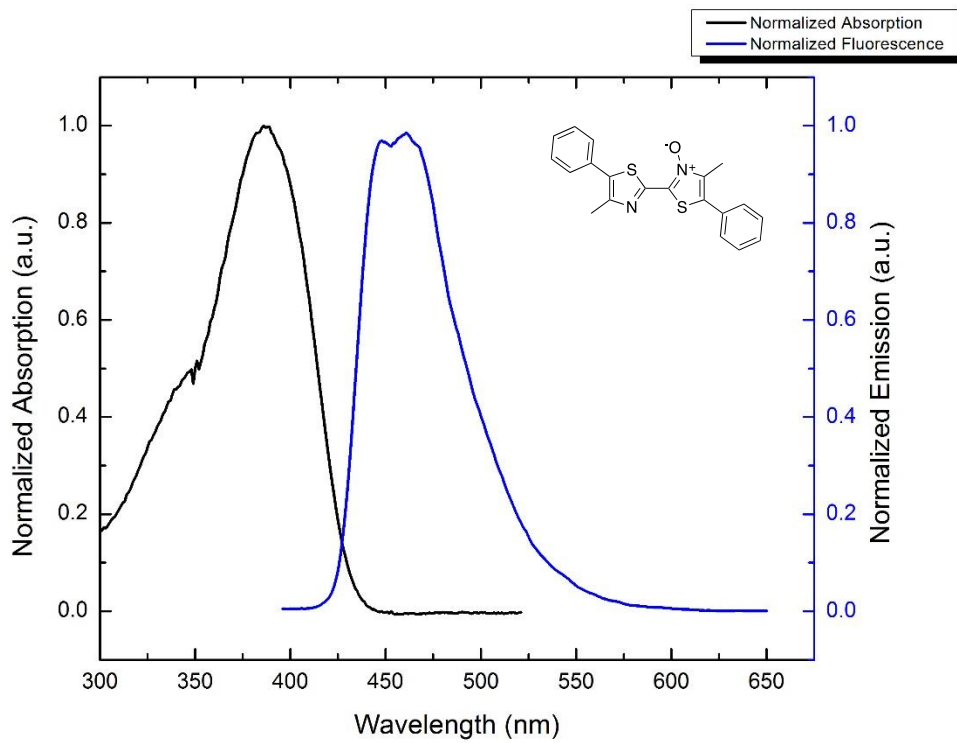


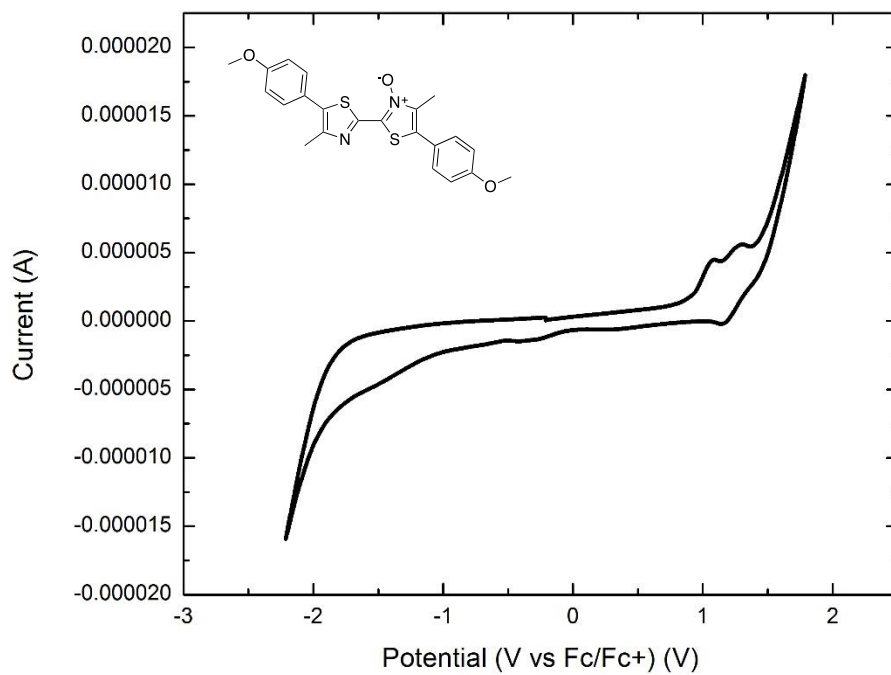
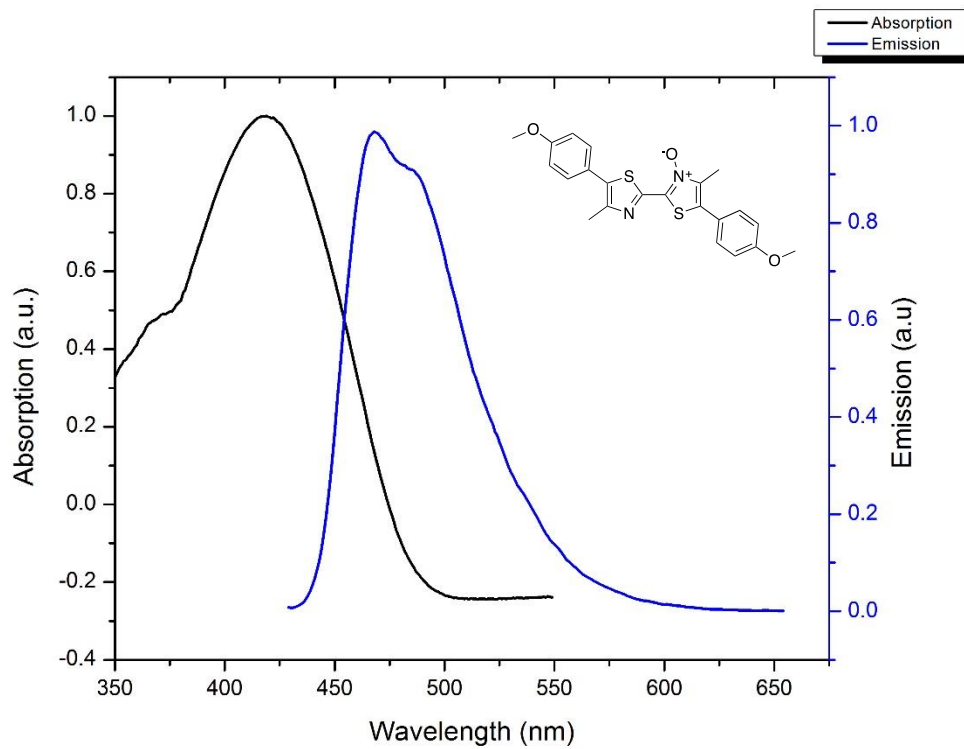


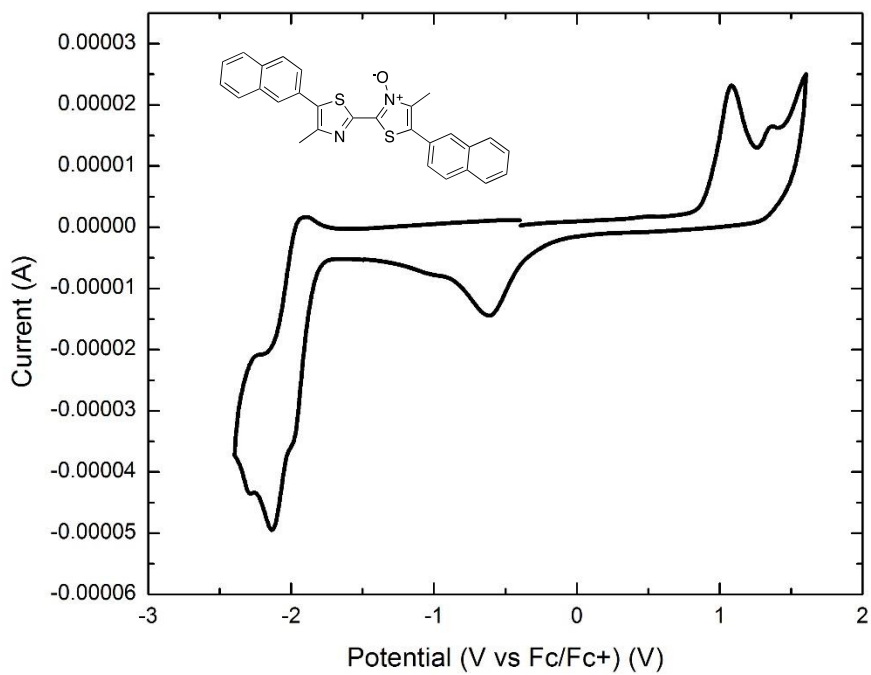
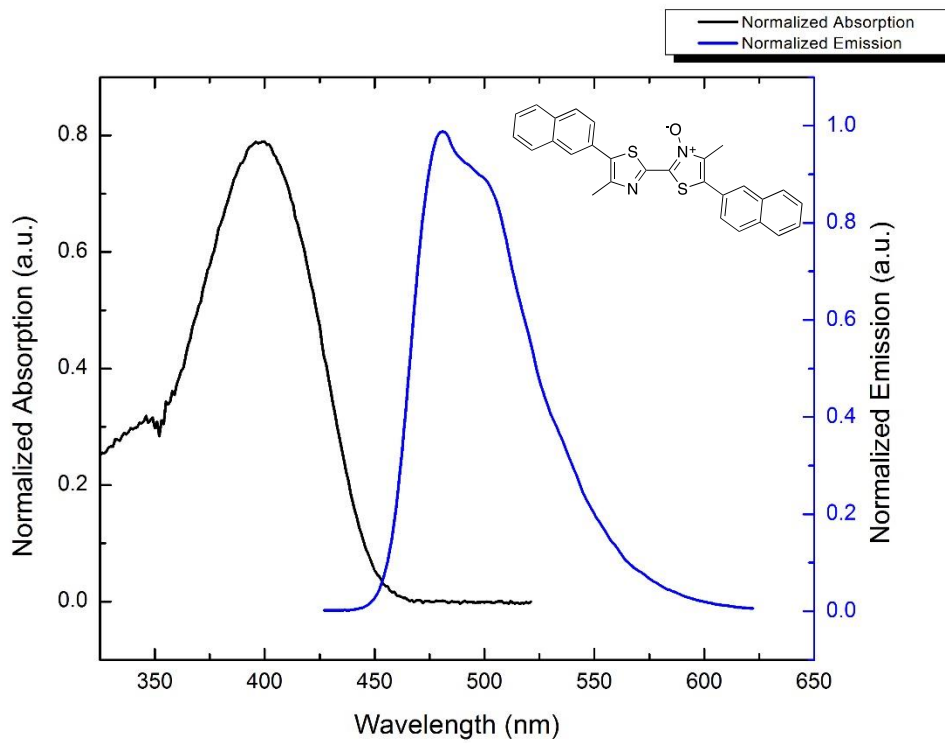


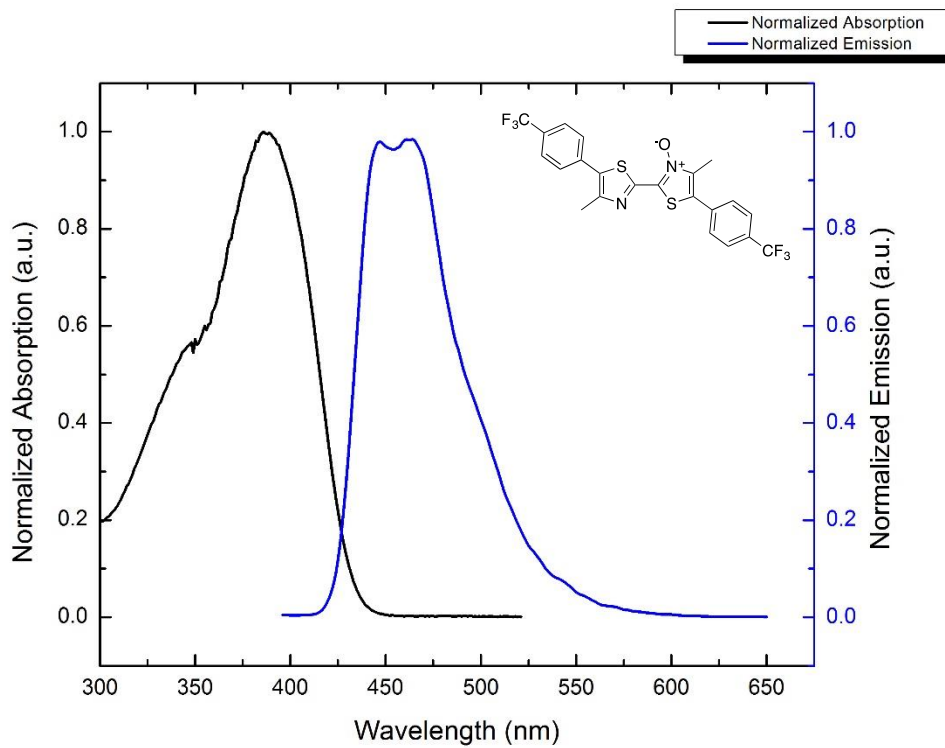
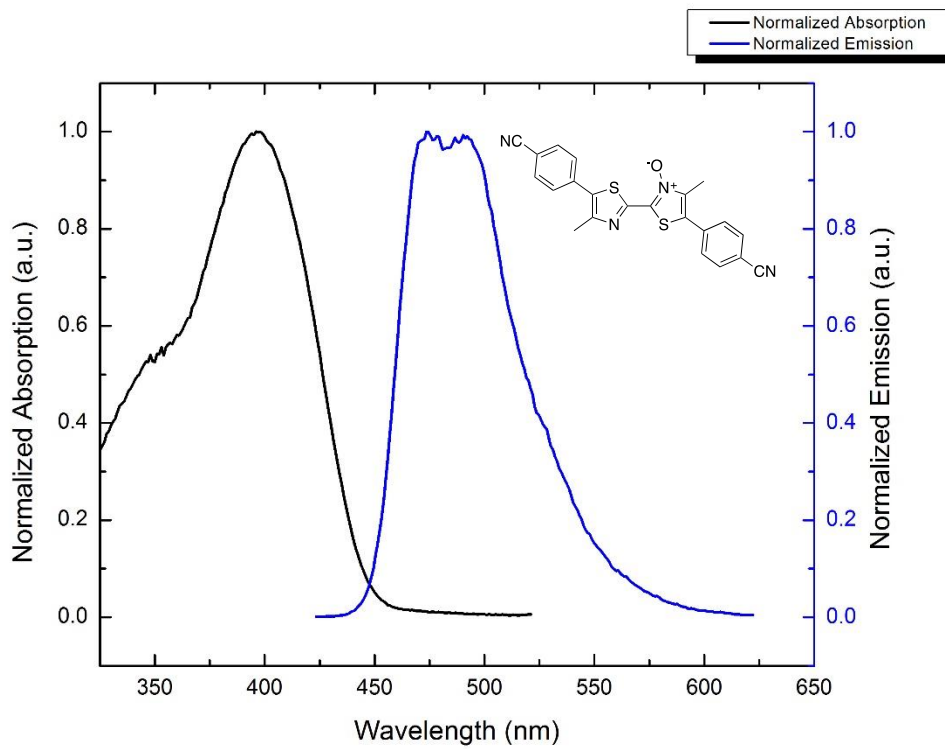


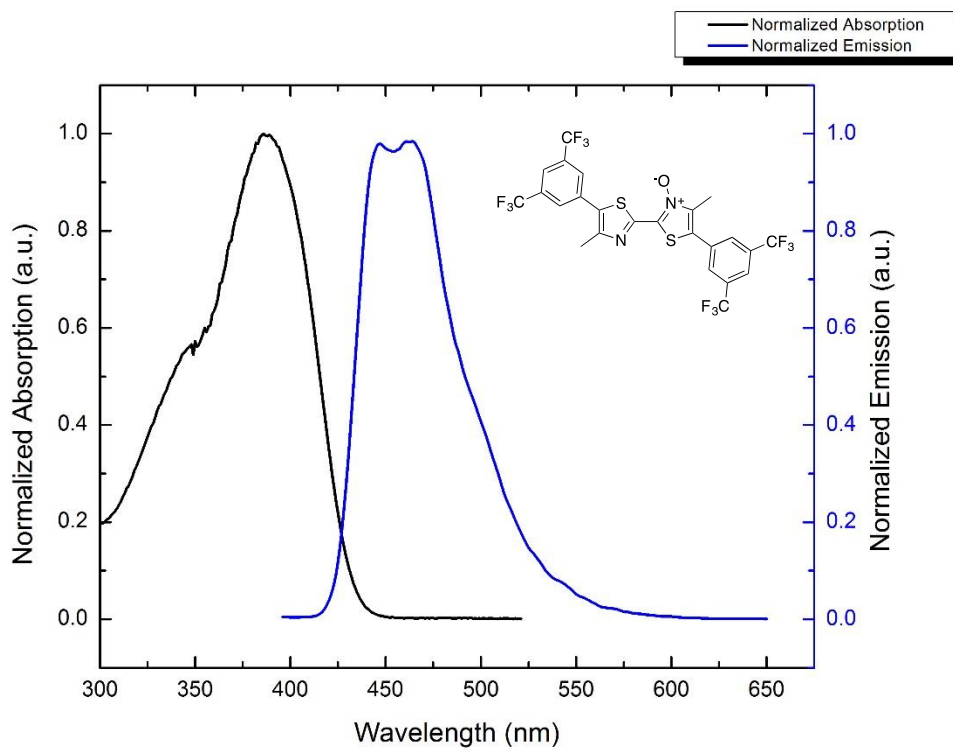
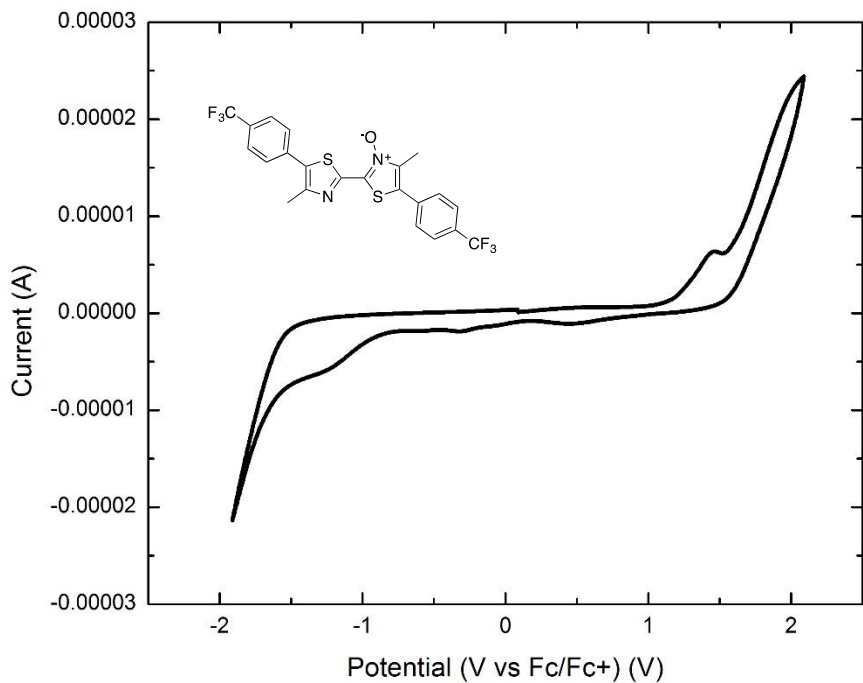


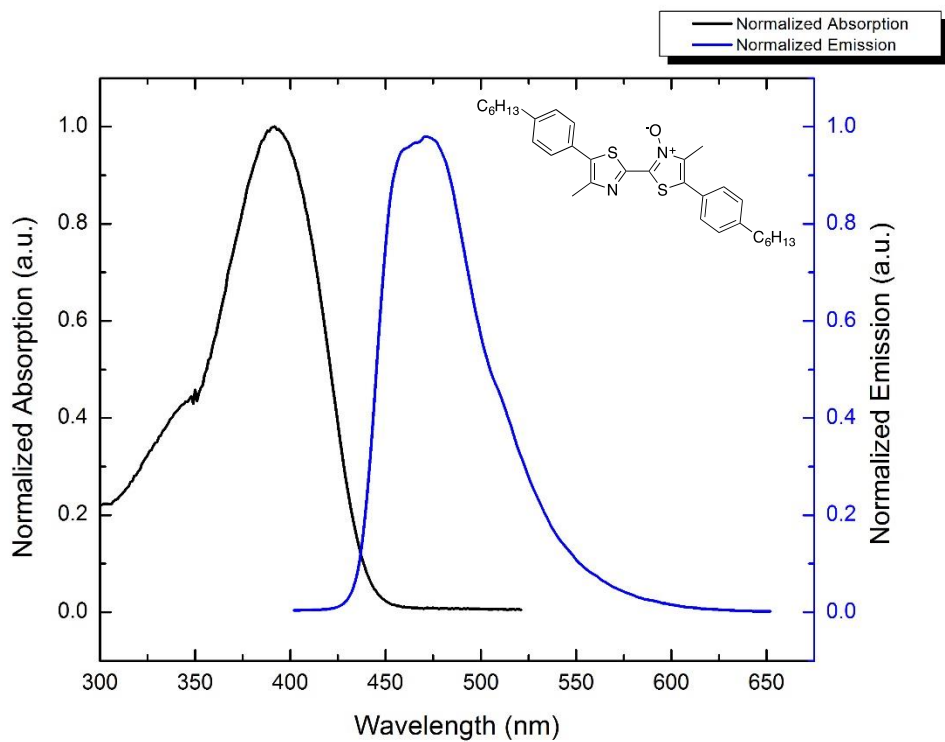
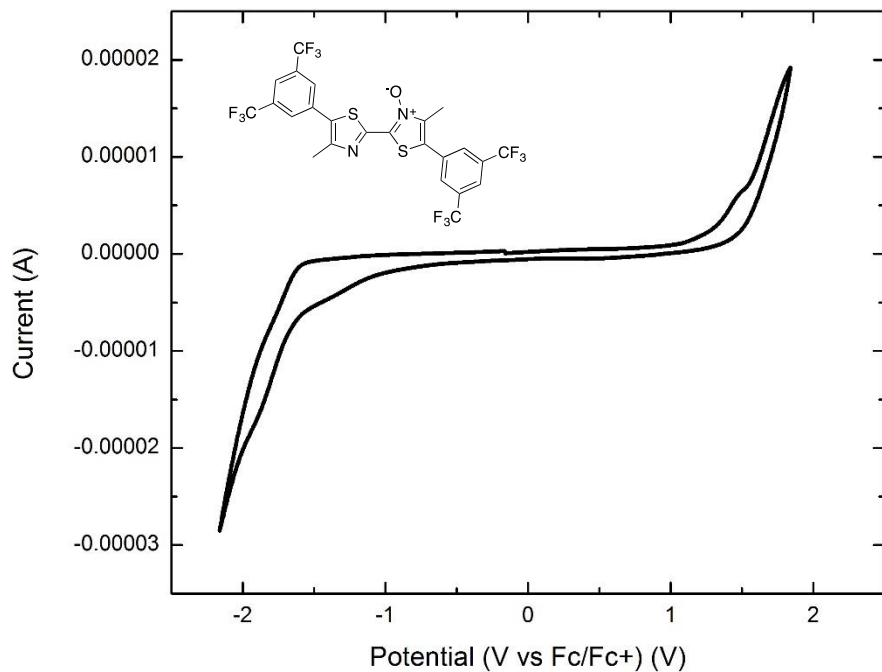


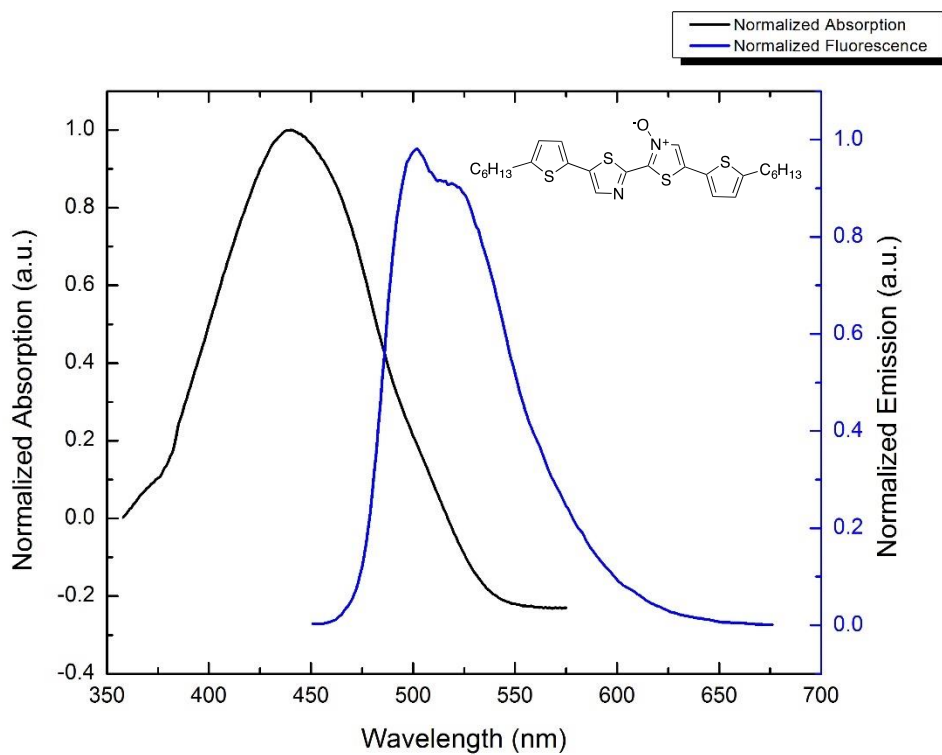
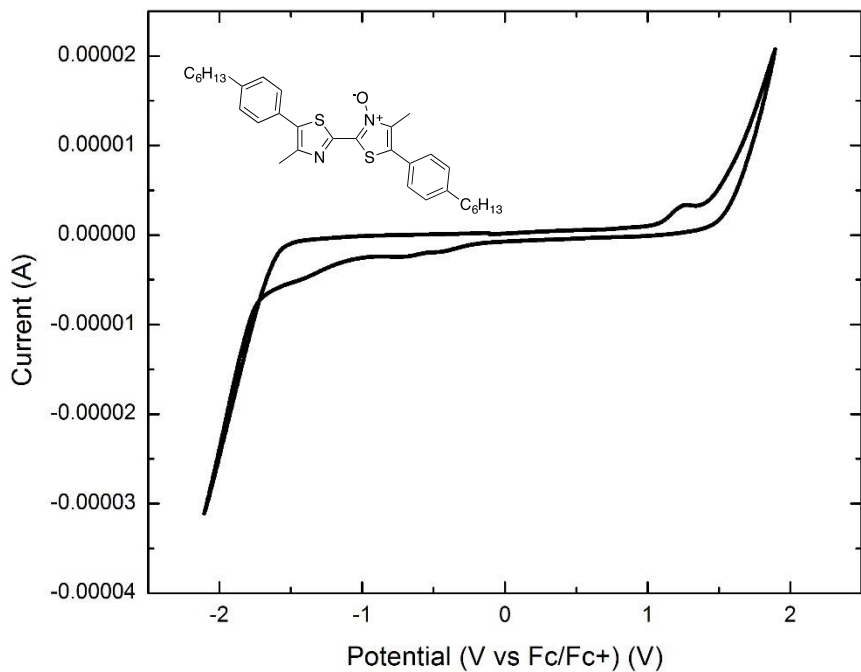


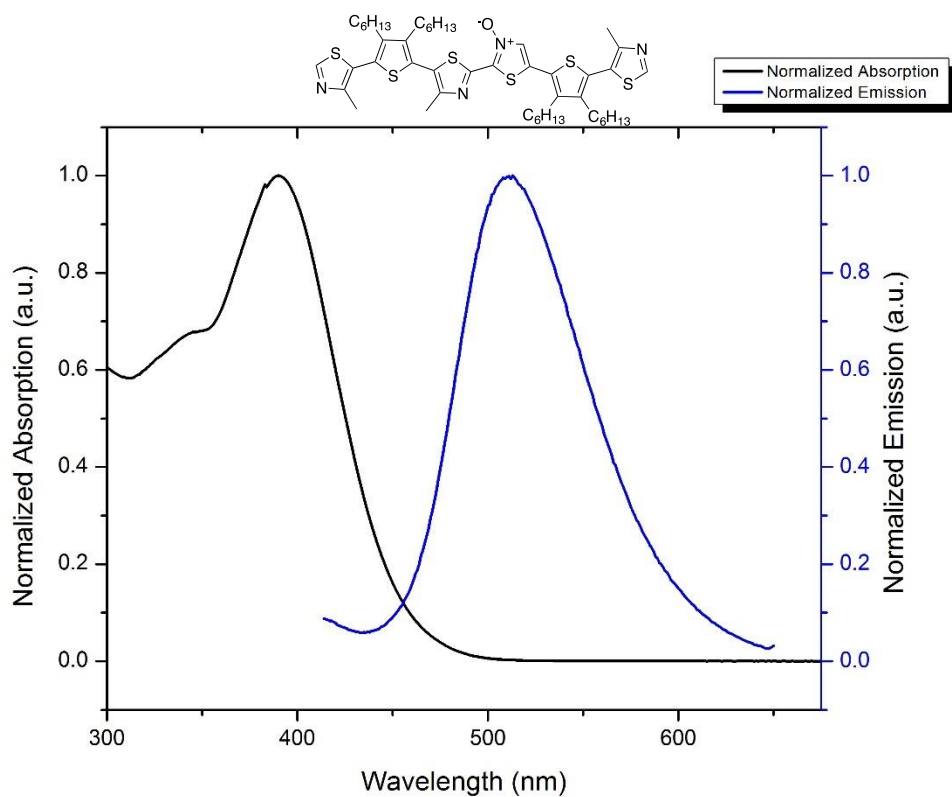
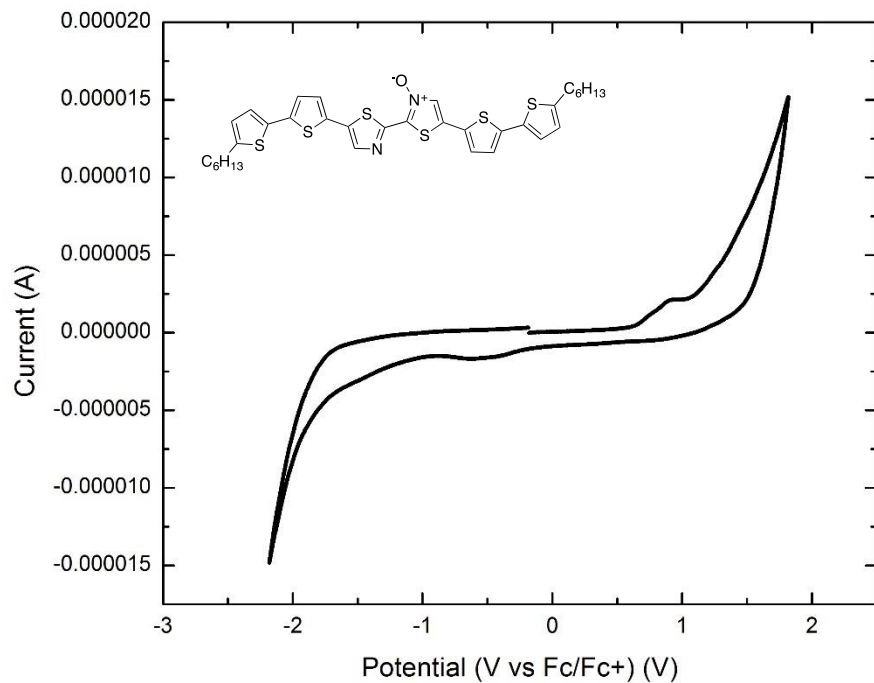


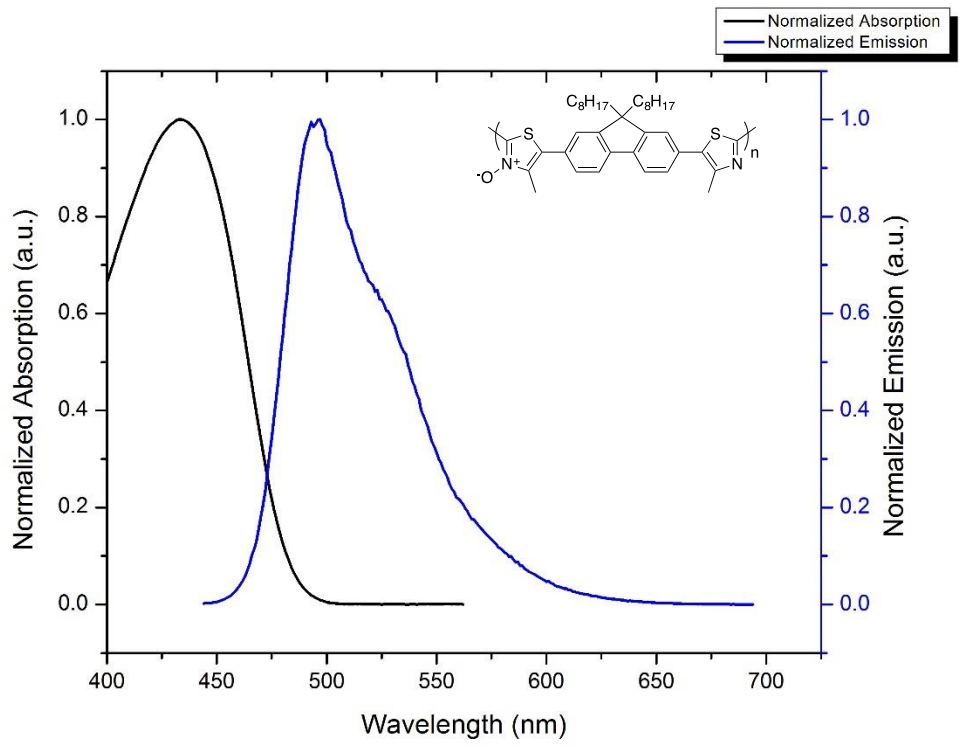
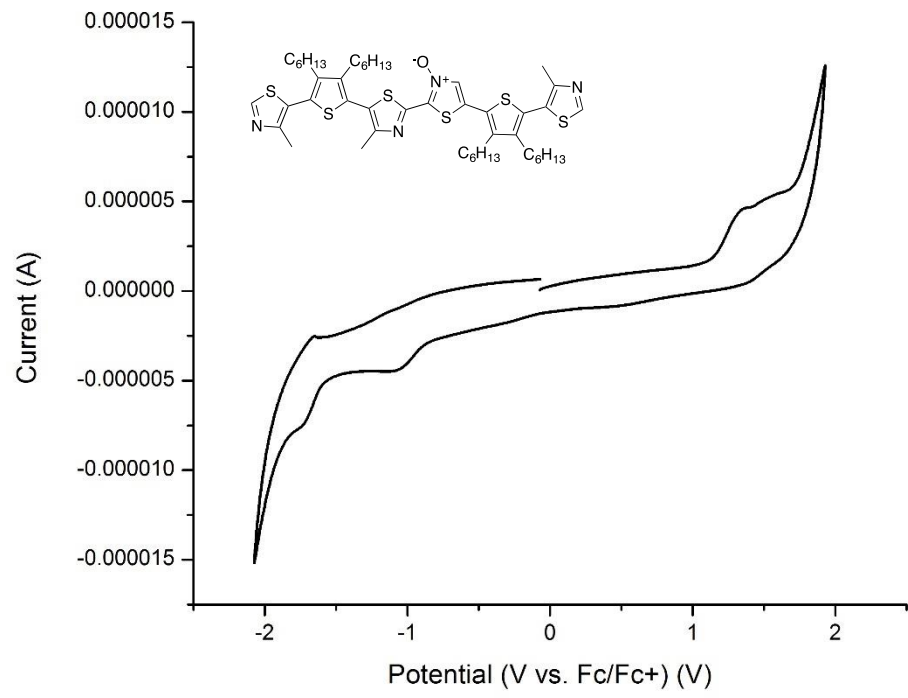


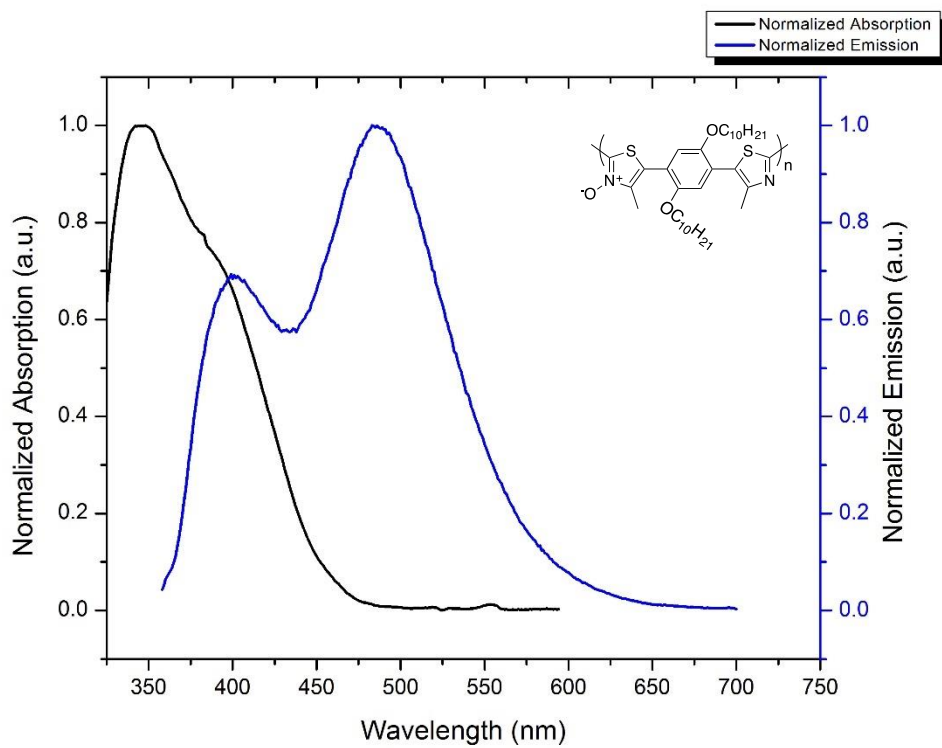
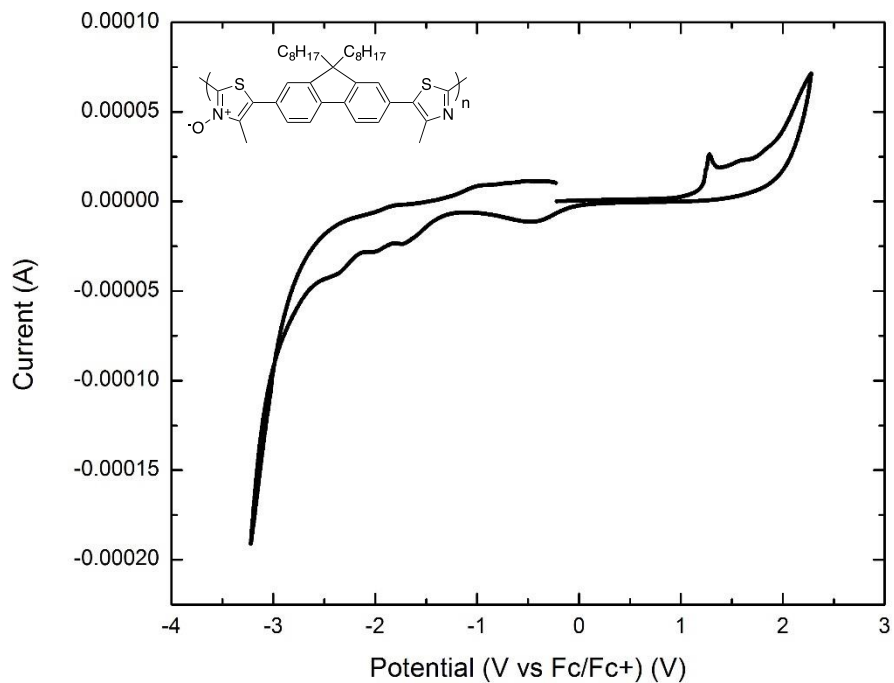


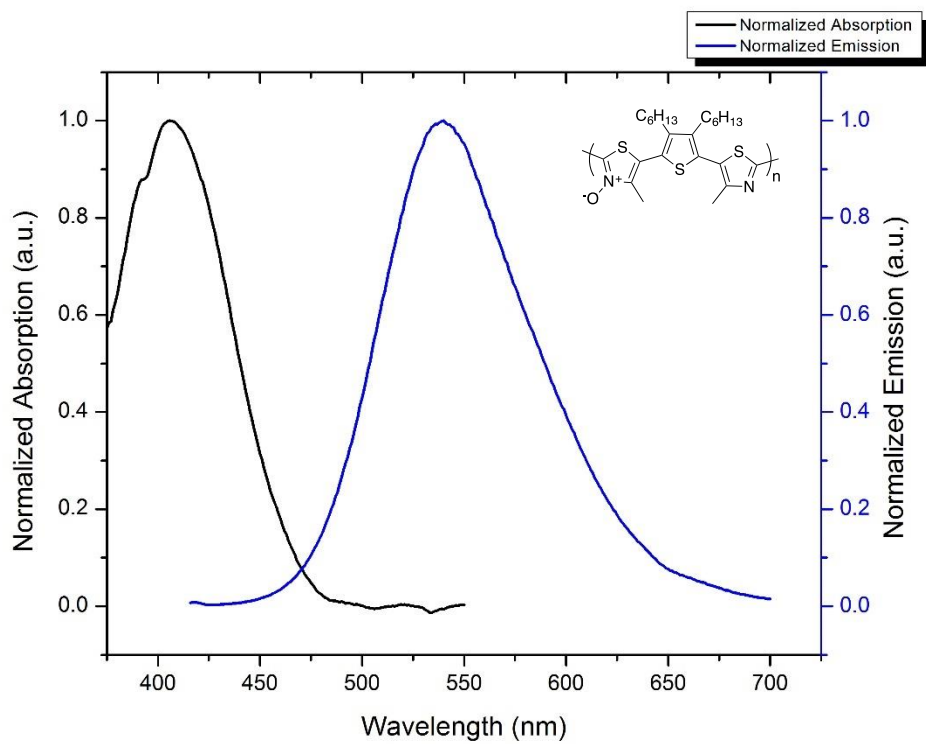
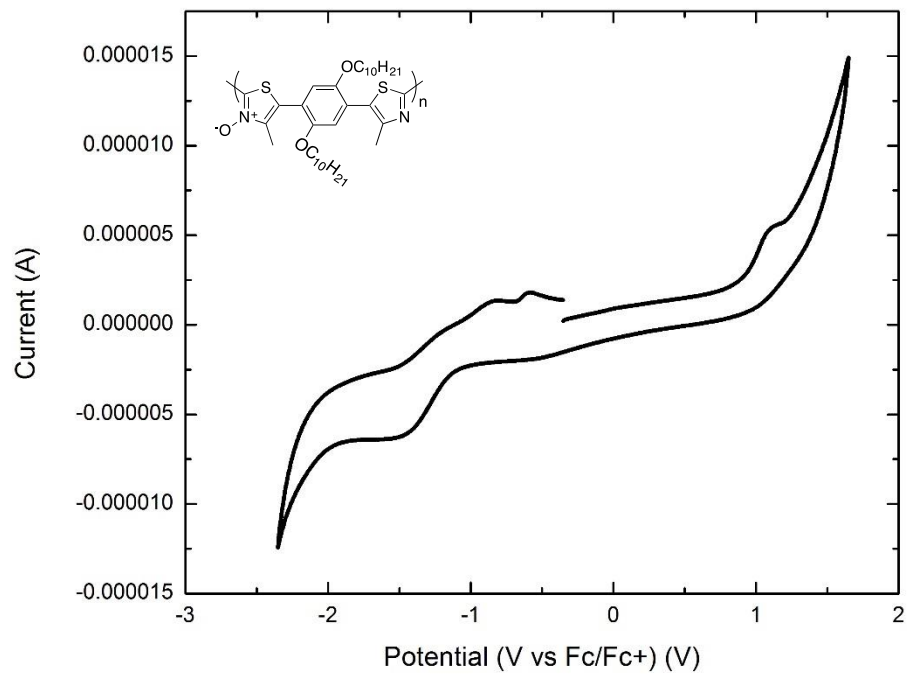


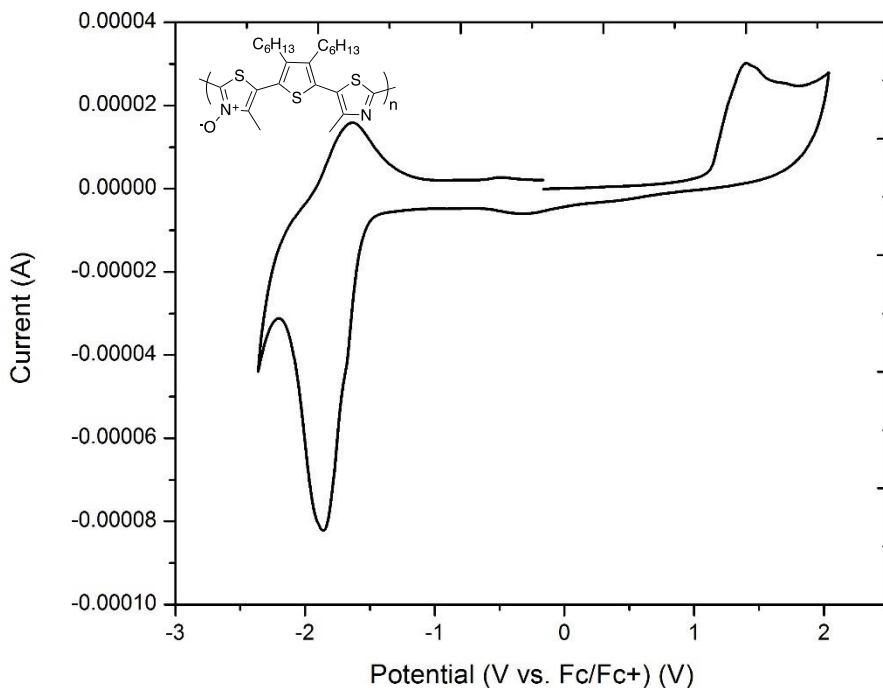








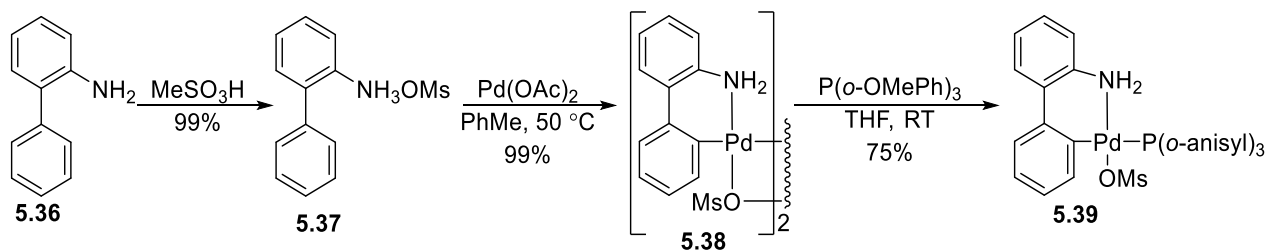




6.4 SYNTHETIC PROCEDURES-CHAPTER 5

Synthesis of $P(o\text{-OMePh})_3$ Precatalyst (**5.39**):

Compounds (**5.37**) and (**5.38**) were synthesized according to the procedure outlined in Buchwald *et al.*³⁸²



$P(o\text{-anisyl})_3$ Palladium Precatalyst (5.39**):** A flame dried 2 mL microwave vial was charged with a magnetic stir bar, compound **5.38** 50 mg (0.07 mmol, 1 equiv), and $P(o\text{-OMePh})_3$ 47.7 mg (0.135 mmol, 2 equiv). The vial was then capped and purged with argon gas 3 times. THF (1.1 mL) was then added under a protective atmosphere and the reaction was allowed to proceed for 1 hour or until an off-white precipitate formed. After the allotted reaction time, 90% of the solvent was removed under vacuum and the remaining residue was triturated with pentane and

isolated via suction filtration. The off-white solid was then further dried under high vacuum for 24 hours. Yield 71.42 mg (73%). Single crystal suitable for X-ray diffraction was grown through slow evaporation in CHCl₃.

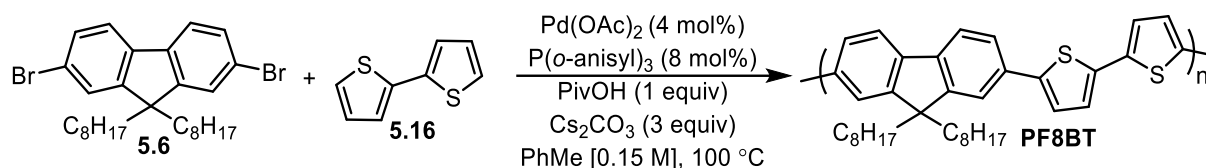
¹H NMR (300 MHz, CDCl₃, 293K, CDCl₃): 7.44 (m, 3H), 7.33 (m, 5H), 7.21 (m, 6H), 6.83 (m, 5H), 6.70 (broad s, 3H), 6.45 (m, 2H), 4.43 (s, 1H), 3.35 (s, 9H), 2.15 (s, 3H)

¹³C NMR (75 MHz, CDCl₃, 293K, CDCl₃): 160.8, 140.2, 138.7, 136.5, 135.5, 135.3, 132.2, 128.0, 127.4, 126.8, 125.4, 125.1, 124.8, 120.6, 120.6, 120.4, 120.2, 116.8, 111.0, 55.3, 38.5

³¹P NMR (121 MHz, CDCl₃, 293K, H₃PO₄): 19.9

Time vs. Molecular weight experiments for of Poly(9,9-dioctyl-2,7-fluorene-alt-2,2'-bithiophene) (PF8BT).

PF8BT synthesized using Pd(OAc)₂/ P(*o*-anisyl)₃:Condition A



The polymerization of PF8BT was done according to the procedure outlined by Leclerc *et al.*¹⁷⁴ A flame dried 5 mL microwave vial with a magnetic stir bar was charged with 50.4 mg (0.300 mmol, 1 equiv) of 2,2'-bithiophene, 165 mg of 9,9-dioctyl-2,7- dibromofluorene (0.300 mmol, 1 equiv), 30.3 mg of pivalic acid (0.300 mmol, 1 equiv), 8.6 mg of P(*o*-OMePh)₃ (0.02 mmol, 0.08 equiv), 3.1 mg of Pd(OAc)₂ (0.010 mmol, 0.05 equiv) and 293 mg of Cs₂CO₃ (0.900 mmol, 3 equiv). The vial was sealed and freeze-dried by repeatedly cooling with liquid nitrogen and then drying under high vacuum. The reaction vessel was then purged twice with argon gas. After purging, dry toluene 2 mL [0.15 M] was added to the reaction vessel under a protective atmosphere and then the reaction was set to stir at 100 °C. At the time intervals listed below an aliquot of approximately 0.1 mL was extracted from the reaction mixture and without further purification analyzed by GPC. The reaction was then repeated as listed above without removing any aliquots to obtain the reaction yield. Upon completing the reaction time, the reaction mixture was

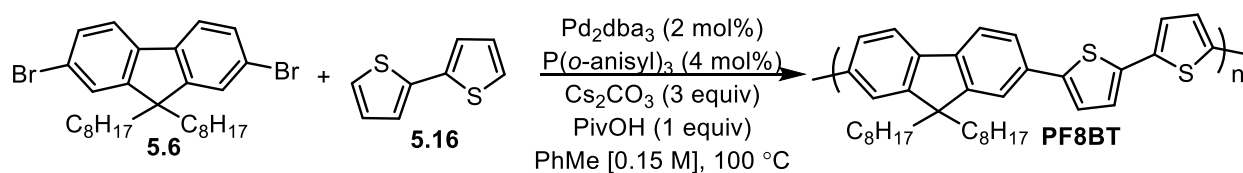
cooled to room temperature and the **PF8BT** was precipitated in a solution of vigorously stirring cold methanol revealing a fibrous yellow polymer. (147 mg, 89%) **PF8BT** displayed identical spectra to previously reported.¹⁷⁴

¹H NMR (300 MHz, TCE, 353K): 7.68 (d, *J* = 7.9 Hz, 2H), 7.69 (d, *J* = 7.7 Hz, 2H), 7.57 (bs, 2H), 7.30 (d, *J* = 2.8 Hz, 2H), 7.21 (d, *J* = 2.8 Hz, 2H), 2.13 (m, 4H), 1.21 (m, 6H), 1.10 (m, 18H), 0.90 (t, *J* = 6.9 Hz, 6H).

Reaction time (min)	M _n (g/mol)	M _w (g/mol)	PDI
10	1536	1568	1.0
20	1866	2124	1.1
30	2001	2441	1.2
40	2454	3287	1.3
60	3803	4925	1.3
90	5534	9388	1.7
120	10584	25016	2.4
150	10733	37372	3.5
210	7918	20446	2.6

Table S10- Time vs. Molecular weight data for **PF8BT** using Pd(OAc)₂/P(*o*-anisyl)₃

PF8BT synthesized using Pd₂dba₃/P(*o*-anisyl)₃: Condition B



The polymerization of **PF8BT** was done according to the procedure outlined by Leclerc *et al.*¹⁷⁴ A flame dried 5 mL microwave vial with a magnetic stir bar was charged with 74.8 mg (0.450 mmol, 1 equiv) of 2,2'-bithiophene, 246 mg of 9,9-dioctyl-2,7-dibromofluorene (0.450 mmol, 1 equiv), 46.0 mg of pivalic acid (0.450 mmol, 1 equiv), 6.5 mg Pd₂dba₃ (9.00 μmol, 0.02 equiv), and 440 mg of Cs₂CO₃ (1.35 mmol, 3 equiv). The vial was sealed and freeze-dried by repeatedly cooling with liquid nitrogen and then drying under high vacuum. The reaction vessel was then purged twice with argon gas. After purging, dry toluene 5 mL [0.15 M] was added to the reaction vessel under a protective atmosphere and then the reaction was set to stir at 100 °C. At the time intervals listed below an aliquot of approximately 0.1 mL was extracted from the reaction mixture and without further purification analyzed by GPC. The reaction was then repeated as listed above without removing any aliquots in order to obtain the reaction yield. Upon completing the reaction time, the reaction mixture was cooled to room temperature and the **PF8BT** was

precipitated in a solution of vigorously stirring cold methanol revealing a fibrous yellow polymer. (231 mg, 93%)

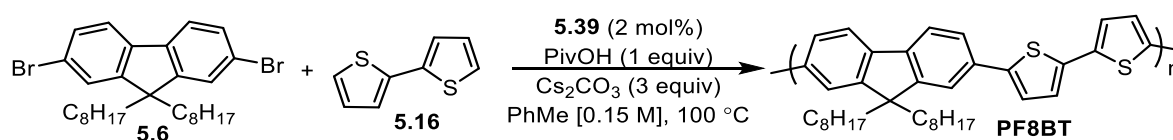
PF8BT displayed identical spectra to previously reported.¹⁷⁴

¹H NMR (300 MHz, TCE, 353K): 7.68 (d, *J* = 7.9 Hz, 2H), 7.69 (d, *J* = 7.7 Hz, 2H), 7.57 (bs, 2H), 7.30 (d, *J* = 2.8 Hz, 2H), 7.21 (d, *J* = 2.8 Hz, 2H), 2.13 (m, 4H), 1.21 (m, 6H), 1.10 (m, 18H), 0.90 (t, *J* = 6.9 Hz, 6H).

Reaction time (min)	M _n (g/mol)	M _w (g/mol)	PDI
60	1472	3375	2.3
120	5841	21013	3.6
150	12838	47026	3.7
180	10679	44448	4.2
210	8789	41363	4.7

Table S11- Time vs. Molecular weight data for **PF8BT** using Pd(OAc)₂/P(*o*-anisyl)₃

PF8BT Synthesized using precatalyst (5.39): Condition C



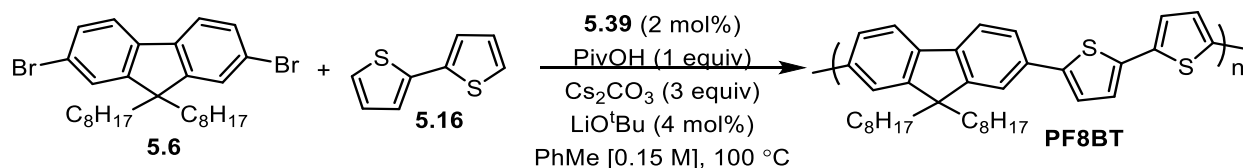
The polymerization of **PF8BT** was done according to the procedure outlined by Leclerc *et al.*¹⁷⁴ A flame dried 5mL microwave vial with a magnetic stir bar was charged with 75.3 mg (0.45 mmol, 1 equiv) of 2,2'-bithiophene, 247 mg of 9,9-dioctyl-2,7- dibromofluorene (0.450 mmol, 1 equiv), 46.0 mg of pivalic acid (0.450 mmol, 1 equiv), 6.5 mg of P(*o*-OMePh)₃ palladium pre-catalyst (9.00 μmol, 0.02 equiv), and 440 mg of Cs₂CO₃ (1.35 mmol, 3 equiv). The vial was sealed and freeze-dried by repeatedly cooling with liquid nitrogen and then drying under high vacuum. The reaction vessel was then purged twice with argon gas. After purging, dry toluene 5 mL [0.15 M] was added to the reaction vessel under a protective atmosphere and then the reaction was set to stir at 100 °C. At the time intervals listed below an aliquot of approximately 0.1 mL was extracted from the reaction mixture and without further purification analyzed by GPC. The reaction was then repeated as listed above without removing any aliquots in order to obtain the reaction yield. Upon completing the reaction time, the reaction mixture was cooled to room temperature and the **PF8BT** was precipitated in a solution of vigorously stirring cold methanol revealing a fibrous yellow polymer. (239 mg, 96%) **PF8BT** displayed identical spectra to previously reported.¹⁷⁴

¹H NMR (300 MHz, TCE, 353K): 7.68 (d, *J* = 7.9 Hz, 2H), 7.69 (d, *J* = 7.7 Hz, 2H), 7.57 (bs, 2H), 7.30 (d, *J* = 2.8 Hz, 2H), 7.21 (d, *J* = 2.8 Hz, 2H), 2.13 (m, 4H), 1.21 (m, 6H), 1.10 (m, 18H), 0.90 (t, *J* = 6.9 Hz, 6H).

Reaction time (min)	M _n (g/mol)	M _w (g/mol)	PDI
60	1600	1636	1.0
120	1743	1808	1.0
180	1999	2219	1.1
240	2273	2687	1.2
300	2652	3440	1.3
360	3629	5226	1.4
420	6173	10719	1.7
480	13592	26376	1.9
540	22629	53992	2.4
600	31447	73154	2.3
660	34371	76634	2.2
720	25594	75424	2.9
780	25594	75424	2.9

Table S12- Time vs. Molecular weight data for **PF8BT** using precatalyst (**5.39**)

PF8BT synthesized using Precatalyst (**5.39**) plus LiO^tBu: Condition D



The polymerization of **PF8BT** was done according to the procedure outlined by Leclerc *et al.*¹⁷⁴ A flame dried 5 mL microwave vial with a magnetic stir bar was charged with 25.4 mg (0.150 mmol, 1 equiv) of 2,2'-bithiophene, 83.4 mg of 9,9-dioctyl-2,7-dibromofluorene (0.150 mmol, 1 equiv), 15.7 mg of pivalic acid (0.15 mmol, 1 equiv), 2.3 mg of P(*o*-OMePh)₃ palladium pre-catalyst (3.0 μmol, 0.02 equiv), 0.5 mg of LiO^tBu (0.006 mmol, 0.04 equiv) and 150 mg of Cs₂CO₃ (0.45 mmol, 3 equiv). The vial was sealed and freeze-dried by repeatedly cooling with liquid nitrogen and then drying under high vacuum. The reaction vessel was then purged twice with argon gas. After purging, dry toluene 1 mL [0.15 M] was added to the reaction vessel under a protective atmosphere and then the reaction was set to stir at 100 °C. At the time intervals listed below an aliquot of approximately 0.05 mL was extracted from the reaction mixture and without further purification analyzed by GPC. The reaction was then repeated as listed above without removing any aliquots in order to obtain the reaction yield. Upon completing the reaction time, the reaction mixture was cooled to room temperature and the **PF8BT** was precipitated in a solution of vigorously stirring cold

methanol revealing a fibrous yellow polymer. (72 mg, 87%) **PF8BT** displayed identical spectra to previously reported.¹⁷⁴

¹H NMR (300 MHz, TCE, 353K): 7.68 (d, *J* = 7.9 Hz, 2H), 7.69 (d, *J* = 7.7 Hz, 2H), 7.57 (bs, 2H), 7.30 (d, *J* = 2.8 Hz, 2H), 7.21 (d, *J* = 2.8 Hz, 2H), 2.13 (m, 4H), 1.21 (m, 6H), 1.10 (m, 18H), 0.90 (t, *J* = 6.9 Hz, 6H).

Reaction time (min)	M _n (g/mol)	M _w (g/mol)	PDI
60	1294	1465	1.1
120	2136	3210	1.5
180	3877	7457	1.9
240	6488	14097	2.2
300	20417	54769	2.6
330	17737	65315	3.7

Table S13- Time vs. Molecular weight data for PF8BT using precatalyst (**5.39**) with LiO^tBu as an additive.

Crystal and structure data for precatalyst (5.39)

Crystal Data Formula	C ₃₄ H ₃₄ N O ₆ P Pd S. 0.5 C ₆ H ₁₂		
Formula Weight	764.13		
Crystal System	monoclinic		
Space group	C2/c (No. 15)		
a, b, c [Angstrom]	27.2958(11)	10.3051(4)	25.7535(10)
alpha, beta, gamma [deg]	90	109.1286(17)	90
V [Ang ³]	6844.1(5)		
Z	8		
D(calc) [g/cm ³]	1.401		
Mu(MoKa) [/mm]	0.697		
F(000)	2960		
Crystal Size [mm]	0.04 x 0.11 x 0.14		

Data Collection

Temperature (K)	296
Radiation [Angstrom]	MoKa 0.71073
Theta Min-Max [Deg]	1.6, 26.0
Dataset	-27: 33 ; -11: 12 ; -31: 31
Tot., Uniq. Data, R(int)	6711, 6711, 0.040
Observed Data [I > 2.0 sigma(I)]	4692

Refinement

Nref, Npar	6711, 403
R, wR2, S	0.0424, 0.0847, 1.33

$$w = \frac{1}{\sigma^2(F_o^2) + (0.0257P)^2} \text{ WHERE } P = \frac{(F_o^2 + 2F_c^2)}{3}$$

Max. and Av. Shift/Error 0.00, 0.00

Min. and Max. Resd. Dens. [e/Ang³] -0.41, 0.91

Table S14- Crystal and structure refinement data for **5.39**. Crystal structure of material was elucidated with the aid of the SQUEEZE function.

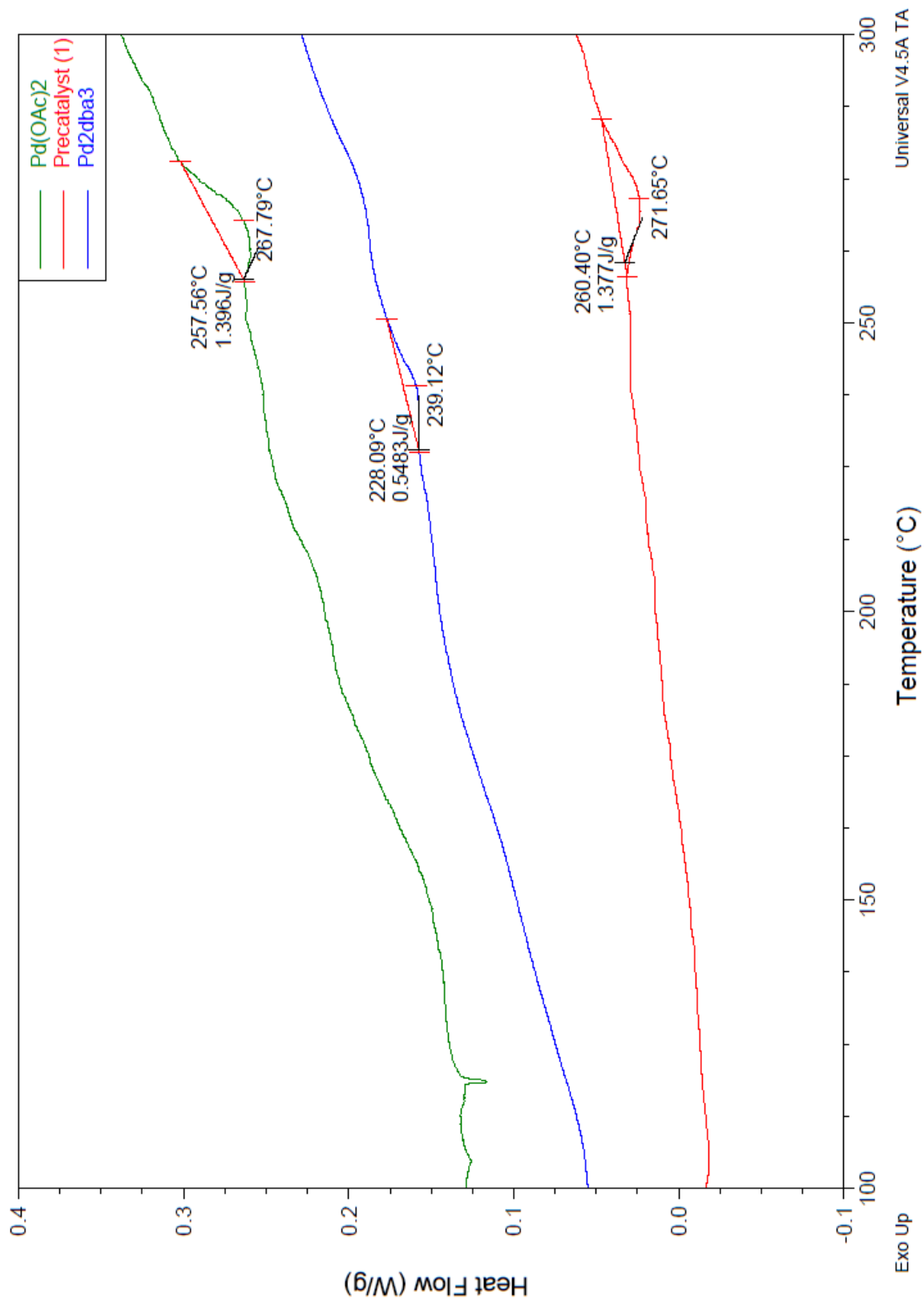
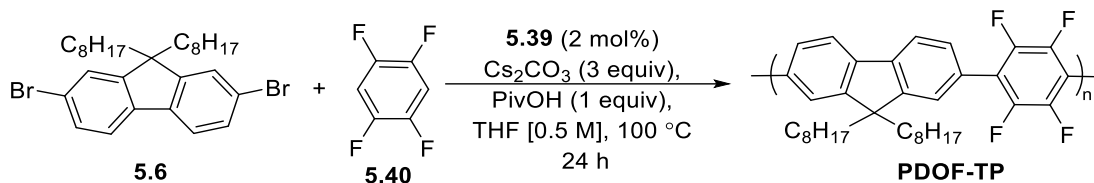


Figure S4- Differential calorimetry data for PF8BT made with conditions A, B, and C.

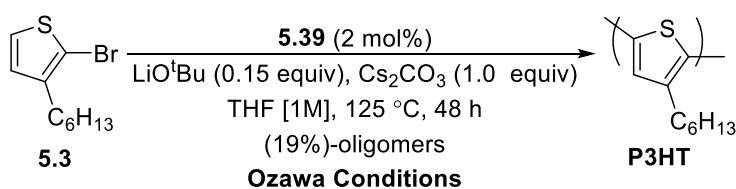
Synthesis of PDOF-TP using precatalyst (5.39)



The polymerization of **PDOF-TP** was done according to the procedure outlined by Ozawa *et al.*³³⁶ **5.6** (100.0 mg, 0.1824 mmol, 1 equiv), **5.40** (27.4 mg, 0.182 mmol, 1 equiv), **5.39** (1.43 mg, 2.00 μmol , 2 mol%), PivOH (18.6 mmol, 0.182 mmol, 1 equiv), and Cs_2CO_3 (178 mg, 0.546 mmol, 3 equiv) were added to a flame dried MW vial with a stir bar. The vial was then sealed and purged 3 times with Ar. THF (0.36 mL, 0.5 M) was then added and the reaction mixture was allowed to first stir for 30 min at room temperature and was then set to stir at 100 $^\circ\text{C}$ for 24 h. Following the reaction time, the mixture was diluted in CHCl_3 , washed twice with water and then 5 M HCl. The organic layer was then dried and concentrated under rotatory evaporation. **PDOF-TP** was then isolated following precipitation from vigorously stirring methanol as a white to light blue solid. (77 mg, 79%, $M_n = 15.0 \text{ kg mol}^{-1}$, $M_w = 53.3 \text{ kg mol}^{-1}$) **PDOF-TP** displayed identical spectra to previously reported.³³⁶

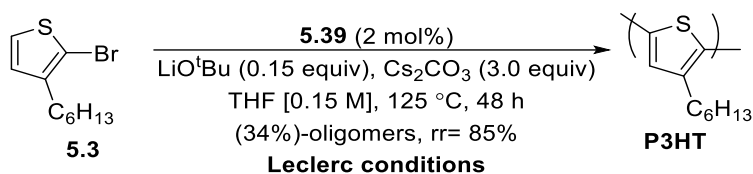
$^1\text{H NMR}$ (300 MHz, CDCl_3): 7.90 (d, $J = 8.1 \text{ Hz}$, 2H), 7.62-7.50 (m, 4H), 2.06 (m, 4H), 1.28-1.02 (m, 20H), 0.86-0.78 (m, 10H).

Synthesis of P3HT using precatalyst (5.39)



The polymerization of **P3HT** was done according to the procedure outlined by Ozawa *et al.*³¹⁹ To a flame dried MW vial **5.39** (5.8 mg, 8.0 μmol , 2 mol%), LiOtBu (4.7 mg, 0.061 mmol, 0.15 equiv), and Cs_2CO_3 (132 mg, 0.405 mmol, 1 equiv) were added. The vial was then sealed and purged with Ar followed by the addition of THF (0.42 mL, 1 M). **5.3** (100 mg, 0.4 mmol, 1 equiv) was then added and the vial was slowly heated to 125 $^\circ\text{C}$ where it was then allowed to stir for 48 h. Following the reaction time, the mixture was diluted in CHCl_3 and washed 3 times with water. The organic layer was dried and concentrated through rotatory evaporation. The solids were then dissolved in a

minimal amount of CHCl_3 and P3HT was precipitated with methanol. The methanol-precipitate solution was then centrifuged at 4000 rpm for 15 min. The supernatant was decanted, and the purple residue was dissolved in CHCl_3 and passed through a membrane filter (0.45 μm). The filtrate was then concentrated under vacuum to yield **P3HT** as a purple goo-like solid. (12 mg, 19%, Oligomers $M_n < 1500$)



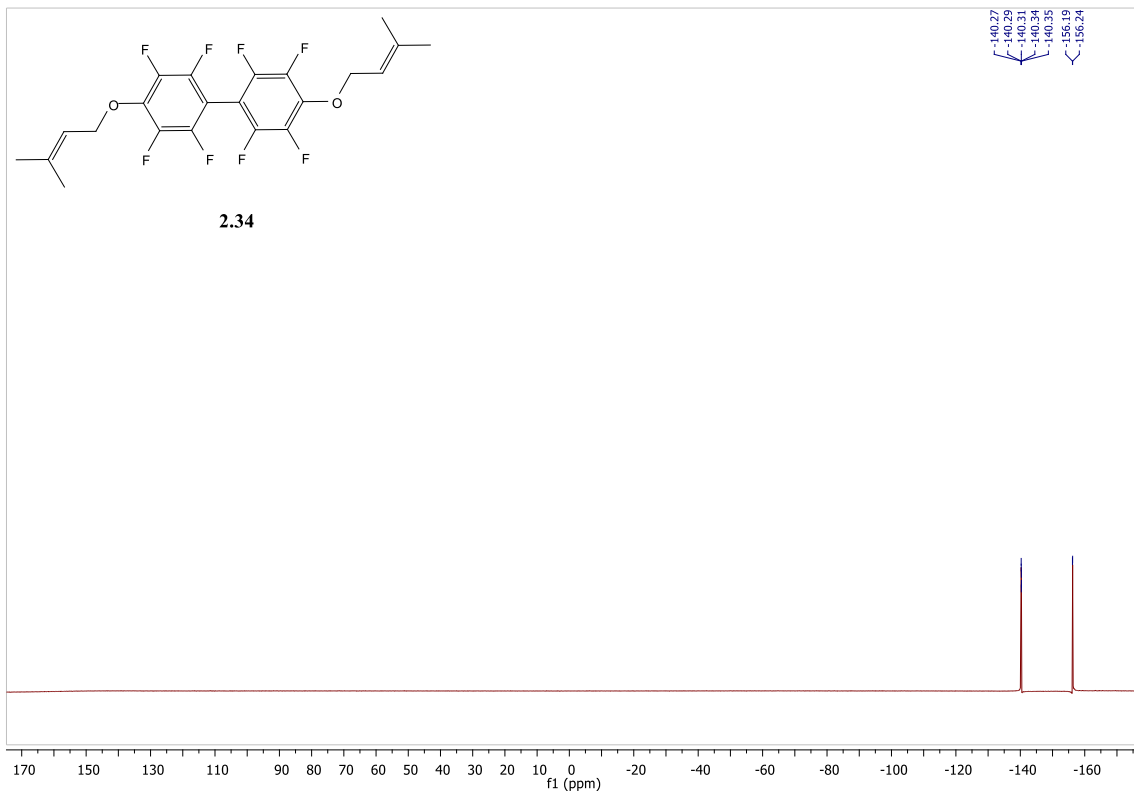
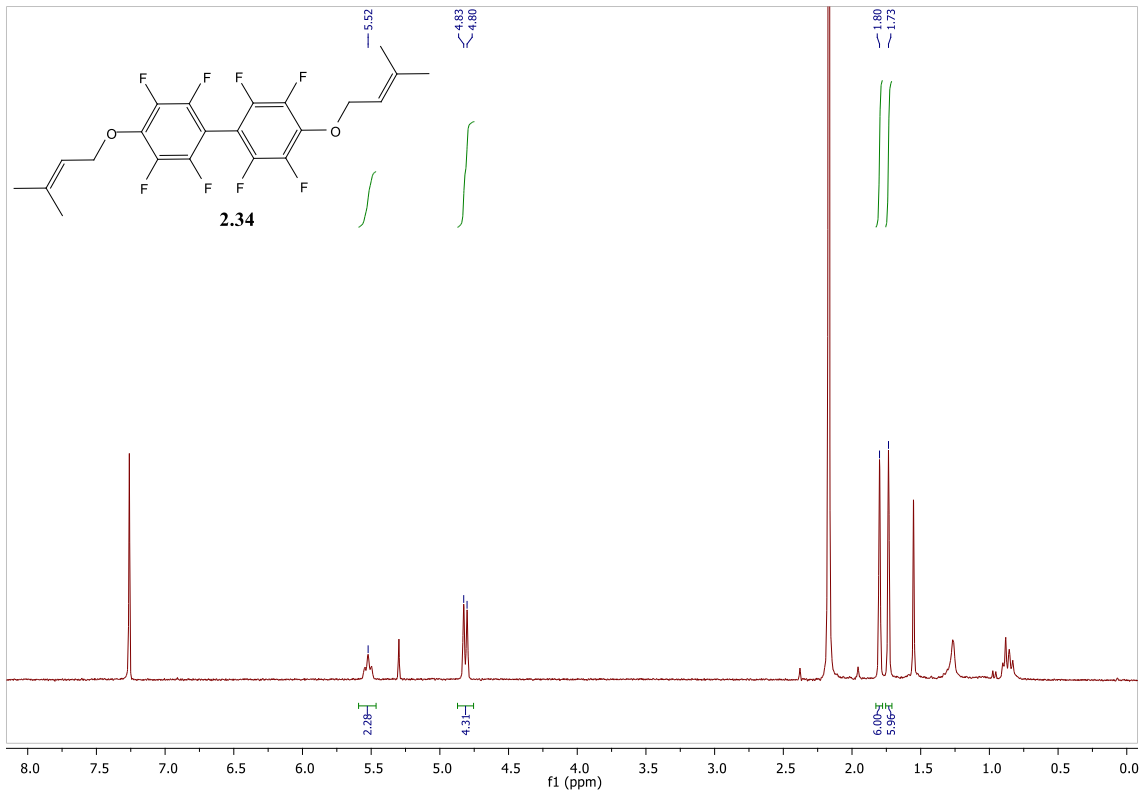
The polymerization of P3HT was done by modifying a procedure previously outlined by Leclerc *et al.*¹⁷⁴ To a flame dried MW vial **5.39** (5.8 mg, 8.0 μmol , 2 mol%), LiO^tBu (4.7 mg, 0.061 mmol, 0.15 equiv), PivOH (41.4 mg, 0.405 mmol, 1 equiv) and Cs_2CO_3 (398 mg, 1.22 mmol, 3 equiv) were added. The vial was then sealed and purged with Ar followed by the addition of THF (2.7 mL, 0.15 M). **5.3** (100 mg, 0.4 mmol, 1 equiv) was then added and the vial was slowly heated to 125 $^\circ\text{C}$ where it was then allowed to stir for 48 h. Following the reaction time, the mixture was diluted in CHCl_3 and washed 3 times with water. The organic layer was then dried and concentrated through rotatory evaporation. The solids were then dissolved in a minimal amount of CHCl_3 and P3HT was precipitated with methanol. The methanol-precipitate solution was then centrifuged at 4000 rpm for 15 min. The supernatant was decanted, and the purple residue was dissolved in CHCl_3 and passed through a membrane filter (0.45 μm). The filtrate was then concentrated under vacuum to yield P3HT as a purple goo-like solid. (23 mg, 34%, Oligomers $M_n < 3000$, rr=85%).

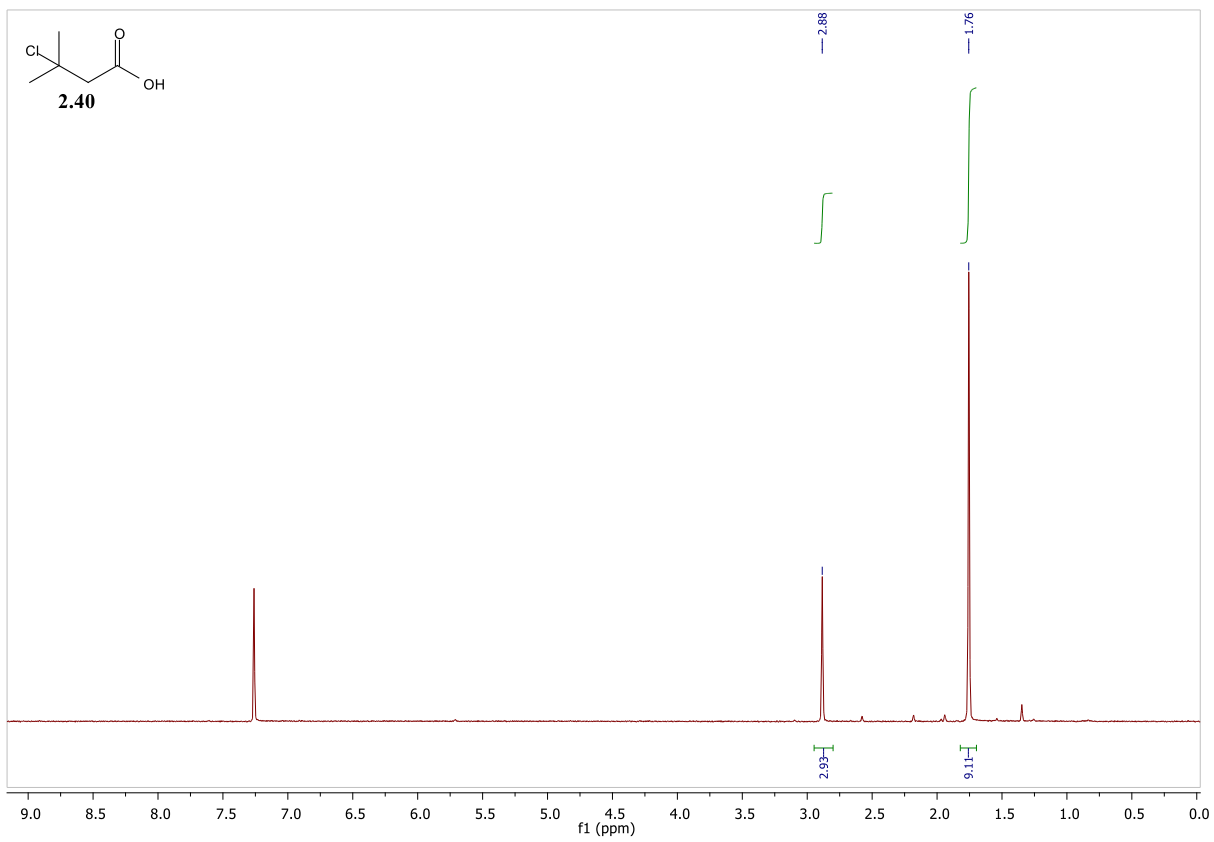
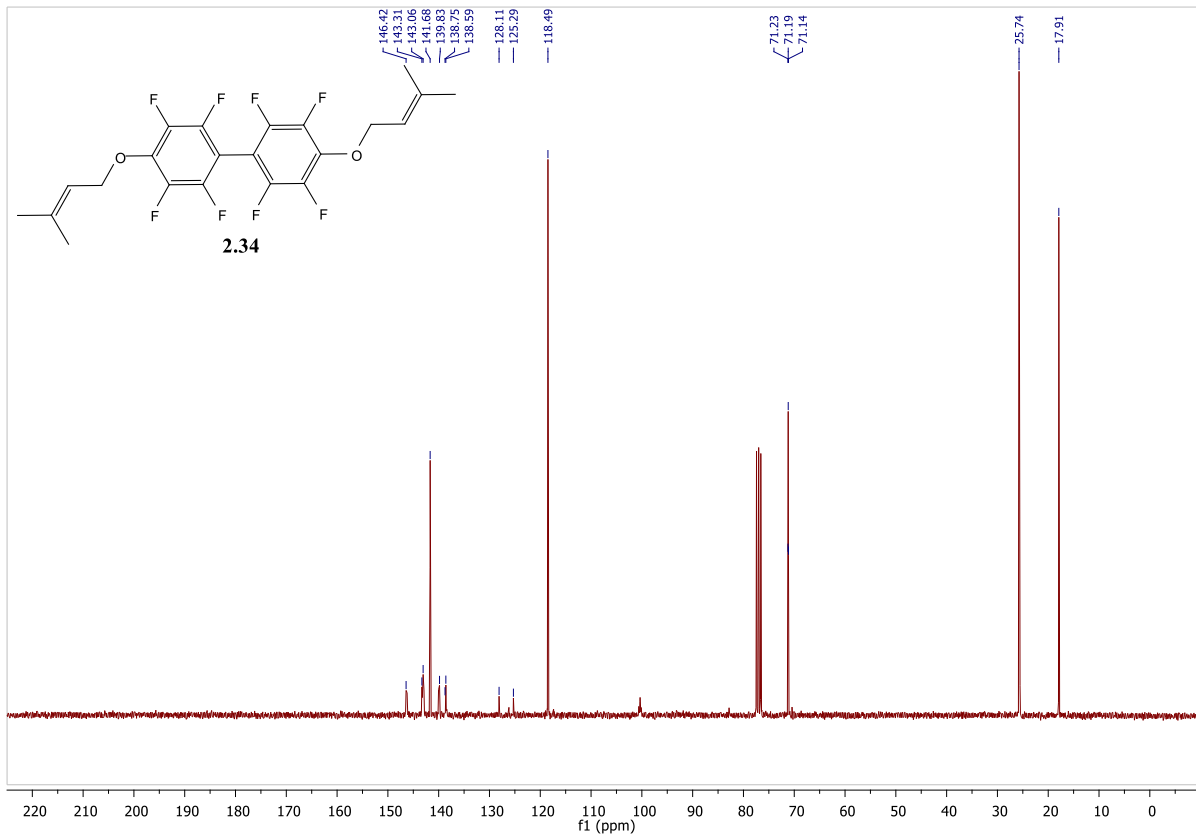
^1H NMR (300 MHz, CDCl_3): 6.98 (app s, 1H), 2.98 (app s, 2H), 1.68 (m, 2H), 1.42 (m, 2H), 0.90 (br s, 3H)

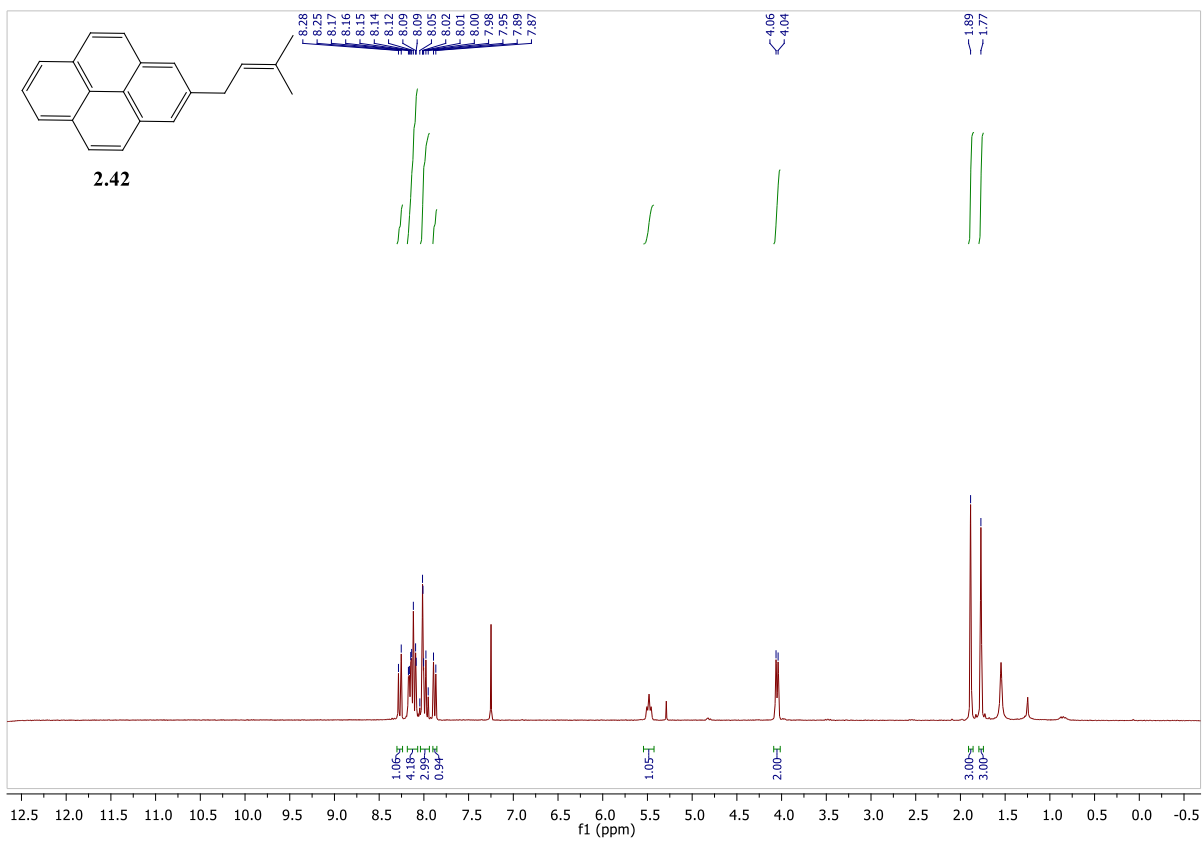
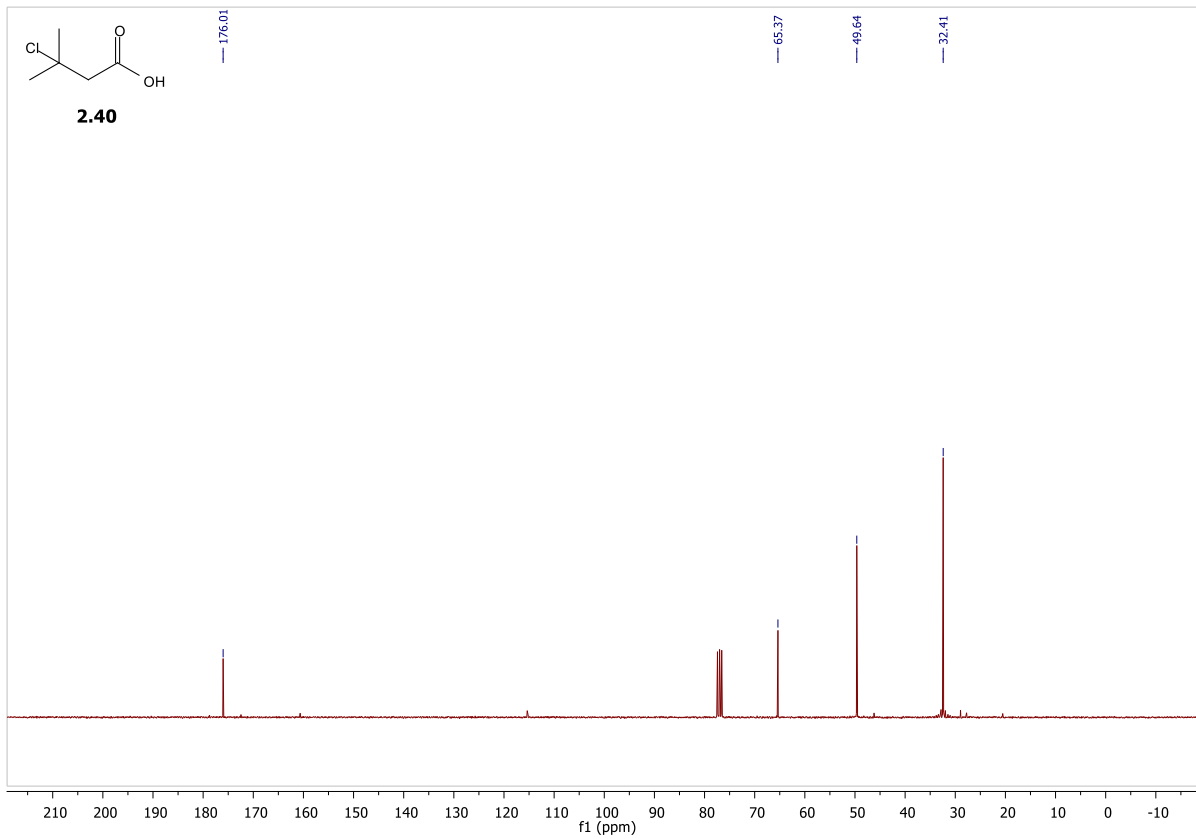
6.5 NMR SPECTRA FOR NOVEL COMPOUNDS

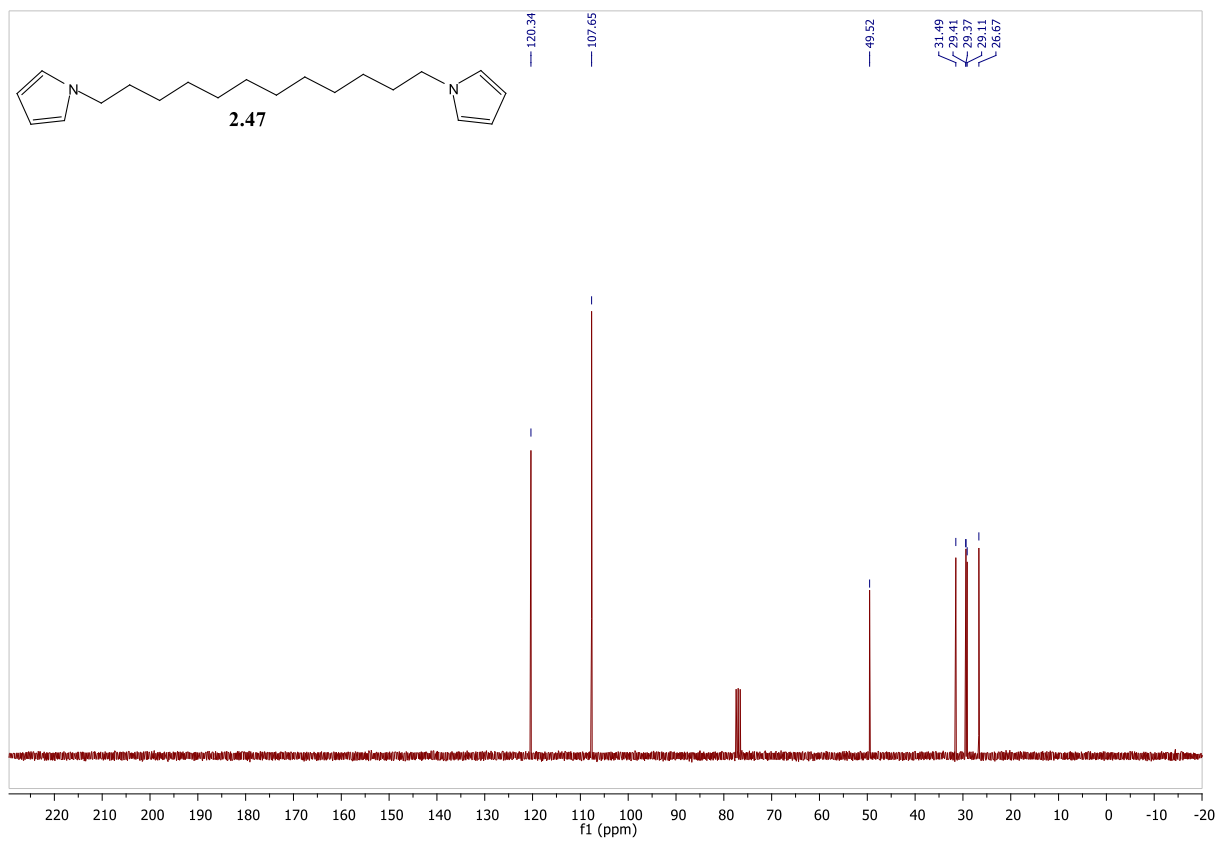
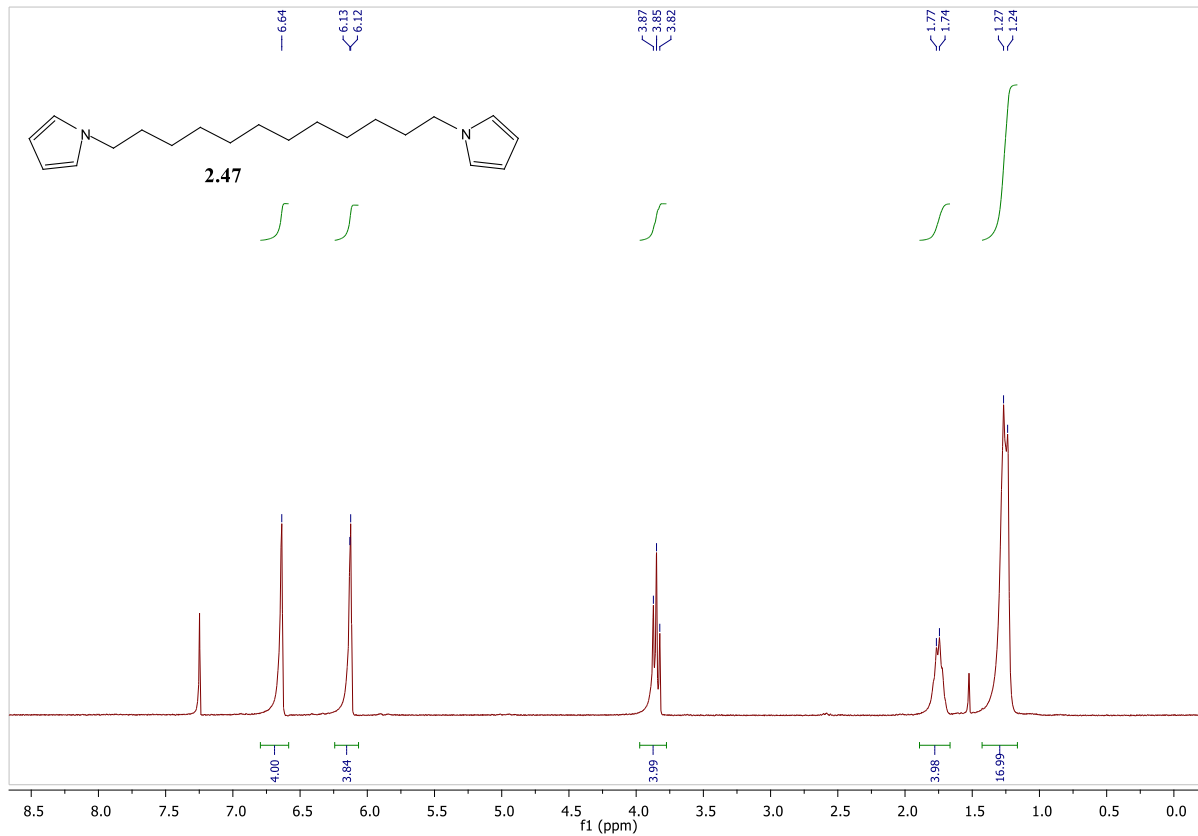
Compound	Page	Compound	Page	Compound	Page
2.34	303	3.140/3.141	340	4.96 + 4.97	386
2.40	304	3.140	341	4.98	387
2.42	305	3.143	342	4.99	388
2.47	306	3.144	345	4.100	389
2.74	307	3.145	346	4.101	389
2.75	308	3.146	347	4.102	390
2.76	309	3.147	348	4.103	390
2.77	310	3.148	349	4.104	391
2.87	310	3.149	350	5.39	392
2.101	311	3.150	351	PF8BT Condition A	394
2.102	312	3.151	353	PF8BT Condition B	394
2.114	313	3.155	353	PF8BT Condition C/D	395
2.220	314	4.49	354	P3HT made with 5.39	395
2.228	314	4.54	355	PDOF-TP made with 5.39	396
2.229	315	4.56	356		
2.236	316	4.57	357		
<i>syn</i> -2.237	317	4.58	358		
<i>anti</i> -2.237	318	4.60	359		
<i>syn</i> 2.238	319	4.61	360		
<i>anti</i> -2.238	319	4.62	361		
<i>syn</i> 2.239	320	4.63	362		
2.241	321	4.64	363		
2.242	321	4.65	364		
2.243	322	4.66	365		
2.253	323	4.67	366		
2.252	324	4.69	367		
3.64	324	4.70	368		
3.65	326	4.71	369		
3.106	328	4.72	369		
3.108	328	4.73	370		
3.109	329	4.74	371		
3.112	329	4.75	372		
3.111	330	4.76	373		
3.112	330	4.84	374		
3.114	331	4.85	375		
3.116	331	4.86	376		
3.117/3.124	332	4.87	377		
3.118	332	4.88	378		
3.119	333	4.89	379		
3.120	334	4.90	380		
3.123/3.138	335	4.91	381		
3.125/3.138	336	4.92	382		
3.126	338	4.93	383		
3.127	338	4.94	384		
3.128	339	4.95	385		

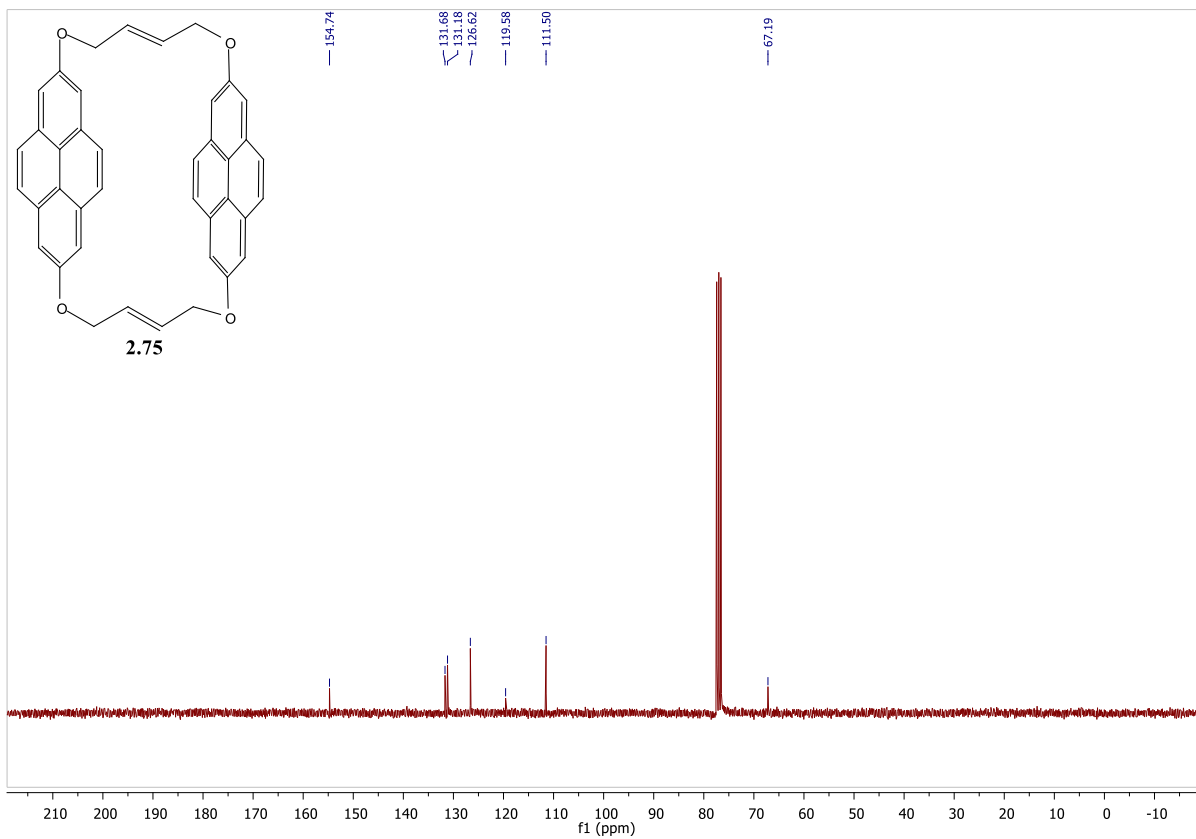
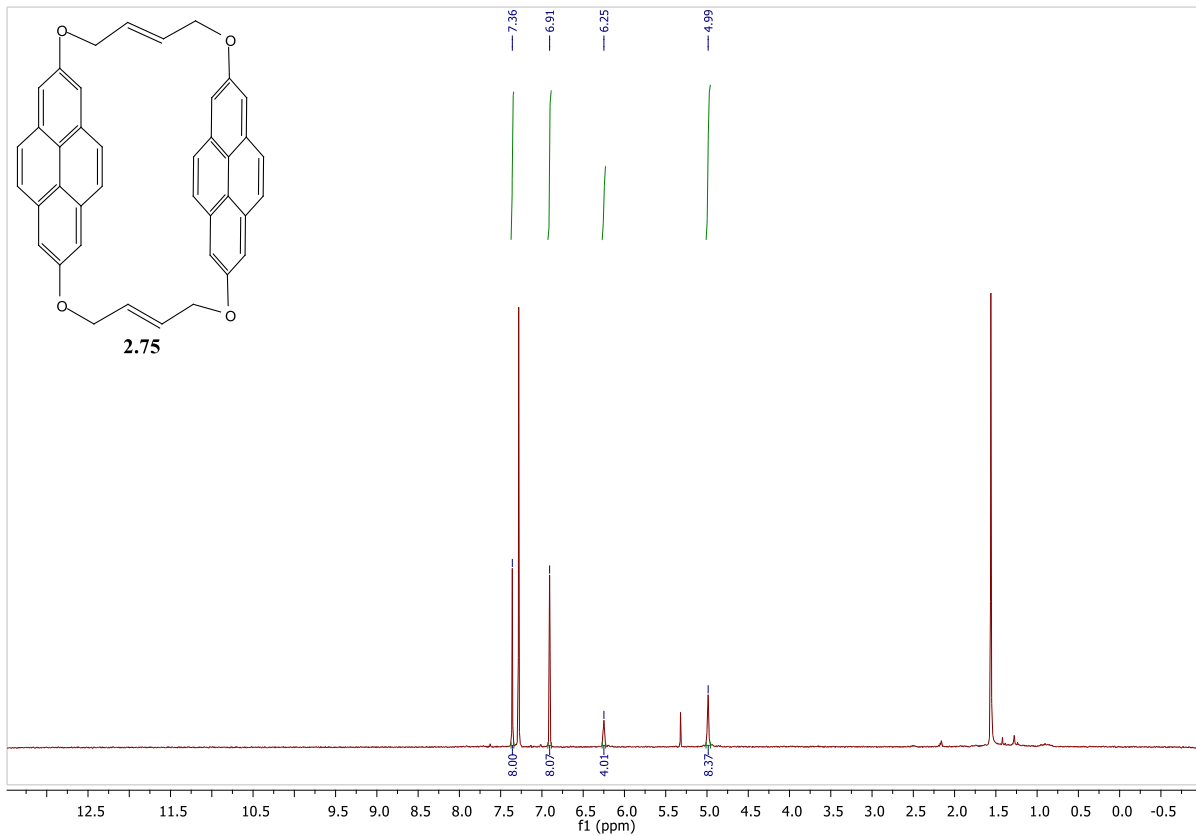
Table S15- Table of contents for compound NMR spectra.

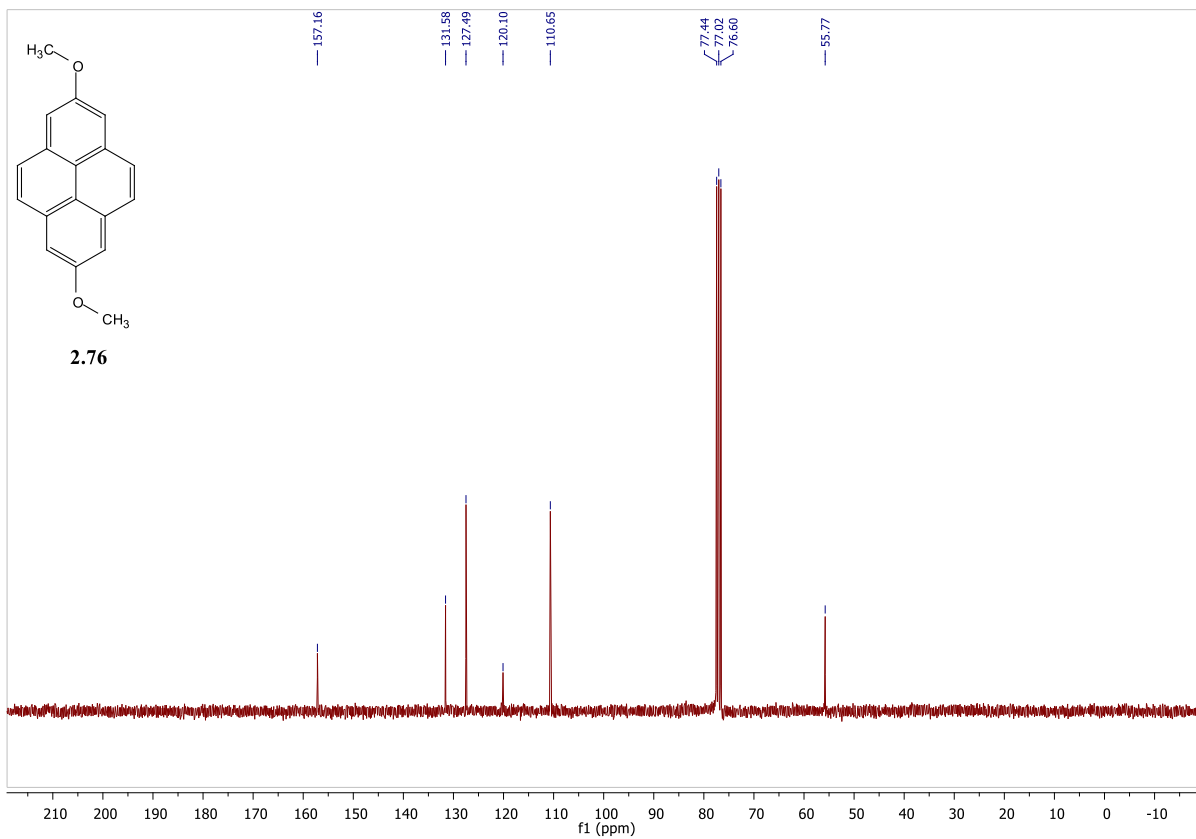
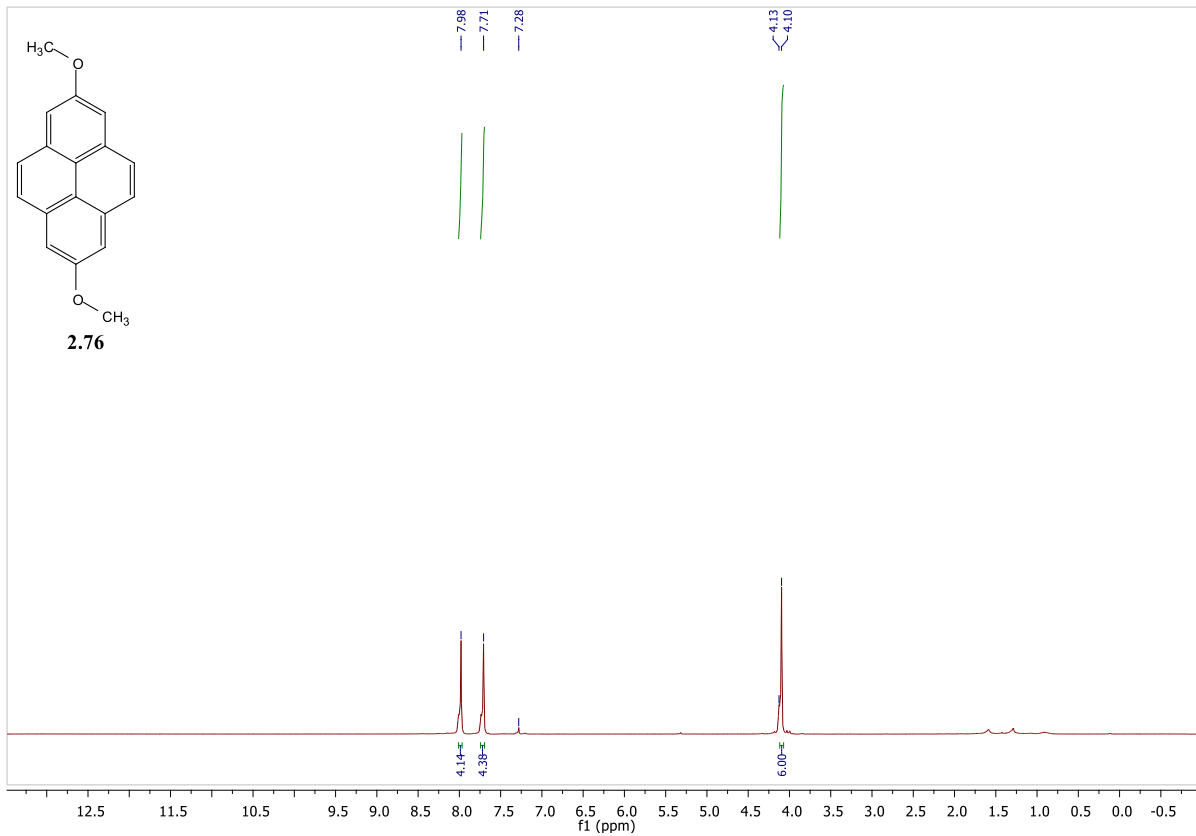


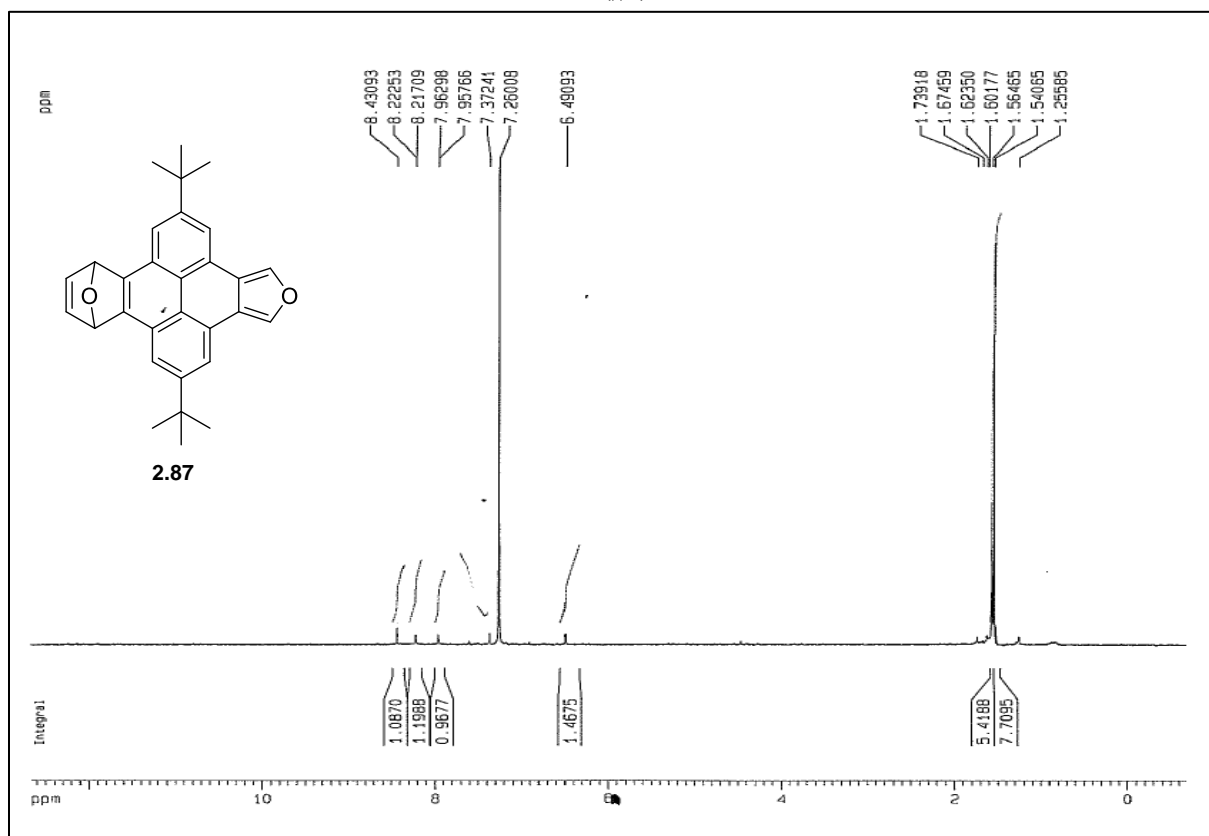
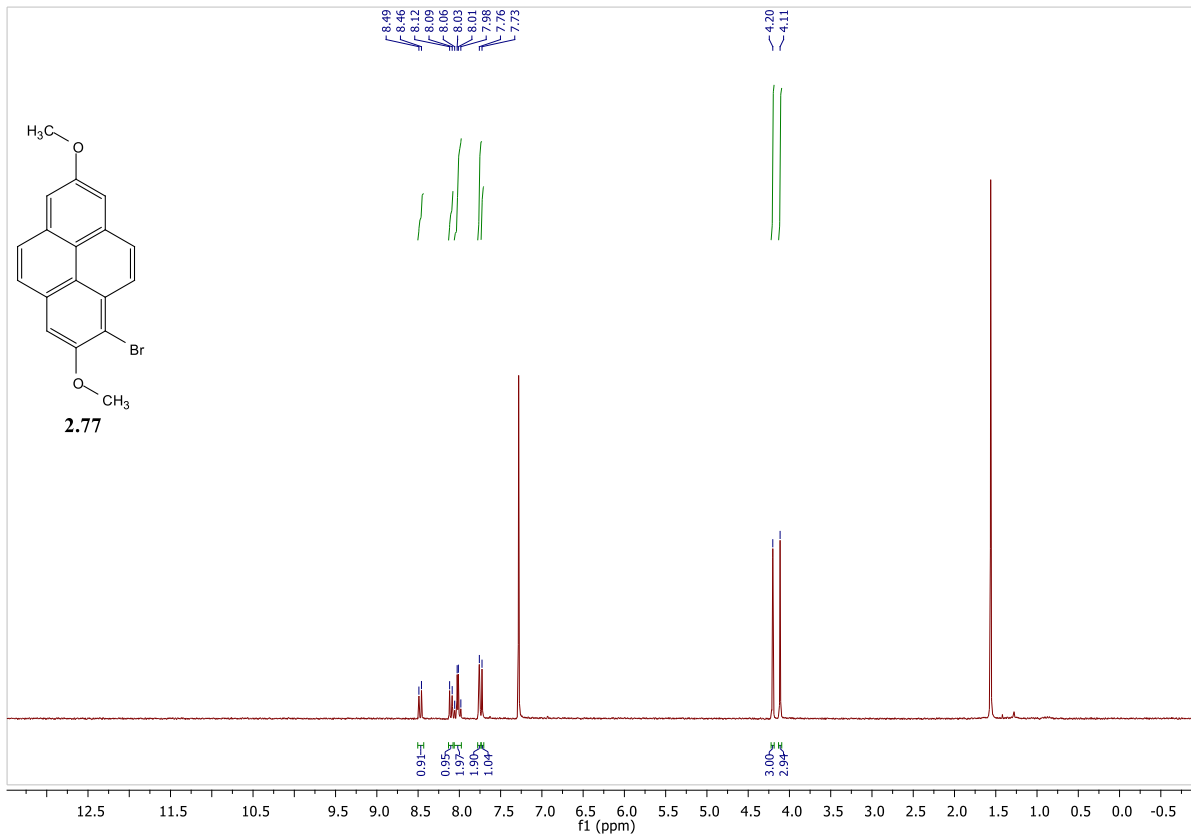


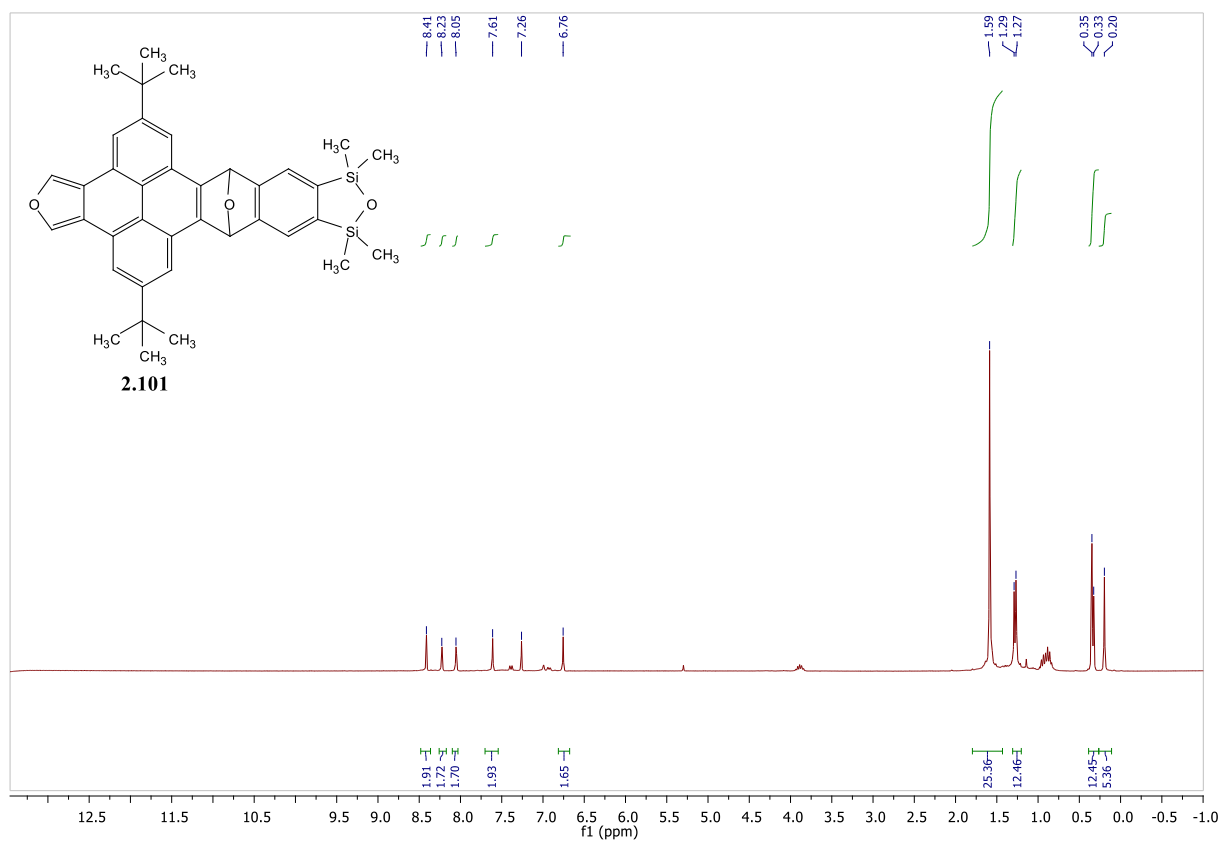
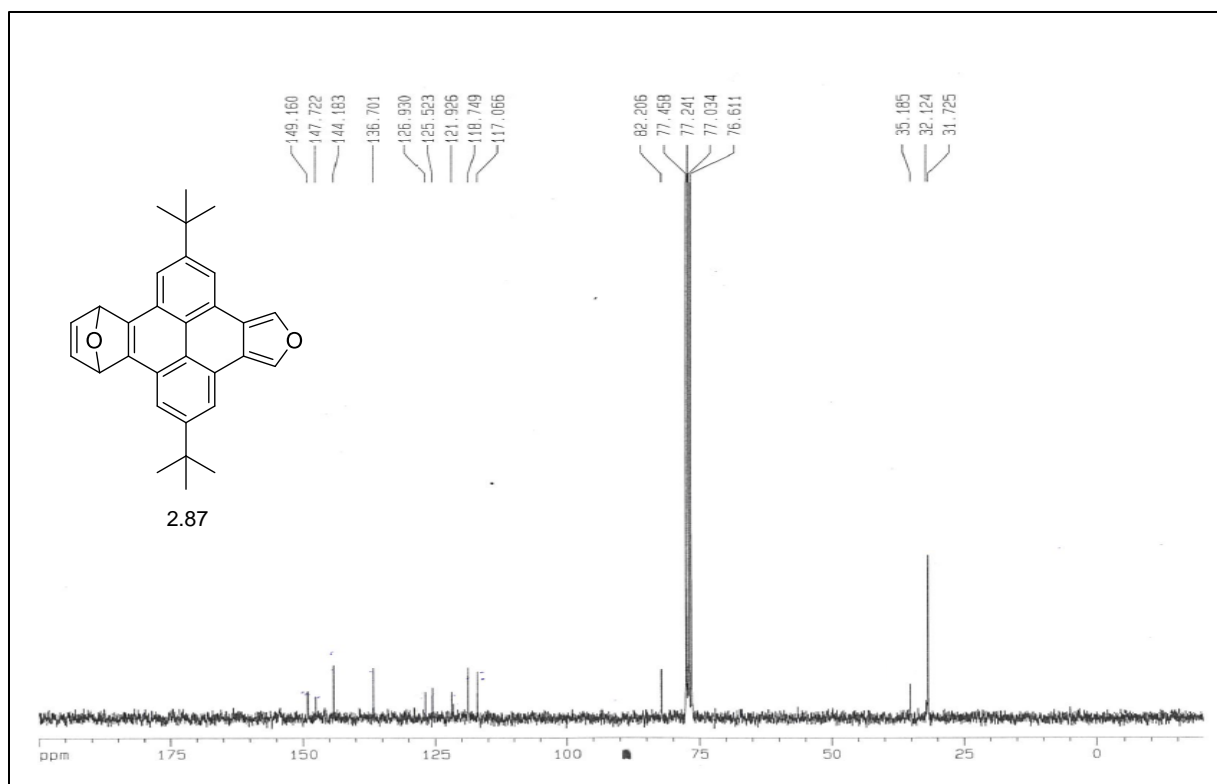


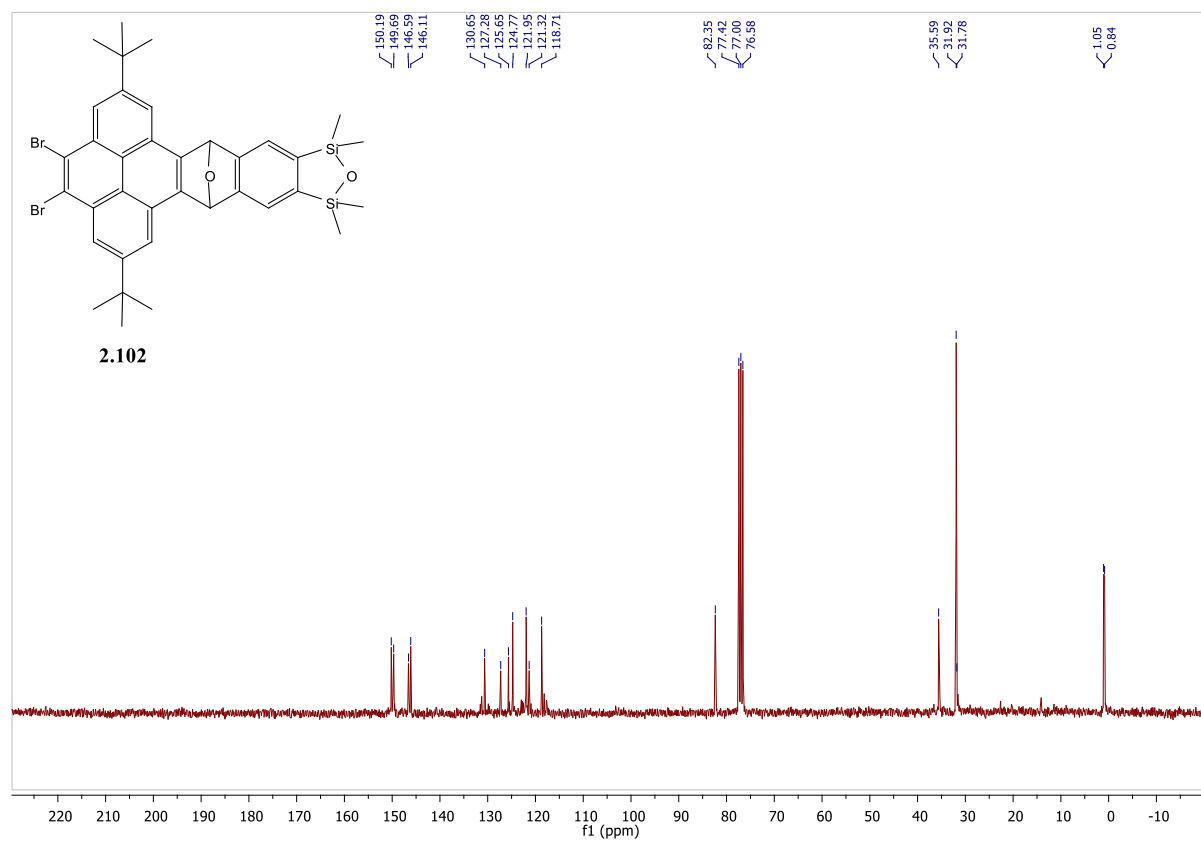
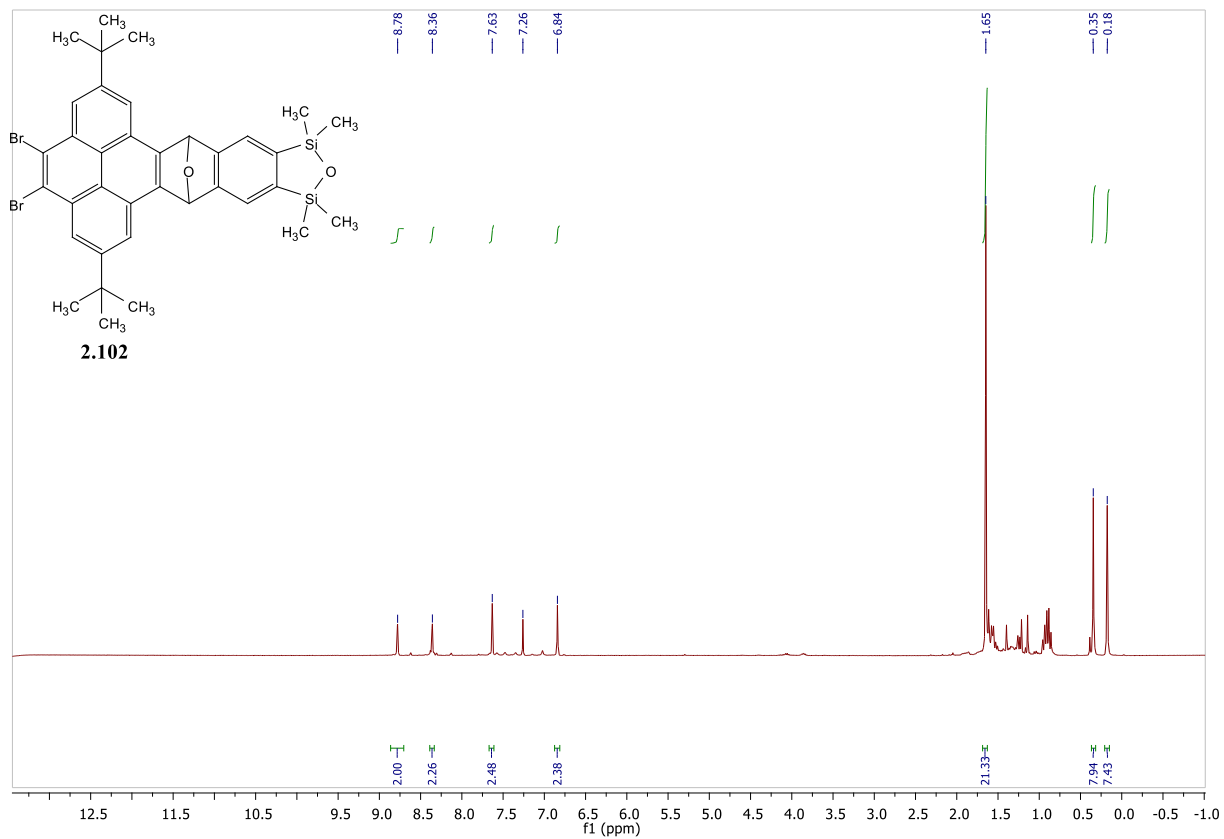


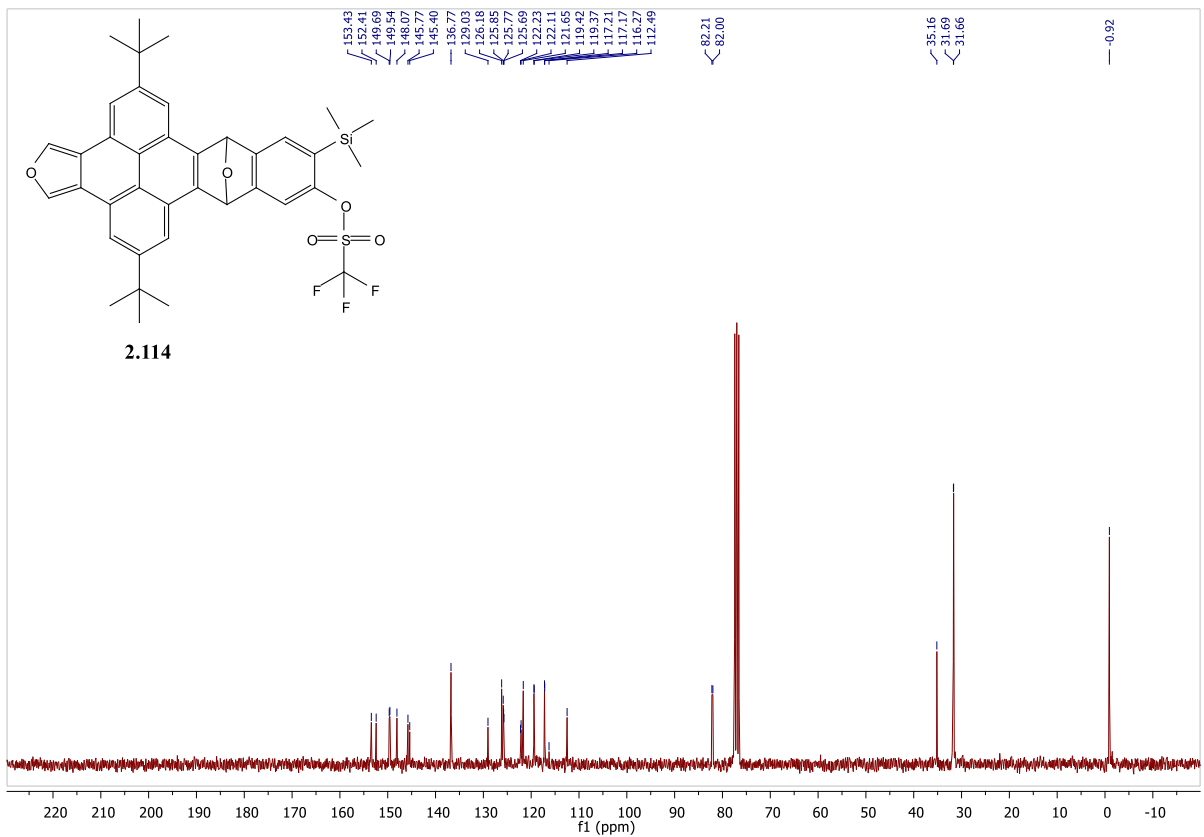
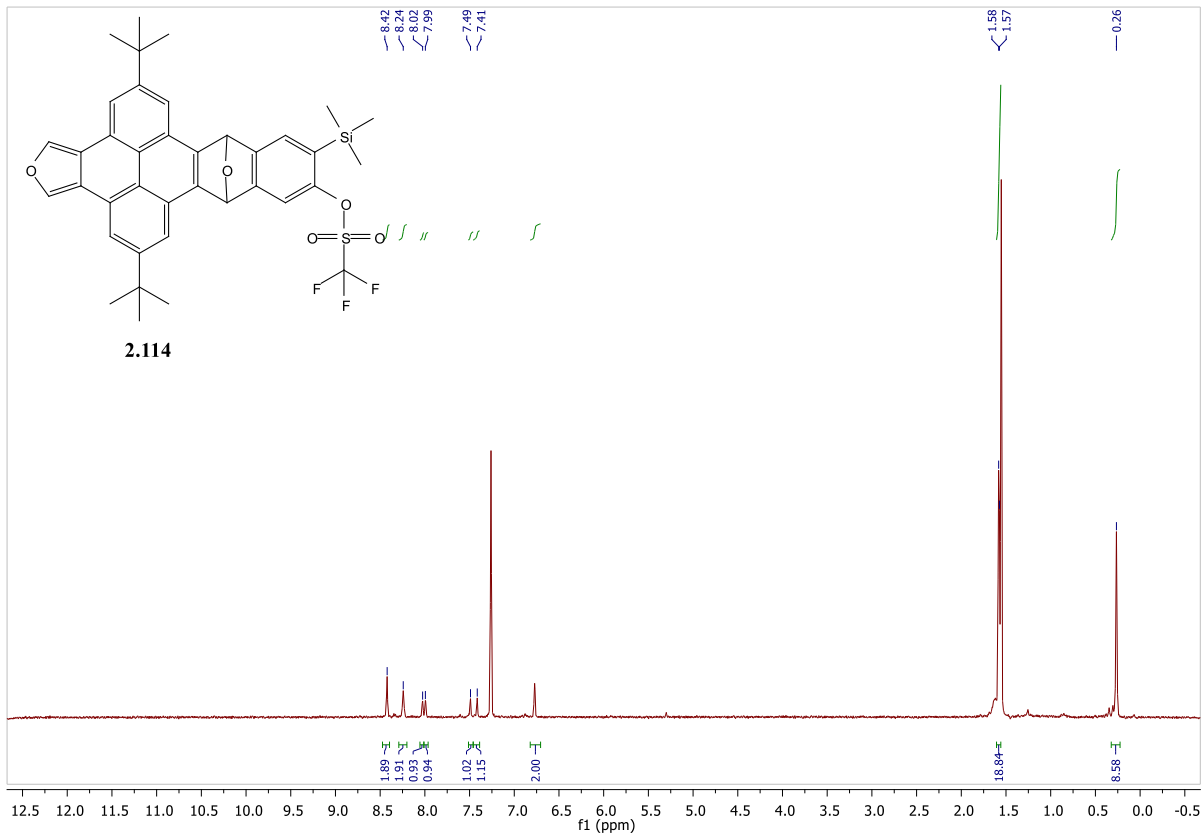


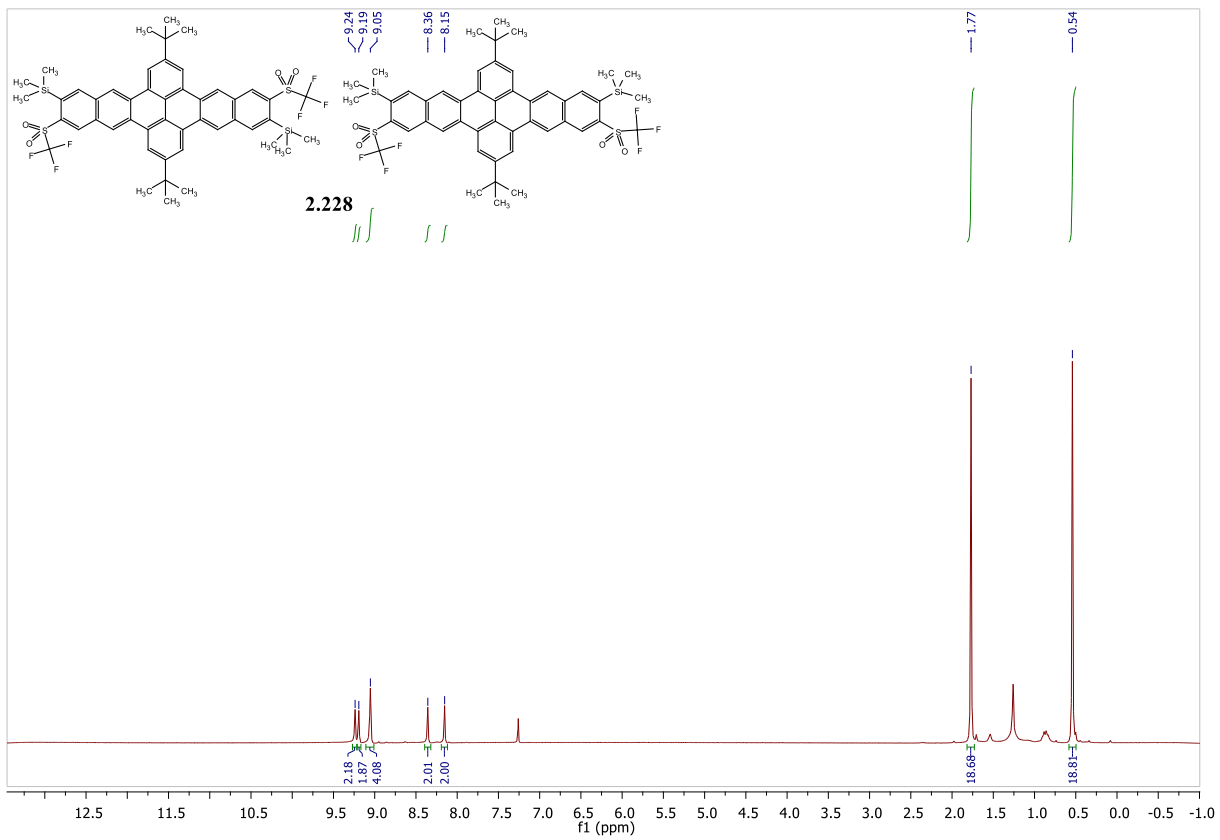
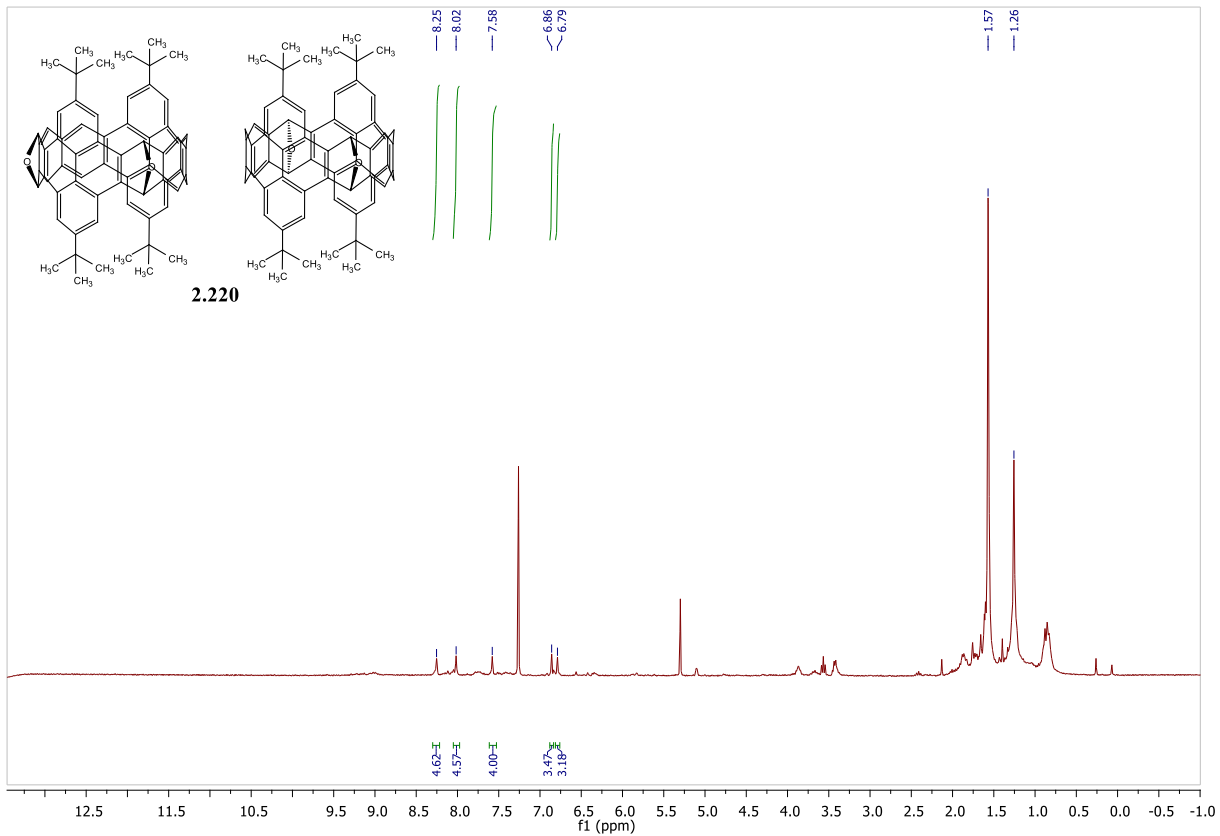


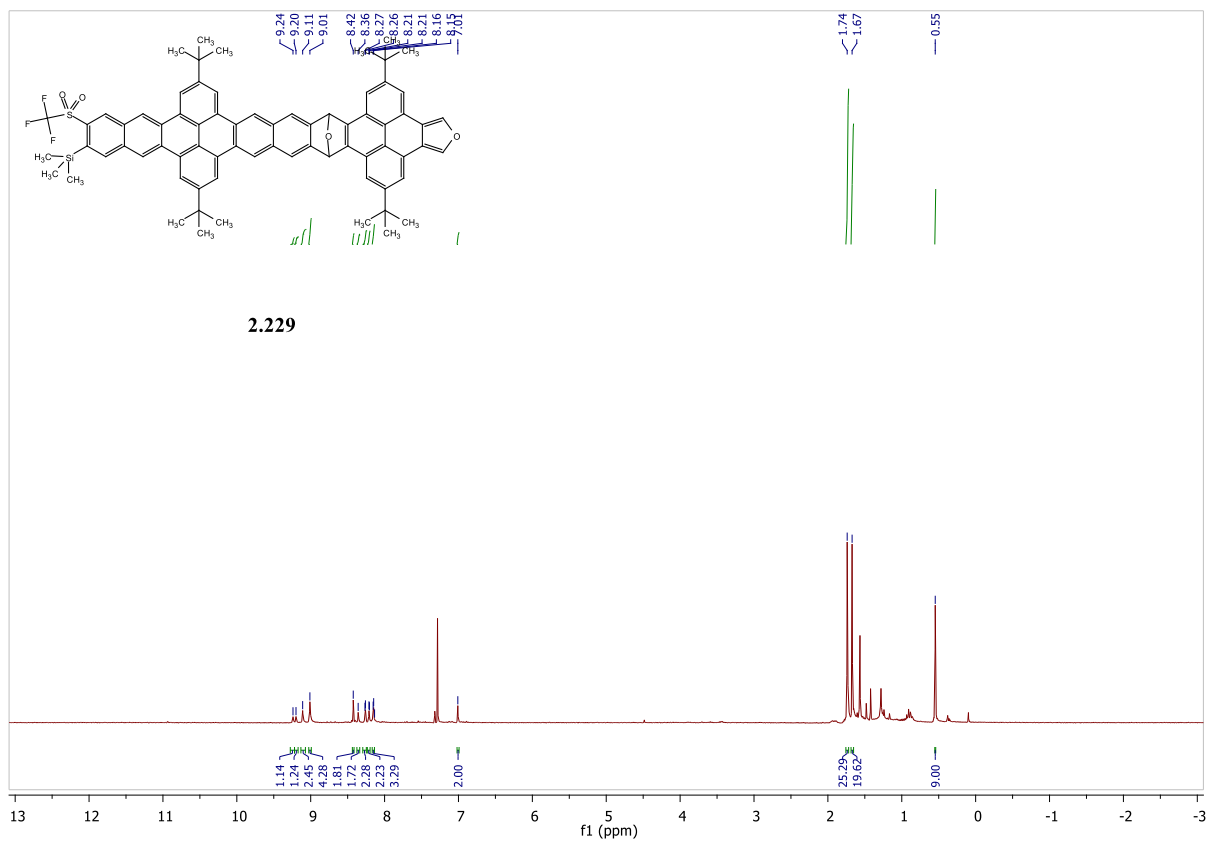
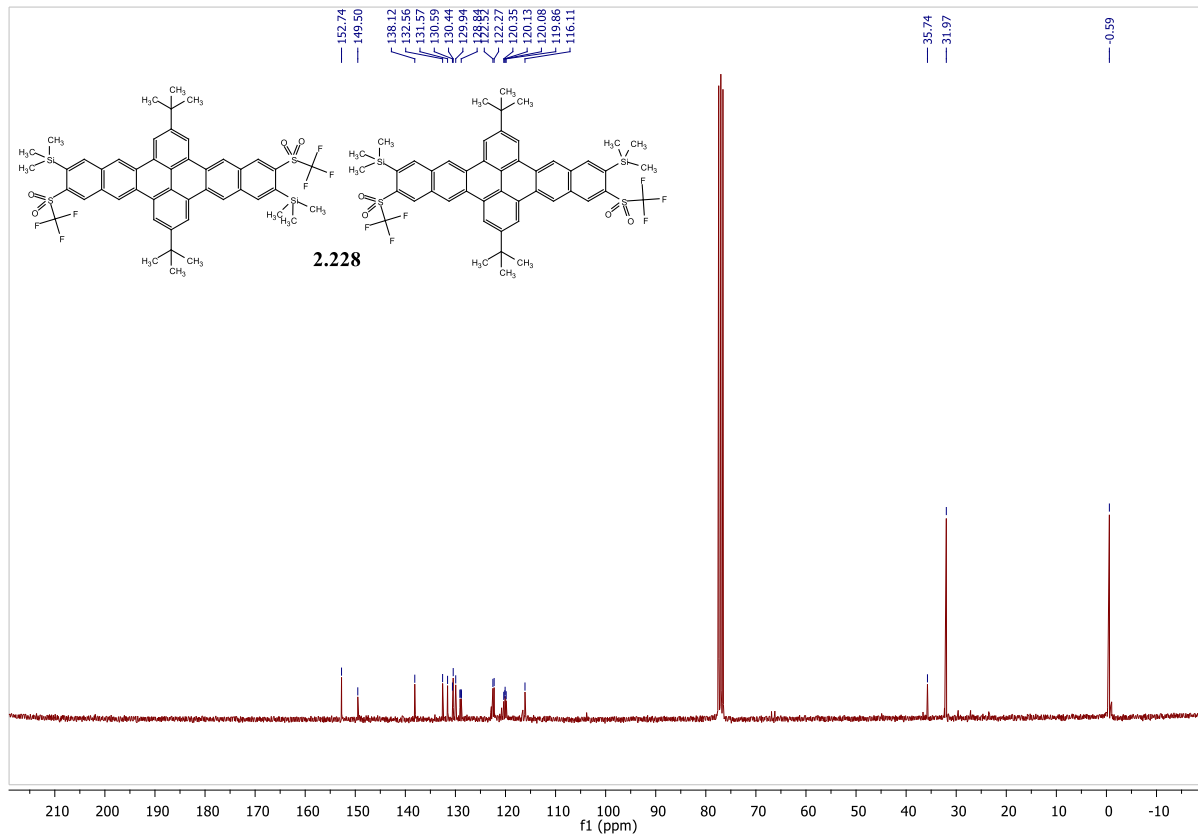


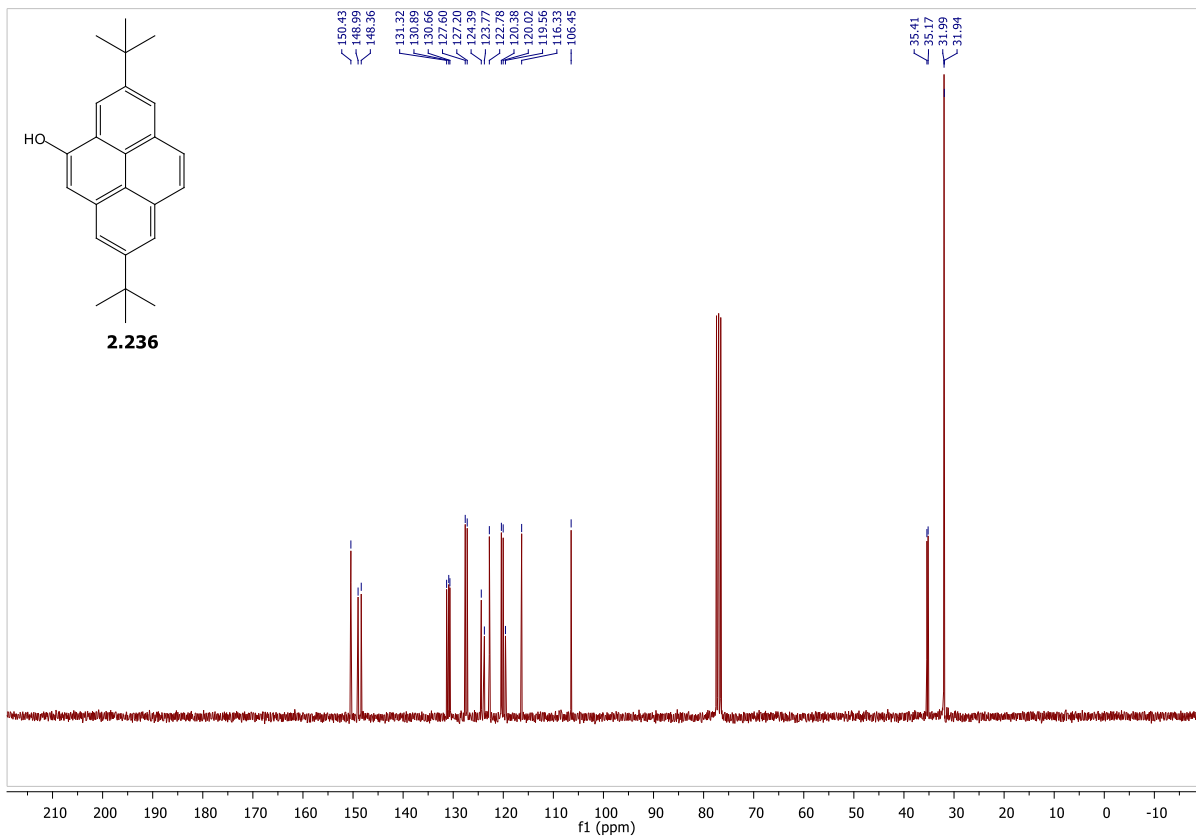
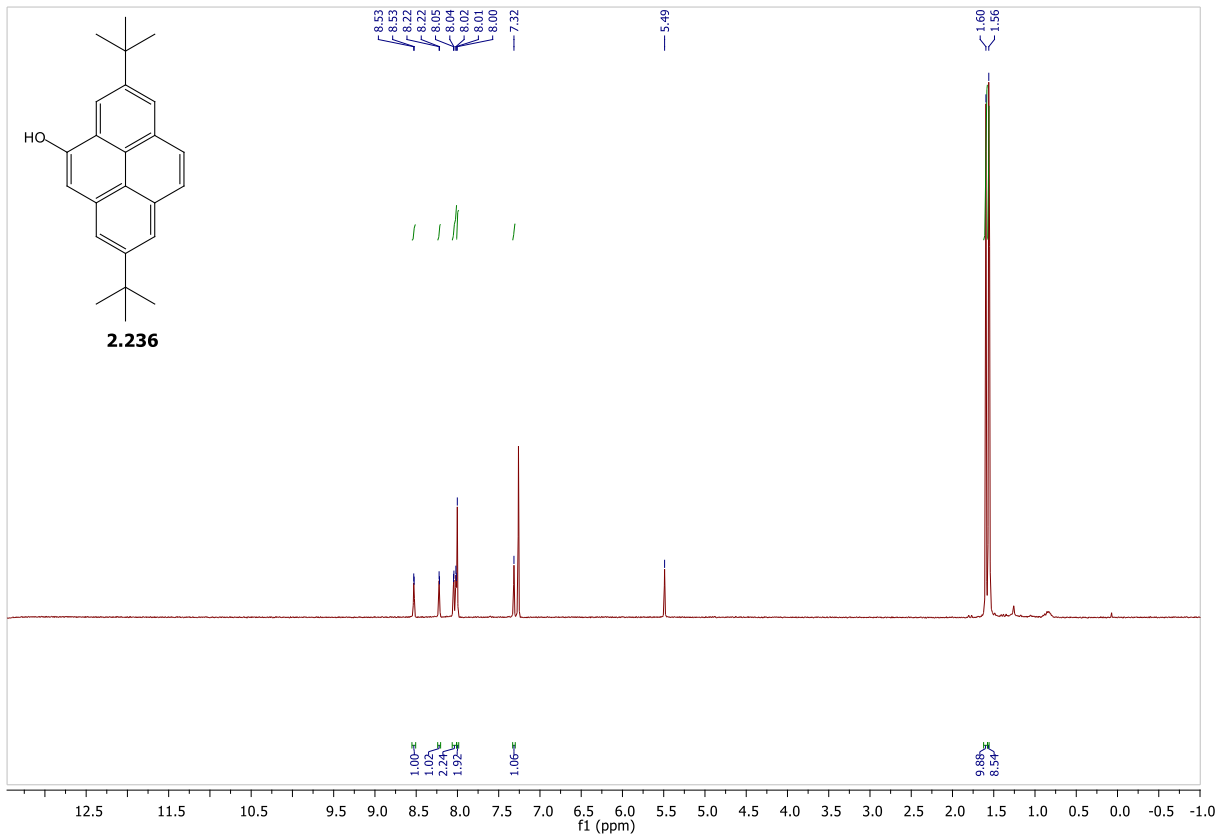


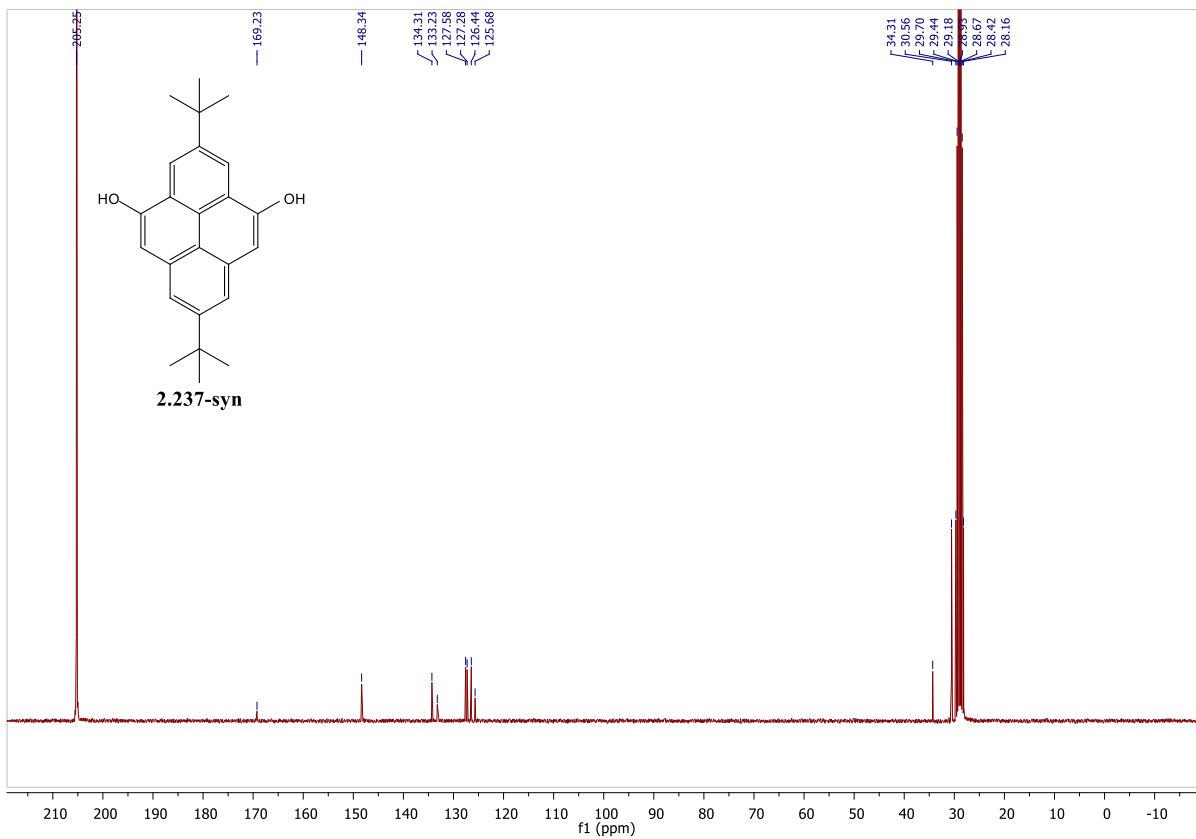
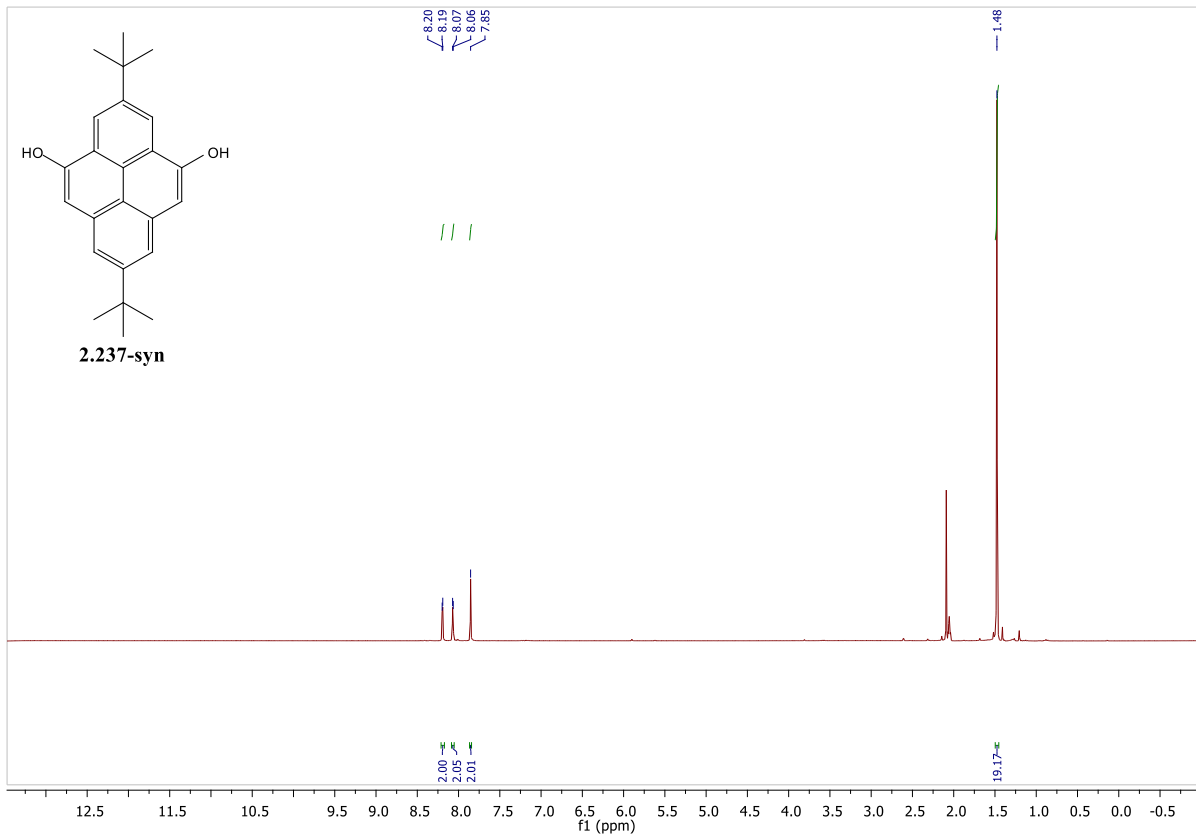


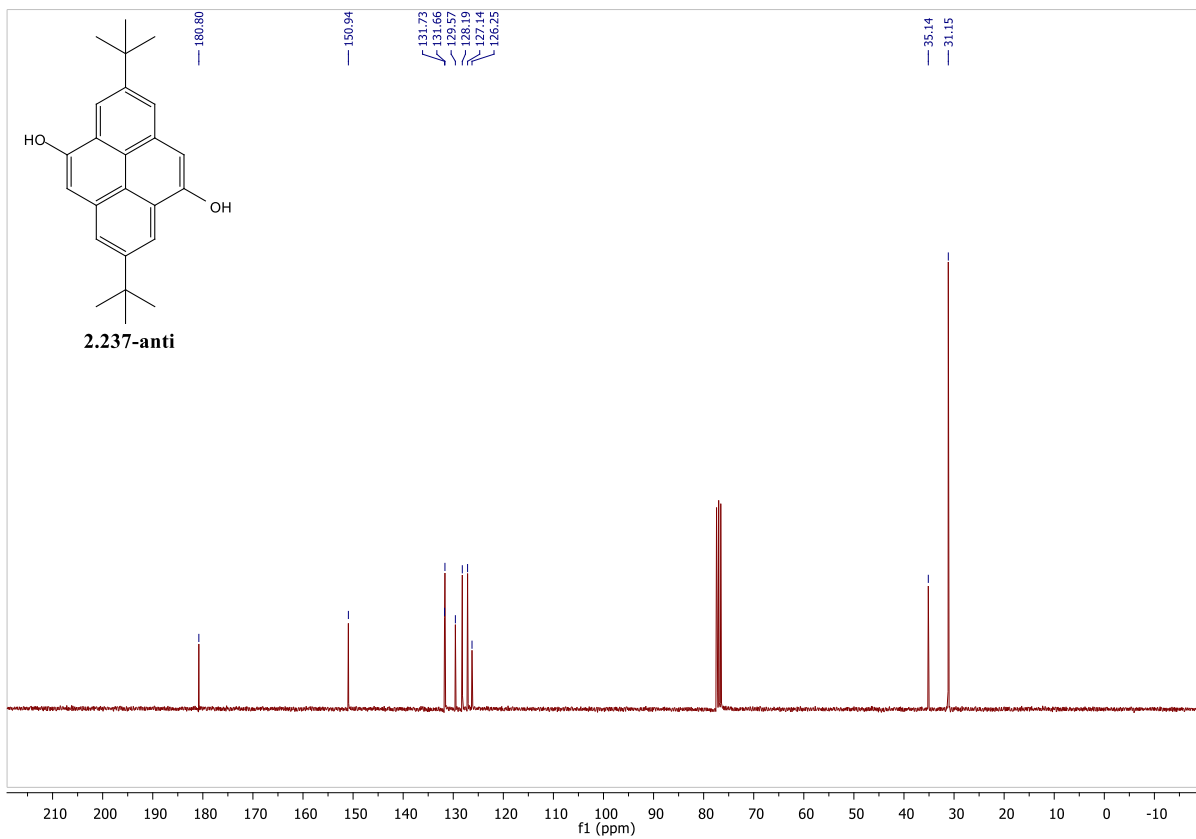
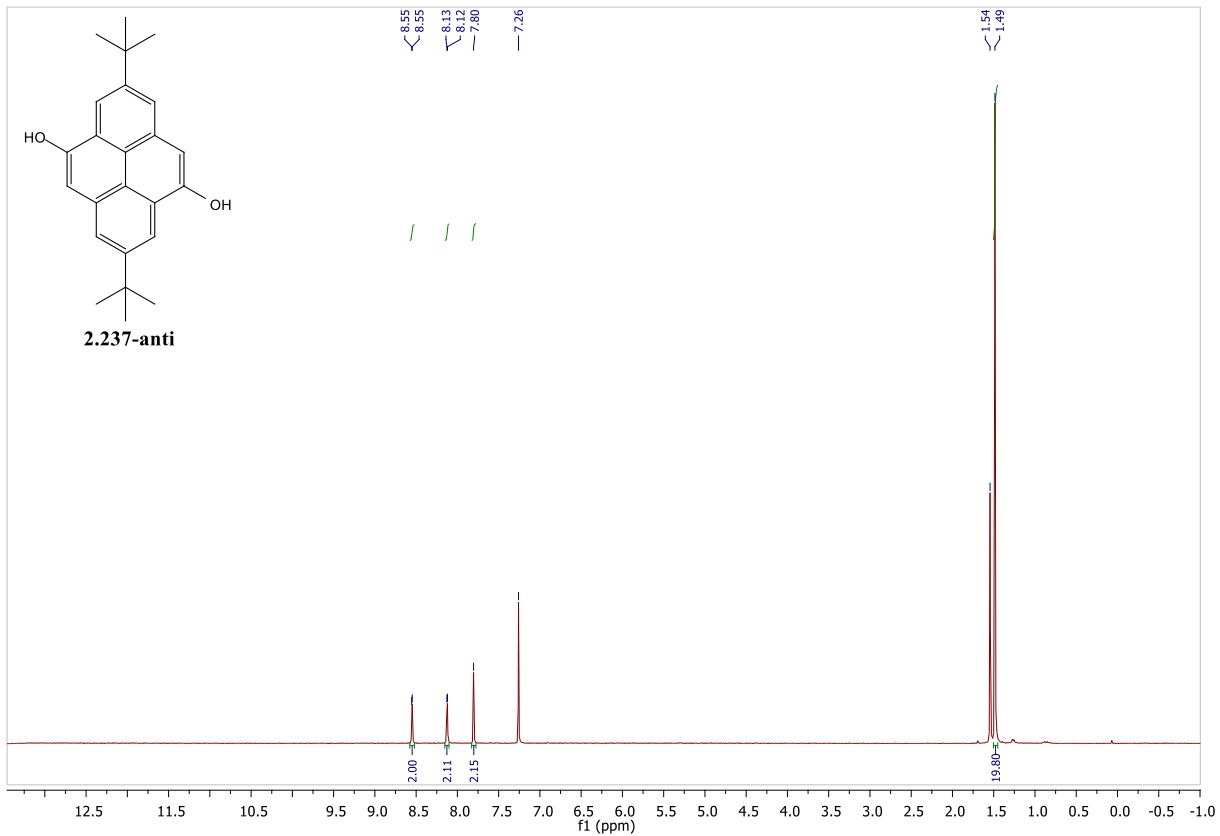


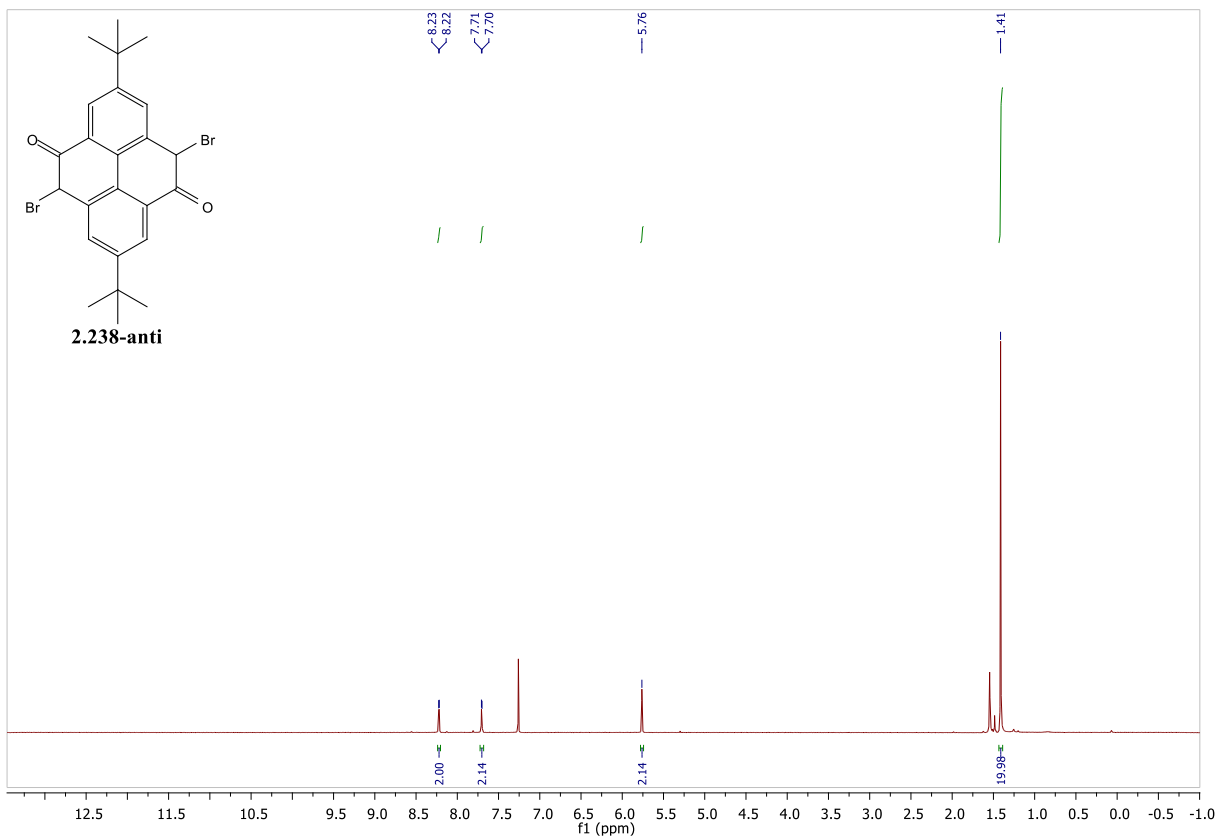
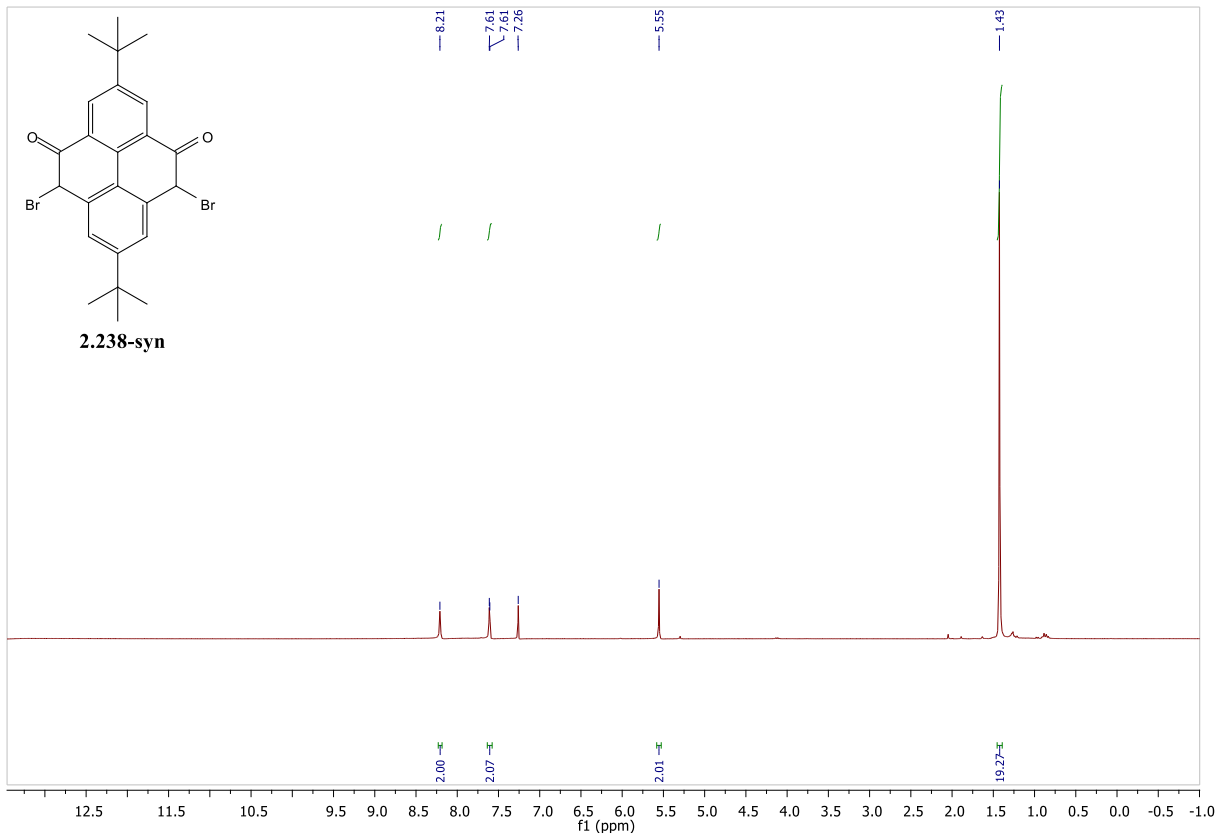


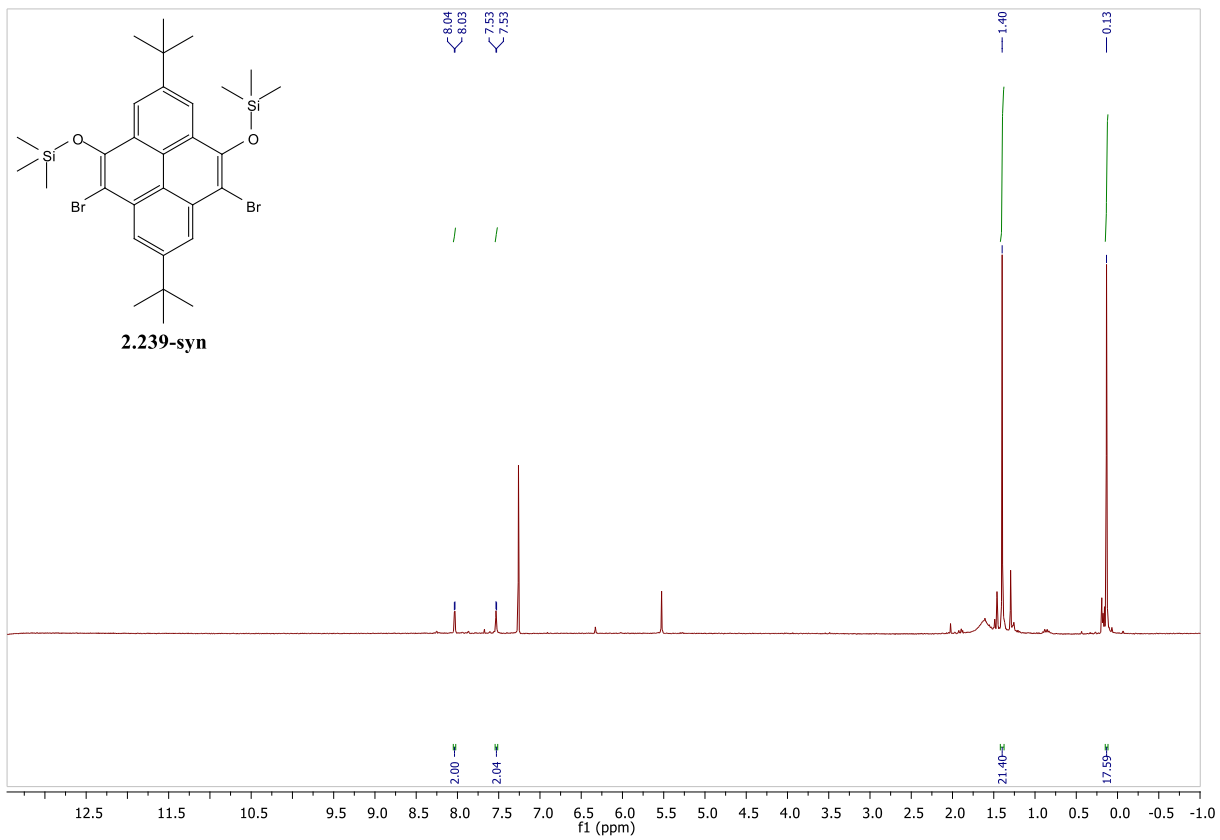
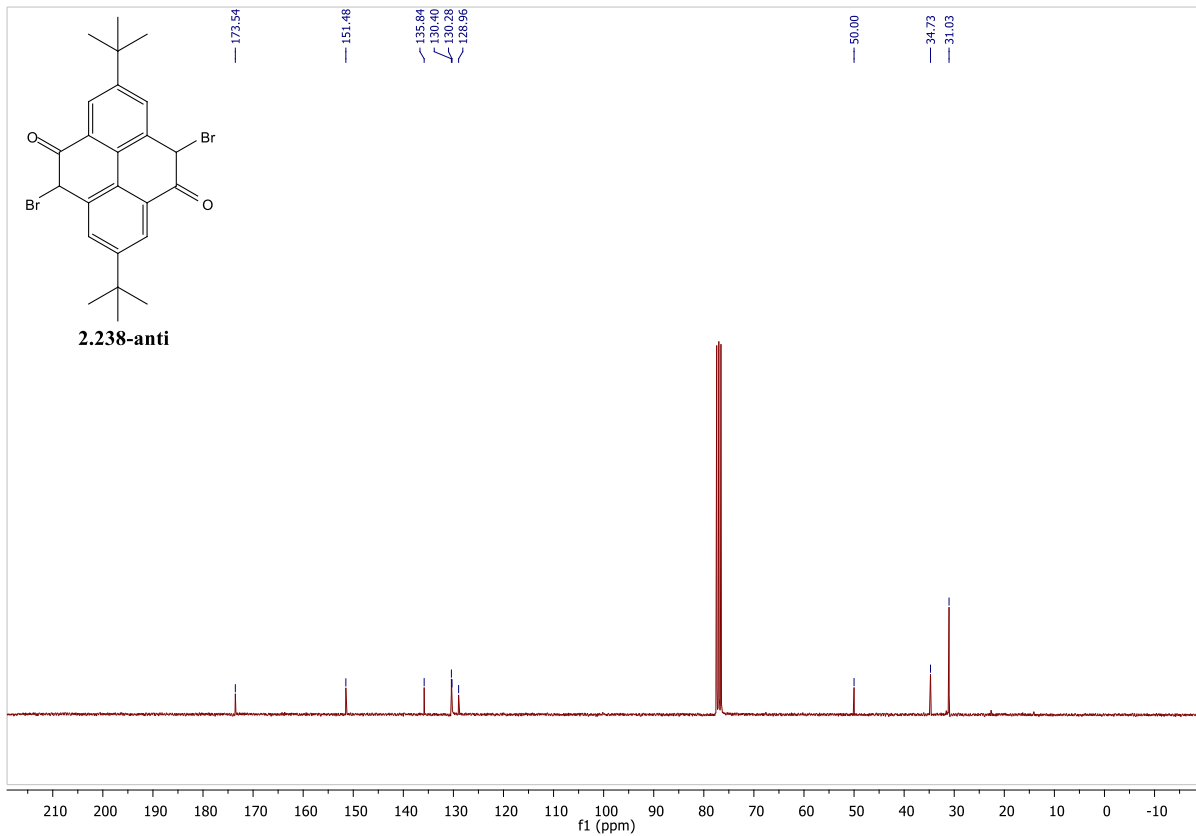


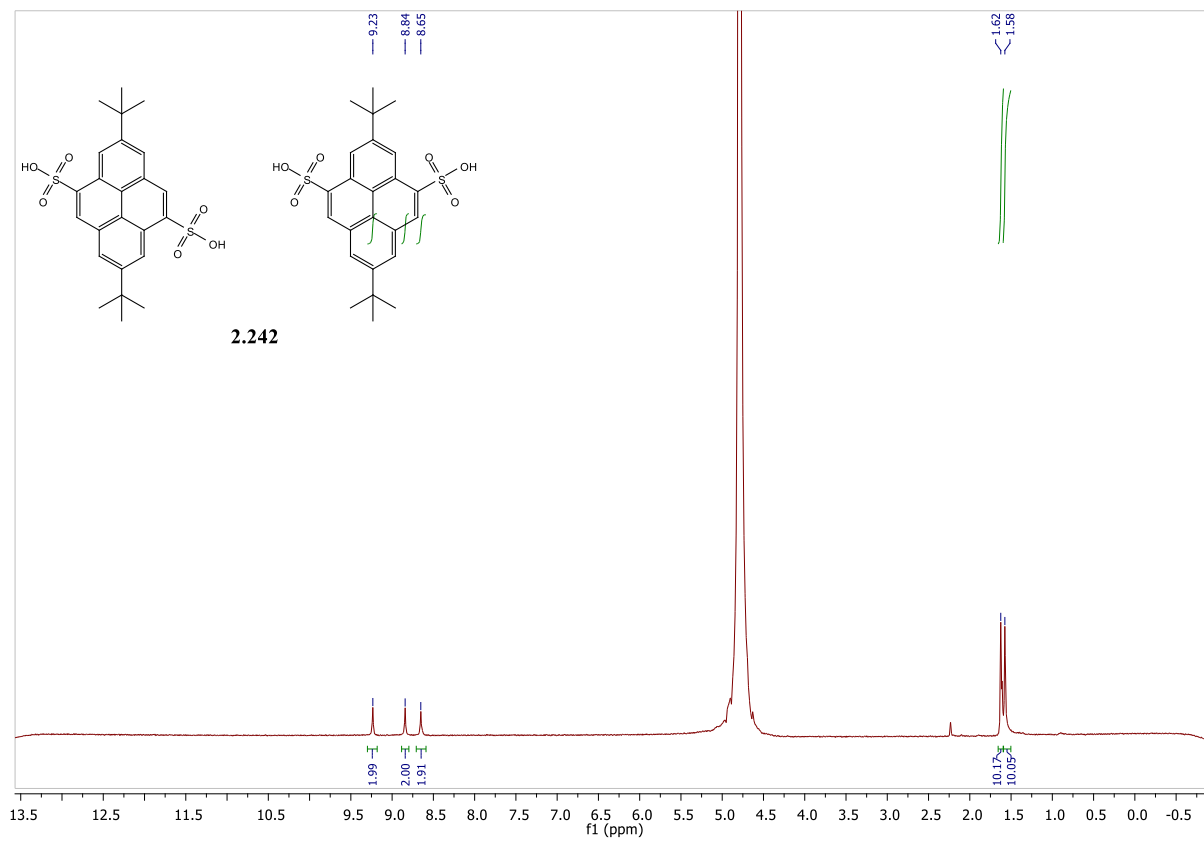
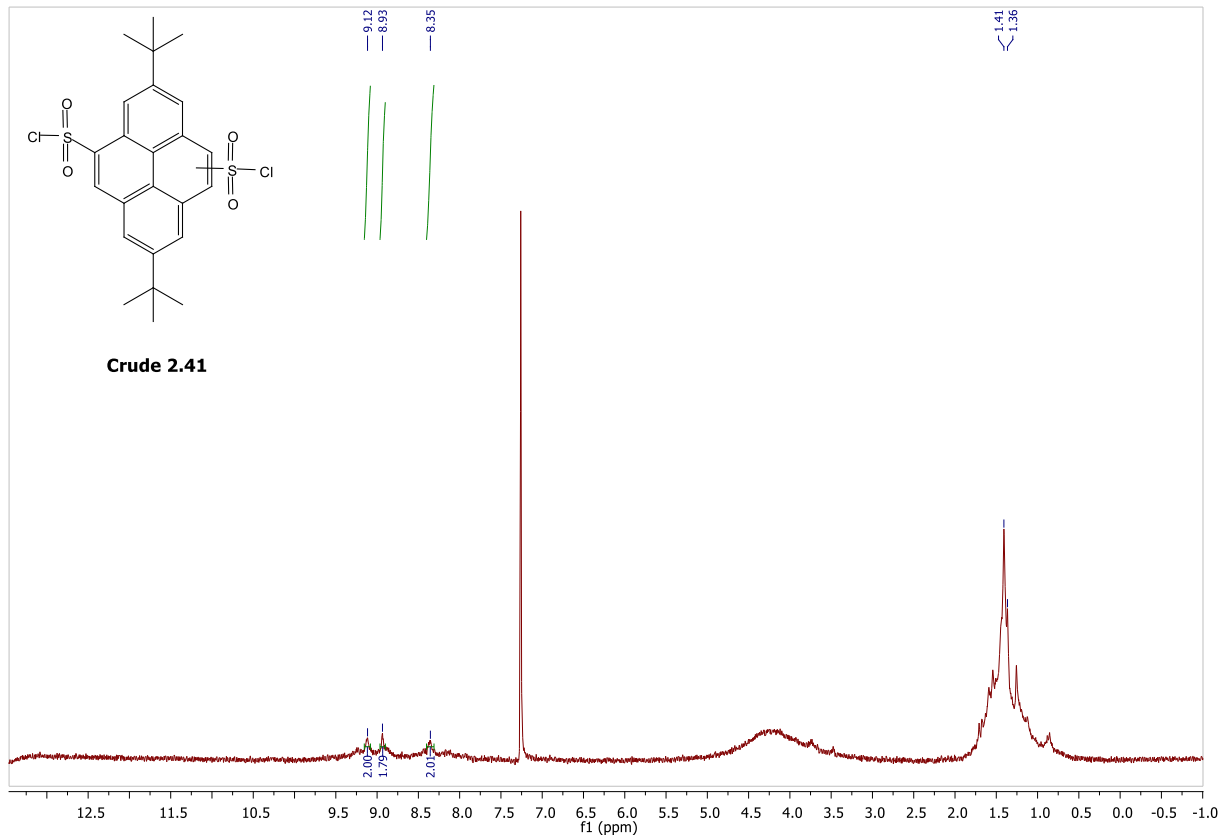


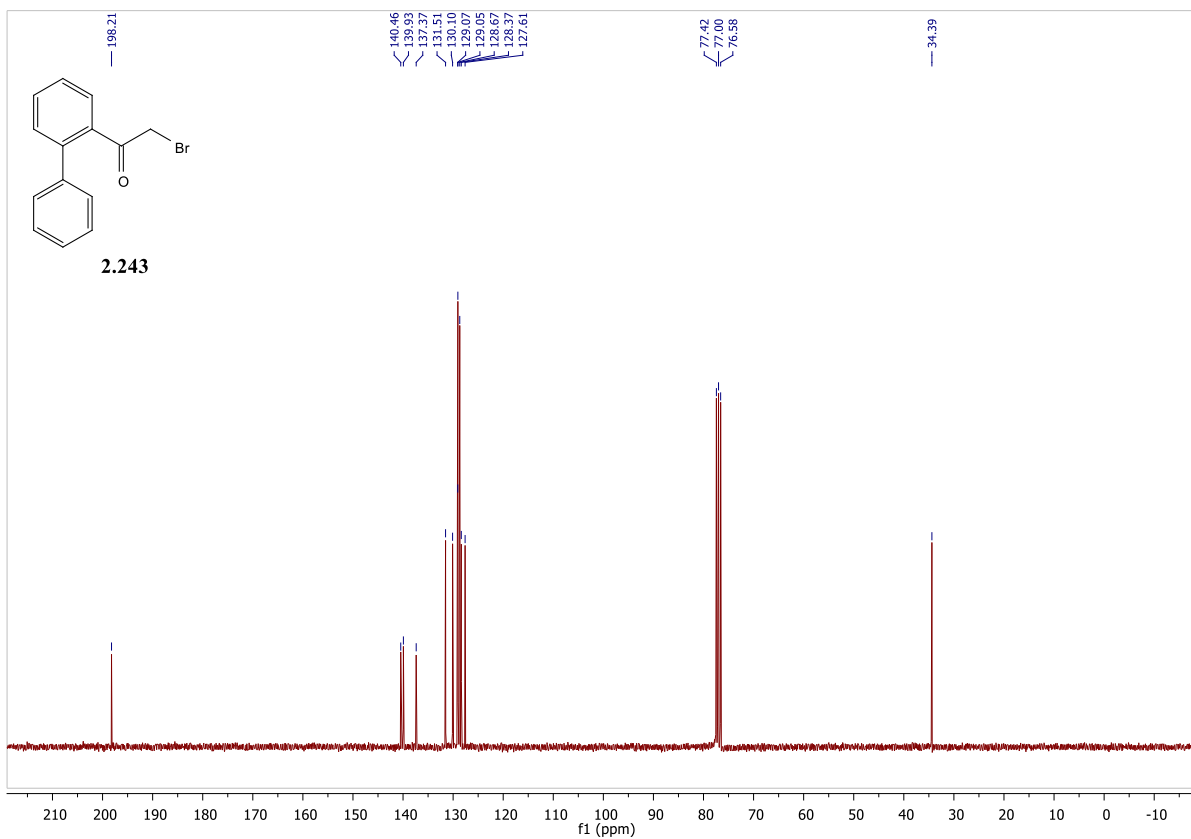
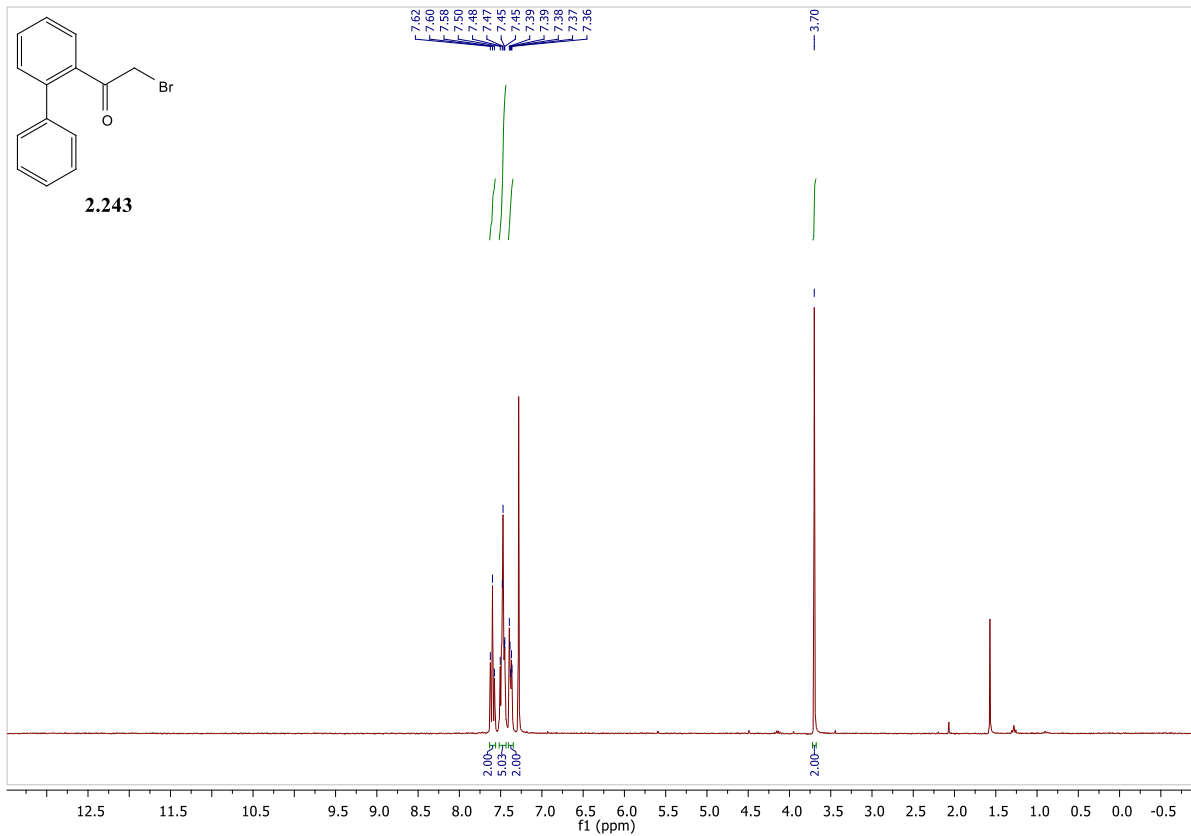


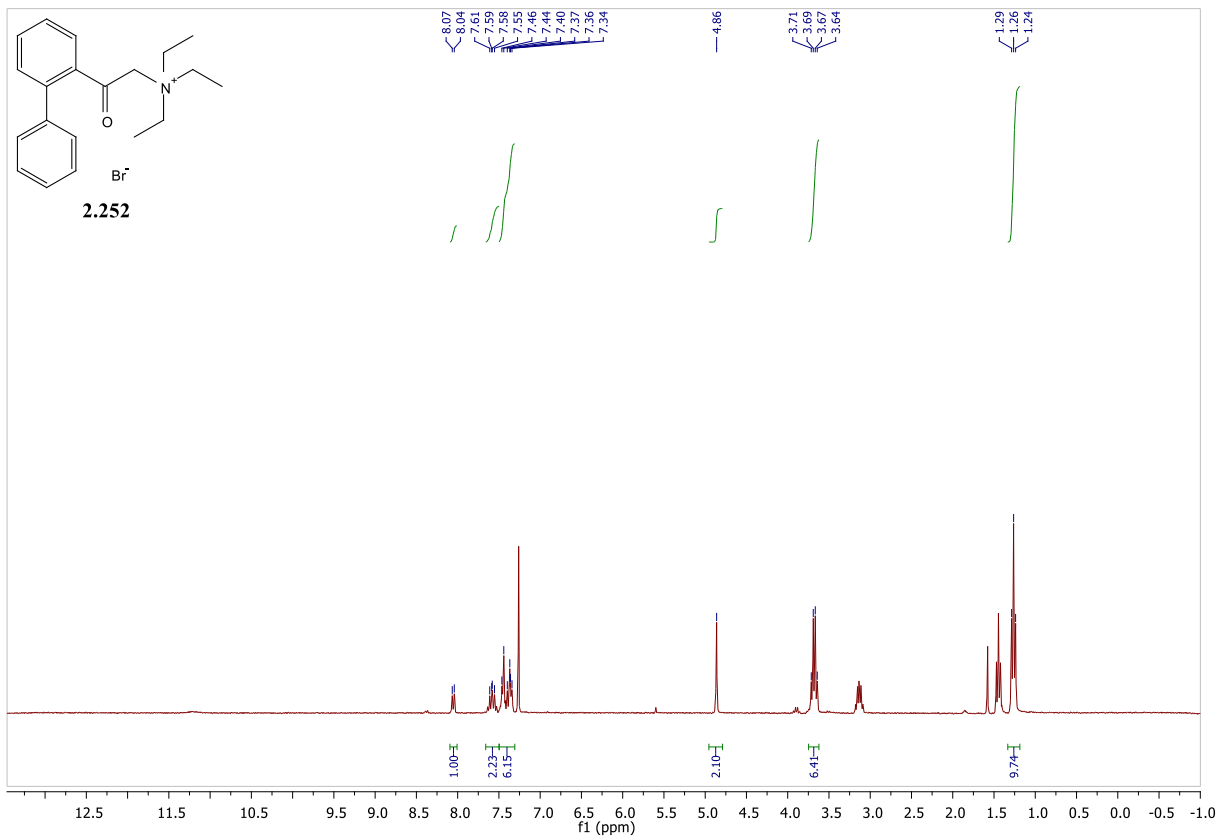
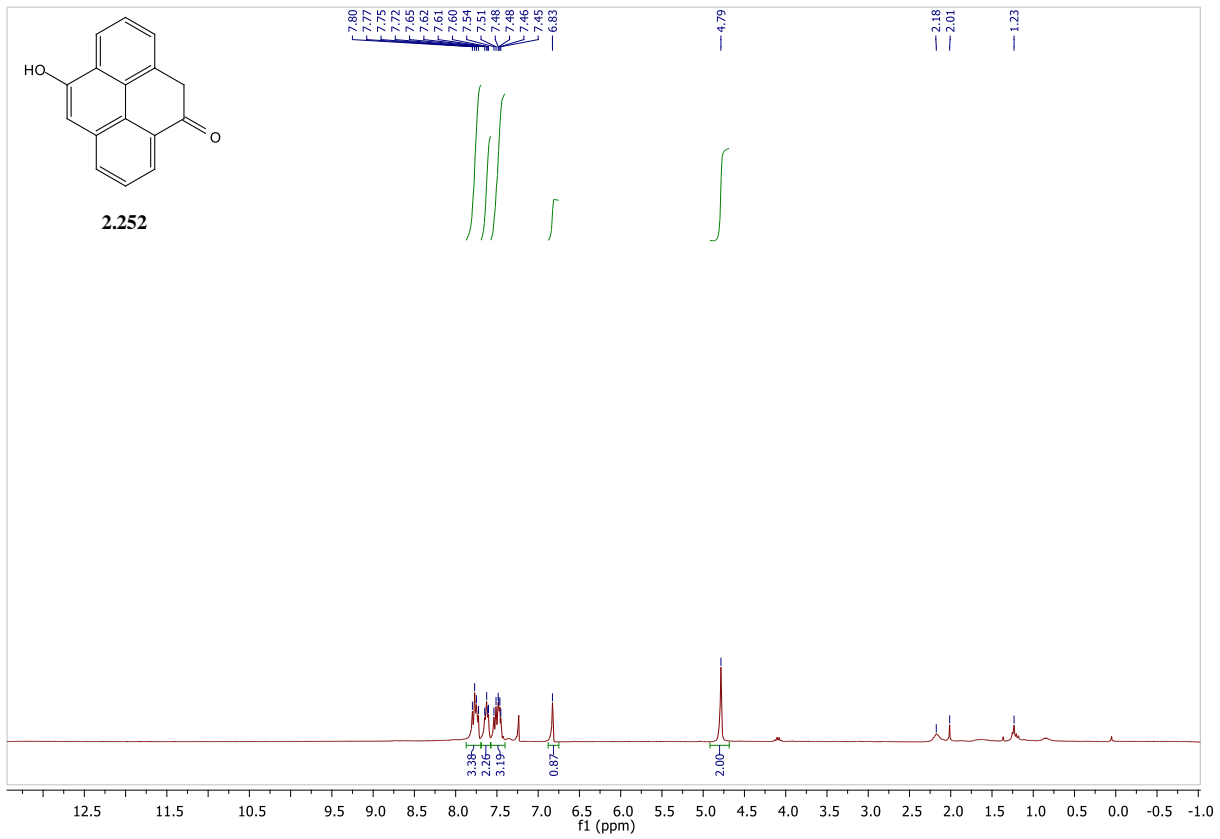


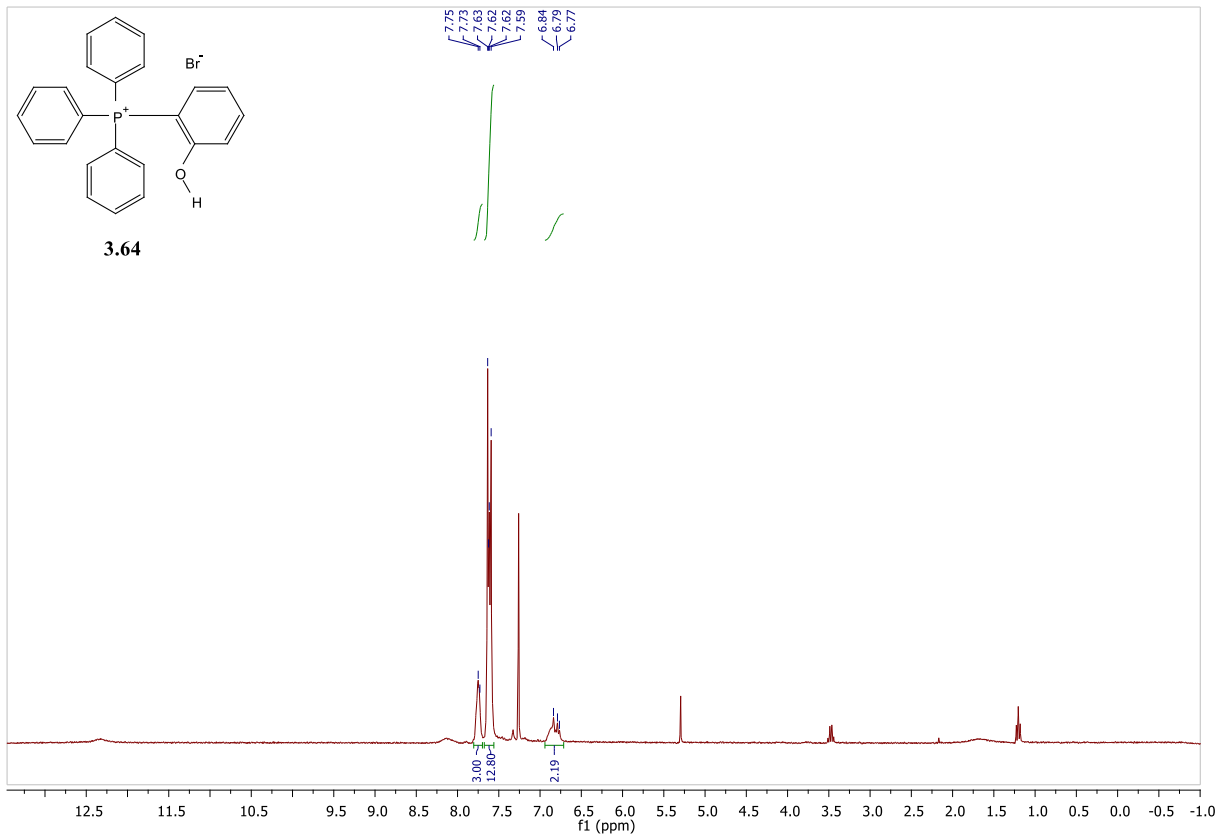


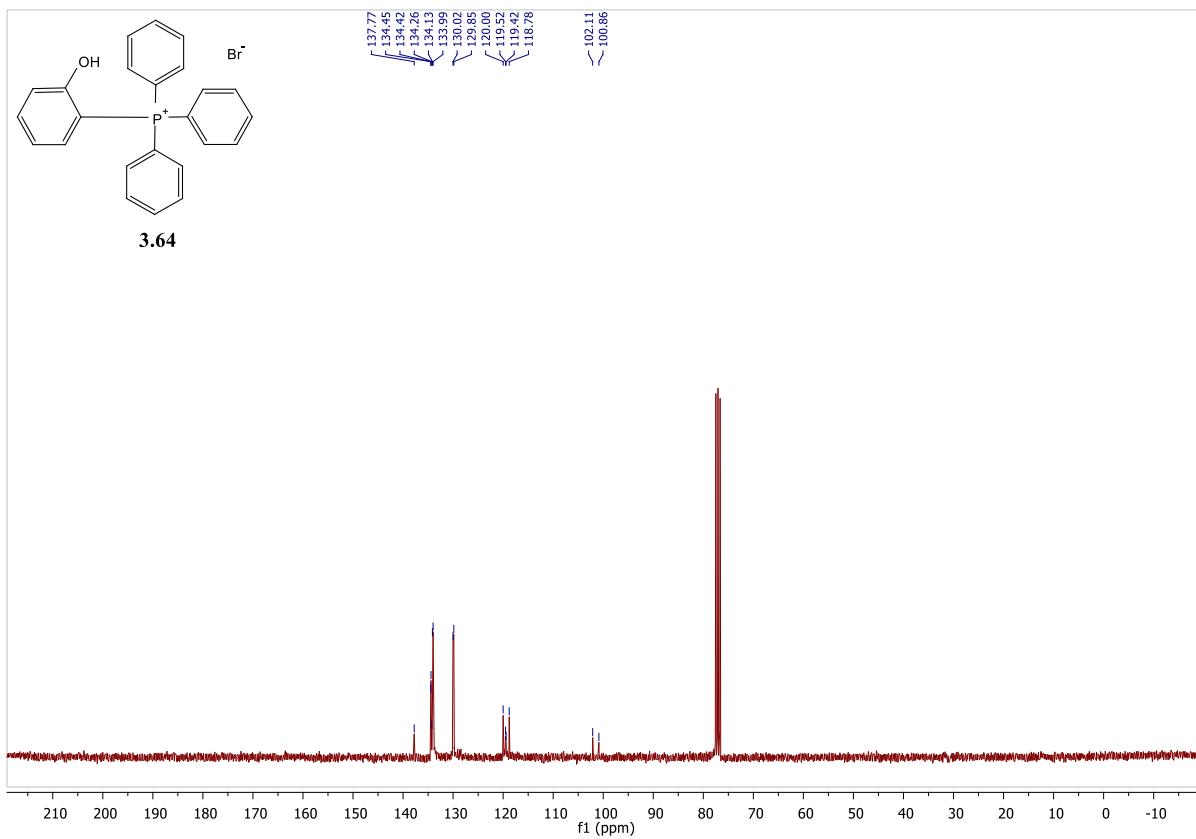
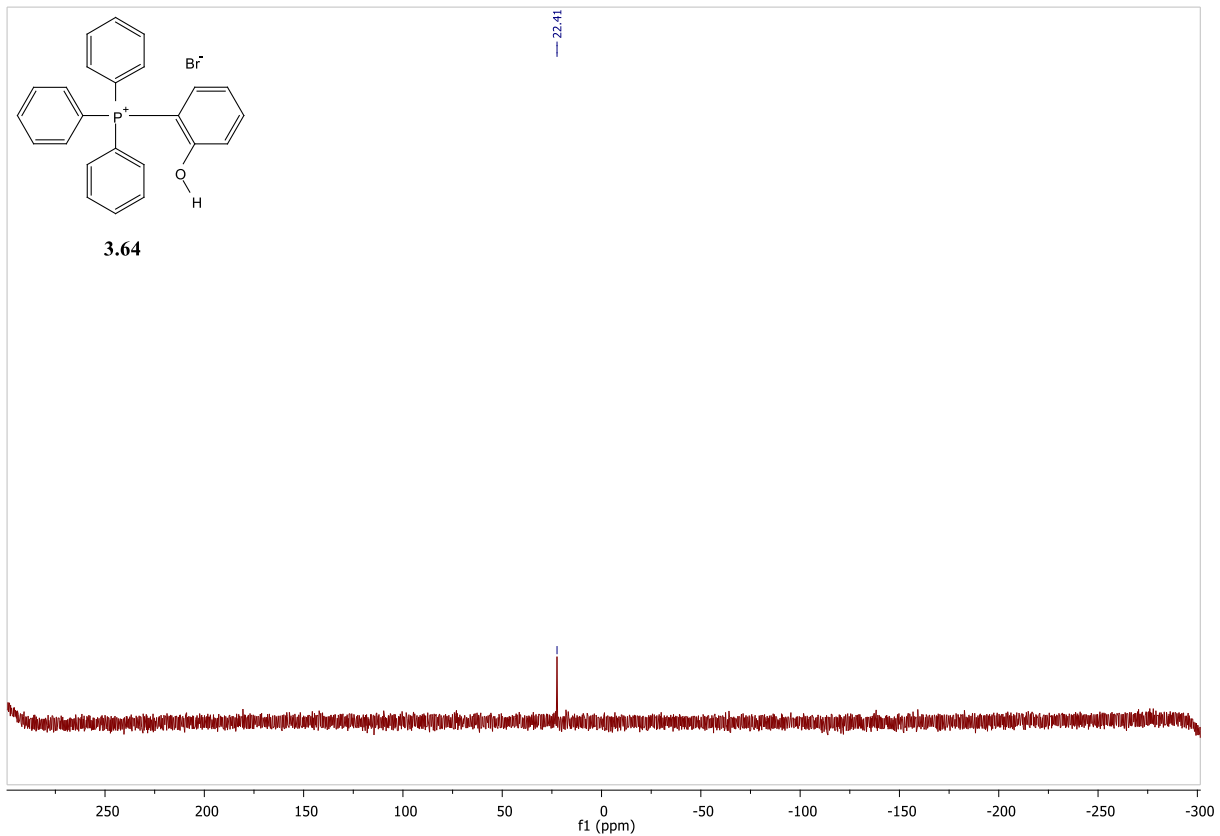


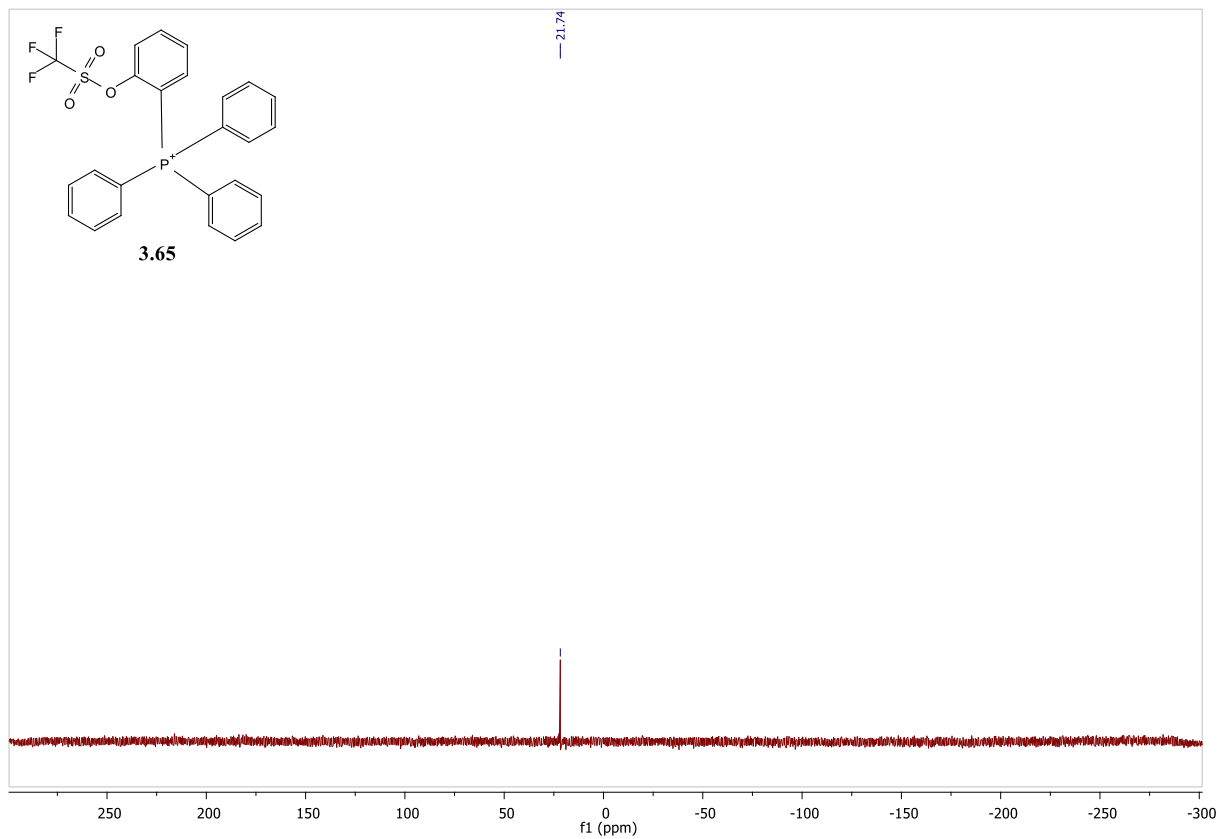
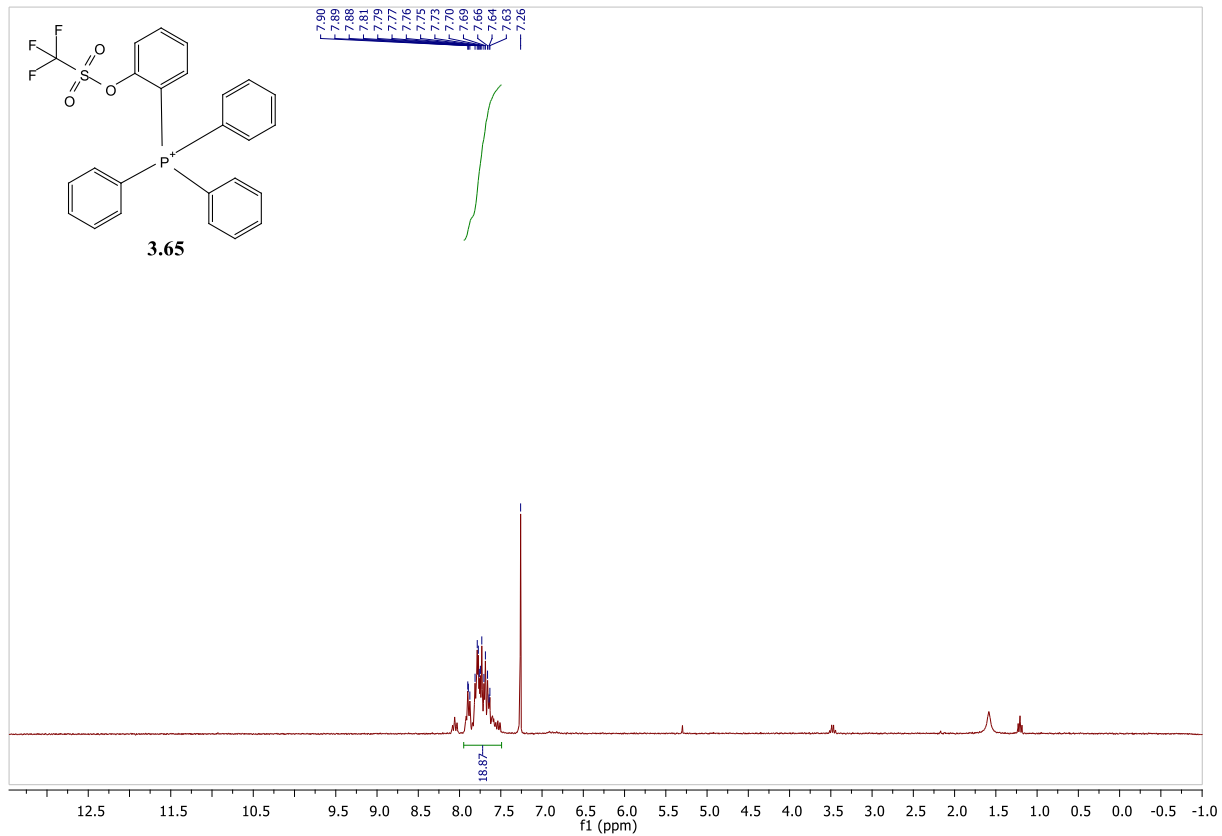


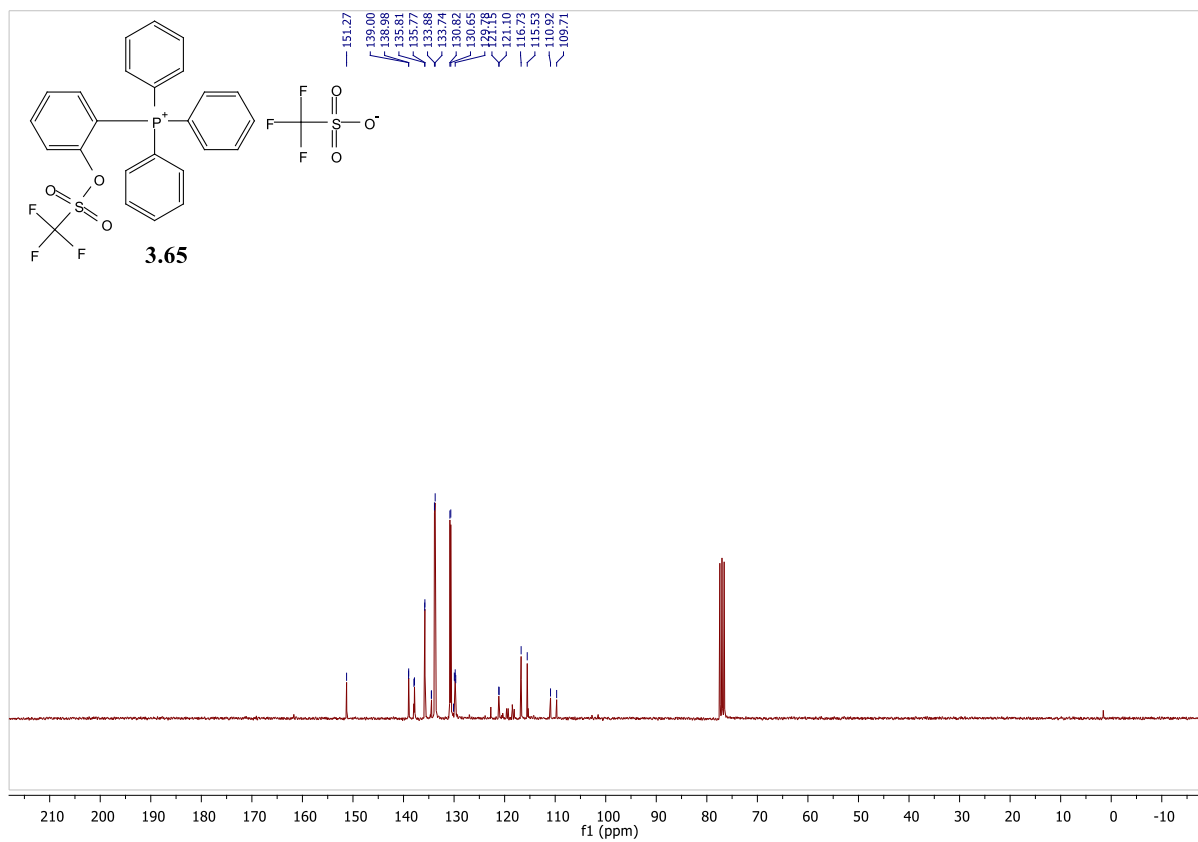
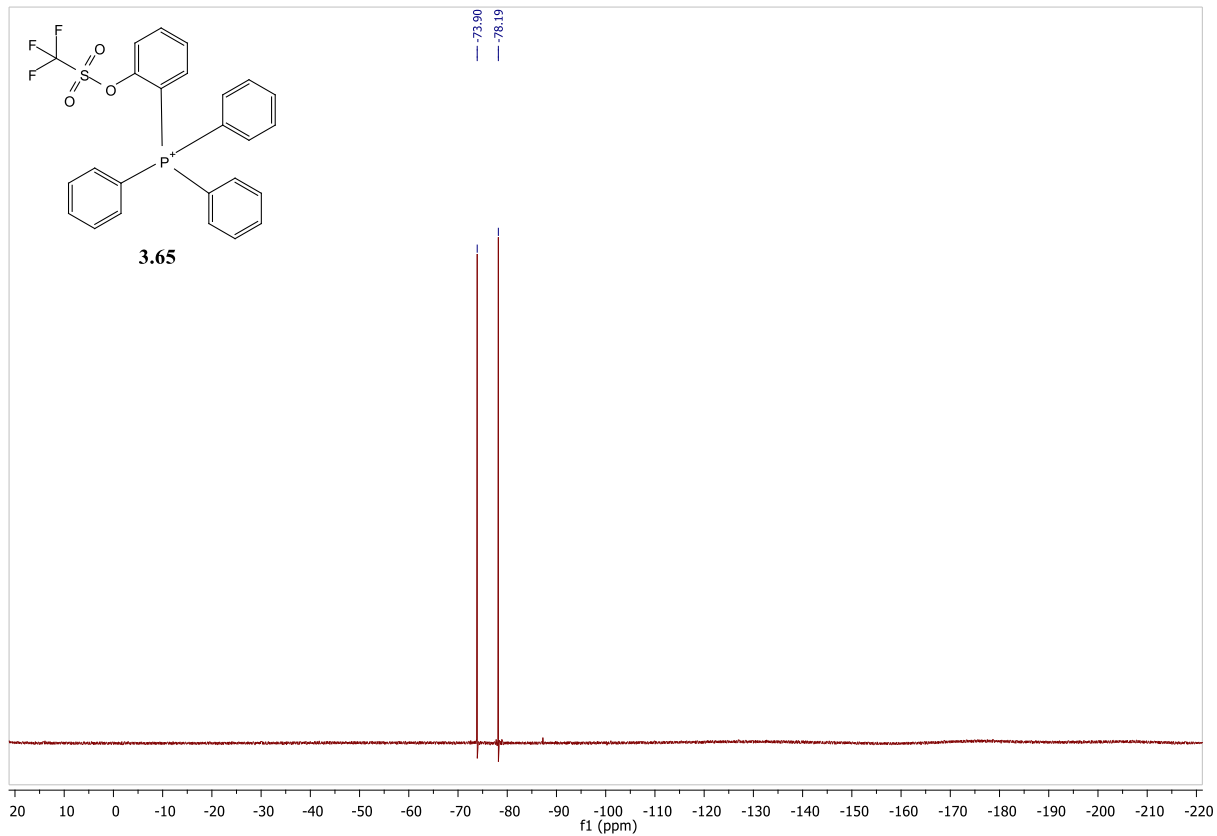


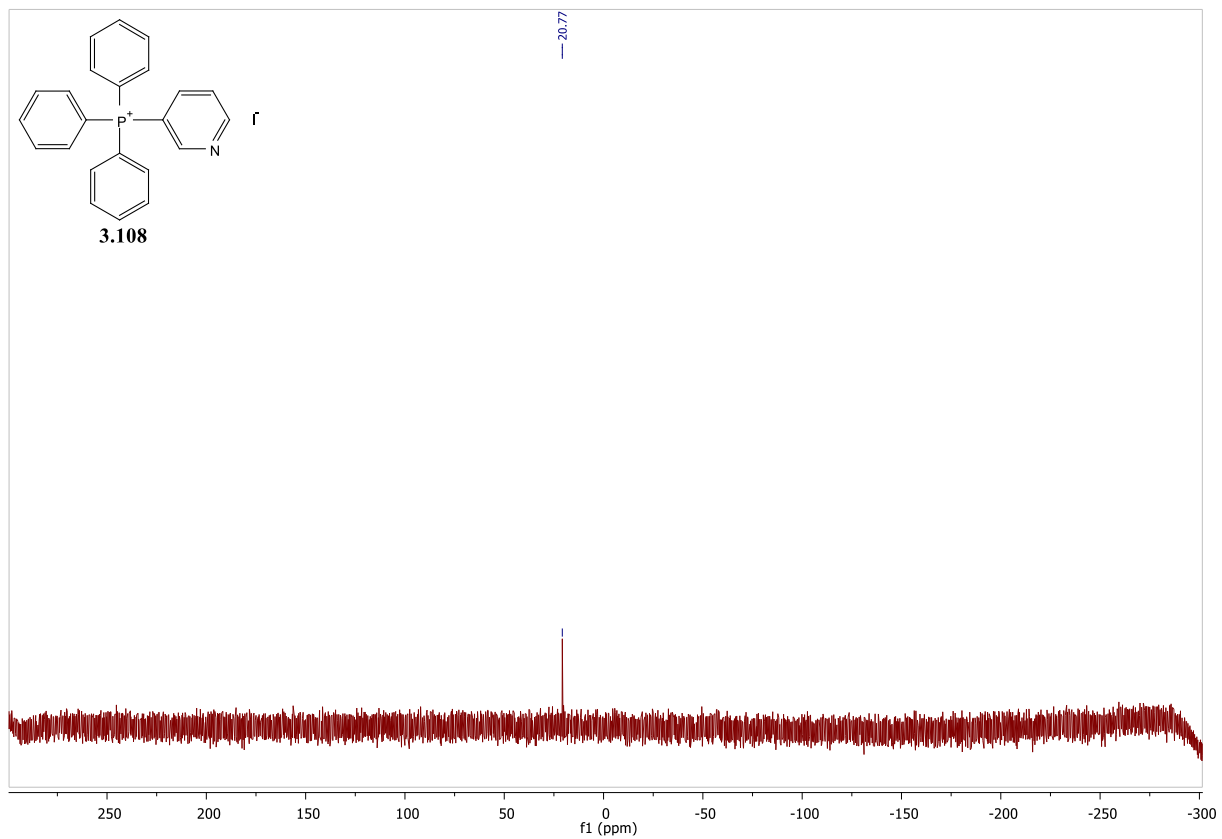
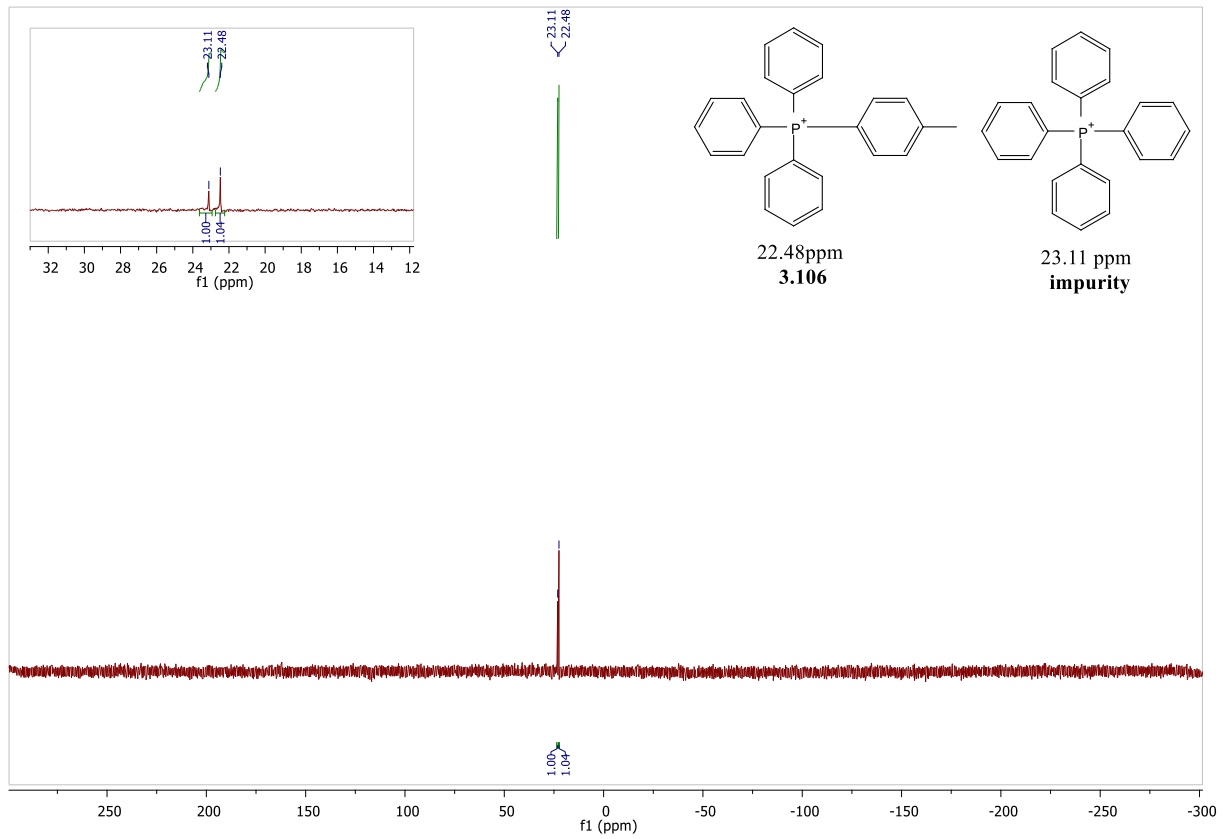


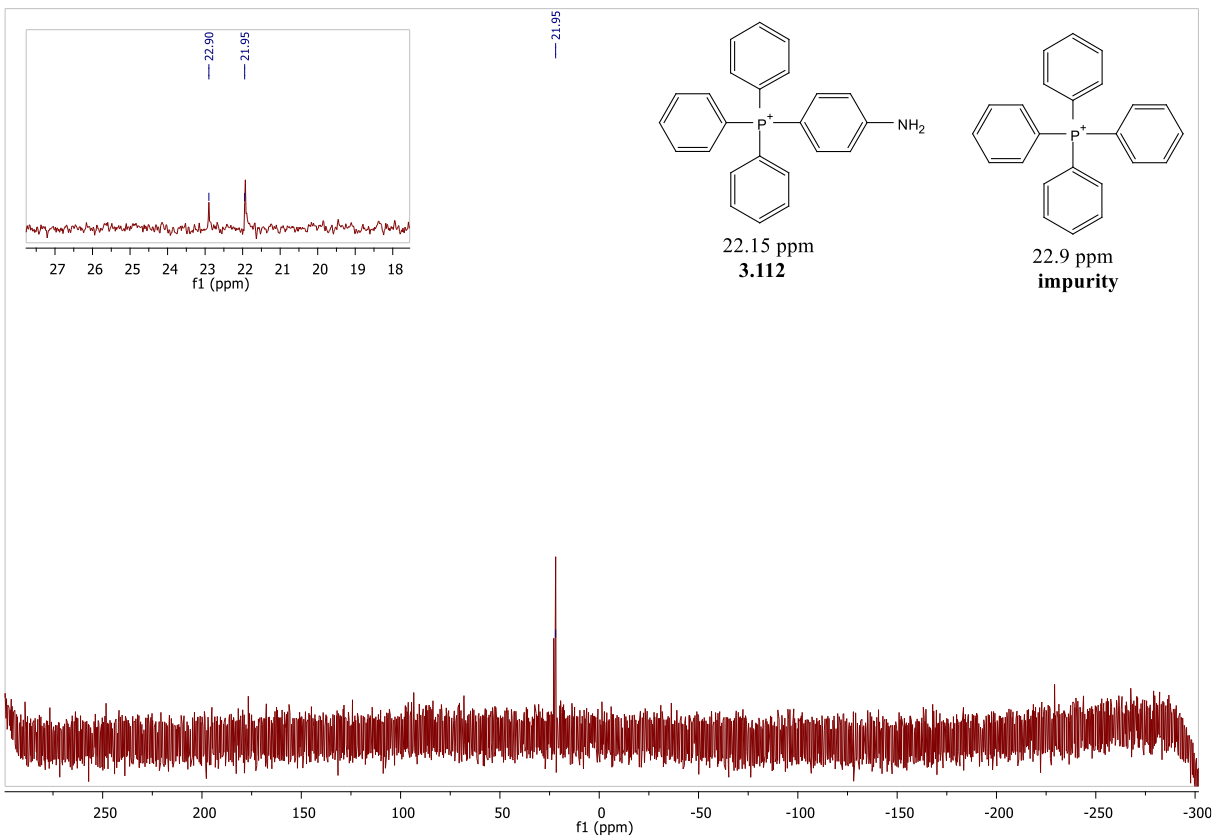
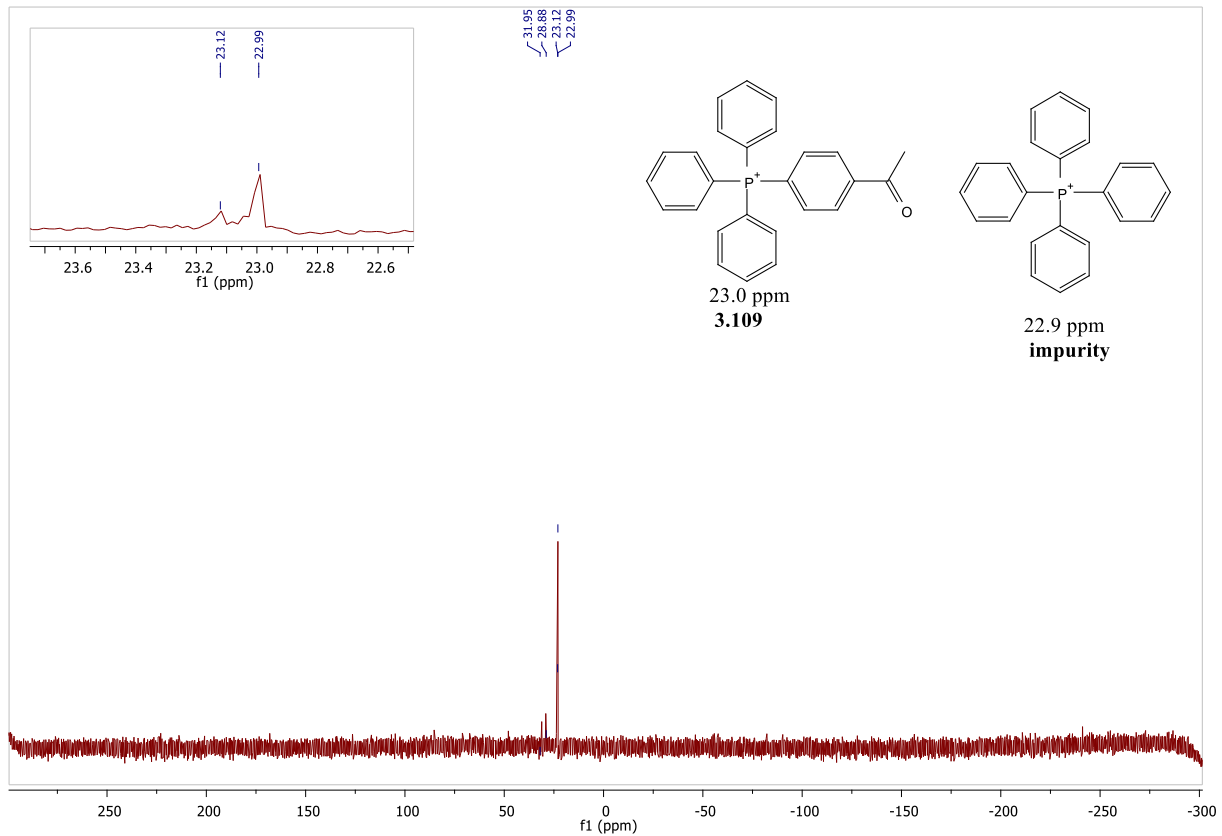


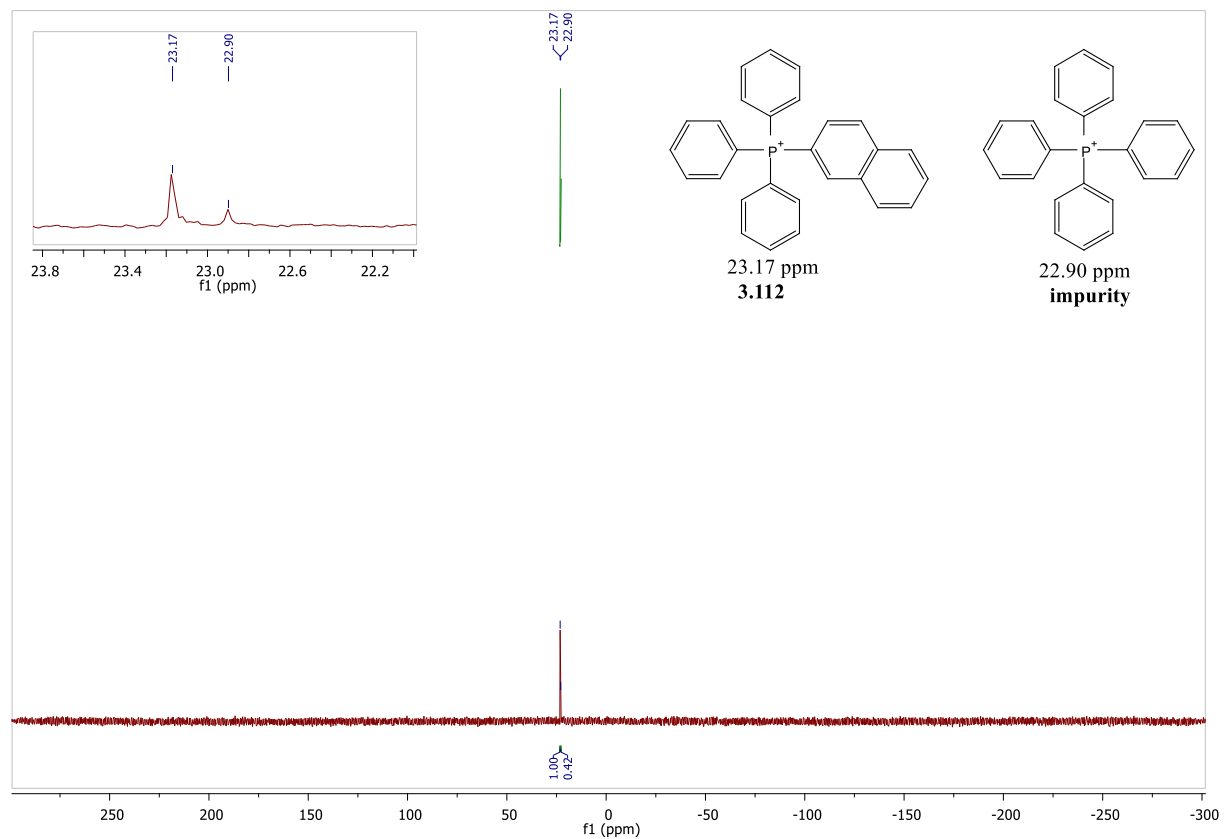
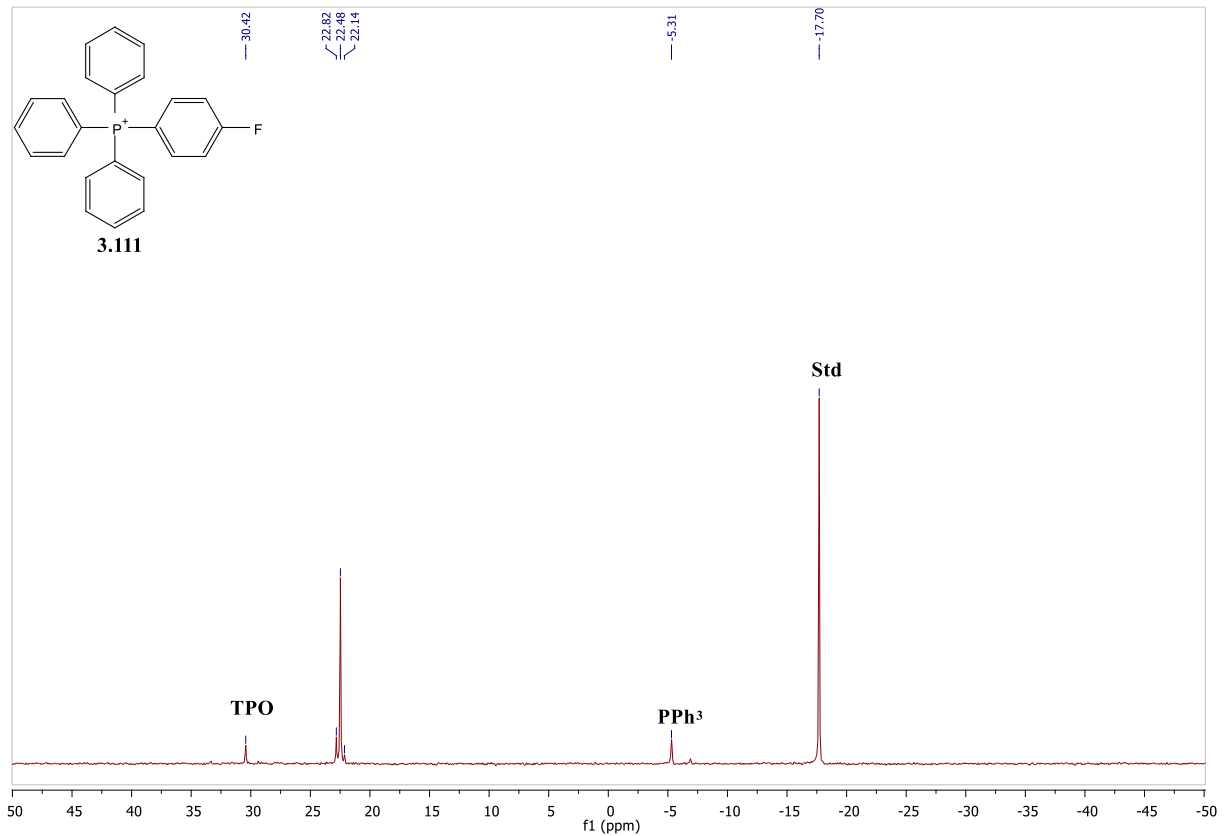


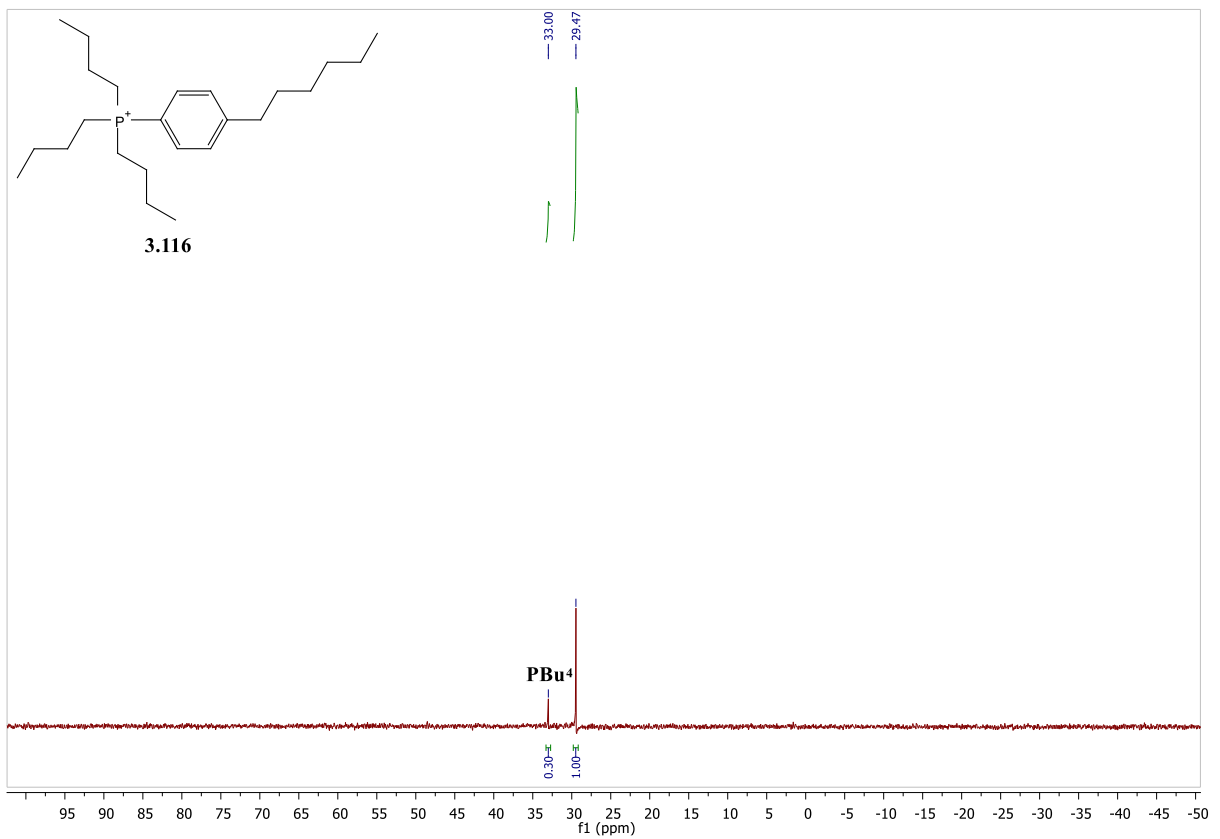
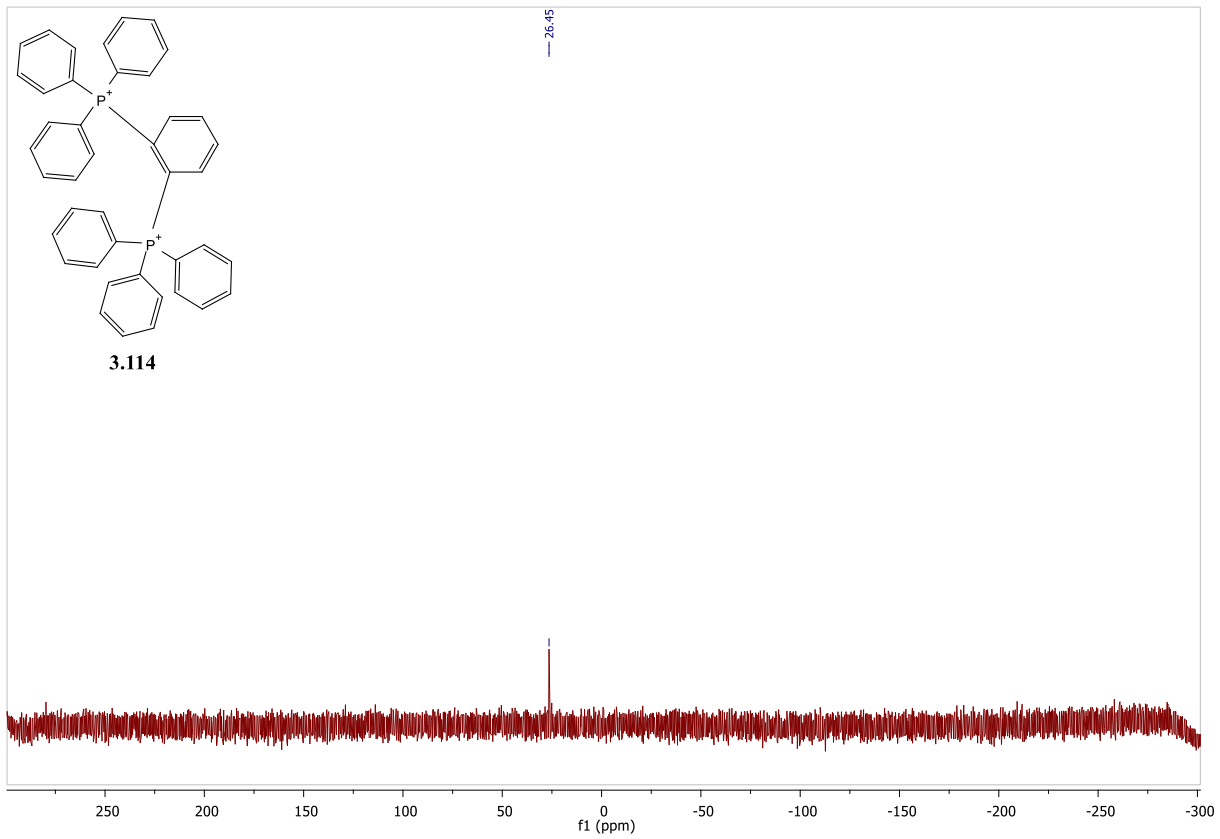


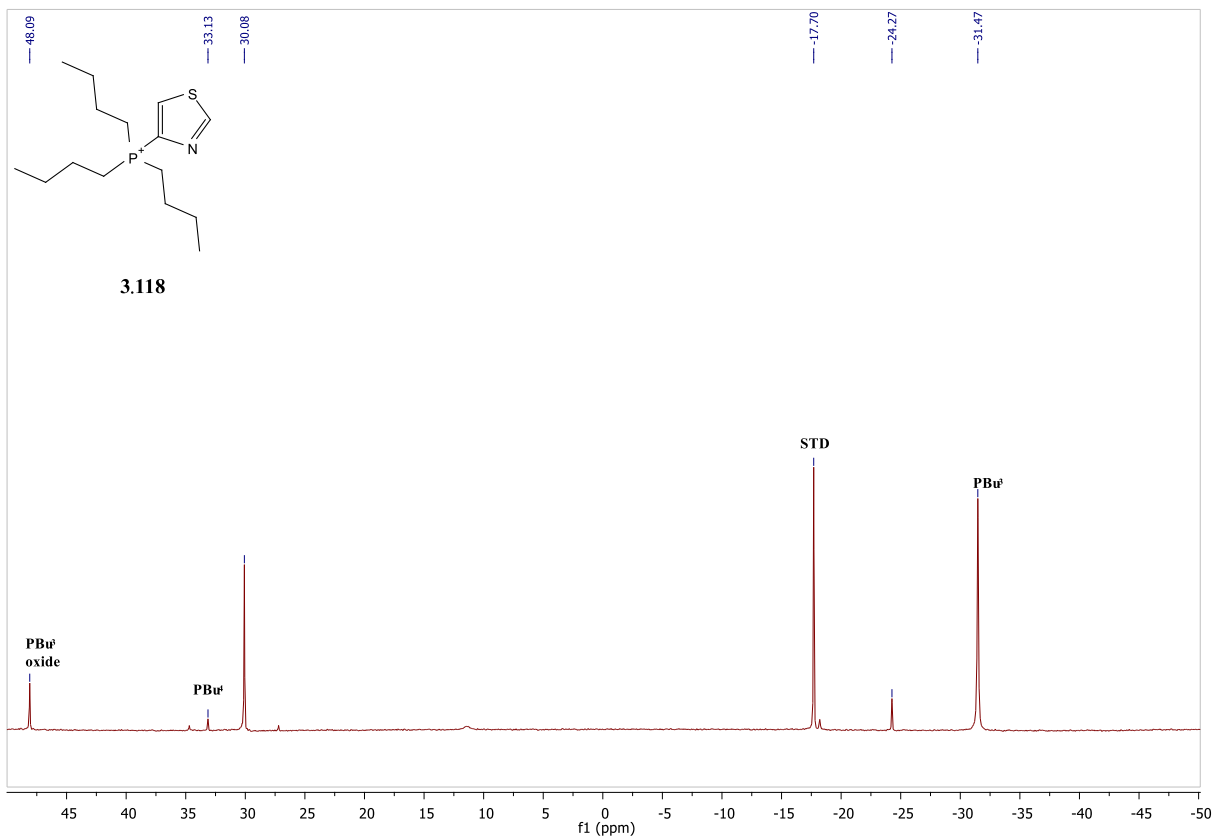
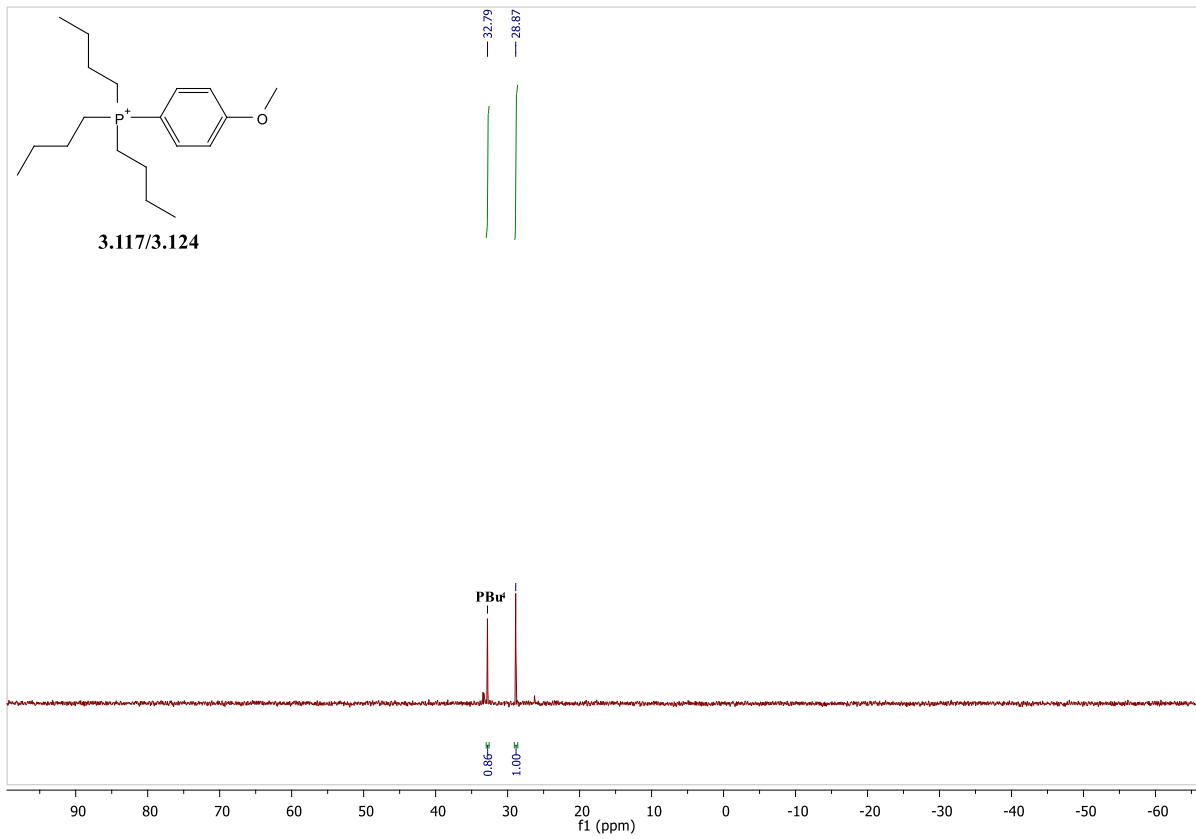


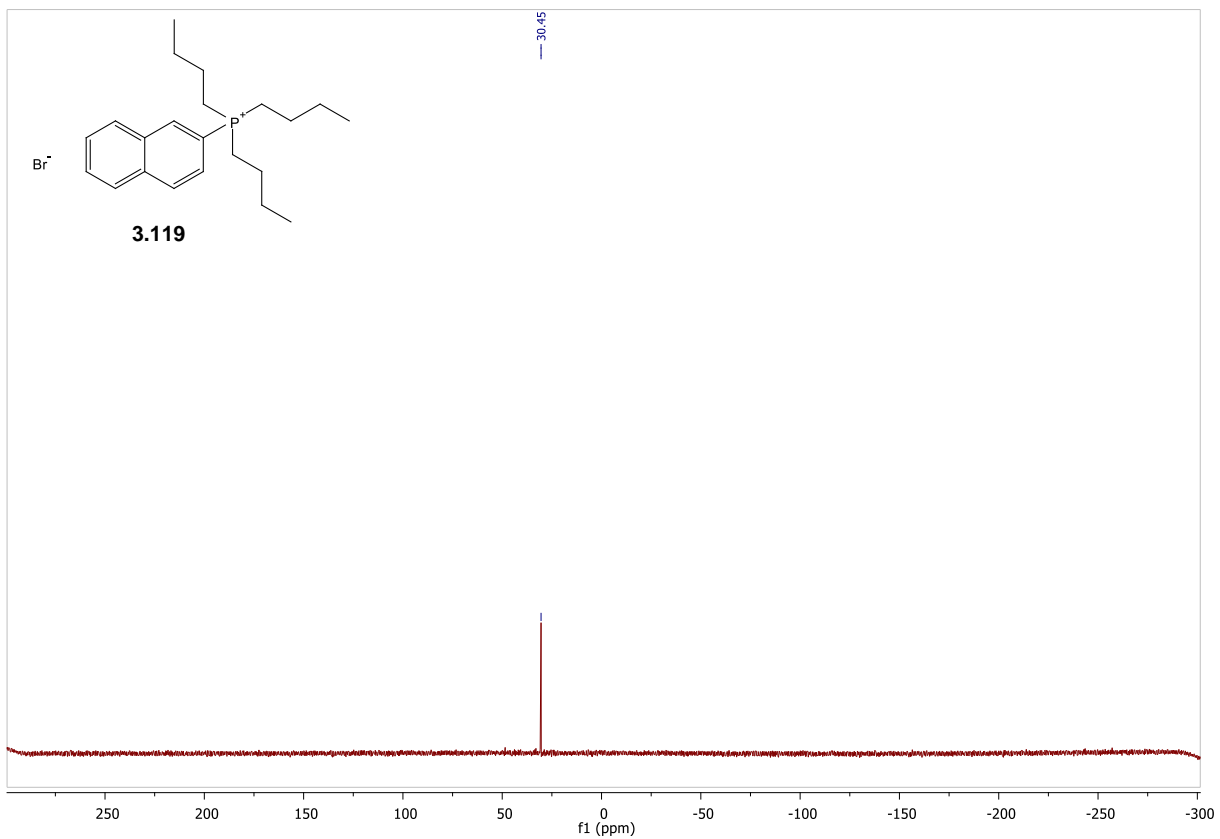
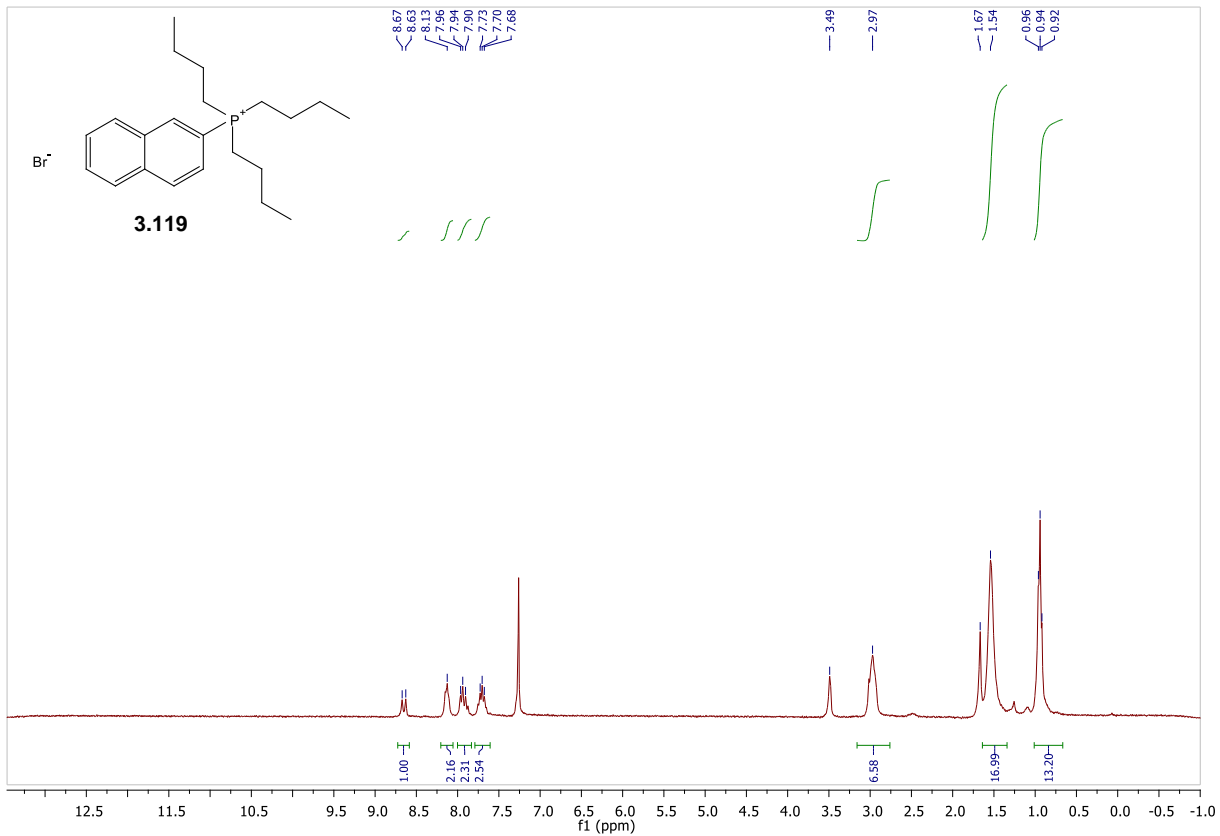


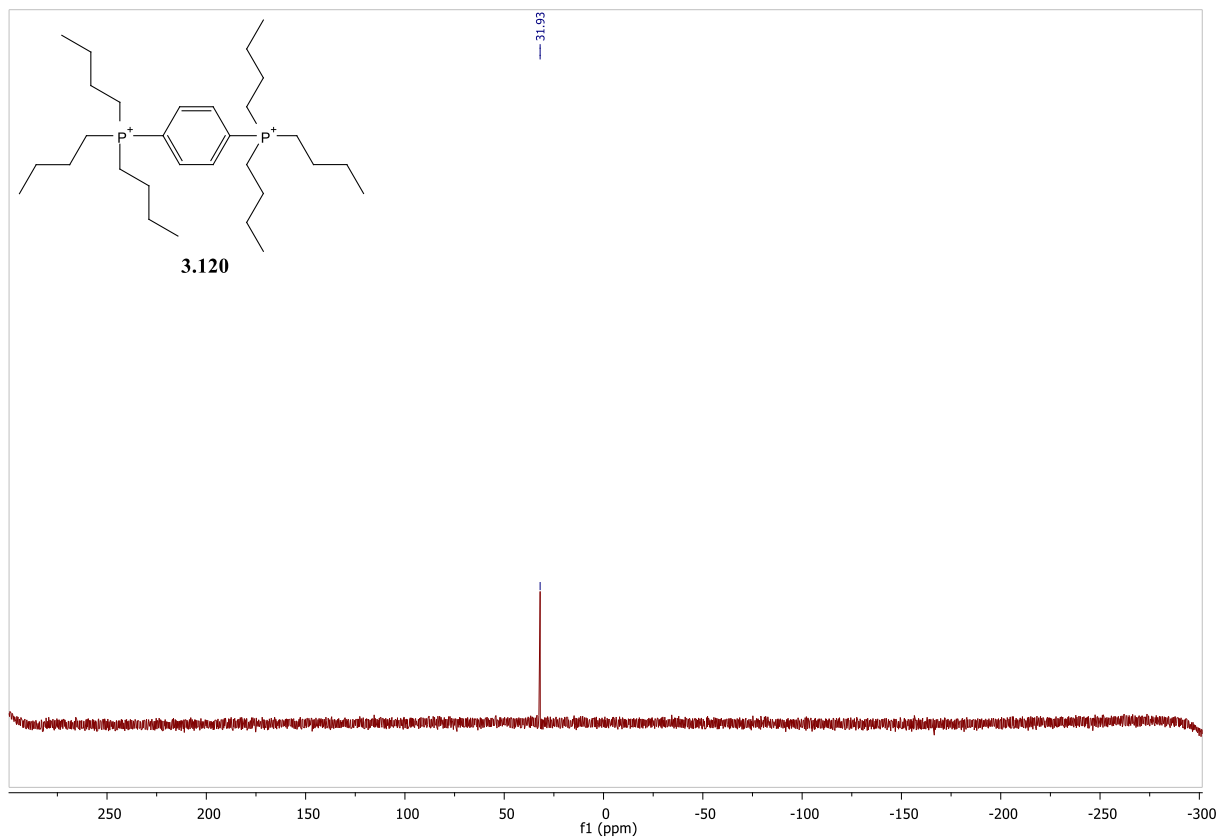
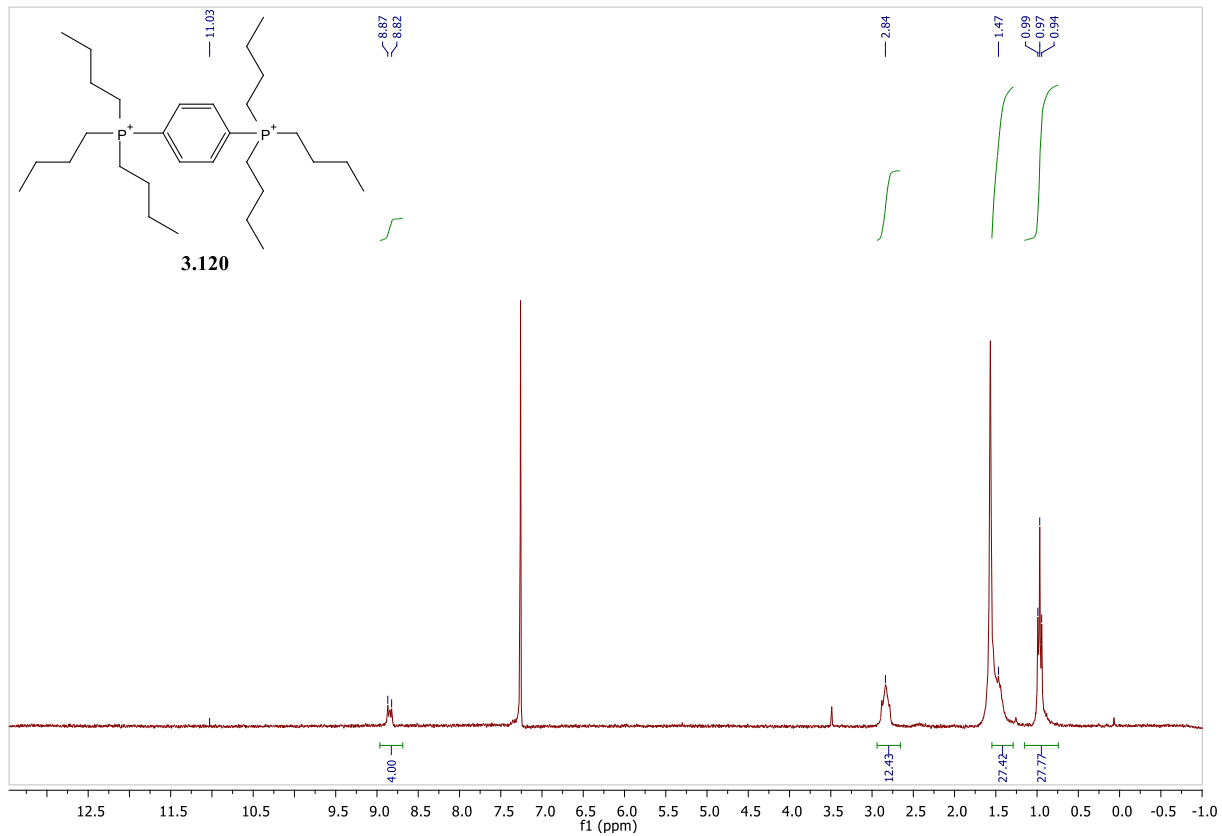


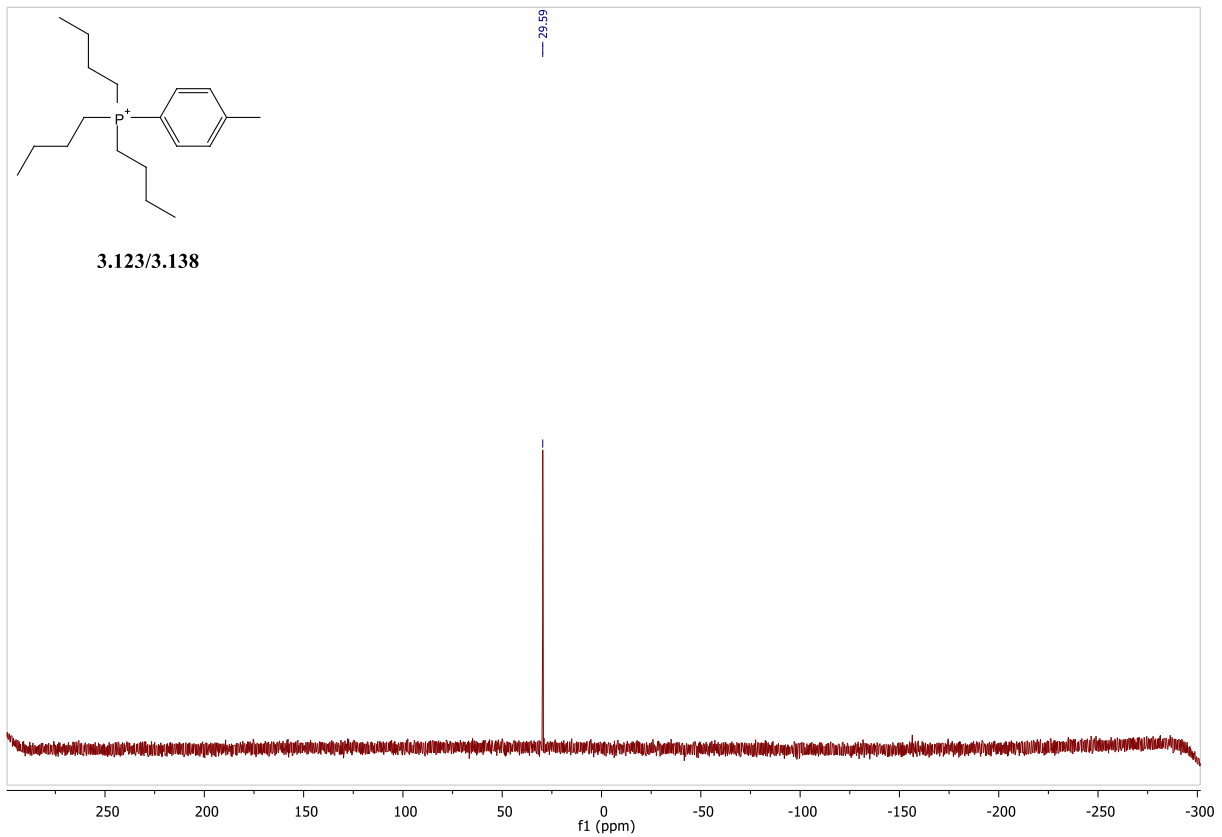
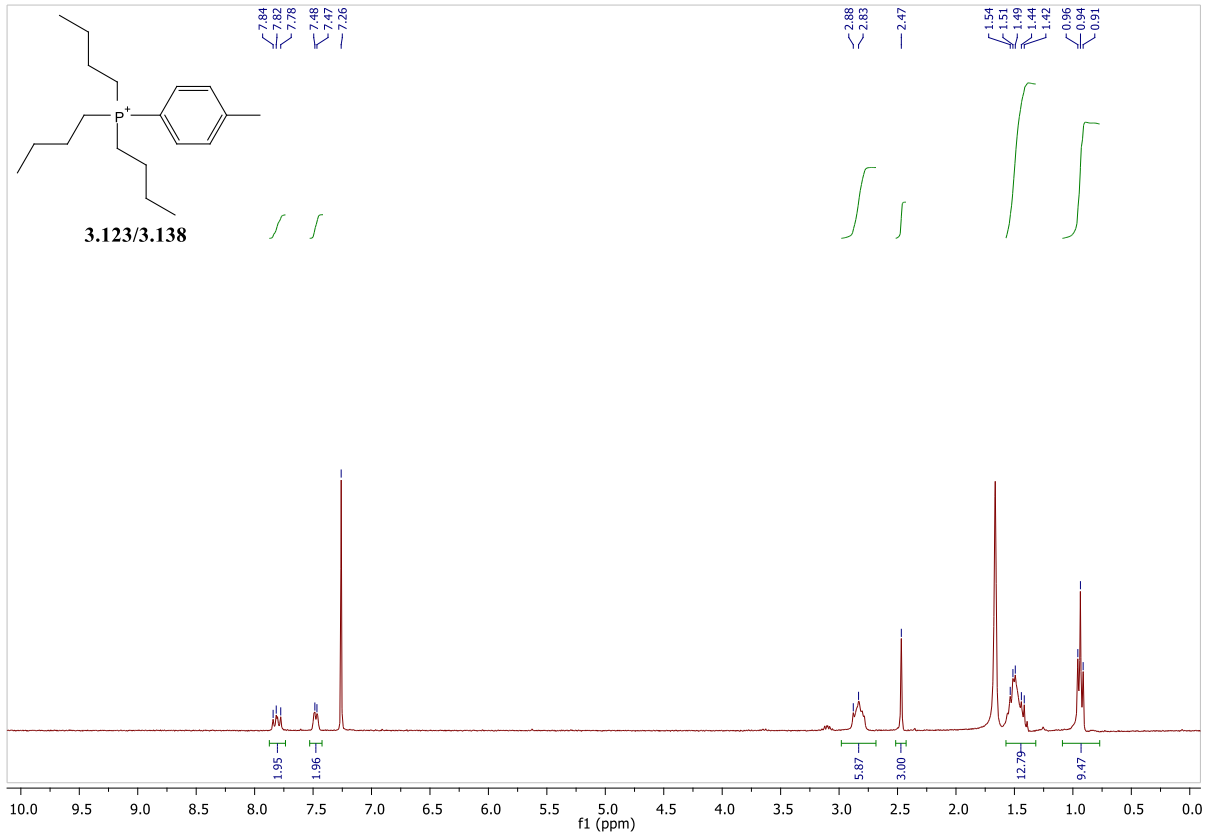


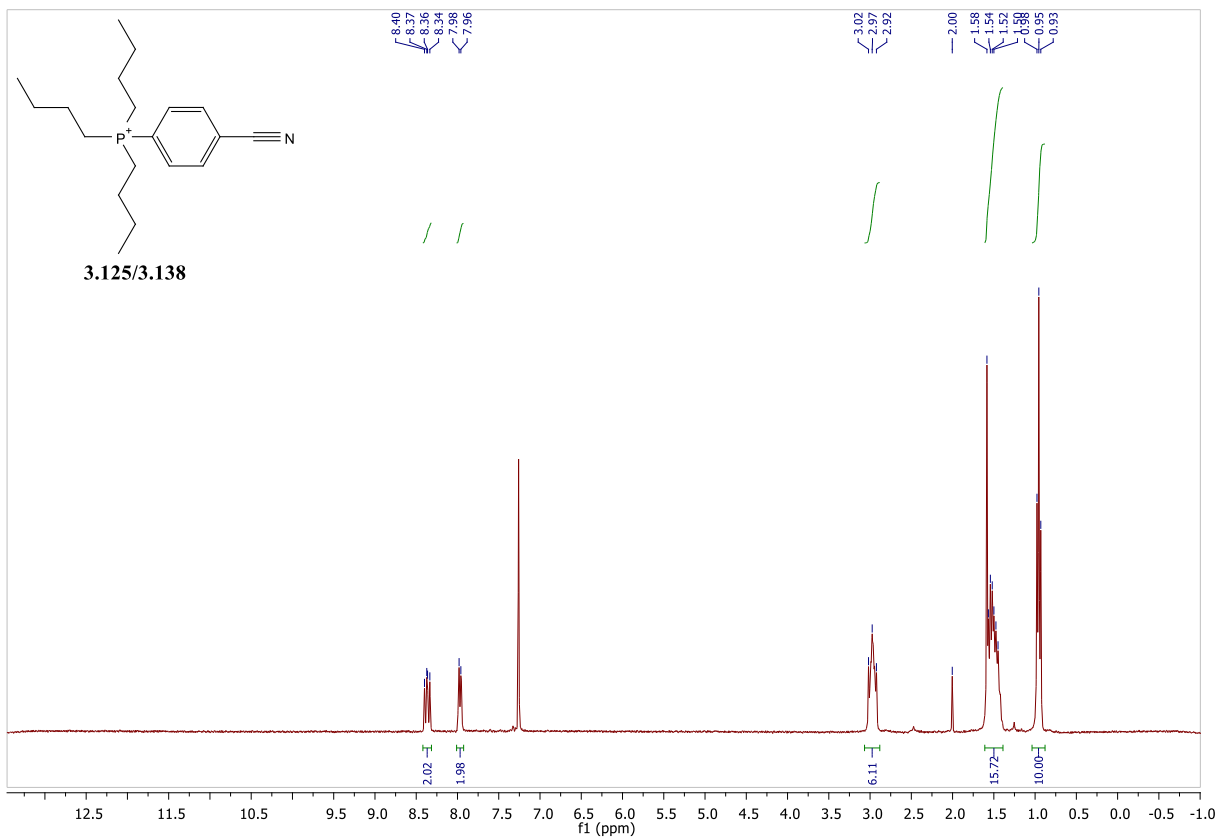
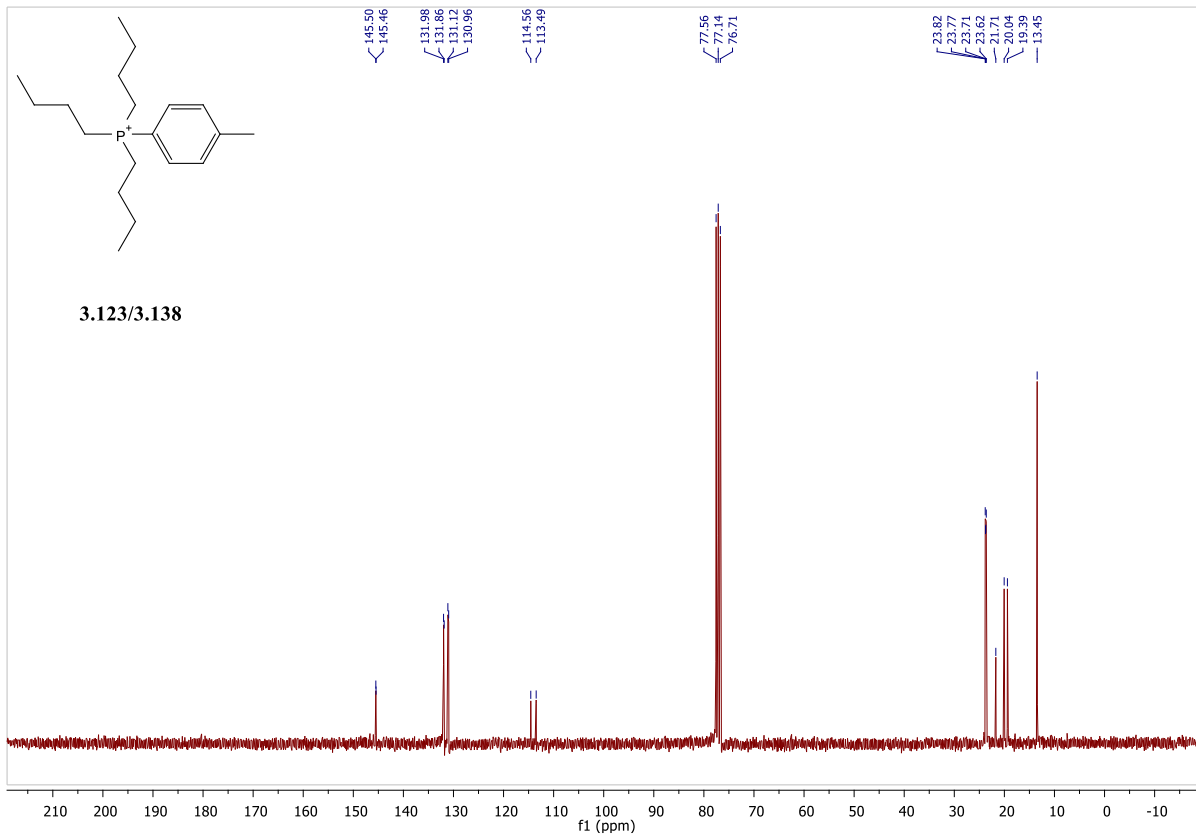


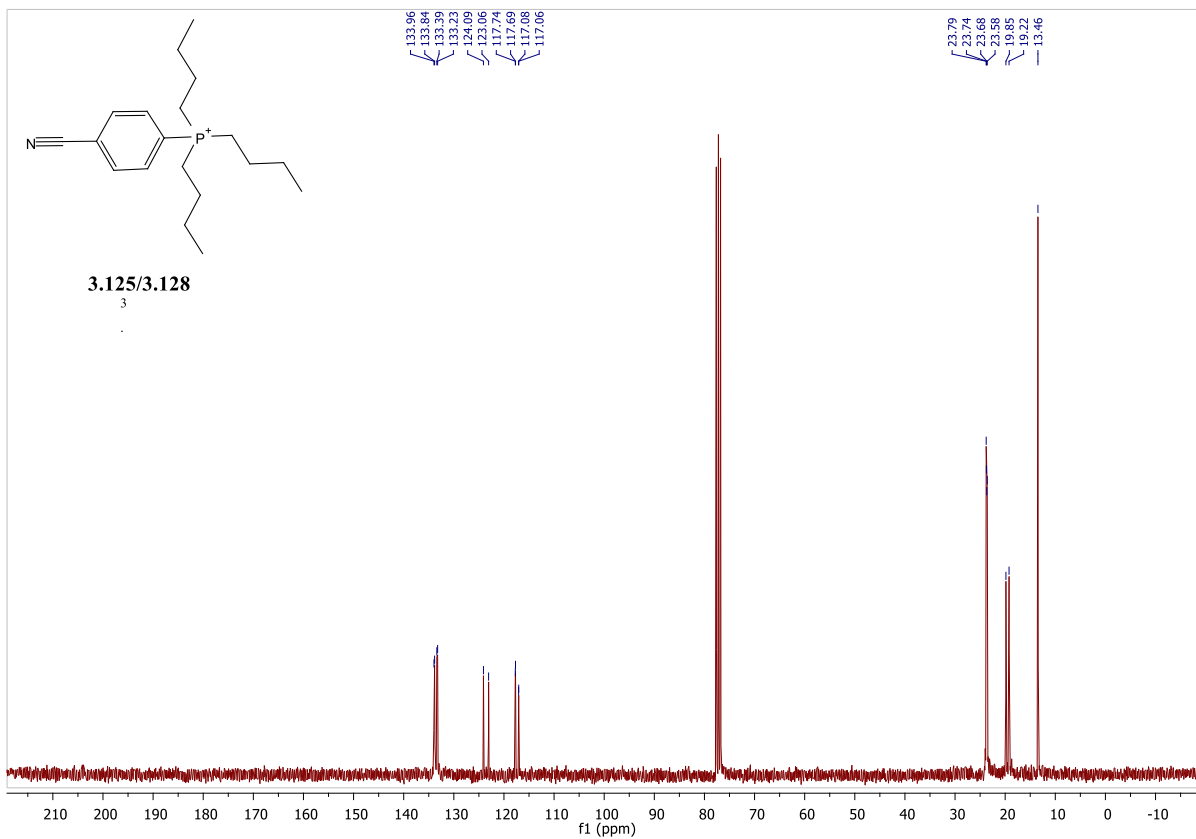
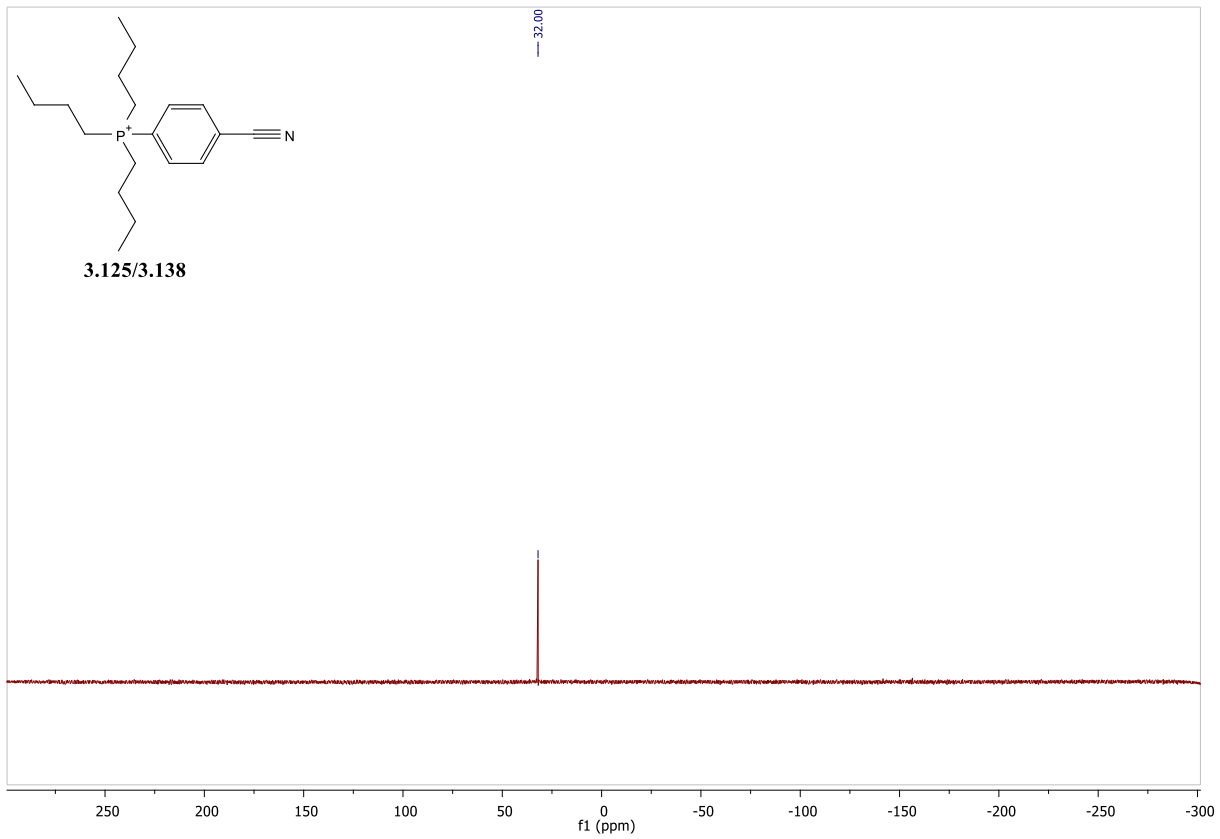


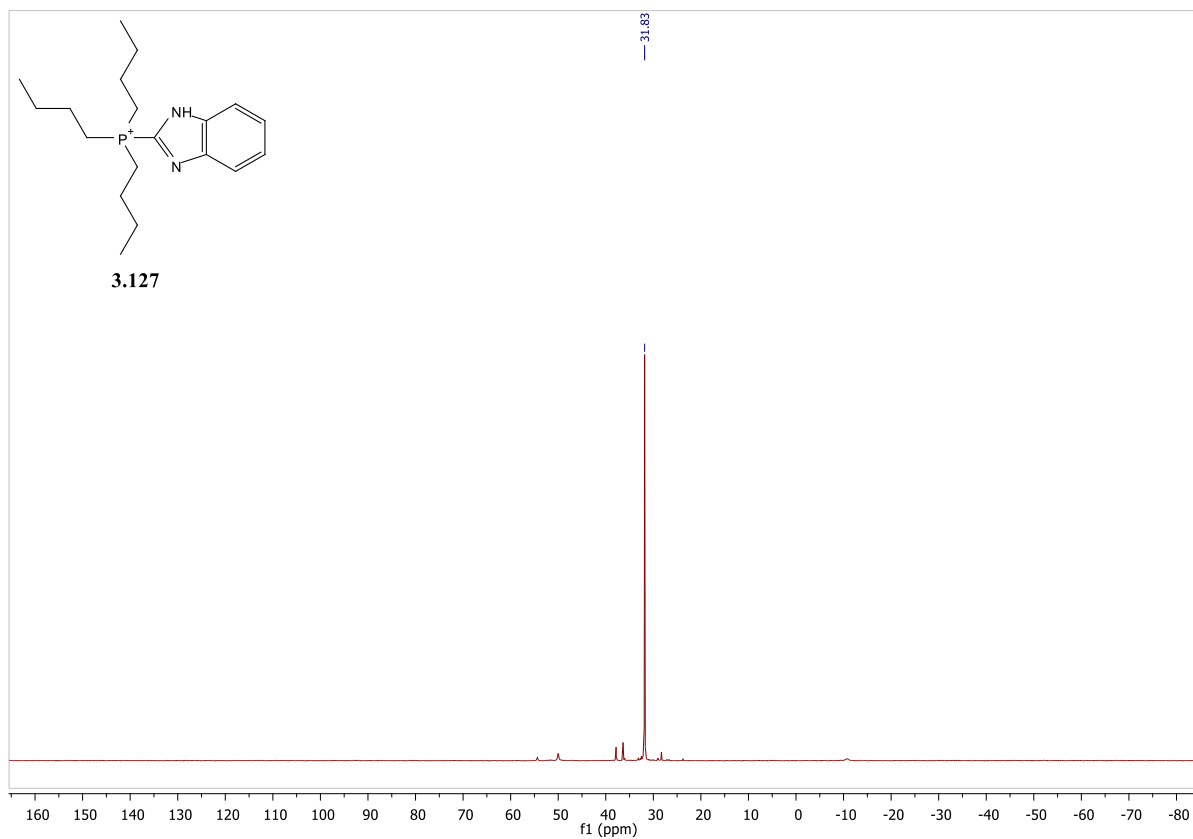
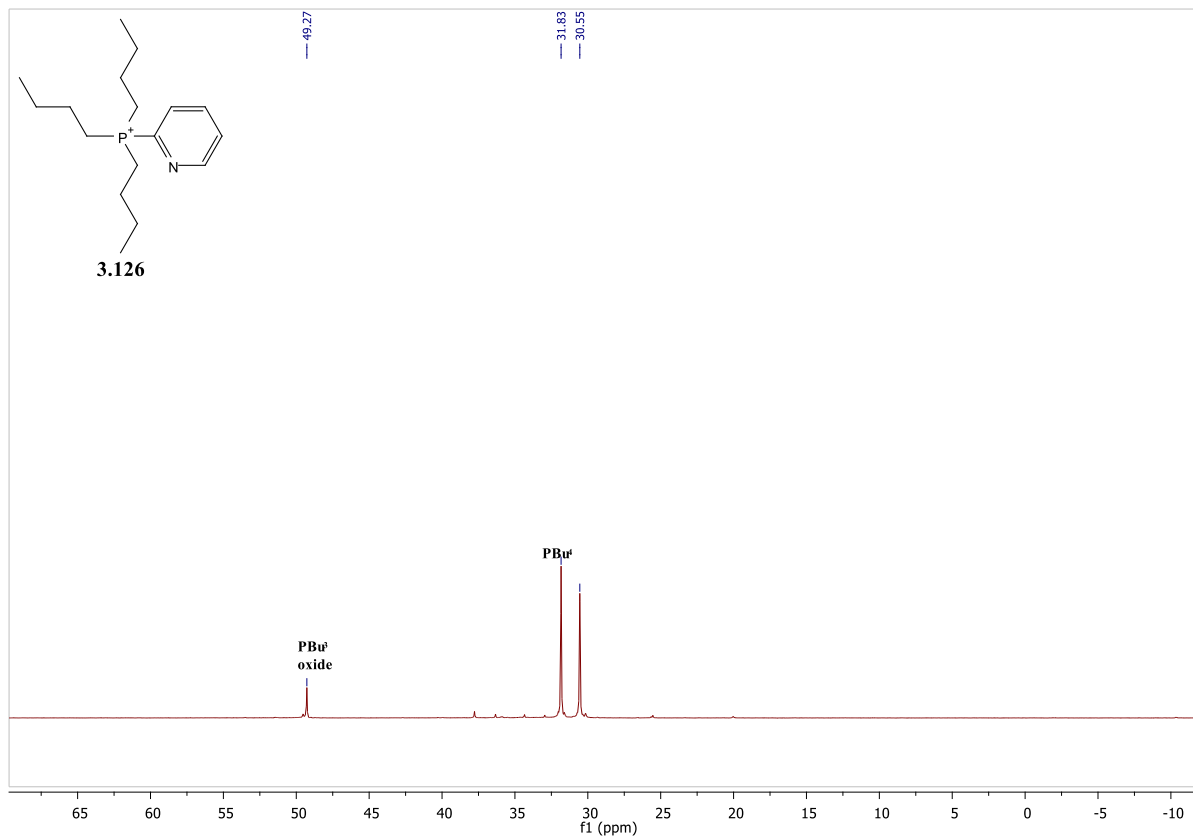


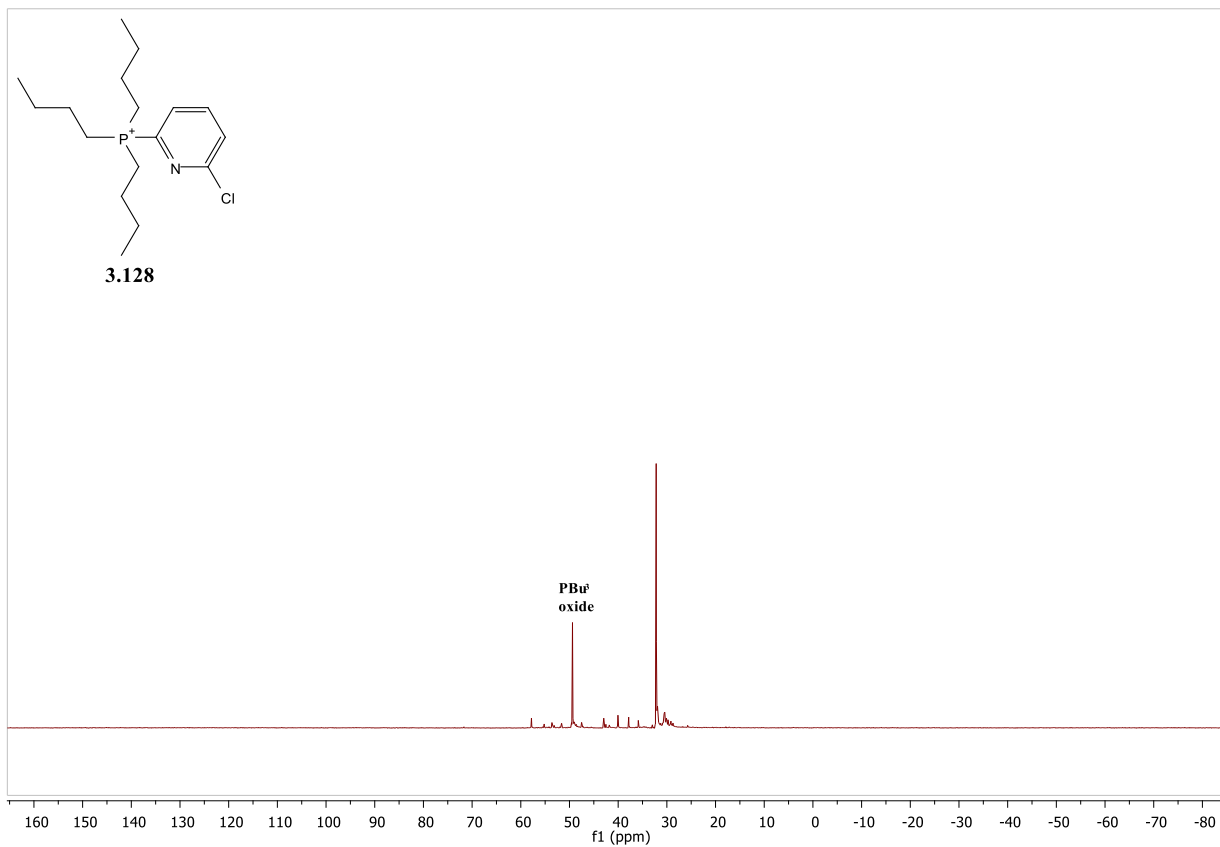
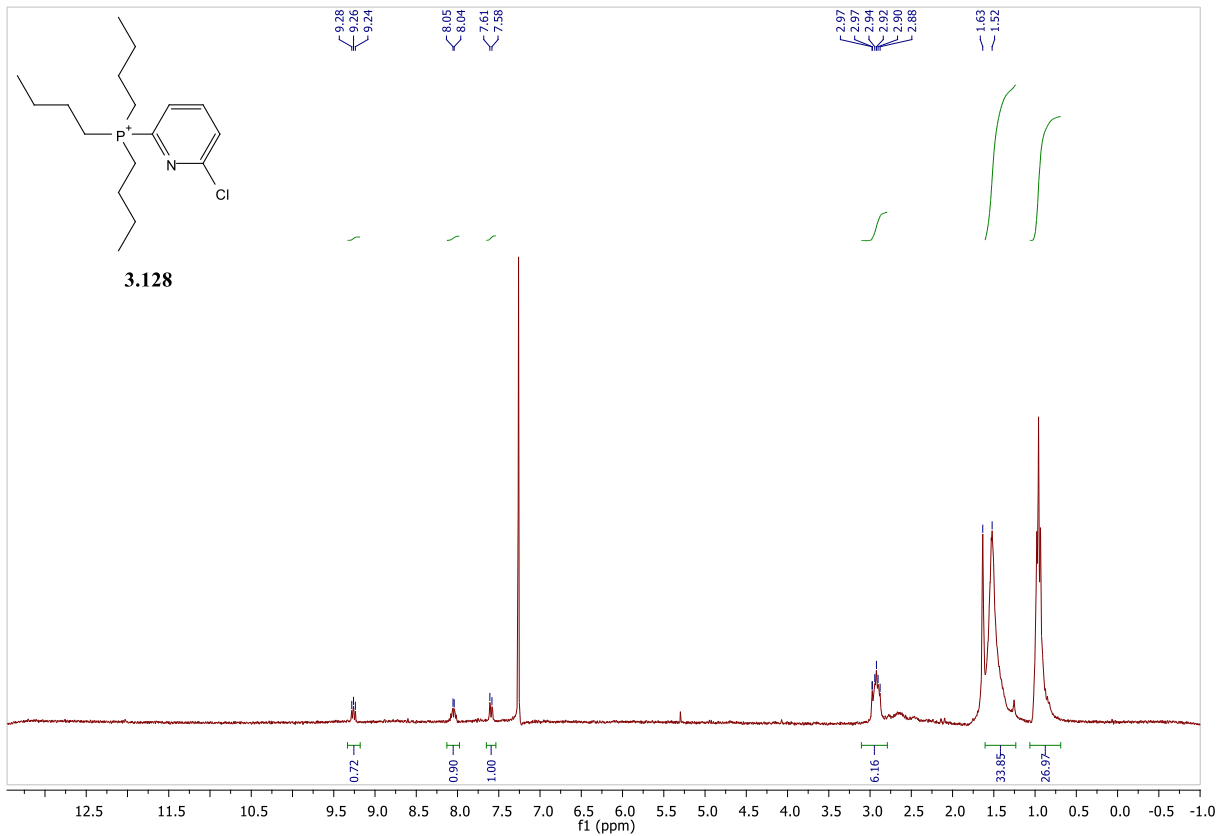


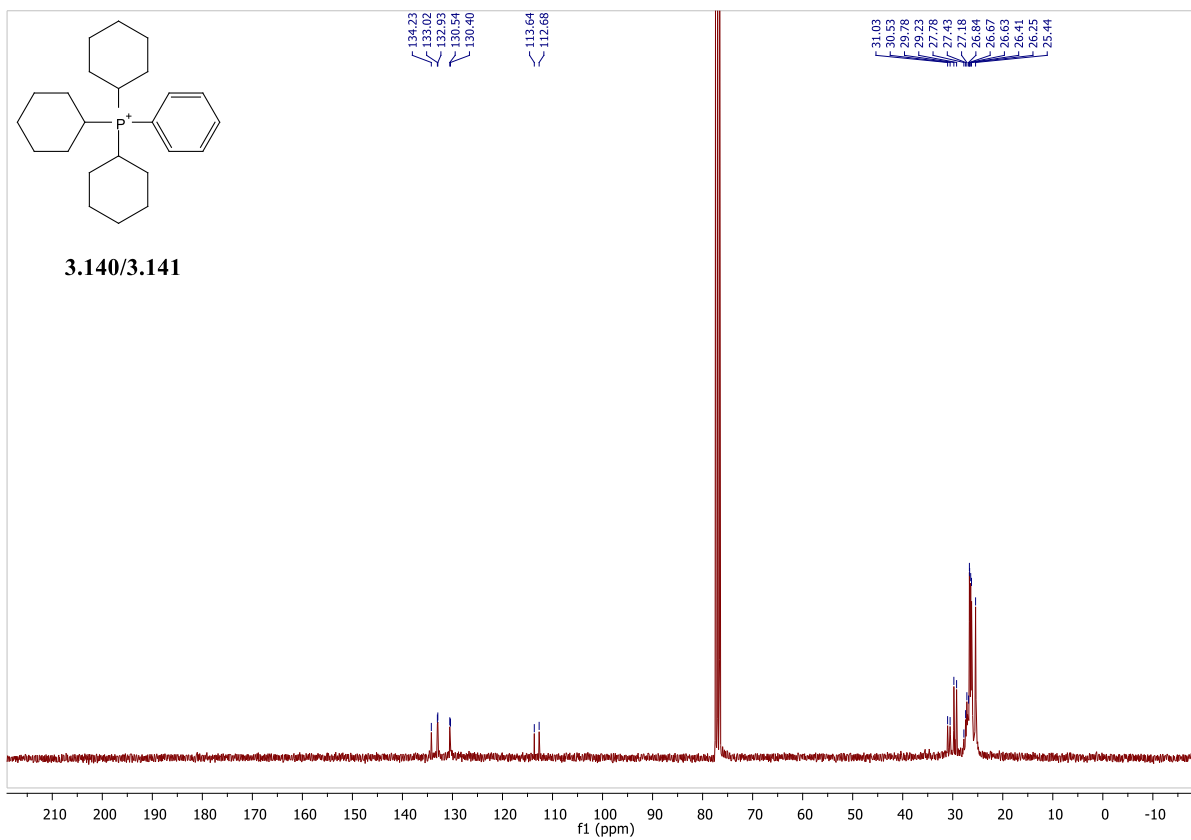
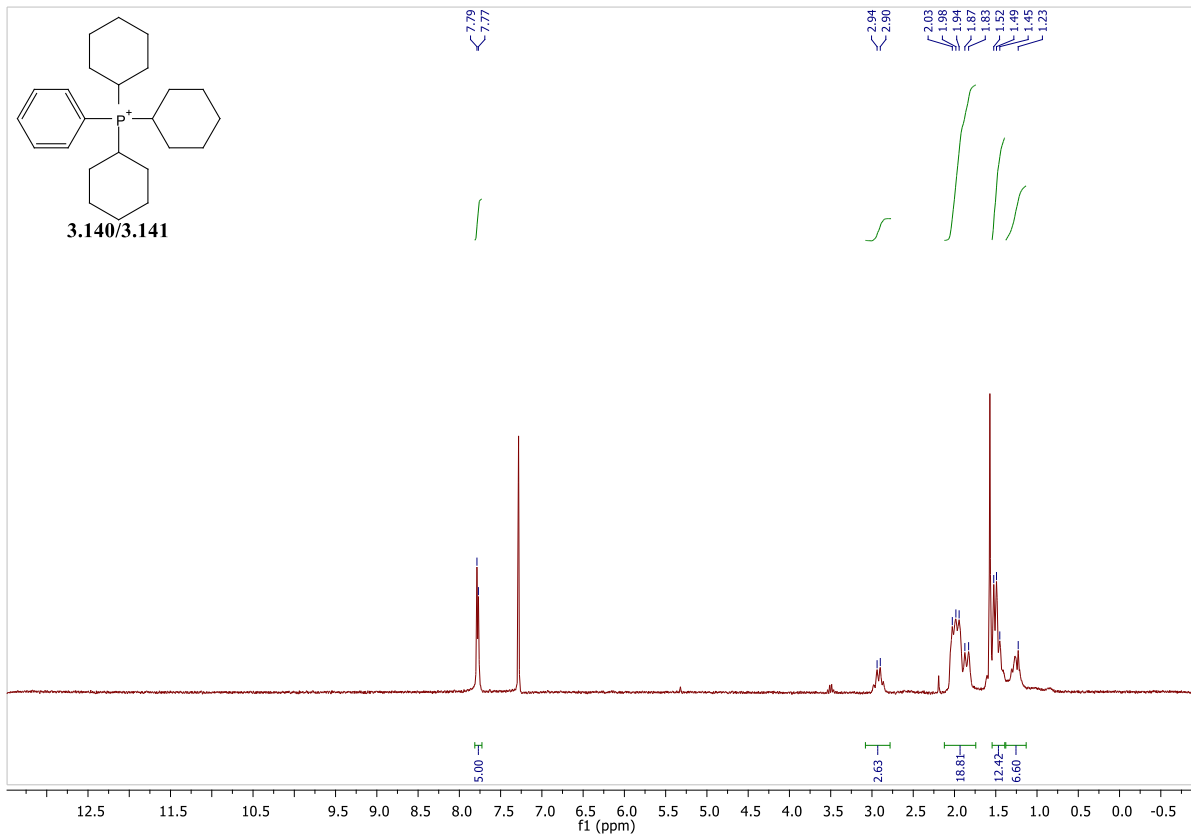


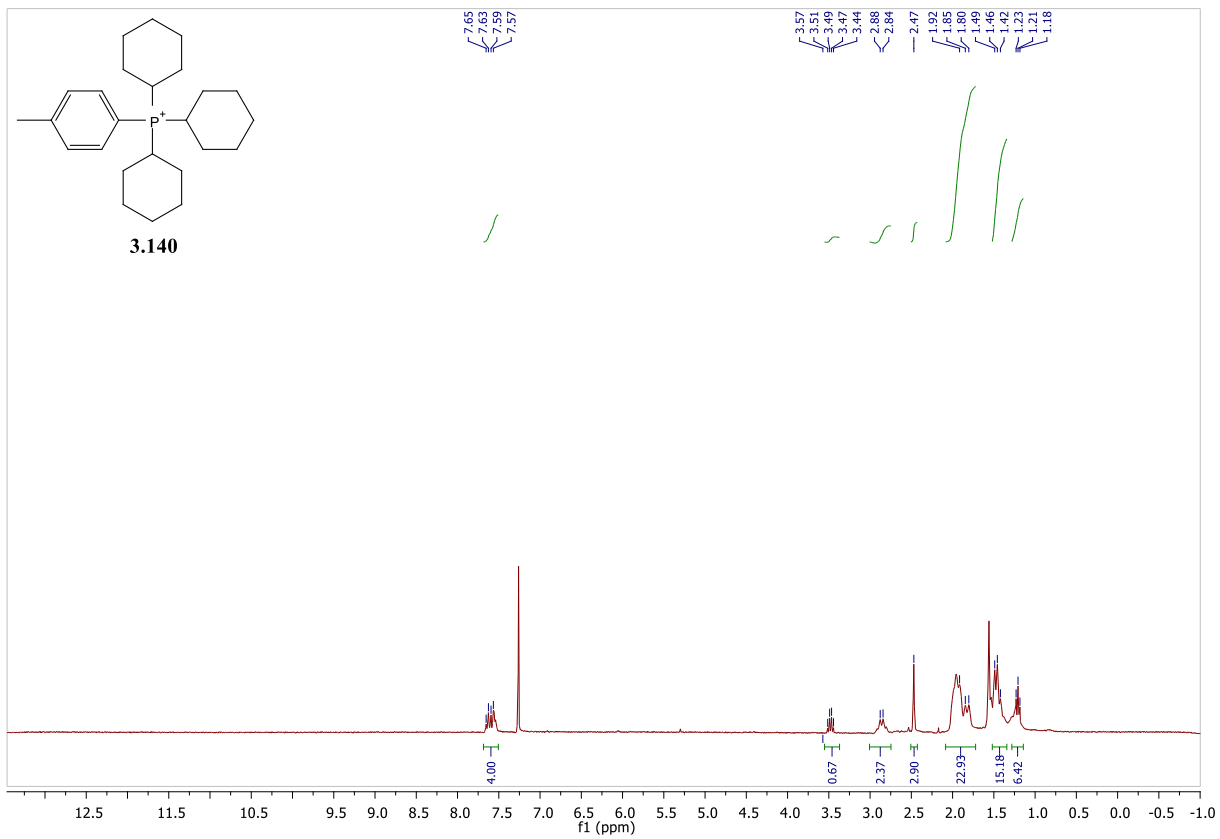
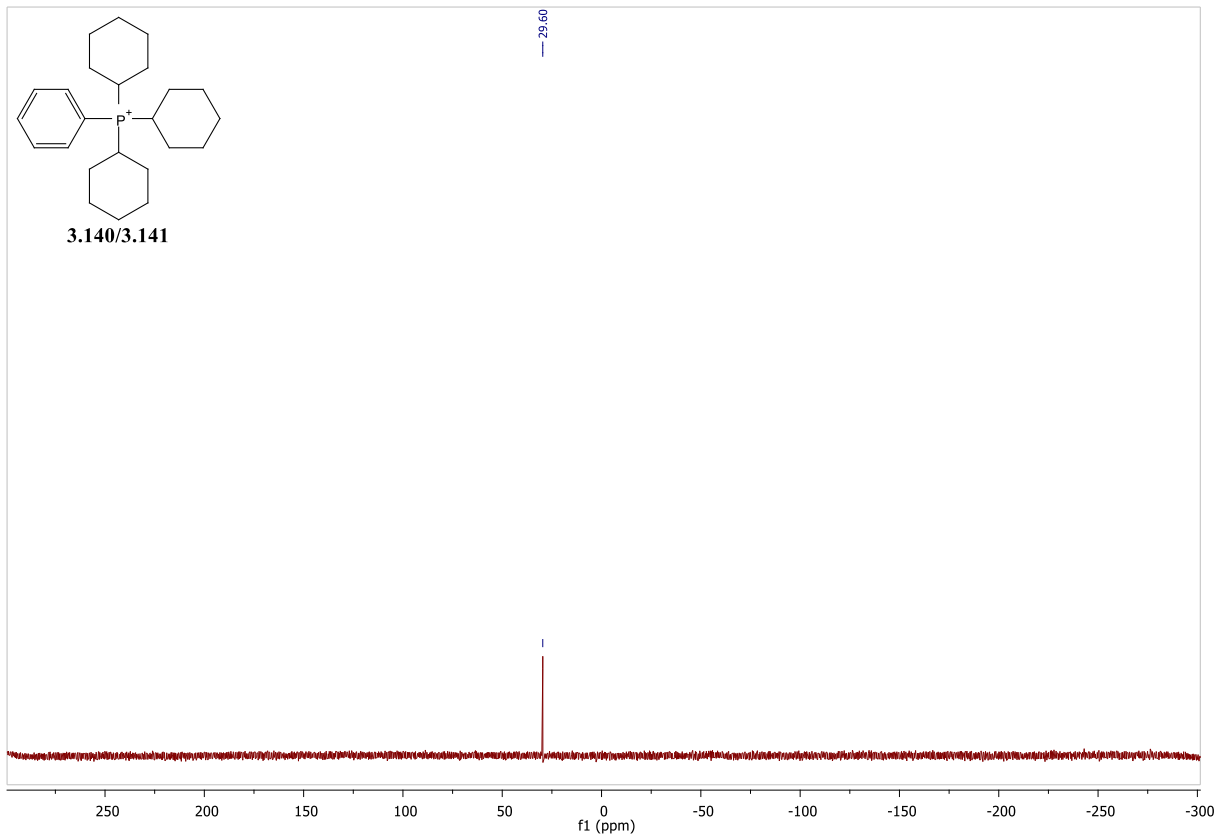


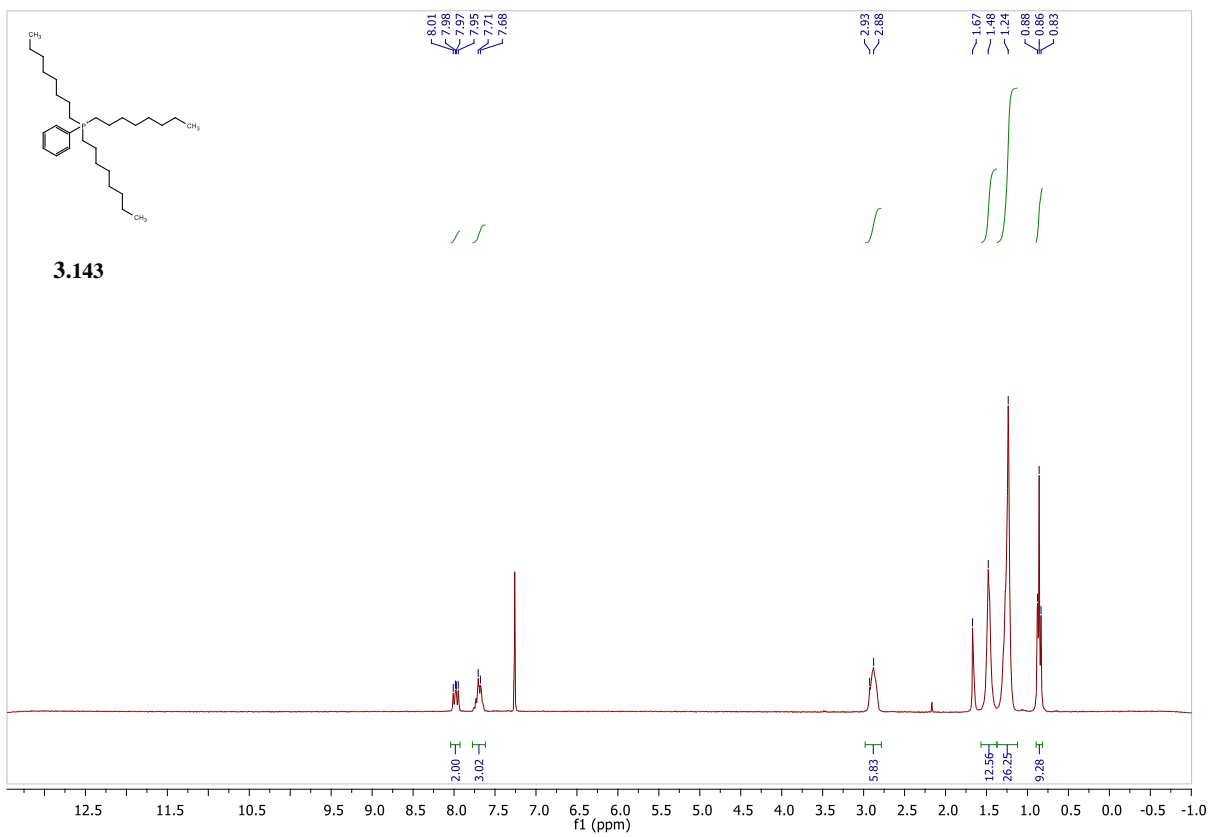
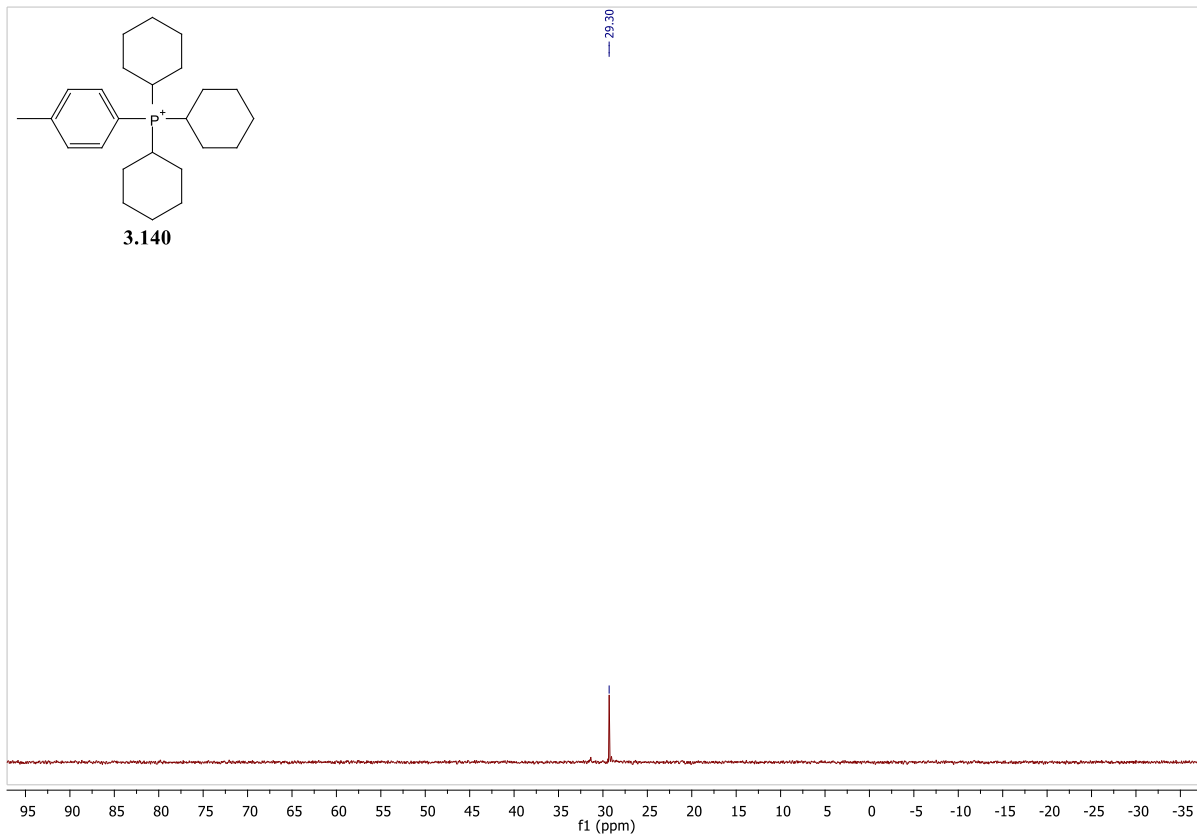


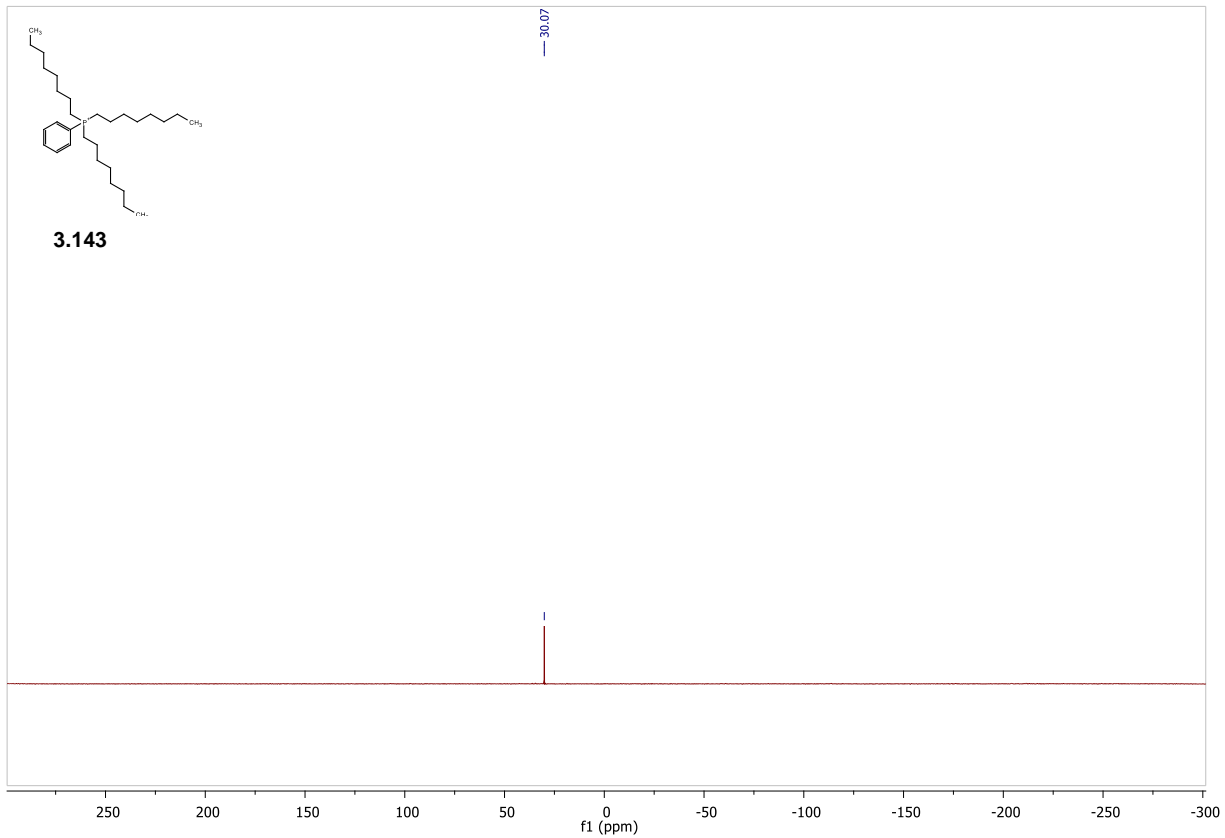
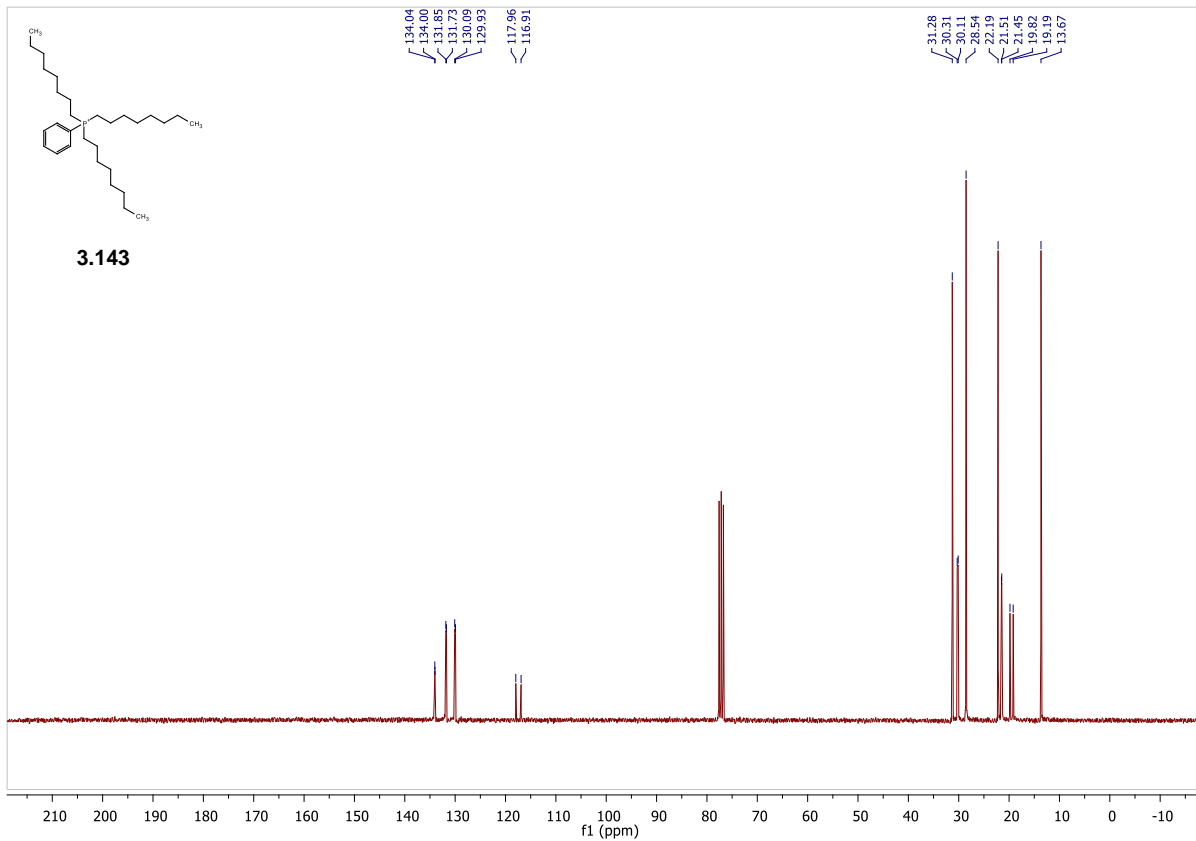


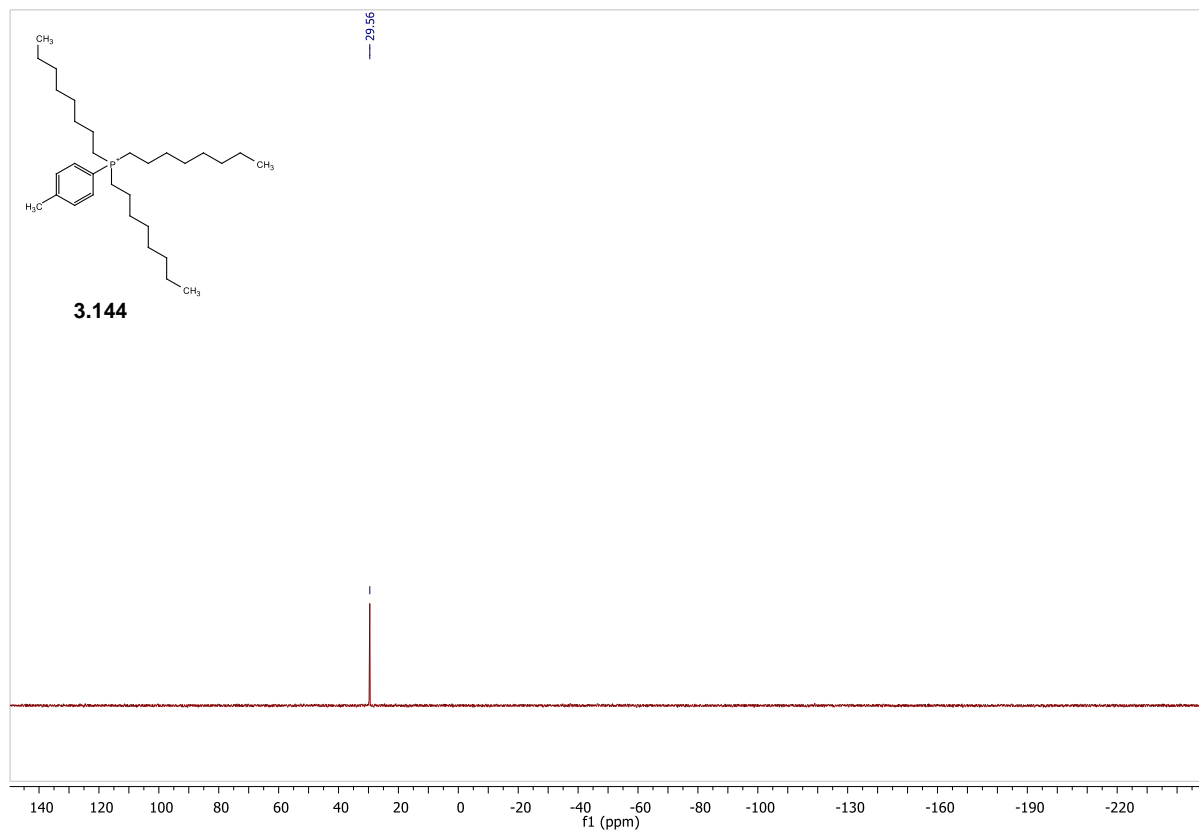
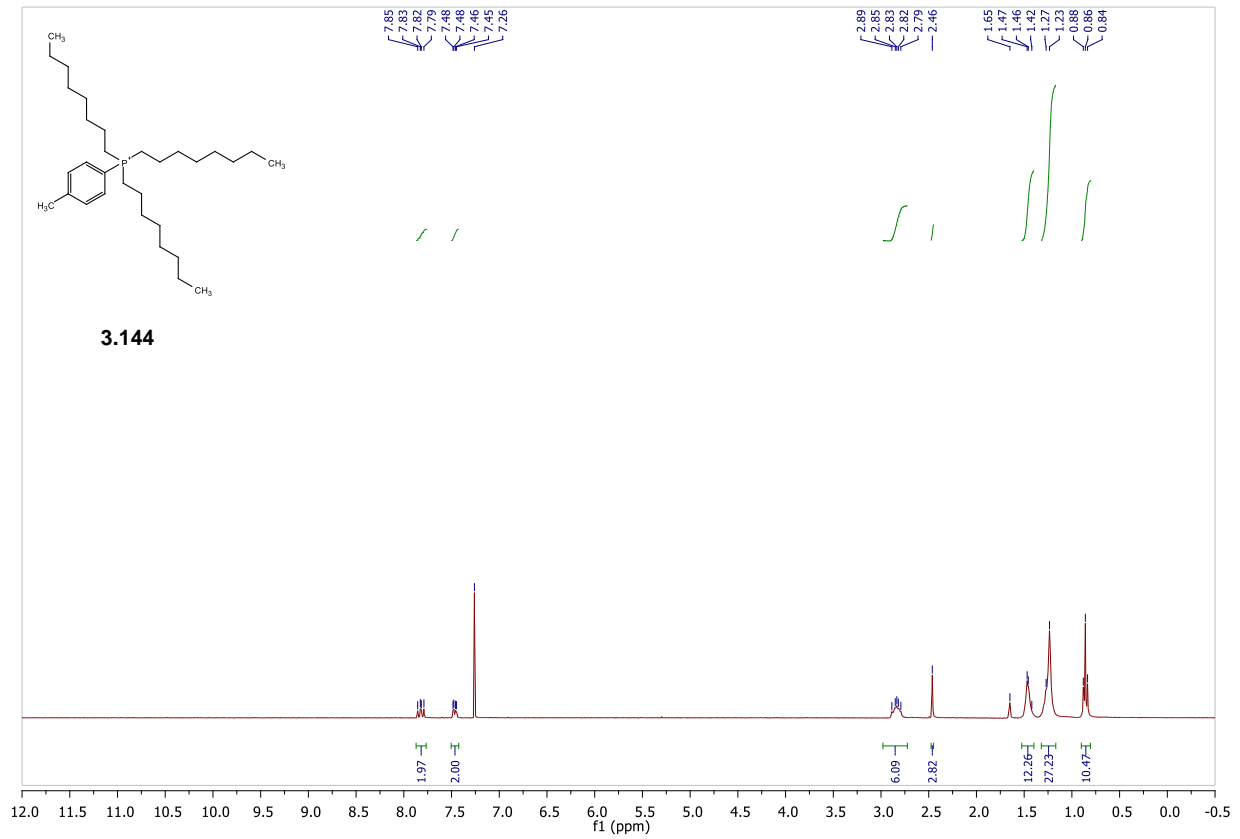


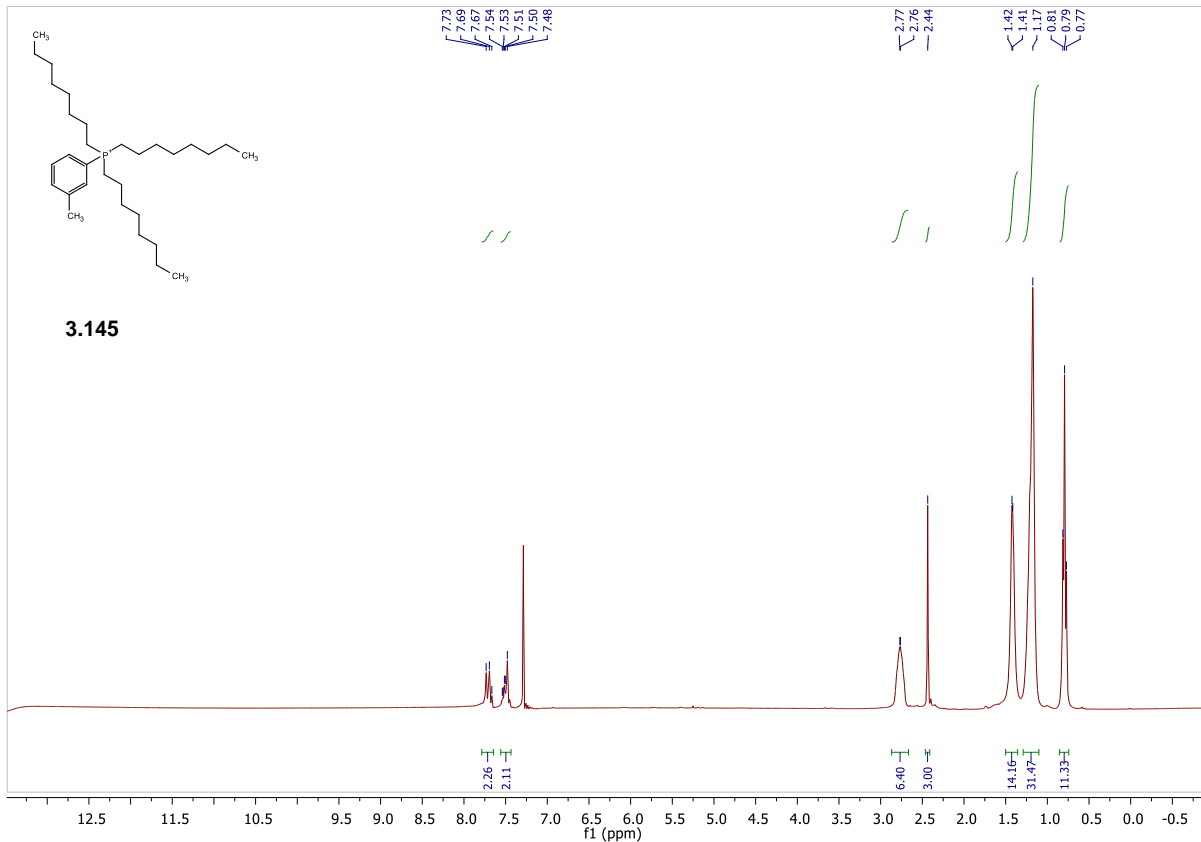
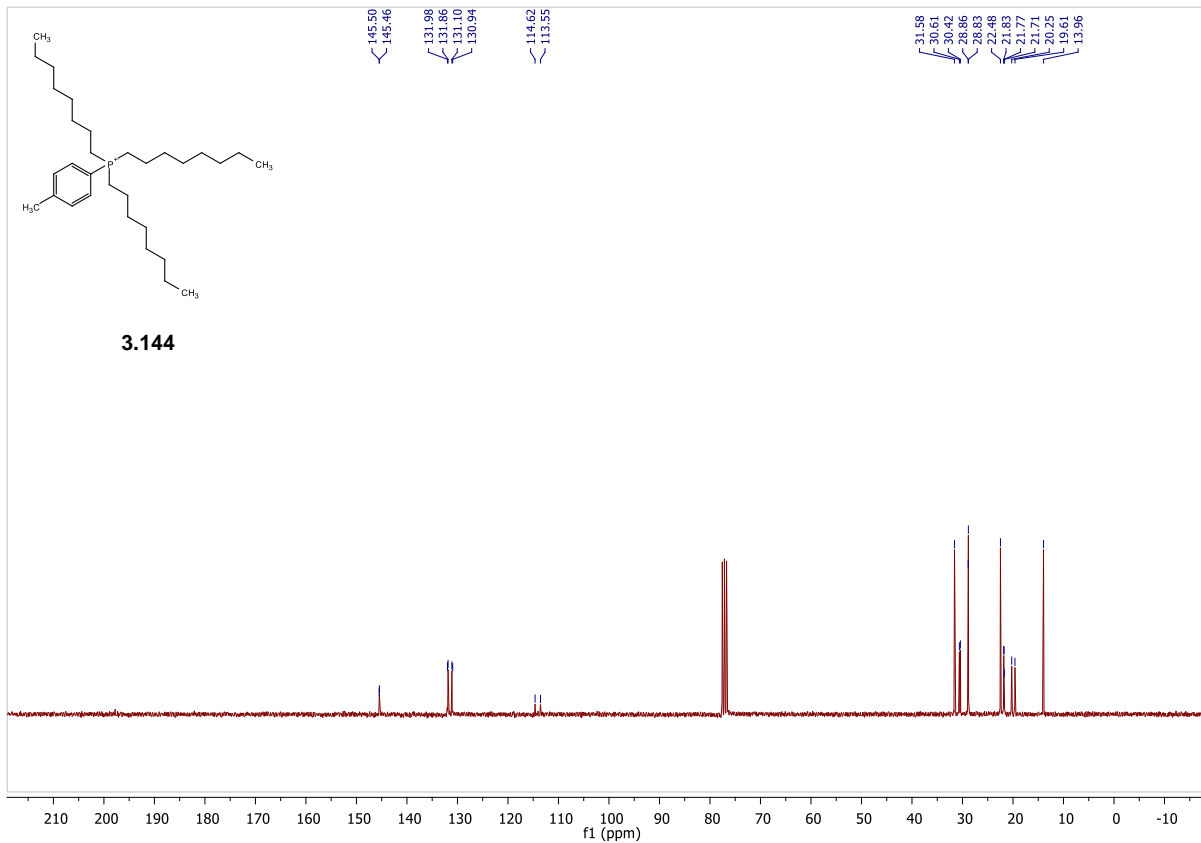


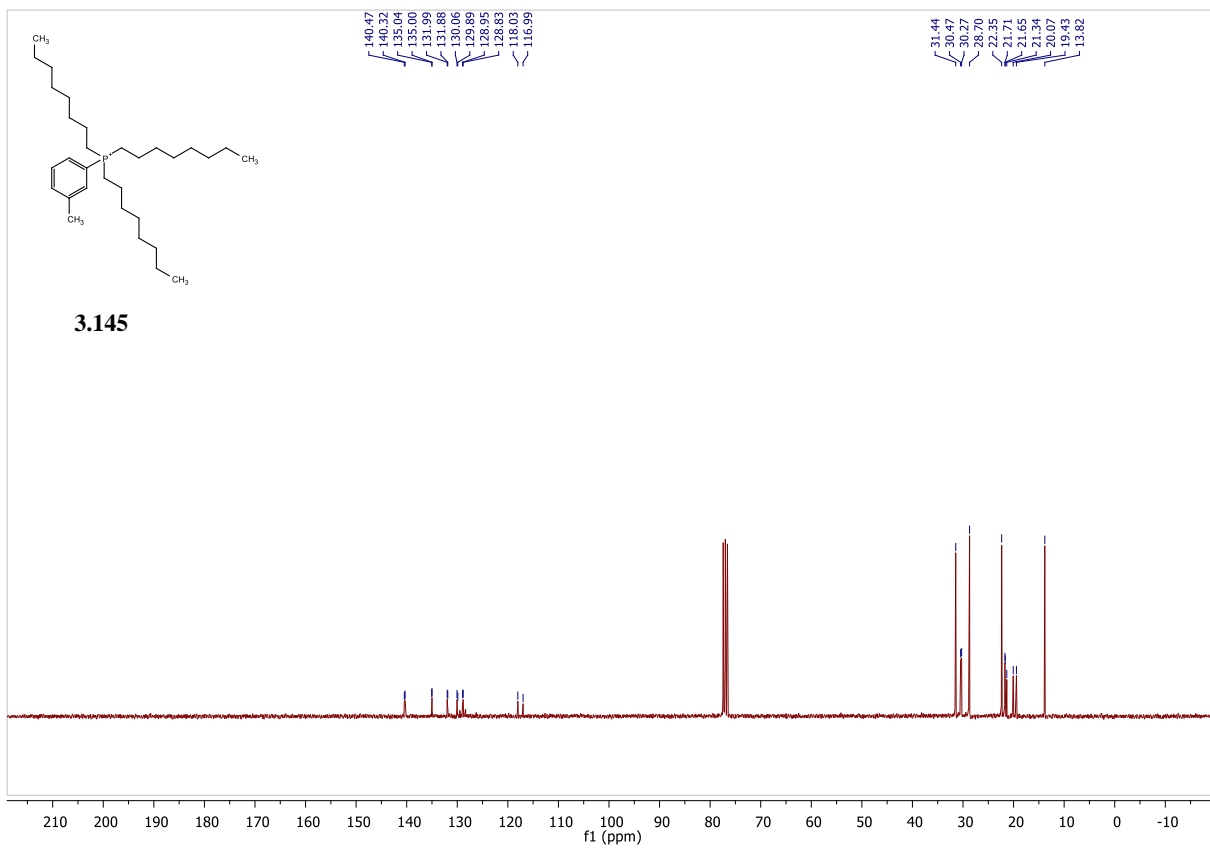
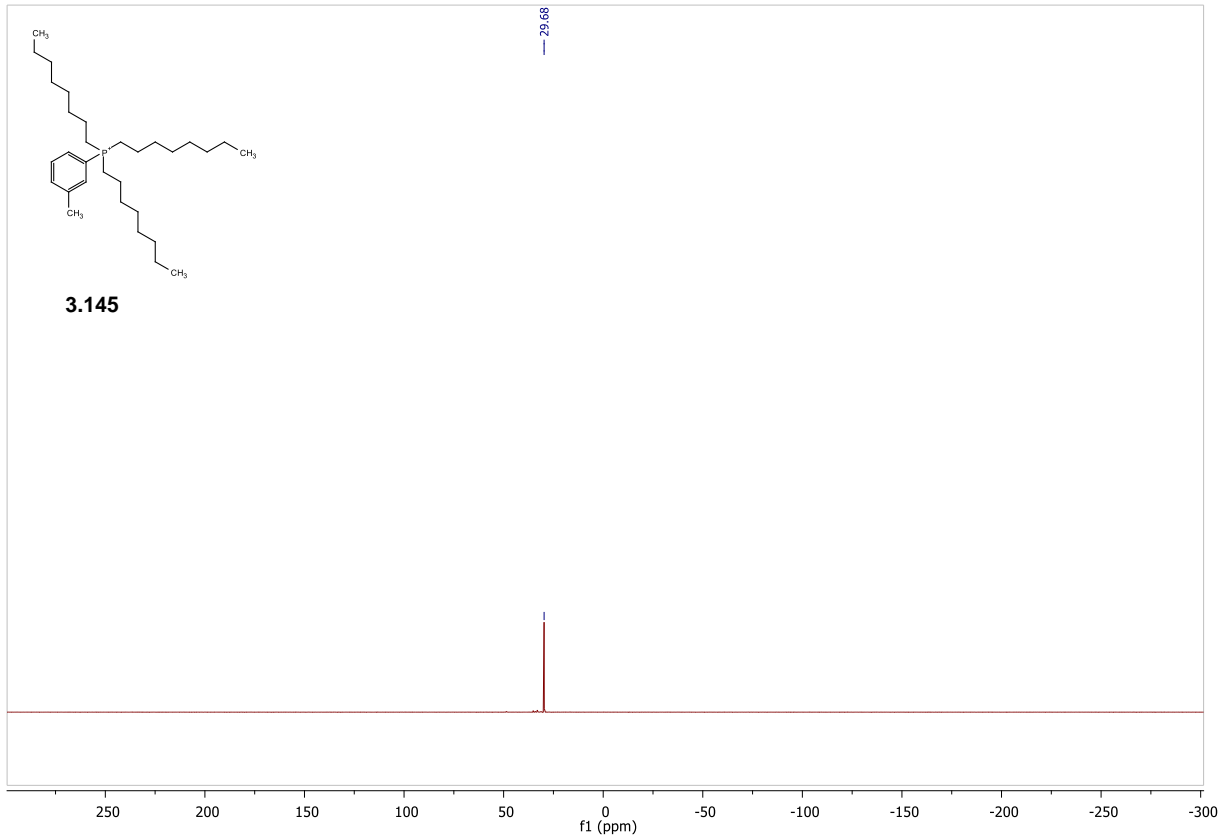


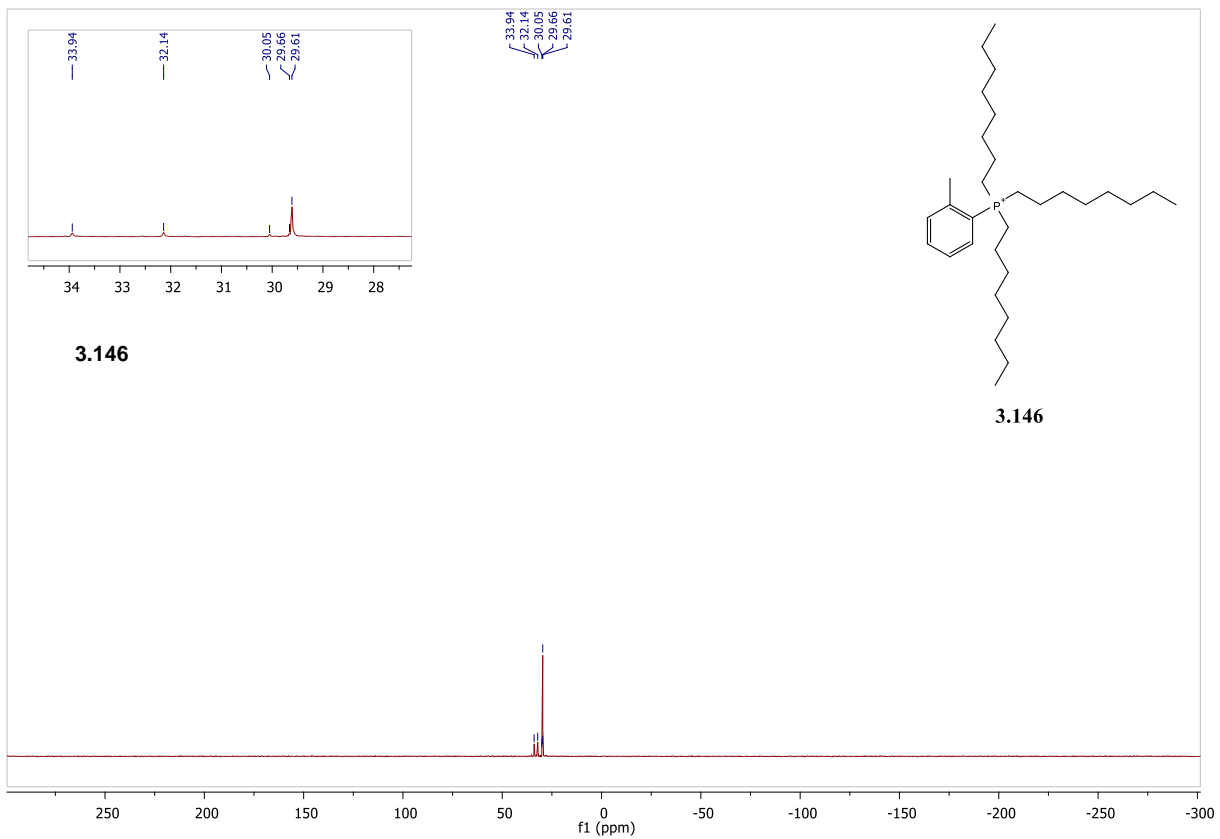
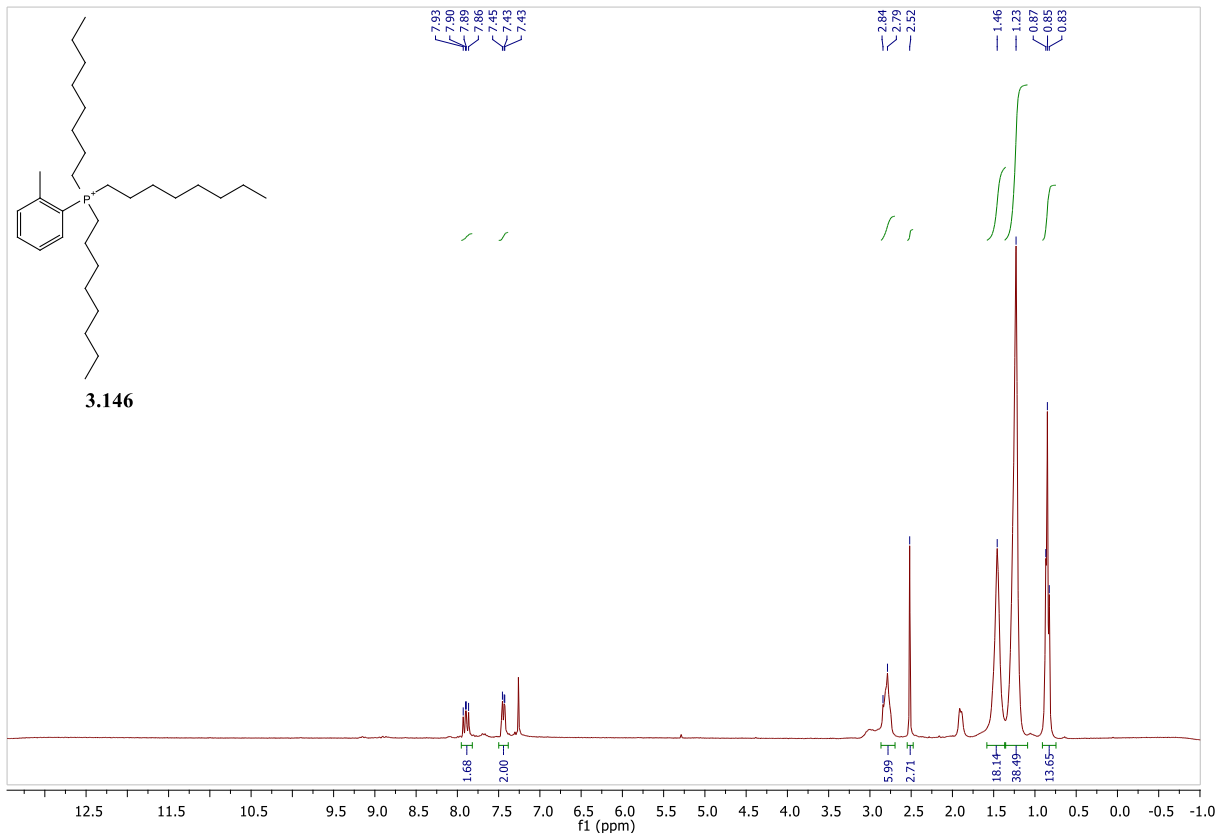


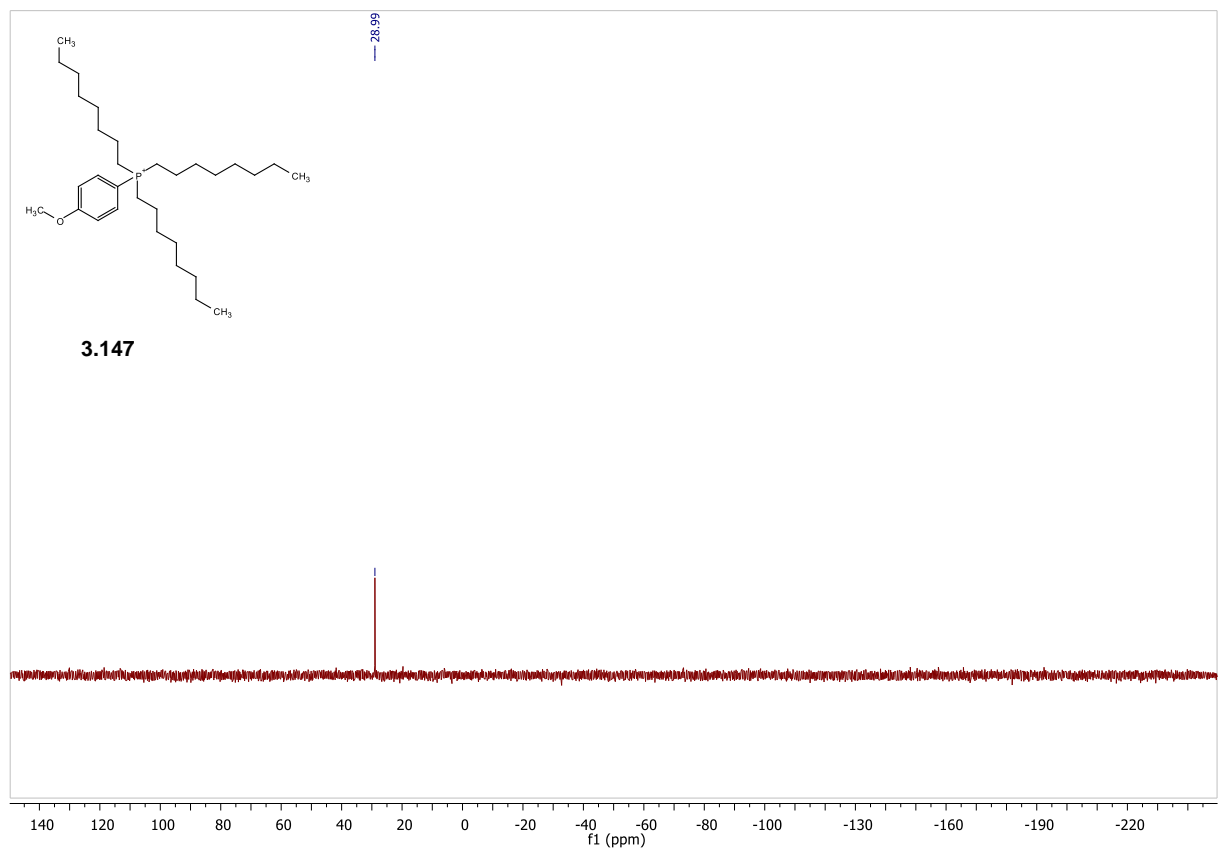
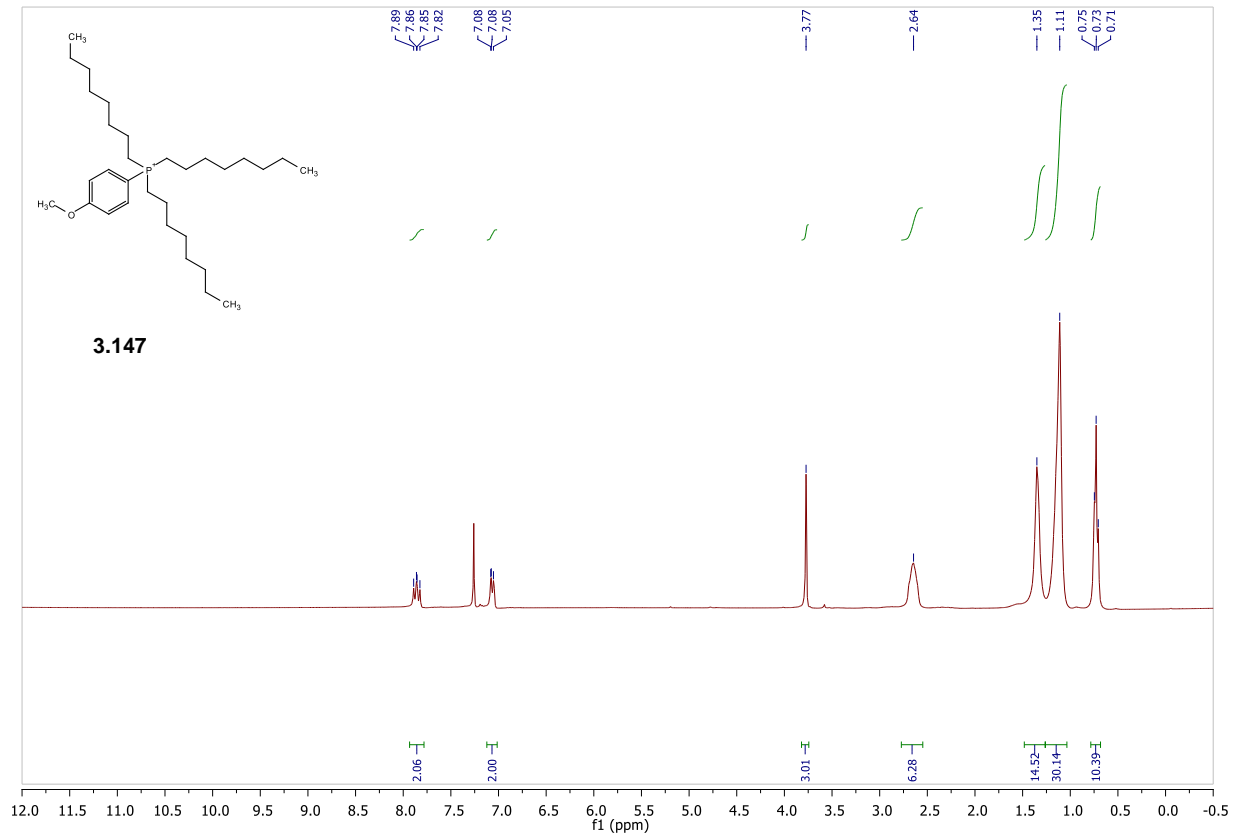


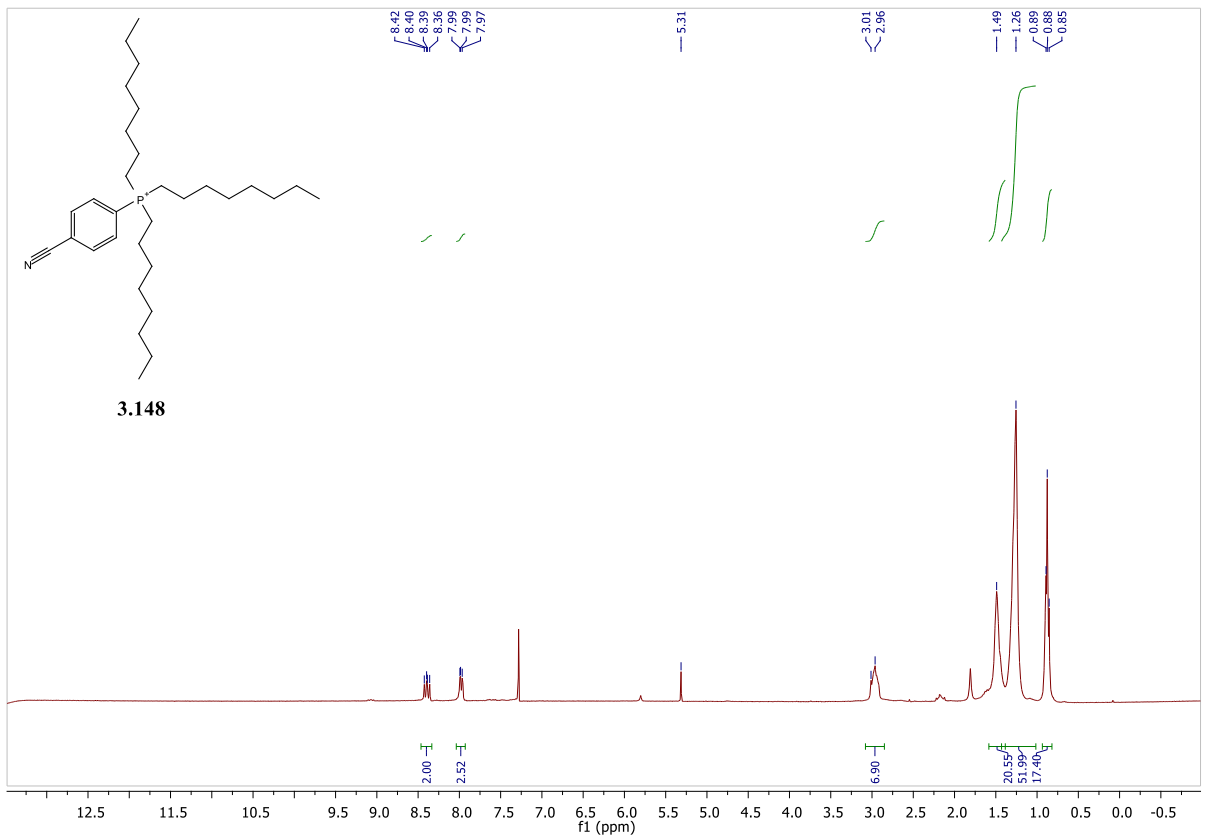
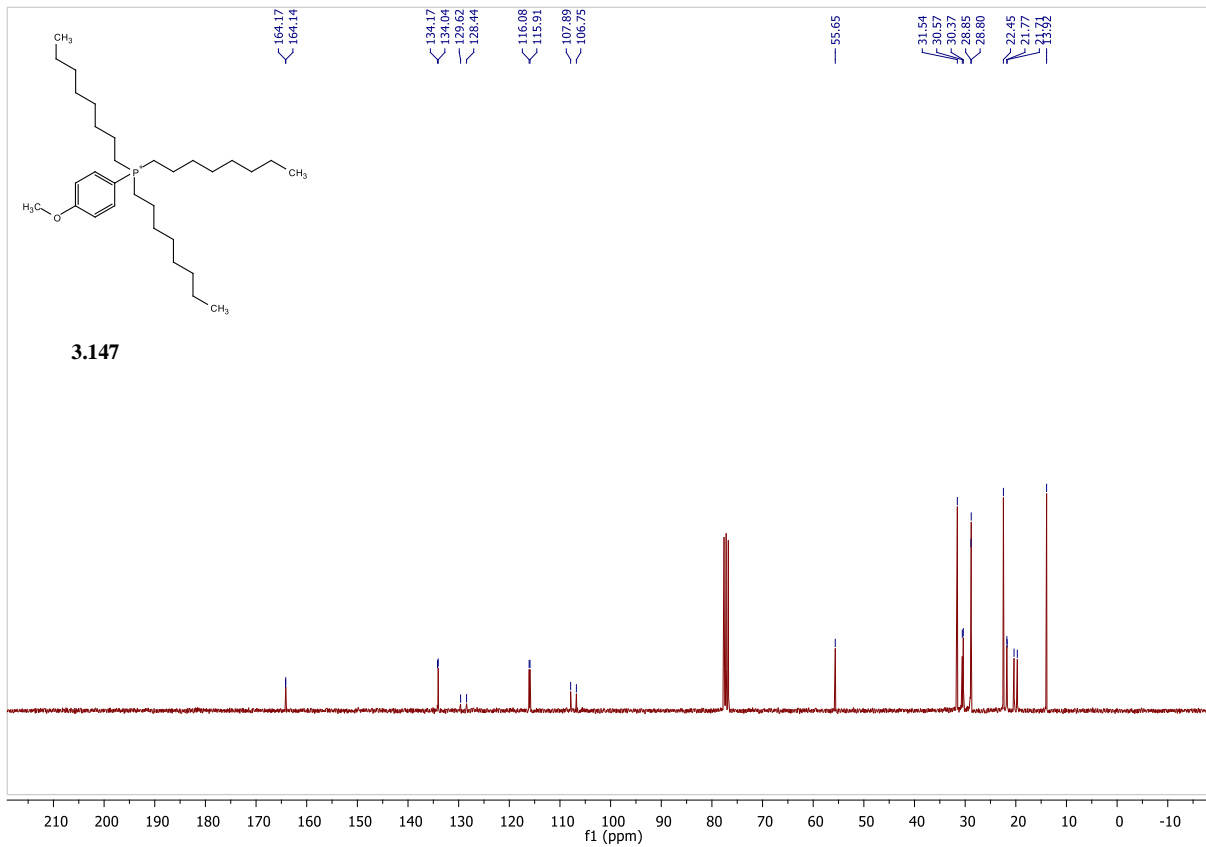


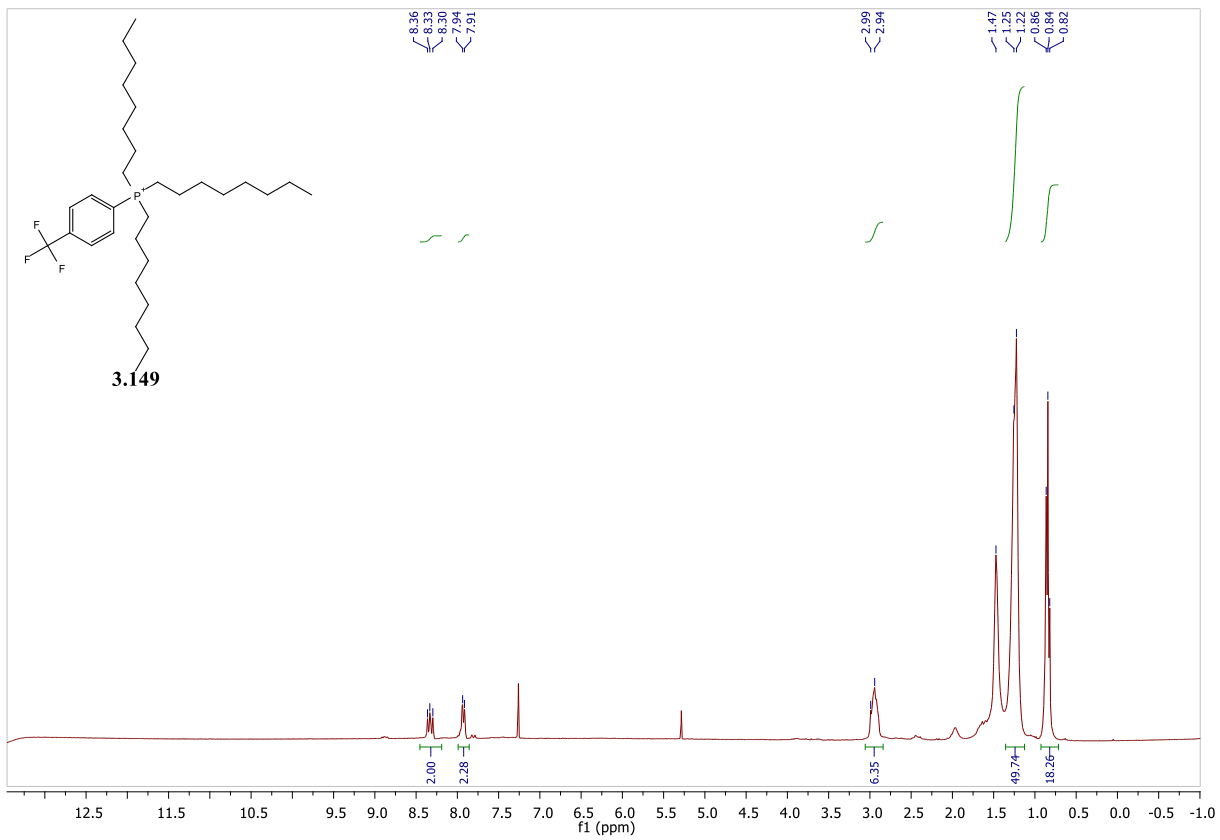
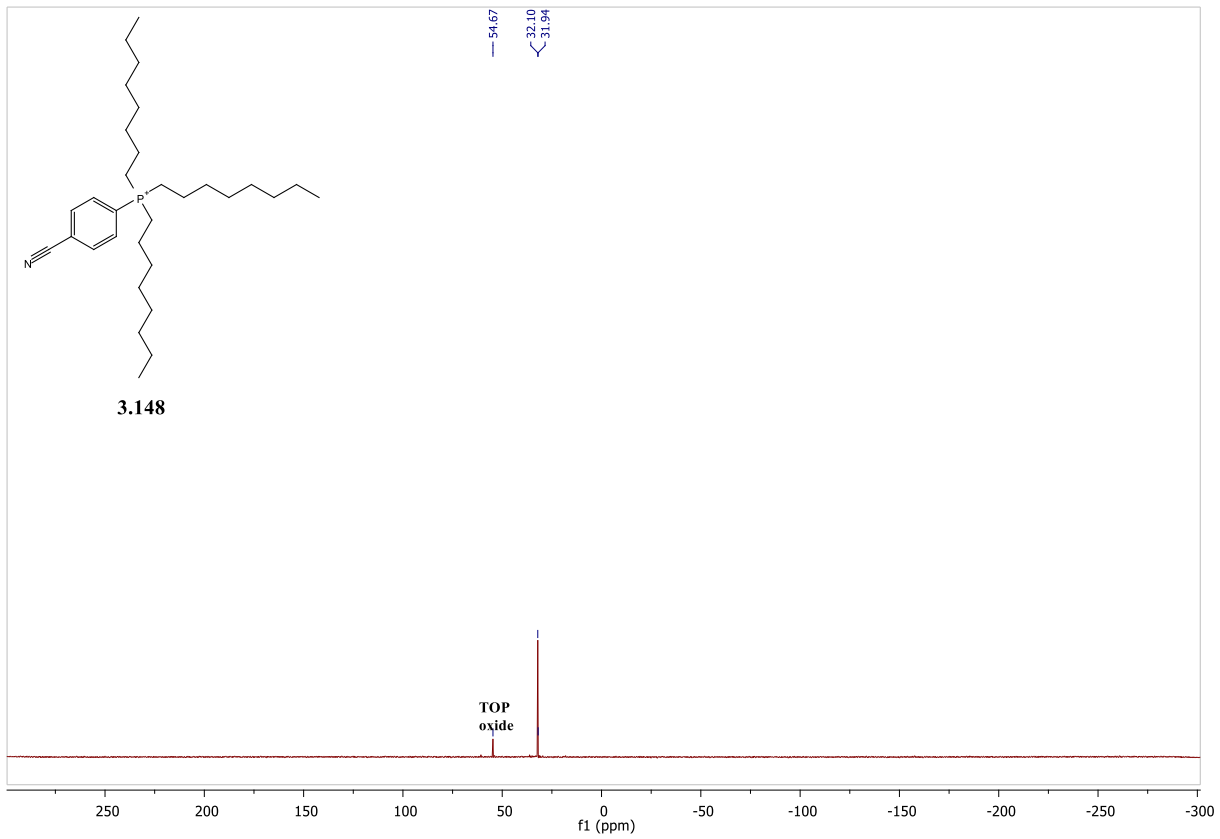


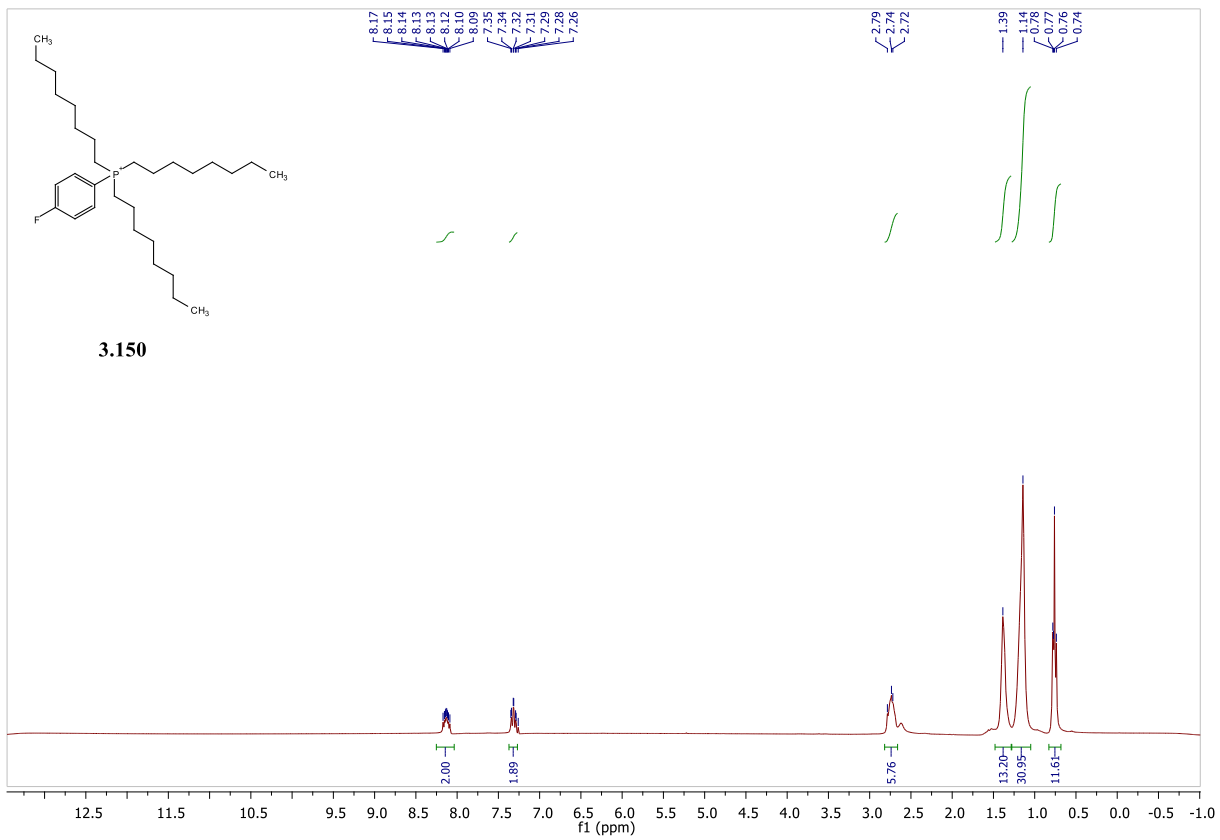
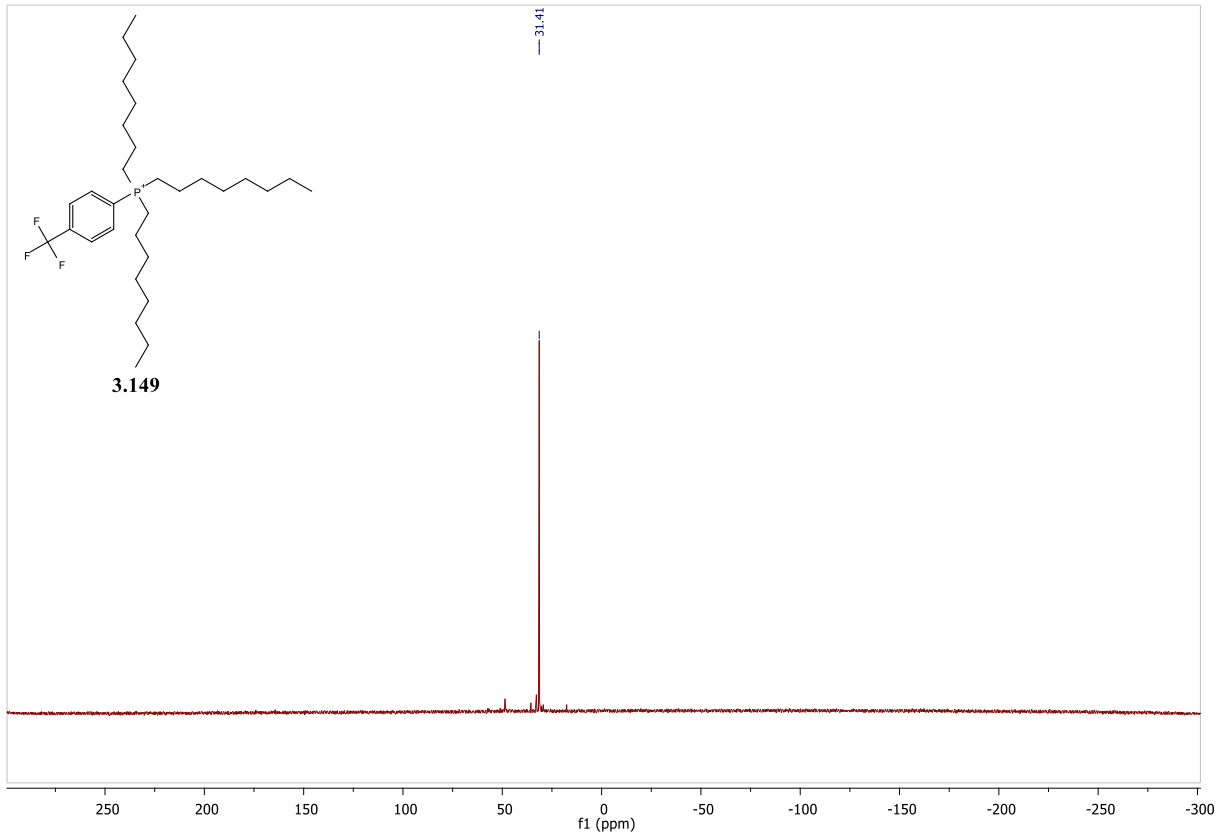


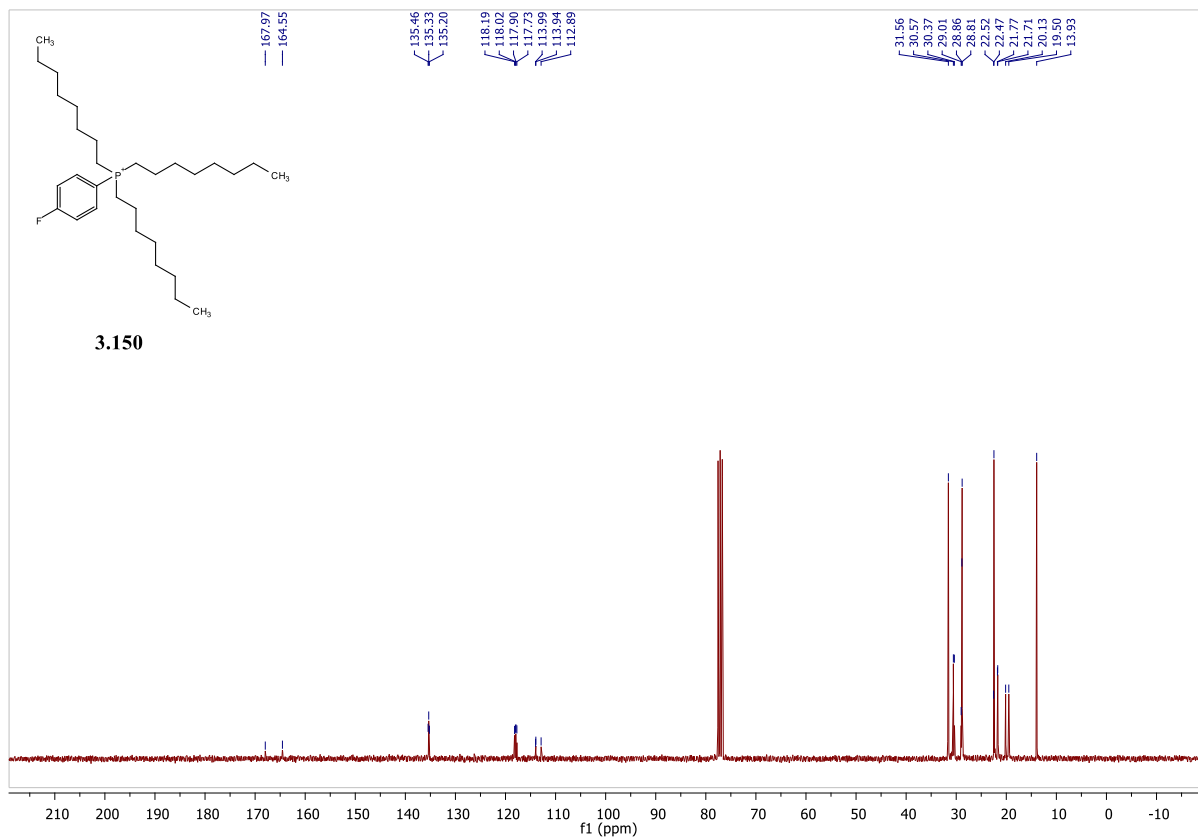
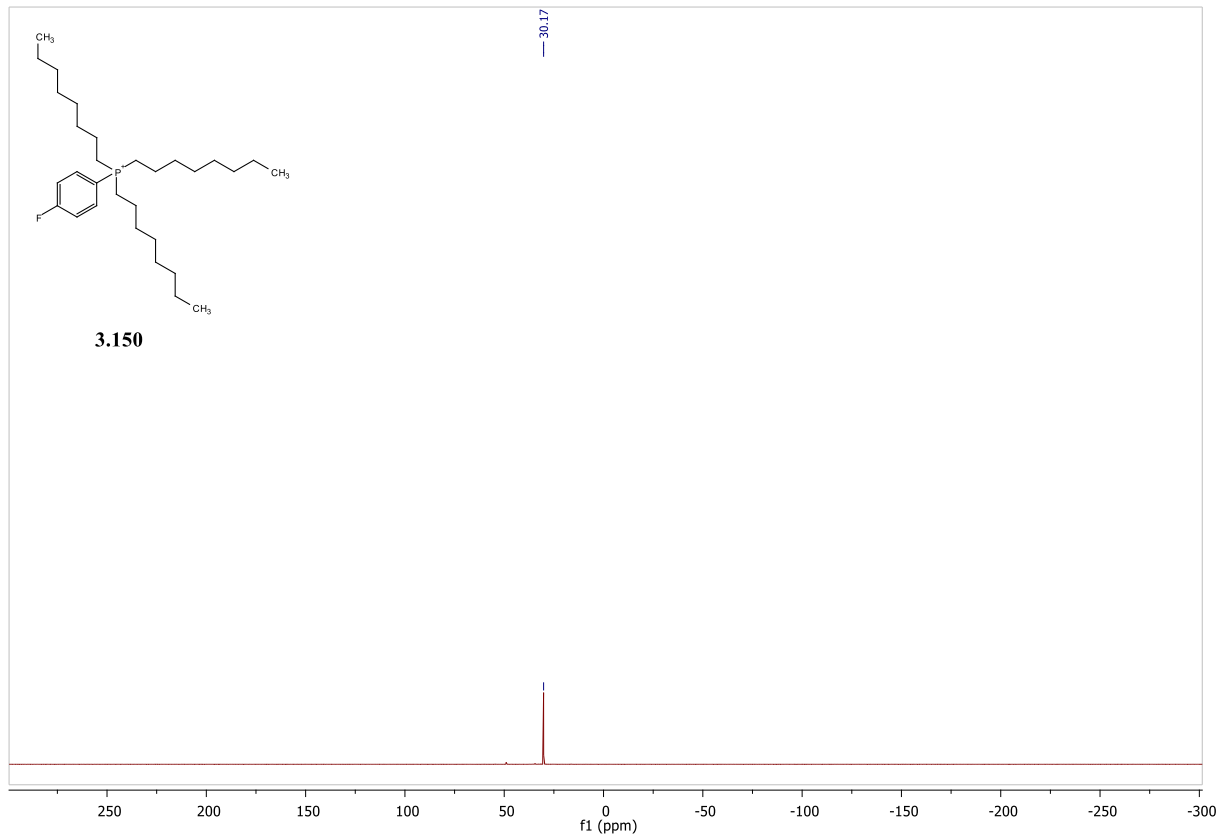


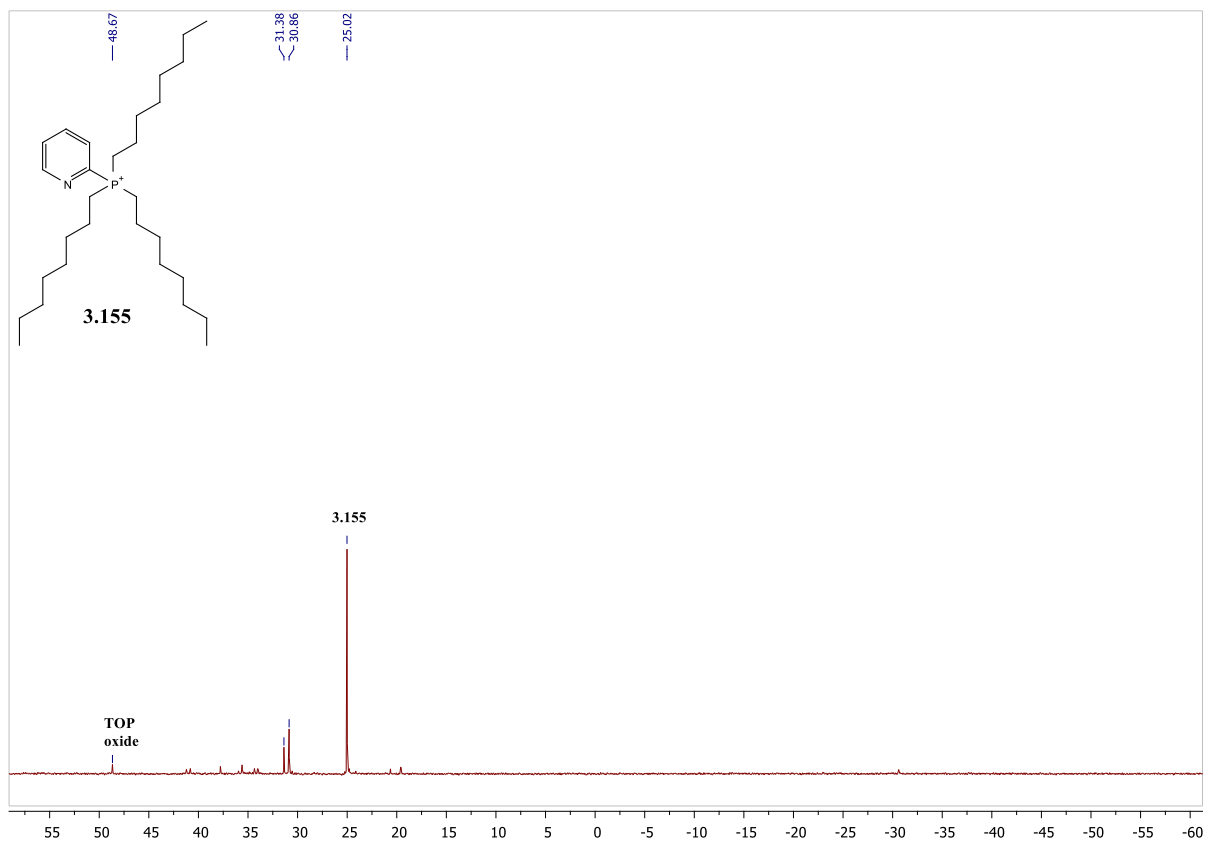
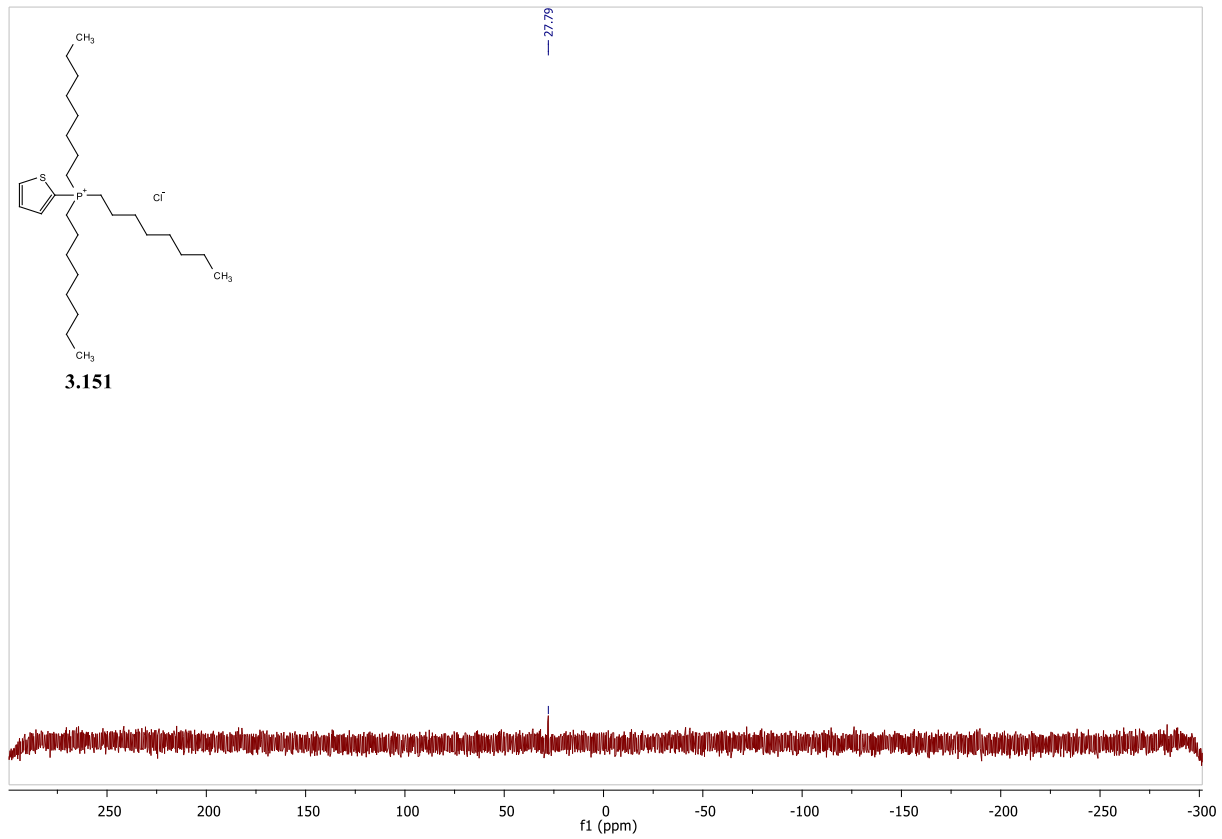


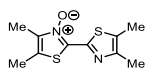




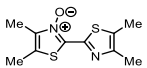
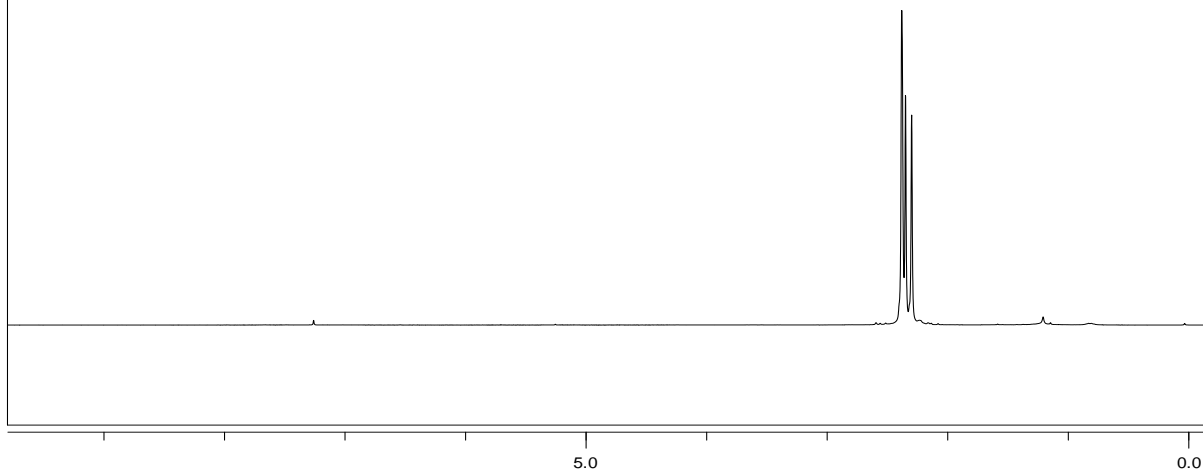




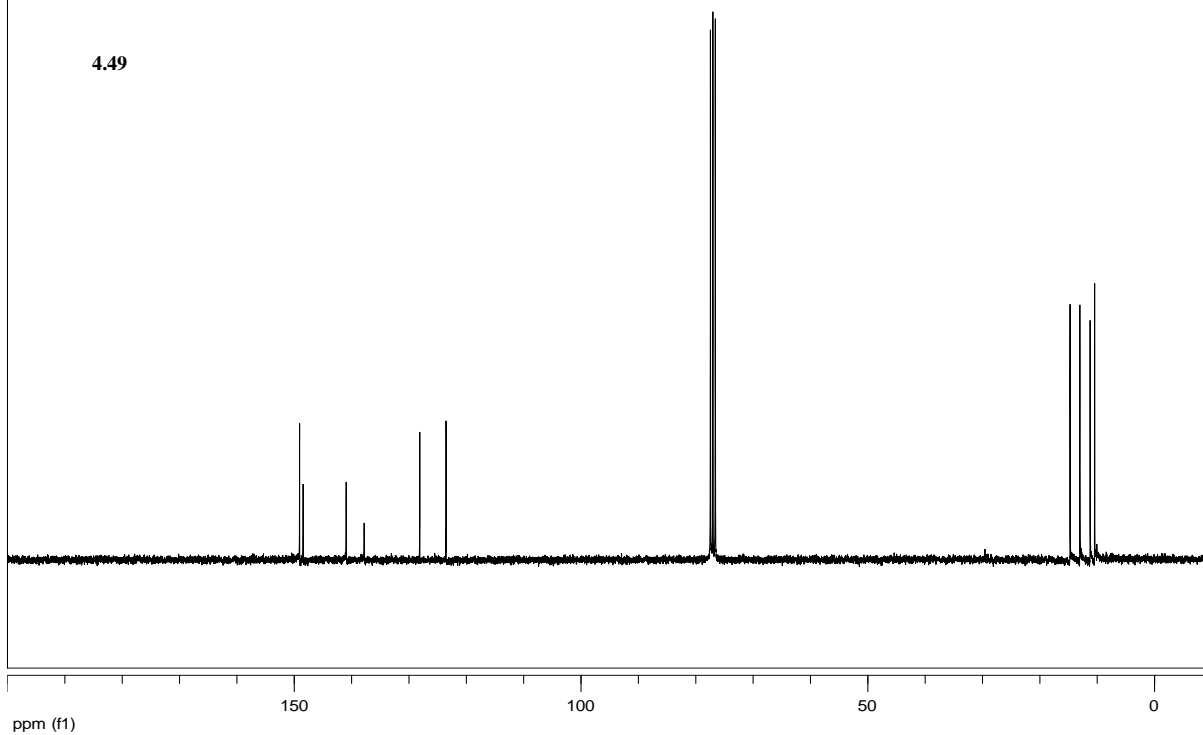


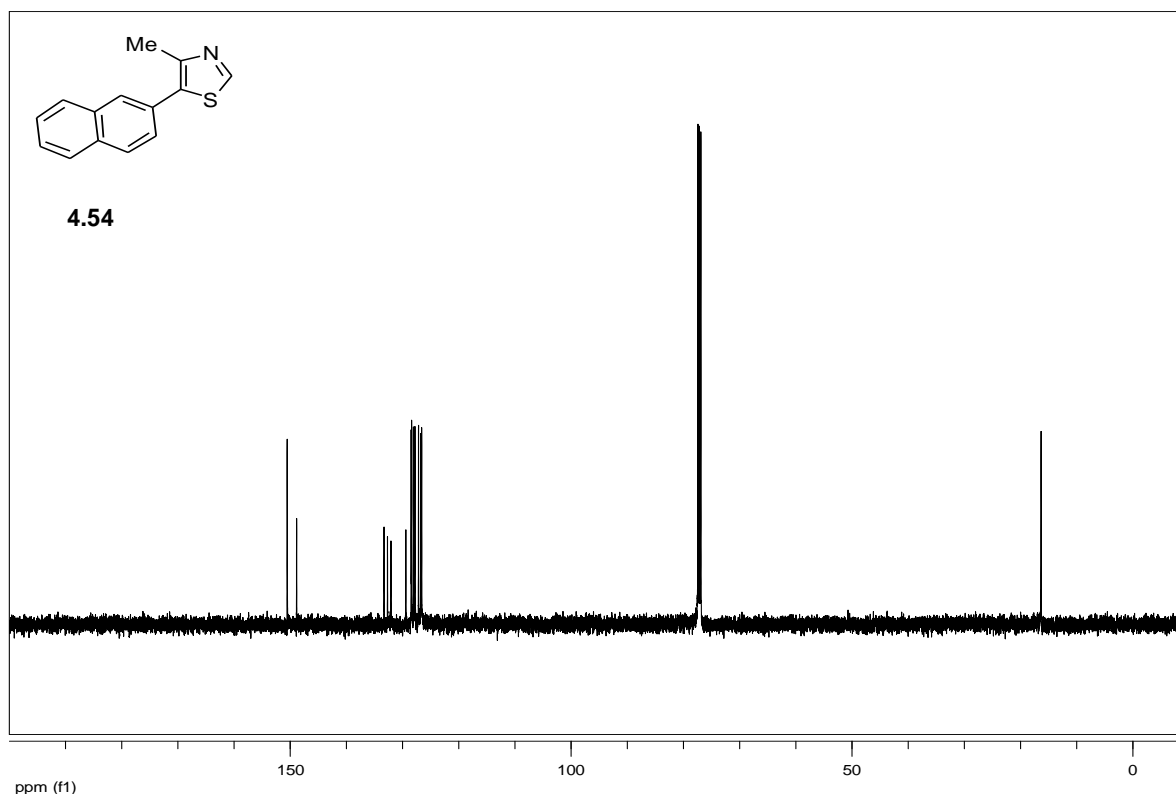
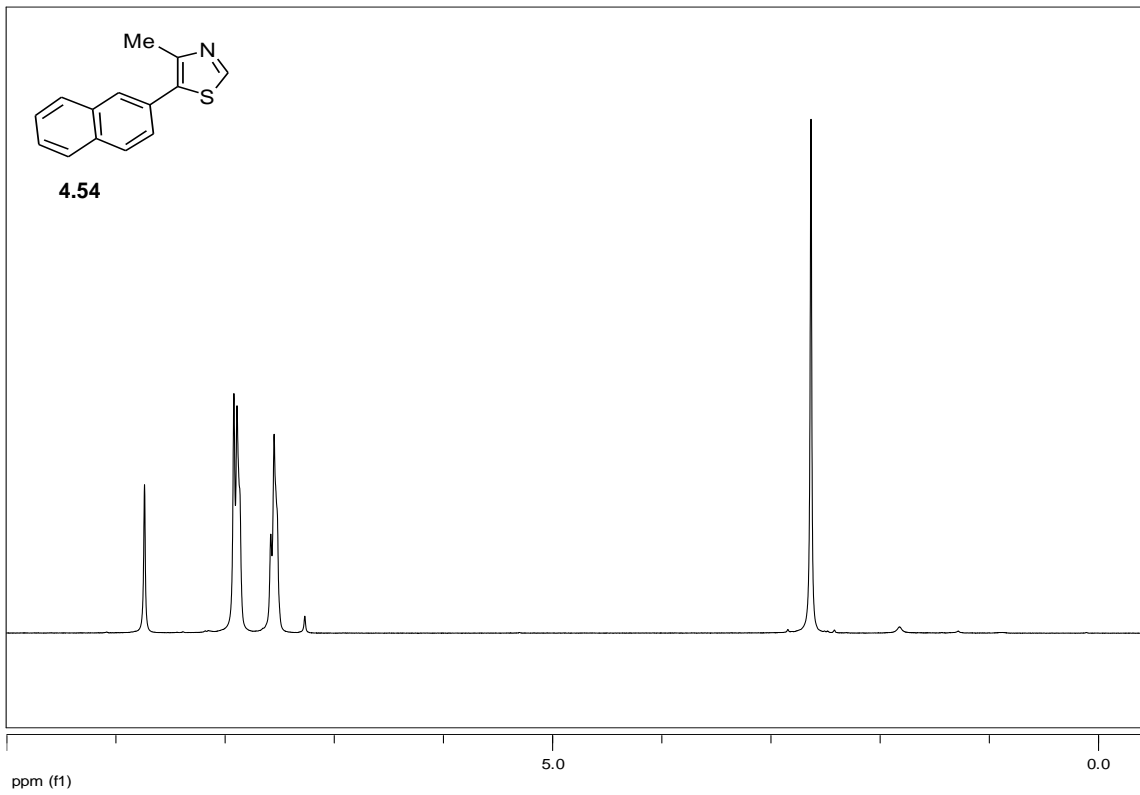


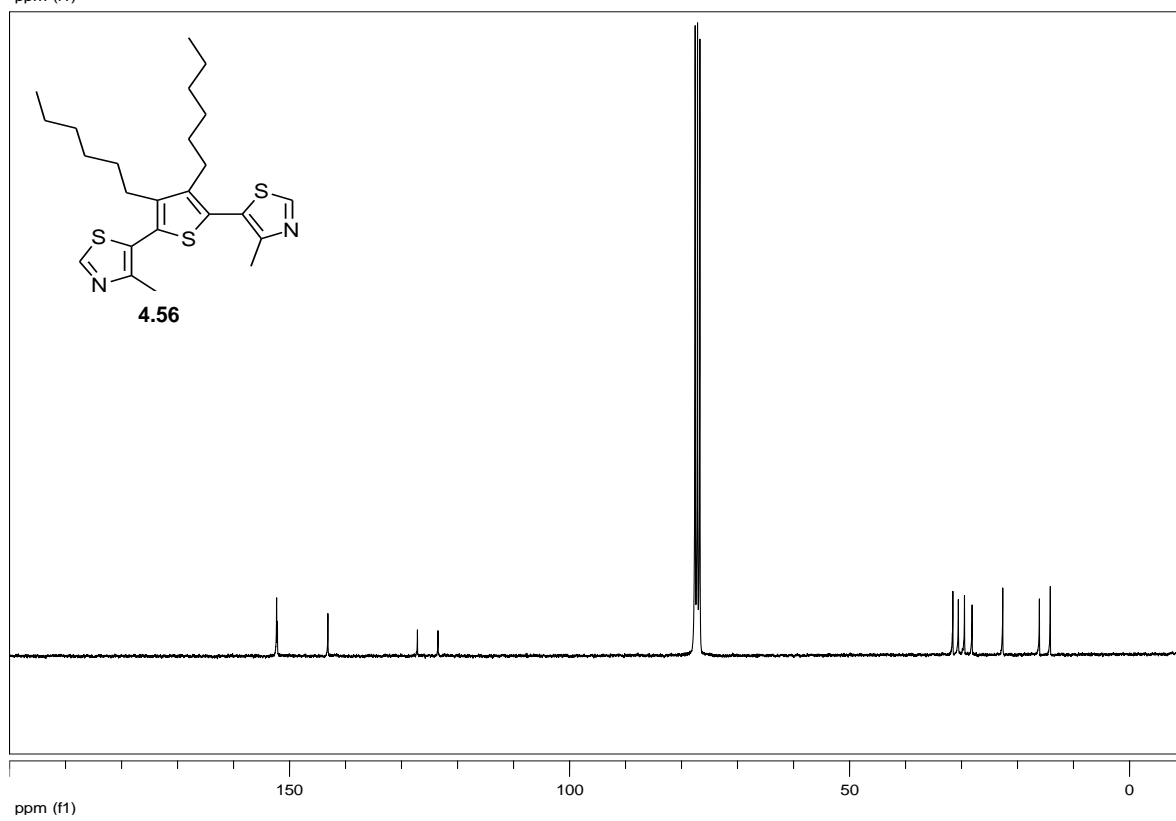
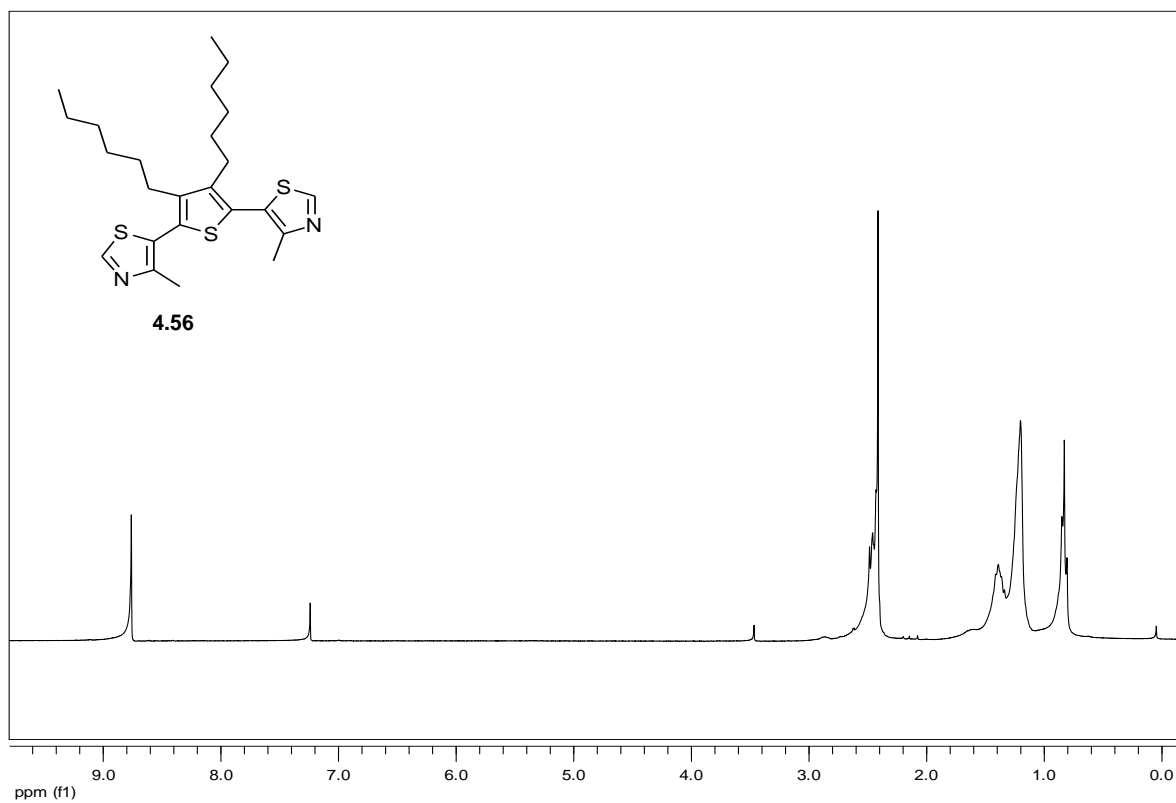
4.49

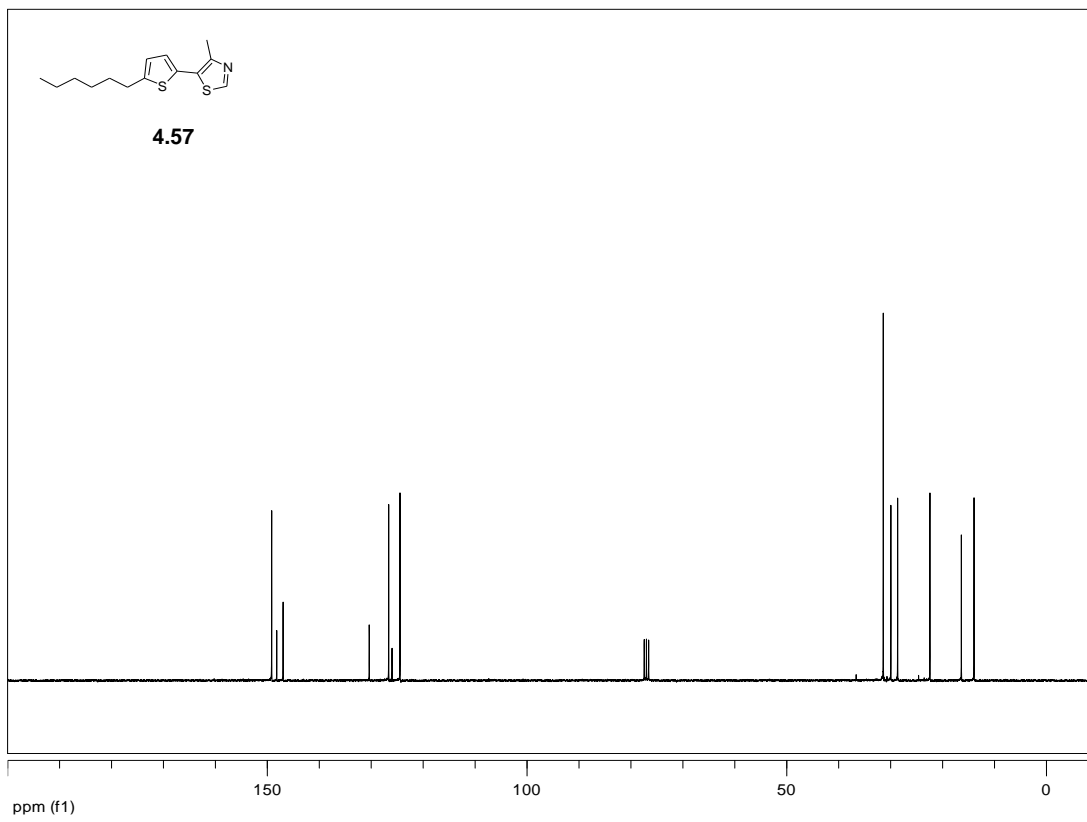
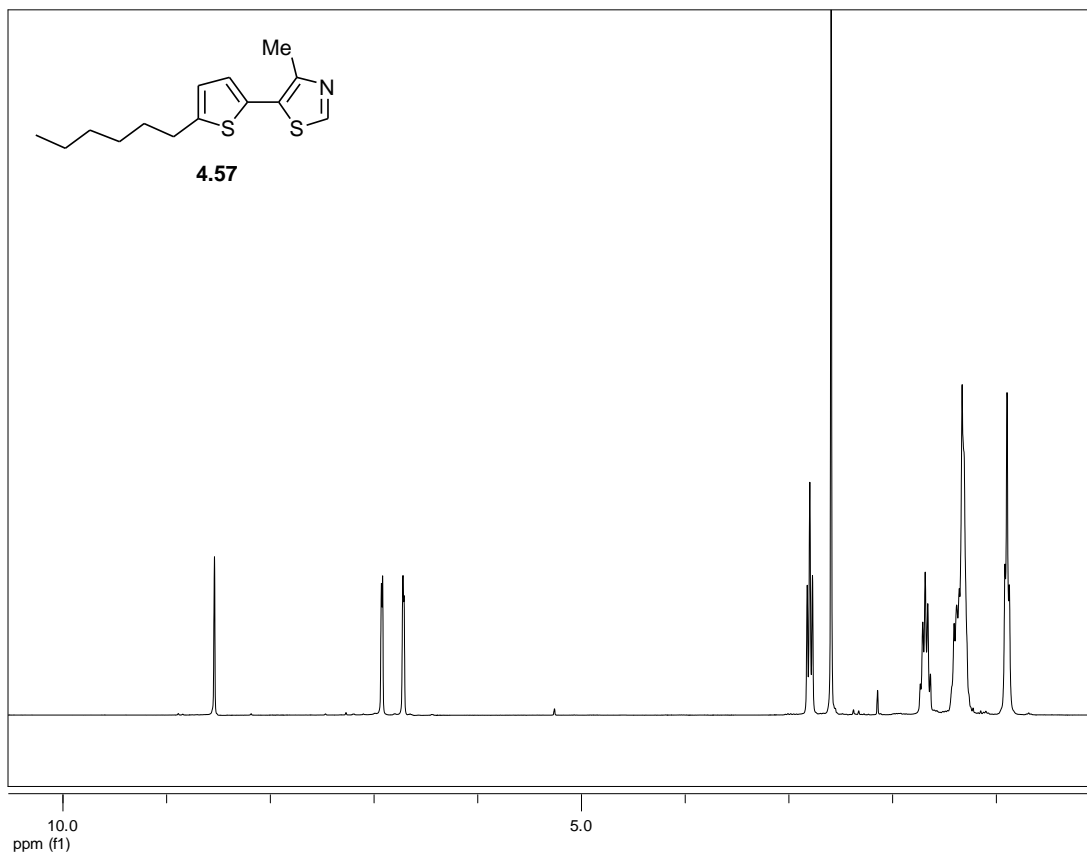


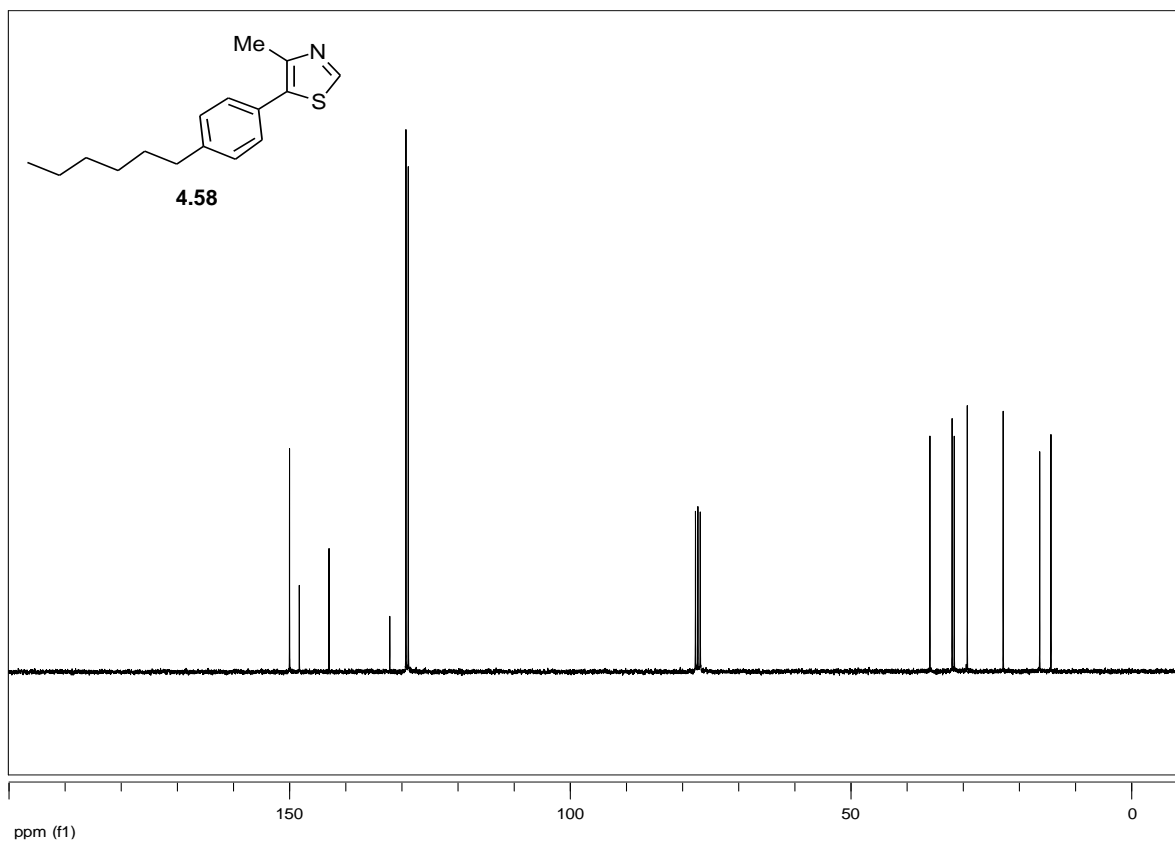
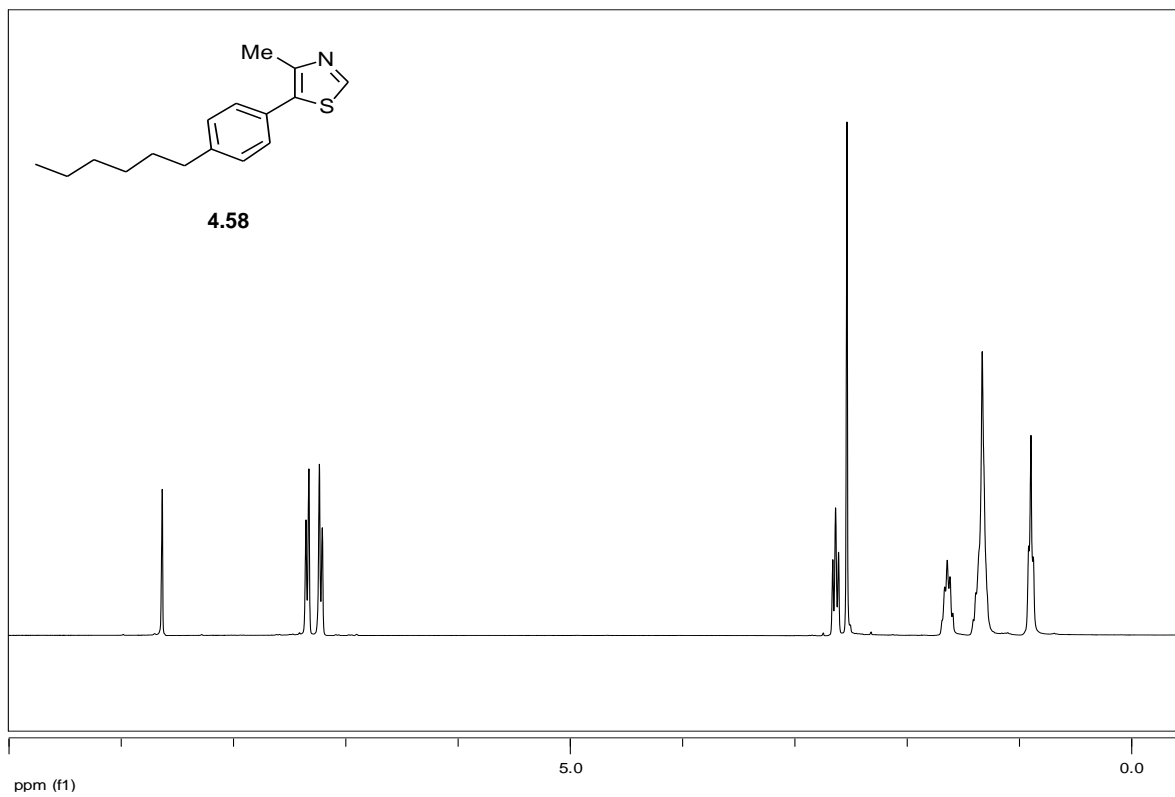
4.49

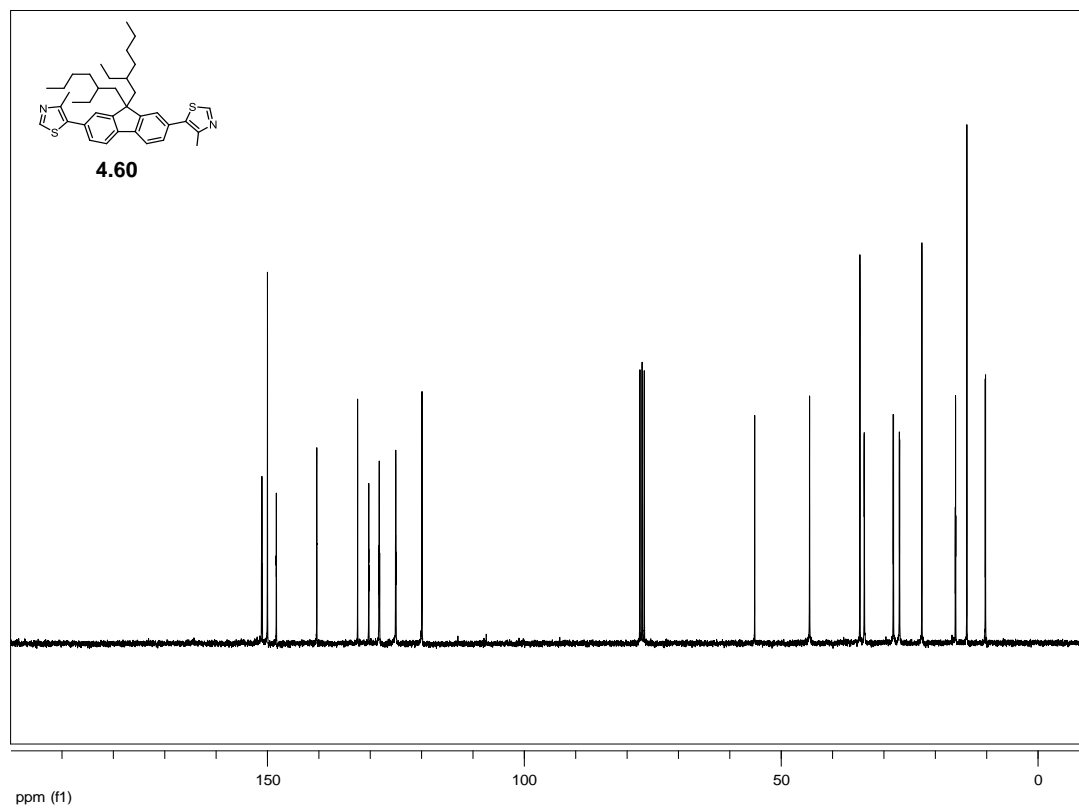
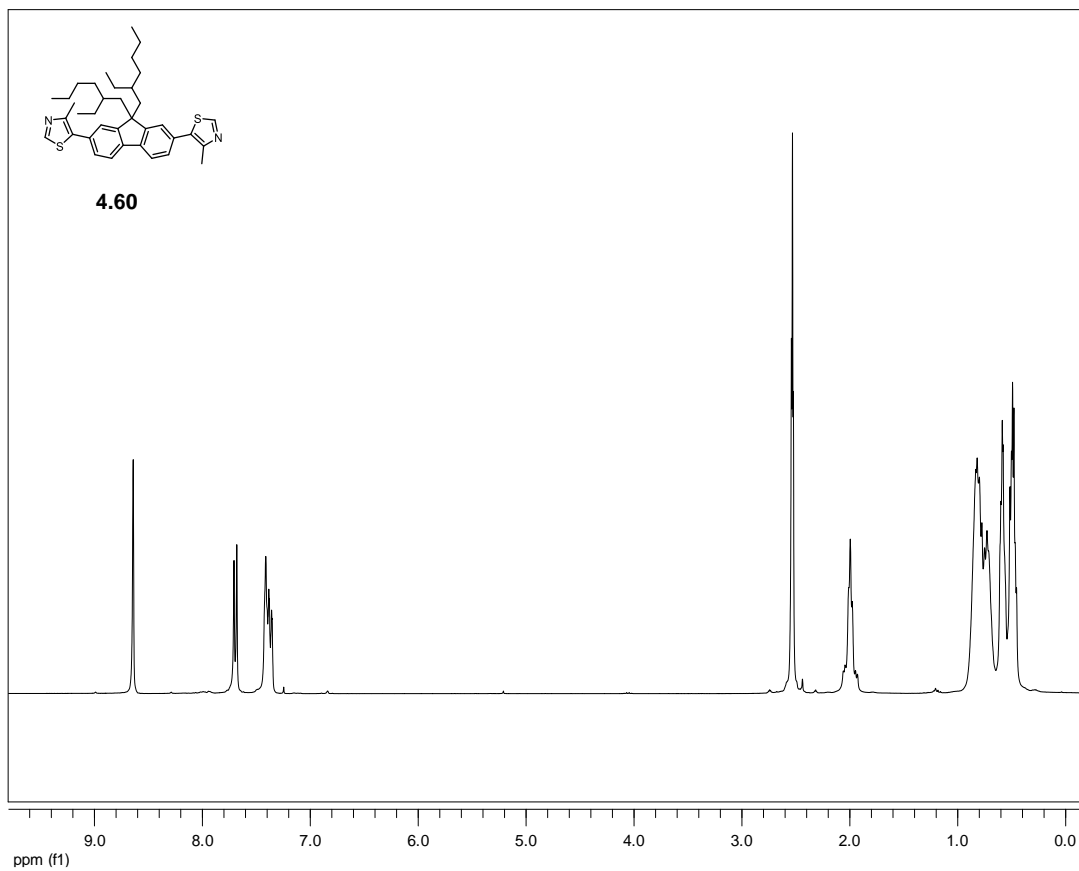


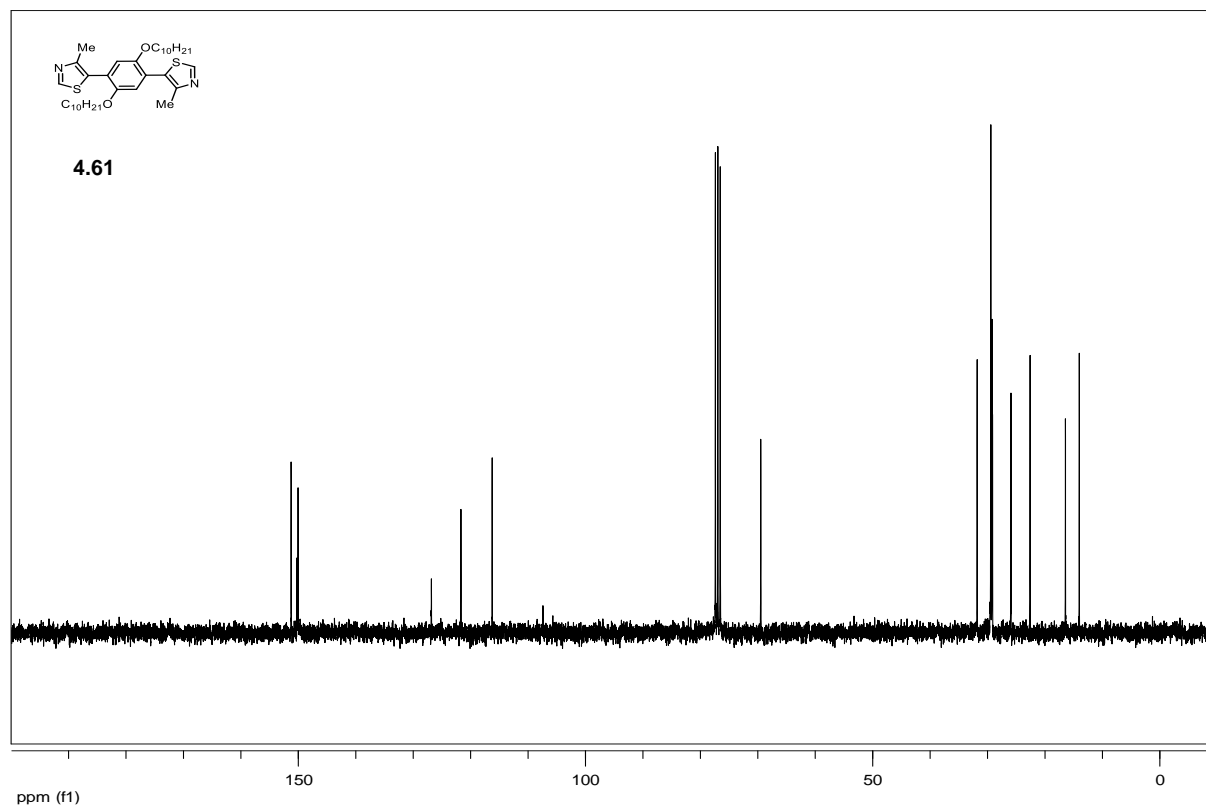
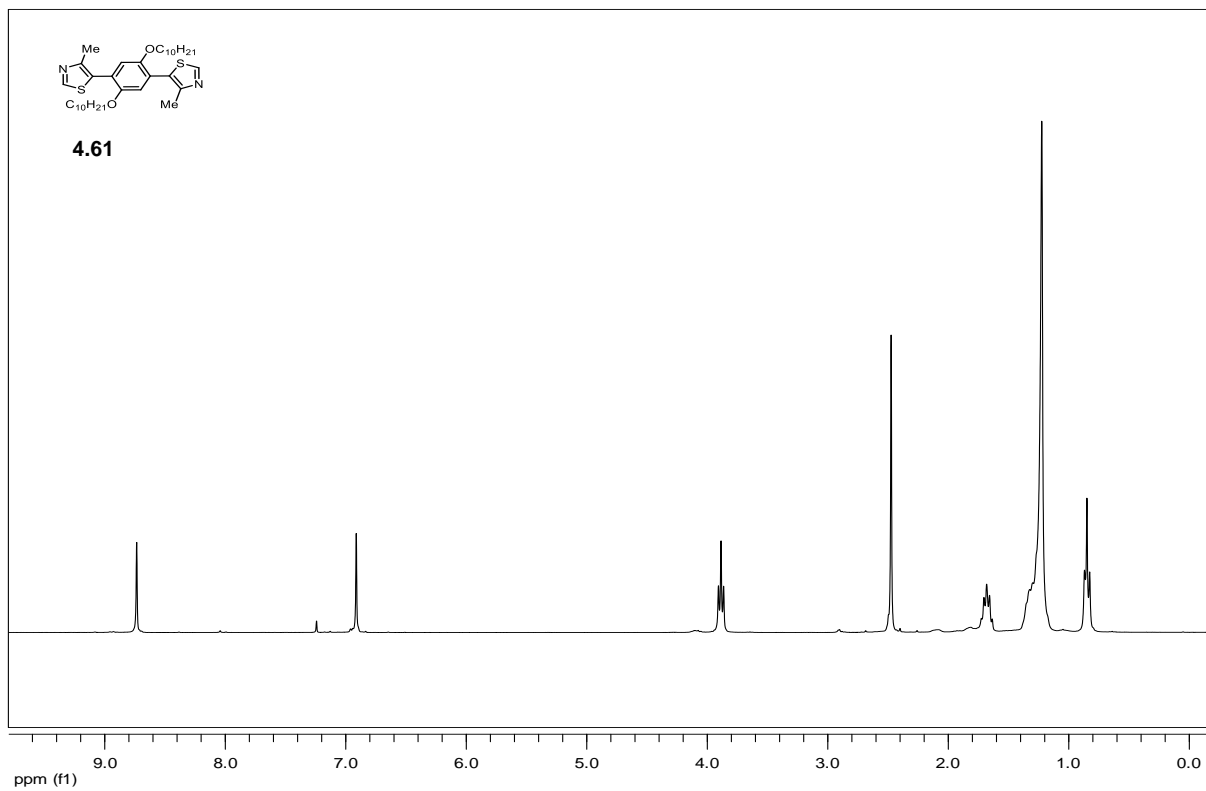


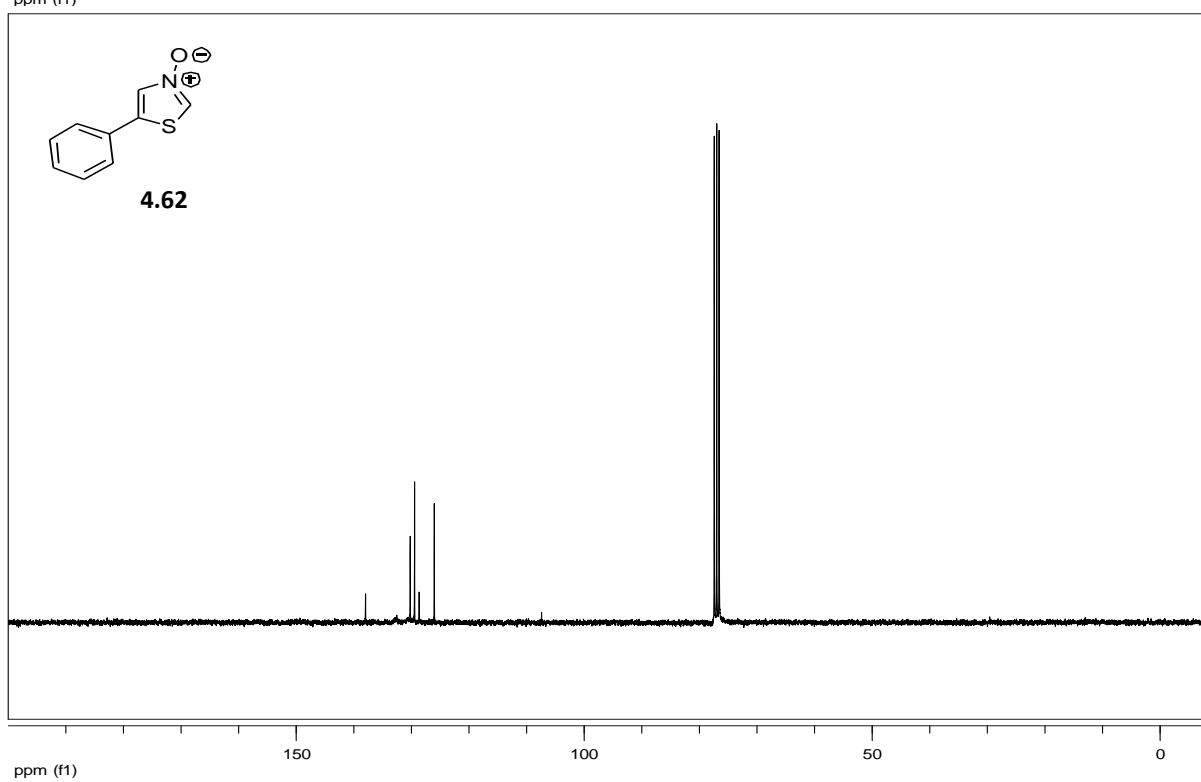
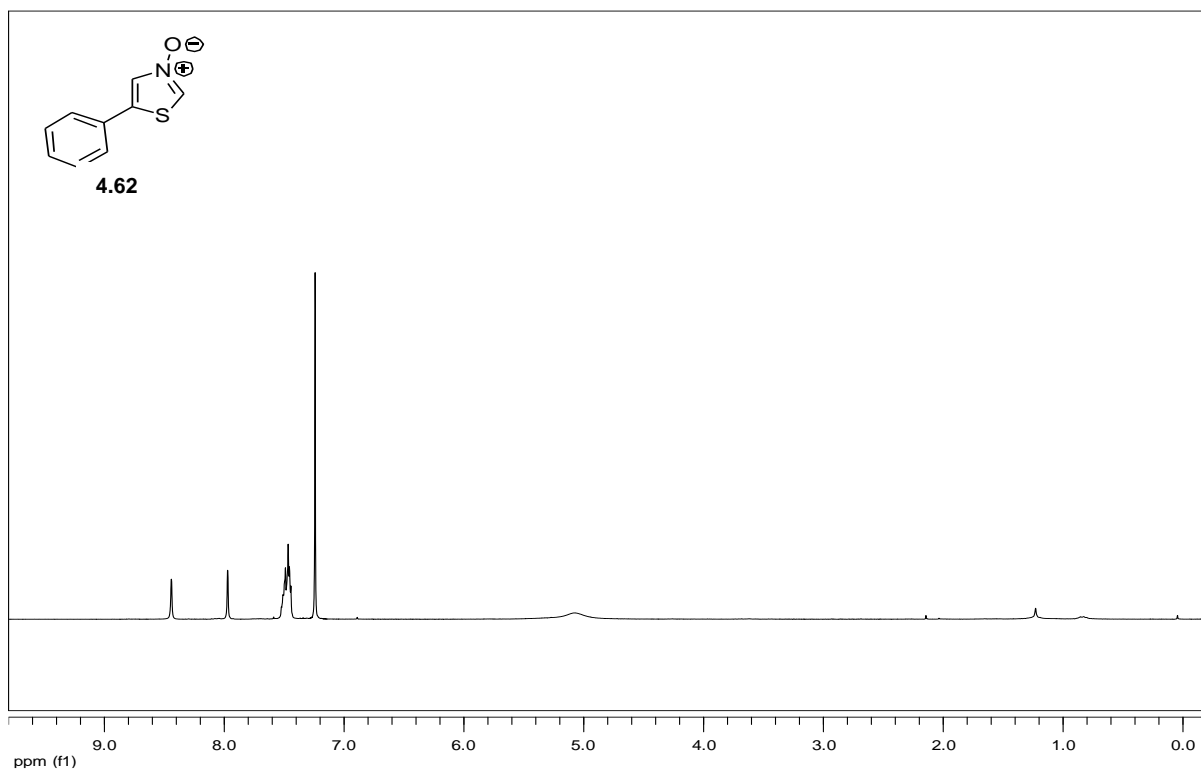


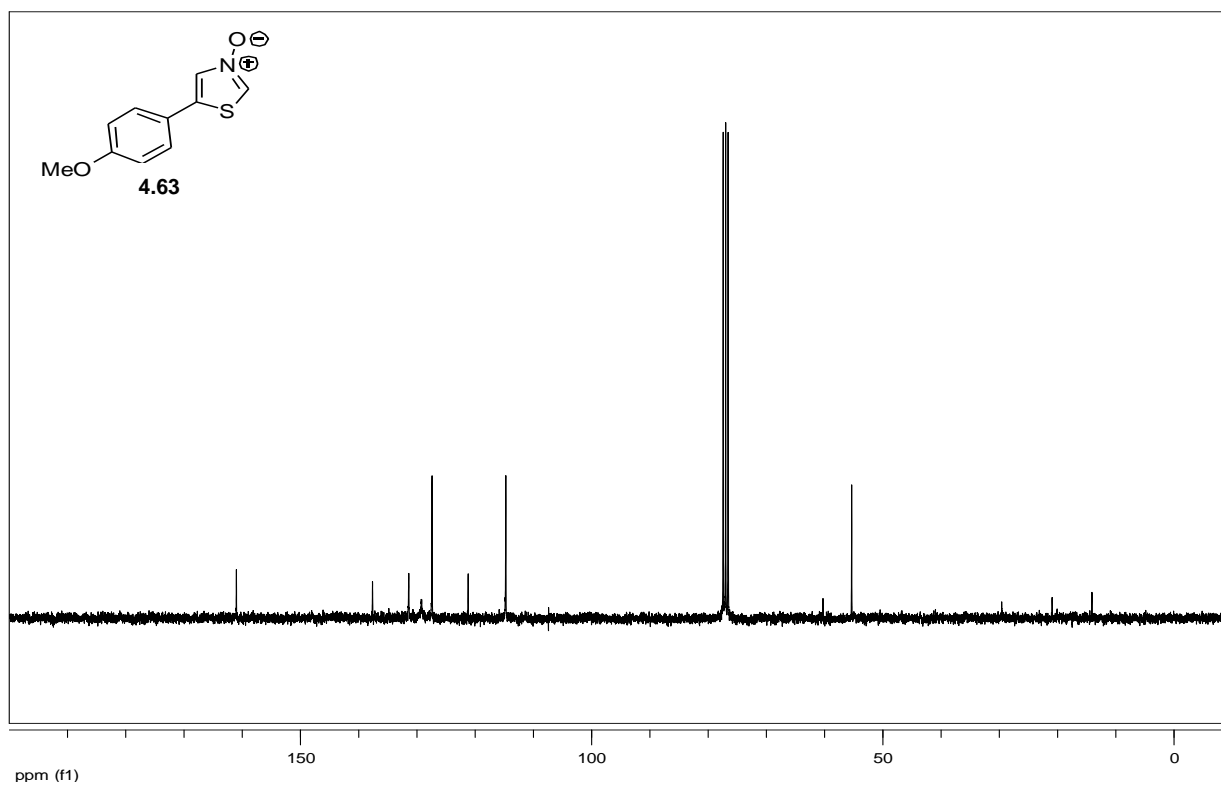
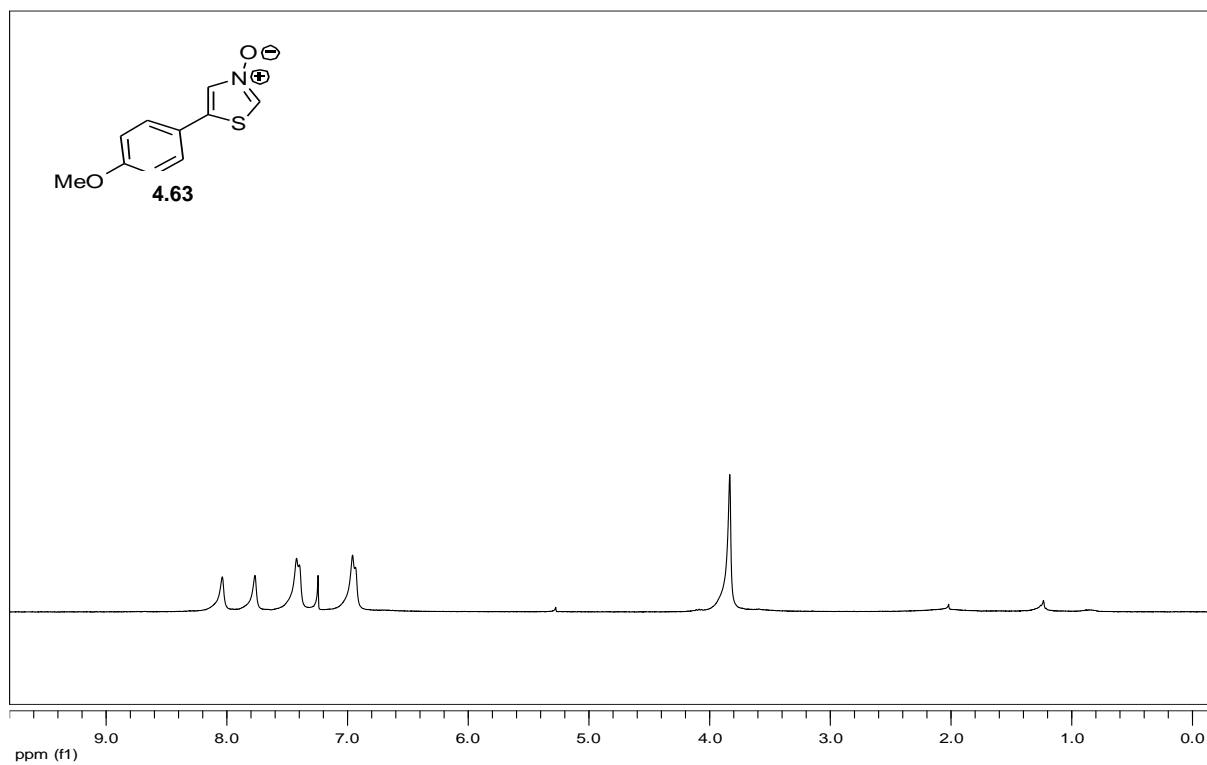


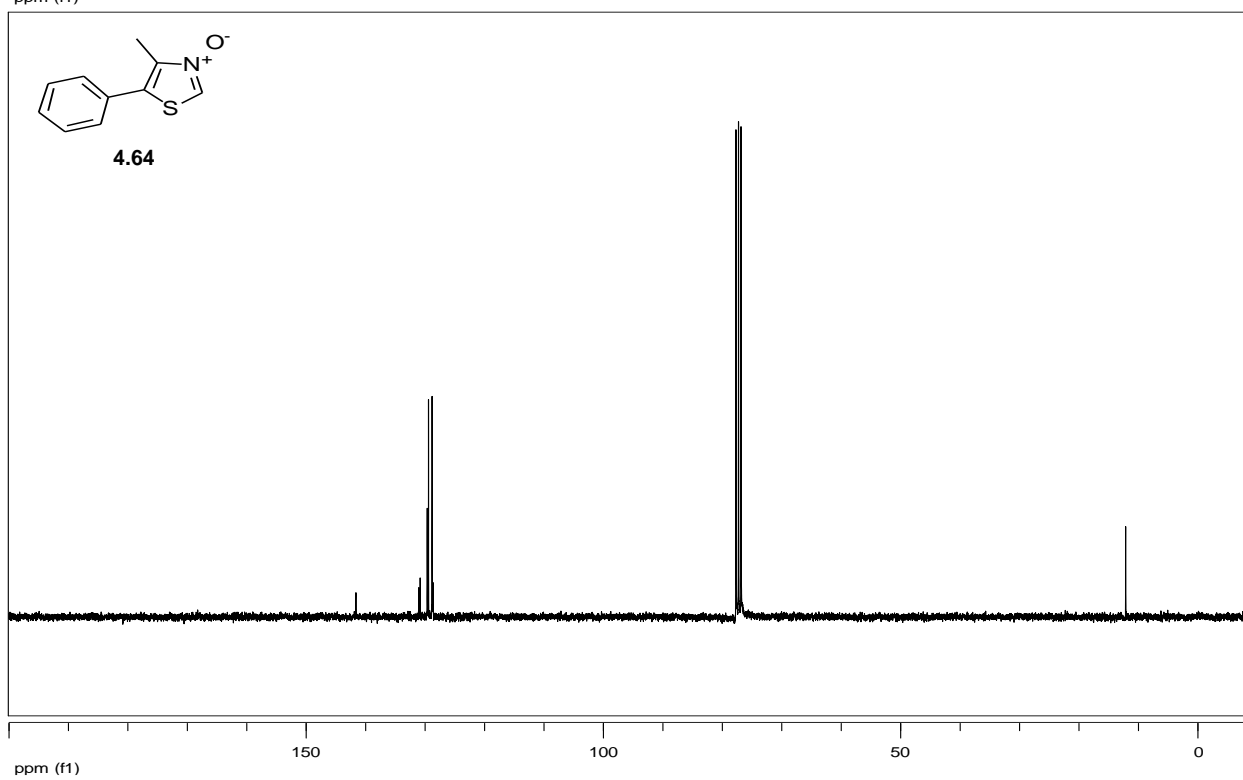
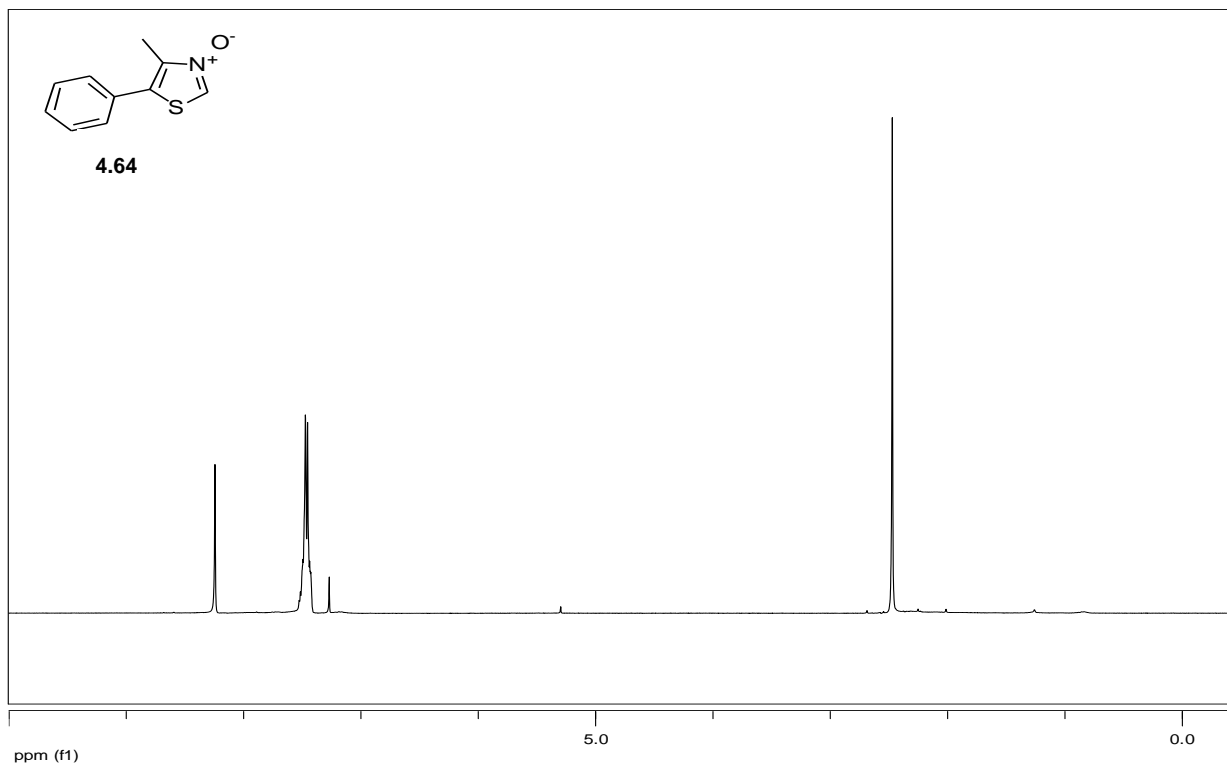


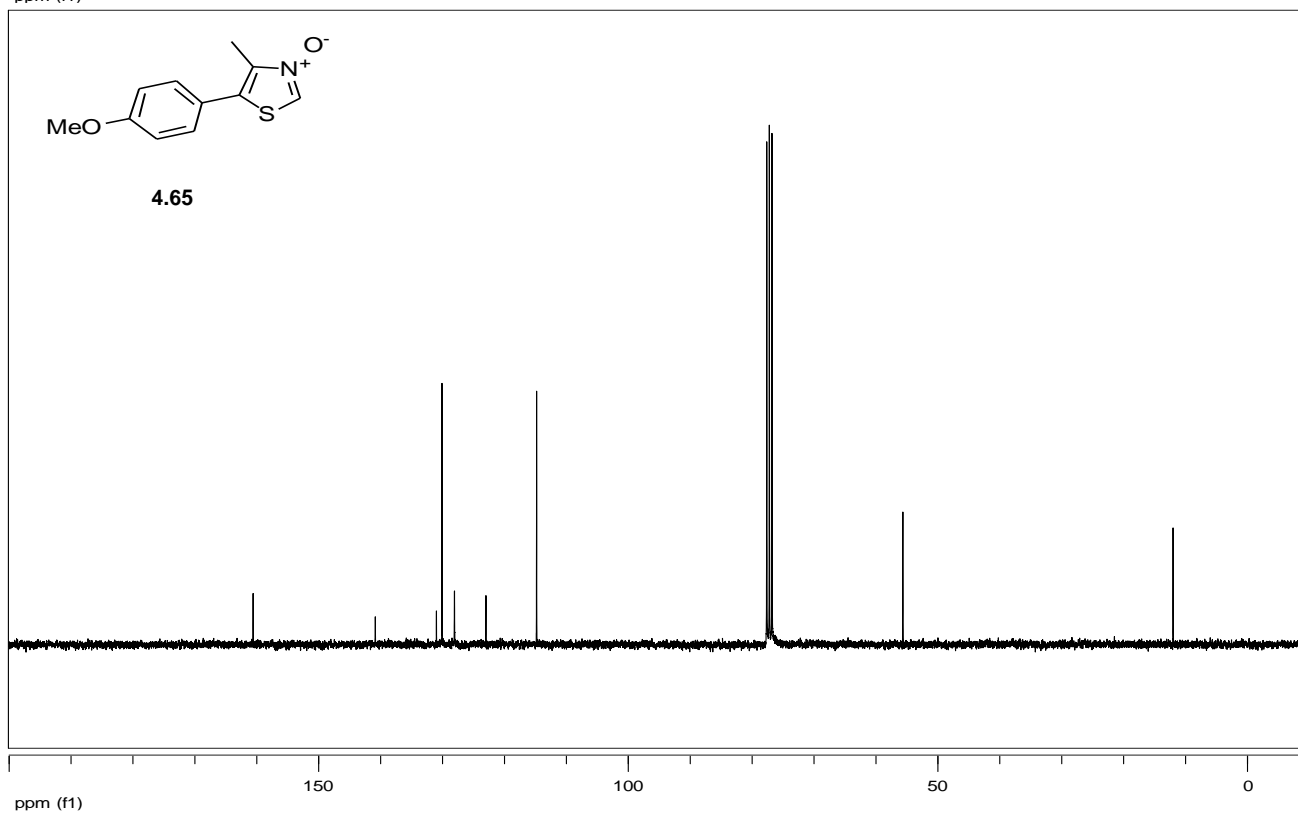
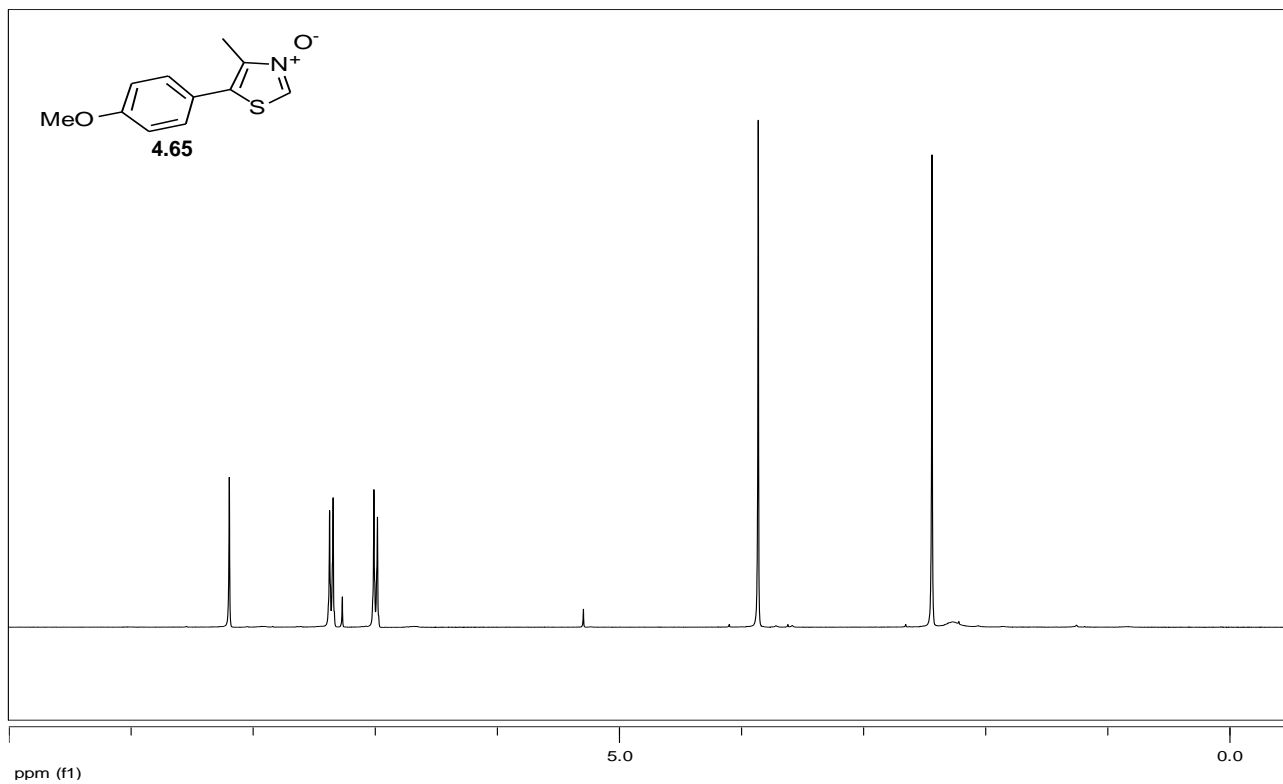


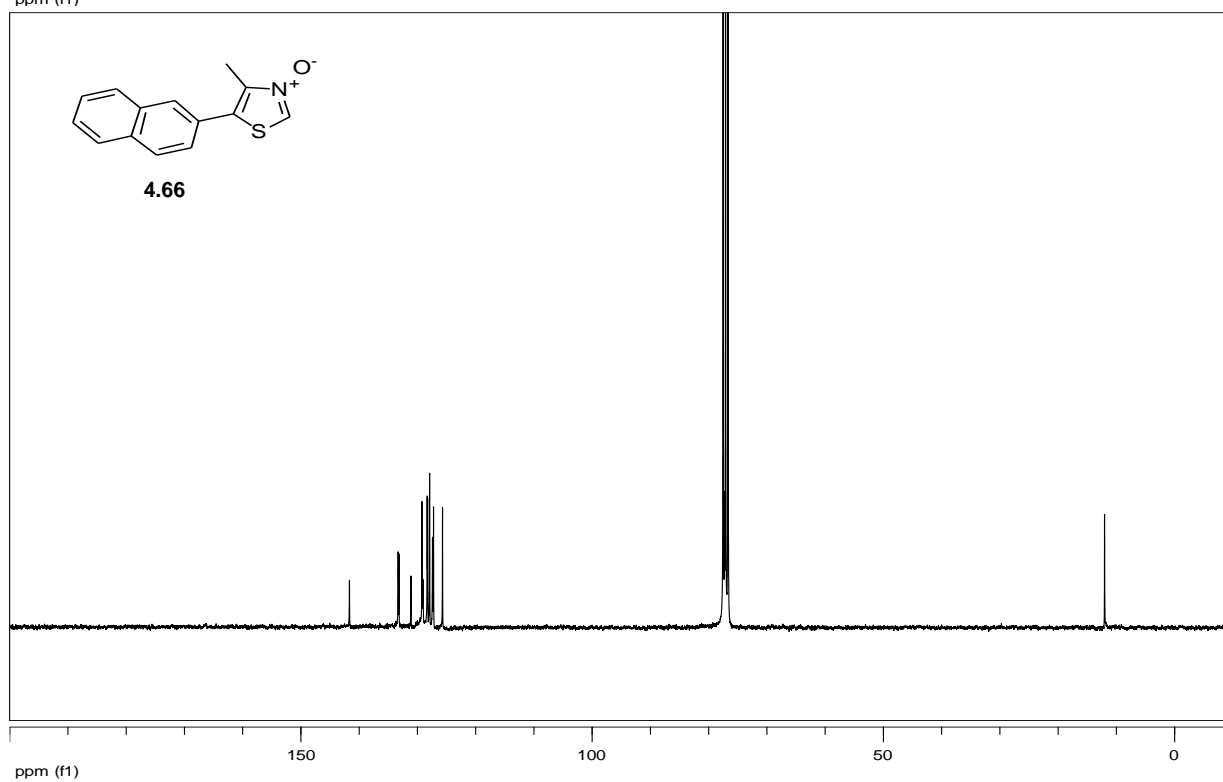
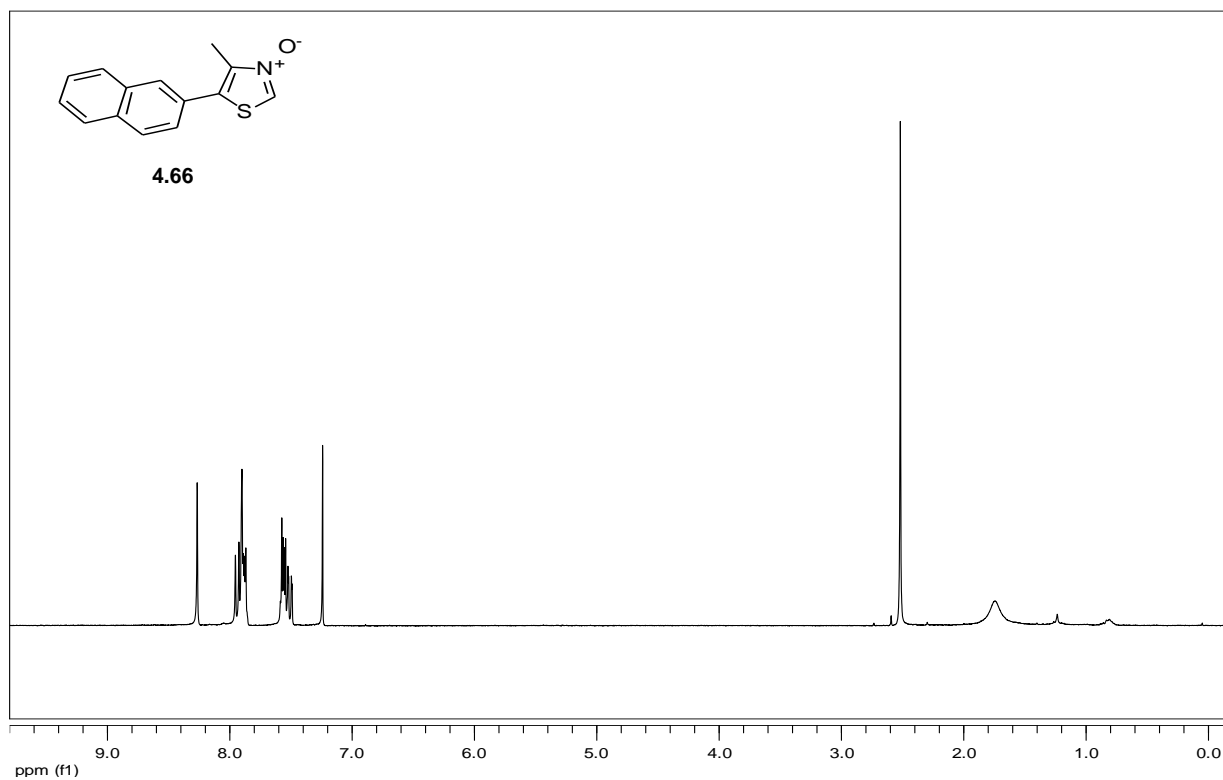


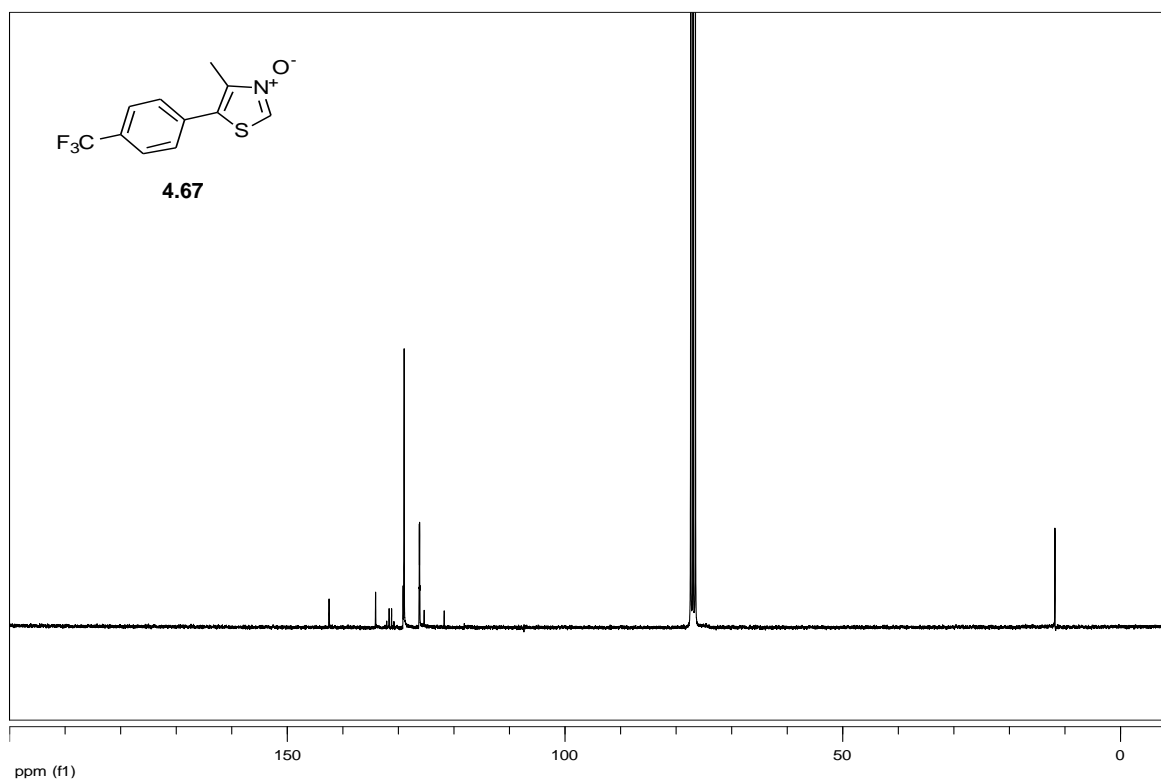
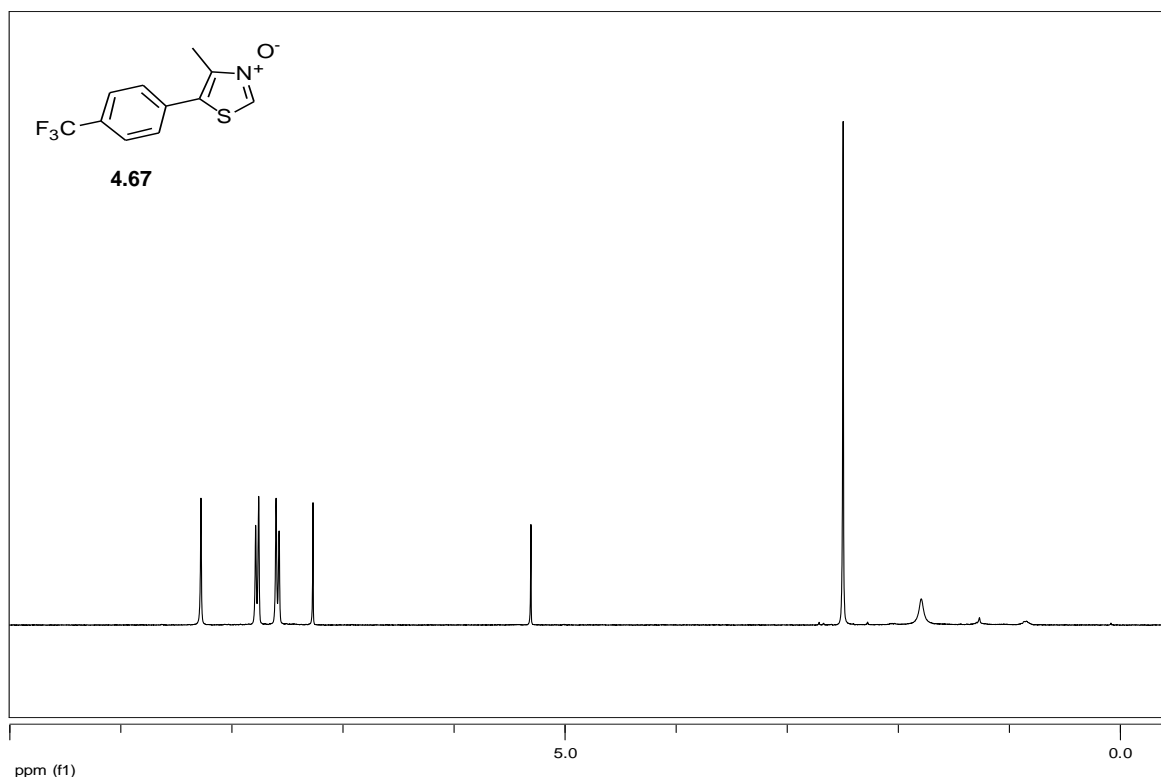


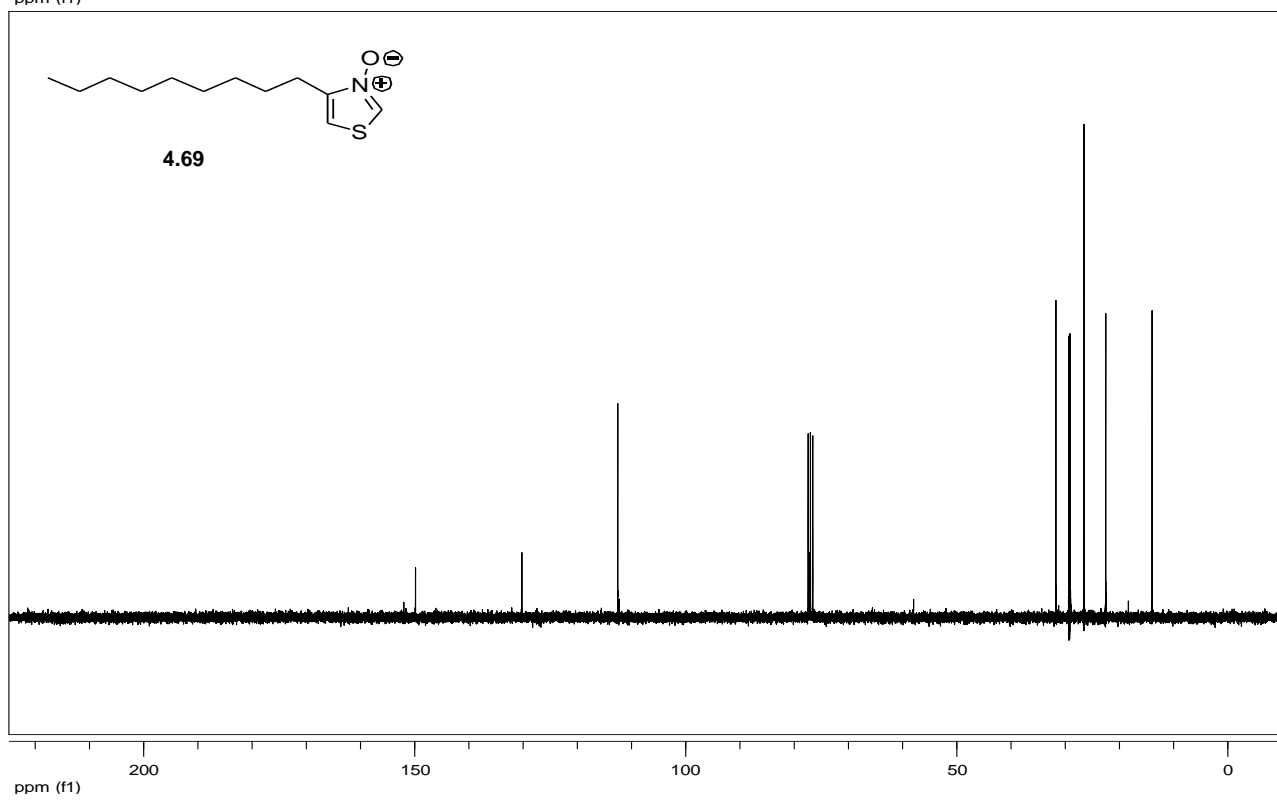
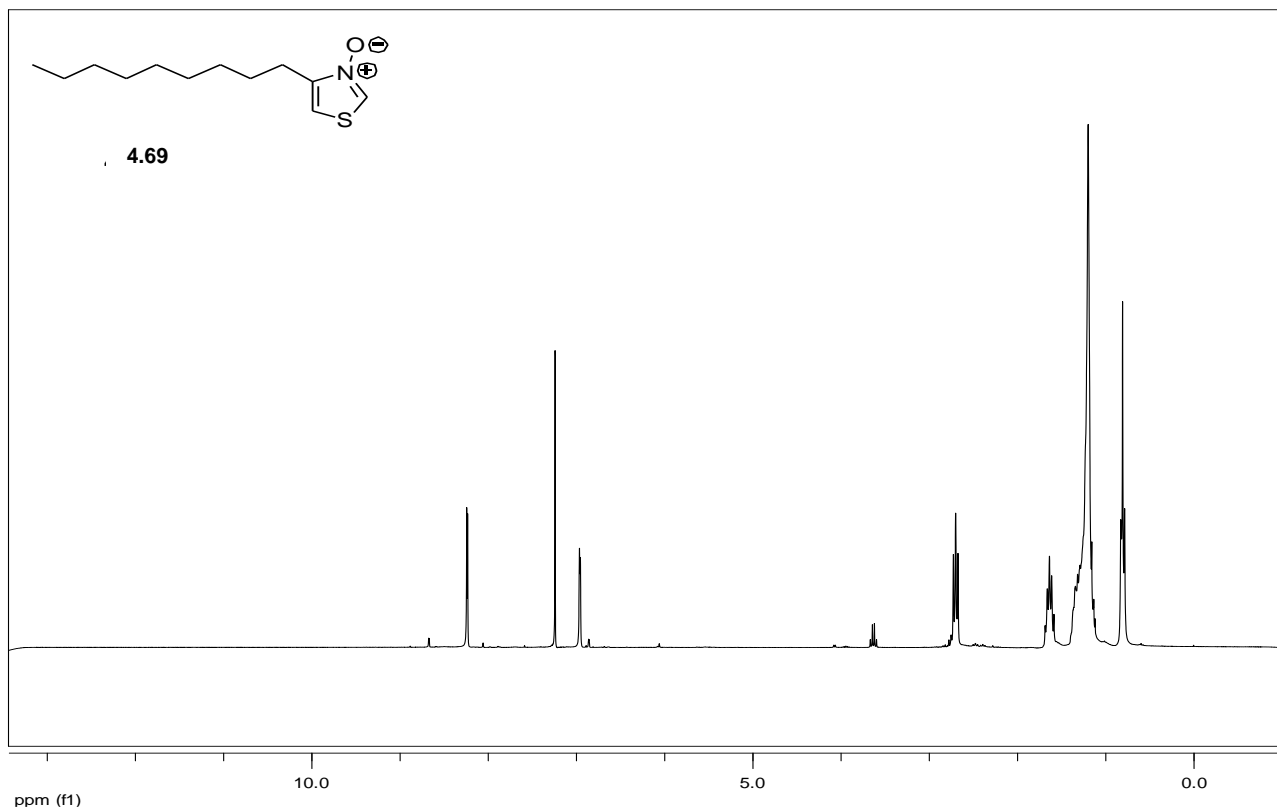


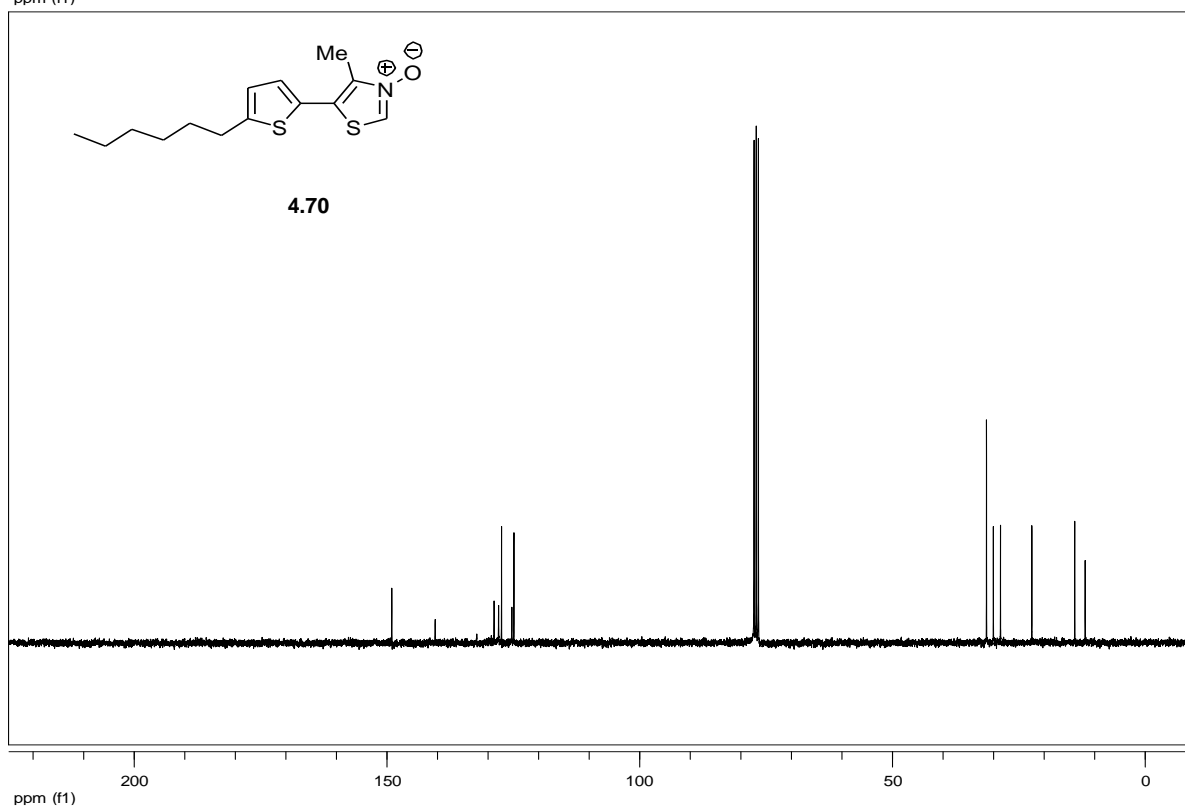
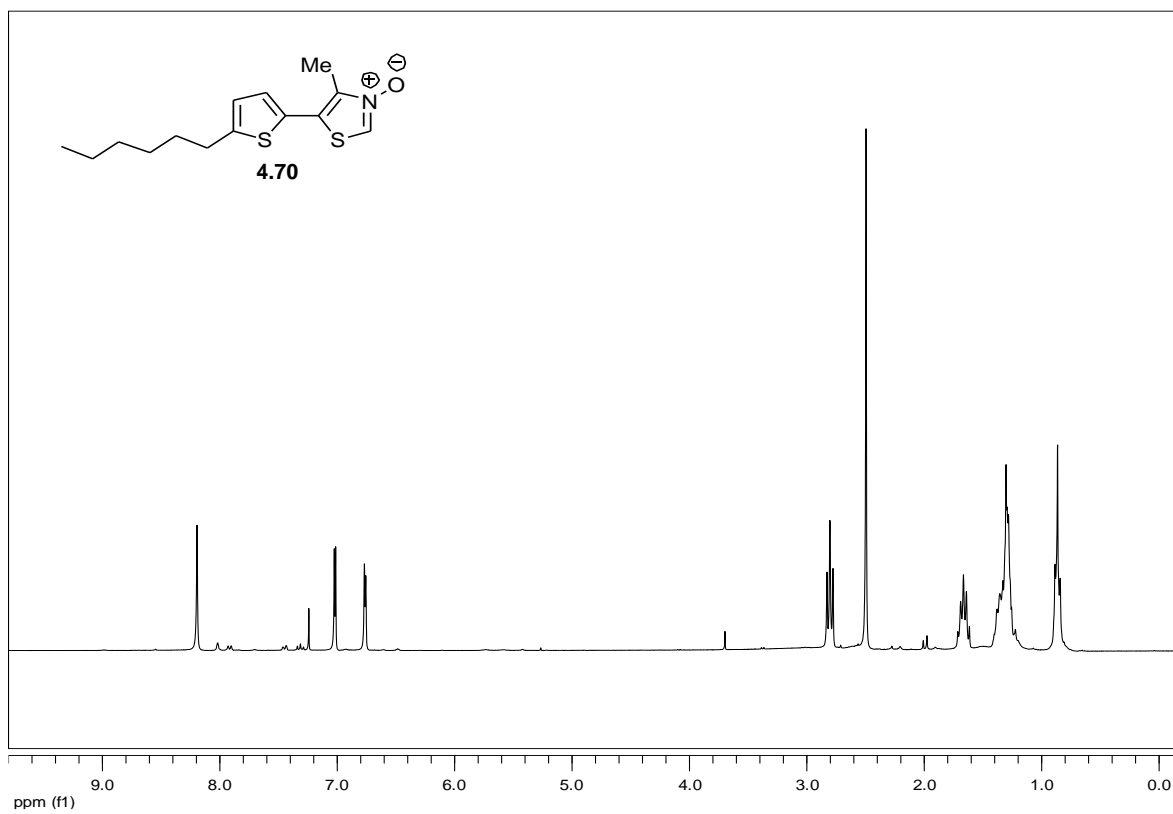


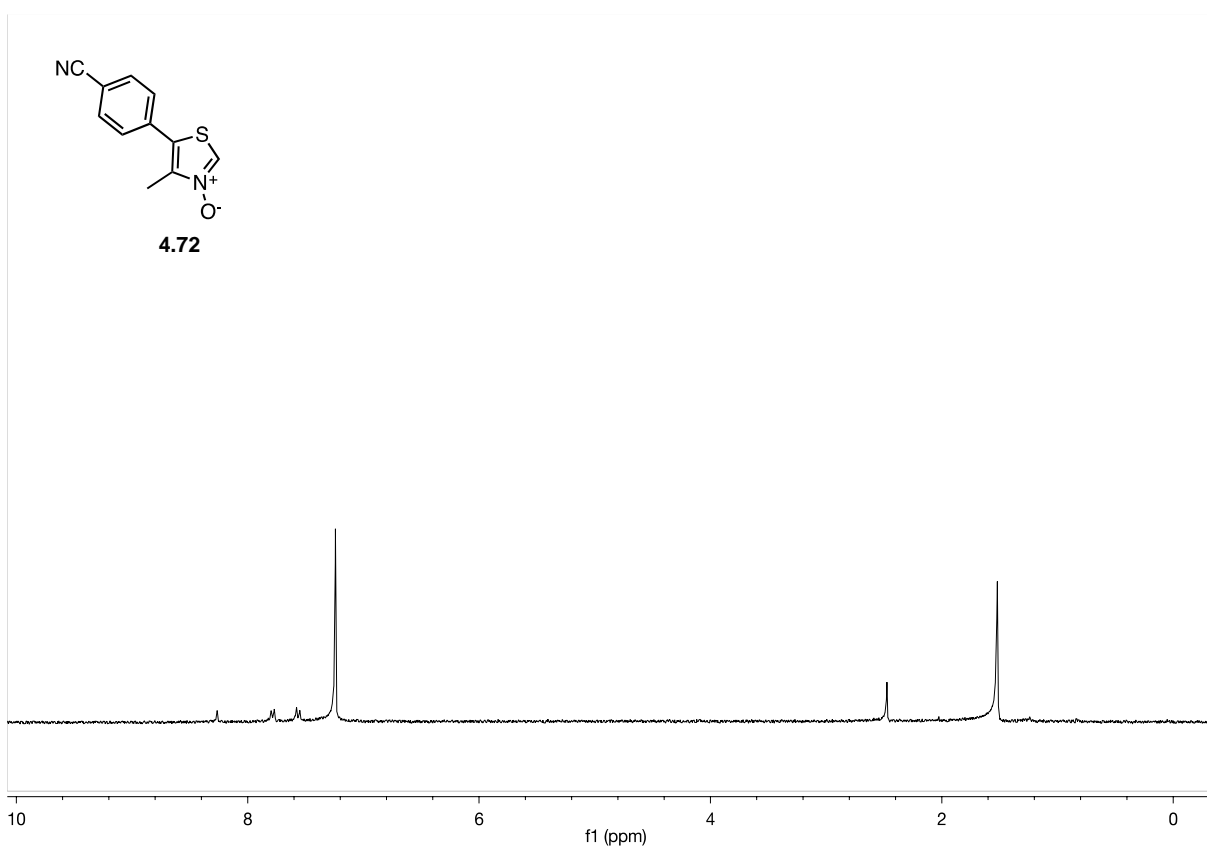
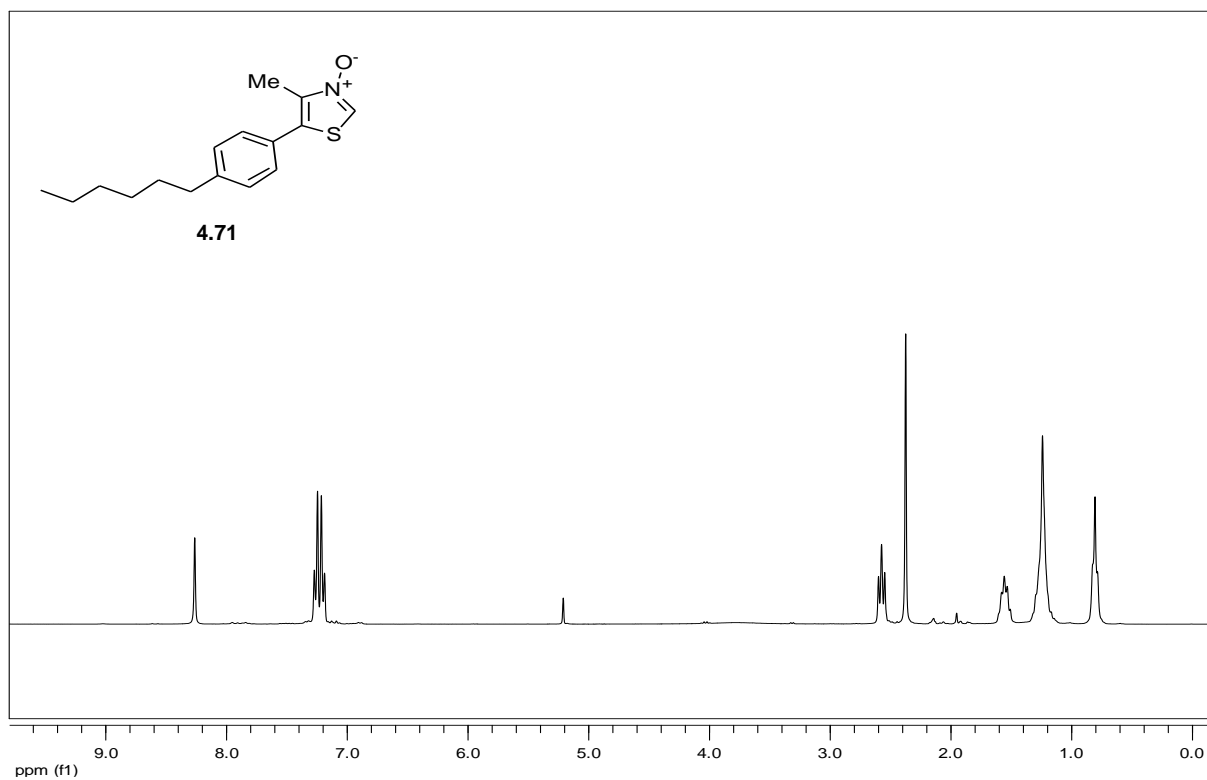


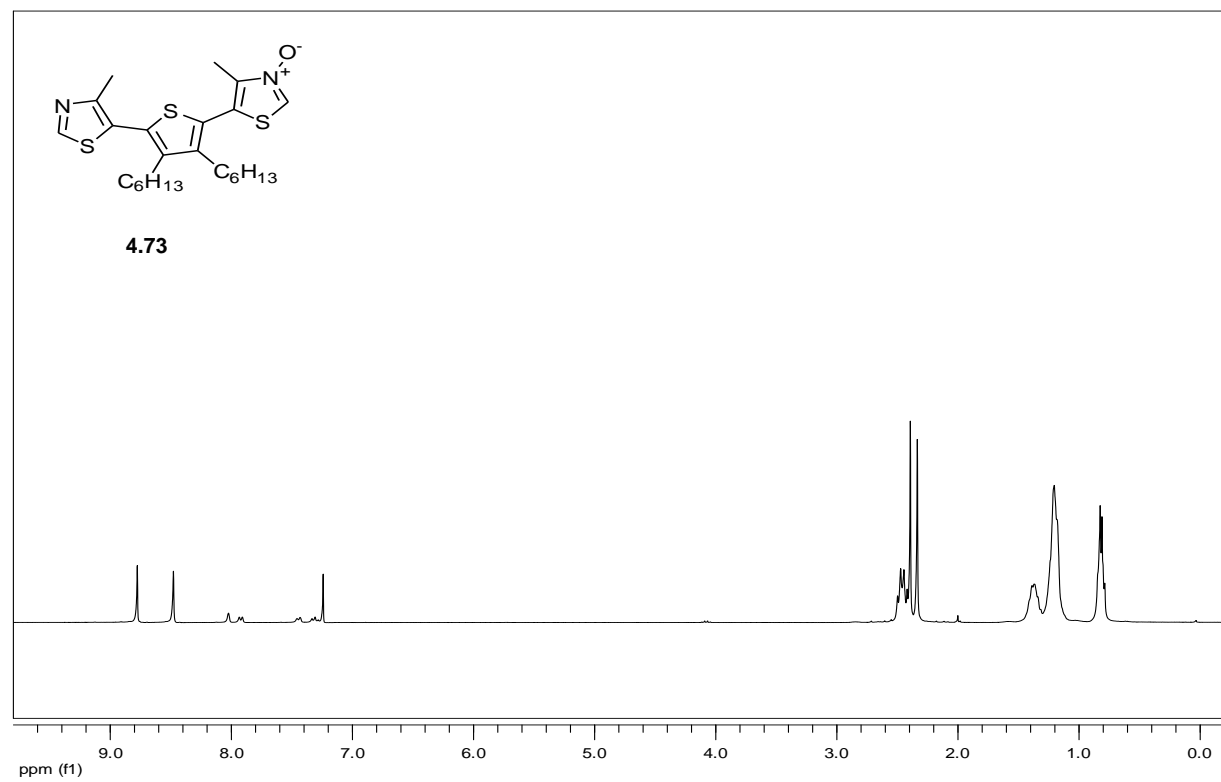
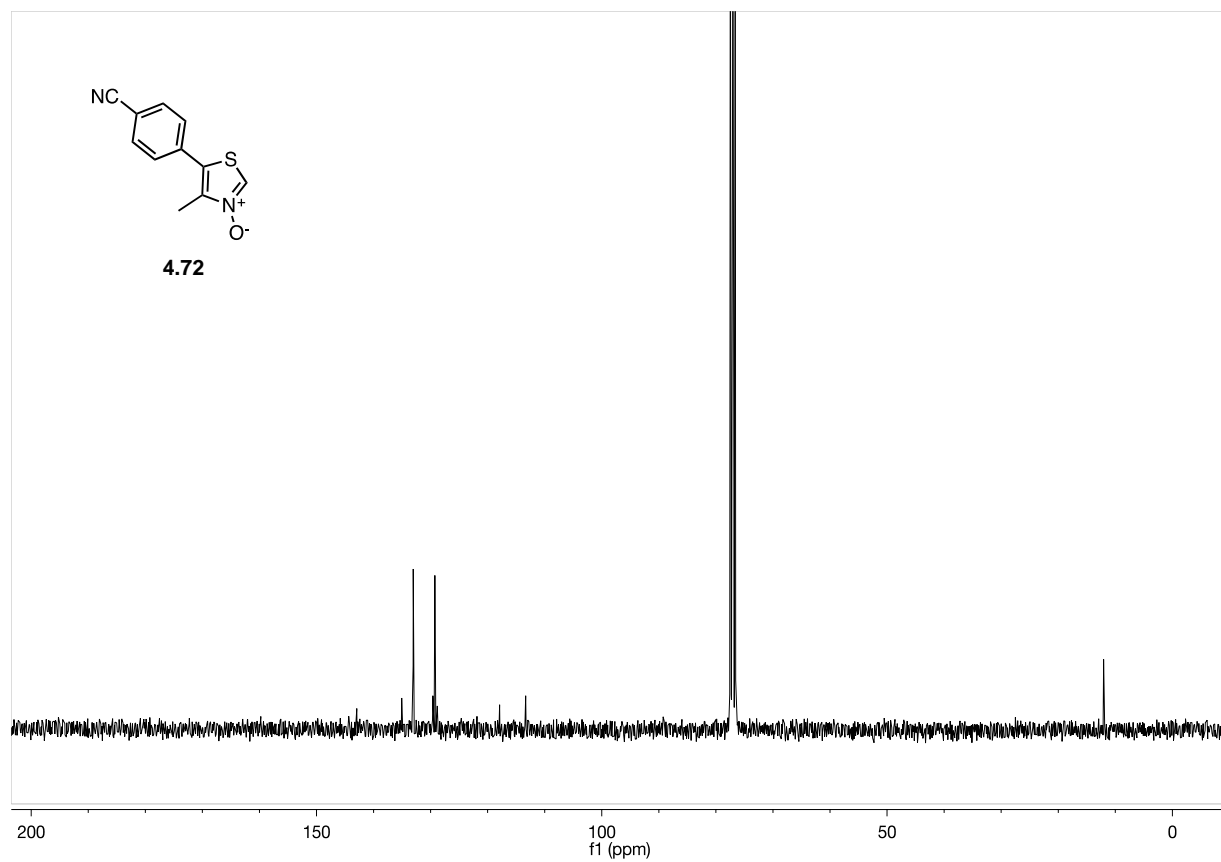


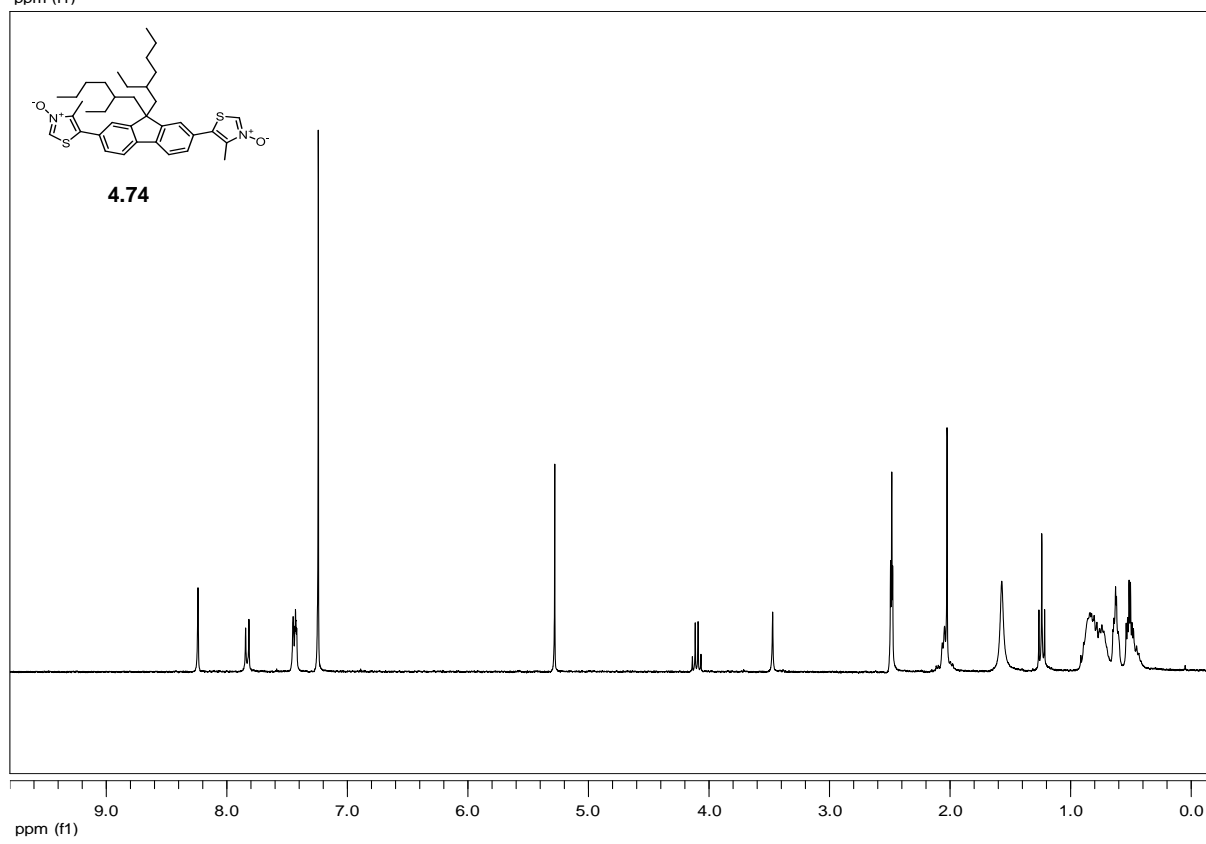
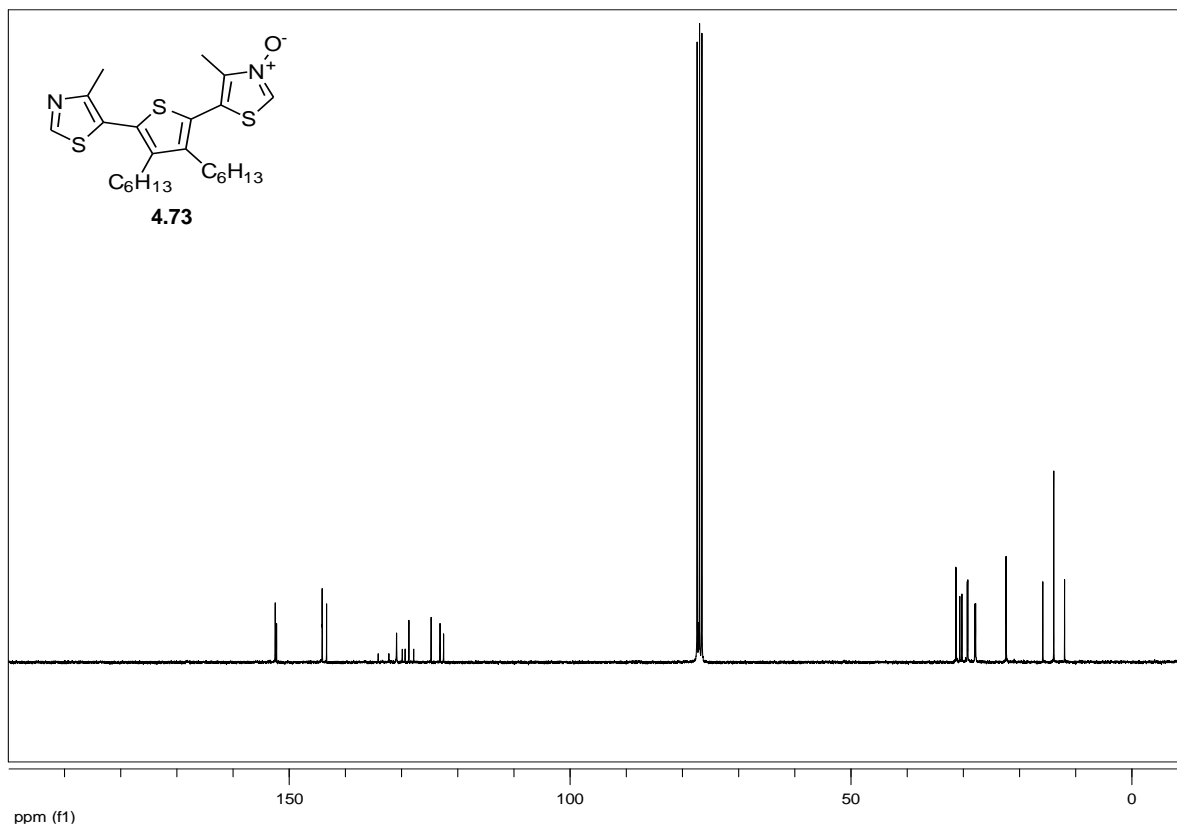


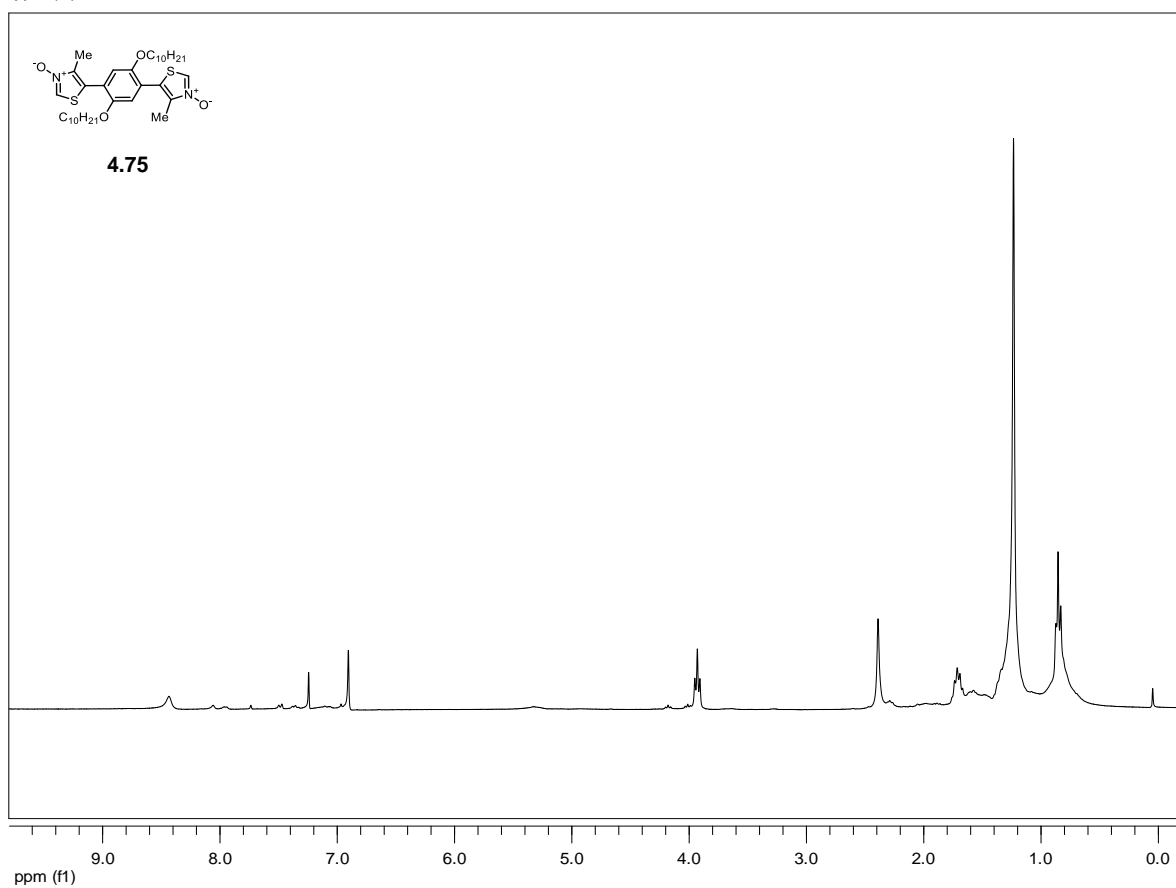
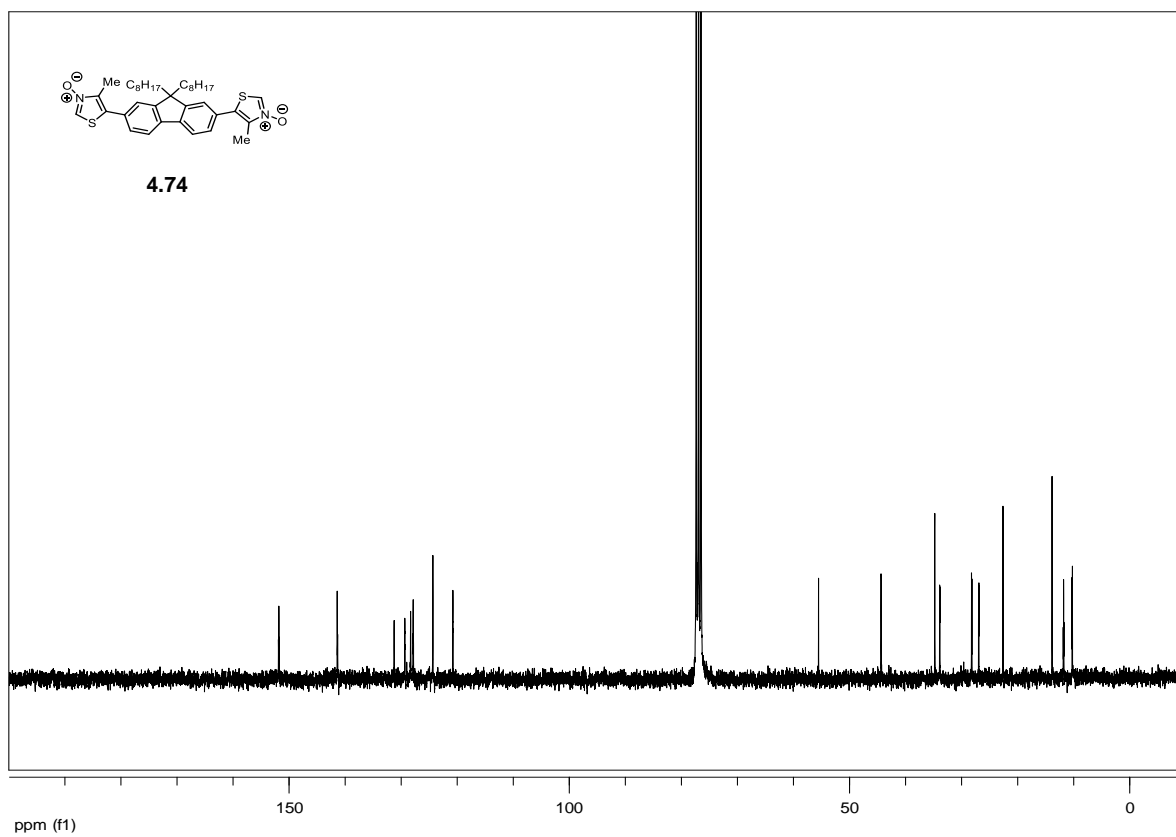


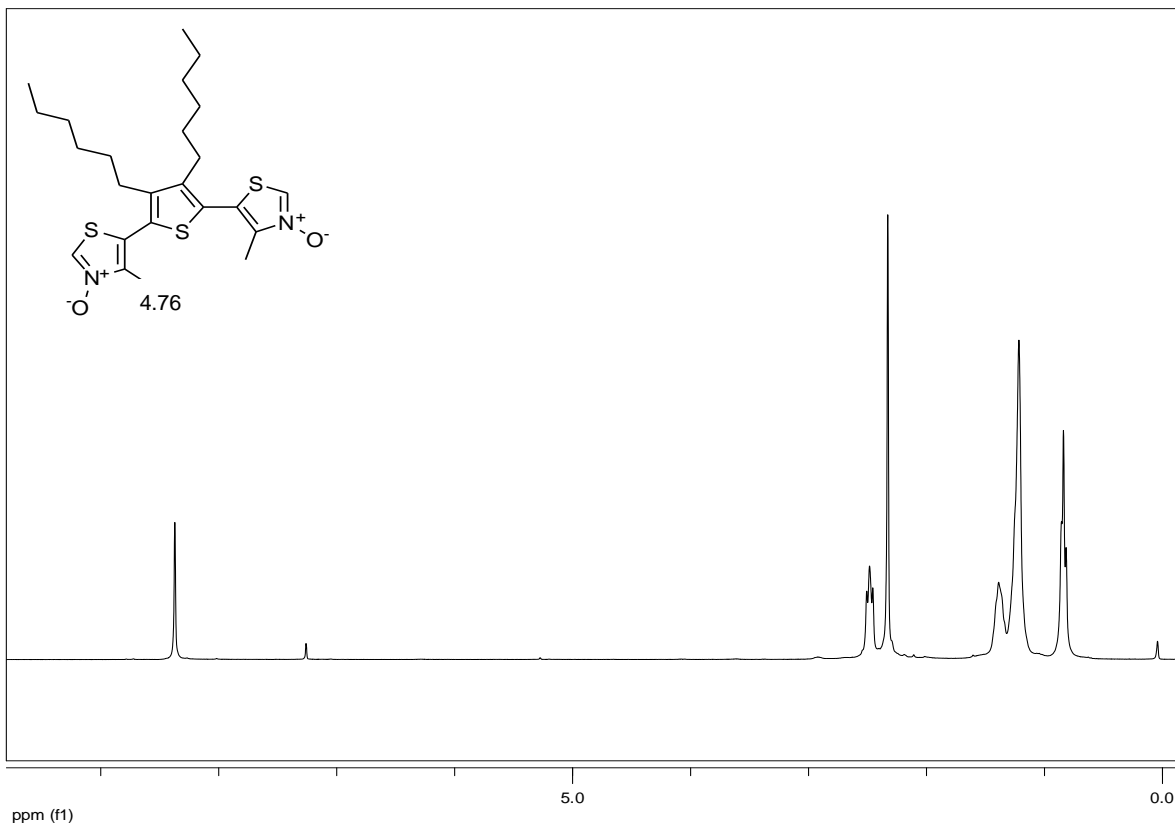
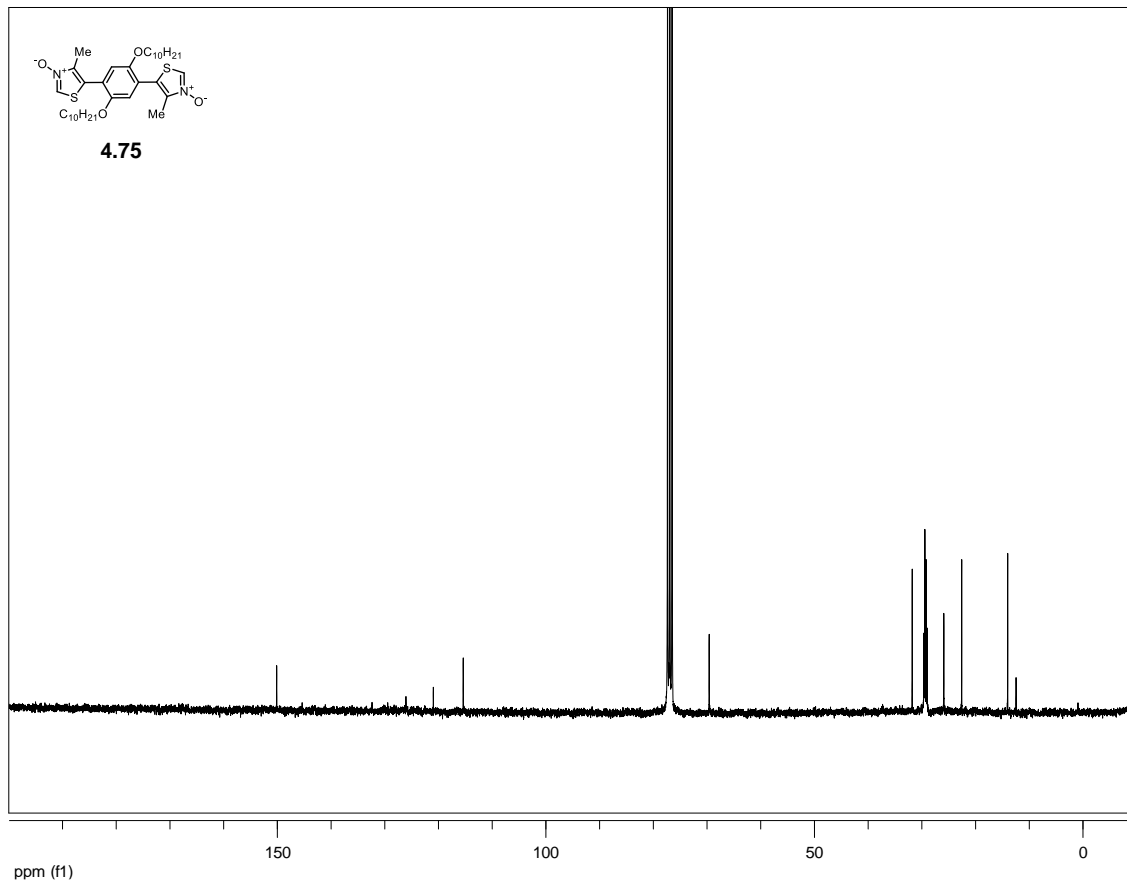


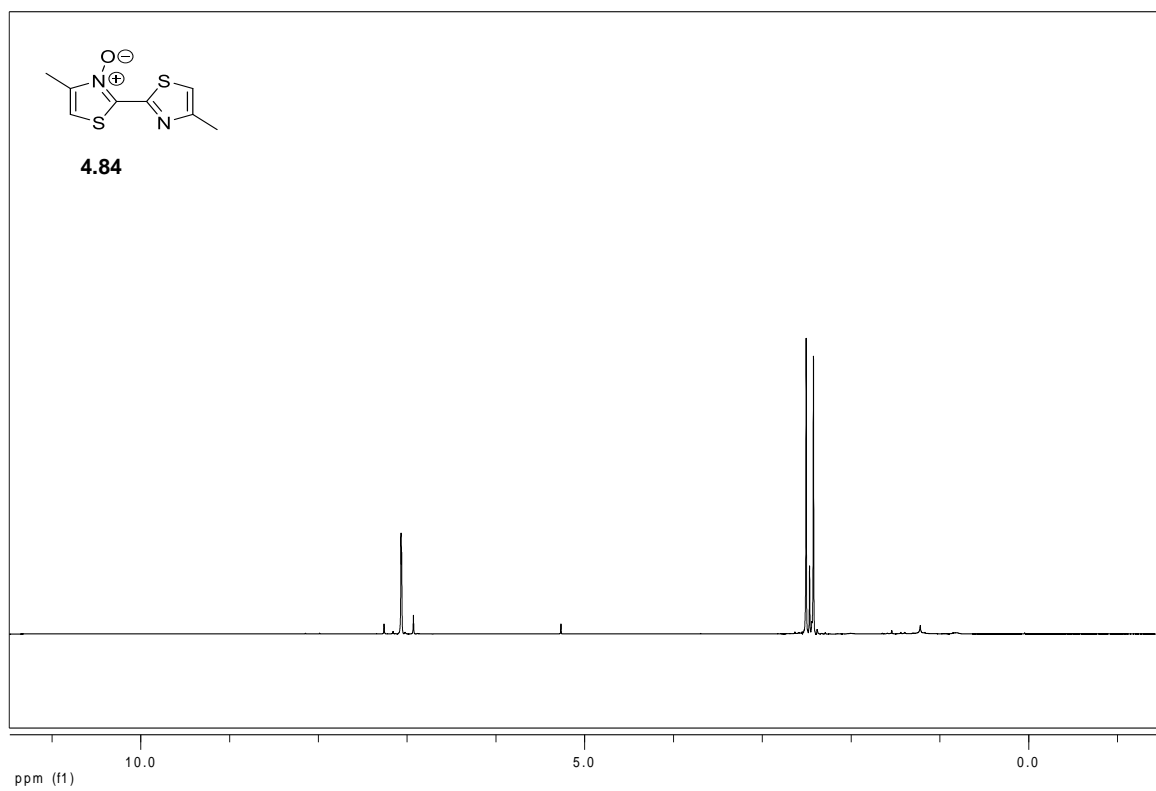
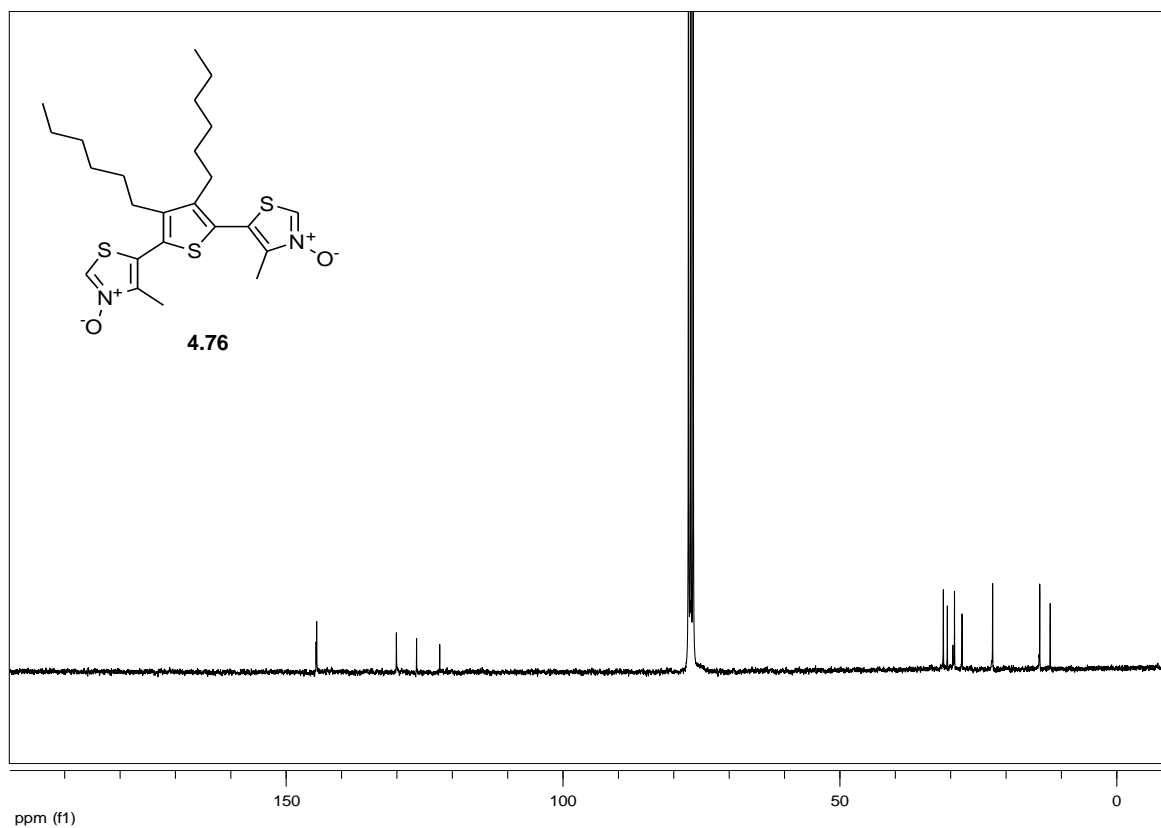


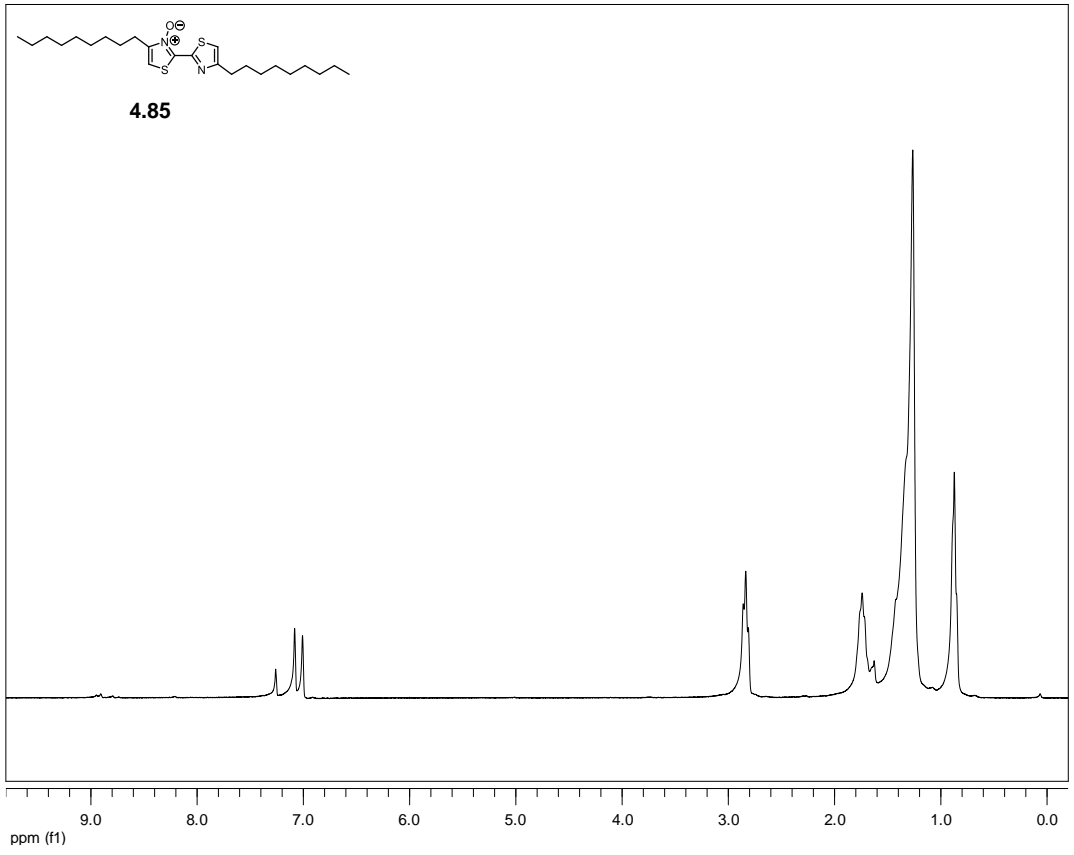
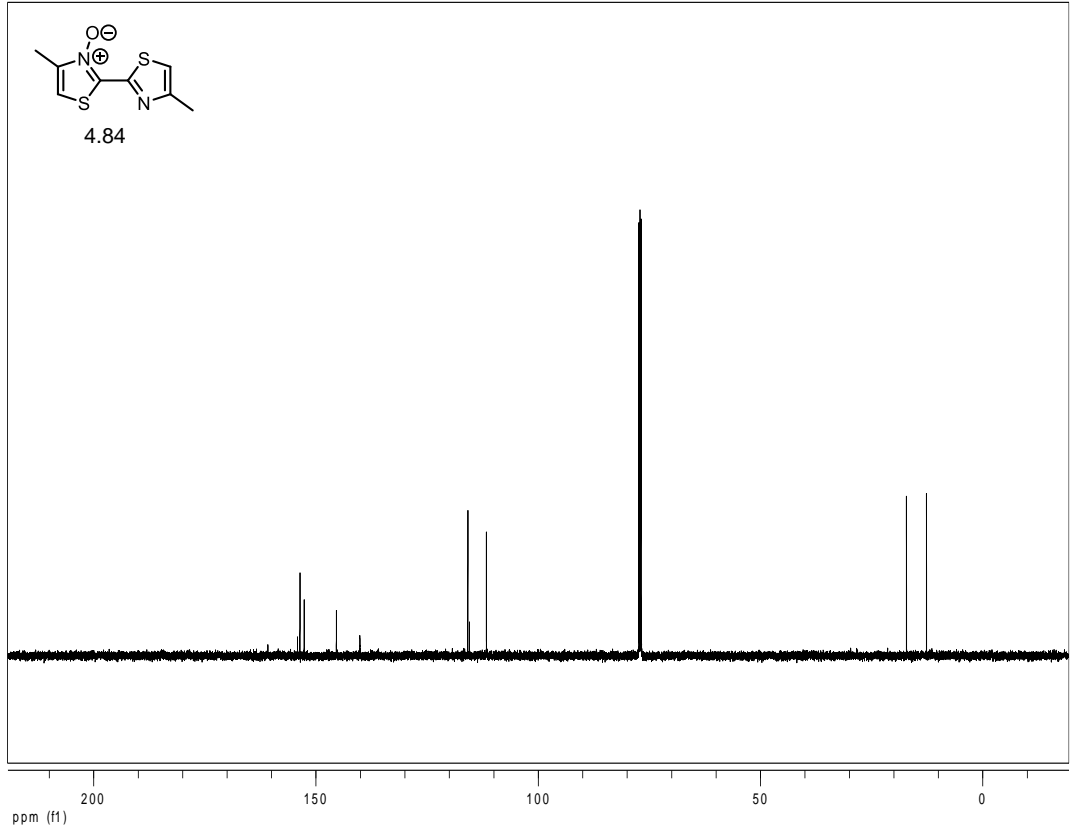


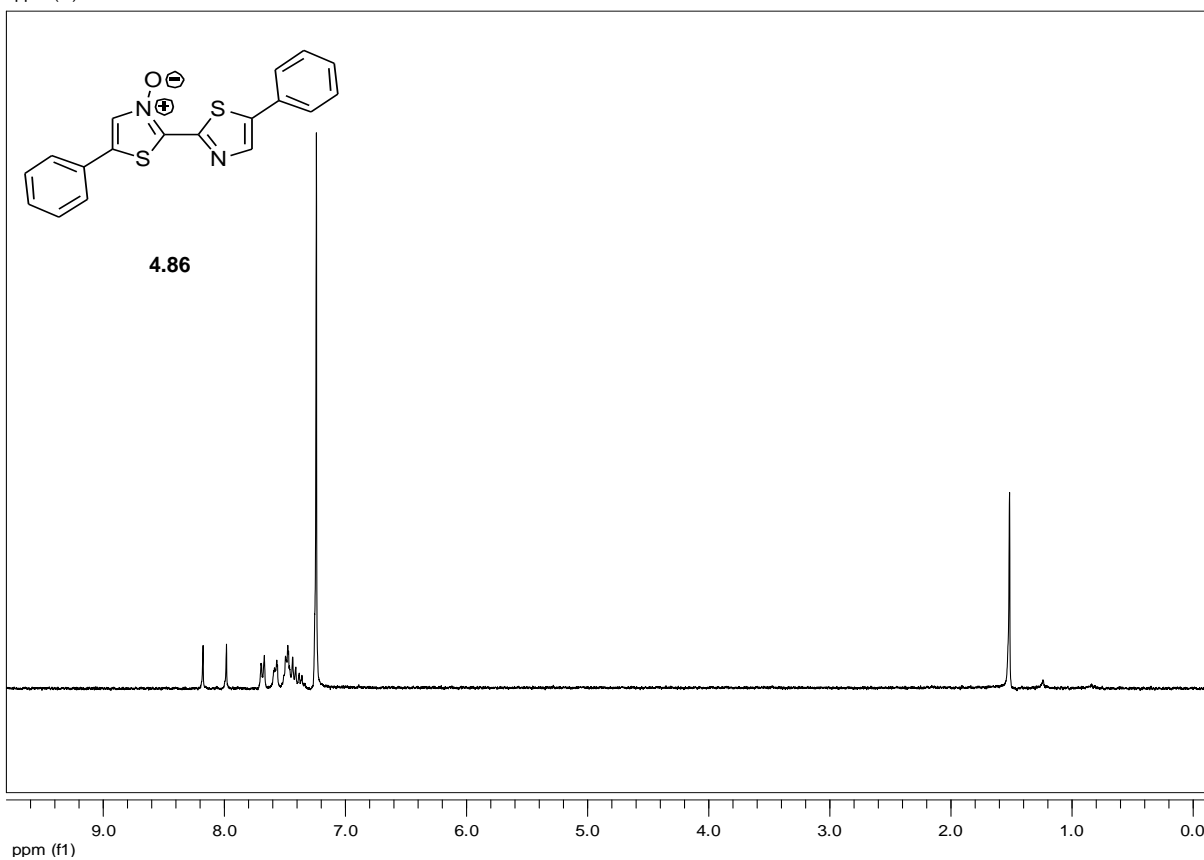
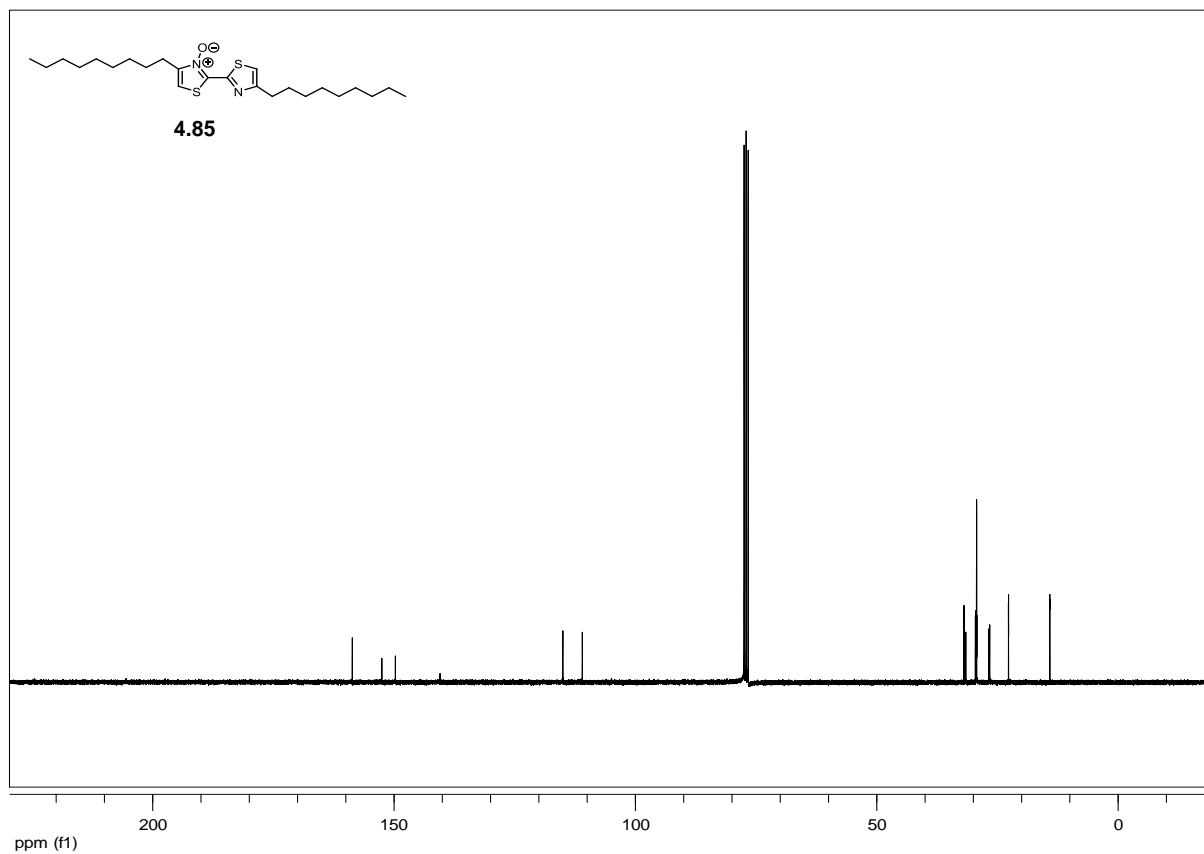


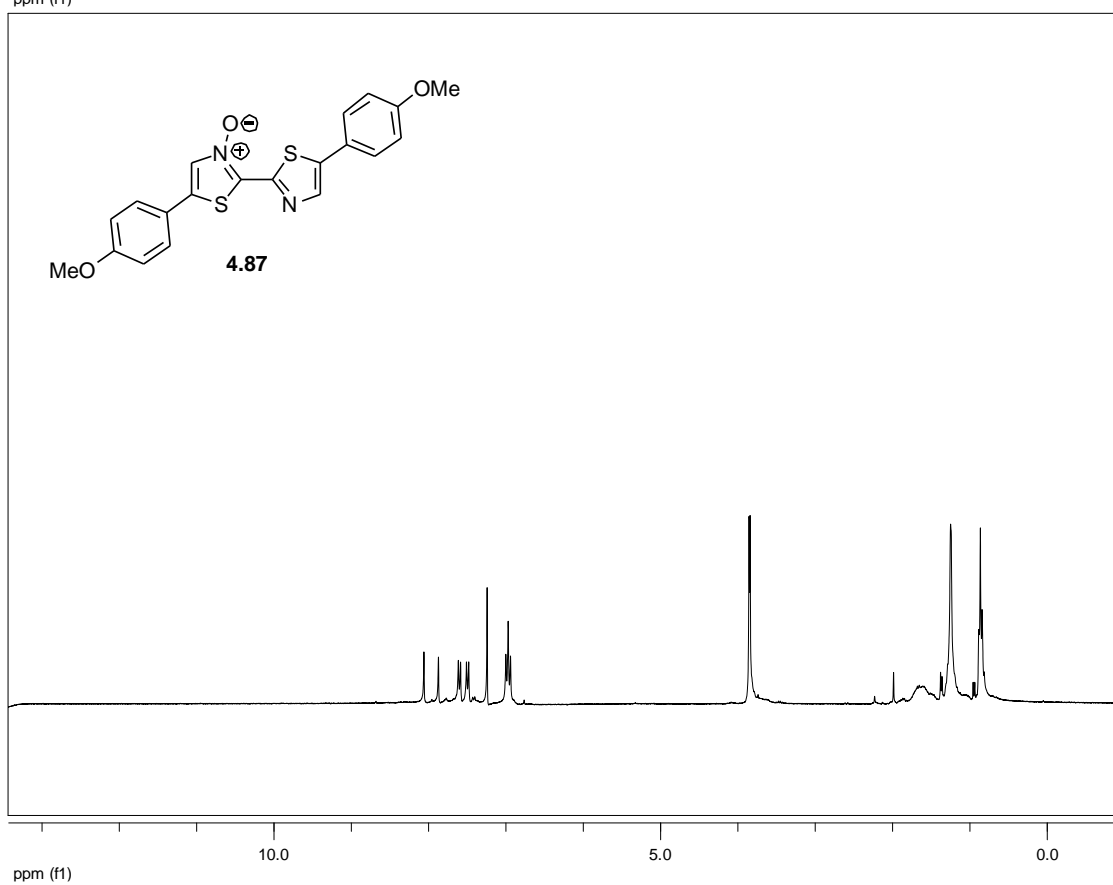
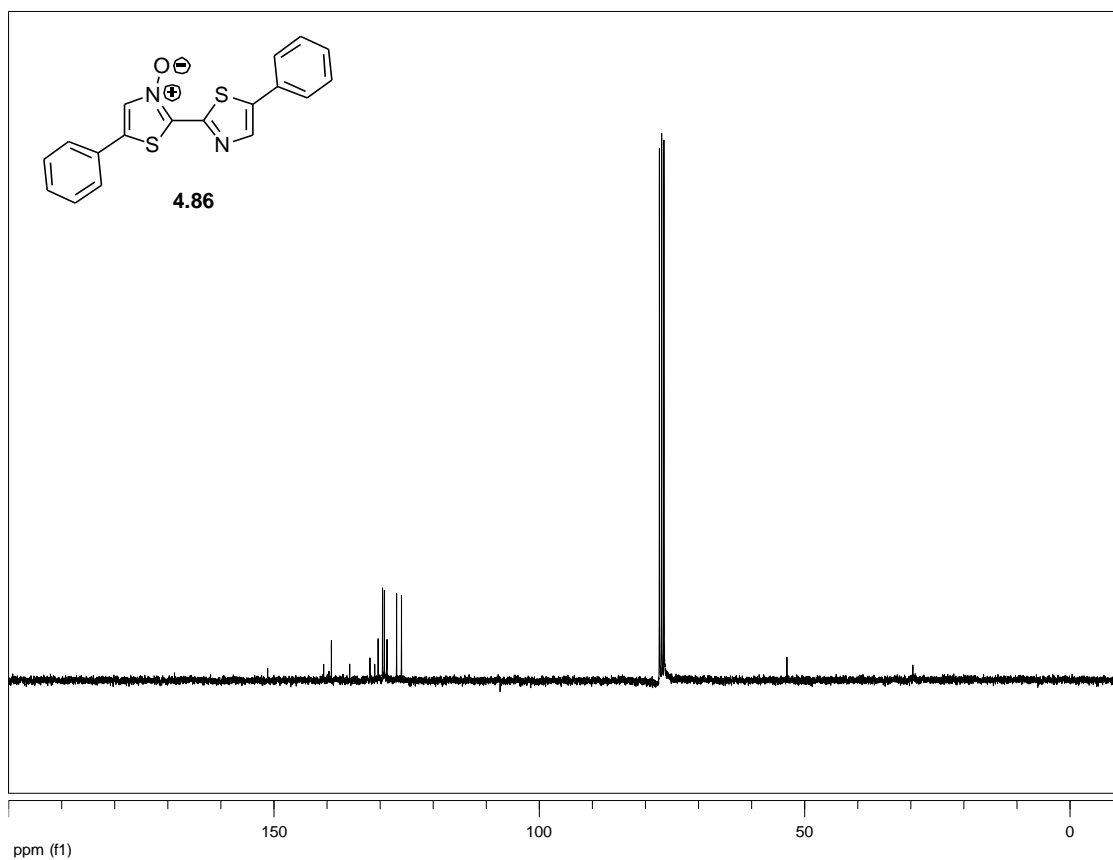


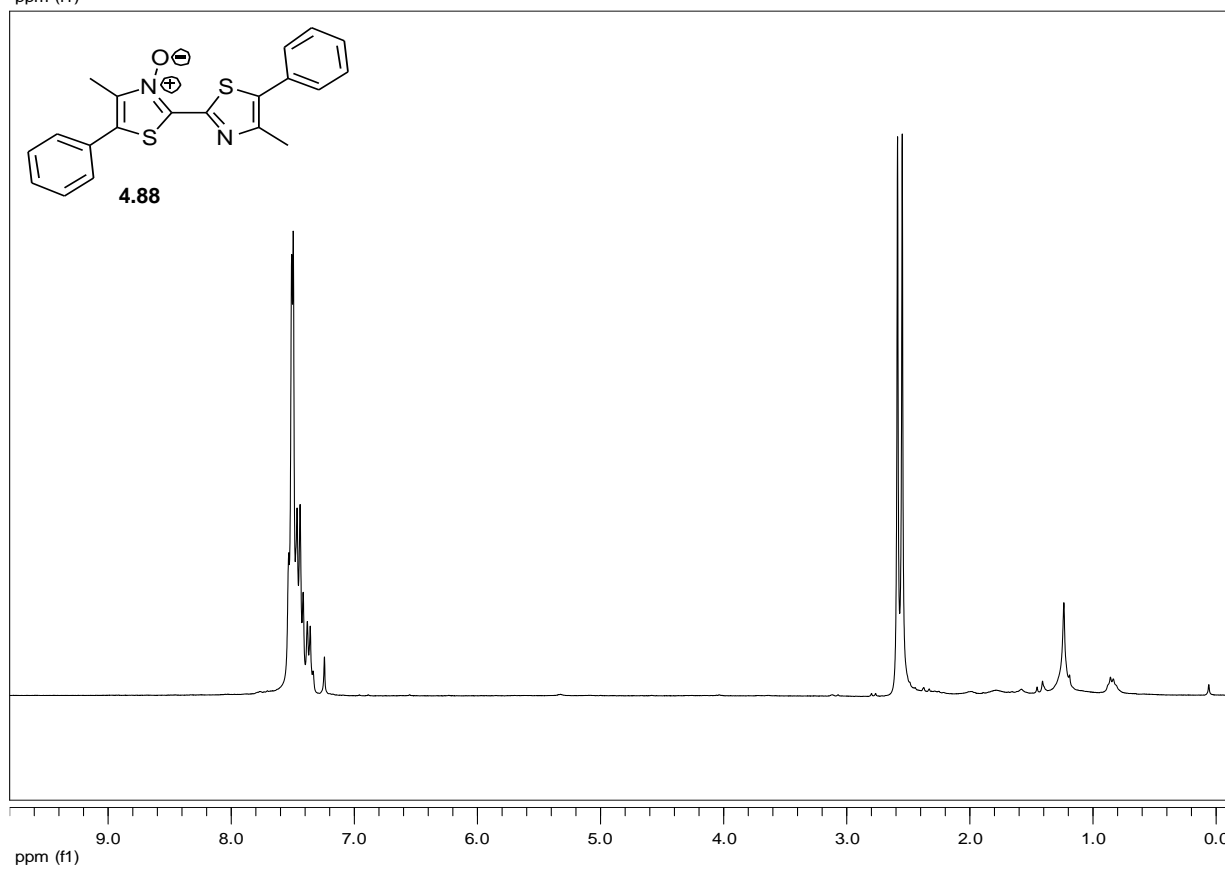
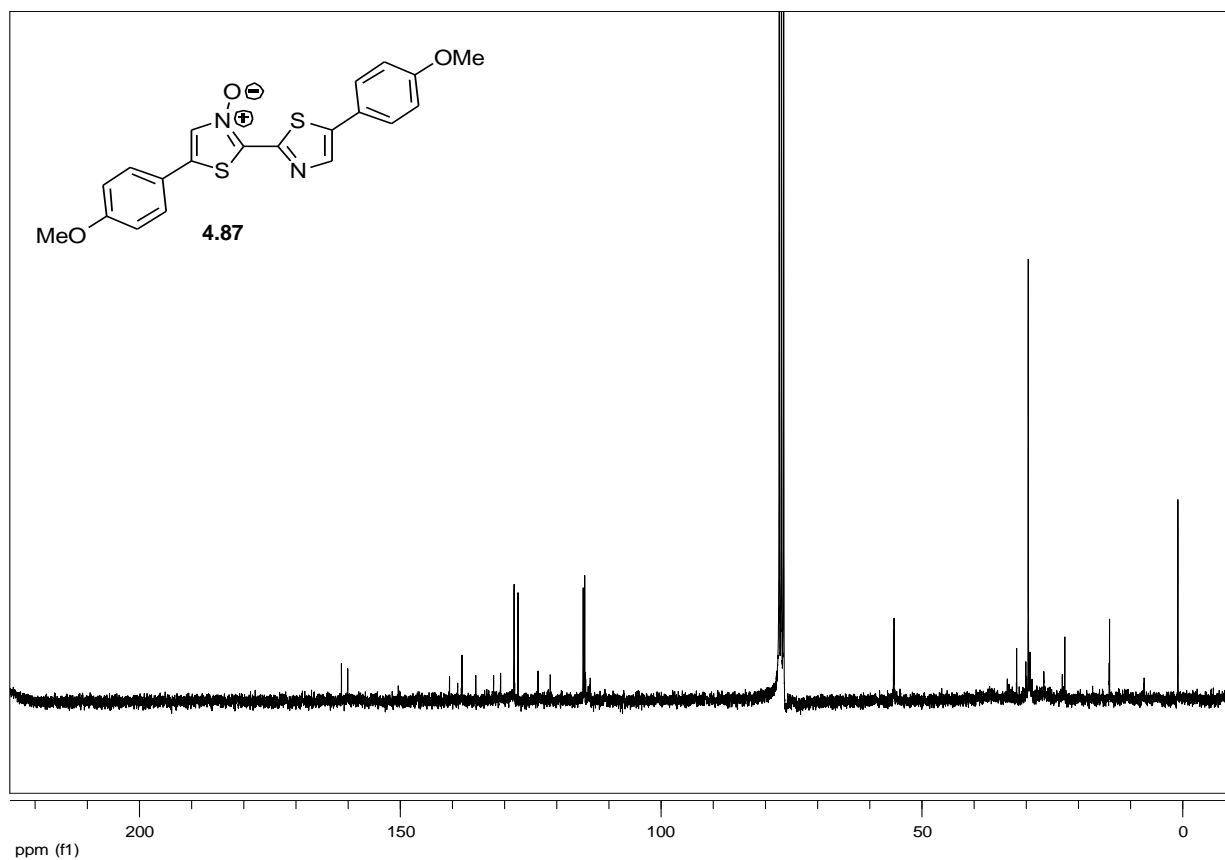


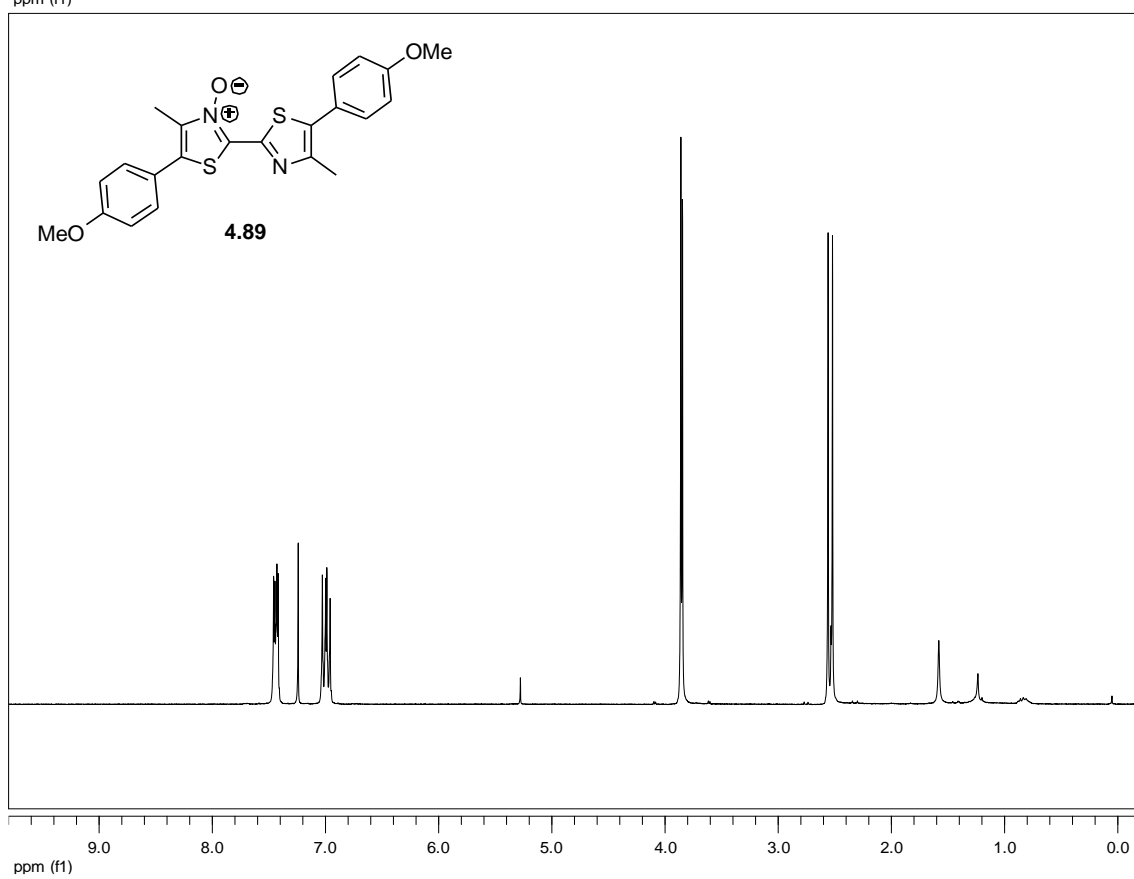
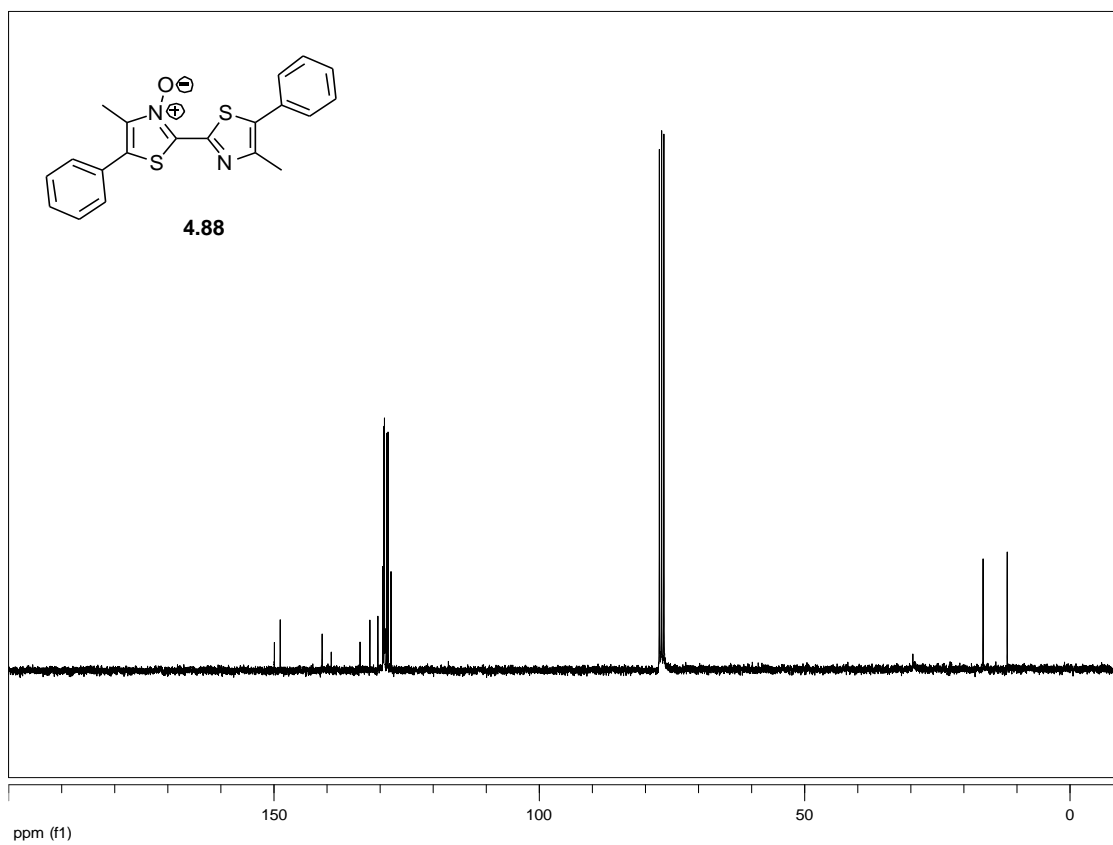


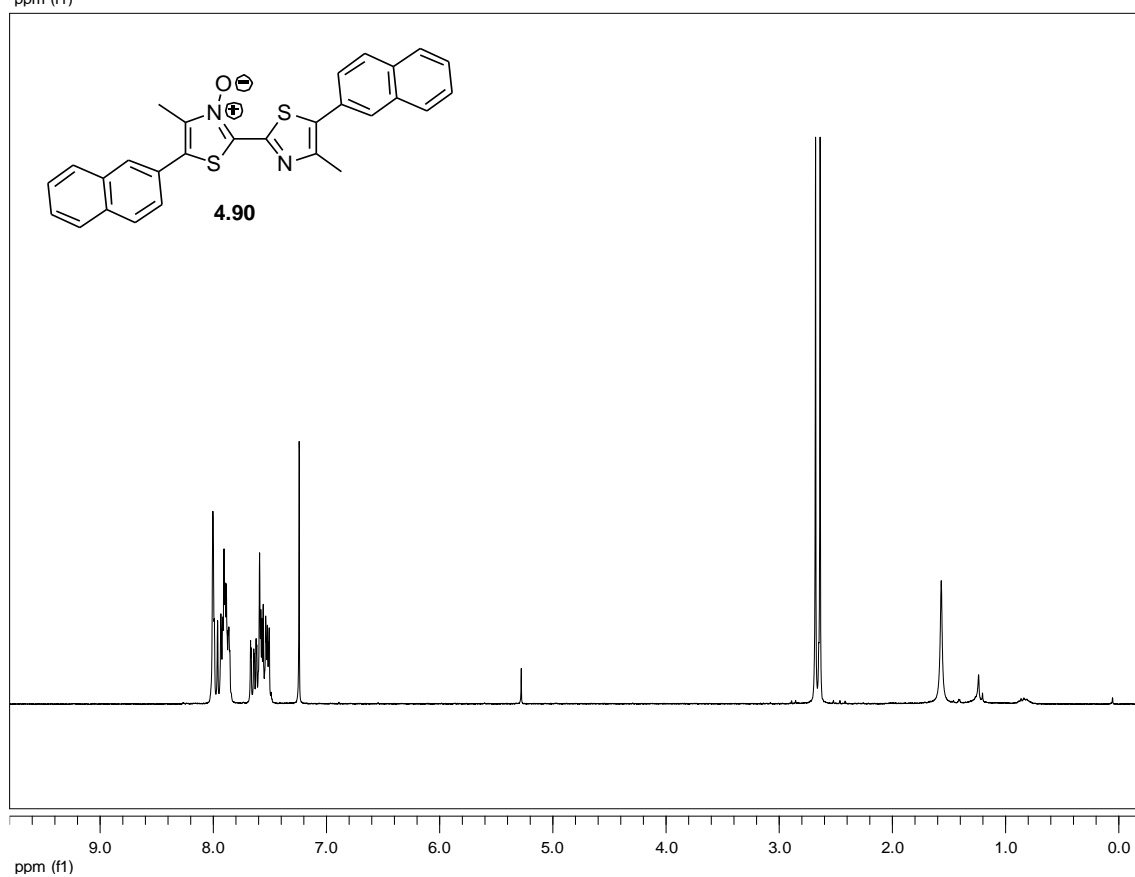
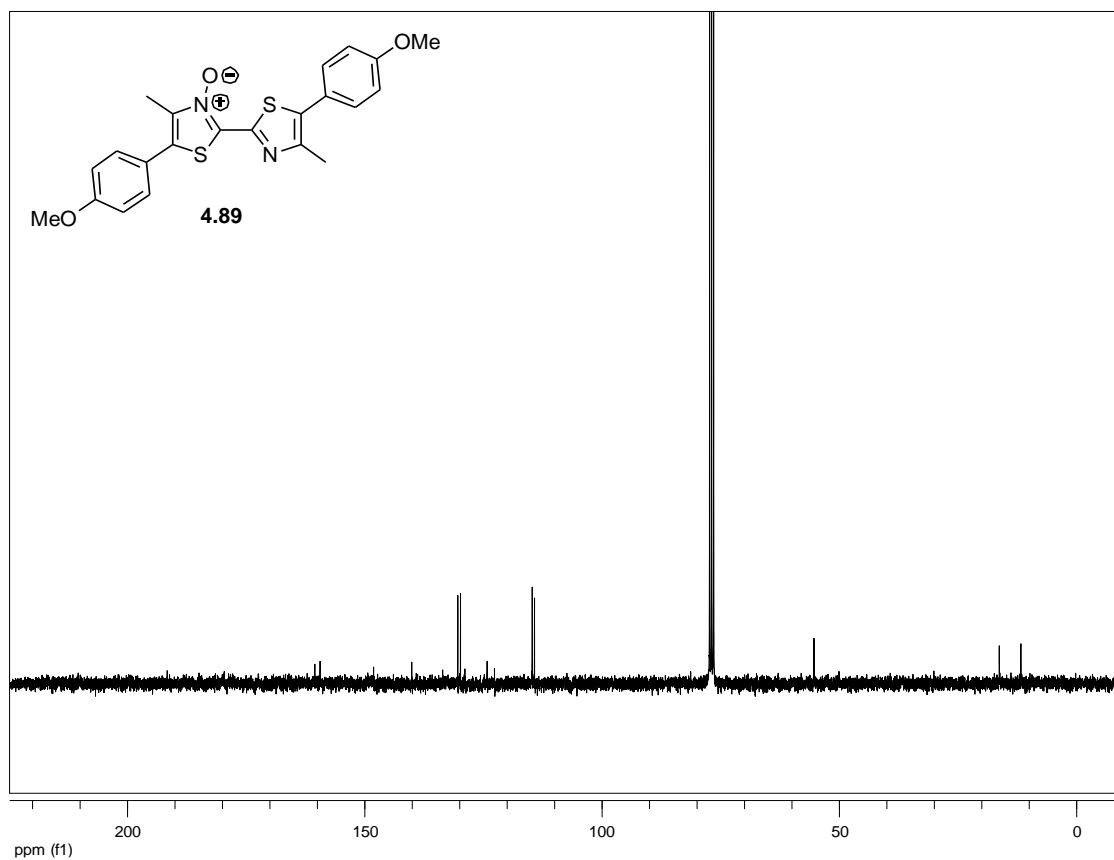


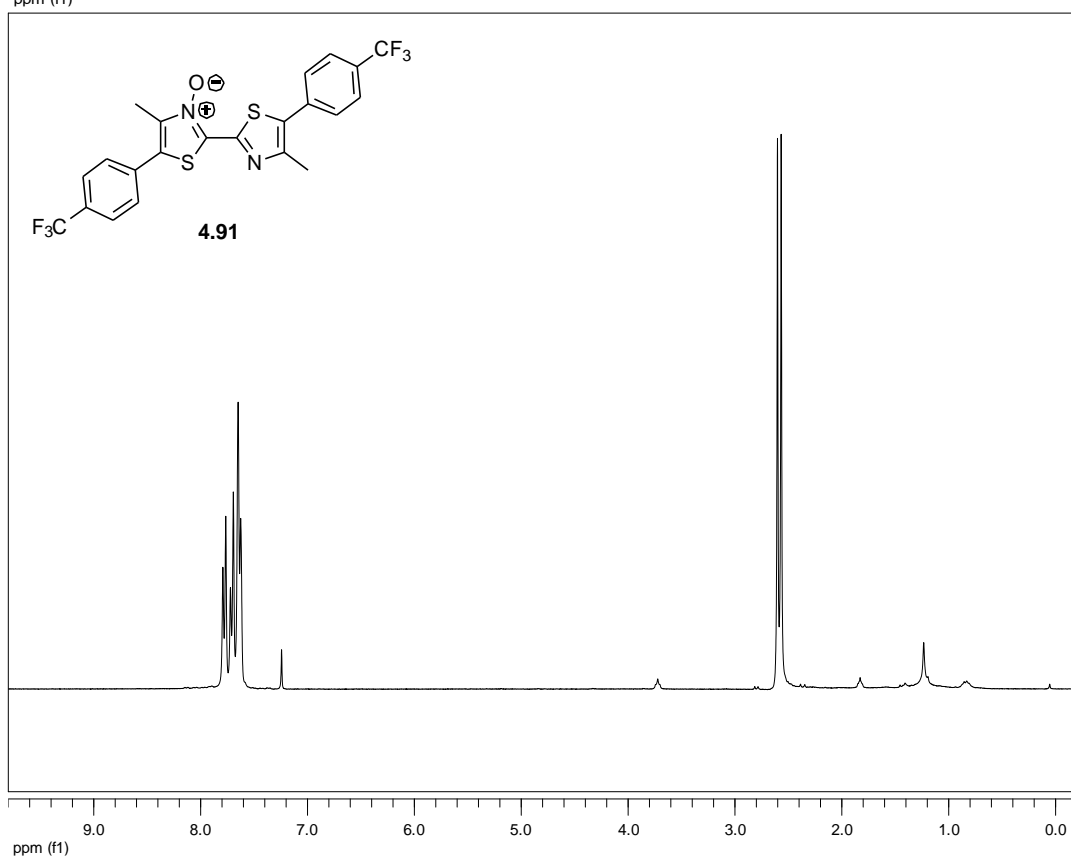
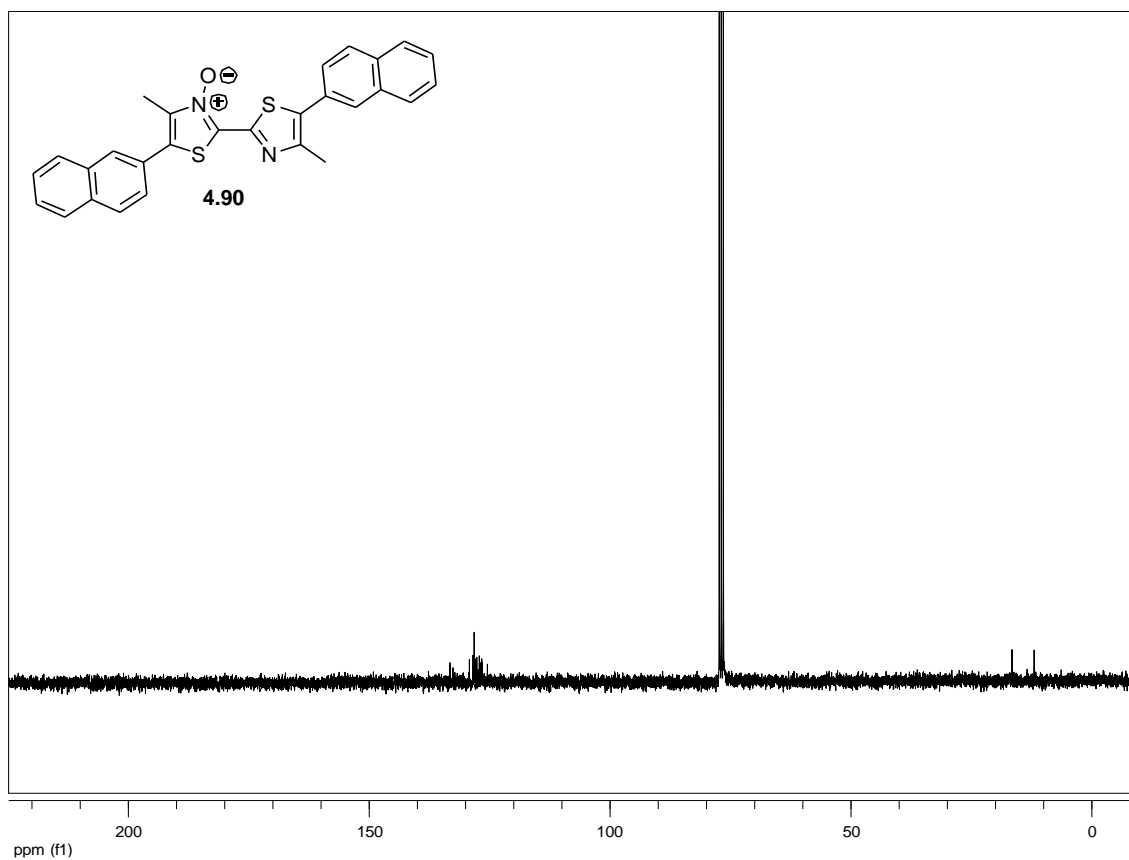


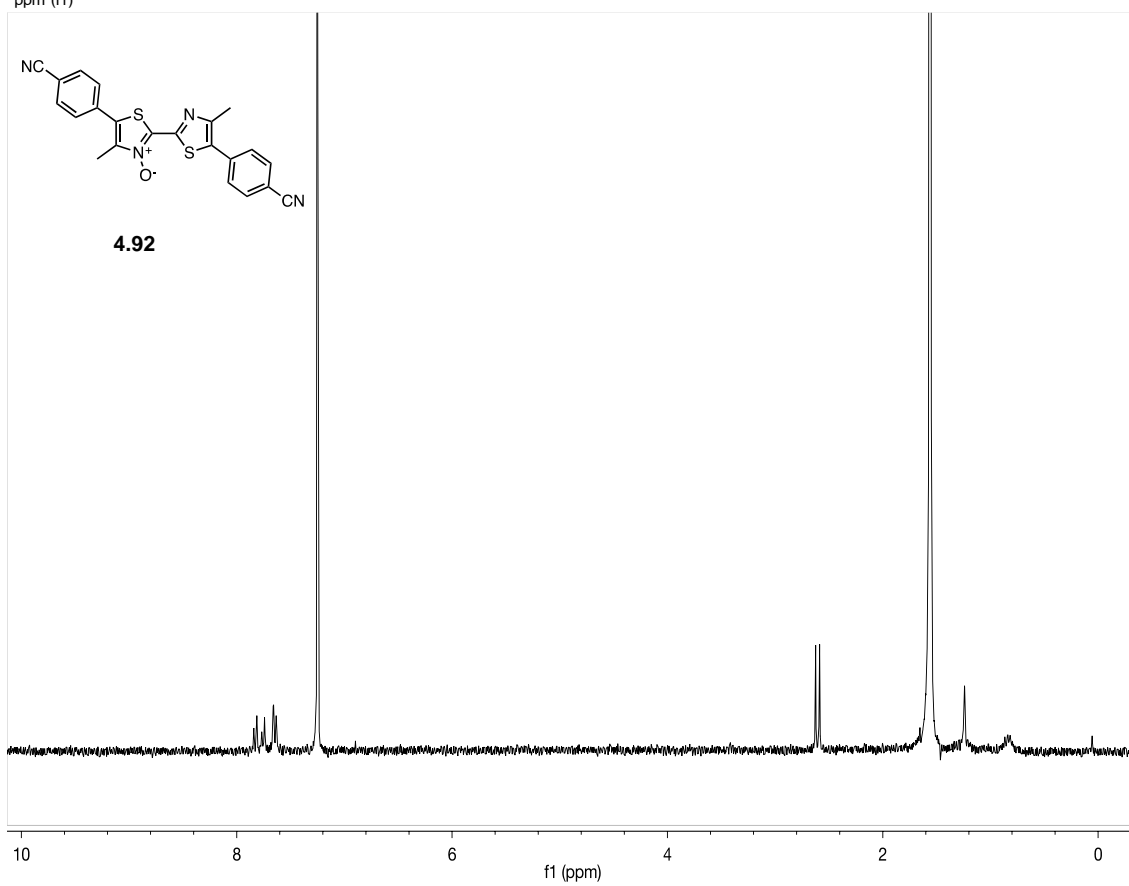
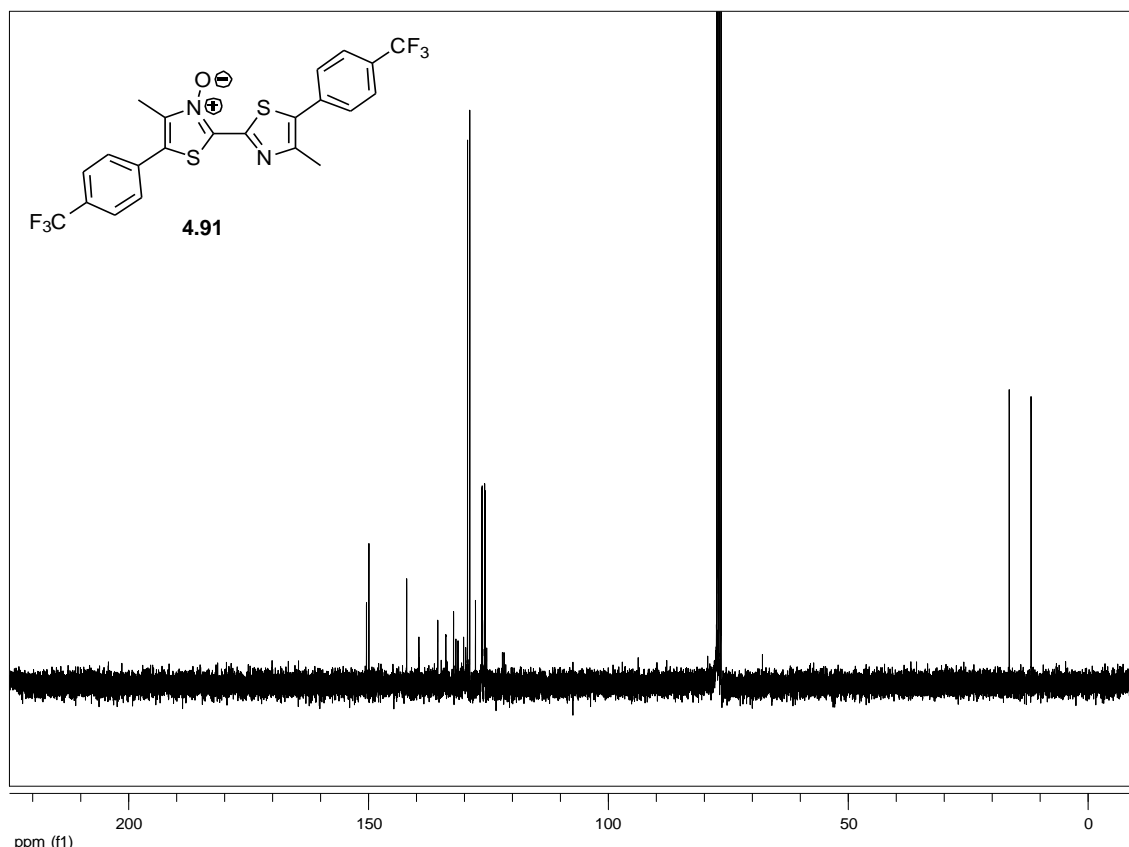


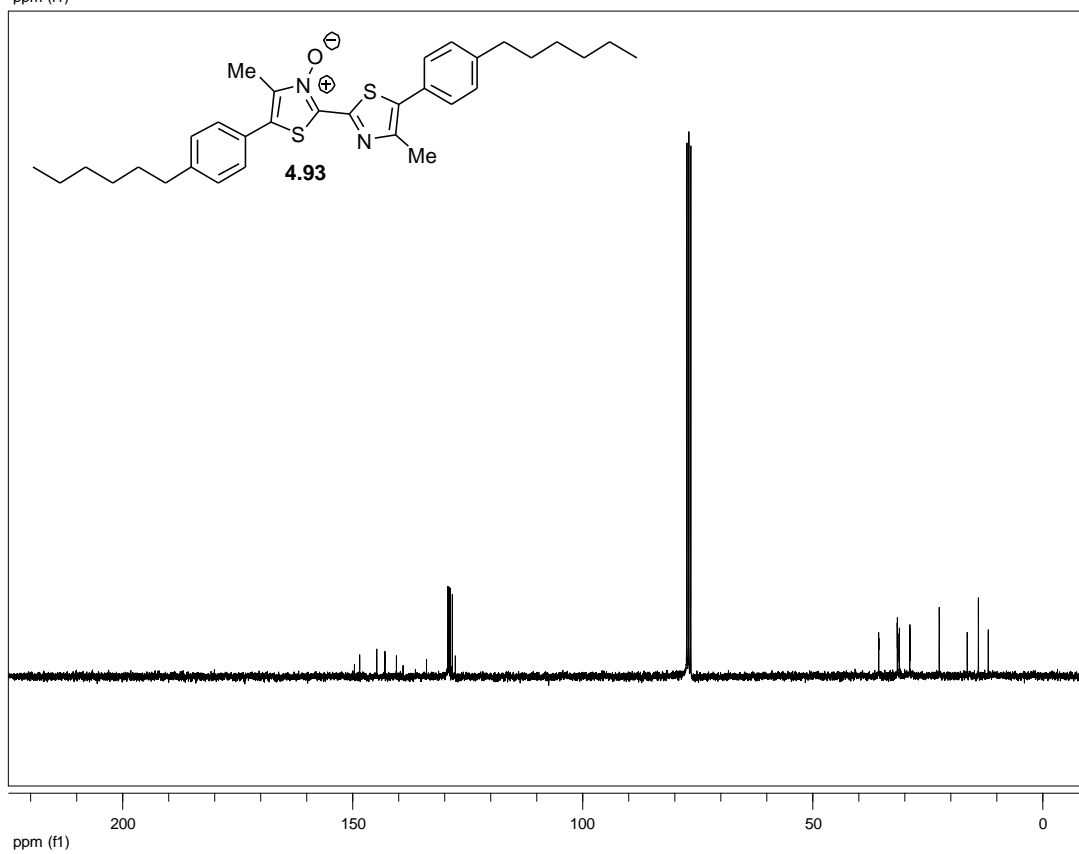
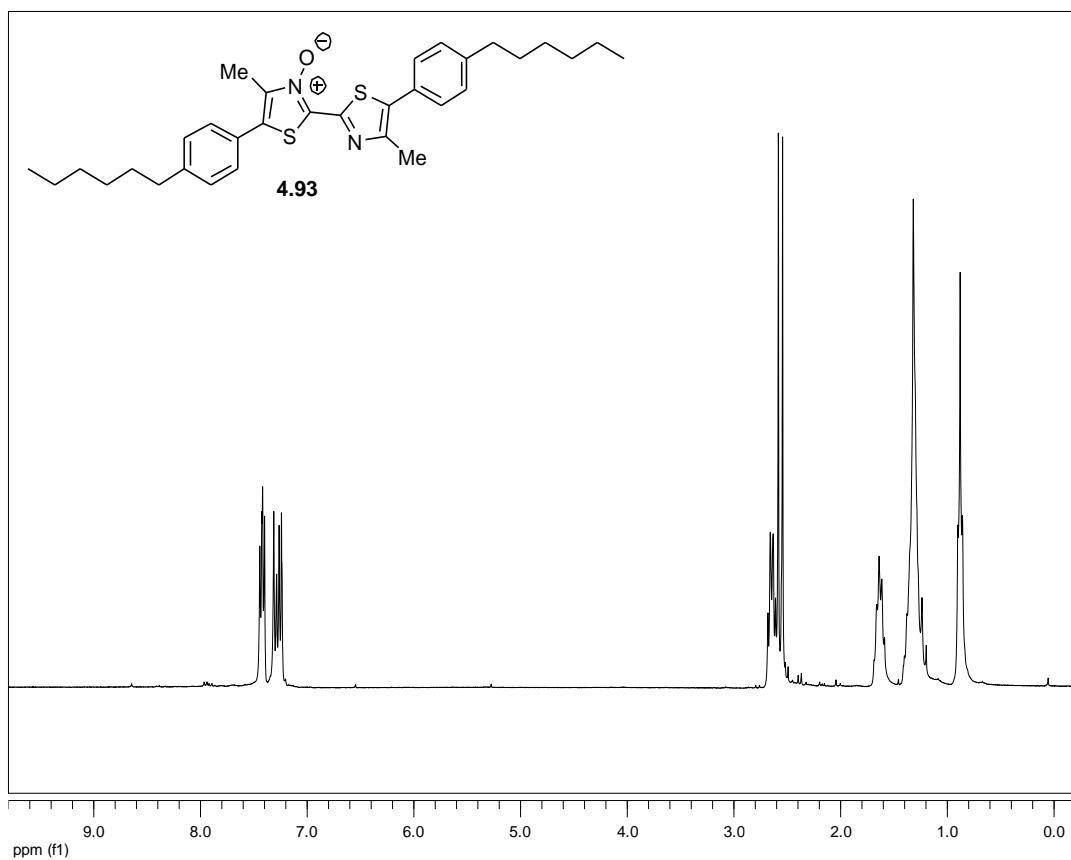


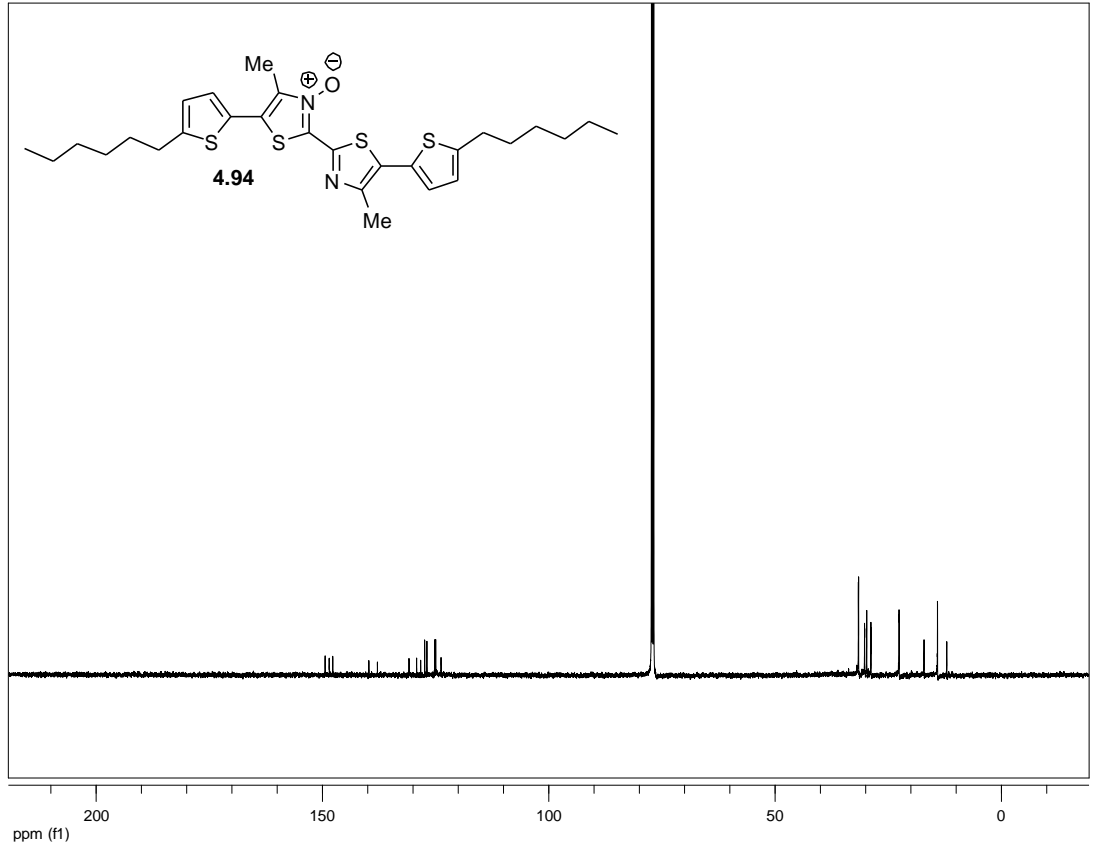
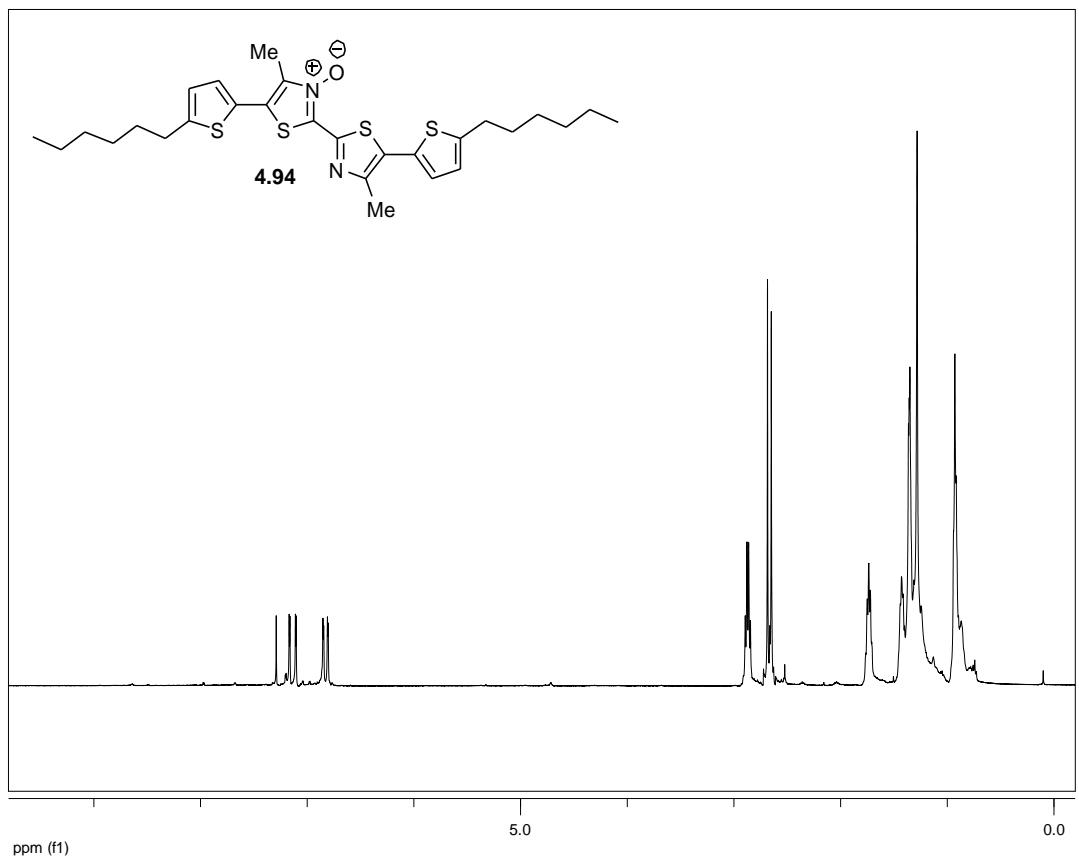


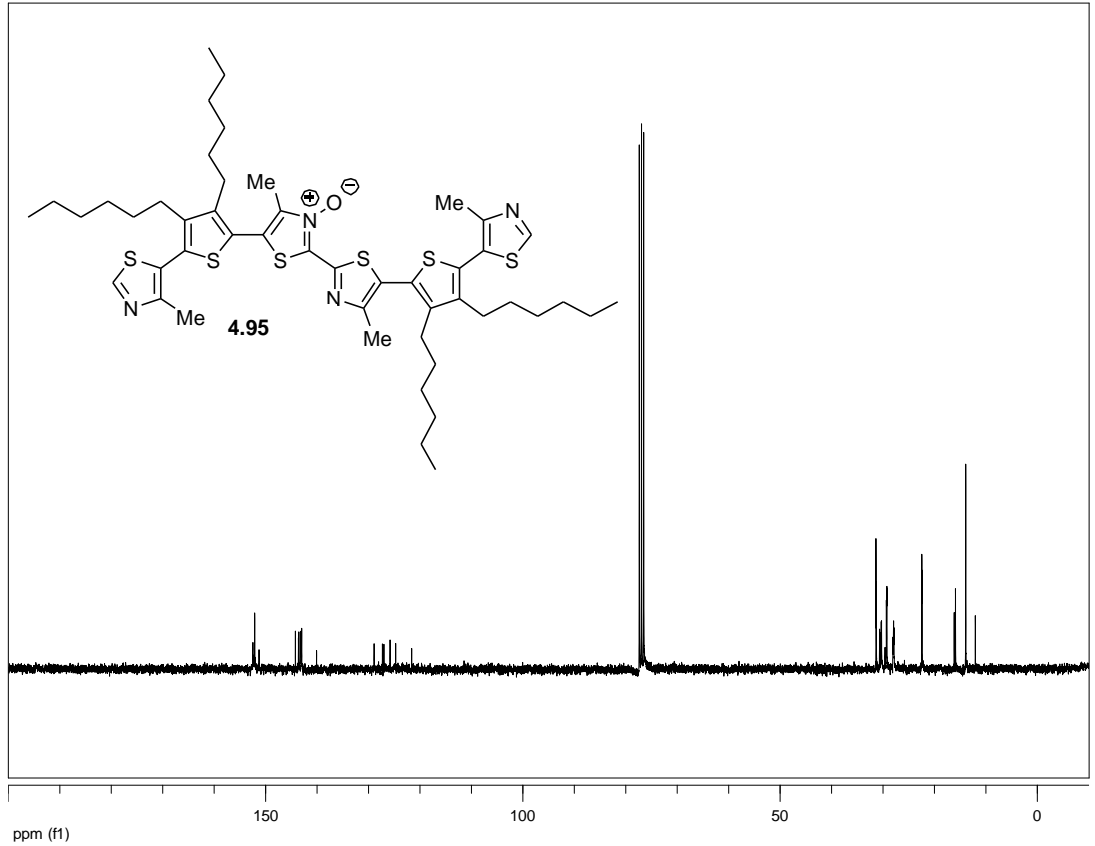
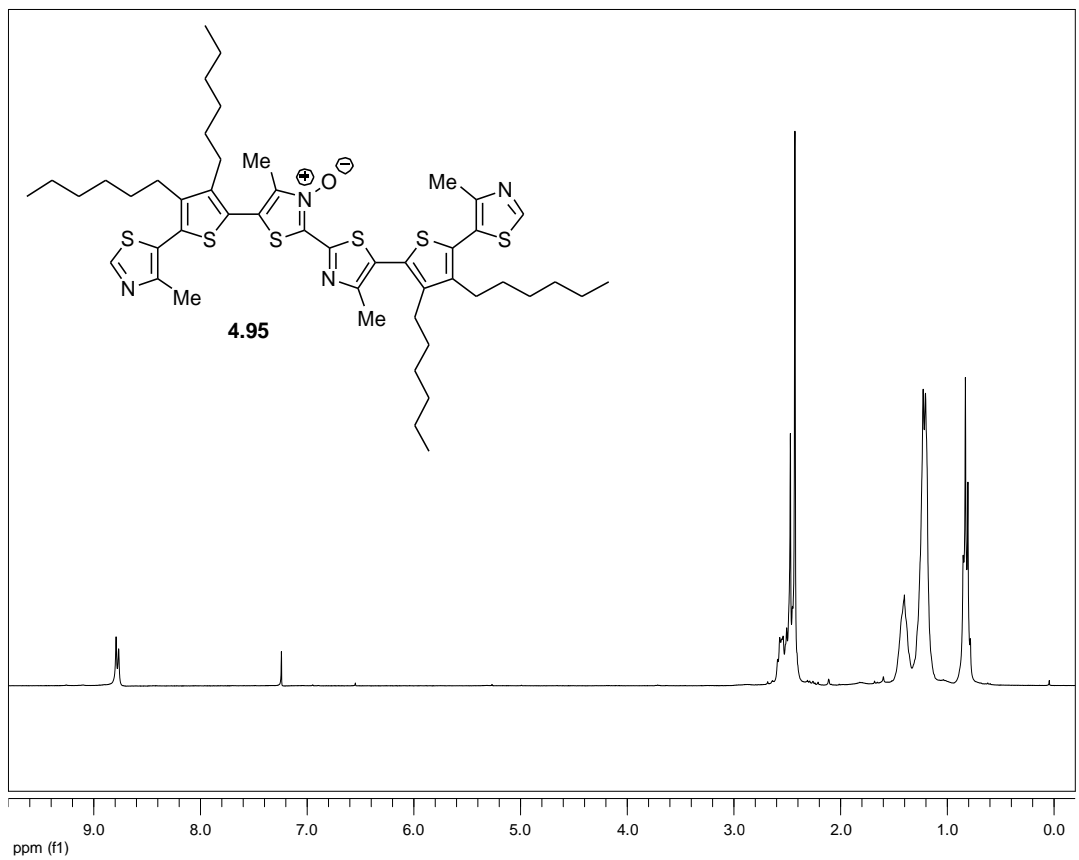


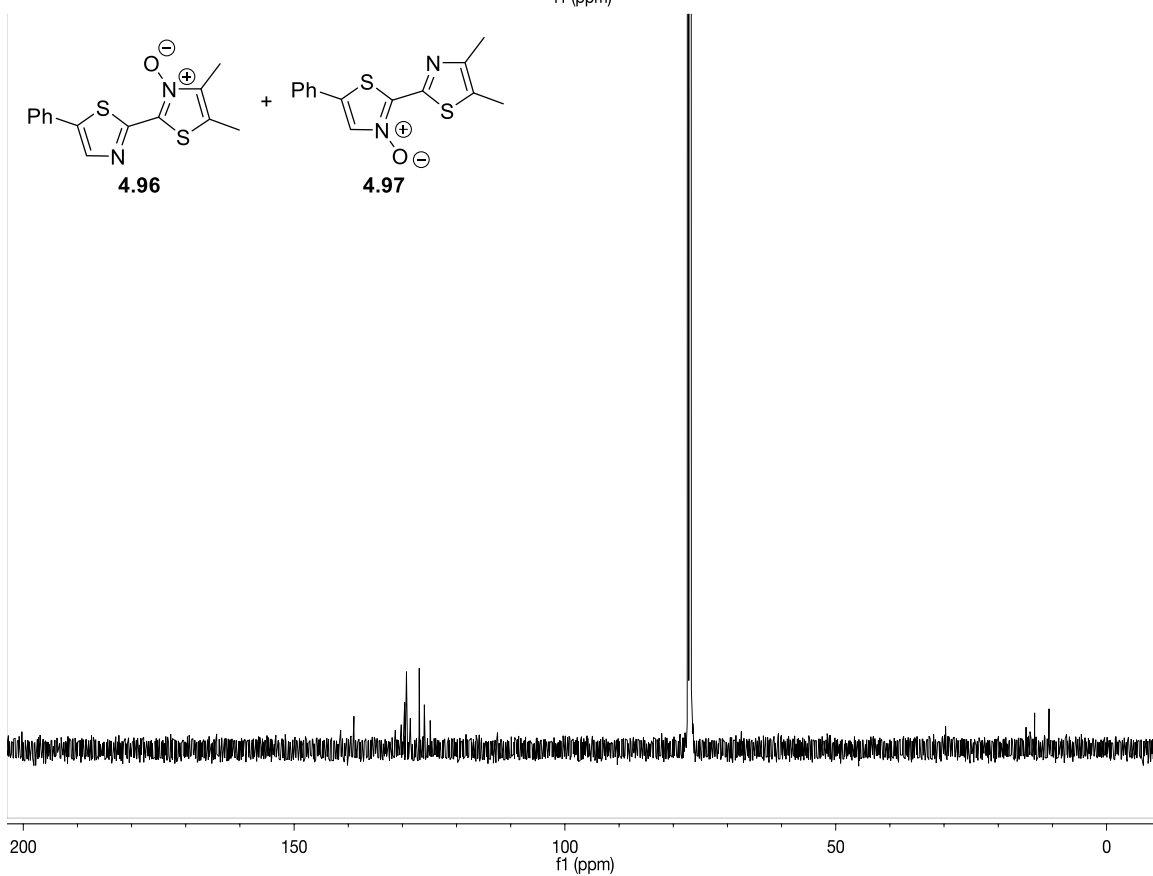
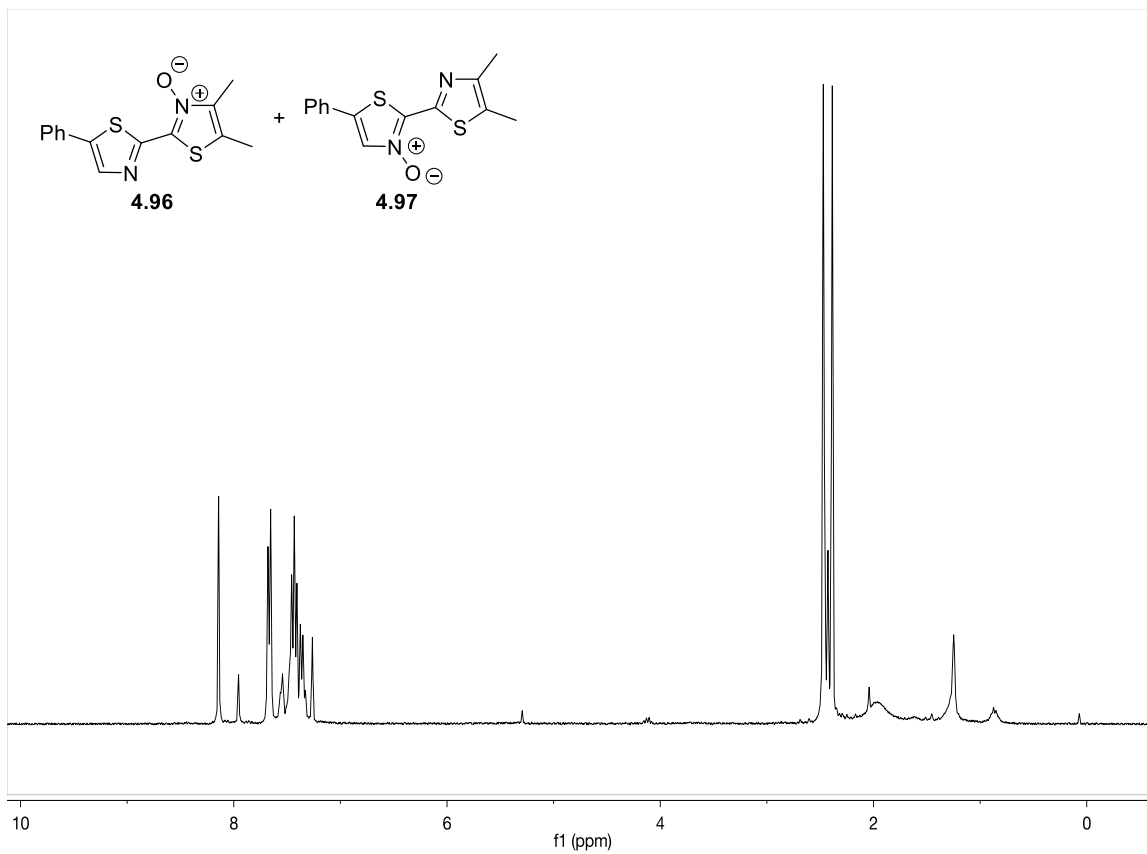


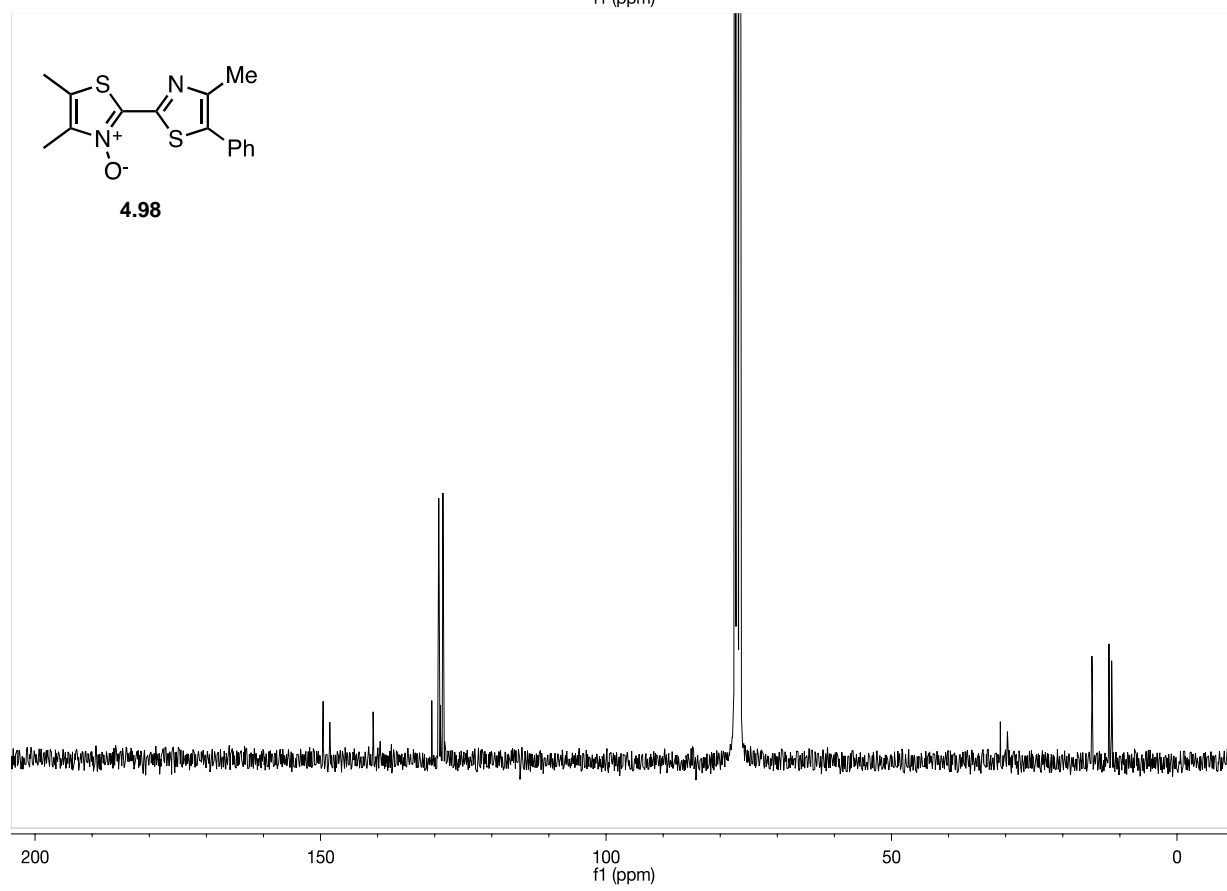
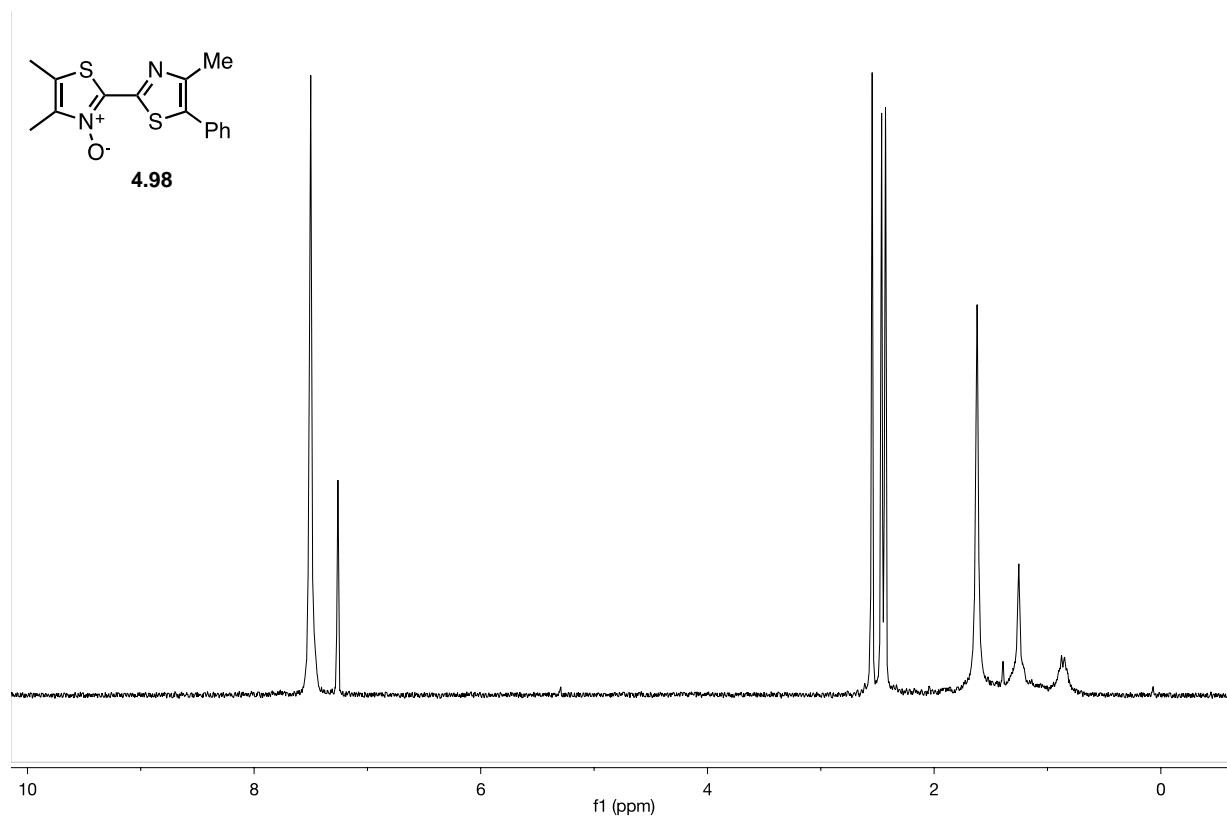


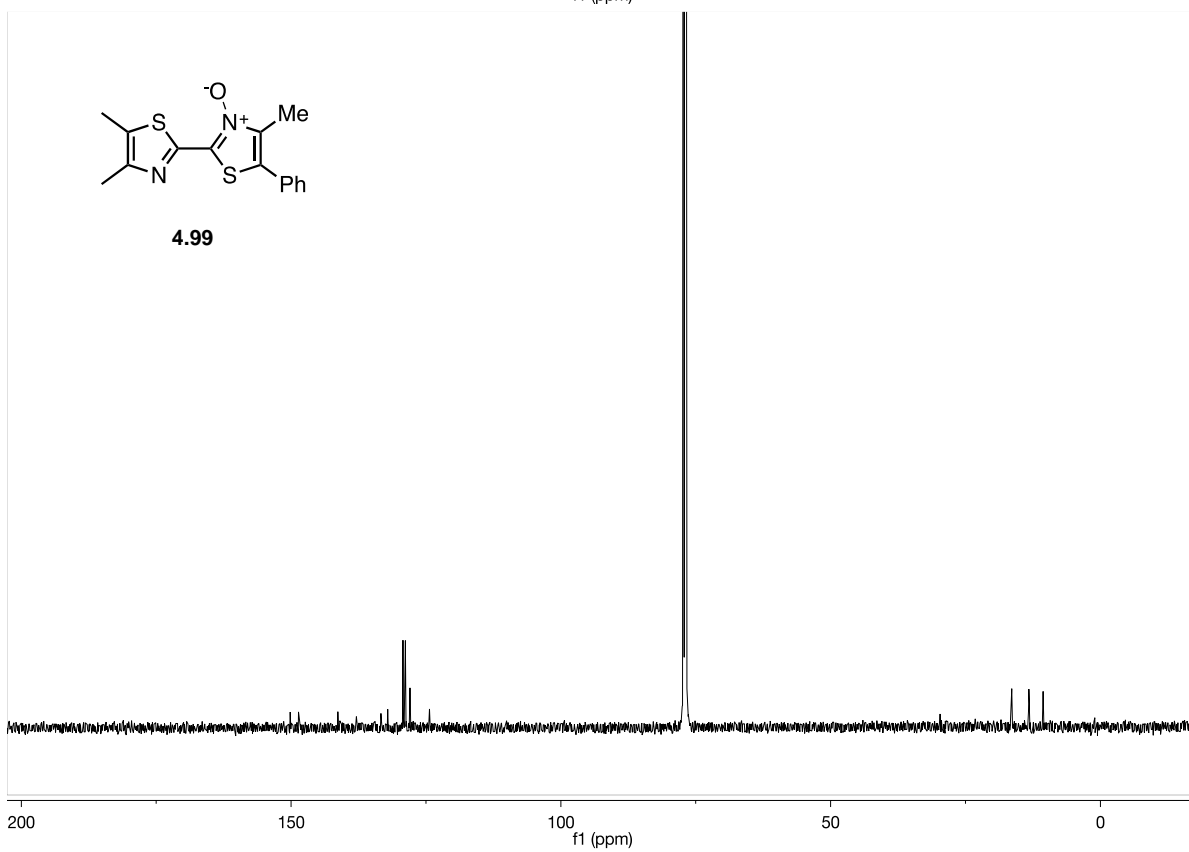
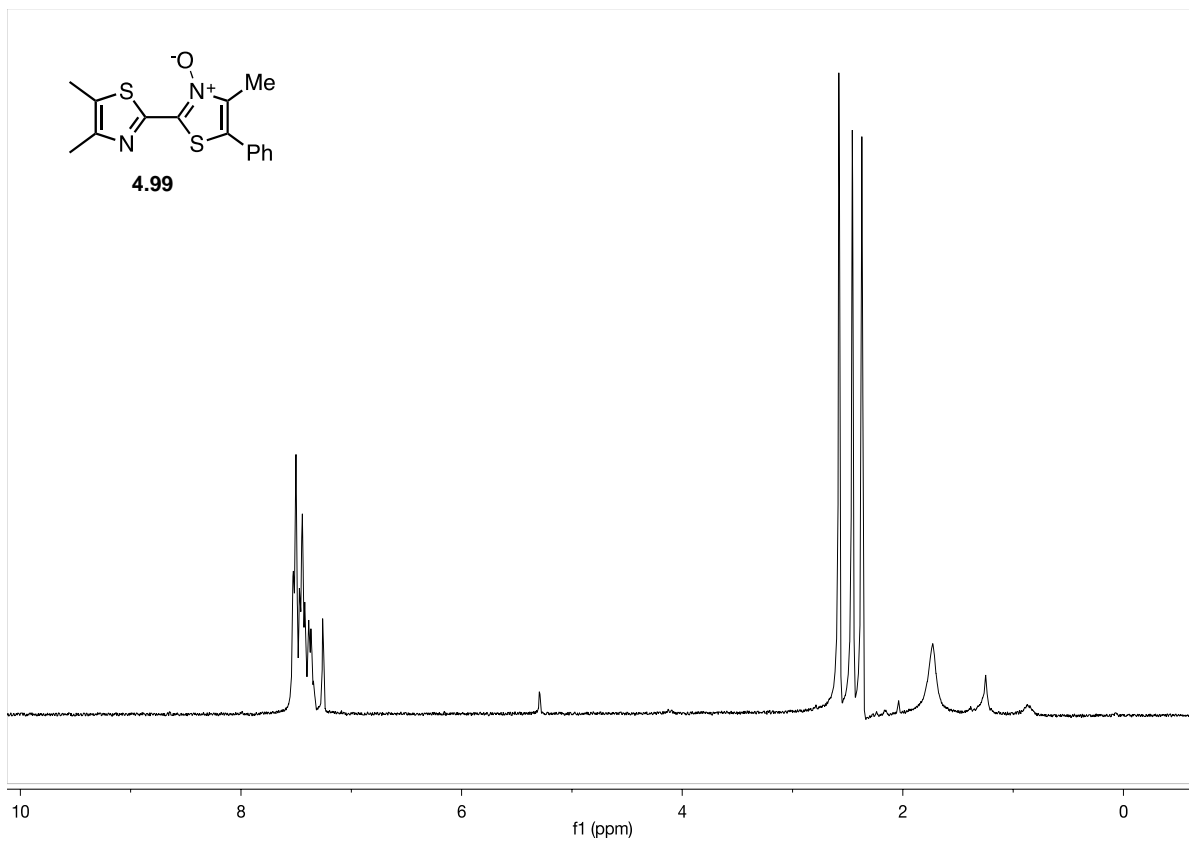


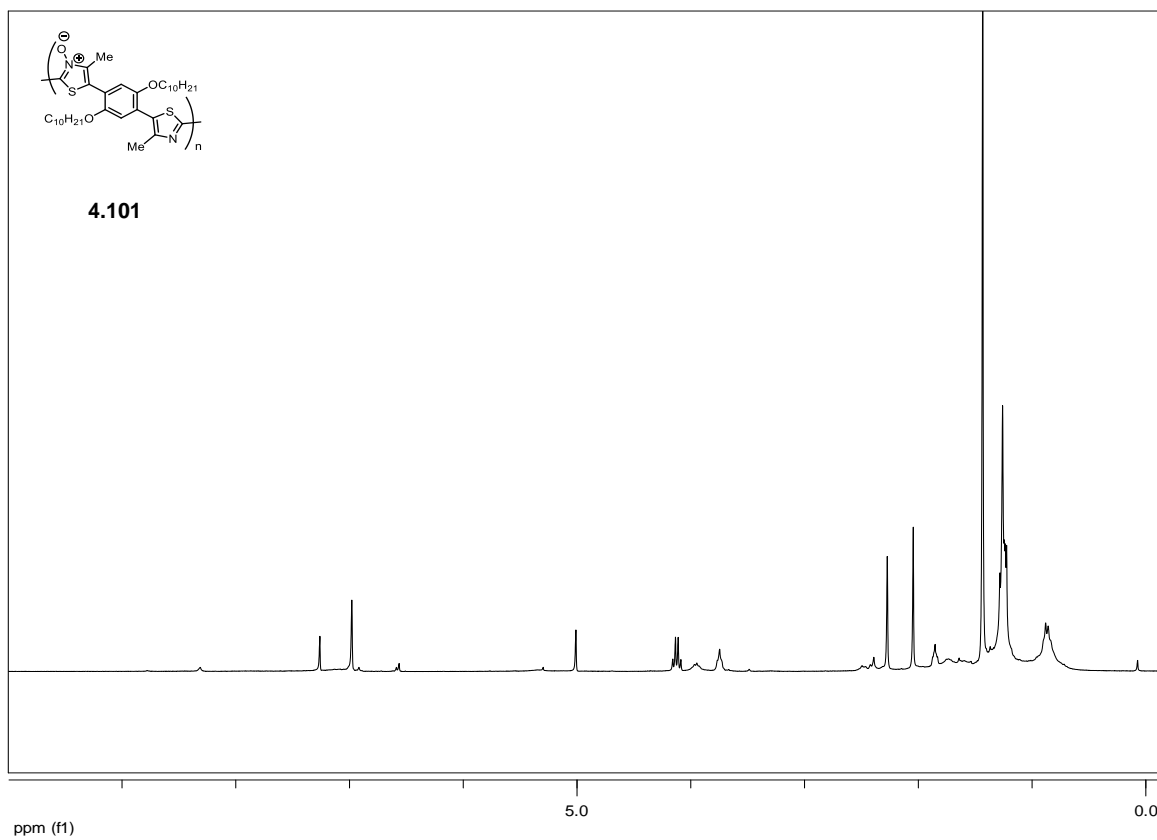
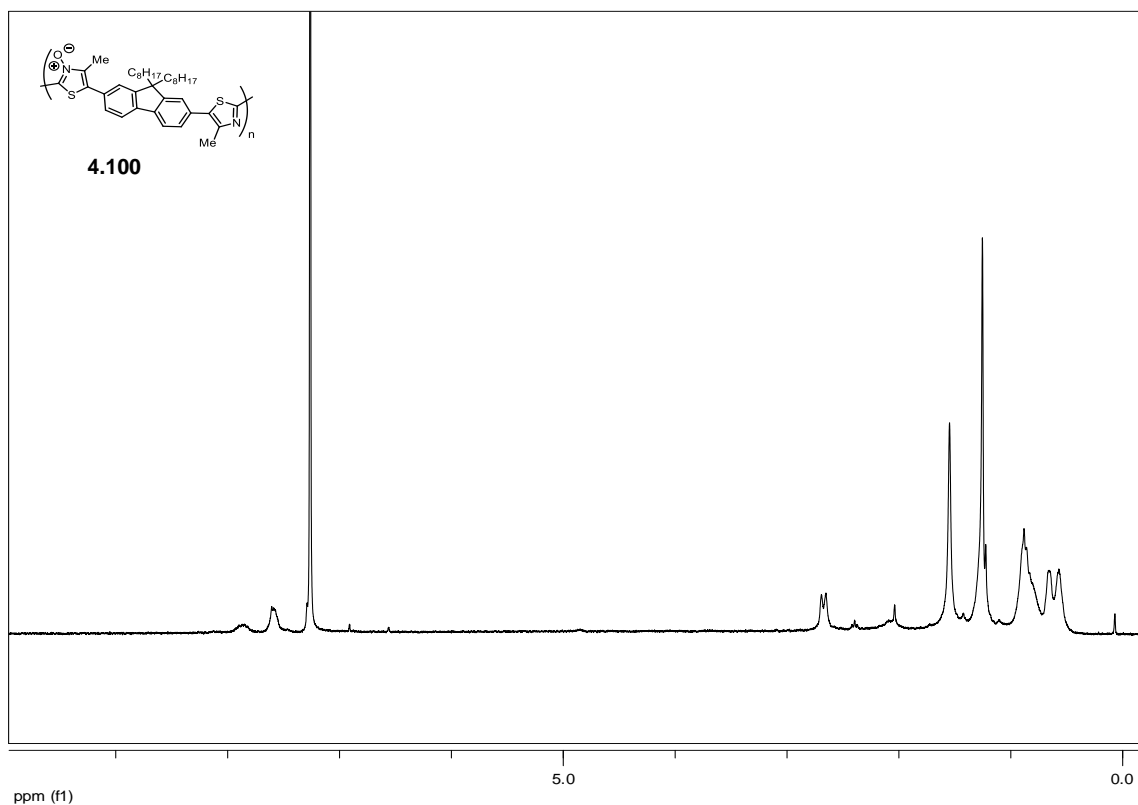


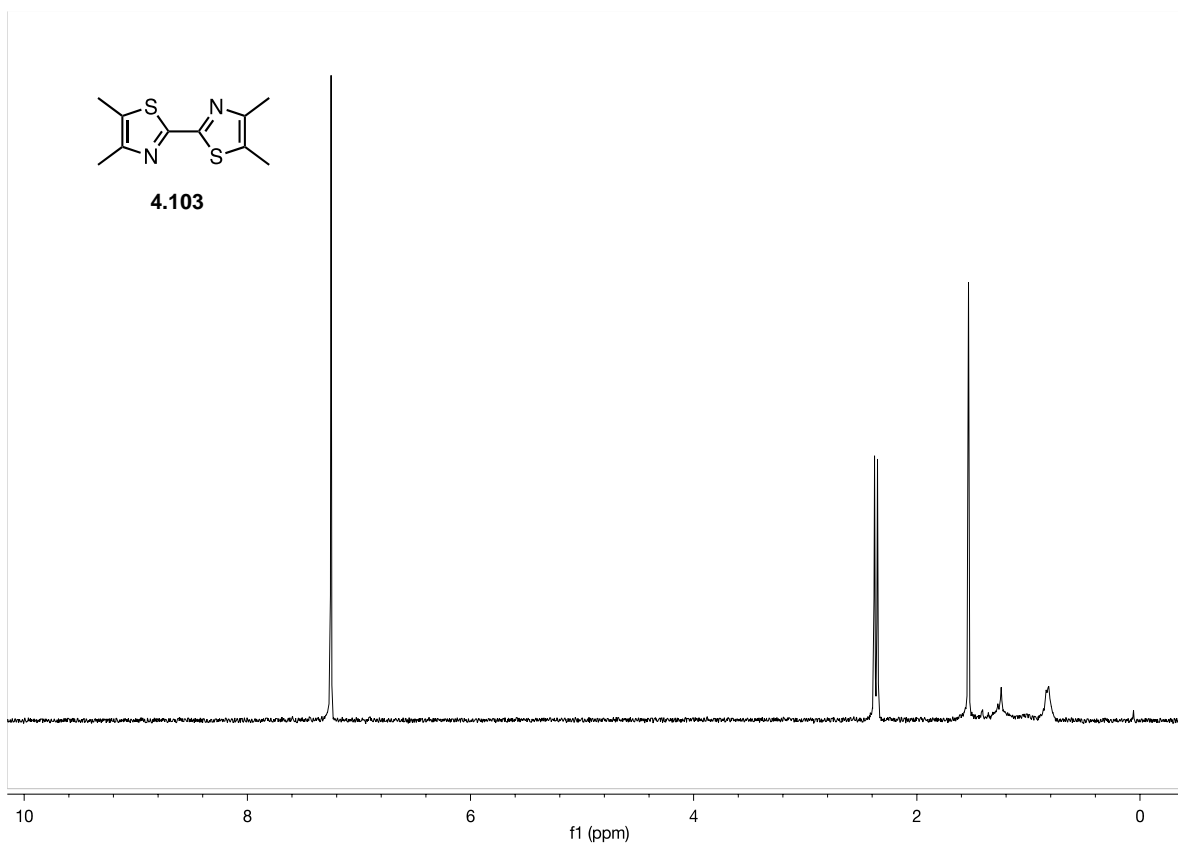
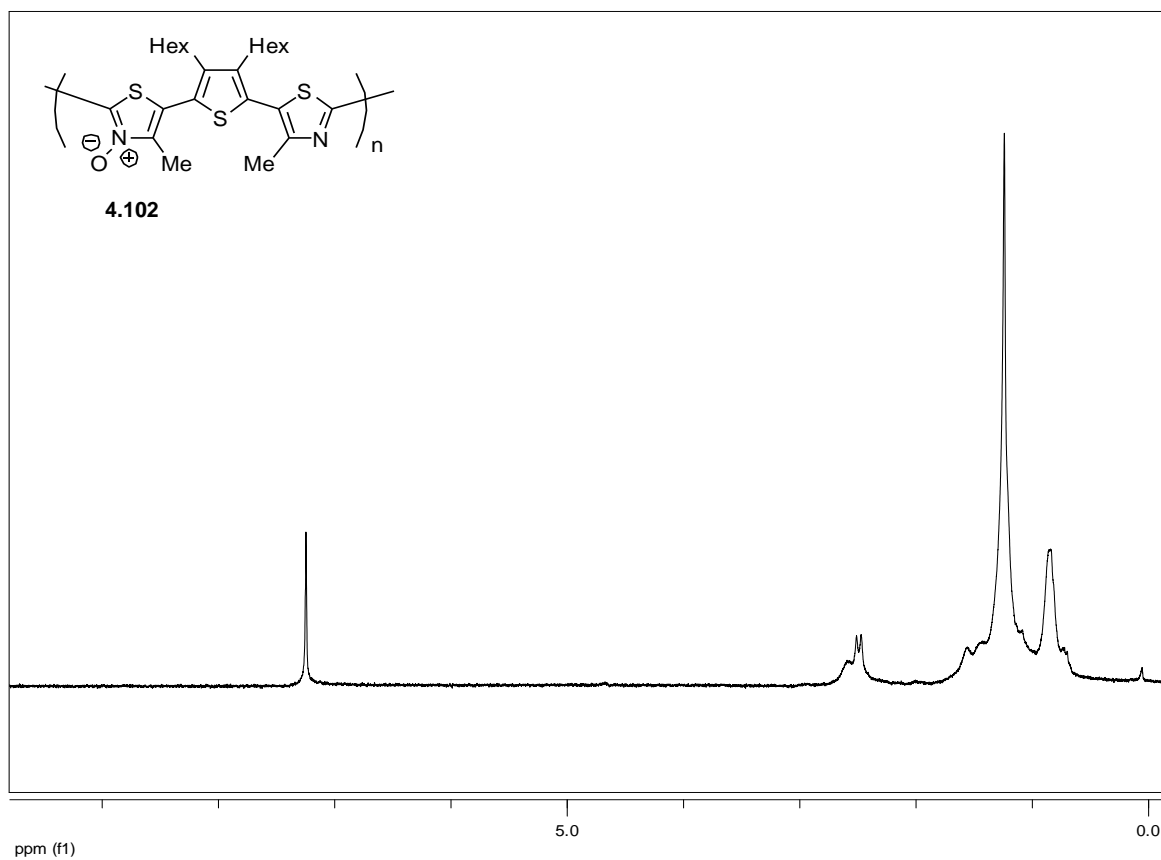


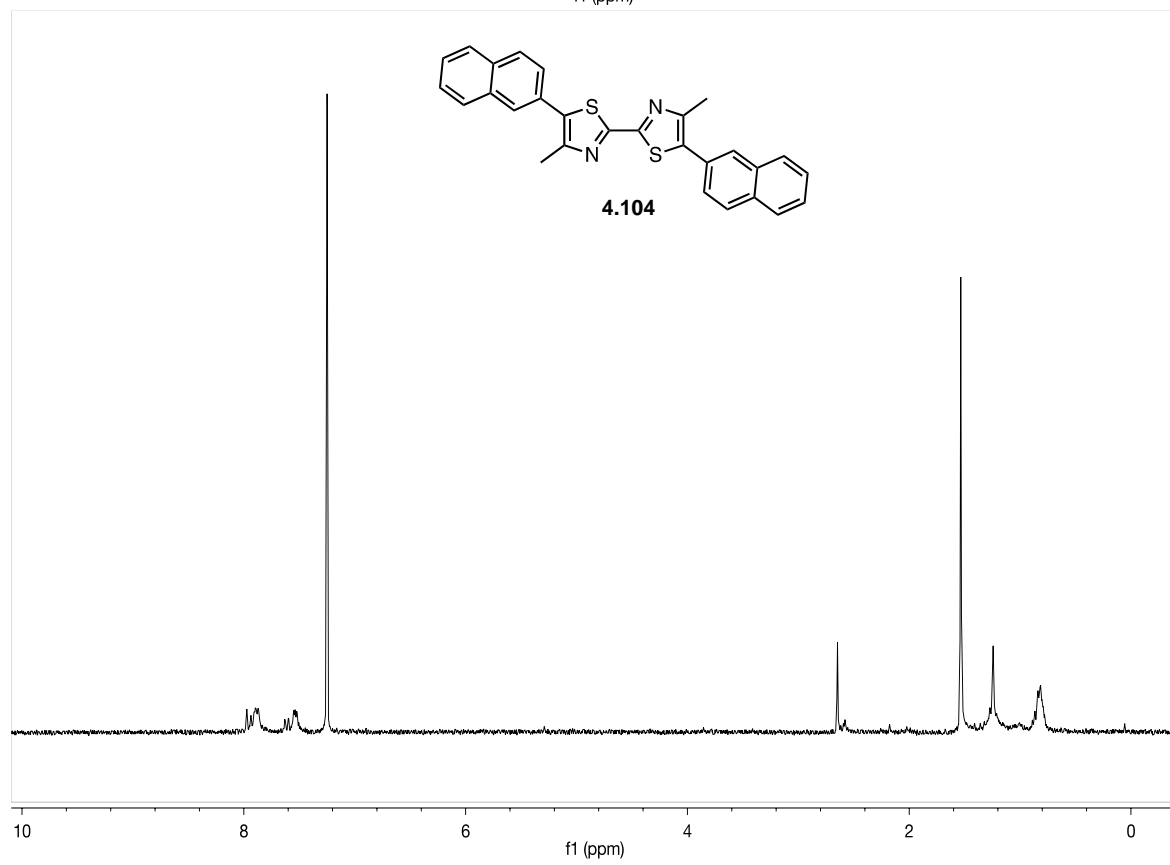
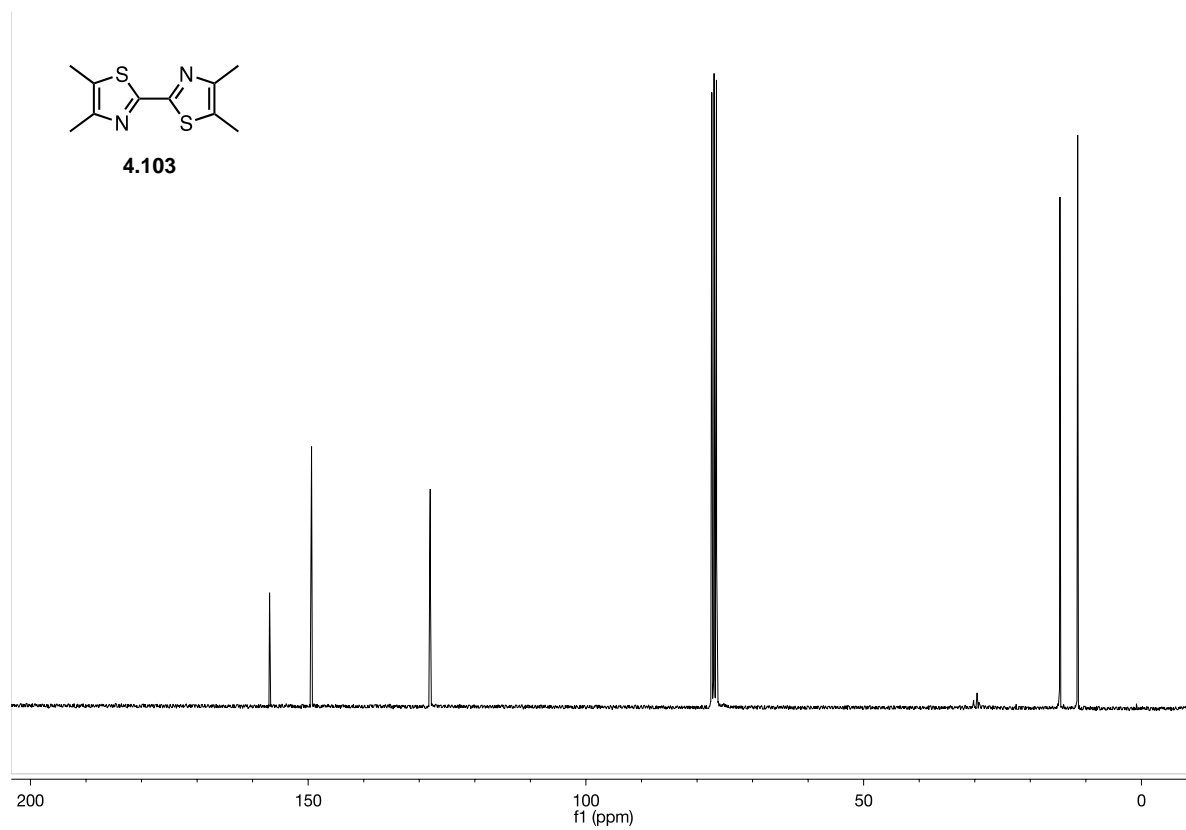


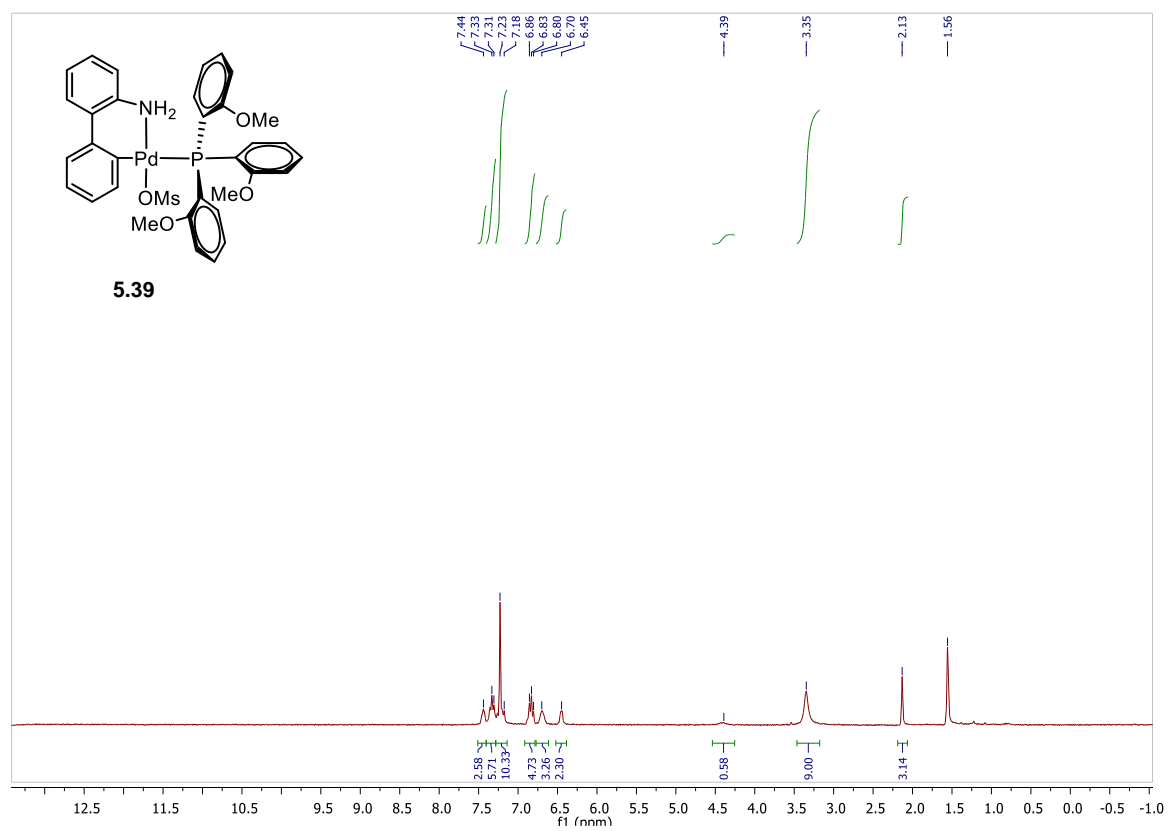
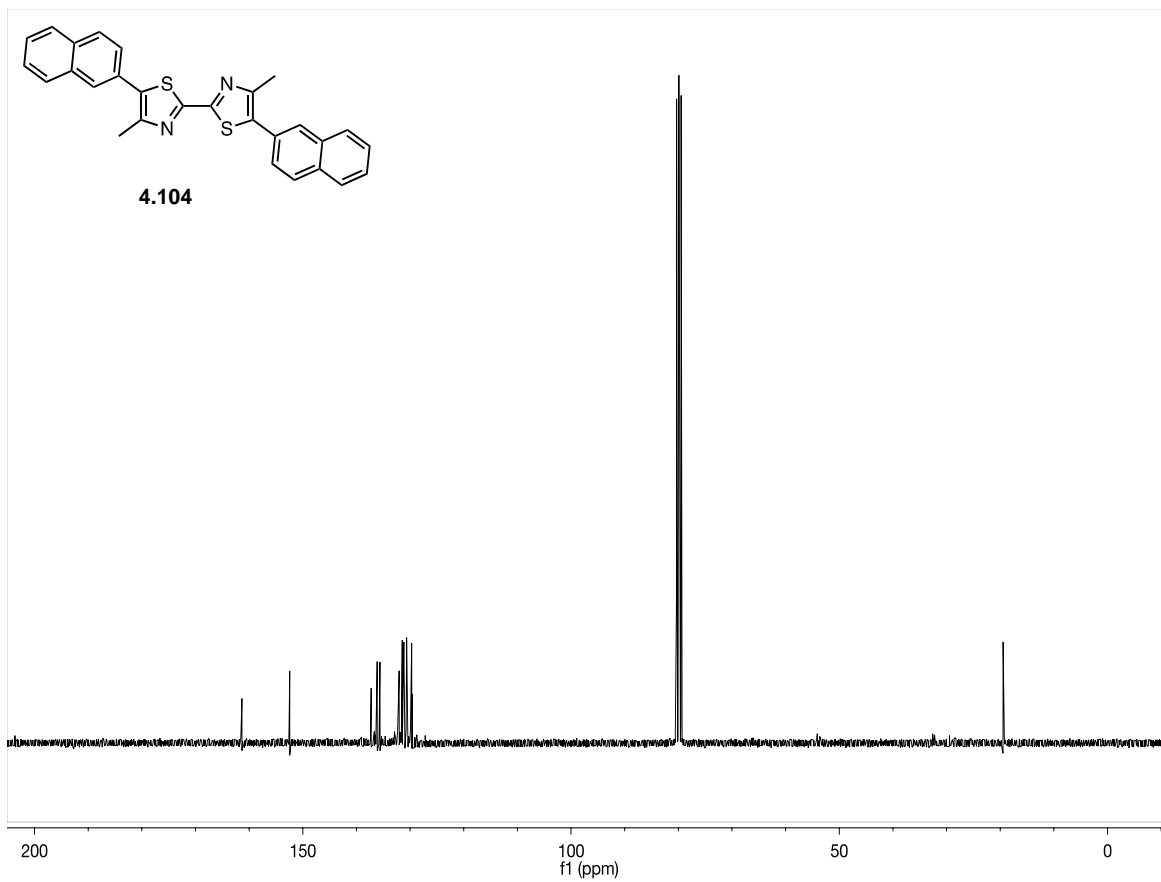


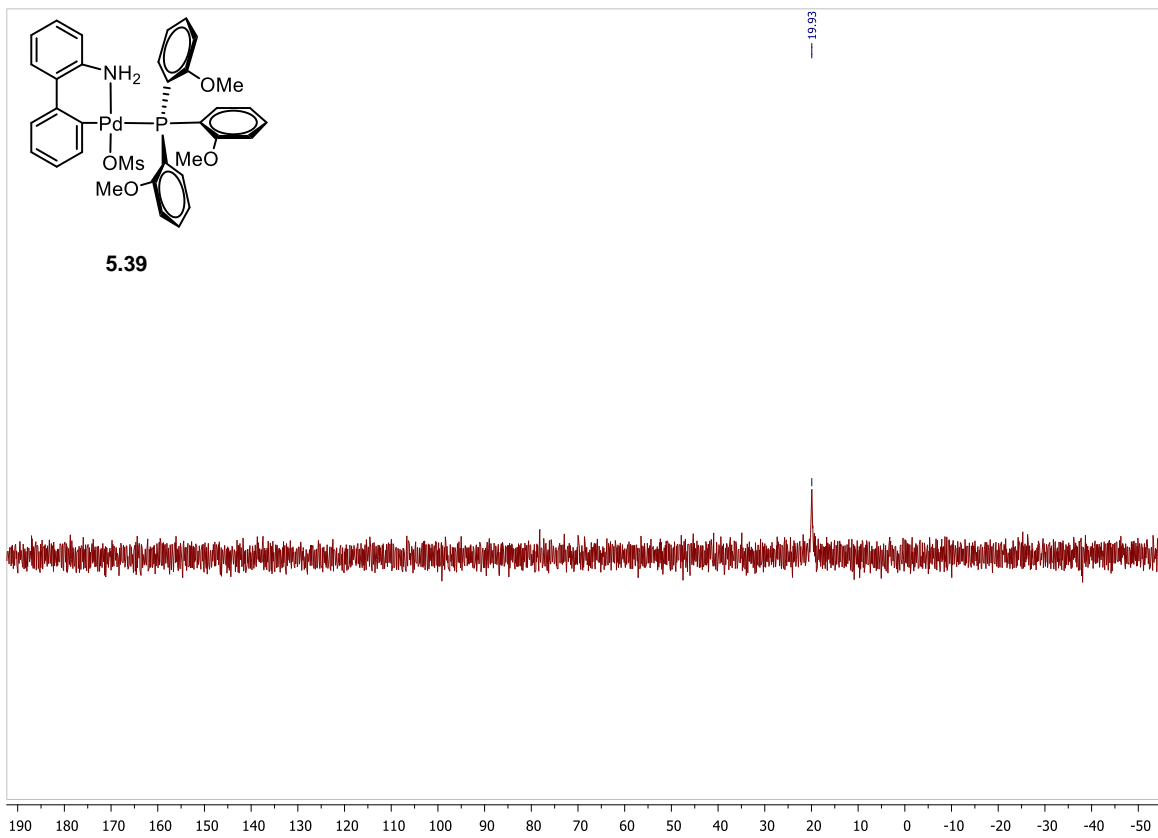
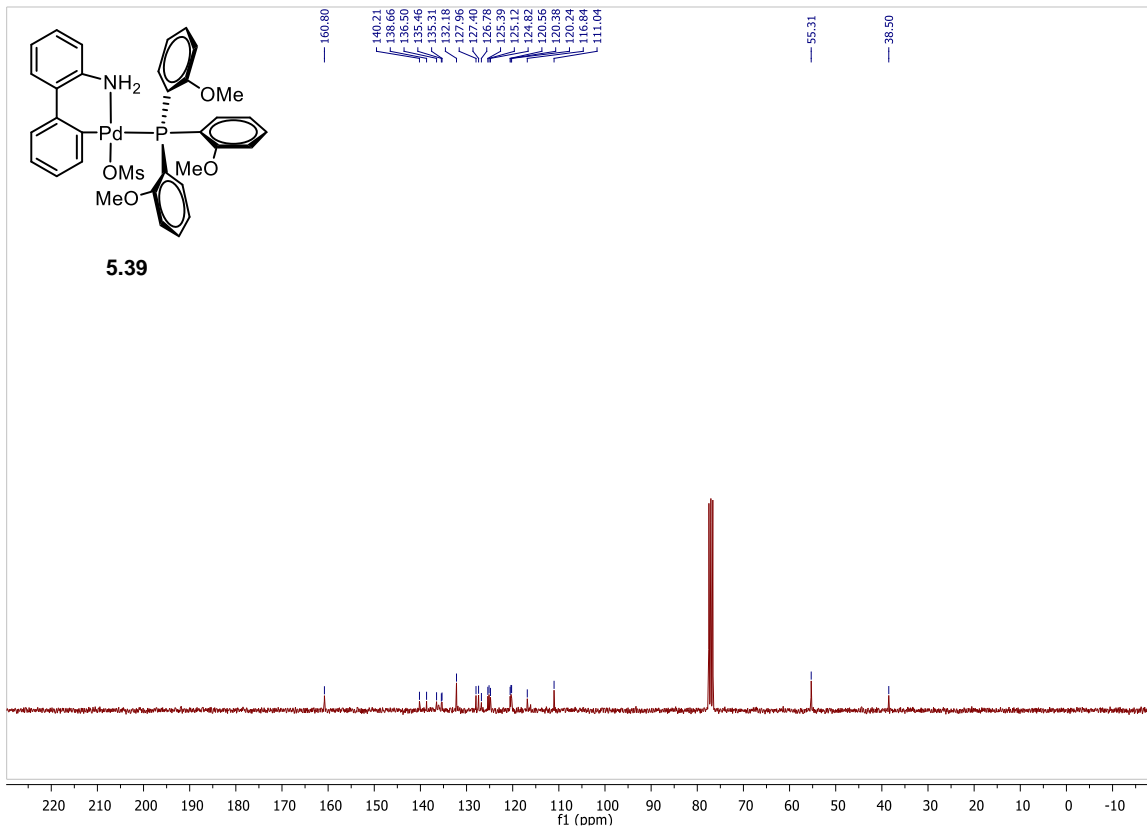


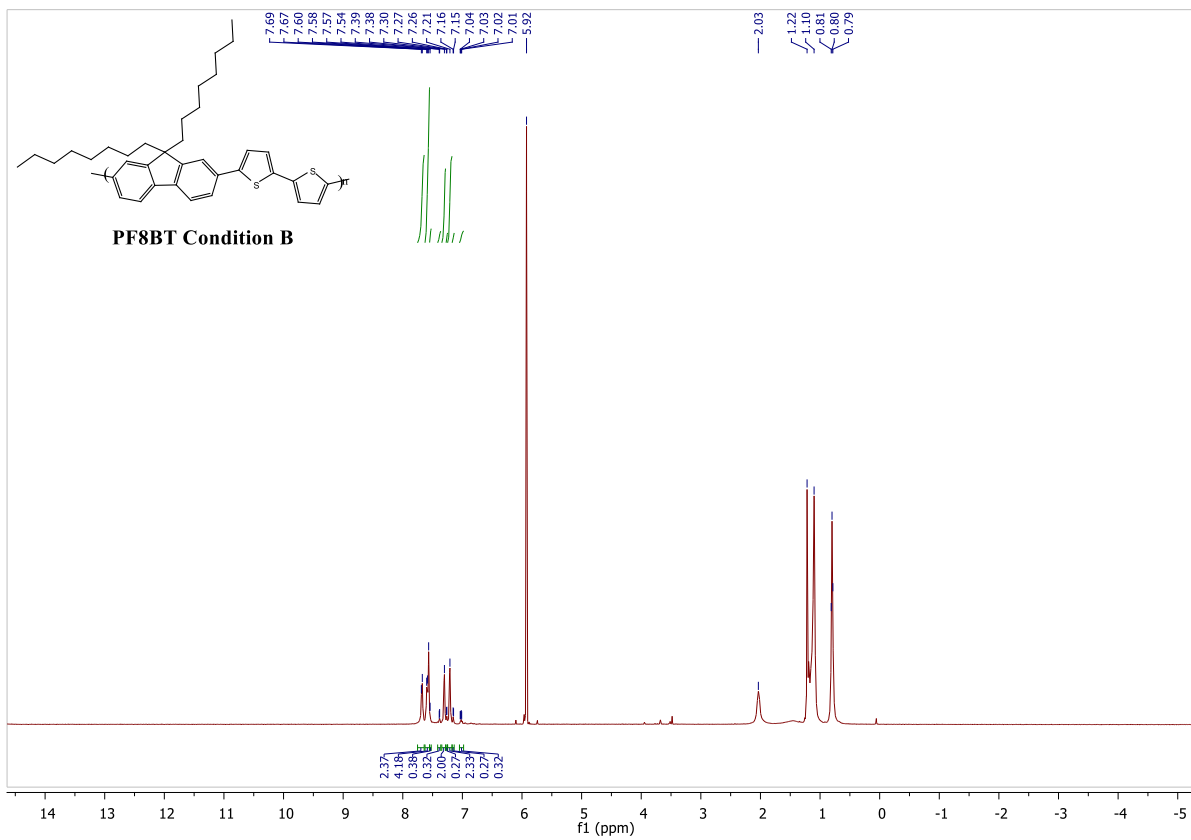
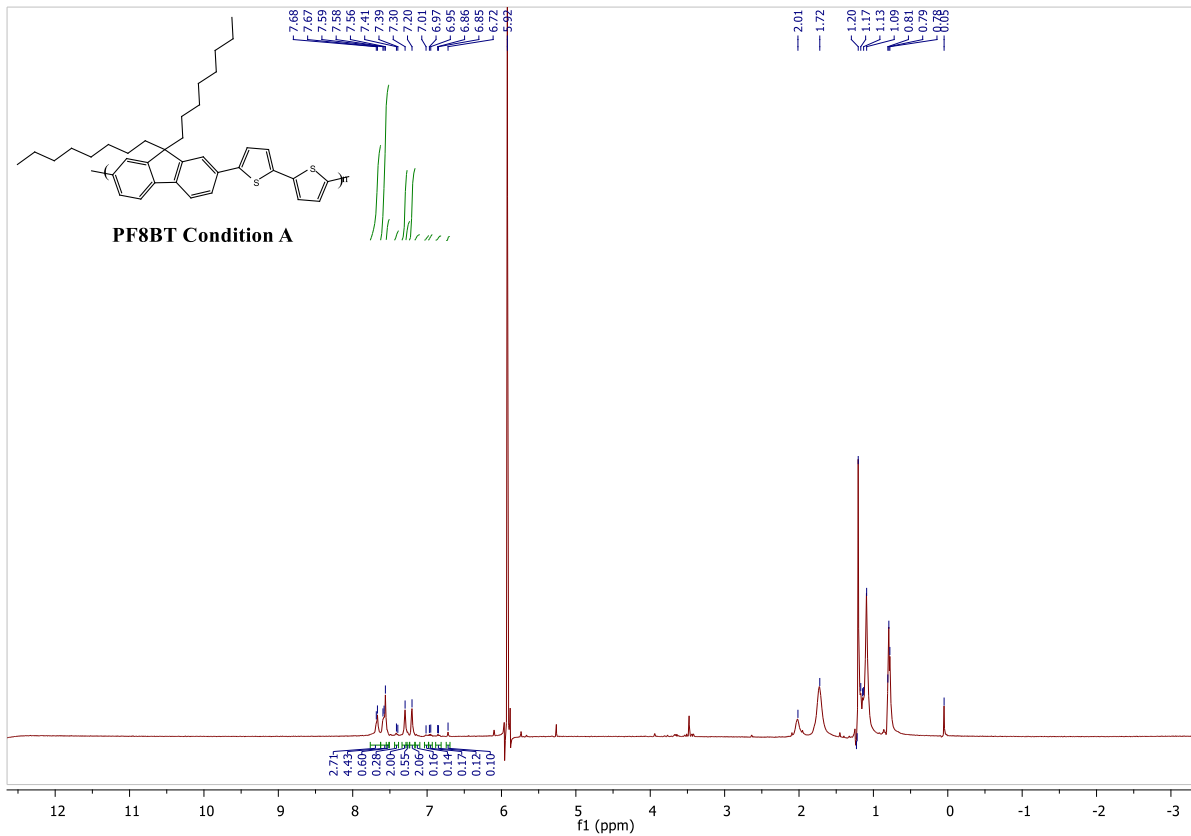


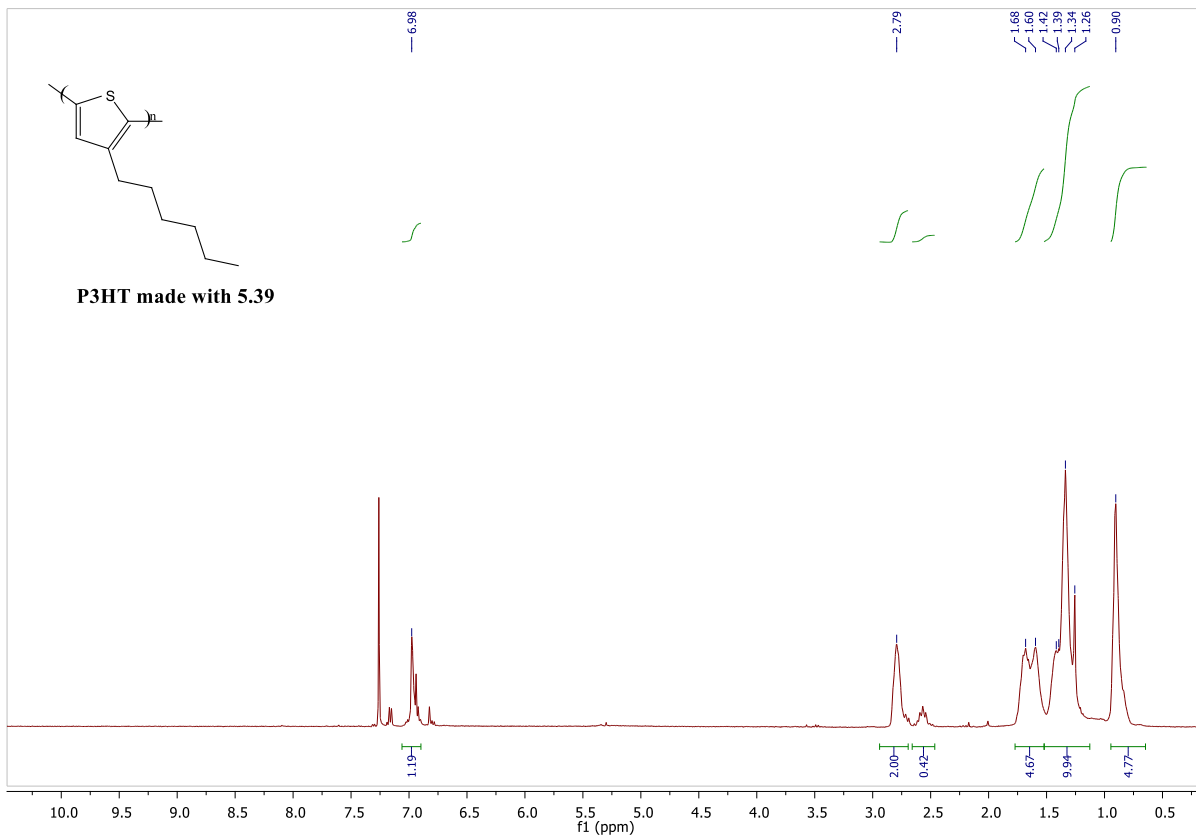
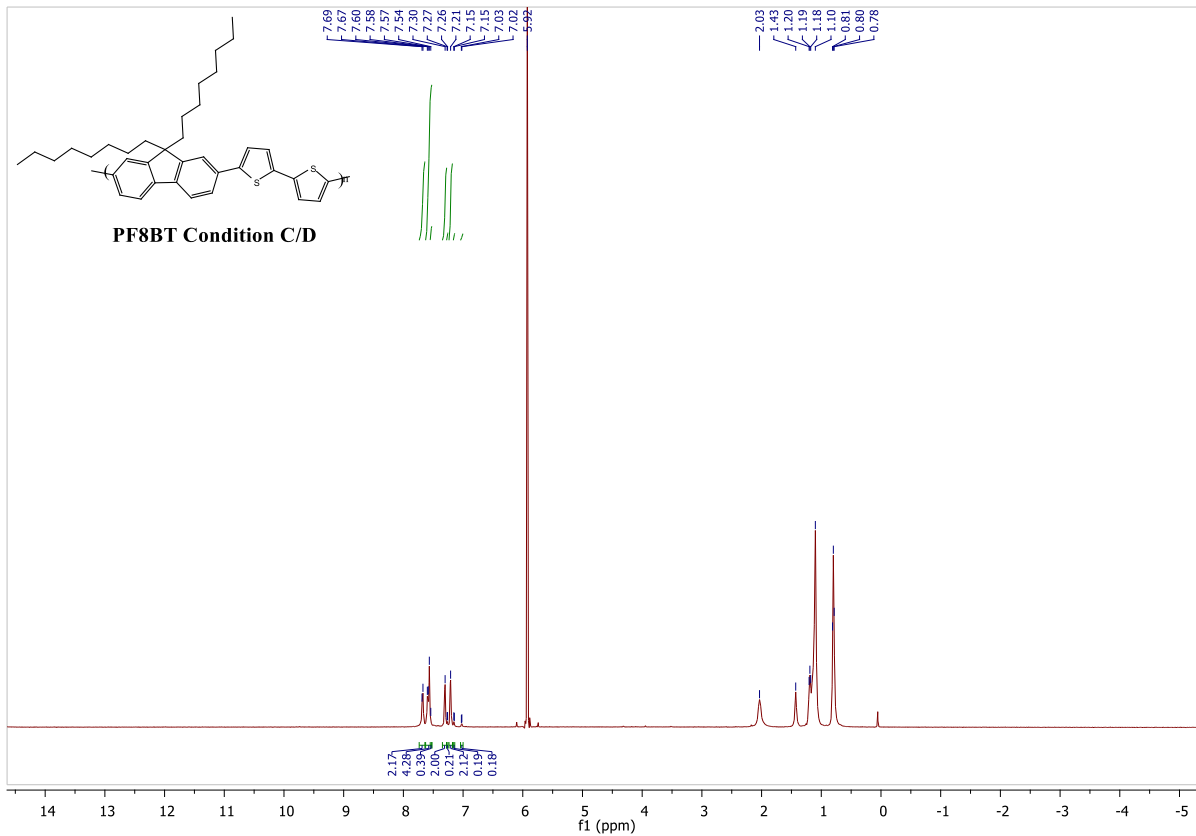


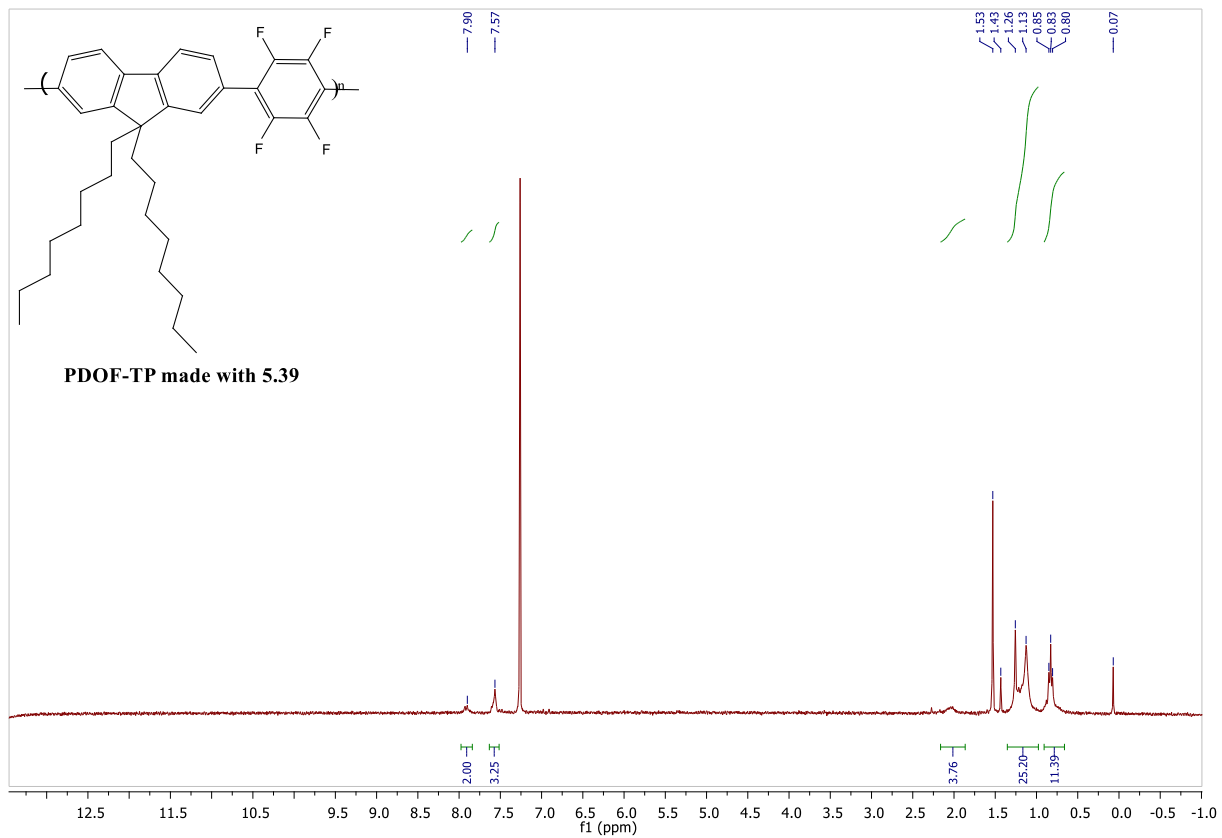












7.0 REFERENCES

- (1) Lijima, S. Helical Microtubules of Graphitic Carbon. *Nature* **1991**, *354*, 56–57.
- (2) Baughman, R. H.; Zakhidov, A. A.; De Heer, W. A. Carbon Nanotubes - The Route toward Applications. *Science* **2002**, *297*, 787–792.
- (3) De Volder, M. F. L.; Tawfick, S. H.; Baughman, R. H.; Hart, A. J. Carbon Nanotubes: Present and Future Commercial Applications. *Science* **2013**, *339*, 535–539.
- (4) Martins-Júnior, P. A.; Alcântara, C. E.; Resende, R. R.; Ferreira, A. J. Carbon Nanotubes: Directions and Perspectives in Oral Regenerative Medicine. *J. Dent. Res.* **2013**, *92*, 575–583.
- (5) Wang, M. S.; Wang, J. Y.; Peng, L. M. Engineering the Cap Structure of Individual Carbon Nanotubes and Corresponding Electron Field Emission Characteristics. *Appl. Phys. Lett.* **2006**, *88*, 10–13.
- (6) Gorantla, S.; Börrnert, F.; Bachmatiuk, A.; Dimitrakopoulou, M.; Schönfelder, R.; Schäffel, F.; Thomas, J.; Gemming, T.; Borowiak-Palen, E.; Warner, J. H.; Jakobson, B. I.; Eckert, J.; Bücher, B.; Rummeli, M. In Situ Observations of Fullerene Fusion and Ejection in Carbon Nanotubes. *Nanoscale* **2010**, *2*, 2077–2079.
- (7) Qin, L. C. Determination of the Chiral Indices (n,m) of Carbon Nanotubes by Electron Diffraction. *Phys. Chem. Chem. Phys.* **2007**, *9*, 31–48.
- (8) Park, J. Y. Band Structure and Electron Transport of One-Dimensional SWNTs. In *Carbon Nanotube Electronics*; 2009; pp 1–42.
- (9) Wallace, P. R. The Band Theory of Graphite. *Phys. Rev.* **1947**, *71*, 622–634.
- (10) Wei, B. Q.; Vajtai, R.; Ajayan, P. M. Reliability and Current Carrying Capacity of Carbon Nanotubes. *Appl. Phys. Lett.* **2001**, *79*, 1172–1174.
- (11) Peng, B. E. I.; Locascio, M.; Zapol, P.; Li, S.; Mielke, S. L.; Schatz, G. C.; Espinosa, H. D. Measurements of Near-Ultimate Strength for Multiwalled Carbon Nanotubes and Irradiation-Induced Crosslinking Improvements. *Nat. Nanotechnol.* **2008**, *3*, 626–631.
- (12) Gao, G.; Cagin, T.; Goddard III, W. A. Energetics, Structure, Mechanical and Vibrational Properties of Single-Walled Carbon Nanotubes. *Nanotechnology* **1998**, *9*, 184–191.
- (13) Wong, E. W.; Sheehan, P. E.; Lieber, C. M. Nanobeam Mechanics: Elasticity, Strength, and Toughness of Nanorods and Nanotubes. *Science* **1997**, *277*, 1971–1976.
- (14) Am, J. A. X. B.; Liang, W.; Bockrath, M.; Bozovic, D.; Hafner, J. H. Fabry-Perot Interference in a Nanotube Electron Waveguide. *Nature* **2001**, *411*, 665–669.
- (15) Frank, S.; Poncharal, P.; Wang, Z. L.; Heer, W. A. De. Carbon Nanotube Quantum Resistors. *Science* **1998**, *280*, 1744–1746.
- (16) Kim, P.; Shi, L.; Majumdar, A.; Mceuen, P. L. Thermal Transport Measurements of Individual Multiwalled Nanotubes. *Phys. Rev. Lett.* **2001**, *87*, 215502.
- (17) Tang, Z. K.; Zhang, L.; Wang, N.; Zhang, X. X.; Wen, G. H.; Li, G. D.; Wang, J. N.; Chan, C. T.; Sheng, P. Superconductivity in 4 Angstrom Single-Walled Carbon Nanotubes. **2001**, *292*, 2462–2466.
- (18) Kumar, S.; Thomas, B.; Ranjan, V. A Comprehensive Review on CNTs and CNT-Reinforced Composites: Syntheses, Characteristics and Applications. *Mater. Today Commun.* **2020**, *25*, 101546.

- (19) Beigbeder, A.; Degee, P.; Conlan, S. L.; Mutton, R. J.; Clare, A. S.; Pettitt, M. E.; Callow, M. E.; Callow, J. A.; Dubois, P. Preparation and Characterisation of Silicone-Based Coatings Filled with Carbon Nanotubes and Natural Sepiolite and Their Application as Marine Fouling- Release Coatings. *Biofouling* **2008**, *24*, 291–302.
- (20) Wu, Z.; Chen, Z.; Du, X.; Logan, J. M.; Sippel, J.; Nikolou, M.; Kamaras, K.; Reynolds, J. R.; Tanner, D. B.; Hebard, A. F.; et al. Transparent, Conductive Carbon Nanotube Films. *Science* **2004**, *305*, 1273–1277.
- (21) Hills, G.; Lau, C.; Wright, A.; Fuller, S.; Bishop, M. D.; Srimani, T.; Kanhaiya, P. Modern Microprocessor Built from Complementary Carbon Nanotube Transistors. *Nature* **2019**, *572*, 595–602.
- (22) Shulaker, M. M.; Hills, G.; Patil, N.; Wei, H.; Chen, H.; Wong, H. P.; Mitra, S. Carbon Nanotube Computer. *Nature* **2013**, *501*, 526–535.
- (23) Aval, L. F.; Ghoranneviss, M.; Pour, G. B. High-Performance Supercapacitors Based on the Carbon Nanotubes , Graphene and Graphite Nanoparticles Electrodes. *Heliyon* **2018**, *4*, e00862.
- (24) Le Goff, A.; Artero, V.; Jusselme, B.; Tran, P. D.; Guillet, N.; Métayé, R.; Fihri, A.; Palacin, S.; Fontecave, M. From Hydrogenases to Noble Metal-Free Catalytic Nanomaterials for H₂ Production and Uptake. *Science* **2009**, *326*, 1384–1388.
- (25) Tilmaci, C.; Morris, M. C. Carbon Nanotube Biosensors. *Front. Chem.* **2015**, *3*, 1–21.
- (26) Chen, Y.; Shaw, David, T.; Bai, X. D.; Wang, E. G.; Lund, C.; Lu, W. M.; Chung, D. D. L. Hydrogen Storage in Aligned Carbon Nanotubes. *Appl. Phys. Lett.* **2001**, *78*, 2128–2130.
- (27) Schroeder, V.; Savagatrup, S.; He, M.; Lin, S.; Swager, T. M. Carbon Nanotube Chemical Sensors. *Chem. Rev.* **2019**, *119*, 599–663.
- (28) Paolini, M.; Cantelli-Forti, G.; Perocco, P.; Pedulli, G. F.; Abdel-Rahman, S. Z.; Legator, M. S. Growth of Nanotubes for Probe Microscopy Tips. *Nature* **1999**, *398*, 761–762.
- (29) Mubarak, N. M.; Abdullah, E. C.; Jayakumar, N. S.; Sahu, J. N. An Overview on Methods for the Production of Carbon Nanotubes. *J. Ind. Eng. Chem.* **2014**, *20*, 1186–1197.
- (30) Ebbesen, T. W. Production and Purification of Carbon Nanotubes. In *Carbon nanotubes: Preparation and properties*; 1997; pp 139–162.
- (31) Ebbesen, T. W.; Ajayan, P. M. Large-Scale Synthesis of Carbon Nanotubes. *Nature* **1992**, *358*, 220–222.
- (32) Journet, C.; Maser, W. K.; Bernier, P.; Loiseau, A.; Lamy de la Chapelle, M.; Lefrant, S.; Deniard, P.; Lee, R.; Fischer, J. E. Large-Scale Production of Single-Walled Carbon Nanotubes by the Electric-Arc Technique. *Nature* **1997**, *388*, 756–758.
- (33) Hatta, N.; Murata, K. Very Long Graphitic Nano-Tubules Synthesized by Plasma-Decomposition of Benzene. *Chem. Phys. Lett.* **1994**, *217*, 398–402.
- (34) Jong, S.; Koo, H.; Yoo, J.; Hoon, J. Large Scale Synthesis of Carbon Nanotubes by Plasma Rotating Arc Discharge Technique. *Diam. Relat. Mater.* **2002**, *11*, 914–917.
- (35) Guo, T.; Nikolaev, P.; Thess, A.; Colbert, D. T.; Smalley, R. E. Catalytic Growth of Single-Walled Nanotubes by Laser Vaporization. *Chem. Phys. Lett.* **1995**, *243*, 49–54.
- (36) Bandow, S.; Asaka, S.; Saito, Y.; Rao, A. M.; Grigorian, L.; Richter, E.; Eklund, P. C. Effect of the Growth Temperature on the Diameter Distribution and Chirality of Single-Wall Carbon Nanotube. *Phys. Rev. Lett.* **1998**, *80*, 3779–3782.

- (37) Thess, A.; Lee, R.; Nikolaev, P.; Dai, H.; Petit, P.; Robert, J.; Xu, C.; Lee, Y. H.; Kim, S. G.; Rinzler, A. G.; et al. Crystalline Ropes of Metallic Carbon Nanotubes. *Science* **1996**, *273*, 483–487.
- (38) Naumov, A. V.; Kuznetsov, O. A.; Harutyunyan, A. R.; Green, A. A.; Hersam, M. C.; Resasco, D. E.; Nikolaev, P. N.; Weisman, R. B. Quantifying the Semiconducting Fraction in Single-Walled Carbon Nanotube Samples through Comparative Atomic Force and Photoluminescence Microscopies. *Nano Lett.* **2009**, *9*, 3203–3208.
- (39) Shah, K. A.; Tali, B. A. Synthesis of Carbon Nanotubes by Catalytic Chemical Vapour Deposition: A Review on Carbon Sources, Catalysts and Substrates. *Mater. Sci. Semicond. Process.* **2016**, *41*, 67–82.
- (40) Hayashi, T.; Kim, Y. A.; Matoba, T.; Esaka, M.; Nishimura, K.; Tsukada, T.; Endo, M.; Dresselhaus, M. S. Smallest Freestanding Single-Walled Carbon Nanotube. *Nano Lett.* **2003**, *3*, 887–889.
- (41) Bachilo, S. M.; Balzano, L.; Herrera, J. E.; Pompeo, F.; Resasco, D. E.; Weisman, R. B. Narrow (n,m)-Distribution of Single-Walled Carbon Nanotubes Grown Using a Solid Supported Catalyst. *J. Am. Chem. Soc.* **2003**, *125*, 11186–11187.
- (42) Qu, L.; Du, F.; Dai, L. Preferential Syntheses of Semiconducting Vertically Aligned Single-Walled Carbon Nanotubes for Direct Use in FETs. *Nano Lett.* **2008**, *8*, 2682–2687.
- (43) Bronikowski, M. J.; Willis, P. A.; Colbert, D. T.; Smith, K. A.; Smalley, R. E. Gas-Phase Production of Carbon Single-Walled Nanotubes from Carbon Monoxide via the HiPco Process: A Parametric Study. *J. Vac. Sci. Technol. A Vacuum, Surfaces, Film.* **2001**, *19*, 1800–1805.
- (44) A Carbon nanotube page <http://www.personal.reading.ac.uk/~scsharip/tubes.htm>.
- (45) Shelimov, K. B.; Esenaliev, R. O.; Rinzler, A. G.; Huffman, C. B.; Smalley, R. E. Purification of Single-Wall Carbon Nanotubes by Ultrasonically Assisted Filtration. *Chem. Phys. Lett.* **1998**, *282*, 429–434..
- (46) Sato, Y.; Ogawa, T.; Motomiya, K.; Shinoda, K.; Jeyadevan, B.; Tohji, K.; Kasuya, A.; Nishina, Y. Purification of MWNTs Combining Wet Grinding, Hydrothermal Treatment, and Oxidation. *J. Phys. Chem. B* **2001**, *105*, 3387–3392.
- (47) Huang, W.; Wang, Y.; Luo, G.; Wei, F. 99.9% Purity Multi-Walled Carbon Nanotubes By Vacuum High-Temperature Annealing. *Carbon* **2003**, *41*, 2585–2590.
- (48) Das, R. *Nanohybrid Catalyst Based on Carbon Nanotube: Carbon Nanotube Purification*; 2017.
- (49) Tunnell, A.; Ballarotto, V.; Cumings, J. The Selective Removal of Metallic Carbon Nanotubes from As-Grown Arrays on Insulating Substrates. *Appl. Phys. Lett.* **2012**, *101*, 193109.
- (50) Tu, X.; Manohar, S.; Jagota, A.; Zheng, M. DNA Sequence Motifs for Structure-Specific Recognition and Separation of Carbon Nanotubes. *Nature* **2009**, *460*, 250–253.
- (51) Zheng, M. Sorting Carbon Nanotubes. *Top. Curr. Chem.* **2017**, *375*, 1–36.
- (52) Selmani, S.; Schipper, D. J. Orientation Control of Molecularly Functionalized Surfaces Applied to the Simultaneous Alignment and Sorting of Carbon Nanotubes. *Angew. Chem. Int. Ed.* **2018**, *57*, 2399–2403.
- (53) Brady, G. J.; Way, A. J.; Safron, N. S.; Evensen, H. T.; Gopalan, P.; Arnold, M. S. Quasi-Ballistic Carbon Nanotube Array Transistors with Current Density Exceeding Si and GaAs. *Sci. Adv.* **2016**, *2*, e1601240.
- (54) Avouris, P.; Chen, Z.; Perebeinos, V. Carbon-Based Electronics. *Nat. Nanotechnol.* **2007**, *2*, 605–615.
- (55) Goh, G. L.; Agarwala, S.; Yeong, W. Y. Directed and On-Demand Alignment of Carbon Nanotube: A Review toward 3D Printing of Electronics. *Adv. Mater. Interfaces* **2019**, *6*, 1801318.

- (56) Tulevski, G. S.; Franklin, A. D.; Afzali, A. High Purity Isolation and Quantification of Semiconducting Carbon Nanotubes via Column Chromatography. *ACS Nano* **2013**, *7*, 2971–2976.
- (57) Smalley, R. E.; Li, Y.; Moore, V. C.; Price, B. K.; Colorado, R.; Schmidt, H. K.; Hauge, R. H.; Barron, A. R.; Tour, J. M. Single Wall Carbon Nanotube Amplification : En Route to a Type-Specific Growth Mechanism. *J. Am. Chem. Soc.* **2006**, *128*, 15824–15829.
- (58) Yao, Y.; Feng, C.; Zhang, J.; Liu, Z. Cloning of Single-Walled Carbon Nanotubes via Open-End Growth Mechanism. *Nano Lett.* **2009**, *9*, 1673–1677.
- (59) Yu, X.; Zhang, J.; Choi, W.; Choi, J. Y.; Kim, J. M.; Gan, L.; Liu, Z. Cap Formation Engineering: From Opened C₆₀ to Single-Walled Carbon Nanotubes. *Nano Lett.* **2010**, *10*, 3343–3349.
- (60) Kroto, H. W.; Heath, J. R.; O'Brien, S. C.; Curl, R. F.; Smalley, R. E. C₆₀: Buckminsterfullerene. *Nature* **1985**, *318*, 162–163.
- (61) Scott, L. T.; Jackson, E. A.; Zhang, Q.; Steinberg, B. D.; Bancu, M.; Li, B. A Short, Rigid, Structurally Pure Carbon Nanotube by Stepwise Chemical Synthesis. *J. Am. Chem. Soc.* **2012**, *134*, 107–110.
- (62) Li, H. B.; Page, A. J.; Irlle, S.; Morokuma, K. Single-Walled Carbon Nanotube Growth from Chiral Carbon Nanorings: Prediction of Chirality and Diameter Influence on Growth Rates. *J. Am. Chem. Soc.* **2012**, *134*, 15887–15896.
- (63) Naha, S.; Puri, I. K. A Model for Catalytic Growth of Carbon Nanotubes. *J. Phys. D: Appl. Phys.* **2008**, *41*, 065304.
- (64) Azam, M. A.; Manaf, N. S. A.; Talib, E.; Bistamam, M. S. A. Aligned Carbon Nanotube from Catalytic Chemical Vapor Deposition Technique for Energy Storage Device: A Review. *Ionics (Kiel)*. **2013**, *19*, 1455–1476.
- (65) Strunk, K.-P.; Abdulkarim, A.; Beck, S.; Marzalek, T.; Bernhardt, J.; Koser, S.; Pisula, W.; Jansch, D.; Freudenberg, J.; Pucci, A.; Bunz, U. H. F.; Melzer, C.; Müllen, K. Pristine Poly(paraphenylene): Relating Semiconducting Behavior to Kinetics of Precursor Conversion. *ACS Appl. Mater. Interfaces* **2019**, *11*, 19481–19488.
- (66) Abdulkarim, A.; Hinkel, F.; Jansch, D.; Freudenberg, J.; Golling, F. E.; Mullen, K. A New Solution to an Old Problem: Synthesis of Unsubstituted Poly(paraphenylene). *J. Am. Chem. Soc.* **2016**, *138*, 16208–16211.
- (67) Jasti, R.; Bhattacharjee, J.; Neaton, J. B.; Bertozzi, C. R. Synthesis, Characterization and Theory of [9]-, [12]-, and [18]Cycloparaphenylene: Carbon Nanohoop Structures. *J. Am. Chem. Soc.* **2008**, *130*, 17646–17647.
- (68) Lewis, S. E. Cycloparaphenylenes and Related Nanohoops. *Chem. Soc. Rev.* **2015**, *44*, 2221–2304.
- (69) Yamago, S.; Watanabe, Y.; Iwamoto, T. Synthesis of [8]Cycloparaphenylene from a Square-Shaped Tetranuclear Platinum Complex. *Angew. Chem. Int. Ed.* **2010**, *49*, 757–759.
- (70) Omachi, H.; Nakayama, T.; Takahashi, E.; Segawa, Y.; Itami, K. Initiation of Carbon Nanotube Growth by Well-Defined Carbon Nanorings. *Nat. Chem.* **2013**, *5*, 572–576.
- (71) Grein, F. Twist Angles and Rotational Energy Barriers of Biphenyl and Substituted Biphenyls. *J. Phys. Chem. A* **2002**, *106*, 3823–3827.
- (72) Iwamoto, T.; Watanabe, Y.; Sakamoto, Y.; Suzuki, T.; Yamago, S. Selective and Random Syntheses of [n] Cycloparaphenylenes (n = 8-13) and Size Dependence of Their Electronic Properties. *J. Am. Chem. Soc.* **2011**, *133*, 8354–8361.
- (73) Iwamoto, T.; Watanabe, Y.; Sadahiro, T.; Haino, T.; Yamago, S. Size Selective Encapsulation of C₆₀ by

- [10]Cycloparaphenylene: Formation of the Shortest Fullerene-Peapod. *Angew. Chem. Int. Ed.* **2011**, *50*, 8342–8344.
- (74) Liu, Y.; Lin, J.; Bo, Y.; Xie, L.; Yi, M.; Zhang, X.; Zhang, H.; Loh, T.; Huang, W. Synthesis and Crystal Structure of Highly Strained [4]Cyclofluorene: Green-Emitting Fluorophore. *Org. Lett.* **2016**, *18*, 172–175.
- (75) Nishiuchi, T.; Feng, X.; Enkelmann, V.; Wagner, M.; Müllen, K. Three-Dimensionally Arranged Cyclic p - Hexaphenylbenzene : Toward a Bottom-Up Synthesis of Size-Defined Carbon Nanotubes. *Chem. Eur. J.* **2012**, *18*, 16621–16625.
- (76) Xia, J.; Golder, M. R.; Foster, M. E.; Wong, B. M.; Jasti, R. Synthesis, Characterization, and Computational Studies of Cycloparaphenylene Dimers. *J. Am. Chem. Soc.* **2012**, *134*, 19709–19715.
- (77) Tonshoff, C.; Bettinger, H. F. Pushing the Limits of Acene Chemistry : The Recent Surge of Large Acenes. *Chem. - A Eur. J.* **2021**, *27*, 3193–3212.
- (78) Anthony, J. E. Functionalized Acenes and Heteroacenes for Organic Electronics. *Chem. Rev.* **2006**, *106*, 5028–5048.
- (79) Han, Y.; Dong, S.; Shao, J.; Fan, W.; Chi, C. Synthesis of a Sidewall Fragment of a (12,0) Carbon Nanotube. *Angew. Chem. Int. Ed.* **2021**, *60*, 2658–2662.
- (80) Cheung, K. Y.; Watanabe, K.; Segawa, Y.; Itami, K. Synthesis of a Zigzag Carbon Nanobelt. *Nat. Chem.* **2021**, *13*, 255–259.
- (81) Lin, Y.; Member, S.; Gundlach, D. J.; Nelson, S. F.; Jackson, T. N. Pentacene-Based Organic Thin-Film Transistors. *IEEE Trans. Electron. Devices* **1997**, *44*, 1325–1331.
- (82) Zimmerman, P. M.; Zhang, Z.; Musgrave, C. B. Singlet Fission in Pentacene through Multi-Exciton Quantum States. *Nat. Chem.* **2010**, *2*, 648–652.
- (83) Thorley, K. J.; Anthony, J. E. The Electronic Nature and Reactivity of the Larger Acenes. *Isr. J. Chem.* **2014**, *54*, 642–649.
- (84) Solà, M. Forty Years of Clar's Aromatic π -Sextet Rule. *Front. Chem.* **2013**, *1*, 22–29.
- (85) Bendikov, M.; Duong, H. M.; Starkey, K.; Houk, K. N.; Carter, E. A.; Wudl, F. Oligoacenes: Theoretical Prediction of Open-Shell Singlet Diradical Ground States. *J. Am. Chem. Soc.* **2004**, *126*, 7416–7417.
- (86) Rivero, P.; Jiménez-Hoyos, C. A.; Scuseria, G. E. Entanglement and Polyradical Character of Polycyclic Aromatic Hydrocarbons Predicted by Projected Hartree-Fock Theory. *J. Phys. Chem. B* **2013**, *117*, 12750–12758.
- (87) Hachmann, J.; Dorando, J. J.; Aviñs, M.; Chan, G. K. L. The Radical Character of the Acenes: A Density Matrix Renormalization Group Study. *J. Chem. Phys.* **2007**, *127*, 134309.
- (88) Zade, S. S.; Zamoshchik, N.; Reddy, A. R.; Fridman-Marueli, G.; Sheberla, D.; Bendikov, M. Products and Mechanism of Acene Dimerization. A Computational Study. *J. Am. Chem. Soc.* **2011**, *133*, 10803–10816.
- (89) Maliakal, A.; Raghavachari, K.; Katz, H.; Chandross, E.; Siegrist, T. Photochemical Stability of Pentacene and a Substituted Pentacene in Solution and in Thin Films. *Chem. Mater.* **2004**, *16*, 4980–4986.
- (90) Coppo, B. P.; Yeates, S. G. Shining Light on a Pentacene Derivative : The Role of Photoinduced Cycloadditions. *Adv. Mater.* **2005**, *17*, 3001–3005.
- (91) Payne, M. M.; Parkin, S. R.; Anthony, J. E. Functionalized Higher Acenes : Hexacene and Heptacene. *J. Am.*

- Chem. Soc.* **2005**, *127*, 8028–8029.
- (92) Mondal, R.; Shah, B. K.; Neckers, D. C. Photogeneration of Heptacene in a Polymer Matrix. *J. Am. Chem. Soc.* **2006**, *128*, 9612–9613.
- (93) Eisenhut, F.; Kühne, T.; García, F.; Fernández, S.; Guitián, E.; Pérez, D.; Trinquier, G.; Cuniberti, G.; Joachim, C.; Peña, D.; et al. Dodecacene Generated on Surface: Reopening of the Energy Gap. *ACS Nano* **2020**, *14*, 1011–1017.
- (94) Clar, E.; Fell, G. S.; Richmond, M. H. 4,5:12,13-Dibenzoheptazenterene and 5,6:8,9:14,15:17,18-Tetrabenzoheptacene. *Tetrahedron* **1960**, *9*, 96–105.
- (95) Duong, H. M.; Bendikov, M.; Steiger, D.; Zhang, Q.; Sonmez, G.; Yamada, J.; Wudl, F. Efficient Synthesis of a Novel, Twisted and Stable, Electroluminescent “Twistacene”. *Org. Lett.* **2003**, *5*, 4433–4436.
- (96) Purushothaman, B.; Bruzek, M.; Parkin, S. R.; Miller, A.; Anthony, J. E. Synthesis and Structural Characterization of Crystalline Nonacenes. *Angew. Chem. Int. Ed.* **2011**, *50*, 7013–7017.
- (97) Pramanik, C.; Miller, G. P. Rapid Access to a Benchmark Organic Semiconductor. *Molecules* **2012**, 4625–4633.
- (98) Meijer, E. J.; De Leeuw, D. M.; Setayesh, S.; Van Veenendaal, E.; Huisman, B.-H.; Lom, P. W. M.; Hummelen, J. C.; Scherf, U.; Klapwijk, T. M. Solution-Processed Ambipolar Organic Field-Effect Transistors and Inverters. *Nat. Mater.* **2003**, *2*, 678–682.
- (99) You, A.; Be, M. A. Y.; In, I. Anthracene Derivatives for Stable Blue-Emitting Organic Electroluminescence Devices. *Appl. Phys. Lett.* **2002**, *80*, 3201–3203.
- (100) Choi, H. S.; Kim, K. S. Structures, Magnetic Properties, and Aromaticity of Cyclacenes. *Angew. Chem. Int. Ed.* **1999**, *38*, 2256–2258.
- (101) Fokin, A. A.; Jiao, H.; Schleyer, P. V. R. From Dodecahedrapentaene to the “[n] Trannulenes”. A New In-Plane Aromatic Family. *J. Am. Chem. Soc.* **1998**, *120*, 9364–9365.
- (102) Houk, K. N.; Lee, P. S.; Nendel, M. Polyacene and Cyclacene Geometries and Electronic Structures: Bond Equalization, Vanishing Band Gaps, and Triplet Ground States Contrast with Polyacetylene. *J. Org. Chem.* **2001**, *66*, 5517–5521.
- (103) Chen, Z.; Jiang, D.; Lu, X.; Bettinger, H. F.; Dai, S.; Rague, P. Von; Houk, K. N. Open-Shell Singlet Character of Cyclacenes and Short Zigzag Nanotubes. *Org. Lett.* **2007**, *9*, 5449–5452.
- (104) Hirst, E. S.; Wang, F.; Jasti, R. Theoretical Analysis of [5.7]_n Cyclacenes: Closed-Shell Cyclacene Isomers. *Org. Lett.* **2011**, *13*, 6220–6223.
- (105) Matsui, K.; Fushimi, M.; Segawa, Y.; Itami, K. Synthesis, Structure, and Reactivity of a Cylinder-Shaped Cyclo[12]Orthophenylene[6]Ethylyene: Toward the Synthesis of Zigzag Carbon Nanobelts. *Org. Lett.* **2016**, *18*, 5352–5355.
- (106) Gould, I. I. R.; Taylor, A. M. G. P.; Walkinshaw, M. D.; Chem, J. A.; Spencer, N.; Stoddart, J. F.; Williams, D. J.; Chem, J. C. S. O. C.; Stoddart, J. F.; Williams, D. J. Molecular Belts and Collars in the Making: A Hexaepoxyoctacosahydro[12]cyclacene Derivative. *Angew. Chem. Int. Ed.* **1987**, *26*, 892–894.
- (107) Ashton, P. R.; Isaacs, N. S.; Kohnke, F. H.; Slawin, A. M. Z.; Spencer, C. M.; Stoddart, J. F.; Williams, D. J. Towards the Making of [12]Collarene. *Angew. Chem. Int. Ed.* **1988**, *27*, 966–969.
- (108) Ashton, P. R.; Brown, G. R.; Isaacs, N. S.; Giuffrida, D.; Kohnke, F. H.; Mathias, J. P.; Slawin, A. M. Z.; Smith, D. R.; Stoddart, J. F.; Williams, D. J. Molecular LEGO. Substrate-Directed Synthesis via Stereoregular Diels-Alder

- Oligomerizations. *J. Am. Chem. Soc.* **1992**, *114*, 6330–6353.
- (109) Kohnke, F. H.; Stoddart, J. F. The Evolution of Molecular Belts and Collars. *Appl. Pure Chem.* **1989**, *61*, 1581–1586.
- (110) Girresera, U.; Giuffrida, D.; Kohnke, F. H.; Mathias, J. P.; Philpa, D.; Stoddart, J. F. The Structure-Directed Synthesis of Cycloacene and Polyacene Derivatives. *Pure Appl. Chem.* **1993**, *65*, 119–125.
- (111) Cory, R. M.; Mcphail, C. L. Transformations of a Macrocyclic Cyclophane Belt into Advanced [8] Cyclacene and [8]Cyclacene Triquinone Precursors. *Tetrahedron Lett.* **1996**, *37*, 1987–1990.
- (112) Cory, R. M.; Mcphail, C. L.; Dikmans, A. J.; Viral, J. J. Macrocyclic Cyclophane Belts via Double Diels-Alder Cycloadditions: Macroannulation of Bisdienes by Bisdienophiles. Synthesis of a Key Precursor to an [8]Cyclacene. *Tetrahedron Lett.* **1996**, *37*, 1983–1986.
- (113) Esser, B.; Rominger, F.; Gleiter, R. Synthesis of [6.8]₃Cyclacene: Conjugated Belt and Model for an Unusual Type of Carbon Nanotube. *J. Am. Chem. Soc.* **2008**, *130*, 6716–6717.
- (114) Li, C. W.; Wang, C. I.; Liao, H. Y.; Chaudhuri, R.; Liu, R. S. Synthesis of Dibenzo[*g,p*]chrysenes from Bis(biaryl)acetylenes via Sequential ICl-Induced Cyclization and Mizoroki-Heck Coupling. *J. Org. Chem.* **2007**, *72*, 9203–9207.
- (115) Mukherjee, A.; Pati, K.; Liu, R. S. A Convenient Synthesis of Tetrabenzo[*de,Hi,Mn,Qr*]naphthacene from Readily Available 1,2-Di(phenanthren-4-yl)ethyne. *J. Org. Chem.* **2009**, *74*, 6311–6314.
- (116) Kintzel, O.; Luger, P.; Weber, M.; Schlüter, A. D. Ring-Chain Equilibrium between an [18]Cyclacene Derivative and a Ladder Oligomer. *Eur. J. Org. Chem.* **1998**, 99–105.
- (117) Povie, G.; Segawa, Y.; Nishihara, T.; Miyauchi, Y.; Itami, K. Synthesis of a Carbon Nanobelt. *Science* **2017**, *356*, 172–175.
- (118) Schulz, F.; Garcia, F.; Kaiser, K.; Perez, D.; Guitian, E.; Gross, L.; Pena, D. Exploring a Route to Cyclic Acenes by On-Surface Synthesis. *Angew. Chem. Int. Ed.* **2019**, *58*, 9038–9042.
- (119) Wang, J.; Miao, Q. A Tetraazapentacene–Pyrene Belt: Toward Synthesis of N-Doped Zigzag Carbon Nanobelts. *Org. Lett.* **2019**, *21*, 10120–10124.
- (120) Shi, T.; Guo, Q.; Tong, S.; Wang, M. Toward the Synthesis of a Highly Strained Hydrocarbon Belt. *J. Am. Chem. Soc.* **2020**, *142*, 4576–4580.
- (121) Endo, M.; Hayashi, T.; Kim, Y. Large-Scale Production of Carbon Nanotubes and Their Applications. *Pure Appl. Chem.* **2006**, *78*, 1703–1713.
- (122) Chen, H.; Gui, S.; Zhang, Y.; Liu, Z.; Miao, Q. Synthesis of a Hydrogenated Zigzag Carbon Nanobelt. *CCS Chem.* **2021**, *3*, 613–619.
- (123) Merner, B. L.; Dawe, L. N.; Bodwell, G. J. 1,1,8,8-Tetramethyl[8](2,11)Teropyrenophane: Half of an Aromatic Belt and a Segment of an (8,8) Single-Walled Carbon Nanotube. *Angew. Chem. Int. Ed.* **2009**, *48*, 5487–5491.
- (124) Franz, D.; Robbins, S. J.; Boere, R. T.; Dibble, P. W. Synthesis and Characterization of 2,7-Di(*tert*-butyl)pyreno[4,5-*c*:9,10-*c'*]difuran and Derived Pyrenophanes. *J. Org. Chem.* **2009**, *74*, 7544–7547.
- (125) Iwamoto, T.; Kayahara, E.; Yasuda, N.; Suzuki, T.; Yamago, S. Synthesis, Characterization, and Properties of [4]Cyclo-2,7-Pyrenylene: Effects of Cyclic Structure on the Electronic Properties of Pyrene Oligomers. *Angew. Chem. Int. Ed.* **2014**, *53*, 6430–6434.

- (126) Ghasemabadi, P. G.; Yao, T.; Bodwell, G. J. Cyclophanes Containing Large Polycyclic Aromatic Hydrocarbons. *Chem. Soc. Rev.* **2015**, *44*, 6494–6518.
- (127) Robbins, S. J.; Thibault, M. E.; Masuda, J. D.; Ward, D. R.; Dibble, P. W. X-Ray Structures of Cyclophanes Derived from Naphtho [1,2-*c*:5,6-*c'*] - Difuran and the Synthesis, Structure, and Reaction Kinetics of Its. *J. Org. Chem.* **2009**, *74*, 5192–5198.
- (128) Miura, Y.; Yamano, E. ESR and ¹H ENDOR Spectra of Partly Deuterated JV-[(4-Nitrophenyl)thio]-2,7-di-*tert*-butyl-1-pyrenylaminy Radical. Assignments of the Pyrene Ring Protons. *J. Org. Chem.* **1995**, *60*, 1070–1073.
- (129) Möhring, D.; Nieger, M.; Lewall, B.; Dötz, K. H. Tricarbonyl(naphthoquinone)chromium: Synthesis and Application in [4+2] Cycloaddition Reactions. *Eur. J. Org. Chem.* **2005**, 2620–2628.
- (130) Rosillo, M.; Domínguez, G.; Pérez-Castells, J. Chromium Arene Complexes in Organic Synthesis. *Chem. Soc. Rev.* **2007**, *36*, 1589–1604.
- (131) Arrais, A.; Diana, E.; Gervasio, G.; Gobetto, R.; Marabello, D.; Stanghellini, P. L. Synthesis, Structural and Spectroscopic Characterization of Four [(η⁶-PAH)Cr(CO)₃] Complexes (PAH= Pyrene, Perylene, Chrysene, 1,2-Benzanthracene). *Eur. J. Inorg. Chem.* **2004**, 1505–1513.
- (132) El-azizi, Y.; Schmitzer, A.; Collins, S. K. Exploitation of Perfluorophenyl-Phenyl Interactions for Achieving Difficult Macrocyclizations by Using Ring-Closing Metathesis. *Angew. Chem. Int. Ed.* **2006**, *45*, 968–973.
- (133) Gurudutt, K. N.; Ravindranath, B.; Srinivas, P. Solvolytic Displacement of Alkyl Halides by Metal Salts. *Tetrahedron* **1982**, *38*, 1843–1846.
- (134) Hart, H.; Lai, C.-Y.; Nwokogu, G.; Shamouilian, S. Tetrahalobenzenes as Di-aryne Equivalents in Polycyclic Arene Synthesis. *Tetrahedron* **1987**, *43*, 5203–5224.
- (135) Davies, J. W.; Durrant, M. L.; Walker, M. P.; Belkacemi, D.; Malpass, J. R. Preparation and Spectroscopic Studies of the 1,4-Dihydro-1,4-iminonaphthalene(7-azabenzonorbornadiene) Ring System. *Tetrahedron* **1992**, *48*, 861–884.
- (136) Shirley, D. A.; Gross, B. H.; Roussel, P. A. Metalation of Pyrrole, 1-Methylpyrrole, and 1-Phenylpyrrole with *n*-Butyllithium. *J. Org. Chem.* **1955**, *20*, 225–231.
- (137) Cant, A. A.; Bertrand, G. H. V.; Henderson, J. L.; Roberts, L.; Greaney, M. F. The Benzyne Aza-Claisen Reaction. *Angew. Chem. Int. Ed.* **2009**, *48*, 5199–5202.
- (138) Ji, L.; Krummenacher, I.; Friedrich, A.; Lorbach, A.; Haehnel, M.; Edkins, K.; Braunschweig, H.; Marder, T. B. Synthesis, Photophysical, and Electrochemical Properties of Pyrenes Substituted with Donors or Acceptors at the 4- or 4,9-Positions. *J. Org. Chem.* **2018**, *83*, 3599–3606.
- (139) Crawford, A. G.; Liu, Z.; Mkhallid, I. A. I.; Thibault, M.; Schwarz, N.; Alcaraz, G.; Steffen, A.; Collings, J. C.; Batsanov, A. S.; Howard, J. A. K.; et al. Synthesis of 2- and 2,7-Functionalized Pyrene Derivatives: An Application of Selective C-H Borylation. *Chem. Eur. J.* **2012**, *18*, 5022–5035.
- (140) Tobisu, M.; Morioka, T.; Ohtsuki, A.; Chatani, N. Nickel-Catalyzed Reductive Cleavage of Aryl Alkyl Ethers to Arenes in Absence of External Reductant. *Chem. Sci.* **2015**, *6*, 3410–3414.
- (141) Chen, Y.; Sun, J.; Wei, X.; Wong, W.; Lee, A. W. M. Generation of Synthetic Equivalents of Benzdiynes from Benzobisoxadisiloles. *J. Org. Chem.* **2004**, *78*, 7190–7197.
- (142) Poater, J.; Fradera, X.; Duran, M.; Solà, M. An Insight into the Local Aromaticities of Polycyclic Aromatic Hydrocarbons and Fullerenes. *Chem. Eur. J.* **2003**, *9*, 1113–1122.

- (143) Aihara, J. I. Nucleus-Independent Chemical Shifts and Local Aromaticities in Large Polycyclic Aromatic Hydrocarbons. *Chem. Phys. Lett.* **2002**, *365*, 34–39.
- (144) Reisi-Vanani, A.; Rezaei, A. A. Evaluation of the Aromaticity of Non-Planar and Bowl-Shaped Molecules by NICS Criterion. *J. Mol. Graph. Model.* **2015**, *61*, 85–88.
- (145) Havenith, R. W. A.; Van Lenthe, J. H.; Dijkstra, F.; Jenneskens, L. W. Aromaticity of Pyrène and Its Cyclopentafused Congeners-Resonance and NICS Criteria. An Ab Initio Valence Bond Analysis in Terms of Kekulé Resonance Structures. *J. Phys. Chem. A* **2001**, *105*, 3838–3845.
- (146) Fowler, P. W.; Soncini, A. Visualising Aromaticity of Bowl-Shaped Molecules. *Phys. Chem. Chem. Phys.* **2011**, *13*, 20637–20643.
- (147) Pasquarello, A.; Schlüter, M.; Haddon, R. C. Ring Currents in Icosahedral C₆₀. *Science* **1992**, *257*, 1660–1661.
- (148) Merz, J.; Dietz, M.; Vonhausen, Y.; Wöber, F.; Friedrich, A.; Sieh, D.; Krummenacher, I.; Braunschweig, H.; Moos, M.; Holzapfel, M.; Lambert, C.; Marder, T. B. Synthesis, Photophysical and Electronic Properties of New Red-to-NIR Emitting Donor–Acceptor Pyrene Derivatives. *Chem. - A Eur. J.* **2020**, *26*, 438–453.
- (149) Agarwal, S. K.; Boyd, D. R.; Jennings, W. B.; McGuckin, R. M.; O’Kane, G. A. General Synthetic Routes to Diarene Oxides of Polycyclic Aromatic Hydrocarbons. *Tetrahedron Lett.* **1989**, *30*, 123–126.
- (150) Agarwal, S. C.; Van Duuren, B. L. Synthesis of Diepoxides and Diphenol Ethers of Pyrene and Dibenz[*a,h*]Anthracene. *J. Org. Chem.* **1975**, *40*, 2307–2310.
- (151) Murray, R. W.; Singh, M.; Rath, N. P. Improved Synthesis and X-Ray Crystallographic Structure Determination of the Stereoisomeric K-Region Arene Dioxides of Pyrene and Dibenz[*a,h*]Anthracene. *Polycycl. Aromat. Compd.* **1999**, *13*, 139–149.
- (152) Moriarty, R. M.; Dansette, P.; Jerina, D. M. Pyrene Derivatives Oxygenated at Both K-Regions of a Bis-arene Oxide. *Tetrahedron Lett.* **1975**, 2557–2560.
- (153) Ji, L.; Krummenacher, I.; Friedrich, A.; Lorbach, A.; Haehnel, M.; Edkins, K.; Braunschweig, H.; Marder, T. B. Synthesis, Photophysical, and Electrochemical Properties of Pyrenes Substituted with Donors or Acceptors at the 4- or 4,9-Positions. *J. Org. Chem.* **2018**, *83*, 3599–3606.
- (154) Moriconi, E. J.; Wallenberger, F. T.; O’Connor, W. F. A New Synthesis of 9-Phenanthrol; Absorption Spectra of the Quinhydrone-Type Molecular Compound between 9-Phenanthrol and Phenanthrenequinone. *J. Org. Chem.* **1959**, *24*, 86–90.
- (155) Tietze, E.; Bayer, O. Die Sulfosäuren Des Pyrens Und Ihre Abkömmlinge. *Justus Liebigs Ann. Chem.* **1939**, *540*, 189–210.
- (156) Boswell, M. C.; Dickson, J. V. The Fusion of Sodium Hydroxide with Some Inorganic Salts. *J. Am. Chem. Soc.* **1918**, *40*, 1773–1779.
- (157) Hartman, W. W. *p*-Cresol. *Org. Synth.* **1923**, *3*, 37.
- (158) Ghaffarzadeh, M.; Bolourtchian, M.; Halvagar, M. R.; Hosseini, M. Synthesis of Phenols and Naphthols by Alkali Metal Hydroxide Fusion under Microwave Irradiation. *J. Chem. Res. - Part S* **2003**, No. 12, 812–813.
- (159) Dudley, M. W.; Frost, J. W. Biocatalytic Desulfurization of Arylsulfonates. *Bioorganic Med. Chem.* **1994**, *2*, 681–690.
- (160) Bunnett, J. F.; Zahler, R. E. Aromatic Nucleophilic Substitution Reactions. *Chem. Rev.* **1951**, *49*, 273–412.

- (161) Hennessy, E. J.; Buchwald, S. L. Synthesis of Substituted Oxindoles from α -Chloroacetanilides via Palladium-Catalyzed C-H Functionalization. *J. Am. Chem. Soc.* **2003**, *125* (40), 12084–12085.
- (162) Iwasaki, M.; Araki, Y.; Iino, S.; Nishihara, Y. Synthesis of Multisubstituted Triphenylenes and Phenanthrenes by Cascade Reaction of *o*-Iodobiphenyls or (Z)- β -Halostyrenes with *o*-Bromobenzyl Alcohols through Two Sequential C-C Bond Formations Catalyzed by a Palladium Complex. *J. Org. Chem.* **2015**, *80*, 9247–9263.
- (163) Ghera, E.; Gaoni, Y.; Shoua, S. Zinc-Induced Reactions of Bromo Ketones. *J. Am. Chem. Soc.* **1975**, *98*, 3627–3632.
- (164) Bergmark, W. R.; Barnes, C.; Clark, J.; Paparian, S.; Marynowski, S. Photoenolization with α -Chloro Substituents. *J. Org. Chem.* **1985**, *50*, 5612–5615.
- (165) Nanjundiah, B. S.; Sonawane, H. R. Photochemistry of the Carbon-Halogen Bond: Some Recent Developments. *Proc. Indian Acad. Sci. - Chem. Sci.* **1985**, *95*, 447–462.
- (166) Swamy, K. C. K.; Kumar, N. N. B.; Balaraman, E.; Kumar, K. V. P. Mitsunobu and Related Reactions: Advances and Applications. *Chem. Rev.* **2009**, *109* (6), 2551–2651.
- (167) But, T. Y. S.; Toy, P. H. The Mitsunobu Reaction: Origin, Mechanism, Improvements, and Applications. *Chem. - An Asian J.* **2007**, *2*, 1340–1355.
- (168) Heravi, M. M.; Ghanbarian, M.; Zadsirjan, V.; Alimadadi Jani, B. Recent Advances in the Applications of Wittig Reaction in the Total Synthesis of Natural Products Containing Lactone, Pyrone, and Lactam as a Scaffold. *Monatshefte fur Chemie* **2019**, *150*, 1365–1407.
- (169) Nicolaou, K. C.; Härter, M. W.; Gunzner, J. L.; Nadin, A. The Wittig and Related Reactions in Natural Product Synthesis. *Liebigs Ann.* **1997**, No. 7, 1283–1301.
- (170) Henrici-Olivé, G.; Olivé, S. Influence of Ligands on the Activity and Specificity of Soluble Transition Metal Catalysts. **1971**, *10*, 105–115.
- (171) Kelly, W. J.; Belabassi, Y.; Gouault-Bironneau, S.; Montchamp, J.-L. 1,1'-Bis(diphenylphosphino)ferrocene. *Encycl. Reagents Org. Synth.* **2006**.
- (172) Westcott, S. A. (Bicyclo[2.2.1]hepta-2,5-diene)[(2S,3S)-bis(diphenylphosphino)butane]rhodium Perchlorate. *Encycl. Reagents Org. Synth.* **2019**.
- (173) Kitamura, M.; Noyori, R.; Tsukamoto, M.; Kitamura, M. (R) and (S)-2,2-Bis(diphenylphosphino)-1,1'-Binaphthyl. *Encycl. Reagents Org. Synth.* **2005**.
- (174) Morin, P. O.; Bura, T.; Sun, B.; Gorelsky, S. I.; Li, Y.; Leclerc, M. Conjugated Polymers à La Carte from Time-Controlled Direct (Hetero)arylation Polymerization. *ACS Macro Lett.* **2015**, *4*, 21–24.
- (175) Bugaenko, D. I.; Volkov, A. A.; Livantsov, M. V.; Yurovskaya, M. A.; Karchava, A. V. Catalyst-Free Arylation of Tertiary Phosphines with Diaryliodonium Salts Enabled by Visible Light. *Chem. Eur. J.* **2019**, *25*, 12502–12506.
- (176) Rémond, E.; Tessier, A.; Leroux, F. R.; Bayardon, J.; Jugé, S. Efficient Synthesis of Quaternary and P-Stereogenic Phosphonium Triflates. *Org. Lett.* **2010**, *12*, 1568–1571.
- (177) Imrie, C.; Modro, T. A.; Van Rooyen, P. H.; Wagener, C. C. P.; Wallace, K.; Hudson, H. R.; McPartlin, M.; Nasirun, J. B.; Powroznyk, L. Structural Study on Quasi-phosphonium Salts Containing Phosphorus–Oxygen, Phosphorus–Oxygen, Phosphorus–Nitrogen and Phosphorus–sulphur Bonds. *J. Phys. Org. Chem.* **1995**, *8*, 41–46.
- (178) Godfrey, S. M.; Mcauli, C. a; Pritchard, R. G.; She, J. M.; Thompson, G. M. Structure of R₃PCl₂ Compounds in

- the Solid State and in Solution: Dependency of Structure on R. Crystal Structures of Trigonal Bipyramidal (C_6F_5)₃PCl₂, Ph₂(C₆F₅)PCl₂ and of Ionic Prⁿ₃PCl₂. *J. Chem. Soc., Dalt. Trans.* **1997**, 4823–4827.
- (179) Godfrey, S. M.; McAuli, C. A.; Mushtaq, I.; Pritchard, R. G.; Sheffield, J. M. The Structure of R₃PBr₂ Compounds in the Solid State and in Solution; Geometrical Dependence on R, the Crystal Structures of Tetrahedral Ionic Et₃PBr₂ and Molecular Trigonal Bipyramidal (C₆F₅)₃PBr₂. *J. Chem. Soc., Dalt. Trans.* **1998**, 3815–3818.
- (180) Godfrey, S. M.; McAuliffe, C. A.; Pritchard, R. G.; Sheffield, J. M. An X-Ray Crystallographic Study of the Reagent Ph₃PCl₂; Not Charge-Transfer, R₃P-Cl-Cl, Trigonal Bipyramidal or [R₃PCl]Cl but an Unusual Dinuclear Ionic Species, [Ph₃PCl+···Cl··· +ClPPh₃]Cl Containing Long Cl-Cl Contacts. *Chem. Commun.* **1996**, 1, 2521–2522.
- (181) Vetter, A. C.; Nikitin, K.; Gilheany, D. G. Exploring an Umpolung Strategy for Quaternization of Phosphorus. *Phosphorus. Sulfur. Silicon Relat. Elem.* **2019**, 194, 339–342.
- (182) Bayne, J. M.; Stephan, D. W. Phosphorus Lewis Acids: Emerging Reactivity and Applications in Catalysis. *Chem. Soc. Rev.* **2016**, 45, 765–774.
- (183) Dupont, J.; De Souza, R. F.; Suarez, P. A. Z. Ionic Liquid (Molten Salt) Phase Organometallic Catalysis. *Chem. Rev.* **2002**, 102, 3667–3692.
- (184) Fraser, K. J.; MacFarlane, D. R. Phosphonium-Based Ionic Liquids: An Overview. *Aust. J. Chem.* **2009**, 62, 309–321.
- (185) Comyns, C.; Karodia, N.; Zeler, S.; Andersen, J. A. Clean Catalysis with Clean Solvents - Phosphonium Tosylates for Transfer Hydrogenation Reactions. *Catal. Letters* **2000**, 67, 113–115.
- (186) Knifton, J. F. Ethylene Glycol from Synthesis Gas via Ruthenium Melt Catalysis. *J. Am. Chem. Soc.* **1981**, 103, 3959–3961.
- (187) Sheu, S.; Nauduri, D.; Anders, M. W. Targeting Antioxidants to Mitochondria: A New Therapeutic Direction. *Biochim. Biophys. Acta* **2006**, 1762, 256–265.
- (188) Khasiyatullina, N. R.; Vazykhova, A. M.; Mironov, V. F.; Krivolapov, D. B.; Voronina, Y. K.; Voloshina, A. D.; Kulik, V.; Strobukina, A. S. Phosphonium Salts with a Dihydroxynaphthyl Substituent: Versatile Synthesis and Evaluation of Antimicrobial Activity. *Mendeleev Commun.* **2017**, 27, 134–136.
- (189) Akutsu, H.; Yamada, J.; Nakatsuji, S. New BEDT-TTF-Based Organic Conductor Including an Organic Anion Derived from the TEMPO Radical, a-(BEDT-TTF)₃(TEMPO–NHCOCH₂SO₃)₂•6H₂O. *Chem. Lett.* **2003**, 32, 1118–1119.
- (190) Stazi, F.; Marcoux, D.; Poupon, J.; Latassa, D.; Charette, A. B. Tetraarylphosphonium Salts as Soluble Supports for the Synthesis of Small Molecules. *Angew. Chem. Int. Ed.* **2007**, 46, 5011–5014.
- (191) Zhang, X.; McNally, A. Phosphonium Salts as Pseudohalides: Regioselective Nickel-Catalyzed Cross-Coupling of Complex Pyridines and Diazines. *Angew. Chem. Int. Ed.* **2017**, 56, 9833–9836.
- (192) Hwang, L. K.; Na, Y.; Lee, J.; Do, Y.; Chang, S. Tetraarylphosphonium Halides as Arylating Reagents in Pd-Catalyzed Heck and Cross-Coupling Reactions. *Angew. Chem. Int. Ed.* **2005**, 44, 6166–6169.
- (193) Kawai, H.; Wolf, W. J.; Dipasquale, A. G.; Winston, M. S.; Toste, F. D. Phosphonium Formation by Facile Carbon – Phosphorus Reductive Elimination from Gold(III). *J. Am. Chem. Soc.* **2016**, 138, 587–593.
- (194) Hilton, M. C.; Zhang, X.; Boyle, B. T.; Alegre-requena, J. V.; Paton, R. S.; McNally, A. Heterobiaryl Synthesis by Contractive C–C Coupling via P(V) Intermediates. *Science* **2018**, 362, 799–804.

- (195) Enders, D.; Nguyen, T. V. Chiral Quaternary Phosphonium Salts : A New Class of Organocatalysts. *Org. Biomol. Chem.* **2012**, *10*, 5327–5331.
- (196) Methot, J. L.; Roush, W. R. Nucleophilic Phosphine Organocatalysis. *Adv. Synth. Catal.* **2004**, *346*, 1035–1050.
- (197) Deng, Z.; Lin, J.; Xiao, J. Nucleophilic Arylation with Tetraarylphosphonium Salts. *Nat. Commun.* **2016**, *7*, 10337.
- (198) Wang, L. C.; Luis, A. L.; Agapiou, K.; Jang, H. Y.; Krische, M. J. Organocatalytic Michael Cycloisomerization of Bis(enones): The Intramolecular Rauhut-Currier Reaction. *J. Am. Chem. Soc.* **2002**, *124*, 2402–2403.
- (199) Huang, J. W.; Shi, M. Polymer-Supported Lewis Bases for the Baylis-Hillman Reaction. *Adv. Synth. Catal.* **2003**, *345*, 953–958.
- (200) Wittig, G.; Schoellkopf, U.; Roberts, J. D.; Vogel, M. Methylene-cyclohexane. *Org. Synth.* **1960**, *40*, 66.
- (201) Aldrich, S. Wittig Reagents <https://www.sigmaaldrich.com/chemistry/chemistry-products.html?TablePage=16279059#:~:text=Wittig reagents are triphenyl phosphonium,base such as n-butyllithium.>
- (202) Horner, L.; Duda, U. M. Phosphororganische Verbindungen 69 Darstellung Und Eigenschaften Einiger Vollaromatischer Phosphoniumsalze Mit *p*-Dimethylamino- Und *p*-Methoxygruppen. *Tetrahedron Lett.* **1970**, *11*, 5177–5181.
- (203) Horner, L.; Mumenthey, G.; Moser, H.; Beck, P. Die Einführung von Arylresten in Tertiäre Phosphine Mit Hilfe von Komplexen Der Übergangsmetalle (Komplexsalzmethode). *Chem. Ber.* **1966**, *99*, 2782–2788.
- (204) von Hirusawa, Y.; Oku, M.; Yamamoto, K. Neue Synthetische Methode Chemie Aus Tertiarem Reihenfolge Betrag an Chlorid Jeder Halogenide. *Bull. Chem. Soc. Jpn.* **1957**, *30*, 667.
- (205) Marcoux, D.; Charette, A. B. Palladium-Catalyzed Synthesis of Functionalized Tetraarylphosphonium Salts. *J. Org. Chem.* **2008**, *73*, 590–593.
- (206) Marcoux, D.; Charette, A. B. Nickel-Catalyzed Synthesis of Phosphonium Salts from Aryl. *Adv. Synth. Catal.* **2008**, *350*, 2967–2974.
- (207) Neog, K.; Dutta, D.; Das, B.; Gogoi, P. Aryne Insertion into the P=O Bond : One-Pot Synthesis of Quaternary Phosphonium Triflates. *Org. Biomol. Chem.* **2019**, *17*, 6450–6460.
- (208) Vetter, A. C.; Nikitin, K.; Gilheany, D. G. Long Sought Synthesis of Quaternary Phosphonium Salts from Phosphine Oxides : Inverse Reactivity Approach. *Chem. Commun.* **2018**, *54*, 5843–5846.
- (209) Stankevi, M.; Pisklak, J.; Katarzyna, W. Aryl Group-a Leaving Group in Arylphosphine Oxides. *Tetrahedron* **2016**, *72*, 810–824.
- (210) Fearnley, A. F.; Jackson, J. A. M.; Lindovska, P.; Denton, R. M. Synthesis of Quaternary Aryl Phosphonium Salts: Photoredox-Mediated Phosphine Arylation. *Chem. Commun.* **2016**, *52*, 4987–4990.
- (211) Dawber, J. G.; Skerratt, R. G.; Tebby, J. C.; Waite, A. A. C. Kinetics of Alkaline Hydrolysis of Quaternary Phosphonium Salts. The Influence of Protic and Aprotic Solvents on the Hydrolysis of Alkyl Phenylphosphonium Salts. *Phosphorus, Sulfur Silicon Relat. Elem.* **2012**, *187*, 1261–1268.
- (212) Marsi, K. L.; Oberlander, J. E. Alkaline Cleavage Reactions of Tetraalkylphosphonium Salts. *J. Am. Chem. Soc.* **1973**, *95*, 200–204.
- (213) Hawes, W.; Trippett, S. Alkaline Hydrolysis of a Phosphonium Salt with Retention of Configuration at

- Phosphorus. *Chem. Commun.* **1968**, No. 6, 295–296.
- (214) Yanagisawa, S.; Ueda, K.; Taniguchi, T.; Itami, K. Potassium *t*-Butoxide Alone Can Promote the Biaryl Coupling of Electron-Deficient Nitrogen Heterocycles and Haloarenes. *Org. Lett.* **2008**, *10*, 4673–4676.
- (215) Shirakawa, E.; Itoh, K.; Higashino, T.; Hayashi, T. *Tert*-Butoxide-Mediated Arylation of Benzene with Aryl Halides in the Presence of a Catalytic 1,10-Phenanthroline Derivative. *J. Am. Chem. Soc.* **2010**, *132*, 15537–15539.
- (216) Barham, J. P.; Coulthard, G.; Emery, K. J.; Doni, E.; Cumine, F.; Nocera, G.; John, M. P.; Berlouis, L. E. A.; Mcguire, T.; Tuttle, T.; et al. KO^tBu: A Privileged Reagent for Electron Transfer Reactions? *J. Am. Chem. Soc.* **2016**, *138*, 7402–7401.
- (217) Sun, C.; Li, H.; Yu, D.; Yu, M.; Zhou, X.; Lu, X.; Huang, K.; Zheng, S.-F.; Li, B.-J.; Shi, Z.-J. An Efficient Organocatalytic Method for Constructing Biaryls through Aromatic C–H Activation. *Nat. Chem.* **2010**, *2*, 1044–1049.
- (218) Boche, G.; Etzrodt, H. The Reaction of *n*-Butyllithium/sodium(potassium) *tert*-Butoxide (Lochmann-Schlosser Base) with a CH-Acid Leads to Organo-Sodium(Potassium) Compounds. An NMR Spectroscopical Study of Several Organo-Lithium, -Sodium and -Potassium Compounds in Tetrahydrofuran-D₈. *Tetrahedron Lett.* **1983**, *24*, 5477–5480.
- (219) Dong, Y.; Lipschutz, M. I.; Tilley, T. D. Regioselective, Transition Metal-Free C–O Coupling Reactions Involving Aryne Intermediates. *Org. Lett.* **2016**, *18*, 1530–1533.
- (220) Zhou, S.; Anderson, G. M.; Mondal, B.; Doni, E.; Ironmonger, V.; Kranz, M.; Tuttle, T.; Murphy, J. A. Organic Super-Electron-Donors: Initiators in Transition Metal-Free Haloarene-Arene Coupling. *Chem. Sci.* **2014**, *5*, 476–482.
- (221) Prier, C. K.; Rankic, D. A.; MacMillan, D. W. C. Visible Light Photoredox Catalysis with Transition Metal Complexes: Applications in Organic Synthesis. *Chem. Rev.* **2013**, *113*, 5322–5363.
- (222) Kim, H.; Lee, C. Visible-Light-Induced Photocatalytic Reductive Transformations of Organohalides. *Angew. Chem. Int. Ed.* **2012**, *51*, 12303–12306.
- (223) Wolf, W.; Kharasch, N. Photolysis of Iodoaromatic Compounds in Benzene. *J. Org. Chem.* **1965**, *30*, 2493–2498.
- (224) Dichiarante, V.; Fagnoni, M.; Albini, A. Metal-Free Synthesis of Sterically Crowded Biphenyls by Direct Ar–H Substitution in Alkyl Benzenes. *Angew. Chem. Int. Ed.* **2007**, *46*, 6495–6498.
- (225) Grimshaw, J.; De Silva, Prasanna, A. Photocyclization of Aryl Halides. Part I. 5-(2-Halogenophenyl)-1,3-diphenylpyrazoles; Homolytic Fission Assisted by Radical Complexation. *Can. J. Chem.* **1980**, 1880–1888.
- (226) Ishiyama, T.; Murata, M.; Miyaura, N. Palladium(0)-Catalyzed Cross-Coupling Reaction of Alkoxydiboron with Haloarenes: A Direct Procedure for Arylboronic Esters. *J. Org. Chem.* **1995**, *60*, 7508–7510.
- (227) Molander, G. A.; Trice, S. L. J.; Dreher, S. D. Palladium-Catalyzed, Direct Boronic Acid Synthesis from Aryl Chlorides: A Simplified Route to Diverse Boronate Ester Derivatives. *J. Am. Chem. Soc.* **2010**, *132*, 17701–17703.
- (228) Mfuh, A. M.; Doyle, J. D.; Chhetri, B.; Arman, H. D.; Larionov, O. V. Scalable, Metal- and Additive-Free, Photoinduced Borylation of Haloarenes and Quaternary Arylammonium Salts. *J. Am. Chem. Soc.* **2016**, *138*, 2985–2988.

- (229) Liu, W.; Yang, X.; Gao, Y.; Li, C. Simple and Efficient Generation of Aryl Radicals from Aryl Triflates: Synthesis of Aryl Boronates and Aryl Iodides at Room Temperature. *J. Am. Chem. Soc.* **2017**, *139*, 8621–8627.
- (230) Zeng, H.; Dou, Q.; Li, C. Photoinduced Transition-Metal-Free Cross-Coupling of Aryl Halides with H-Phosphonates. *Org. Lett.* **2019**, *21*, 1301–1305.
- (231) Li, L.; Liu, W.; Zeng, H.; Mu, X.; Cosa, G.; Mi, Z.; Li, C. Photo-Induced Metal-Catalyst-Free Aromatic Finkelstein Reaction. *J. Am. Chem. Soc.* **2015**, *137*, 8328–8331.
- (232) Miyaura, N.; Suzuki, A. Palladium-Catalyzed Cross-Coupling Reactions of Organoboron Compounds. *Chem. Rev.* **1995**, *95*, 2457–2483.
- (233) Littke, A. F.; Fu, G. C. A Versatile Catalyst for Heck Reactions of Aryl Chlorides and Aryl Bromides under Mild Conditions. *J. Am. Chem. Soc.* **2001**, *123*, 6989–7000.
- (234) Littke, A. F.; Dai, C.; Fu, G. C. Versatile Catalysts for the Suzuki Cross-Coupling of Arylboronic Acids with Aryl and Vinyl Halides and Triflates under Mild Conditions. *J. Am. Chem. Soc.* **2000**, *122*, 4020–4028.
- (235) Kalmus, C. E.; Hercules, D. M. A Mechanistic Study of the Photo-Fries Rearrangement of Phenyl Acetate. *J. Am. Chem. Soc.* **1974**, *96*, 449–456.
- (236) Siano, G.; Crespi, S.; Mella, M.; Bonesi, S. M. Selectivity in the Photo-Fries Rearrangement of Some Aryl Benzoates in Green and Sustainable Media. Preparative and Mechanistic Studies. *J. Org. Chem.* **2019**, *84*, 4338–4352.
- (237) Norrish, R. G. W.; Bamford, C. H. Photo-Decomposition of Aldehydes and Ketones. *Nature* **1937**, *140*, 195–196.
- (238) Batesky, D. C.; Goldfogel, M. J.; Weix, D. J. Removal of Triphenylphosphine Oxide by Precipitation with Zinc Chloride in Polar Solvents. *J. Org. Chem.* **2017**, *82*, 9931–9936.
- (239) Netherton, M. R.; Fu, G. C. Air-Stable Trialkylphosphonium Salts: Simple, Practical, and Versatile Replacements for Air-Sensitive Trialkylphosphines. Applications in Stoichiometric and Catalytic Processes. *Org. Lett.* **2001**, *3*, 4295–4298.
- (240) Diver, S. T. Tributylphosphine. *Encycl. Reagents Org. Synth.* **2016**, 1–7.
- (241) The Nobel prize in chemistry 2000. NobelPrize.org. Nobel Prize Outreach AB 2021. Sun. 19 Sep 2021. <<https://www.nobelprize.org/prizes/chemistry/2000/summary/>>
- (242) Inzelt, G. *Conducting Polymers: A New Era in Electrochemistry*; 2008; Vol. 1.
- (243) Ito, S. Printable Solar Cells. *Wiley Interdiscip. Rev. Energy Environ.* **2015**, *4*, 51–73.
- (244) Reale, A.; LaNotte, L.; Salamandra, L.; Polino, G.; Susanna, G.; Brown, T. M.; Brunetti, F.; DiCarlo, A. Spray Coating for Polymer Solar Cells: An Up-to-Date Overview. *Energy Technol.* **2015**, *3*, 385–406.
- (245) Hösel, M.; Dam, H. F.; Krebs, F. C. Development of Lab-to-Fab Production Equipment Across Several Length Scales for Printed Energy Technologies, Including Solar Cells. *Energy Technol.* **2015**, *3*, 293–304.
- (246) Cheng, Y. J.; Yang, S. H.; Hsu, C. S. Synthesis of Conjugated Polymers for Organic Solar Cell Applications. *Chem. Rev.* **2009**, *109*, 5868–5923.
- (247) Liu, C.; Wang, K.; Gong, X.; Heeger, A. J. Low Bandgap Semiconducting Polymers for Polymeric Photovoltaics. *Chem. Soc. Rev.* **2016**, *45*, 4825–4846.

- (248) Grimsdale, A. C.; Chan, K. L.; Martin, R. E.; Jokisz, P. G.; Holmes, A. B. Synthesis of Light-Emitting Conjugated Polymers for Applications in Electroluminescent Devices. *Chem. Rev.* **2009**, *109*, 897–1091.
- (249) Perepichka, I. F.; Perepichka, D. F.; Meng, H.; Wudl, F. Light-Emitting Polythiophenes. *Adv. Mater.* **2005**, *17*, 2281–2305.
- (250) Thomas, S. W.; Joly, G. D.; Swager, T. M. Chemical Sensors Based on Amplifying Fluorescent Conjugated Polymers. *Chem. Rev.* **2007**, *107*, 1339–1386.
- (251) Facchetti, A. π -Conjugated Polymers for Organic Electronics and Photovoltaic Cell Applications. *Chem. Mater.* **2011**, *23*, 733–758.
- (252) Dou, L.; Liu, Y.; Hong, Z.; Li, G.; Yang, Y. Low-Bandgap Near-IR Conjugated Polymers/Molecules for Organic Electronics. *Chem. Rev.* **2015**, *115*, 12633–12665.
- (253) Khim, D.; Ryu, G.; Park, W.; Kim, H.; Lee, M. Precisely Controlled Ultrathin Conjugated Polymer Films for Large Area Transparent Transistors and Highly Sensitive Chemical Sensors. *Adv. Mater.* **2016**, *28*, 2752–2759.
- (254) Lee, J. U.; Jung, J. W.; Jo, J. W.; Jo, W. H. Degradation and Stability of Polymer-Based Solar Cells. *J. Mater. Chem.* **2012**, *22*, 24265–24283.
- (255) Shockley, W.; Queisser, H. J. Detailed Balance Limit of Efficiency of p-n Junction Solar Cells. *J. Appl. Phys.* **1961**, *32*, 510–519.
- (256) Yoshikawa, K.; Kawasaki, H.; Yoshida, W.; Irie, T.; Konishi, K.; Nakano, K.; Uto, T.; Adachi, D.; Kanematsu, M.; Uzu, H.; et al. Silicon Heterojunction Solar Cell with Interdigitated Back Contacts for a Photoconversion Efficiency over 26%. *Nat. Energy* **2017**, *2*, 17032.
- (257) Bhattacharya, S.; John, S. Beyond 30% Conversion Efficiency in Silicon Solar Cells: A Numerical Demonstration. *Sci. Rep.* **2019**, *9*, 1–15.
- (258) Zhan, X.; Zhu, D. Conjugated Polymers for High-Efficiency Organic Photovoltaics. *Polym. Chem.* **2010**, *1*, 409–419.
- (259) Fan, Q.; Zhu, Q.; Xu, Z.; Su, W.; Chen, J.; Wu, J.; Guo, X.; Ma, W.; Zhang, M.; Li, Y. Chlorine Substituted 2D-Conjugated Polymer for High-Performance Polymer Solar Cells with 13.1% Efficiency via Toluene Processing. *Nano Energy* **2018**, *48*, 413–420.
- (260) Rudin, A.; Choi, P. Basic Principles of Polymer Molecular Weights. *Elem. Polym. Sci. Eng.* **2013**, 63–87.
- (261) Tu, G.; Bilge, A.; Adamczyk, S.; Forster, M.; Heiderhoff, R.; Balk, L. J.; Mühlbacher, D.; Morana, M.; Koppe, M.; Scharber, M. C.; et al. The Influence of Interchain Branches on Solid State Packing, Hole Mobility and Photovoltaic Properties of Poly(3-hexylthiophene) (P3HT). *Macromol. Rapid Commun.* **2007**, *28*, 1781–1785.
- (262) Okamoto, K.; Housekeeper, J. B.; Michael, F. E.; Luscombe, C. K. Thiophene Based Hyperbranched Polymers with Tunable Branching Using Direct Arylation Methods. *Polym. Chem.* **2013**, *4*, 3499–3506.
- (263) Kohn, P.; Huettner, S.; Steiner, U.; Sommer, M. Fractionated Crystallization of Defect-Free Poly(3-hexylthiophene). *ACS Macro Lett.* **2012**, *1*, 1170–1175.
- (264) Rudenko, A. E.; Wiley, C. A.; Tannaci, J. F.; Thompson, B. C. Optimization of Direct Arylation Polymerization Conditions for the Synthesis of Poly(3-Hexylthiophene). *J. Polym. Sci. Part A Polym. Chem.* **2013**, *51*, 2660–2668.
- (265) Dou, J.; Chen, Z.; Ma, C. Regioregularity and Properties of the Poly(3-hexylthiophene) Synthesized by Palladium Catalyzed Direct C-H Arylation Polycondensation under Different Reaction Conditions. *Synth. Met.*

- 2014**, 196, 117–124.
- (266) Rangel, M.; Güizado-Rodríguez, M.; Maldonado, J. L.; Olayo-Valles, R.; Barba, V.; Reveles, J. U. Eco-Friendly Synthesis of Regioregular Poly(3-hexylthiophene) by Direct Arylation Polymerization: Analysis of the Properties That Determine Its Performance in BHJ Solar Cells. *Polymer (Guildf)*. **2020**, 193, 122348.
- (267) Adachi, T.; Brazard, J.; Ono, R. J.; Hanson, B.; Traub, M. C.; Wu, Z. Q.; Li, Z.; Bolinger, J. C.; Ganesan, V.; Bielawski, C. W.; Vanden Bout, D. A.; Barbara, P. F. Regioregularity and Single Polythiophene Chain Conformation. *J. Phys. Chem. Lett.* **2011**, 2, 1400–1404.
- (268) Bredas, J. L. Mind the Gap! *Mater. Horizons* **2014**, 1, 17–19.
- (269) Rudolf, P. Less Can Be More: Semiconductors. In *Conductors, semiconductors, superconductors: An introduction to solid state physics*; 2014; pp 73–96.
- (270) Brédas, J. L. Relationship between Band Gap and Bond Length Alternation in Organic Conjugated Polymers. *J. Chem. Phys.* **1985**, 82, 3808–3811.
- (271) Kitamura, C.; Tanaka, S.; Yamashita, Y. Design of Narrow-Bandgap Polymers. Syntheses and Properties of Monomers and Polymers Containing Aromatic-Donor and o-Quinoid-Acceptor Units. *Chem. Mater.* **1996**, 8, 570–578.
- (272) Wudl, F.; Kobayashi, M.; Heeger, A. J. Poly(isothianaphthene). *J. Org. Chem.* **1984**, 49, 3382–3384.
- (273) Dell, E. J.; Campos, L. M. The Preparation of Thiophene-S,S-Dioxides and Their Role in Organic Electronics. *J. Mater. Chem.* **2012**, 22, 12945–12952.
- (274) Brisset, H.; Thobie-Gautier, C.; Gorgues, A.; Jubault, M.; Roncali, J. Novel Narrow Bandgap Polymers from Sp³ Carbon-Bridged Bithienyls: Poly(4,4-ethylenedioxy-4H-cyclopenta[2,1-b;3,4-b']dithiophene). *J. Chem. Soc. Chem. Commun.* **1994**, 11, 1305–1306.
- (275) Wang, E.; Wang, L.; Lan, L.; Luo, C.; Zhuang, W.; Peng, J.; Cao, Y. High-Performance Polymer Heterojunction Solar Cells of a Polysilfluorene Derivative. *Appl. Phys. Lett.* **2008**, 92, 90–93.
- (276) Chen, H. Y.; Hou, J.; Hayden, A. E.; Yang, H.; Houk, K. N.; Yang, Y. Silicon Atom Substitution Enhances Interchain Packing in a Thiophene-Based Polymer System. *Adv. Mater.* **2010**, 22, 371–375.
- (277) Sinclair, G. S.; Claridge, R. C. M.; Kukor, A. J.; Hopkins, W. S.; Schipper, D. J. N-Oxide S-O Chalcogen Bonding in Conjugated Materials. *Chem. Sci.* **2021**, 12, 2304–2312.
- (278) Huang, Y.; Huo, L.; Zhang, S.; Guo, X.; Han, C. C.; Li, Y.; Hou, J. Sulfonyl: A New Application of Electron-Withdrawing Substituent in Highly Efficient Photovoltaic Polymer. *Chem. Commun.* **2011**, 47, 8904–8906.
- (279) Chen, H. Y.; Hou, J.; Zhang, S.; Liang, Y.; Yang, G.; Yang, Y.; Yu, L.; Wu, Y.; Li, G. Polymer Solar Cells with Enhanced Open-Circuit Voltage and Efficiency. *Nat. Photonics* **2009**, 3, 649–653.
- (280) Brédas, J. L.; Heeger, A. J. Influence of Donor and Acceptor Substituents on the Electronic Characteristics of Poly(paraphenylene Vinylene) and Poly(paraphenylene). *Chem. Phys. Lett.* **1994**, 217, 507–512.
- (281) Brocks, G.; Tol, A. Small Band Gap Semiconducting Polymers Made from Dye Molecules: Polysquaraines. *J. Phys. Chem.* **1996**, 100, 1838–1846.
- (282) Zhang, Q. T.; Tour, J. M. Alternating Donor/Acceptor Repeat Units in Polythiophenes. Intramolecular Charge Transfer for Reducing Band Gaps in Fully Substituted Conjugated Polymers. *J. Am. Chem. Soc.* **1998**, 120, 5355.

- (283) Hutchison, G. R.; Ratner, M. A.; Marks, T. J. Intermolecular Charge Transfer between Heterocyclic Oligomers. Effects of Heteroatom and Molecular Packing on Hopping Transport in Organic Semiconductors. *J. Am. Chem. Soc.* **2005**, *127*, 16866–16881.
- (284) Martinez, C. R.; Iverson, B. L. Rethinking the Term “Pi-Stacking.” *Chem. Sci.* **2012**, *3*, 2191–2201.
- (285) Steyrlleuthner, R.; Schubert, M.; Howard, I.; Klaumünzer, B.; Schilling, K.; Chen, Z.; Saalfrank, P.; Laquai, F.; Facchetti, A.; Neher, D. Aggregation in a High-Mobility n-Type Low-Bandgap Copolymer with Implications on Semicrystalline Morphology. *J. Am. Chem. Soc.* **2012**, *134*, 18303–18317.
- (286) Hou, J.; Tan, Z.; Yan, Y.; Youjun, H.; Yang, C.; Li, Y. Synthesis and Photovoltaic Properties of Two-Dimensional D-A Copolymers with Conjugated Side Chains. *J. Am. Chem. Soc.* **2006**, *128*, 4911–4916.
- (287) Scharsich, C.; Lohwasser, R. H.; Sommer, M.; Asawapirom, U.; Scherf, U.; Thelakkat, M.; Neher, D.; Köhler, A. Control of Aggregate Formation in Poly(3-hexylthiophene) by Solvent, Molecular Weight, and Synthetic Method. *J. Polym. Sci. Part B Polym. Phys.* **2012**, *50*, 442–453.
- (288) Traiphol, R.; Charoenthai, N.; Sriksirin, T.; Kerdcharoen, T.; Osotchan, T.; Maturros, T. Chain Organization and Photophysics of Conjugated Polymer in Poor Solvents: Aggregates, Agglomerates and Collapsed Coils. *Polymer (Guildf)*. **2007**, *48*, 813–826.
- (289) Perepichka, I. F.; Levillain, E.; Roncali, J. Effect of Substitution of 3,4-Ethylenedioxythiophene (EDOT) on the Electronic Properties of the Derived Electrogenerated Low Band Gap Conjugated Polymers. *J. Mater. Chem.* **2004**, *14*, 1679–1681.
- (290) Mei, J.; Bao, Z. Side Chain Engineering in Solution-Processable Conjugated Polymers. *Chem. Mater.* **2014**, *26*, 604–615.
- (291) Katsouras, A.; Gasparini, N.; Koulogiannis, C.; Spanos, M.; Ameri, T.; Brabec, C. J.; Chochos, C. L.; Avgeropoulos, A. Systematic Analysis of Polymer Molecular Weight Influence on the Organic Photovoltaic Performance. *Macromol. Rapid Commun.* **2015**, *36*, 1778–1797.
- (292) Lu, L.; Zheng, T.; Xu, T.; Zhao, D.; Yu, L. Mechanistic Studies of Effect of Dispersity on the Photovoltaic Performance of PTB7 Polymer Solar Cells. *Chem. Mater.* **2015**, *27*, 537–543.
- (293) Rudenko, A. E.; Thompson, B. C. Optimization of Direct Arylation Polymerization (DAP) through the Identification and Control of Defects in Polymer Structure. *J. Polym. Sci. Part A Polym. Chem.* **2015**, *53*, 135–147.
- (294) Hendriks, K. H.; Li, W.; Heintges, G. H. L.; Van Pruissen, G. W. P.; Wienk, M. M.; Janssen, R. A. J. Homocoupling Defects in Diketopyrrolopyrrole-Based Copolymers and Their Effect on Photovoltaic Performance. *J. Am. Chem. Soc.* **2014**, *136*, 11128–11133.
- (295) Lombeck, F.; Komber, H.; Fazzi, D.; Nava, D.; Kuhlmann, J.; Stegerer, D.; Strassel, K.; Brandt, J.; de Zerio Mendaza, A. D.; Müller, C.; Thiel, W.; Caironi, M.; Friend, R.; Sommer, M. On the Effect of Prevalent Carbazole Homocoupling Defects on the Photovoltaic Performance of PCDTBT:PC71BM Solar Cells. *Adv. Energy Mater.* **2016**, *6*, 1–9.
- (296) Pouliot, J. R.; Grenier, F.; Blaskovits, J. T.; Beaupré, S.; Leclerc, M. Direct (Hetero)Arylation Polymerization: Simplicity for Conjugated Polymer Synthesis. *Chem. Rev.* **2016**, *116*, 14225–14274.
- (297) Ito, T.; Shirakawa, H.; Ikeda, S. Simultaneous Polymerization and Formation of Polyacetylene. *J. Polym. Sci. Polym. Chem. Ed.* **1974**, *12*, 11–19.
- (298) Dieck, A.; Heck, R. F. Organophosphinepalladium Complexes as Catalysts for Vinylic Hydrogen Substitution

- Reactions. *J. Am. Chem. Soc.* **1974**, *96*, 1133–1136.
- (299) Heck, K. F.; Nolley, J. P. Palladium-Catalyzed Vinylic Hydrogen Substitution Reactions with Aryl, Benzyl, and Styryl Halides. *J. Org. Chem.* **1972**, *37*, 2320–2322.
- (300) de Meijere, A.; Diederich, F. *Metal Catalyzed Cross-Couplings*, 2nd ed.; Wiley-VCH, 2004.
- (301) Huo, S.; Mroz, R.; Carroll, J. Negishi Coupling in the Synthesis of Advanced Electronic, Optical, Electrochemical, and Magnetic Materials. *Org. Chem. Front.* **2015**, *2*, 416–445.
- (302) Geng, Y.; Huang, L.; Wu, S.; Wang, F. Kumada Chain-Growth Polycondensation as a Universal Method for Synthesis of Well-Defined Conjugated Polymers. *Sci. China Chem.* **2010**, *53*, 1620–1633.
- (303) McCullough, R. D.; Lowe, R. D.; Jayaraman, M.; Anderson, D. L. Design, Synthesis, and Control of Conducting Polymer Architectures: Homogeneous Poly(3-Alkylthiophene). *J. Org. Chem.* **1993**, *58*, 904–912.
- (304) Bryan, Z. J.; McNeil, A. J. Conjugated Polymer Synthesis via Catalyst-Transfer Polycondensation (CTP): Mechanism, Scope, and Applications. *Macromolecules* **2013**, *46*, 8395–8405.
- (305) Slagt, V. F.; De Vries, A. H. M.; De Vries, J. G.; Kellogg, R. M. Practical Aspects of Carbon–Carbon Cross-Coupling Reactions Using Heteroarenes. *Org. Process Res. Dev.* **2010**, *14*, 30–47.
- (306) Carsten, B.; He, F.; Son, H. J.; Xu, T.; Yu, L. Stille Polycondensation for Synthesis of Functional Materials. *Chem. Rev.* **2011**, *111*, 1493–1528.
- (307) Farina, V. New Perspectives in the Cross-Coupling Reactions of Organostannanes. *Pure Appl. Chem.* **1996**, *68*, 73–78.
- (308) Zhou, D.; Doumon, N. Y.; Abdu-Aguye, M.; Bartesaghi, D.; Loi, M. A.; Koster, L. J. A.; Chiechi, R. C.; Hummelen, J. C. High-Quality Conjugated Polymers via One-Pot Suzuki–Miyaura Homopolymerization. *RSC Adv.* **2017**, *7*, 27762–27769.
- (309) Padalkar, V. S.; Tsutsui, Y.; Sakurai, T.; Sakamaki, D.; Tohnai, N.; Kato, K.; Takata, M.; Akutagawa, T.; Sakai, K. I.; Seki, S. Optical and Structural Properties of ES IPT Inspired HBT-Fluorene Molecular Aggregates and Liquid Crystals. *J. Phys. Chem. B* **2017**, *121*, 10407–10416.
- (310) Yu, L.; Bao, Z.; Cai, R. Conjugated, Liquid Crystalline Polymers. *Angew. Chem. Int. Ed.* **1993**, *32*, 1345–1347.
- (311) Cox, P. A.; Leach, A. G.; Campbell, A. D.; Lloyd-Jones, G. C. Protodeboronation of Heteroaromatic, Vinyl, and Cyclopropyl Boronic Acids: pH-Rate Profiles, Autocatalysis, and Disproportionation. *J. Am. Chem. Soc.* **2016**, *138*, 9145–9157.
- (312) Nielsen, K. T.; Bechgaard, K.; Krebs, F. C. Removal of Palladium Nanoparticles from Polymer Materials. *Macromolecules* **2005**, *38*, 658–659.
- (313) Bura, T.; Blaskovits, J. T.; Leclerc, M. Direct (Hetero)Arylation Polymerization: Trends and Perspectives. *J. Am. Chem. Soc.* **2016**, *138*, 10056–10071.
- (314) Lapointe, D.; Caron, L.; Vlassova, A.; Fagnou, K. Establishment of Broadly Applicable Reaction Conditions for the Palladium-Catalyzed Direct Arylation of Heteroatom-Containing Aromatic Compounds. *J. Org. Chem.* **2009**, *74*, 1826–1834.
- (315) Mercier, L. G.; Leclerc, M. Direct (Hetero) Arylation : A New Tool for Polymer Chemists. *Acc. Chem. Res.* **2013**, *46*, 1597–1605.
- (316) Schipper, D. J.; Fagnou, K. Direct Arylation as a Synthetic Tool for the Synthesis of Thiophene-Based Organic

- Electronic Materials. *Chem. Mater.* **2011**, *23*, 1594–1600.
- (317) Gorelsky, S. I.; Lapointe, D.; Fagnou, K. Analysis of the Palladium-Catalyzed (Aromatic)C – H Bond Metalation – Deprotonation Mechanism Spanning the Entire Spectrum of Arenes. *J. Org. Chem.* **2012**, *77*, 658–668.
- (318) Berrouard, P.; Najari, A.; Pron, A.; Gendron, D.; Morin, O.; Pouliot, J.; Veilleux, J.; Leclerc, M. Synthesis of 5-Alkyl[3,4-c]thienopyrrole-4,6-Dione-Based Polymers by Direct Heteroarylation. *Angew. Chem. Int. Ed.* **2012**, *51*, 2068–2071.
- (319) Wang, Q.; Takita, R.; Kikuzaki, Y.; Ozawa, F. Palladium-Catalyzed Dehydrohalogenative Polycondensation of 2-Bromo-3-Hexylthiophene: An Efficient Approach to Head-to-Tail Poly(3-hexylthiophene). *J. Am. Chem. Soc.* **2010**, *132*, 11420–11421.
- (320) Klemm, D.; Heublein, B.; Fink, H. P.; Bohn, A. Cellulose: Fascinating Biopolymer and Sustainable Raw Material. *Angew. Chem. Int. Ed.* **2005**, *44*, 3358–3393.
- (321) Palmer, R. J. Polyamides, Plastics. *Encycl. Polym. Sci. Technol.* **2001**, *3*, 618–643.
- (322) Mirabal, R. A.; Vanderzwet, L.; Abuadas, S.; Emmett, M. R.; Schipper, D. Dehydration Polymerization for Poly(Hetero)Arene Conjugated Polymers. *Chem. - A Eur. J.* **2018**, *24*, 12231–12235.
- (323) Campeau, L. C.; Stuart, D. R.; Leclerc, J. P.; Bertrand-Laperle, M.; Villemure, E.; Sun, H. Y.; Lasserre, S.; Guimond, N.; Lecavallier, M.; Fagnou, K. Palladium-Catalyzed Direct Arylation of Azine and Azole *N*-Oxides: Reaction Development, Scope and Applications in Synthesis. *J. Am. Chem. Soc.* **2009**, *131*, 3291–3306.
- (324) Campeau, L. C.; Bertrand-Laperle, M.; Leclerc, J. P.; Villemure, E.; Gorelsky, S.; Fagnou, K. C2, C5, and C4 Azole *N*-Oxide Direct Arylation Including Room-Temperature Reactions. *J. Am. Chem. Soc.* **2008**, *130*, 3276–3277.
- (325) Piel, I.; Pawelczyk, M. D.; Hirano, K.; Fröhlich, R.; Glorius, F. A Family of Thiazolium Salt Derived *N*-Heterocyclic Carbenes (NHCs) for Organocatalysis: Synthesis, Investigation and Application in Cross-Benzoin Condensation. *Eur. J. Org. Chem.* **2011**, No. 28, 5475–5484.
- (326) Moreira, R. E.; Sinclair, G. S.; Schipper, D. J. Oxidative Ring-Opening of Benzothiazole Derivatives. *Can. J. Chem.* **2019**, *97*, 360–365.
- (327) Sinclair, G. S.; Kukor, A. J.; Imperial, K. K. G.; Schipper, D. J. Transition-Metal-Free *Ips*o-Arylative Condensation. *Macromolecules* **2020**, *53*, 5169–5176.
- (328) Amir, E.; Rozen, S. Easy Access to the Family of Thiazole *N*-Oxides Using HOF·CH₃CN. *Chem. Commun.* **2006**, No. 21, 2262–2264.
- (329) Pearson, D. L.; Schumm, J. S.; Tour, J. M. Iterative Divergent/Convergent Approach. *Macromolecules* **1994**, *27*, 2348–2350.
- (330) Abuadas, S. Synthesis of Molecularly Defined Conjugated Oligomers and Polymers through Dehydrative Coupling, University of Waterloo, 2019.
- (331) Guo, Q.; Jiang, R.; Wu, D.; You, J. Rapid Access to 2,2' -Bithiazole-Based Copolymers via Sequential Palladium-Catalyzed C – H / C – X and C – H / C – H Coupling Reactions. *Macromol. Rapid Commun.* **2016**, *37*, 794–798.
- (332) Rudin, A.; Choi, P. *Step-Growth Polymerizations*, 3rd ed.; Elsevier Inc., 2013.
- (333) Wei, S.; Xia, J.; Dell, E. J.; Jiang, Y.; Song, R.; Lee, H.; Rodenbough, P.; Briseno, A. L.; Campos, L. M. Bandgap Engineering through Controlled Oxidation of Polythiophenes. *Angew. Chem. Int. Ed.* **2014**, *53*, 1832–1836.
- (334) Sévignon, M.; Papillon, J.; Schulz, E.; Lemaire, M. New Synthetic Method for the Polymerization of

- Alkylthiophenes. *Tetrahedron Lett.* **1999**, *40*, 5873–5876.
- (335) Alberico, D.; Scott, M. E.; Lautens, M. Aryl-Aryl Bond Formation by Transition-Metal-Catalyzed Direct Arylation. *Chem. Rev.* **2007**, *107*, 174–238.
- (336) Wakioka, M.; Kitano, Y.; Ozawa, F. A Highly Efficient Catalytic System for Polycondensation of 2,7-Dibromo-9,9-Dioctylfluorene and 1,2,4,5-Tetrafluorobenzene via Direct Arylation. *Macromolecules* **2013**, *46*, 370–374.
- (337) Lu, W.; Kuwabara, J.; Kanbara, T. Polycondensation of Dibromofluorene Analogues with Tetrafluorobenzene via Direct Arylation. *Macromolecules* **2011**, *44*, 1252–1255.
- (338) Kowalski, S.; Allard, S.; Scherf, U. Synthesis of Poly(4,4-Dialkyl-cyclopenta[2,1-*b*:3,4-*b'*]dithiophene-Alt-2,1,3-Benzothiadiazole) (PCPDTBT) in a Direct Arylation Scheme. *ACS Macro Lett.* **2012**, *1*, 465–468.
- (339) Roger, J.; Požgan, F.; Doucet, H. Ligand-Free Palladium-Catalyzed Direct Arylation of Thiazoles at Low Catalyst Loadings. *J. Org. Chem.* **2009**, *74*, 1179–1186.
- (340) Matsidik, R.; Komber, H.; Luzio, A.; Caironi, M.; Sommer, M. Defect-Free Naphthalene Diimide Bithiophene Copolymers with Controlled Molar Mass and High Performance via Direct Arylation Polycondensation. *J. Am. Chem. Soc.* **2015**, *137*, 6705–6711.
- (341) Ackermann, L. Carboxylate-Assisted Transition-Metal-Catalyzed C-H Bond Functionalizations: Mechanism and Scope. *Chem. Rev.* **2011**, *111*, 1315–1345.
- (342) Tan, Y.; Hartwig, J. F. Assessment of the Intermediacy of Arylpalladium Carboxylate Complexes in the Direct Arylation of Benzene: Evidence for C-H Bond Cleavage by “Ligandless” Species. *J. Am. Chem. Soc.* **2011**, *133*, 3308–3311.
- (343) Rudenko, A. E.; Wiley, C. A.; Stone, S. M.; Tannaci, J. F.; Thompson, B. C. Semi-Random P3HT Analogs via Direct Arylation Polymerization. *J. Polym. Sci. Part A Polym. Chem.* **2012**, *50*, 3691–3697.
- (344) Kuwabara, J.; Sakai, M.; Zhang, Q.; Kanbara, T. Mechanistic Studies and Optimisation of a Pd-Catalysed Direct Arylation Reaction Using Phosphine-Free Systems. *Org. Chem. Front.* **2015**, *2*, 520–525.
- (345) Iizuka, E.; Wakioka, M.; Ozawa, F. Mixed-Ligand Approach to Palladium-Catalyzed Direct Arylation Polymerization: Synthesis of Donor-Acceptor Polymers with Dithienosilole (DTS) and Thienopyrroledione (TPD) Units. *Macromolecules* **2015**, *48*, 2989–2993.
- (346) Wakioka, M.; Yamashita, N.; Mori, H.; Nishihara, Y.; Ozawa, F. Synthesis of a 1,2-Dithienylethene-Containing Donor-Acceptor Polymer via Palladium-Catalyzed Direct Arylation Polymerization (DARp). *Molecules* **2018**, *23*, 981.
- (347) Wakioka, M.; Morita, H.; Ichihara, N.; Saito, M.; Osaka, I.; Ozawa, F. Mixed-Ligand Approach to Palladium-Catalyzed Direct Arylation Polymerization: Synthesis of Donor-Acceptor Polymers Containing Unsubstituted Bithiophene Units. *Macromolecules* **2020**, *53*, 158–164.
- (348) Calò, V.; Nacci, A.; Monopoli, A.; Cotugno, P. Palladium-Nanoparticle-Catalysed Ullmann Reactions in Ionic Liquids with Aldehydes as the Reductants: Scope and Mechanism. *Chem. Eur. J.* **2009**, *15*, 1272–1279.
- (349) Grushin, V. V.; Marshall, W. J. Trans -Difluoro Complexes of Palladium (II). *J. Am. Chem. Soc.* **2009**, *131*, 918–919.
- (350) Yagyu, T.; Hamada, M.; Osakada, K.; Yamamoto, T. Cationic Arylpalladium Complexes with Chelating Diamine Ligands, [PdAr(N-N)(Solv)]BF₄(N-N = N,N,N',N'- Tetramethylethylenediamine, 2,2'-Bipyridine, 4,4'-Dimethyl-

- 2,2'-Bipyridine). Preparation, Intermolecular Coupling of the Aryl Ligands, and Insertion. *Organometallics* **2001**, *20*, 1087–1101.
- (351) Remy, M. S.; Cundari, T. R.; Sanford, M. S. Computational and Experimental Studies of Methyl Group Exchange between Palladium(II) Centers. *Organometallics* **2010**, *29*, 1522–1525.
- (352) Suzuki, Y.; Osakada, K. Cyclization of Dinuclear Aryl- and Arylpalladium Complexes with the Metal Centers Tethered by an Oligo(ethylene oxide)Chain. Intramolecular Transmetalation of the Cationic Dinuclear Arylpalladium Complexes. *Organometallics* **2003**, *22*, 2193–2195.
- (353) Kohn, P.; Huettner, S.; Komber, H.; Senkovskyy, V.; Tkachov, R.; Kiriya, A.; Friend, R. H.; Steiner, U.; Huck, W. T. S.; Sommer, J. U.; Sommer, M. On the Role of Single Regiodefects and Polydispersity in Regioregular Poly(3-hexylthiophene): Defect Distribution, Synthesis of Defect-Free Chains, and a Simple Model for the Determination of Crystallinity. *J. Am. Chem. Soc.* **2012**, *134*, 4790–4805.
- (354) Rahimi, K.; Botiz, I.; Agumba, J. O.; Motamen, S.; Stingelin, N.; Reiter, G. Light Absorption of Poly(3-hexylthiophene) Single Crystals. *RSC Adv.* **2014**, *4*, 11121–11123.
- (355) Woo, C. H.; Thompson, B. C.; Kim, B. J.; Toney, M. F.; Fréchet, J. M. J. The Influence of Poly(3-hexylthiophene) Regioregularity on Fullerene-Composite Solar Cell Performance. *J. Am. Chem. Soc.* **2008**, *130*, 16324–16329.
- (356) Poelking, C.; Andrienko, D. Effect of Polymorphism, Regioregularity and Paracrystallinity on Charge Transport in Poly(3-hexylthiophene) [P3HT] Nanofibers. *Macromolecules* **2013**, *46*, 8941–8956.
- (357) Sivaraman, P.; Mishra, S. P.; Bhattacharyya, A. R.; Thakur, A.; Shashidhara, K.; Samui, A. B. Effect of Regioregularity on Specific Capacitance of Poly(3-hexylthiophene). *Electrochim. Acta* **2012**, *69*, 134–138.
- (358) Mauer, R.; Kastler, M.; Laquai, F. The Impact of Polymer Regioregularity on Charge Transport and Efficiency of P3HT:PCBM Photovoltaic Devices. *Adv. Funct. Mater.* **2010**, *20*, 2085–2092.
- (359) Hendriks, K. H.; Li, W.; Heintges, G. H. L.; Pruisen, G. W. P. Van; Wienk, M. M.; Janssen, R. A. J. Homocoupling Defects in Diketopyrrolopyrrole-Based Copolymers and Their Effect on Photovoltaic Performance. *J. Am. Chem. Soc.* **2014**, *136*, 11128–11133.
- (360) Lombeck, F.; Komber, H.; Gorelsky, S. I.; Sommer, M. Identifying Homocouplings as Critical Side Reactions in Direct Arylation Polycondensation. *ACS Macro Lett.* **2014**, *3*, 819–823.
- (361) Okamoto, K.; Housekeeper, J. B.; Michael, E.; Luscombe, C. K. Polymer Chemistry Branching Using Direct Arylation Methods. *Polym. Chem.* **2013**, *4*, 3499–3506.
- (362) Fujinami, Y.; Kuwabara, J.; Lu, W.; Hayashi, H.; Kanbara, T. Synthesis of Thiophene- and Bithiophene-Based Alternating Copolymers via Pd-Catalyzed Direct C – H Arylation. *ACS Macro Lett.* **2012**, *1*, 67–70.
- (363) Gurau, M. C.; Delongchamp, D. M.; Vogel, B. M.; Lin, E. K.; Fischer, D. A.; Sambasivan, S.; Richter, L. J. Measuring Molecular Order in Poly(3-alkylthiophene)Thin Films with Polarizing Spectroscopies. *Langmuir* **2007**, *23*, 834–842.
- (364) Zagórska, M.; Krische, B. Chemical Synthesis and Characterization of Soluble Poly(4,4'-dialkyl-2,2'-bithiophenes). *Polymer (Guildf)*. **1990**, *31*, 1379–1383.
- (365) Dudnik, A. S.; Aldrich, T. J.; Eastham, N. D.; Chang, R. P. H.; Facchetti, A.; Marks, T. J. Tin-Free Direct C-H Arylation Polymerization for High Photovoltaic Efficiency Conjugated Copolymers. *J. Am. Chem. Soc.* **2016**, *138*, 15699–15709.
- (366) Bura, T.; Beaupré, S.; Légaré, M. A.; Quinn, J.; Rochette, E.; Blaskovits, J. T.; Fontaine, F. G.; Pron, A.; Li, Y.;

- Leclerc, M. Direct Heteroarylation Polymerization: Guidelines for Defect-Free Conjugated Polymers. *Chem. Sci.* **2017**, *8*, 3913–3925.
- (367) Lu, W.; Kuwabara, J.; Kanbara, T. Synthesis of π -Conjugated Polymer Consisting of Pyrrole and Fluorene Units by Ru-Catalyzed Site-Selective Direct Arylation Polycondensation. *Macromol. Rapid Commun.* **2013**, *34*, 1151–1156.
- (368) Nakabayashi, K.; Mori, H. Palladium-Catalyzed Direct Arylation Approach to Synthesize Naphthalene Bisimide-Based Low-Band-Gap Polymers. *Chem. Lett.* **2013**, *42*, 717–718.
- (369) Yamazaki, K.; Kuwabara, J.; Kanbara, T. Detailed Optimization of Polycondensation Reaction via Direct C-H Arylation of Ethylenedioxythiophene. *Macromol. Rapid Commun.* **2013**, *34*, 69–73.
- (370) Wang, Q.; Zhang, B.; Liu, L.; Chen, Y.; Qu, Y.; Zhang, X.; Yang, J.; Xie, Z.; Geng, Y.; Wang, L.; Wang, F. Effect of End Groups on Optoelectronic Properties of Poly(9,9-dioctylfluorene): A Study with Hexadecylfluorenes as Model Polymers. *J. Phys. Chem. C* **2012**, *116*, 21727–21733.
- (371) Wakioka, M.; Ichihara, N.; Kitano, Y.; Ozawa, F. A Highly Efficient Catalyst for the Synthesis of Alternating Copolymers with Thieno[3,4-c]Pyrrole-4,6-Dione Units via Direct Arylation Polymerization. *Macromolecules* **2014**, *47*, 626–631.
- (372) Krebs, F. C.; Nyberg, R. B.; Jørgensen, M. Influence of Residual Catalyst on the Properties of Conjugated Polyphenylenevinylene Materials: Palladium Nanoparticles and Poor Electrical Performance. *Chem. Mater.* **2004**, *16*, 1313–1318.
- (373) Estrada, L. A.; Deininger, J. J.; Kamenov, G. D.; Reynolds, J. R. Direct (Hetero)arylation Polymerization: An Effective Route to 3,4-Propylenedioxythiophene-Based Polymers with Low Residual Metal Content. *ACS Macro Lett.* **2013**, *2*, 869–873.
- (374) Kuwabara, J.; Yasuda, T.; Choi, S. J.; Lu, W.; Yamazaki, K.; Kagaya, S.; Han, L.; Kanbara, T. Direct Arylation Polycondensation: A Promising Method for the Synthesis of Highly Pure, High-Molecular-Weight Conjugated Polymers Needed for Improving the Performance of Organic Photovoltaics. *Adv. Funct. Mater.* **2014**, *24*, 3226–3233.
- (375) Mercier, L. G.; Aich, B. R.; Najari, A.; Beaupré, S.; Berrouard, P.; Pron, A.; Robitaille, A.; Tao, Y.; Leclerc, M. Direct Heteroarylation of β -Protected Dithienosilole and Dithienogermole Monomers with Thieno[3,4-c]Pyrrole-4,6-Dione and Furo[3,4-c]Pyrrole-4,6-Dione. *Polym. Chem.* **2013**, *4*, 5252–5260.
- (376) Gildner, P. G.; Colacot, T. J. Reactions of the 21st Century: Two Decades of Innovative Catalyst Design for Palladium-Catalyzed Cross-Couplings. *Organometallics* **2015**, *34*, 5497–5508.
- (377) Balcells, D.; Nova, A. Designing Pd and Ni Catalysts for Cross-Coupling Reactions by Minimizing Off-Cycle Species. *ACS Catal.* **2018**, *8*, 3499–3515.
- (378) Dudnik, A. S.; Aldrich, T. J.; Eastham, N. D.; Chang, R. P. H.; Facchetti, A.; Marks, T. J. Tin-Free Direct C – H Arylation Polymerization for High Photovoltaic Efficiency Conjugated Copolymers. *J. Am. Chem. Soc.* **2016**, *138*, 15699–15709.
- (379) Lee, J. A.; Luscombe, C. K. Dual-Catalytic Ag-Pd System for Direct Arylation Polymerization to Synthesize Poly(3-hexylthiophene). *ACS Macro Lett.* **2018**, *7*, 767–771.
- (380) Suraru, S.; Lee, J. A.; Luscombe, C. K. Preparation of an Arylated Alkylthiophene Monomer via C – H Activation for Use in Pd-PEPPSI-IPr Catalyzed-Controlled Chain Growth Polymerization. *ACS Macro Lett.* **2016**, *5*, 533–536.

- (381) Lee, Y.; Gomez, E. D. Challenges and Opportunities in the Development of Conjugated Block Copolymers for Photovoltaics. *Macromolecules* **2015**, *48*, 7385–7395.
- (382) Bruno, N. C.; Tudge, T.; Buchwald, S. L. Design and Preparation of New Palladium Precatalysts for C–C and C–N Cross-Coupling Reactions. *Chem. Sci.* **2013**, *4*, 916–920.
- (383) Cong, M.; Fan, Y.; Raimundo, J.-M.; Tang, J.; Peng, L. Pd(Dba)₂ vs Pd₂(Dba)₃: An in-Depth Comparison of Catalytic Reactivity and Mechanism via Mixed-Ligand Promoted C–N and C–S Coupling Reactions. *Org. Lett.* **2005**, *16*, 4074–4077.
- (384) Zalesskiy, S. S.; Ananikov, V. P. Pd₂(Dba)₃ as a Precursor of Soluble Metal Complexes and Nanoparticles: Determination of Palladium Active Species for Catalysis and Synthesis. *Organometallics* **2012**, *31*, 2302–2309.
- (385) Carole, W. A.; Bradley, J.; Sarwar, M.; Colacot, T. J. Can Palladium Acetate Lose Its “Saltiness”? Catalytic Activities of the Impurities in Palladium Acetate. *Org. Lett.* **2015**, *17*, 5472–5475.
- (386) Bruneau, A.; Roche, M.; Alami, M.; Messaoudi, S. 2-Aminobiphenyl Palladacycles: The “Most Powerful” Precatalysts in C-C and C-Heteroatom Cross-Couplings. *ACS Catal.* **2015**, *5*, 1386–1396.
- (387) Hameury, S.; Kunz, S.; Sommer, M. Expanding the Scope of Electron-Deficient C–H Building Blocks: Direct Arylation of Pyromellitic Acid Diimide. *ACS Omega* **2017**, *2*, 2483–2488.
- (388) Chen, X.; Ichige, A.; Chen, J.; Fukushima, I.; Kuwabara, J.; Kanbara, T. Facile Access to Conjugated Polymers under Aerobic Conditions via Pd-Catalyzed Direct Arylation and Aryl Amination Polycondensation. *Polymer (Guildf)*. **2020**, *207*, 122927.
- (389) Mirabal, R. A.; Buratynski, J. A.; Schipper, D. J. Design of Palladium Precatalysts for Direct(Hetero)Arylation Polymerization. *Manuscr. Prep.* **2021**.
- (390) Matthews, J. R.; Niu, W.; Tandia, A.; Wallace, A. L.; Hu, J.; Lee, W. Y.; Giri, G.; Mannsfeld, S. C. B.; Xie, Y.; Cai, S.; et al. Scalable Synthesis of Fused Thiophene-Diketopyrrolopyrrole Semiconducting Polymers Processed from Non-chlorinated Solvents into High Performance Thin Film Transistors. *Chem. Mater.* **2013**, *25*, 782–789.
- (391) Matsidik, R.; Komber, H.; Luzio, A.; Caironi, M.; Sommer, M. Defect-Free Naphthalene Diimide Bithiophene Copolymers with Controlled Molar Mass and High Performance via Direct Arylation Polycondensation. *J. Am. Chem. Soc.* **2015**, *137*, 6705–6711.
- (392) Kissel, P.; Murray, D. J.; Wulftange, W. J.; Catalano, V. J.; King, B. T. A Nanoporous Two-Dimensional Polymer by Single-Crystal-to-Single-Crystal Photopolymerization. *Nat. Chem.* **2014**, *6*, 774–778.
- (393) Mailley, P.; Cosnier, S.; Coche-Guérente, L. Amperometric Glucose Biosensors Based on Composite Polymeric Structures to Prevent Interferences. *Anal. Lett.* **2000**, *33*, 1733–1753.
- (394) Zhu, W.; Tao, S.; Tao, C. A.; Li, W.; Lin, C.; Li, M.; Wen, Y.; Li, G. Hierarchically Imprinted Porous Films for Rapid and Selective Detection of Explosives. *Langmuir* **2011**, *27*, 8451–8457.
- (395) Zou, W.; Chen, C. Influence of Backbone Substituents on the Ethylene (Co)Polymerization Properties of α -Diimine Pd(II) and Ni(II) Catalysts. *Organometallics* **2016**, *35* (11), 1794–1801.
- (396) Pavlicek, N.; Schuler, B.; Collazos, S.; Moll, N.; Pérez, D.; Guitián, E.; Meyer, G.; Peña, D.; Gross, L. On-Surface Generation and Imaging of Arynes by Atomic Force Microscopy. *Nat. Chem.* **2015**, *7*, 623–628.
- (397) Chan, S.; Yick, C.; Wong, H. N. C. 5, 6-Bis (Trimethylsilyl)Benzo[c] Furan : An Isolable Versatile Building Block

- for Linear Polycyclic Aromatic Compounds. *Tetrahedron* **2002**, *58*, 9413–9422.
- (398) Atkinson, E. R.; Lawler, H. J. Diphenic Acid. *Org. Synth.* **1927**, *7*, 30.
- (399) Su, X.; Fox, D. J.; Blackwell, D. T.; Tanaka, K.; Spring, D. R. Copper Catalyzed Oxidation of Organozinc Halides. *Chem. Commun.* **2006**, 3883–3885.
- (400) Günther, M.; Lategahn, J.; Juchum, M.; Döring, E.; Keul, M.; Engel, J.; Tumbrink, H. L.; Rauh, D.; Laufer, S. Trisubstituted Pyridinylimidazoles as Potent Inhibitors of the Clinically Resistant L858R/T790M/C797S EGFR Mutant: Targeting of Both Hydrophobic Regions and the Phosphate Binding Site. *J. Med. Chem.* **2017**, *60*, 5613–5637.
- (401) Voss, J.; Sarafidis, A.; Sawluk, A.; Schmidt, G.; Adiwidjaja, G. Preparation of New Dialkyl Benzene-, Biphenyl-, and Naphthalene-Bis(α -Oxoethanedithioates). *Phosphorus, Sulfur Silicon Relat. Elem.* **2010**, *185*, 2249–2276.
- (402) Zheng, L.; Zhou, B.; Jin, H.; Li, T.; Liu, Y. Radical-Triggered Tandem Cyclization of 1,6-Enynes with H₂O: A Way to Access Strained 1 H-Cyclopropa[b]Naphthalene-2,7-Diones. *Org. Lett.* **2018**, *20*, 7053–7056.
- (403) Schröder, N.; Wencel-Delord, J.; Glorius, F. High-Yielding, Versatile, and Practical [Rh(III)Cp*]-Catalyzed Ortho Bromination and Iodination of Arenes. *J. Am. Chem. Soc.* **2012**, *134*, 8298–8301.
- (404) Chang, M. Y.; Tsai, Y. L.; Chen, H. Y. CuBr₂-Mediated One-Pot Synthesis of Sulfonyl 9-Fluorenylidenes. *J. Org. Chem.* **2020**, *85*, 6897–6909.
- (405) Sapountzis, I.; Lin, W.; Kofink, C. C.; Despotopoulou, C.; Knochel, P. Iron-Catalyzed Aryl-Aryl Cross-Couplings with Magnesium-Derived Copper Reagents. *Angew. Chem. Int. Ed.* **2005**, *44*, 1654–1658.
- (406) Lin, S. zheng; You, T. pa. An Efficient One-Pot Approach to Phenanthrene Derivatives Using a Catalyzed Tandem Ullmann-Pinacol Coupling Reaction. *Tetrahedron* **2008**, *64*, 9906–9910.
- (407) Segawa, Y.; Yagi, A.; Ito, H.; Itami, K. A Theoretical Study on the Strain Energy of Carbon Nanobelts. *Org. Lett.* **2016**, *18*, 1430–1433.
- (408) Toda, Y.; Gomyou, S.; Tanaka, S.; Komiyama, Y.; Kikuchi, A.; Suga, H. Tetraarylphosphonium Salt-Catalyzed Synthesis of Oxazolidinones from Isocyanates and Epoxides. *Org. Lett.* **2017**, *19*, 5786–5789.
- (409) Ha, S.; Lee, Y.; Kwak, Y.; Mishra, A.; Yu, E.; Ryou, B.; Park, C. M. Alkyne–Alkene [2+2] Cycloaddition Based on Visible Light Photocatalysis. *Nat. Commun.* **2020**, *11*, 1–12.
- (410) Guo, X.; Fan, H.; Zhang, M.; Huang, Y.; Tan, S.; Li, Y. Synthesis and Characterizations of Poly(4-alkylthiazole Vinylene) Xia. *J. Appl. Polym. Sci.* **2011**, *124*, 847–854.
- (411) Guo, Q.; Wu, D.; You, J. Oxidative Direct Arylation Polymerization Using Oxygen as the Sole Oxidant: Facile, Green Access to Bithiazole-Based Polymers. *ChemSusChem* **2016**, *9*, 2765–2768.
- (412) Lapointe, D.; Markiewicz, T.; Whipp, C. J.; Toderian, A.; Fagnou, K. Predictable and Site-Selective Functionalization of Poly(hetero)arene Compounds by Palladium Catalysis. *J. Org. Chem.* **2011**, *76*, 749–759.
- (413) Primas, N.; Bouillon, A.; Lancelot, J. C.; El-Kashef, H.; Rault, S. Synthesis of 5-Arylthiazoles. Comparative Study between Suzuki Cross-Coupling Reaction and Direct Arylation. *Tetrahedron* **2009**, *65*, 5739–5746.
- (414) Liu, X. W.; Shi, J. L.; Yan, J. X.; Wei, J. B.; Peng, K.; Dai, L.; Li, C. G.; Wang, B. Q.; Shi, Z. J. Regioselective Arylation of Thiazole Derivatives at 5-Position via Pd Catalysis under Ligand-Free Conditions. *Org. Lett.* **2013**, *15*, 5774–5777.

- (415) Forgione, P.; Brochu, M. C.; St.-Onge, M.; Thesen, K. H.; Bailey, M. D.; Bilodeau, F. Unexpected Intermolecular Pd-Catalyzed Cross-Coupling Reaction Employing Heteroaromatic Carboxylic Acids as Coupling Partners. *J. Am. Chem. Soc.* **2006**, *128*, 11350–11351.

APPENDIX-CARTESIAN COORDINATES FOR COMPOUNDS IN COMPUTATIONAL STUDY

Table S16- Cartesian coordinates for [10]pyrenecyclacene

0 1

C	-5.60442901	0.84775668	2.53261450
C	-5.27667801	0.86085168	1.17159950
C	-5.26310601	-0.36489632	0.46321950
C	-5.27667801	-1.59064432	1.17159950
C	-5.60442901	-1.57754932	2.53261450
C	-5.82506701	-0.36489632	3.18931250
C	-5.26310601	-0.36489632	-0.98921050
C	-5.27667801	-1.59064432	-1.69759050
C	-4.66138001	-2.72784632	-0.98656650
C	-4.66138001	-2.72784632	0.46057550
C	-4.66138001	1.99805368	0.46057550
C	-4.66138001	1.99805368	-0.98656650
C	-5.27667801	0.86085168	-1.69759050
C	-5.60442901	0.84775668	-3.05860550
C	-5.82506701	-0.36489632	-3.71530350
C	-5.60442901	-1.57754932	-3.05860550
C	-3.76515501	-3.53459832	-1.66422950
C	-2.65670301	-4.12112232	-0.98503450
C	-2.65670301	-4.12112232	0.45904350
C	-3.76515501	-3.53459832	1.13823850
C	-1.44046801	-4.28913632	-1.66934550
C	-0.22423301	-4.12112232	-0.98503450
C	-0.22423301	-4.12112232	0.45904350
C	-1.44046801	-4.28913632	1.14335450
C	-3.76515501	2.80480568	1.13823850

C	-2.65670301	3.39132968	0.45904350
C	-2.65670301	3.39132968	-0.98503450
C	-3.76515501	2.80480568	-1.66422950
C	-1.44046801	3.55934368	1.14335450
C	-0.22423301	3.39132968	0.45904350
C	-0.22423301	3.39132968	-0.98503450
C	-1.44046801	3.55934368	-1.66934550
C	2.72349299	0.84775668	2.53261450
C	2.39574199	0.86085168	1.17159950
C	2.38216999	-0.36489632	0.46321950
C	2.39574199	-1.59064432	1.17159950
C	2.72349299	-1.57754932	2.53261450
C	2.94413099	-0.36489632	3.18931250
C	2.38216999	-0.36489632	-0.98921050
C	2.39574199	-1.59064432	-1.69759050
C	1.78044399	-2.72784632	-0.98656650
C	1.78044399	-2.72784632	0.46057550
C	1.78044399	1.99805368	0.46057550
C	1.78044399	1.99805368	-0.98656650
C	2.39574199	0.86085168	-1.69759050
C	2.72349299	0.84775668	-3.05860550
C	2.94413099	-0.36489632	-3.71530350
C	2.72349299	-1.57754932	-3.05860550
C	0.88421899	-3.53459832	-1.66422950
C	0.88421899	-3.53459832	1.13823850
C	0.88421899	2.80480568	1.13823850
C	0.88421899	2.80480568	-1.66422950
H	-5.67130001	1.78359668	3.08038950
H	-5.67130001	-2.51338932	3.08038950

H	-5.67130001	1.78359668	-3.60638050
H	-5.67130001	-2.51338932	-3.60638050
H	-3.70866501	-3.46782832	-2.74693350
H	-3.70866501	-3.46782832	2.22094250
H	-1.44046801	-4.23643932	-2.75608750
H	-1.44046801	-4.23643932	2.23009650
H	-3.70866501	2.73803568	2.22094250
H	-3.70866501	2.73803568	-2.74693350
H	-1.44046801	3.50664668	2.23009650
H	-1.44046801	3.50664668	-2.75608750
H	2.79036399	1.78359668	3.08038950
H	2.79036399	-2.51338932	3.08038950
H	2.79036399	1.78359668	-3.60638050
H	2.79036399	-2.51338932	-3.60638050
H	0.82772899	-3.46782832	-2.74693350
H	0.82772899	-3.46782832	2.22094250
H	0.82772899	2.73803568	2.22094250
H	0.82772899	2.73803568	-2.74693350
H	3.22958099	-0.36489632	4.23768850
H	-6.11051701	-0.36489632	4.23768850
H	-6.11051701	-0.36489632	-4.76367950
H	3.22958099	-0.36489632	-4.76367950

Table S17- Cartesian coordinates for [15]pyrenecyclacene

0 1

C	-6.01691400	0.41945900	-1.43516100
C	-5.81248300	-0.79102400	-0.72684000
C	-5.68595700	-2.01210500	-1.43516700
C	-6.00269900	-2.03772600	-2.79960200
C	-6.36550100	-0.86629400	-3.46278500

C	-5.81247800	-0.79102600	0.72687500
C	-5.68594700	-2.01210700	1.43519900
C	-5.05911000	-3.13691200	0.72378500
C	-5.05911500	-3.13691100	-0.72375900
C	-5.71345300	1.67087900	-0.72375100
C	-5.71344800	1.67087800	0.72378900
C	-6.01690400	0.41945700	1.43519900
C	-6.32899700	0.35948400	2.79963400
C	-6.36547800	-0.86630000	3.46282300
C	-6.00268100	-2.03773000	2.79963600
C	-4.25951200	-4.03864900	1.39955500
C	-3.29932300	-4.84088400	0.72261300
C	-3.29932700	-4.84088200	-0.72260200
C	-4.25952000	-4.03864600	-1.39953500
C	-2.20877300	-5.39834700	1.40654700
C	-1.04007400	-5.76466600	0.72260800
C	-1.04007800	-5.76466400	-0.72261200
C	-2.20878100	-5.39834300	-1.40654300
C	0.20711500	-5.86508400	1.39954300
C	1.40944100	-5.78223500	0.72376000
C	1.40943600	-5.78223400	-0.72377900
C	0.20710600	-5.86508100	-1.39955400
C	2.64495200	-5.41943700	1.43517200
C	3.59121800	-4.63735600	0.72684400
C	3.59121400	-4.63735500	-0.72687400
C	2.64494400	-5.41943500	-1.43519700
C	4.58568000	-3.91757100	-1.43519300
C	4.76618400	-4.17915800	-2.79962600
C	3.93282300	-5.07882500	-3.46280500

C	2.85286400	-5.65980800	-2.79962100
C	4.58568900	-3.91757300	1.43515800
C	5.24668200	-2.81247000	0.72375600
C	5.24667800	-2.81246900	-0.72379200
C	2.85288100	-5.65981200	2.79959500
C	3.93284400	-5.07883000	3.46277300
C	4.76620000	-4.17916300	2.79959000
C	5.62803700	-1.66921000	1.39952100
C	5.84297900	-0.43658900	0.72259100
C	5.84297400	-0.43658800	-0.72262700
C	5.62802900	-1.66920800	-1.39955800
C	5.78061100	0.78659500	1.40651900
C	5.51351200	1.98188700	0.72259300
C	5.51350800	1.98188800	-0.72262300
C	5.78060300	0.78659700	-1.40655200
C	4.97674600	3.11212800	1.39952700
C	4.30367300	4.11184800	0.72376000
C	4.30366900	4.11185000	-0.72377900
C	4.97673800	3.11213100	-1.39955200
C	3.37154200	5.00025800	1.43518100
C	2.22100300	5.42842200	0.72685500
C	2.22099900	5.42842300	-0.72686000
C	3.37153300	5.00026000	-1.43519300
C	1.10022900	5.92933900	1.43518300
C	-0.18730200	5.94887300	0.72377500
C	-0.18730600	5.94887400	-0.72376500
C	1.10022100	5.92934100	-1.43518000
C	1.23638500	6.21647300	-2.79961900
C	2.43225600	5.94493100	-3.46282900

C	3.47559500	5.30047800	-2.79964300
C	3.47561200	5.30047400	2.79963100
C	2.43227700	5.94492500	3.46282400
C	1.23640200	6.21646900	2.79962100
C	-1.36804600	5.70741400	1.39955500
C	-2.54301400	5.27729100	0.72262100
C	-2.54301800	5.27729200	-0.72259800
C	-1.36805500	5.70741600	-1.39953700
C	-3.57126300	4.61190100	1.40655700
C	-4.47313600	3.78323700	0.72262500
C	-4.47314100	3.78323800	-0.72259200
C	-3.57127200	4.61190300	-1.40652800
C	-5.18394200	2.75351700	-1.39952100
C	-5.18393300	2.75351500	1.39955700
H	-6.55151600	1.27325800	-3.34242600
H	-5.97284800	-2.97772800	-3.34242500
H	-6.64135800	-0.90384200	-4.51297800
H	-6.55149300	1.27325300	3.34246900
H	-6.64132900	-0.90384900	4.51301800
H	-5.97282700	-2.97773300	3.34245700
H	-4.19914500	-3.99435100	2.48304200
H	-4.19916000	-3.99434600	-2.48302300
H	-2.19482300	-5.36425200	2.49402400
H	-2.19483800	-5.36424600	-2.49402000
H	0.19510800	-5.79125500	2.48303800
H	0.19509400	-5.79125000	-2.48305000
H	5.56549600	-3.68358400	-3.34245100
H	4.10323300	-5.29904200	-4.51298500
H	2.17261600	-6.30924600	-3.34243600

H	2.17263600	-6.30925100	3.34241200
H	4.10326000	-5.29905000	4.51295100
H	5.56551600	-3.68358900	3.34241100
H	5.55944200	-1.63905700	2.48300600
H	5.55942700	-1.63905300	-2.48304300
H	5.74403200	0.78160900	2.49399200
H	5.74401700	0.78161400	-2.49402500
H	4.91876300	3.06478100	2.48301400
H	4.91874900	3.06478500	-2.48303900
H	0.40740700	6.66064500	-3.34244300
H	2.53765200	6.20261100	-4.51302200
H	4.37820000	5.03630800	-3.34247600
H	4.37822100	5.03630300	3.34245800
H	2.53768000	6.20260400	4.51301600
H	0.40742700	6.66063900	3.34245200
H	-1.35990400	5.63306000	2.48304900
H	-1.35991900	5.63306300	-2.48303200
H	-3.54868600	4.58272800	2.49403200
H	-3.54870100	4.58273100	-2.49400300
H	-5.11397500	2.72697900	-2.48301400
H	-5.11396000	2.72697700	2.48304900
C	-6.32901600	0.35948900	-2.79959400

Table S18- Cartesian coordinates for [20]pyrenecyclacene.

0 1

C	7.77460400	-0.86875700	1.39804900
C	7.77460400	-0.86875800	-1.39805000
C	4.00247800	-7.28398400	-2.80423000
C	3.91501400	-6.99235800	-1.43621200
C	2.74745700	-7.37512700	-0.72736500

C	1.61397600	-7.84939600	-1.43621500
C	1.73856500	-8.12719500	-2.80422800
C	2.93584300	-7.88097900	-3.47185800
C	2.74745800	-7.37512700	0.72736600
C	1.61397600	-7.84939600	1.43621700
C	0.32955500	-7.90921400	0.72380000
C	0.32955500	-7.90921400	-0.72379800
C	4.92561600	-6.19733800	-0.72380100
C	4.92561600	-6.19733800	0.72380200
C	3.91501400	-6.99235700	1.43621300
C	4.00247900	-7.28398300	2.80423200
C	2.93584400	-7.88097800	3.47185900
C	1.73856600	-8.12719400	2.80423000
C	-0.86875700	-7.77460200	1.39805000
C	-2.09130800	-7.51258400	0.72273200
C	-2.09130800	-7.51258400	-0.72273000
C	-0.86875700	-7.77460200	-1.39804800
C	-3.23174200	-7.06898000	1.40671000
C	-4.31341900	-6.49683800	0.72273200
C	-4.31341900	-6.49683800	-0.72273000
C	-3.23174200	-7.06898000	-1.40670800
C	5.74373800	-5.31147500	-1.39804700
C	6.49683900	-4.31341900	-0.72273100
C	6.49683900	-4.31341900	0.72273100
C	5.74373800	-5.31147400	1.39804700
C	7.06898200	-3.23174300	-1.40670900
C	7.51258600	-2.09130800	-0.72273200
C	7.51258600	-2.09130800	0.72273100
C	7.06898200	-3.23174200	1.40670900

C	-5.31147500	-5.74373700	1.39804800
C	-6.19733900	-4.92561500	0.72380300
C	-6.19733900	-4.92561500	-0.72380100
C	-5.31147500	-5.74373700	-1.39804600
C	-6.99235800	-3.91501300	1.43621300
C	-7.37512800	-2.74745700	0.72736600
C	-7.37512800	-2.74745700	-0.72736500
C	-6.99235900	-3.91501400	-1.43621100
C	-7.84939800	-1.61397600	1.43621700
C	-7.90921600	-0.32955500	0.72379900
C	-7.90921600	-0.32955500	-0.72379800
C	-7.84939800	-1.61397600	-1.43621600
C	-8.12719700	-1.73856600	-2.80422800
C	-7.88098100	-2.93584400	-3.47185800
C	-7.28398500	-4.00247900	-2.80423000
C	-7.28398400	-4.00247800	2.80423200
C	-7.88098000	-2.93584300	3.47185900
C	-8.12719700	-1.73856500	2.80423000
C	-4.00247900	7.28398300	-2.80423200
C	-3.91501300	6.99235700	-1.43621300
C	-2.74745700	7.37512700	-0.72736600
C	-1.61397600	7.84939600	-1.43621700
C	-1.73856600	8.12719500	-2.80423000
C	-2.93584400	7.88097800	-3.47185900
C	-2.74745700	7.37512700	0.72736500
C	-1.61397600	7.84939700	1.43621500
C	-0.32955500	7.90921500	0.72379800
C	-0.32955500	7.90921500	-0.72379900
C	-4.92561500	6.19733800	-0.72380200

C	-4.92561600	6.19733800	0.72380100
C	-3.91501300	6.99235800	1.43621200
C	-4.00247900	7.28398400	2.80423000
C	-2.93584300	7.88097900	3.47185800
C	-1.73856500	8.12719600	2.80422800
C	0.86875700	7.77460200	1.39804800
C	2.09130800	7.51258400	0.72273100
C	2.09130800	7.51258400	-0.72273200
C	0.86875700	7.77460200	-1.39805000
C	3.23174200	7.06898000	1.40670800
C	4.31341900	6.49683800	0.72273000
C	4.31341900	6.49683800	-0.72273200
C	3.23174200	7.06898000	-1.40671000
C	-5.74373800	5.31147400	-1.39804800
C	-5.74373800	5.31147500	1.39804700
C	5.31147500	5.74373700	1.39804600
C	6.19733800	4.92561500	0.72380100
C	6.19733800	4.92561500	-0.72380200
C	5.31147500	5.74373700	-1.39804800
C	6.99235800	3.91501300	1.43621200
C	7.37512800	2.74745700	0.72736500
C	7.37512800	2.74745700	-0.72736600
C	6.99235800	3.91501300	-1.43621300
C	7.84939800	1.61397600	1.43621600
C	7.90921600	0.32955500	0.72379800
C	7.90921600	0.32955500	-0.72379900
C	7.84939700	1.61397600	-1.43621700
C	8.12719600	1.73856500	-2.80423000
C	7.88097900	2.93584300	-3.47185900

C	7.28398400	4.00247800	-2.80423200
C	7.28398400	4.00247900	2.80423000
C	7.88098000	2.93584400	3.47185800
C	8.12719700	1.73856600	2.80422800
C	-7.77460400	0.86875800	1.39805000
C	-7.51258500	2.09130800	0.72273100
C	-7.51258500	2.09130800	-0.72273100
C	-7.77460400	0.86875700	-1.39804900
C	-7.06898100	3.23174200	1.40670900
C	-6.49683900	4.31341900	0.72273100
C	-6.49683900	4.31341900	-0.72273100
C	-7.06898100	3.23174200	-1.40670900
H	7.70592000	-0.87319200	2.48174400
H	7.70591900	-0.87319300	-2.48174500
H	4.91557400	-7.05969500	-3.34658300
H	0.90120200	-8.55486400	-3.34655800
H	4.91557400	-7.05969400	3.34658400
H	0.90120200	-8.55486300	3.34656000
H	-0.87319200	-7.70591700	2.48174600
H	-0.87319200	-7.70591700	-2.48174400
H	-3.22019300	-7.04371000	2.49449700
H	-3.22019300	-7.04371000	-2.49449500
H	5.70205600	-5.25658100	-2.48173400
H	5.70205600	-5.25658100	2.48173400
H	7.04371100	-3.22019300	-2.49449600
H	7.04371200	-3.22019300	2.49449600
H	-5.25658100	-5.70205500	2.48173500
H	-5.25658200	-5.70205500	-2.48173300
H	-8.55486600	-0.90120300	-3.34655900

H	-7.05969600	-4.91557400	-3.34658200
H	-7.05969600	-4.91557300	3.34658400
H	-8.55486500	-0.90120200	3.34656000
H	-4.91557400	7.05969500	-3.34658400
H	-0.90120200	8.55486400	-3.34656000
H	-4.91557400	7.05969500	3.34658300
H	-0.90120200	8.55486400	3.34655800
H	0.87319200	7.70591800	2.48174400
H	0.87319200	7.70591800	-2.48174600
H	3.22019300	7.04371000	2.49449500
H	3.22019300	7.04371000	-2.49449700
H	-5.70205600	5.25658000	-2.48173500
H	-5.70205600	5.25658100	2.48173400
H	5.25658100	5.70205500	2.48173300
H	5.25658100	5.70205500	-2.48173500
H	8.55486500	0.90120200	-3.34656000
H	7.05969500	4.91557300	-3.34658400
H	7.05969600	4.91557400	3.34658200
H	8.55486500	0.90120300	3.34655900
H	-7.70591900	0.87319300	2.48174500
H	-7.70591900	0.87319200	-2.48174500
H	-7.04371100	3.22019300	2.49449600
H	-7.04371100	3.22019200	-2.49449600
H	-8.13180500	-3.02926100	-4.52480600
H	-3.02926000	8.13180200	-4.52480800
H	3.02925900	-8.13180300	-4.52480600
H	8.13180300	3.02925900	-4.52480800
H	-3.02926000	8.13180300	4.52480600
H	-8.13180400	-3.02925900	4.52480800

H	8.13180400	3.02926000	4.52480600
H	3.02926000	-8.13180100	4.52480800

Table S19- Cartesian coordinates for [25]pyrenecyclacene.

O 1

C	-3.32950700	9.72015300	2.80782800
C	-3.18397800	9.46663600	1.43682900
C	-4.26825700	8.88707400	0.72743600
C	-5.39840600	8.40316300	1.43691100
C	-5.50519400	8.67528100	2.80790800
C	-4.49357700	9.35648700	3.47859100
C	-4.26828200	8.88701600	-0.72799200
C	-5.39845600	8.40305000	-1.43739000
C	-6.36581600	7.55748500	-0.72394200
C	-6.36579100	7.55754200	0.72356400
C	-1.91922900	9.69290000	0.72340500
C	-1.91925400	9.69284200	-0.72410800
C	-3.18402800	9.46652200	-1.43746900
C	-3.32960500	9.71993100	-2.80848300
C	-4.49369900	9.35621200	-3.47917600
C	-5.50529200	8.67505900	-2.80840400
C	-7.16854000	6.65660900	-1.39708000
C	-7.93381700	5.66840800	-0.72279200
C	-7.93379300	5.66846500	0.72261800
C	-7.16849200	6.65672000	1.39680100
C	-8.55938300	4.61731800	-1.40685700
C	-9.09474500	3.51759700	-0.72268900
C	-9.09472100	3.51765500	0.72272700
C	-8.55933500	4.61743000	1.40678900
C	-9.50077100	2.33545500	-1.39687400

C	-9.81318700	1.17003500	-0.72362900
C	-9.81316200	1.17009300	0.72388000
C	-9.50072400	2.33556700	1.39702000
C	-9.98885600	-0.10277700	-1.43696900
C	-9.77272500	-1.31302300	-0.72748800
C	-9.77270000	-1.31296500	0.72793500
C	-9.98880700	-0.10266200	1.43732700
C	-9.66154600	-2.53732000	1.43742100
C	-9.95322300	-2.55478800	2.80844600
C	-10.28850500	-1.38218300	3.47913300
C	-10.27476900	-0.16271600	2.80835100
C	-9.66159700	-2.53743500	-1.43688000
C	-9.15610600	-3.71864700	-0.72344400
C	-9.15607900	-3.71858900	0.72406200
C	-10.27486600	-0.16294100	-2.80797800
C	-10.28862500	-1.38246100	-3.47866200
C	-9.95332000	-2.55501200	-2.80789300
C	-8.54705900	-4.76027500	-1.39660400
C	-7.84333400	-5.79322100	-0.72233700
C	-7.84330700	-5.79316100	0.72307600
C	-8.54700700	-4.76016000	1.39728400
C	-7.03664800	-6.71265600	-1.40643000
C	-6.15583400	-7.56129700	-0.72229700
C	-6.15580700	-7.56123700	0.72311700
C	-7.03659400	-6.71254000	1.40721300
C	-5.15684900	-8.31250300	-1.39652300
C	-4.14483700	-8.96953200	-0.72332600
C	-4.14481000	-8.96947300	0.72418500
C	-5.15679600	-8.31238800	1.39736700

C	-2.98861400	-9.52988300	-1.43671900
C	-1.77078700	-9.69837500	-0.72729900
C	-1.77076000	-9.69831800	0.72813000
C	-2.98856100	-9.52976800	1.43758000
C	-0.57204300	-9.97130600	-1.43674400
C	0.70761100	-9.85575000	-0.72337400
C	0.70763700	-9.85569400	0.72412800
C	-0.57199100	-9.97119300	1.43755300
C	-0.64547800	-10.25414200	2.80854200
C	-1.86426300	-10.21052000	3.47928600
C	-3.01976900	-9.82039000	2.80858900
C	-3.01987000	-9.82061300	-2.80770300
C	-1.86438800	-10.21079600	-3.47841100
C	-0.64557900	-10.25436400	-2.80770700
C	1.88648400	-9.59867700	-1.39660400
C	3.08646400	-9.24890100	-0.72239600
C	3.08649000	-9.24884700	0.72301600
C	1.88653500	-9.59857000	1.39729400
C	4.21029000	-8.76617000	-1.40654700
C	5.28979300	-8.19102500	-0.72247600
C	5.28982000	-8.19097000	0.72293500
C	4.21034200	-8.76606400	1.40708900
C	-0.71427100	9.75602100	1.39657400
H	-0.69570200	9.69316800	-2.48101900
C	-0.71432000	9.75590800	-1.39732400
C	8.40800500	-5.90708800	2.80823000
C	8.14122600	-5.78763000	1.43723000
C	8.67776000	-4.68150800	0.72774400
C	9.30764000	-3.62566500	1.43712600

C	9.55404400	-3.78294500	2.80812300
C	9.13604600	-4.92862400	3.47890000
C	8.67773500	-4.68156500	-0.72767900
C	9.30759100	-3.62577700	-1.43716500
C	9.59298600	-2.37299300	-0.72383000
C	9.59301000	-2.37293700	0.72368300
C	7.25095300	-6.71409900	0.72389300
C	7.25092700	-6.71415400	-0.72361900
C	8.14117500	-5.78774200	-1.43706000
C	8.40790600	-5.90730800	-2.80805900
C	9.13592400	-4.92889600	-3.47883100
C	9.55394600	-3.78316500	-2.80815900
C	9.71251800	-1.17236300	-1.39707300
C	9.75049100	0.07698400	-0.72287800
C	9.75051400	0.07704000	0.72253400
C	9.71256200	-1.17225300	1.39682800
C	9.63848000	1.29495500	-1.40703200
C	9.42498500	2.49934200	-0.72296700
C	9.42500800	2.49939900	0.72244300
C	9.63852400	1.29506500	1.40659600
C	9.05856300	3.69429900	-1.39725500
C	8.62631900	4.82083200	-0.72409500
C	8.62634300	4.82088900	0.72341400
C	9.05860800	3.69440900	1.39664800
C	8.02032500	5.95378200	-1.43751600
C	7.13406200	6.80586300	-0.72810300
C	7.13408700	6.80592100	0.72731600
C	8.02037400	5.95389600	1.43676600
C	6.32457300	7.73121500	1.43672900

C	6.55037400	7.91699600	2.80770700
C	7.51092000	7.16552100	3.47843000
C	8.21654500	6.17077900	2.80773500
C	6.32452300	7.73110000	-1.43756200
C	5.22127000	8.38966500	-0.72418000
C	5.22129500	8.38972300	0.72333300
C	8.21644900	6.17055700	-2.80851000
C	7.51080000	7.16524500	-3.47925800
C	6.55027700	7.91677300	-2.80856200
C	6.31315000	-7.47325900	1.39713200
C	6.31309900	-7.47336600	-1.39676600
C	4.11629200	8.87432500	-1.39737300
C	2.93983300	9.29644200	-0.72312400
C	2.93985800	9.29650000	0.72228400
C	4.11634100	8.87443800	1.39652600
C	1.74680700	9.56620400	-1.40722400
C	0.53541700	9.73525500	-0.72310100
C	0.53544200	9.73531300	0.72230900
C	1.74685600	9.56631800	1.40640400
H	-2.53790700	10.22618700	3.35074300
H	-6.39499300	8.37384300	3.35090200
H	-4.60501200	9.58859600	4.53405900
H	-2.53802500	10.22592200	-3.35146500
H	-4.60517100	9.58823900	-4.53465800
H	-6.39511000	8.37357800	-3.35134300
H	-7.13136400	6.60288000	-2.48078200
H	-7.13127900	6.60307800	2.48050700
H	-8.54031300	4.60697500	-2.49478500
H	-8.54022900	4.60717500	2.49471600

H	-9.43539600	2.33374100	-2.48057100
H	-9.43531300	2.33394000	2.48071500
H	-9.94134500	-3.49418000	3.35145500
H	-10.54358200	-1.41643000	4.53462700
H	-10.51138700	0.74651600	3.35128000
H	-10.51150300	0.74624900	-3.35097200
H	-10.54373900	-1.41679200	-4.53414500
H	-9.94146100	-3.49444700	-3.35082800
H	-8.48442400	-4.74143300	-2.48030000
H	-8.48433000	-4.74122900	2.48097700
H	-7.02094800	-6.69769700	-2.49435800
H	-7.02085300	-6.69749100	2.49514000
H	-5.13512100	-8.25089400	-2.48022600
H	-5.13502700	-8.25069000	2.48106400
H	0.25159200	-10.53337400	3.35145500
H	-1.91052000	-10.46382000	4.53475000
H	-3.95758600	-9.76444400	3.35156300
H	-3.95770700	-9.76471000	-3.35064900
H	-1.91068300	-10.46417900	-4.53385400
H	0.25147200	-10.53363900	-3.35063000
H	1.88789600	-9.53340900	-2.48030900
H	1.88798800	-9.53322000	2.48099500
H	4.20088500	-8.74667400	-2.49447600
H	4.20097700	-8.74648500	2.49501700
H	-0.69561500	9.69336700	2.48027400
H	8.06501600	-6.78172000	3.35121900
H	10.09671100	-3.01599100	3.35103200
H	9.36265200	-5.05083400	4.53437000
H	8.06489800	-6.78198200	-3.35096800

H	9.36249300	-5.05118900	-4.53430000
H	10.09659500	-3.01625400	-3.35114700
H	9.65073200	-1.15085300	-2.48077000
H	9.65081100	-1.15065900	2.48052500
H	9.61695900	1.29202400	-2.49496000
H	9.61703800	1.29222000	2.49452400
H	9.00464600	3.65717600	-2.48094900
H	9.00472600	3.65737200	2.48034800
H	5.98865500	8.67009200	3.35063800
H	7.69725400	7.34333700	4.53387500
H	8.94247500	5.57437200	3.35067400
H	8.94236000	5.57410600	-3.35142600
H	7.69709800	7.34297700	-4.53472500
H	5.98853900	8.66982600	-3.35153400
H	6.26127000	-7.43345400	2.48083100
H	6.26117900	-7.43364200	-2.48046600
H	4.07672300	8.82225500	-2.48107100
H	4.07681000	8.82245600	2.48022900
H	1.74289800	9.54485400	-2.49515200
H	1.74298600	9.54505500	2.49433400

Table S20- Cartesian coordinates for [10]-cyclacene

O 1

C	1.22067900	3.75686500	1.40875900
C	3.19578000	2.32187000	1.40875900
C	3.95020100	0.00000000	1.40875900
C	3.19578000	-2.32187000	1.40875900
C	1.22067900	-3.75686500	1.40875900
C	-1.22067900	-3.75686500	1.40875900
C	-3.19578000	-2.32187000	1.40875900

C	-3.95020100	0.00000000	1.40875900
C	-3.19578000	2.32187000	1.40875900
C	-1.22067900	3.75686500	1.40875900
C	0.00000000	3.93809600	-0.73170400
C	0.00000000	3.93809600	0.73170400
C	1.22067900	3.75686500	-1.40875900
C	2.31475500	3.18598700	-0.73170400
C	2.31475500	3.18598700	0.73170400
C	3.19578000	2.32187000	-1.40875900
C	3.74535200	1.21693900	-0.73170400
C	3.74535200	1.21693900	0.73170400
C	3.95020100	0.00000000	-1.40875900
C	3.74535200	-1.21693900	-0.73170400
C	3.74535200	-1.21693900	0.73170400
C	3.19578000	-2.32187000	-1.40875900
C	2.31475500	-3.18598700	-0.73170400
C	2.31475500	-3.18598700	0.73170400
C	1.22067900	-3.75686500	-1.40875900
C	0.00000000	-3.93809600	-0.73170400
C	0.00000000	-3.93809600	0.73170400
C	-1.22067900	-3.75686500	-1.40875900
C	-2.31475500	-3.18598700	-0.73170400
C	-2.31475500	-3.18598700	0.73170400
C	-3.19578000	-2.32187000	-1.40875900
C	-3.74535200	-1.21693900	-0.73170400
C	-3.74535200	-1.21693900	0.73170400
C	-3.95020100	0.00000000	-1.40875900
C	-3.74535200	1.21693900	-0.73170400
C	-3.74535200	1.21693900	0.73170400

C	-3.19578000	2.32187000	-1.40875900
C	-2.31475500	3.18598700	-0.73170400
C	-2.31475500	3.18598700	0.73170400
C	-1.22067900	3.75686500	-1.40875900
H	3.92588700	0.00000000	2.49660800
H	3.17610900	2.30757800	2.49660800
H	1.21316600	3.73374000	2.49660800
H	-1.21316600	3.73374000	2.49660800
H	3.92588700	0.00000000	-2.49660800
H	3.17610900	2.30757800	-2.49660800
H	3.17610900	-2.30757800	-2.49660800
H	1.21316600	3.73374000	-2.49660800
H	1.21316600	-3.73374000	-2.49660800
H	-1.21316600	3.73374000	-2.49660800
H	-1.21316600	-3.73374000	-2.49660800
H	-3.17610900	2.30757800	-2.49660800
H	-3.17610900	2.30757800	2.49660800
H	-3.92588700	0.00000000	2.49660800
H	-3.17610900	-2.30757800	2.49660800
H	-1.21316600	-3.73374000	2.49660800
H	1.21316600	-3.73374000	2.49660800
H	3.17610900	-2.30757800	2.49660800
H	-3.92588700	0.00000000	-2.49660800
H	-3.17610900	-2.30757800	-2.49660800

Table S21- Cartesian Coordinates for [20]cyclacene

O 1

C	7.83813500	0.04485700	0.73421700
C	7.83813600	0.04485700	-0.73421400
C	7.73946900	1.27126400	-1.41150200

C	7.44048100	2.46471000	-0.73421700
C	7.44048100	2.46471000	0.73422100
C	7.73946700	1.27126500	1.41150600
C	6.96763600	3.60059400	-1.41150400
C	6.31453600	4.64325600	-0.73421200
C	6.31453600	4.64325600	0.73421600
C	6.96763500	3.60059600	1.41150700
C	7.75366600	-1.18256400	1.41150300
C	7.46843300	-2.37942400	0.73421800
C	7.46843400	-2.37942400	-0.73421600
C	7.75366800	-1.18256500	-1.41150100
C	5.51399500	5.57755900	-1.41150700
C	4.57071300	6.36746000	-0.73421800
C	4.57071400	6.36746000	0.73422200
C	5.51399500	5.57756100	1.41151100
C	3.52062400	7.00863900	-1.41150700
C	2.37942100	7.46837400	-0.73421600
C	2.37942200	7.46837500	0.73421900
C	3.52062300	7.00864000	1.41151100
C	1.18256600	7.75360100	-1.41150100
C	-0.04486000	7.83807000	-0.73421300
C	-0.04486000	7.83806900	0.73421700
C	1.18256400	7.75360200	1.41150500
C	-1.27126400	7.73940000	-1.41150200
C	-2.46471400	7.44042200	-0.73421700
C	-2.46471400	7.44042100	0.73422000
C	-1.27126500	7.73939900	1.41150600
C	-3.60060200	6.96758700	-1.41150500
C	-4.64327000	6.31450000	-0.73421300

C	-4.64327000	6.31449900	0.73421600
C	-3.60060300	6.96758500	1.41150800
C	7.00869400	-3.52061800	1.41150900
C	6.36750100	-4.57070700	0.73422000
C	6.36750100	-4.57070700	-0.73422000
C	7.00869500	-3.52061900	-1.41150800
C	5.57759600	-5.51397500	1.41150900
C	4.64327200	-6.31450500	0.73421400
C	4.64327300	-6.31450500	-0.73421600
C	5.57759500	-5.51397500	-1.41151000
C	3.60060900	-6.96758700	1.41150400
C	2.46471100	-7.44042000	0.73421700
C	2.46471100	-7.44041900	-0.73422100
C	3.60060800	-6.96758600	-1.41150700
C	1.27127000	-7.73939300	1.41150100
C	0.04485500	-7.83805900	0.73421300
C	0.04485600	-7.83805900	-0.73421800
C	1.27126900	-7.73939200	-1.41150500
C	-1.18255900	-7.75359100	1.41150000
C	-2.37942600	-7.46836100	0.73421500
C	-2.37942600	-7.46836100	-0.73422000
C	-1.18256000	-7.75359000	-1.41150500
C	-3.52061900	-7.00863200	1.41150600
C	-4.57072100	-6.36745300	0.73421700
C	-4.57072000	-6.36745200	-0.73422300
C	-3.52061900	-7.00863000	-1.41151200
C	-5.57758400	5.51396900	-1.41150900
C	-6.36749400	4.57069800	-0.73421900
C	-6.36749400	4.57069700	0.73422100

C	-5.57758500	5.51396600	1.41151100
C	-5.51399800	-5.57756300	1.41150700
C	-6.31454700	-4.64325500	0.73421200
C	-6.31454700	-4.64325400	-0.73421700
C	-5.51399800	-5.57756100	-1.41151200
C	-7.00868400	3.52061100	-1.41150900
C	-7.46842900	2.37941800	-0.73421700
C	-7.46843000	2.37941700	0.73421700
C	-7.00868400	3.52060900	1.41151000
C	-7.75366800	1.18256000	-1.41150400
C	-7.83814200	-0.04485900	-0.73421500
C	-7.83814200	-0.04486000	0.73421300
C	-7.75366800	1.18255700	1.41150300
C	-6.96764300	-3.60060200	1.41150400
C	-7.44049100	-2.46471100	0.73421600
C	-7.44049100	-2.46471000	-0.73422000
C	-6.96764300	-3.60059900	-1.41150900
C	-7.73947300	-1.27127100	1.41150300
C	-7.73947300	-1.27126800	-1.41150600
H	7.72409300	1.26878500	-2.49946700
H	7.72409000	1.26878500	2.49947000
H	6.95379300	3.59349700	-2.49946800
H	6.95379200	3.59349800	2.49947200
H	7.73830000	-1.18017000	2.49946800
H	7.73830400	-1.18017100	-2.49946600
H	5.50307800	5.56657900	-2.49947300
H	5.50307800	5.56658200	2.49947700
H	3.51359400	6.99475800	-2.49947100
H	3.51359400	6.99476000	2.49947500

H	1.18017000	7.73823400	-2.49946600
H	1.18016900	7.73823500	2.49947000
H	-1.26878300	7.72401200	-2.49946600
H	-1.26878500	7.72401000	2.49947000
H	-3.59350300	6.95374300	-2.49946900
H	-3.59350400	6.95373900	2.49947200
H	6.99481800	-3.51359200	2.49947300
H	6.99481900	-3.51359300	-2.49947200
H	5.56661800	-5.50306300	2.49947400
H	5.56661800	-5.50306200	-2.49947500
H	3.59351100	-6.95374600	2.49946800
H	3.59351000	-6.95374400	-2.49947100
H	1.26878700	-7.72400600	2.49946500
H	1.26878700	-7.72400400	-2.49947000
H	-1.18016600	-7.73822400	2.49946500
H	-1.18016700	-7.73822200	-2.49947000
H	-3.51358900	-6.99474600	2.49947000
H	-3.51359000	-6.99474400	-2.49947600
H	-5.56660400	5.50305300	-2.49947400
H	-5.56660500	5.50304900	2.49947600
H	-5.50308100	-5.56658200	2.49947200
H	-5.50308200	-5.56657900	-2.49947800
H	-6.99480000	3.51358200	-2.49947300
H	-6.99480100	3.51357800	2.49947400
H	-7.73830500	1.18016600	-2.49946900
H	-7.73830600	1.18016300	2.49946800
H	-6.95380300	-3.59350400	2.49946900
H	-6.95380300	-3.59350000	-2.49947300
H	-7.72409000	-1.26879000	2.49946700

H -7.72408900 -1.26878600 -2.49947000